JOURNAL OF THE MECHANICS AND PHYSICS OF SOLIDS

EDITORIAL ADVISORY BOARD

J. F. BAKER—Cambridge W. M. BALDWIN—Cleveland
E. BRANDENBERGER—Zürich G. BUSCH—Zürich
A. H. COTTRELL—Birmingham C. CRUSSARD—Paris M. J. DRUYVESTEYN—Delft
A. KOCHENDÖRFER—Düsseldorf N. F. MOTT—Bristol A. NADAI—Pittsburgh, Pa.
G. SACHS—Syracuse, N.Y. E. SIEBEL—Stuttgart H. W. SWIFT—Sheffield

EDITOR-IN-CHIEF

R. HILL
University of Nottingham

Volume 3
1954 — 55

PERGAMON PRESS LTD · LONDON & NEW YORK

Vol
3
1954/

Contents of Volume 3

NUMBER 1 PAGE

A. P. GREEN: A theory of the plastic yielding due to bending of cantilevers and fixed-ended beams. Part I 1

B. B. HUNDY and A. P. GREEN: A determination of plastic stress-strain relations 16

A. J. WANG and H. G. HOPKINS: On the plastic deformation of built-in circular plates under impulsive load 22

D. B. C. TAYLOR: The dynamic straining of metals having definite yield points 38

R. HILL: The mechanics of machining: A new approach 47

J. D. CAMPBELL: The yield of mild steel under impact loading 54

P. M. NAGHDI and J. C. ROWLEY: An experimental study of biaxial stress-strain relations in plasticity 63

Book reviews:

"Les fonctions orthogonales dans les problemes aux limites de la physique mathématique" by T. VOGEL (reviewed by G. POWER) 81

"Formulas for Stress and Strain" by R. J. ROARK (reviewed by M. R. HORNE) .. 81

"Dislocations in Crystals" by W. T. READ (reviewed by T. BROOM) 82

"Crystal Growth and Dislocations" by AJIT RAM VERMA (reviewed by C. W. BUNN) 82

"Stress Waves in Solids" by H. KOLSKY (reviewed by E. H. LEE) 83

NUMBER 2

J. E. DORN: Some fundamental experiments on high temperature creep .. 85

H. G. HOPKINS and A. J. WANG: Load-carrying capacities for circular plates of perfectly-plastic material with arbitrary yield conditions 117

J. F. W. BISHOP: A theory of the tensile and comprehensive textures of face-centred cubic metals 130

A. P. GREEN: A theory of the plastic yielding due to bending of cantilevers and beams. Part II 143

C. STEELE: The plastic bending and twisting of square section numbers .. 156

Book reviews:

"Twinning and Diffusionless Transformations in Metals" by E. O. HALL (reviewed by A. H. COTTRELL) 167

"Structure and Properties of Solid Surfaces" Ed. by ROBERT GOMER and CYRIL STANLEY SMITH (reviewed by F. C. FRANK) 167

NUMBER 3

A. J. WANG and W. PRAGER: Plastic twisting of a circular ring sector .. 169

P. G. HODGE, Jr.: Impact pressure loading of rigid-plastic cylindrical shells 176

A. P. GREEN: An unsymmetrical extrusion in plane strain 189

D. S. DUGDALE: Experiments with pyramidal indenters. Part I 197

Vol.
3
54/55

NUMBER 3 (*Cont'd*) PAGE

D. S. DUGDALE: Experiments with pyramidal indenters. Part II 206

LO-CHING CHANG: X-ray microbeam studies of brittle fractures of metals .. 212

W. JOHNSON: Extrusion through wedge-shaped dies. Part I 218

W. JOHNSON: Extrusion through wedge-shaped dies. Part II 224

Book reviews:

" Dynamical Theory of Crystal Lattices " by MAX BORN and KUN HUANG (reviewed by J. D. ESHELBY) 231

" Theoretical Elasticity " by A. E. GREEN and W. ZERNA (reviewed by R. HILL) .. 231

" Progress in Metal Physics," Vol. 5, Ed. by B. CHALMERS and R. KING (reviewed by by N. F. MOTT) 231

" Magnetic Cooling " by C. G. B. GARRETT (reviewed by L. F. BATES) 232

" Relaxation Methods " by D. N. DE G. ALLEN (reviewed by W. M. SHEPHERD) .. 232

NUMBER 4

J. M. ALEXANDER: The effect of coulomb friction in the plane-strain compression of a plastic-rigid material.. 233

R. T. SHIELD: Plastic flow in a converging conical channel 246

J. F. W. BISHOP: On the contribution of crystallographic fibring to hardening under uniaxial straining conditions 259

A. H. CHILVER: Average warping in the torsion of thin-walled open-section beams 267

F. GAROFALO and J. R. LOW, Jr.: The effect of prestraining in simple tension and biaxial tension on flow and fracture behaviour of a low carbon deep drawing steel sheet 275

Book reviews:

" Analysis of Deformation, Volume 2 " by K. SWAINGER (reviewed by J. F. W. BISHOP) 295

" Strength and Resistance of Metals " by J. M. LESSELLS ((reviewed by J. A. POPE) .. 295

Author Index

(B) denotes a book review

ALEXANDER, J. M. p. 233.
BATES, L. F. p. 232 (B).
BISHOP, J. F. W. pp. 130, 259, 295 (B).
BROOM, T. p. 82 (B).
BUNN, C. W. p. 82 (B).
CAMPBELL, J. D. p. 54.
CHANG, LO-CHING. p. 212.
CHILVER, A. H. p. 267.
COTTRELL, A. H. p. 167 (B).
DORN, J. E. p. 85.
DUGDALE, D. S. pp. 197, 206.
ESHELBY, J. D. p. 231 (B).
FRANK, F. C. p. 167 (B).
GAROFALO, F. p. 275.
GREEN, A. P. pp. 1, 16, 143, 189.
HILL, R. p. 47, 231.
HODGE, P. G., Jr. p. 176.
HOPKINS, H. G. pp. 22, 117.
HORNE, M. R. p. 81 (B).
HUNDY, B. B. p. 16.
JOHNSON, W. pp. 218, 224.
LEE, E. H. p. 83 (B).
LOW, J. R., Jr. p. 275.
MOTT, N. F. p. 231 (B).
NAGHDI, P. M. p. 63.
POPE, J. A. p. 295 (B).
POWER, G. p. 81 (B).
PRAGER, W. p. 169.
ROWLEY, J. C. p. 63.
SHEPHERD, W. M. p. 232 (B).
SHIELD, R. T. p. 246.
STEELE, C. p. 156.
TAYLOR, D. B. C. p. 38.
WANG, A. J. pp. 22, 117, 169.

Vol 3 1954/

Journal of the Mechanics and Physics of Solids, 1954, Vol. 3, pp. 1 to 15. Pergamon Press Ltd., London.

A THEORY OF THE PLASTIC YIELDING DUE TO BENDING OF CANTILEVERS AND FIXED-ENDED BEAMS. PART I.

By A. P. Green
British Iron and Steel Research Association Metal Working Laboratories, Sheffield

(*Received* 14*th May*, 1954)

Summary

Plane strain and plane stress solutions are obtained for the plastic yielding of horizontal uniformly tapering cantilevers of rectangular section carrying a vertical end load. An isotropic plastic-rigid material is assumed, and, for the plane stress solutions, a Mises yield criterion. The effects of weak end support, and of axial loading in addition to vertical loading, are analysed for uniform cantilevers in plane strain.

VOL. 3 54/55

1. Introduction

The simple theory of plastic bending of a uniform beam by equal and opposite couples with or without axial load is well known (see for example Nadai 1931, Roderick 1948, Hill 1950, p. 81), and is well supported by experiment (Roderick and Phillips 1949, Baker *et al.* 1949, Neal 1950). The same theory is often applied to the calculation of bending moments in beams bent under shearing loads. It is in fact assumed, at present, in the plastic limit design of structures (Baker 1949, Symonds and Neal 1951) that the effect of shearing loads on the bending moment is negligible for most practical purposes. The assumption is known to be incorrect, however, if the mean shear stress across a transverse section is high (Hendry 1950).

The present work is an attempt to assess theoretically the effect of shearing loads. In Part I, plain strain and plain stress solutions are described for the problem of a cantilever of rectangular transverse section bent under end loading. Only those solutions are considered for which yielding does not extend to the loaded end of the cantilever. The only published work on this problem appears to be a paper by Horne (1951) to which more detailed reference is made below.

An isotropic plastic-rigid material is assumed, i.e. the rigidity modulus is assigned an indefinitely large value. The yield-point for a given loading system is precisely defined, therefore, as the moment when local distortion first begins. The yield-point load has the practical significance that the load for an actual material with a finite rigidity may be raised very near to it and yet cause a permanent distortion of elastic order of magnitude only (Hill and Siebel 1953).

In Part II, the solutions for uniform cantilevers are applied to the problems

of yielding of a centrally loaded simply supported beam, and of centrally or uniformly loaded fixed-ended beams. All the plane stress solutions for uniformly thick cantilevers and fixed-ended beams are then applied to corresponding problems for I-beams bent about axes perpendicular to their webs. Finally, some of the theoretical results, both yield-point loads and modes of deformation, are compared with experiment.

2. Formulation of the problem

Consider a uniformly tapering horizontal cantilever of length l which is symmetrical about a horizontal plane through Oy (Fig. 1). Its horizontal width w is constant, and any transverse section perpendicular to Oy is rectangular. Its thick-

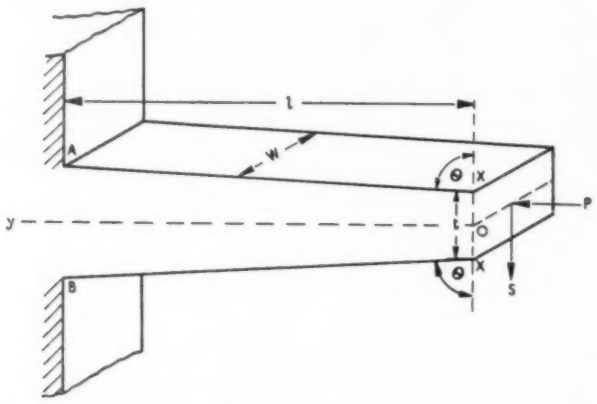

Fig. 1. Uniformly tapering cantilever of rectangular cross-section.

ness is a minimum t at the unsupported end O. It is supported in position and direction at one end AB and the other end XOX carries a uniform shearing stress S and a uniform axial pressure P, just sufficient to cause yielding. The weight of the cantilever itself is neglected since it is small in comparison with the yield-point loads.

Solutions are obtained under the two extreme conditions of plane strain and plane stress,* corresponding to a wide and a narrow beam respectively. The approximation to one or other of these conditions should be very close if w is larger or smaller than the thickness of the beam at the regions of deformation by a factor of at least six. The plane strain solutions are valid for any yield criterion; in the plane stress solutions a Mises yield criterion is assumed. The possibility of buckling in a narrow beam is not considered here.

Most of the solutions obtained are incomplete in that no stress distribution is constructed in the non-deforming regions. Hence, according to Hill's (1951) extremum principles for a plastic-rigid body,the yield-point loads may be overestimated, though this is unlikely, especially in view of the experimental confirmation obtained for deformation modes.

* For a detailed account of the theories of plane plastic strain and plane plastic stress see R. Hill, *The Mathematical Theory of Plasticity*, Chs. 6 and 11 (Clarendon Press, Oxford). The same notation is used in this paper.

HORNE (1951) considered a uniformly thick cantilever carrying a vertical load at one end. He assumed plane stress conditions and a Tresca yield criterion. His solutions are incomplete, however, because he did not construct a mode of deformation compatible with his stress distribution. They are equilibrium states of stress which obey the stress boundary conditions and which do not violate the yield criterion except in two very small areas. Such solutions tend to underestimate the yield-point loads (HILL 1951). They are not compared here with the present solutions because a different yield criterion was assumed.

3. PLANE STRAIN SOLUTIONS

(a) *Shearing without axial load*

First let us suppose that the cantilever is rigidly fixed at AB and yields under a vertical load St only at the other end (Fig. 2). S depends on θ and the ratio l/t i.e. on the geometry of the cantilever.

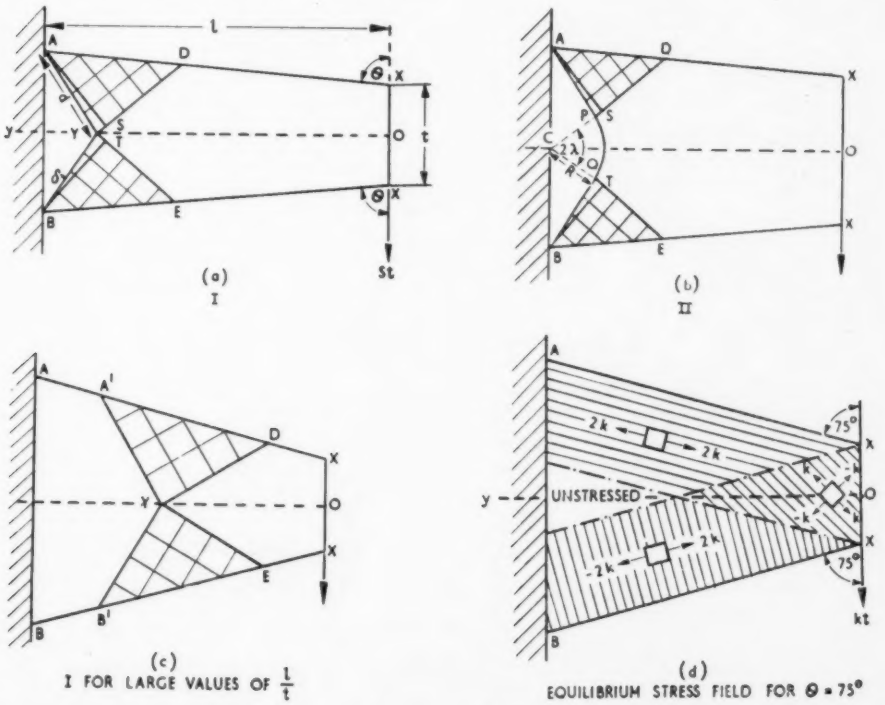

Fig. 2. Plate strain solutions for strongly supported tapering cantilevers under shear loading. (a) I ; (b) II ; (c) I for large values of l/t ; (d) Equilibrium stress field for $\theta = 75°$.

If l/t and θ are sufficiently large the cantilever may be expected to yield by the formation of a plastic ' hinge ' at its fixed end where the bending moment is greatest, while the rest of it remains rigid. This suggests the slip-line fields I and II shown in Figs. 2a and 2b. These fields are similar to those devised for the bending of a wide bar notched symmetrically on opposite sides with deep wedge

shaped notches (GREEN 1953a). In the present problem, solution I applies to the higher values of l/t and solution II to the lower values.

In ADS and BET the field, which is determined by the straight stress-free edge, consists of straight lines inclined at angles $\pi/4$ to the edge. It is extended round the singularities at A and B to form the regions AYS and BYT (on APS and BQT), consisting of straight lines and circular acrs. These regions meet at a point Y in I, but in II they are connected by the single curved slip-line PYQ. Relative to its rigid support the cantilever yields by the rotation of its rigid end, in I about Y, and in II by sliding over the arc PYQ. Therefore, PYQ must be a circular arc, and $APYQB$ a continuous slip-line across which there is a velocity discontinuity. The material in $AYSD$ (or $APSD$) is extended and in $BYTE$ (or $BQTE$) is compressed. Hence, the mean compressive stress p is equal to $-k$ in ADS and to k in BET, where k is the yield stress in pure shear of the material. In I there is a stress discontinuity across the point Y.

TABLE 1. PLANE STRAIN.

Strongly supported cantilevers with uniform taper yielding under shear load.

θ	l/t	S/k	d/t	R/t	δ
90°	∞	0	0·707	0	0
	13·73	0·038	0·625	0	8° 10′
	5·00	0·108	0·560	0·086	8° 10′
	2·00	0·281	0·401	0·298	8° 10′
	1·00	0·518	0·183	0·590	8° 10′
	0·73	0·635	0·076	0·733	8° 10′
85°	6·62	0·347	1·409	0	0
	5·32	0·351	1·169	0	5° 40′
	3·00	0·406	0·788	0·199	5° 40′
	2·00	0·485	0·564	0·371	5° 40′
	0·88	0·715	0·164	0·782	5° 40′
80°	3·63	0·684	1·393	0	0
	3·41	0·684	1·298	0	3° 10′
	2·50	0·702	0·962	0·233	3° 10′
	1·50	0·775	0·532	0·593	3° 10′
	1·17	0·820	0·362	0·754	3° 10′

Let us denote the angle SBY $(= SAP)$ by δ, the length AS $(= BT)$ by d, the radius of curvature of the arc PQ by R and its angular span by 2λ. These dimensions are uniquely determined by the stress boundary conditions and the shape of the cantilever.

The fields must be symmetrical about Oy because the cantilever is symmetrical and $P = 0$. Therefore, in I Y lies on Oy, and in II OYC, the line which joins O to C the centre of curvature of the arc PQ, coincides with Oy. It follows that the initial direction of motion of O is vertically downwards.

In II p varies from $-k$ to $+k$ along $SPQT$, and by applying the Hencky relations (HILL 1950, p. 135) we find that $2\delta = \theta - \frac{1}{4}\pi - \frac{1}{2}$ and $2\lambda = \theta - \frac{1}{4}\pi + \frac{1}{2}$. In I δ is only limited by the condition that the yield criterion must not be violated

in the corner of the rigid region between SY and YT, i.e. the change in p in turning through the angle of this corner must not exceed that prescribed by the Hencky relations along a slip line turning through such an angle (HILL 1954). Hence, $2\delta \leqslant \theta - \frac{1}{4}\pi - \frac{1}{2}$, and solution I changes over to II when the equality sign holds and $R = 0$.

The shapes of the fields are finally determined by taking moments about Y or C for the portion of the cantilever to the right of AYB. Their dimensions and the corresponding values of S/k are given in Table 1 for values of $\theta = 90°$, $85°$, $80°$ and $75°$. The relations between S/k and l/t are shown in Fig. 3. When

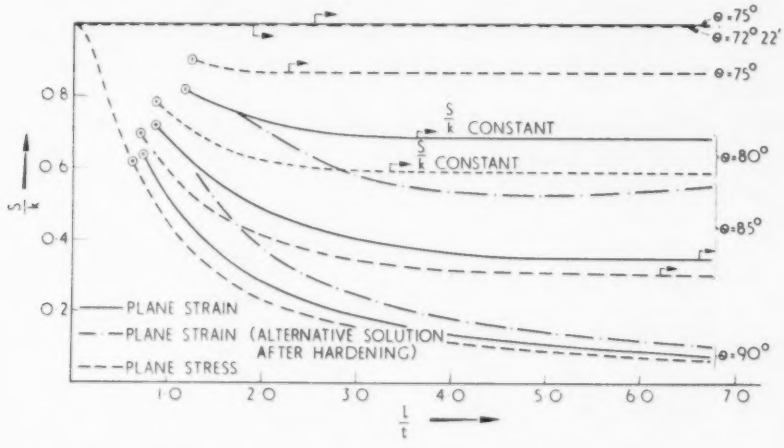

Fig. 3. Relations between S/k and l/t for strongly supported tapering cantilevers under shear loading.

$\theta = 75°$, $S = k$ for all values of l/t. For higher values of θ S/k varies and, as we would expect, decreases as l/t increases. The solutions are discussed below in further detail.

Solution I

For a given θ, as l/t increases, δ decreases. When $\delta = 0$

$$l/t = \tfrac{1}{2} \tan\theta\,(\sin 2\theta - \cos 2\theta), \text{ and } S/k = 2\sin 2\theta. \qquad (1)$$

This limiting solution is also valid for all greater values of l/t since, with $S = 0$, the corners A', B' of the field do not have to be anchored at the corners of the cantilever (Fig. 2c). When $\theta = \frac{1}{2}\pi$, $\delta \to 0$ only as $l/t \to \infty$, and in the limit $S = 0$. As θ is decreased the minimum value of l/t for which $\delta = 0$ also decreases, while the corresponding value of S increases, finally becoming equal to k when $\theta = 75°$. Fig. 2d shows an equilibrium stress field, involving stress discontinuities across the lines XY, which covers the whole cantilever. This is, therefore, a complete solution. It is clear that all cantilevers with $\theta \leqslant 75°$ yield when $S = k$ by shearing at the face XOX.

Solution II

For a given θ, as l/t decreases, R/t increases, and d/t decreases (see Table 1). The solution breaks down when yielding extends to the end XOX. It can be shown (by symmetry and other arguments) that the maximum average shear stress across a plane section of the (assumed) rigid cantilever occurs across YO. This means shear stress increases as l/t decreases and becomes equal to k, with d still finite. Let us denote the variables in this limiting solution by the subscript 0 (their values are given in Table 1 in the last line for each value of θ). As θ decreases, l_0/t_0 and S_0 increase while R_0/d_0 decreases, until for $\theta = 75°\ 0{\cdot}76'$ $l_0/t_0 = 2{\cdot}53$, $S_0/k = 0{\cdot}9998$, and $R = 0$. Over the minute range $75°\ 0{\cdot}76' > \theta > 75°$ the mean shear stress reaches the value k across YO for solutions of type 1. Finally, for $\theta = 75°$ the limit occurs when $S = 0$, the same slip-line field as that discussed above (Fig. 2d). Solutions for which $l/t < l_0/t_0$ are discussed in another paper (GREEN 1954).

Solutions for other shapes of cantilever may be constructed in similar manner. Calculations have been made by the writer (GREEN 1953b) for cantilevers with concave circular sides instead of a uniform taper.

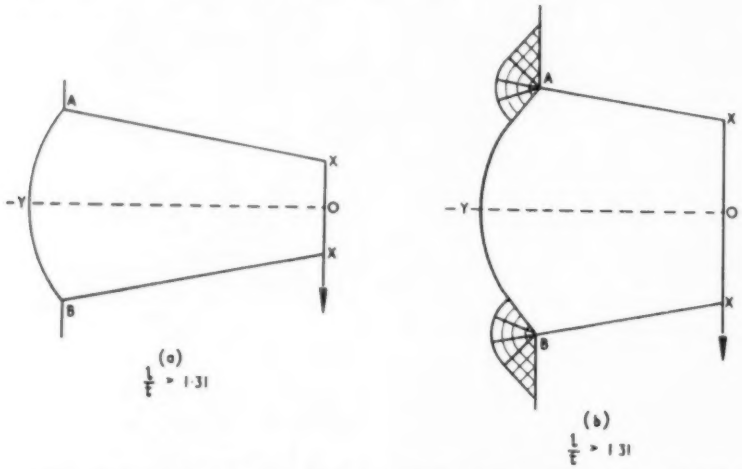

Fig. 4. Alternative modes of deformation in plane strain : (a) $l/t' > 1{\cdot}31$; (b) $l/t' > 1{\cdot}31$.

Alternative Modes of Deformation

Any mode of deformation is only instantaneously valid if the shape of the body and/or the distribution of hardness in the deforming region is changing. If the rate of hardening is rapid, deformation quickly spreads outwards from the original regions in which yielding commences. Some parts may cease to deform and may even unload elastically, particularly when deformation can proceed under falling loads. If, however, the applied loads must be increased in order to continue yielding, an entirely new mode of deformation may be initiated in regions which were previously rigidly constrained throughout. If, in the present problem, the cantilever and its vertical support are one piece of material of uniform width, an alternative mode involving deformation of the support may occur, as shown in Fig. 4. The slip-line field depends on the value of $l\ t'$ (where $t' = AB$)

but not of θ. If $l/t' > 1{\cdot}31$ it consists of a circular arc, AYB (Fig. 4a) with $p = 0$ at its mid-point, Y. The rigid material to the right of AYB rotates by sliding over the arc. Assuming that the change in shape of the cantilever is negligible up to the moment when this alternative deformation begins, the relations between S/k and l/t for $\theta = 90°$ and $85°$ have been calculated, and are shown in Fig. 3. It can be seen that S/k is always greater than its corresponding value for the solutions discussed previously, and the smaller θ the greater the difference. When $\theta = 90°$, the differences are small if l/t is large, and consequently the alternative mode soon comes into operation after initial yielding, if the rate of hardening is high. This has been confirmed by experiment (HUNDY 1954).

When $l/t' < 1{\cdot}31$ the slip-line field (Fig. 4b) includes regions of tension and compression near A and B adjacent to the horizontal faces of the blocks. No calculations have been made for this solution.

Effect of Weaker Support

Naturally the load which a cantilever can carry depends on the precise manner in which it is suppported at its fixed end. The solutions so far described have been for perfectly strong rigid support. In order to find out how sensitive to the end conditions the yield-point loads are likely to be, we now consider a weaker method of support.

Suppose that a uniformly thick cantilever fits into a horizontal slot $AJKB$ in a rigid vertical support (Fig. 5). Provided that the length of cantilever in the

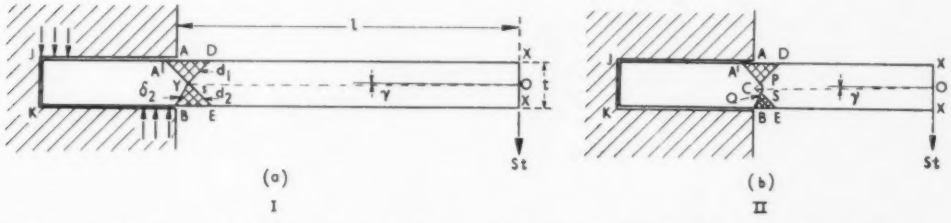

Fig. 5. Plane strain solutions for weakly supported uniform cantilevers under shear loading. (a) I ; (b) II.

slot is sufficiently long, it is reasonable to assume that yielding does not extend to the end JK. The beam is supported by an upward pressure over some region to the left of B and a downward pressure over some region to the right of J. The surface of the beam in the region of A is assumed to be clear of the support.

Possible slip-line field solutions of types I and II are shown in Fig. 5. They differ from those described above in that there is no singularity on the stress-free upper surface (i.e., $\delta_1 = 0$), and they are not therefore, symmetrical about Oy.*

In II, $\delta_2 = \frac{1}{4}\pi - \frac{1}{2}$ and $2\lambda = \frac{1}{4}\pi + \frac{1}{2}$. The change-over from II to I occurs when $l/t = 7{\cdot}59$. When $l/t = 0{\cdot}71$ the mean shear stress across CO is k. Since the solutions are unsymmetrical this may not be the precise value of l/t at which solution II breaks down, but it is probably a close approximation. The lack of

* Notation : lengths and angles which are equal in the symmetrical solutions I and II are denoted in similar but *unsymmetrical* solutions by the subscripts 1 and 2 in the tensile and compressive regions respectively.

symmetry also means that O no longer moves vertically downwards when yielding commences, but instead moves slightly outwards in a direction inclined at the small angle γ (say) to the vertical. The calculated dimensions of the fields and the corresponding values of S/k and γ are given in Table 2. Comparing these results with those for strong support, the reduction in S/k is only about 4% for the smallest values of l/t considered and decreases to about 1% when $l/t \sim 6$ and to zero as $l/t \to \infty$.

TABLE 2. PLANE STRAIN.
Weakly supported uniform cantilevers yielding under shear load.

l/t	S/k	d_1/t	d_2/t	R/t	γ^c
16·69	0·0307	0·717	0·598	0	
13·81	0·0372	0·719	0·588	0	
11·64	0·0443	0·720	0·579	0	
9·97	0·0520	0·723	0·570	0	
8·65	0·0602	0·725	0·562	0	
7·59	0·0689	0·727	0·553	0	0·002
5·84	0·0906	0·706	0·534	0·027	0·003
3·66	0·147	0·651	0·484	0·097	0·008
2·34	0·234	0·567	0·408	0·204	0·019
1·64	0·330	0·473	0·322	0·322	0·035
1·35	0·393	0·412	0·267	0·400	0·047
0·847	0·558	0·251	0·121	0·604	0·079
0·710	0·620	0·190	0·065	0·681	0·091

The solutions of Fig. 5 may be applied to other common conditions of support such as those shown in Figs. 6 and 7. The cantilever in Fig. 6 is welded or firmly clamped to the flat top of a rigid pillar. Fig. 7 shows a simply supported beam

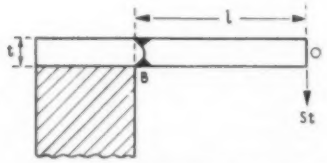

Fig. 6. Uniform cantilever firmly clamped to the top of a rigid vertical pillar.

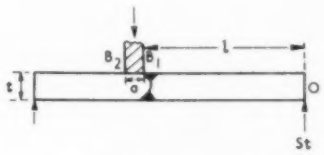

Fig. 7. Simply supported beam under concentrated load.

carrying a vertical load over a finite length $B_1 B_2 = a$. More detailed examination is required of the stresses in the (assumed) rigid region below $B_1 B_2$ to determine how large the ratio a/d_1 must be to avoid violating the yield criterion there. The solution is clearly invalid if a/d is very small but is probably valid if $a > \sqrt{2}\, d_1$. Since the bending moments are equal across the beam at B_1 and B_2, yielding takes place on the side for which the yield-point bending moment is least. This is not necessarily the side for which S is least (i.e. l greatest) as will be seen later in the discussion of results (Part II).

(b) *Uniform cantilever sheared under axial load*

The material is assumed to be isotropic and hence solutions with tensile axial loads are identical to those with compressive loads of equal magnitude and S reversed, except that the stresses and strain-rates are reversed at every point in the body. It is sufficient therefore to consider only compressive loading. Solutions are obtained for a cantilever of uniform thickness t firmly supported in position and direction at the end AB.

The application of pressure upsets the symmetry of loading, and consequently, the slip-line fields, are also unsymmetrical. The solutions I and II with $P = 0$ are modified by expanding the compressive and contracting the tensile regions* (Fig. 8), and may be conveniently subdivided into two different kinds, which are labelled (a) and (b) according to whether δ_1 is respectively greater than or equal to zero. As the pressure is increased on a given cantilever δ_1 decreases. If P is sufficiently large, $\delta_1 = 0$, the corner of the tensile region A need not be anchored at the corner of the cantilever, and its distance increases as the pressure is increased.

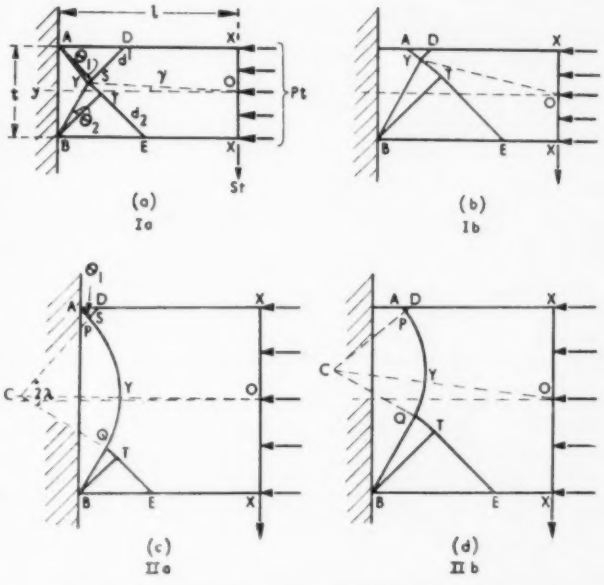

Fig. 8. Plane strain solutions for strongly supported uniform cantilevers under combined shear and axial loading : (a) Ia ; (b) Ib ; (c) IIa ; (d) IIb.

In the slip-line fields of solution I, $(\delta_1 + \delta_2)$ must be less than $(\frac{1}{4}\pi - \frac{1}{2})$ to avoid violating the yield criterion in the rigid corner to the right of Y. In solution II, the Hencky relations determine that $\delta_1 + \delta_2 = \frac{1}{4}\pi - \frac{1}{2}$ and the angular span of the circular arc PQ is $2\lambda = \frac{1}{4}\pi + \frac{1}{2}$.

The ranges of validity of the different types of solution are shown in Fig. 9 in terms of l/t and P. The transition from I to II occurs when $R = 0$, and the greater P the smaller is the value of l/t at which it occurs. R decreases with increasing l/t for a given pressure, or with increasing pressure for a given l/t. Both R and δ_1 are zero when $l/t = 5{\cdot}3$ and $P/k = 0{\cdot}66$.

In solution I (b) as P is increased on a given cantilever both δ_1 and d_1 decrease, becoming zero simultaneously when $S = 0$, $P = 2k$, and $\gamma = \tan^{-1}[t/2(l-t)] = \gamma_0$ say. The limiting slip-line field then consists only of the compressive region BEY and l/t must be greater than 2 for E to lie inside the cantilever. The mode of deformation (rotation about Y) is unique when $d_1 > 0$ but in the limit $d_1 = S = 0$,

* See footnote on p. 7 for notation.

there are an infinite number of possible modes. Provided that there is no constraint on the motion, γ can take any value between γ_0 and $-\gamma_0$ (the condition that the plastic work must be positive precludes the possibility of $\gamma < \gamma_0$). In practice the situation would be unstable and the slightest deviation from unsymmetrical loading would lead to bending of the cantilever with $\gamma = \mp \gamma_0$.

Below certain critical values of l/t, which depend on P, yielding extends to the end XOX, and solutions I and II are not valid. A close approximation to

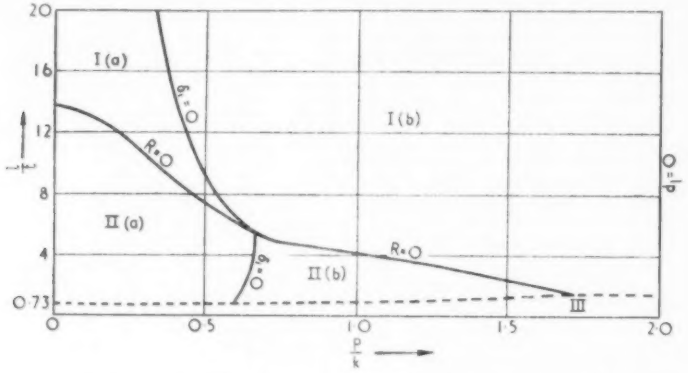

Fig. 9. Range of validity of the different plane strain solutions for a strongly supported uniform cantilever.

this limit is probably provided by calculating the values of l/t and P at which the mean shear stress across OY is equal to k. The dashed line in Fig. 9 is the result of such calculations; below this line solutions I and II are certainly not valid.

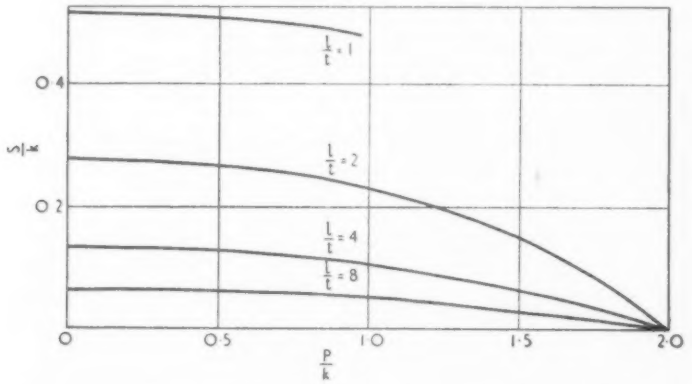

Fig. 10. Relations between S/k and P/k (i.e. yield loci) for strongly supported uniform cantilevers in plane strain.

All results, including the dimensions of the slip-line fields are tabulated in Table 3 (no results have been calculated for solution I (b)). The relations between S/k and P/k for various values of l/t are shown in Fig. 10. These curves may be

regarded as part of the yield loci for the cantilevers, representing possible yield-point states. A complete locus would be symmetrical about both axes since the cantilever is of symmetrical shape and the material is assumed to be isotropic.

TABLE 3. PLANE STRAIN.

Strongly supported uniform cantilevers yielding under combined shear and axial pressure.

l/t	S/k	P/k	δ_1^c	δ_2^c	d_1/t	d_2/t	R/t	γ^c
8·0	0·0656	0·093	0·123	0·163	0·583	0·616	0·033	0·003
	0·0646	0·279	0·083	0·203	0·537	0·657	0·021	0·008
	0·0602	0·614	0	0·23)	0·508	0·754	0	0·018
	0·0348	1·401	0	0·15)	0·223	1·047	0	0·046
	0·009)	1·867	0	0·07)	0·050	1·278	0	0·065
4·0	0·136	0·092	0·123	0·163	0·518	0·552	0·120	0·005
	0·134	0·275	0·083	0·203	0·493	0·593	0·107	0·014
	0·131	0·459	0·043	0·243	0·477	0·643	0·082	0·025
	0·124	0·658	0	0·285	0·469	0·706	0·041	0·038
	0·105	1·039	0	0·285	0·370	0·841	0	0·066
	0·068	1·481	0	0·210	0·204	1·020	0	0·103
	0·034	1·769	0	0·14)	0·093	1·170	0	0·131
	0·009	1·942	0	0·07)	0·024	1·303	0	0·152
2·0	0·280	0·089	0·123	0·163	0·385	0·419	0·297	0·007
	0·278	0·267	0·083	0·203	0·361	0·461	0·284	0·021
	0·273	0·445	0·043	0·243	0·345	0·512	0·257	0·036
	0·264	0·638	0	0·285	0·340	0·577	0·214	0·057
	0·245	0·891	0	0·285	0·280	0·672	0·179	0·095
	0·222	1·090	0	0·285	0·240	0·753	0·143	0·129
	0·184	1·340	0	0·285	0·200	0·864	0·085	0·178
	0·125	1·618	0	0·285	0·171	1·001	0	0·244
	0·068	1·820	0	0·2 0	0·085	1·128	0	0·309
	0·019	1·957	0	0·1 0	0·021	1·272	0	0·386
1·0	0·518	0·084	0·123	0·163	0·167	0·200	0·589	0·005
	0·517	0·252	0·083	0·203	0·141	0·241	0·577	0·014
	0·513	0·421	0·043	0·243	0·123	0·290	0·554	0·026
	0·507	0·603	0	0·285	0·114	0·351	0·515	0·043
	0·499	0·736	0	0·285	0·080	0·399	0·500	0·072
	0·497	0·769	0	0·285	0·072	0·411	0·496	0·079
	0·483	0·980	0	0·285	0·020	0·488	0·470	0·129

4. PLANE STRESS SOLUTIONS

Solutions have been obtained only for shearing without axial load, though it is intended to extend the result to include combined shear and pressure on a uniformly thick cantilever. The symmetrical characteristic fields in plane stress for tapering cantilevers are analogous to the slip-line fields described in § 3a, and reference will be made to the same Fig. 2, though the precise shapes of the fields are slightly different (Fig. 11).

Vol. 3 54/55

In ASD the field determined by the straight stress-free edge, consists of straight lines inclined to the edge at the angle $\beta = \tan^{-1}\sqrt{2} = 54°44'$; the state of stress is uniaxial tension $Y = \sqrt{3}\,k$ parallel to the edge. HILL (1952) has shown that the stresses in the extension of this field round the singularity A, are

$$\sigma_r = k\cos\phi, \qquad \sigma_\phi = 2k\cos\phi, \qquad \tau_{r\phi} = k\sin\phi, \tag{2}$$

where the polar angle ϕ is measured from the base-line indicated in Fig. 11, which is inclined at the angle 2β to the edge AB. The curved characteristics such as SP have the equation $r^2\sin\phi = \text{const}$ while the other family are straight lines through A.

As in the plane strain solutions, O moves vertically downwards at yielding, and deformation takes place by rotation of the rigid cantilever either about the point of stress discontinuity Y (solution I. Fig. 2a) or about a centre of rotation C lying on Oy (solution II, Figs. 2b and 11). The latter solution involves local necking along PY and local bulging along YQ, with pure shear at Y the mid-point of this arc. Local necking along a narrow band through the thickness of the material (through the width of the cantilever in this problem) can only occur along a characteristic (HILL 1952). The vector representing the relative velocity of the material on either side of the neck is perpendicular to the other characterstic direction and is inclined to the neck at an angle ψ which varies with the stress state along the neck (e.g. $\psi = 0$ is pure shear and $\psi = \sin^{-1}(1/3)$ in pure tension). The same applies to local bulging (i.e., thickening instead of thinning) though this can only occur with a strain-softening material or with a metal like annealed mild steel* that has a sharp drop in yield stress after the initial yield-point. Whether or not local bulging is in fact possible, solution II provides at least an upper bound to yield-point loads (HILL 1951). The diffuse mode of deformation for a strain hardening material is not known.

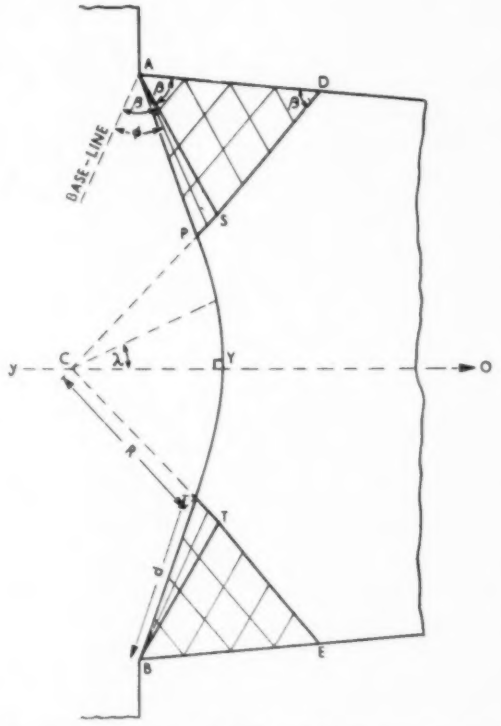

Fig. 11. Characteristic field for a strongly supported uniform cantilever in plane stress.

The equation linking the state of stress to the state of strain-rate along PYQ is found to be

$$\tan\lambda = 2\tan\psi, \tag{3}$$

* Local bulging has been observed in a mild steel pressing by B. P. GREEN and B. B. HUNDY (unpublished).

and hence the polar equation of the arc referred to C as origin is $r^2 \cos \lambda =$ constant, where the polar angle λ is measured from CYO. This is, of course, the same type of curve as that round the singularity at A. For the purpose of calculating the resultant forces acting across the arc PYQ it is convenient to regard $CPYQ$ as a

TABLE 4. PLANE STRESS.

Strongly supported cantilevers with uniform taper yielding under shear load.

θ	l/t	S/k	d/t	R/t	$\delta°$
90°	∞	0	0·612	0	0
	5·65	0·0799	0·530	0	15° 54′
	4·48	0·102	0·509	0·0254	15° 54′
	3·77	0·122	0·489	0·0489	15° 54′
	2·67	0·173	0·439	0·110	15° 54′
	1·94	0·240	0·375	0·187	15° 54′
	1·41	0·327	0·290	0·290	15° 54′
	1·07	0·420	0·200	0·400	15° 54′
	0·865	0·499	0·123	0·492	15° 54′
	0·750	0·555	0·070	0·557	15° 54′
	0·675	0·595	0·030	0·605	15° 54′
	0·636	0·618	0·008	0·632	15° 54′
85°	6·33	0·301	1·220	0	0
	3·88	0·319	0·887	0	11° 30′
	3·37	0·331	0·809	0·0404	11° 30′
	3·01	0·344	0·749	0·0749	11° 30′
	2·34	0·380	0·624	0·156	11° 30′
	1·81	0·431	0·502	0·251	11° 30′
	1·36	0·501	0·370	0·370	11° 30′
	1·04	0·579	0·246	0·492	11° 30′
	0·839	0·646	0·148	0·594	11° 30′
	0·724	0·691	0·085	0·662	11° 30′
80°	3·35	0·592	1·206	0	0
	2·83	0·595	1·050	0	7° 21′
	2·41	0·605	0·907	0·0907	7° 11′
	2·02	0·623	0·764	0·191	7° 11′
	1·65	0·653	0·613	0·306	7° 21′
	1·29	0·698	0·446	0·446	7° 21′
	1·00	0·751	0·293	0·587	7° 21′
	0·875	0·780	0·219	0·659	7° 21′
75°	2·28	0·866	1·183	0	0
	2·16	0·866	1·126	0	3° 24′
	2·05	0·868	1·061	0·0530	3° 24′
	1·72	0·874	0·863	0·216	3° 24′
	1·47	0·885	0·704	0·352	3° 24′
	1·24	0·901	0·550	0·490	3° 24′

fully plastic region in stress equilibrium, the stresses being given by equation (2) with $\phi = \frac{1}{2}\pi - \lambda$. The resultant forces are then evaluated over the boundaries CP and CQ instead of integrating them over the arc PYQ. The angular span

Vol. 3 54/55

of the arc is given by the condition that the stress-state should be continuous along the continuous characteristic $APYQB$. Hence it is related to the angle of taper of the cantilever by the equation

$$2\lambda - \tan^{-1}(\tfrac{1}{2}\tan\lambda) = \theta + \tfrac{1}{2}\pi - 2\beta. \qquad (4)$$

The dimensions of the characteristic fields and values of S/k which have been calculated are given in Table 4. The length of $AP = BQ$ is denoted by d, and of $CP = CQ$ by R. The relations between S/k and l/t are compared in Fig. 3 with those for plane strain. For a given cantilever the plane stress value of S/k is about 14% less than the plane strain value over the whole range of l/t for $\theta > 75°$. This was to be expected for long thin cantilevers with a MISES yield criterion because there is the same difference between the corresponding yield stresses in compression or tension. It is interesting, however, that the percentage difference remains almost the same even for the smallest value of l/t considered; in plane stress the stress state in the deforming region then varies between pure tension at the edge and pure shear at the centre, whereas in plane strain it is pure shear throughout.

Since the general outlines of the plane stress and plane strain solutions are very similar only the points of difference are mentioned in the following discussion of the two types of solution.

Solution I

When $\delta = 0$,

$$l/t = \tan\theta\,(\sin 2\theta - \sqrt{2}\cos 2\theta)/2\sqrt{2}, \quad S/k = \sqrt{3}\sin 2\theta, \qquad (5)$$

and, as with (3) in plane strain, this limiting solution is valid for all greater values of l/t. When $\theta = 72°22'$, $S = k$ for all values of l/t and a stress field can be constructed over the whole cantilever similar to that shown in Fig. 2d, the magnitude of the stress parallel to the surfaces being $Y = \sqrt{3}k$ instead of $2k$.

The relation between l/t and S/k for a uniformly thick cantilever ($\theta = \frac{1}{2}\pi$) in the range of solution I (i.e. $l/t > 5{\cdot}65$) is given by the equations

$$l/t = \tfrac{1}{2}\cot\delta\left[1 + \frac{1}{\sqrt{3}\sin\delta\sin(\beta+\delta)}\right], \quad \text{and} \quad S/k = \frac{\sin^2\delta}{\sin(\beta+\delta)}. \qquad (6)$$

Solution II

The variables in the limiting solution when the mean shear stress across Oy is equal to k are again denoted by the subscript 0. When $\theta = 72°24'$, $R_0 = 0$, $l_0/t_0 = 1{\cdot}89$ and $S_0/k = 0{\cdot}9985$. Only over the minute range $72°24' > \theta > 72°22'$ is this limit reached for solutions of type I. An alternative mode of deformation similar to that shown in Fig. 4a can be constructed but no calculations have been made.

ACKNOWLEDGMENTS

I am grateful to Mr. D. SPENCELEY of the General Plasticity Section of B.I.S.R.A. for his assistance in calculating the results and drawing the diagrams for this paper which is based on B.I.S.R.A. Reports MW/B/14/53 and MW/B/9/54.

REFERENCES

BAKER, J. F.	1949	*J. Inst. Civ. Eng.*, **31**, 188.
BAKER, J. F., HORNE, M. R. and RODERICK, J. W.	1949	*Proc. Roy. Soc.* A, **198**, 493.
GREEN, A. P.	1953a	*Quart. J. Mech. App. Maths.*, **6**, 228.
	1953b	*B.I.S.R.A. Report* MW/B/14/53.
	1954	*J. Mech. Phys. Solids*, **2**, 197.
HENDRY, A. W.	1950	*The Structural Engineer*, **28**, 311.
HILL, R.	1950	*The Mathematical Theory of Plasticity* (Clarendon Press, Oxford).
	1951	*Phil. Mag.*, **42**, 868.
	1952	*J. Mech. Phys. Solids*, **1**, 19.
	1954	*J. Mech. Phys. Solids*, **2**, 000.
HILL, R. and SIEBEL, M. P. L.	1953	*J. Mech. Phys. Solids*, **1**, 207.
HORNE, M. R.	1951	*Proc. Roy. Soc.* A, **207**, 216.
HUNDY, B. B.	1954	*Metallurgia*, 109.
NADAI, A.	1931	*Plasticity*, Ch. 22 (McGraw-Hill).
NEAL, B. G.	1950	*Phil. Trans.* A, **242**, 197.
RODERICK, J. W.	1948	*Phil. Mag.*, **39**, 529.
RODERICK, J. W. and PHILLIPS, I. H.	1949	*Research Engineering Structures Supplement*, p. 9.
SYMONDS, P. S. and NEAL, B. G.	1951	*J. Franklin Inst.*, **252**, 383 and 469.

Vol. 3 54/55

Journal of the Mechanics and Physics of Solids, 1954, Vol. 3, pp. 16 to 21. Pergamon Press Ltd., London.

A DETERMINATION OF PLASTIC STRESS-STRAIN RELATIONS

By B. B. Hundy and A. P. Green
British Iron and Steel Research Association, Sheffield.

(*Received 17th June*, 1954)

Summary

A method suggested recently by Hill (1953), involving the pulling of notched strips past their plastic yield point, has been used to determine the plastic potentials of copper, zinc and stainless steel. It was found that all three metals had a Mises potential (i.e. Lode's parameters, μ and ν, were equal).

1. Introduction

The purpose of the experiments described here was to investigate the plastic stress-strain relation of copper, zinc, and 18/8 stainless steel. It was originally planned to include mild steel also, so that materials with the most common crystal structures (face-centred cubic, body-centred cubic and close-packed hexagonal) would all be represented. However, it was found during the tests that the method would not work for mild steel. 18/8 stainless steel was chosen as an example of a metal that undergoes a crystallographic transformation during plastic deformation.

The method of investigation was suggested recently by Hill (1953) and is based on his theory of local necking in thin sheets (Hill 1952). The specimen is in the form of a strip notched in its plane by wedge-shaped notches which are asymmetrically disposed on either side, so that a line joining their roots AB makes an angle θ with the longitudinal axis of the strip (Fig. 1). It is pulled in tension along its axis until, providing that the rate of work hardening is not too high, plastic yielding takes place by the formation of a straight local neck connecting the roots of the notches. The purpose of the notches is merely to enforce the formation of such straight necks at various angles to the tensile axis ; Hill (1953) suggested that this could also be done by machining shallow grooves in the strip at the desired angles but this method has not yet been tried. The state of stress and strain-rate in the neck at yielding varies from pure tension when $\theta = 55°$ to pure shear when

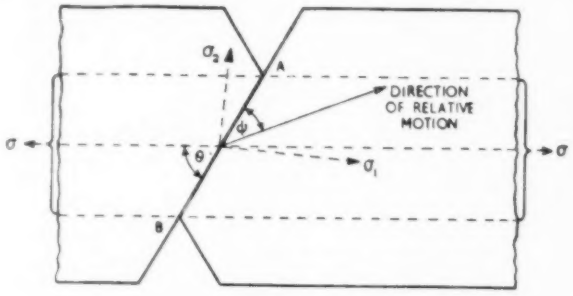

Fig. 1.

$\theta = 90°$ (see equation (1) below). If the relative direction of motion of the two halves of the strip on either side of the neck at yielding makes an angle ψ with the neck, then the plastic stress-strain relations are determined from the relation between θ and ψ as θ takes various values between 55° and 90°. In addition, if the yield point is sufficiently well-defined, the yield criterion may be obtained by measuring the load at which yielding begins. For the theory to be valid it is essential that the neck should be straight, well defined, and narrow in relation to its length. This kind of neck was obtained in copper, zinc and stainless steel, but not in mild steel. In the latter, yielding started by necks spreading out a short distance from each notch at *right angles* to the axis. Before they had spread far, a straight oblique neck formed between the roots of the notches. This mode of yielding is due, presumably, to the discontinuous yield-point in mild steel. It precludes application of the present method to this metal though it may be possible to use the alternative grooving method.

Most previous experiments to obtain the stress-strain relations of a material have been carried out on thin-walled tubes, the tubes being subjected to various combinations of tension and torsion (or internal pressure) in order to produce a variety of states of uniform stress and strain-rate (Taylor and Quinney 1931 ; Schmidt 1932 ; Davis 1943 ; Fraenkel 1948 ; Morrison 1948). Such experiments are difficult to perform and the apparatus needed is expensive and complex. It is also difficult to produce thin tubes which have a prefectly uniform cross-section and to check whether the material is isotropic.

Vol. 3 54/55

The difficulties inherent in the use of tubes underline the comparative simplicity of the present method of pulling notched strip. The state of anisotropy in strip is more easily controlled and can be measured without difficulty. The experimental quantities required can be measured to moderate accuracy without elaborate apparatus.

The method has its limitations, however. If the metal work-hardens too rapidly, the thinning during yielding is diffuse instead of being sharply localized in a neck. This difficulty can be overcome with most metals by prestraining to an amount just sufficient to give a local neck, taking care not to introduce any appreciable anisotropy. This limitation, of course, would not apply to grooved specimens where local yielding would be ensured. It should be noticed that only the initial yielding can be investigated with either method. To follow changes in the shape of the yield criterion or potential as a specified stress (or strain) path is followed, an apparatus is required which is capable of applying any combination of ratios of tension, torque and pressure to a thin tube.

2. Theoretical Formulae

The theory of the method is given in detail by Hill (1953) and only its conclusions are stated here. It is assumed that the metal is isotropic and that the state of stress and strain-rate in the straight neck, AB (Fig. 1), is uniform.

The experimental relations between states of stress and strain-rate are plotted in terms of Lode's parameters μ and ν, which, expressed in terms of the principal stresses and strain-rates, are

$$\mu = \frac{2\sigma_2 - \sigma_1 - \sigma_3}{\sigma_1 - \sigma_3}, \qquad \text{where} \qquad \sigma_1 > \sigma_2 > \sigma_3,$$

and

$$\nu = \frac{2\dot{\epsilon}_2 - \dot{\epsilon}_1 - \dot{\epsilon}_3}{\dot{\epsilon}_1 - \dot{\epsilon}_3}, \qquad \text{where} \qquad \dot{\epsilon}_1 > \dot{\epsilon}_2 > \dot{\epsilon}_3.$$

Both μ and ν vary between 0 and -1 as the state of stress and strain-rate varies between pure shear and uniaxial tension in an isotropic material. It can be shown that in the incipient neck, if $\psi > \sin^{-1}(\frac{1}{3})$,

$$\left.\begin{aligned} \mu &= -\frac{3\cos\theta - \sin(\theta - \psi)}{\cos\theta + \sin(\theta - \psi)}, \\ \text{and} \qquad \nu &= -\frac{3(1 - \sin\psi)}{1 + 3\sin\psi}. \end{aligned}\right\} \qquad (1)$$

3. Experimental Procedure

Strip specimens that were approximately isotropic were produced by rolling from about 0·1″ thick to 0·055″ with process anneals after each 15-20% reduction in thickness. Before annealing, the strips were roller levelled with the aim of reducing any preferred orientation introduced by the rolling. The annealed strip thus prepared was then rolled 10% and roller levelled in order to reduce the rate of work hardening. Each metal was tested for anisotropy by measuring the strain variations in the width and thickness directions during the straining of tensile specimens cut at 0°, 30°, 60°, and 90° to the rolling direction. The anisotropy parameters (Hill 1950) obtained are given in the Table. An isotropic material has $F = G = H = N/3$, so it appears that all these metals were moderately isotropic. Calculations suggested by Hill (1953) showed that the plastic stress-strain relations would not be much affected by the anisotropy in these metals, except for the copper. In the latter the anisotropy was serious enough to mask significant deviations from the relation $\mu = \nu$ towards $\nu = -1$ (tension end).

Table 1.

	F/H	G/H	N/H
Copper	1·12	0·82	2·82
Zinc	0·97	1·02	3·10
Stainless Steel	0·94	0·98	2·90

The method described of using a sequence of moderate cold rolling reductions followed by annealing is a satisfactory way of producing isotropic strip in many metals, but in some, such as copper, it is rather uncertain. In copper, with reductions greater than 10-15%, annealing may not completely remove the anisotropy. Unfortunately, lighter reductions cannot be used because they lead to an undesirable increase in the grain size on annealing. Thus, the choice of the reductions and annealing temperatures is critical, and it would require a careful and detailed

investigation to produce copper strip as isotropic as the other metal strips used in the present experiments. A possible alternative method would be to hot-roll the strip to the required dimensions, but this method, too, requires detailed investigation.

The type of specimen used is shown in Fig. 2. It had two pairs of notches placed so that two necks were formed simultaneously in opposite directions, but both inclined at the same angle θ to the tensile axis. This arrangement eliminates relative rotation of the rigid material on either side of the necks which, if there is only one neck, tends to reduce the accuracy with which ψ can be measured. It has the added advantage, that each specimen gives two tests for the same value of θ. Eleven specimens were prepared from each metal with necking angles spread over the range $\theta = 55°$ to $\theta = 90°$. θ was determined to an accuracy of $\pm$ 0·25° by measuring the specimens with a travelling microscopic reading to 0·01 mm. One face of each specimen was polished with metal polish so that the local necking could be seen as soon as it began and stopped before it went too far. The specimens were strained in a Hounsfield Tensometer which provided autographic load extension curves. Care was taken to ensure axial loading.

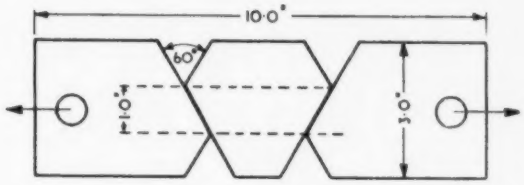

Fig. 2.

A simple but effective method was devised for measuring ψ, the angle which the relative direction of motion of the two halves of the strip makes with the neck. First the angle was roughly estimated by assuming that $\mu = \nu$ when, from equation (1), $\tan\theta = 4\tan\psi$. Once face of the test piece was then painted with marking out blue and fine straight lines were carefully scribed on it at angles dispersed at 1° intervals around the estimated angle. When necking occurred across the minimum section of the strip there was a lateral displacement of the halves of a line on opposite sides of the neck, unless the line coincided with the direction of relative motion (Fig. 3). The lateral displacement of each scribed line and the angle made by the line with the neck were both measured with the travelling microscope after the experiment. By plotting the relation between the angle which a line makes with the neck and its

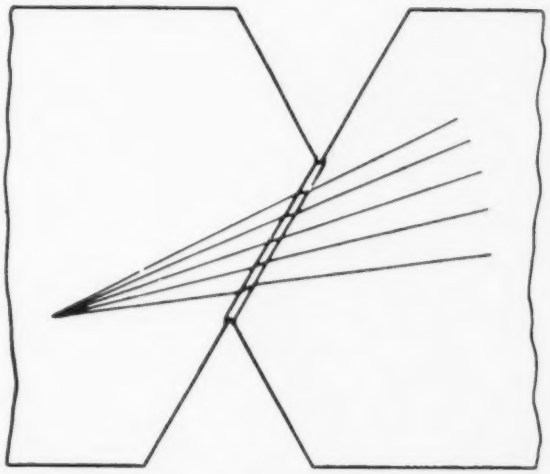

Fig. 3.

lateral displacement, the angle ψ corresponding to no lateral displacement could be interpolated. This angle was, of course, measured after a finite deformation in the neck, whereas the desired angle was that corresponding to the onset of necking. However, measurements made on specimens with various degrees of necking showed that the measured angle varied by only about 0·5°, as the specimen was strained almost to fracture. To minimize any slight error due to this, all specimens were strained to give the smallest amount of necking compatible with accurate interpolation of ψ. The lateral displacement of the lines across the neck varied from about 0·01 mm to 0·08 mm, and it is estimated that ψ could be measured to $\pm$ 0·5°.

The accuracy of measurement quoted for θ and ψ means that any particular (μ, ν) point should be within about 0·035 of its true position (Hill 1953).

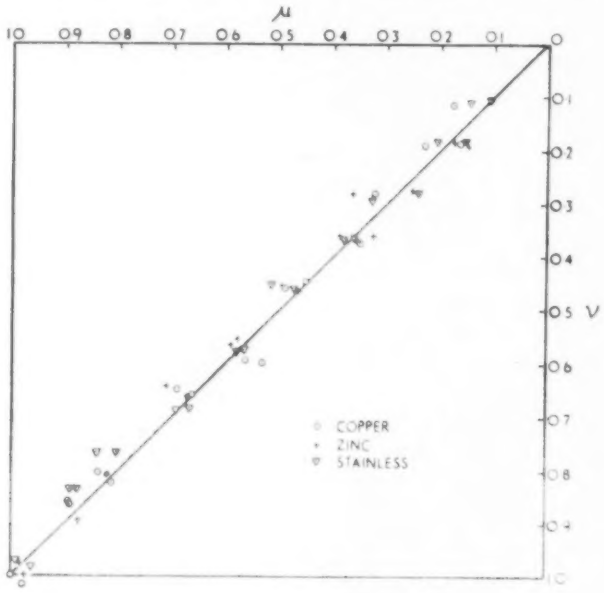

Fig. 4.

4. Experimental Results

The results of the experiments are shown in Fig. 4. It can be seen that, to a close approximation, $\mu = \nu$ for all three metals and that therefore they have a Mises plastic potential. This differs slightly from the results obtained by Taylor and Quinney (1931) who found a small deviation from $\mu = \nu$ (using copper, aluminium and mild steel). This might be due to anisotropy in their tubes, a possibility which has been discussed in some detail by Pugh (1953).

The yield criteria of the metals could not be deduced, mainly because the load-extension curves were so rounded that accurate extrapolation back to zero strain was impossible. Yield-point loads might be taken to correspond to a fixed extension but this is not very reliable when the shapes of the curves differ. Such differences may occur because the type of deformation differs, and were accentuated in the

present experiments because sometimes yielding took place more rapidly at one neck than at the the other. The latter source of error would be eliminated if a separate extensometer was used to span each neck. However, in so far as the yield point loads selected in this way were valid, the yield criterion of copper appeared to lie much closer to a Mises than to a Tresca criterion. The scatter with the other two metals was too great to make any deductions. This was due to creep between readings with the zinc and slipping in the grips of the tensometer with the stainless steel.

Clearly, whatever the experimental method, a well-defined yield-point is required if an accurate yield criterion is to be obtained. Hence a greater pre-strain is necessary; but this entails the danger of introducing serious anisotropy. The same difficulty arises if a grooved strip is used.

5. Acknowledgments

The authors would like to thank Messrs. T. D. Boxall, D. Burton, and B. Coldwell for their help with the experimental work and Mr. D. Spenceley for his help with the computations. This paper is based on B.I.S.R.A. Report MW/B/6/54.

Vol. 3 54/55

References

Bishop, J. F. W. and Hill, R.	1951	*Phil. Mag.*, **42**, 1298.
Davis, E. A.	1943	*Trans. Am. Soc. Mech. Eng.*, **65**, A 187.
Fraenkel, S. J.	1948	*J. Appl. Mech.*, **15**, 193.
Hill, R.	1950	*Mathematical Theory of Plasticity* (Clarendon Press)
	1952	*J. Mech. Phys. Solids*, **1**, 19.
	1953	*J. Mech. Phys. Solids*, **1**, 271.
Morrison, J. L. M.	1948	*Proc. Inst. Mech. Eng.*, **159**, 81.
Pugh, H. Ll. D.	1953	*J. Mech. Phys. Solids*, **1**, 284.
Schmidt, R.	1932	*Ingenieur – Archiv*, **3**, 215.
Taylor, G. I. and Quinney, H.	1931	*Phil. Trans. Roy. Soc.* A., **230** 323

Journal of the Mechanics and Physics of Solids, 1954, Vol. 3, pp. 22 to 37. Pergamon Press Ltd., London.

ON THE PLASTIC DEFORMATION OF BUILT-IN CIRCULAR PLATES UNDER IMPULSIVE LOAD

By A. J. Wang and H. G. Hopkins
Division of Applied Mathematics, Brown University

(*Received 29th March*, 1954)

Summary

This paper concerns a particular problem in the study of the behaviour of structures under dynamic loads of sufficient intensity to cause plastic deformation. A theoretical analysis is given of the plastic deformation of a circular plate. The plate is made of a perfectly-plastic rigid material that obeys the yield condition of Tresca and the associated flow rule. The dynamic load is supposed to be such that at some given time a uniform transverse velocity is instantaneously imparted to the entire plate, save at the edge where the velocity is zero, and thereafter the plate is subject only to edge forces which effect built-in conditions of support. The most important numerical results obtained are estimates of the time that elapses before the plate comes to rest and of the plate central deflection at that time.

1. Introduction

The behaviour of structures under dynamic loads that are of sufficient intensity to cause plastic deformation is a subject of considerable interest, and it is also one of great complexity both from a theoretical as well as from an experimental standpoint. So far only the simple possible physical situations have been treated theoretically. These include the propagation of plane waves along a rod; the propagation of spherical waves in an infinite medium; and transverse impact on cables and membrames, and on beams and frames. The compilation of a bibliography of published work in this field is not within the scope of this paper, but the reader may note that some representative references are given in a recent paper by Hopkins and Prager (1954).

The subject of the paper is a particular problem in this general field. A theoretical analysis is given of the plastic deformation of a built-in circular plate under impulsive load. The precise specification of this problem will be delayed, and attention will first be given to a review of the relevant work on plates that has already been published. The only theoretical work on the dynamic loading of plastic plates of which the present authors are aware is that of Bakhshiyan (1948), Kochetkov (1950), Hopkins (1953) Hopkins and Prager (1954), and Wang (1953). Bakhshiyan and Kochetkov were primarily interested in the problem of the piercing of armour plate by a projectile. In their analysis they neglect all bending stresses in the plate, and account is taken only of the shearing stresses along the generators of coaxial cylinders around the path of the projectile which is supposed to be normal to the plate. In contrast, Hopkins, Prager and Wang adopted

the usual assumption of the theory of thin plates according to which the resultant effect of the bending and shearing stresses parallel to the plate surface far exceeds that of the shearing stresses normal to the plate surface. This assumption is also made in the present paper. However, although the shear force resulting from the latter shearing stresses is taken into account in the equation of motion, these same shearing stresses are neglected in the yield condition. The analyses of these authors, despite the fact that dynamic considerations apply, rest essentially upon an earlier paper by HOPKINS and PRAGER (1953). This latter paper discussed the load-carrying capacities of thin circular plates made of a perfectly-plastic rigid material that obeys Tresca's yield condition and associated flow rule, various conditions of rotationally symmetric loading and edge support being considered. Quasi-static problems of incipient plastic flow were solved. HOPKINS and PRAGER (1954) applied the same type of analysis to discuss the dynamic behaviour of a simply-supported circular plate subjected to a uniformly distributed load which is brought on suddenly and then removed suddenly after being kept constant during a certain interval of time. The concept of a hinge circle (analogous to that of a yield hinge familiar in the plastic analysis of framed structures) was first introduced by HOPKINS and PRAGER (1953). The elaboration to a moving hinge circle was undertaken by HOPKINS and PRAGER (1954). The impact loading of circular plates made of ductile metal was discussed along similar lines by HOPKINS (1953) In this paper the impact loading was produced by a right circular cylinder made of rigid material that impinges centrally on the plate, and then moves normal to, and in contact with, the plate with prescribed velocity. The solution of this problem was found, subject to certain conditions on the prescribed velocity, for simple support and built-in edge conditions. WANG adapted the analysis of HOPKINS and PRAGER to discuss the problem of the plastic deformation of a simply-supported circular plate under impulsive load. The impulsive load was supposed to be such that at some given time a uniform transverse velocity is instantaneously imparted to the entire plate, save at the edge where the velocity is zero, and thereafter the plate is subject only to edge forces which effect simple-support conditions.

In the present paper we shall discuss the problem of the plastic deformation of a built-in circular plate under impulsive load. In its mathematical formulation, this new problem differs from the problem solved by WANG only in respect of the edge conditions of support.

As yet there is available no direct information on the circumstances in which an analysis based upon a perfectly-plastic rigid model is likely to provide results that are a satisfactory approximation to those obtaining in experimental studies of the permanent deformation of a plate of ductile material subjected to transverse load. The assessment of the reliability of such an analysis must perforce rest ultimately upon comparison with either experimental results or predictions of more complete elastic-plastic solutions when these are developed. However, the results may be expected to be valid when the plastic deformations are large enough, and accordingly the plate must be sufficiently thick for bending action to predominate over membrane action.

Briefly, in this paper, analysis similar to that of HOPKINS and PRAGER is applied to solve the problem described above. The presentation of the analysis

Vol. 3 54/55

and the results obtained is arranged in the following way. Attention is first given to a description of the essential features of the analysis and of the results obtained. The complete analysis is given in the final section of the paper.

2. NOTATION

Let r denote the distance of an arbitrary point in the plate middle surface from the plate centre, and let t be the time. The mass per unit area of the plate middle surface is denoted by μ. Furthermore, let $w(r, t)$ be the downwards deflection of material points lying in the middle surface; and let $M(r, t)$, $N(r, t)$ be the radial and circumferential bending moments, respectively, being reckoned positive when the tendency is to cause tension in the lower layer of the plate. Let M_0 denote the conventional fully-plastic bending moment for the plate, i.e., $M_0 = \sigma_0 h^2$ where σ_0 is the yield stress in simple tension (and compression) and $2h$ is the plate thickness. Let R be the plate radius, and v_0 be the uniform transverse velocity imparted to the plate.

3. SOME PRELIMINARY CONSIDERATIONS

The present problem is essentially a simplification of the exceedingly complicated problem of the inter-action between a plane shock wave and a solid object. During the short time that the shock acts the object is subjected to very high pressures. Now HOPKINS and PRAGER established that if an impulsive pressure acts upon a simply-supported plate then a uniform transverse velocity is instantaneously imparted to the entire plate, save at the edge where the velocity is zero. The same result may be shown to apply if the edge is built-in. These considerations have influenced the simplification of the actual effect of the shock wave. It is not within the scope of this paper to examine the relationship between the shock strength and the transmission of kinetic energy to the object in its path. The present task is to examine the mechanism by which this imparted kinetic energy is dissipated. Clearly if the shock strength be high enough then there will be plastic deformation, and attention is directed towards this situation.

4. ESSENTIAL FEATURES OF THE ANALYSIS

The analysis is in the spirit of thin plate theory, and the effects of shear deformation and rotatory inertia are neglected. Bending action is supposed always to predominate over membrane action. Immediately prior to yielding the plate is flat. Throughout any time during which there is yielding, the fundamental problem is to determine associated bending moment $[M(r, t), N(r, t)]$ and velocity distributions $[v(r, t)]$ defined over the plate middle surface. The quantities M, N and v must satisfy an equation of motion, and M and N must not violate the yield condition. In any region where the yield condition is satisfied then plastic deformation may occur, and the velocity distribution is subject to the flow rule associated with the yield condition. Here Tresca's yield condition has been taken, and the corresponding yield locus, drawn in an M, N-plane, is shown in Fig. 1. In addition M, N and v must satisfy certain other conditions, and, in particular, those appertaining to the manner in which the plate is supported.

The analytical procedure is necessarily similar to that adopted in related work. The correct set of plastic regimes is assumed, and then the associated bending moment and velocity distributions are determined subject to various required conditions. Happily there is comparatively little freedom in the choice of this set of plastic regimes. This choice is largely dictated by previous results, and is now described. Two phases of the motion are distinguished each of which is characterized by its own set of plastic regimes. In both phases, regimes *A* through *C* apply (see Fig. 1). In phase I the region in which regimes *AB* and *BC* apply (the edge always being in regime *C*) expands from the edge to cover the entire plate, and the remaining region of the plate is throughout this time moving with the initial uniform velocity; for simplicity (but without essential restriction) this region is assumed to be in regime *A*. Furthermore, in this phase, there is motion of the boundaries between the regions in regimes *A*, *AB* and *BC*. In phase II, only the plate centre is in regime *A*; the central velocity steadily decreases to zero at which time the entire plate comes to rest. In this phase there is motion of the boundary between the regions in regimes *AB* and *BC*.

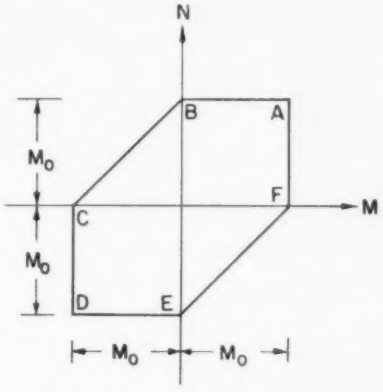

Fig. 1. Tresca yield condition.

5. Discussion of Results

The most important numerical results obtained concern the time that elapses before the plate comes to rest and the plate central deflection at that time. These results and one other are discussed here. The reader should consult the next section for results appertaining to the motion of boundaries between the various regimes. The final shape of the plate has not been found because the necessary computation, although straightforward, is lengthy.

The first phase occupies a time $0{\cdot}57(\mu v_0 R^2/12M_0)$, and the second phase occupies a time $0{\cdot}51(\mu v_0 R^2/12M_0)$. These results may be compared with the corresponding results for the same problem when the edge is simply-supported (Wang 1953); there the first and second phases each occupy a time $\mu v_0 R^2/12M_0$. Thus changing from simple to built-in support edge conditions decreases the time of plastic deformation by about 46%, i.e., by almost one-half. The final central deformation of the plate is $0{\cdot}84\,(\mu v_0^2 R^2/12M_0)$. The corresponding result found by Wang is $1{\cdot}5\ (\mu v_0^2 R^2/12M_0)$. Thus the change in edge support conditions decreases the final central deformation of the plate by about 44%, i.e., by almost one-half. The final shape of the plate may be expected to be somewhat similar to that of a pointed dome as found in related work (Hopkins and Prager, 1954; Wang, 1953). The central velocity of the plate during the second phase, to a very high degree of accuracy, decreases linearly in time. This result is exact for the problem solved by Wang.

6. MATHEMATICAL ANALYSIS

(*i*) *The mathematical problem*

Attention is first given to the formulation of the mathematical problem. Let r, ϕ, z be cylindrical polar coordinates, the origin being at the centre of the undeformed plate's middle surface, and with the z-axis pointing vertically downwards; and let t be the time. Attention is confined here to problems of rotational symmetry, and all mechanical quantities are therefore independent of ϕ. The quantities μ, $M(r, t)$, $N(r, t)$, M_0, R and v_0 were defined in Section 2. Subscripts are used to denote differentiation.

The analysis given here is in the spirit of thin plate theory. For conciseness the basic concepts and fundamental equations needed in the analysis are stated only, and the reader is referred to the papers by HOPKINS and PRAGER for their derivation.

The deformation of the plate is represented solely through the quantities $w(r, t)$, $M(r, t)$ and $N(r, t)$. The fundamental dynamical equation is

$$(rM)_r - N = \mu \int_0^r w_{tt}\, r dr, \tag{1}$$

the plate surface being free from applied load, and effects of shearing deformation and rotatory inertia being neglected. The yield locus is the Tresca hexagon $ABCDEF$ shown in Fig. 1. Let

$$\kappa = -w_{rrt}, \qquad \lambda = -\frac{1}{r} w_{rt} \tag{2}$$

be the radial and circumferential curvature rates, respectively. The flow rule results are required only for the plastic regimes A through C, and are as follows.

Regime
$$\begin{cases} A : M = N = M_0 ; & \kappa, \lambda \geqslant 0 ; & (3) \\ AB : 0 < M < M_0 ; \quad N = M_0 ; & \lambda \geqslant \kappa = 0 ; & (4) \\ B : M = 0, \quad N = M_0 ; & \lambda \geqslant -\kappa \geqslant 0 ; & (5) \\ BC : -M_0 < M < 0, \quad N = M_0 + M ; & \lambda = -\kappa > 0 ; & (6) \\ C : M = -M_0, \quad N = 0 ; & -\kappa \geqslant \lambda \geqslant 0. & (7) \end{cases}$$

In any part of the plate, whether or not it is plastic but which is not yielding, there is instantaneously rigid body motion, i.e., $\kappa = \lambda \equiv 0$ in r, and hence, according to (2), $w_i = w_i(t)$ at such a time.

The plastic deformation is such that the plate middle surface is divided into a central circular region together with surrounding annular regions, each of these regions being in a different plastic regime. The number and position of these regions varies with time. The various mechanical quantities within any such region must satisfy the appropriate relations from (1)-(7), and must at the common boundary between any two such regions satisfy certain continuity or discontinuity relations. In addition, relations appropriate to the prescribed initial conditions and edge support must be satisfied.

At time $t = 0$ let the plate be flat and have the uniform velocity v_0, save at the edge where the velocity is zero. Then

$$w(r, 0) = 0 \qquad (0 \leqslant r \leqslant R), \tag{8}$$

$$w_t(r, 0) = \begin{cases} v_0 & (0 \leqslant r < R), \\ 0 & (r = R). \end{cases} \tag{9}$$

The plate starts to yield at time $t = 0$, and w, M and N are to be determined so that the following conditions are satisfied throughout $0 \leqslant r \leqslant R$ for all $t \geqslant 0$.

(1) w and w_t are continuous in r and t; w_r, w_{rr}, w_{rt} and w_{tt} are piece-wise continuous in r and continuous in t, r-discontinuities being only at hinge circles. Across a stationary hinge circle w_r, w_{rr} and w_{rt} are discontinuous, and w_{tt} is continuous. Across a moving hinge circle of radius $r_0(t)$, w_r is continuous, and w_{rr}, w_{rt} and w_{tt} are discontinuous but such that

$$[w_{rt}] + (r_0)_t [w_{rr}] = 0, \tag{10}$$

$$[w_{tt}] + (r_0)_t [w_{rt}] = 0, \tag{11}$$

the brackets denoting discontinuities of the enclosed quantities.

(2) M is continuous in r and t; M_r and M_t are piece-wise continuous in r and t, r-discontinuites being only at hinge circles, and satisfying

$$[M_t] + (r_0)_t [M_r] = 0; \tag{12}$$

N is piece-wise continuous in r and continuous in t.

(3) w, M and N satisfy the dynamical equation (1). At the plate centre, $M = N = M_0$ always unless a neighbourhood of the centre moves as a rigid body with $w_{rt} \equiv 0$ in r.

(4) The point (M, N) lies inside or on the yield hexagon of Fig. 1. In the first case $w_{rt} \equiv 0$ throughout the region in which the state of stress is represented by interior points of the yield hexagon. In the second case, M, N, κ and λ satisfy the flow rule Eqs. (3)-(7).

(5) The edge is built-in; thus $w(R, t) = 0$, and either $w_{rt}(R, t) = 0$ or $|M(R, t)| = M_0$, and in the latter case the edge is a hinge circle.

(6) The initial conditions (8), (9) are satisfied.

(*ii*) *Solution of the problem*

The method of analysis proceeds in the manner already described in Section 4.

Phase I: $0 < t < t_1$.

Consider the motion described by

$$w_t/v_0 = \begin{cases} 1 & (0 \leqslant r \leqslant r_0(t)), \\ 1 - \sigma(r - r_0)/r_1 & (r_0(t) \leqslant r \leqslant r_1(t)), \\ \sigma \ln(R/r) & (r_1(t) \leqslant r \leqslant R). \end{cases} \tag{13}$$

This motion will satisfy the initial condition $w_t(r, 0) = v_0$ if $r_0(0) = r_1(0) = R$, and the condition $w_t(R, t) = 0$ is also satisfied; further w_t and w_{rt} are continuous throughout $0 < r < R$ if σ is given by

$$1/\sigma = \ln(R/r_1) + (1 - r_0/r_1) \ (\geqslant 0). \tag{14}$$

It is supposed that r_0 and r_1 are monotonically decreasing functions of the time, and then the end of the first phase is defined by

$$r_0(t) = 0, \text{ say } t = t_1. \tag{15}$$

According to (13),

$$\left.\begin{aligned} &\kappa = \lambda = 0 && && (0 < r < r_0), \\ &\kappa = 0, && \lambda = \sigma v_0/r_1 r \quad (\geqslant 0) && (r_0 < r < r_1), \\ &\kappa = -\lambda = -\sigma v_0/r^2 && (\leqslant 0) && (r_1 < r < R), \end{aligned}\right\} \tag{16}$$

so that λ is discontinuous only at $r = r_0, R$ where by definition there must be moving and stationary hinge circles, respectively. Further from the flow rules (3)-(7), the regions $0 \leqslant r < r_0$, $r_0 < r < r_1$ and $r_1 < r < R$ are in regimes A, AB and BC, respectively; the edge of the plate is in regime C. Thus

$$\left.\begin{aligned} &M = N = M_0 && && (0 \leqslant r < r_0), \\ &0 < M < M_0, && N = M_0 && (r_0 < r < r_1). \\ &-M_0 < M < 0, && N = M_0 + M && (r_1 < r < R); \end{aligned}\right\} \tag{17}$$

Also from (13),

$$w_{tt}/v_0 = \begin{cases} 0 & (0 \leqslant r < r_0), \\ -\left[\sigma (r - r_0)/r_1\right]_t & (r_0 < r < r_1), \\ \sigma_t \ln (R/r) & (r_1 < r < R); \end{cases} \tag{18}$$

it is straightforward to verify that the condition (11) is satisfied at the moving hinge circle $r = r_0(t)$, and also of course $w_{tt}(R, t)$ is correctly zero.

Subsequent analysis is simplified through the use of certain non-dimensional variables, viz.,

$$\left.\begin{aligned} &\rho = r/R, && \tau = t/(\mu v_0 R^2/12M_0); \\ &\rho_0 = r_0/R, && \rho_1 = r_1/R; \\ &\xi = \ln (1/\rho_1), && \eta = 1 - \rho_0/\rho_1; \end{aligned}\right\} \tag{19}$$

in what follows w_t/v_0, M and N are regarded principally as functions of ρ and τ, and ξ and η are functions of τ. The basic equations are now re-written. The equation of motion (1) becomes

$$\{(\rho M)_\rho - N\}/M_0 = 12 \int_0^\rho (w_t/v_0)_\tau \, \rho d\rho. \tag{20}$$

The velocity distribution Eqs. (13) becomes

$$w_t/v_0 = \begin{cases} 1 & (0 \leqslant \rho \leqslant \rho_0 = (1 - \eta)e^{-\xi}), \\ (1 + \xi - \rho e^{\xi})/(\xi + \eta) & (\rho_0 \leqslant \rho \leqslant \rho_1 = e^{-\xi}), \\ -(\ln \rho)/(\xi + \eta) & (\rho_1 \leqslant \rho \leqslant 1). \end{cases} \tag{21}$$

The end of this phase is defined by

$$\eta(\tau) = 1, \quad \text{say} \quad \tau = \tau_1. \tag{22}$$

The conditions (17) on the bending moment distributions become

$$\left.\begin{aligned} &M/M_0 = N/M_0 = 1 && && (0 < \rho < \rho_0),\\ &0 < M/M_0 < 1, && N/M_0 = 1 && (\rho_0 < \rho < \rho_1),\\ &-1 < M/M_0 < 0, && N/M_0 = M/M_0 + 1 && (\rho_1 < \rho < 1). \end{aligned}\right\} \tag{23}$$

The dynamical equation (20) is now integrated. First note that throughout the region $0 \leqslant \rho < \rho_0$, $M = N = M_0$ and $w_{tt} = 0$, and therefore the equation is identically satisfied. Now integrate (20) throughout the region $\rho_0 < \rho < \rho_1$, and use (21), (23) and the condition $M(\rho_0, \tau) = M_0$. This gives

$$\left.\begin{aligned} &M/M_0 = 1 + \left\{2\alpha(\rho^2 - 3\rho_0^2 + 2\rho_0^3/\rho) - \beta e^{\xi}(\rho^3 - 4\rho_0^3 + 3\rho_0^4/\rho)\right\} \quad (\rho_0 < \rho < \rho_1),\\ &\text{where} \qquad -\alpha(\xi+\eta)^2 = (1-\eta)\xi_\tau + (1+\xi)\eta_\tau,\\ &\qquad\qquad -\beta(\xi+\eta)^2 = (1-\xi)\xi_\tau + (\eta_\tau - \eta\xi_\tau). \end{aligned}\right\} \tag{24}$$

Now the regime AB terminates when $M(\rho, \tau) = 0$, i.e., $\rho = \rho_1$. Then from (24) and the relations $\rho_0 = (1-\eta)e^{-\xi}$, $\rho_1 = e^{-\xi}$ it follows that ξ and η satisfy the first order, non-linear, ordinary differential equation

$$\left.\begin{aligned} &A_1(\xi,\eta)\,\xi_\tau + B_1(\xi,\eta)\,\eta_\tau = e^{2\xi}(\xi+\eta)^2/\eta^2 \qquad (0 \leqslant \eta \leqslant 1),\\ &\text{where} \quad A_1(\xi,\eta) = (3-2\eta)(1+\xi-\eta) + 3(\xi+\eta-1)(1-\eta)^2,\\ &\qquad B_1(\xi,\eta) = (3-2\eta)(1+2\xi) - 3(1-\eta)^2. \end{aligned}\right\} \tag{25}$$

Next integrate (20) throughout the region $\rho_1 < \rho < 1$, and use (21), (23) and the condition $M(\rho_1, \tau) = 0$. This gives

$$\begin{aligned} M/M_0 = {} & \left\{1 + 6\alpha(\rho_1^2 - \rho_0^2) - 4\beta e^{\xi}(\rho_1^3 - \rho_0^3)\right\} \ln(\rho/\rho_1)\\ & + \frac{3(\xi+\eta)_\tau}{(\xi+\eta)^2}\left\{\rho^2 \ln(\rho/e) - \rho_1^2 \ln(\rho_1/e) - \rho_1^2 \ln(\rho_1^2/e)\ln(\rho/\rho_1)\right\} \qquad (26)\\ & (\rho_1 < \rho < 1). \end{aligned}$$

Now the regime BC terminates when $M(\rho, \tau) = -M_0$; this must correspond to the plate edge, and so $\rho = 1$. Then from (26) and as $M(1, \tau) = -M_0$, it follows that ξ and η satisfy a second equation similar in type to Eq. (25), viz.,

$$\left.\begin{aligned} &A_2(\xi,\eta)\,\xi_\tau + B_2(\xi,\eta)\,\eta_\tau = -(1+\xi)(\xi+\eta)^2 e^{2\xi} \qquad (0 \leqslant \eta \leqslant 1),\\ &\text{where}\\ &A_2(\xi,\eta) = 3(1+2\xi+2\xi^2 - e^{2\xi}) - 2\xi\eta\left[3(1-\eta)(2\xi+\eta)\right.\\ &\qquad\qquad \left. - 2(1-\xi-\eta)\eta^2\right],\\ &B_2(\xi,\eta) = 3(1+2\xi+2\xi^2 - e^{2\xi}) + 2\xi\eta\left[2(1-\eta)^2 - (1+3\xi)(2-\eta)\right]. \end{aligned}\right\} \tag{27}$$

The fundamental analytical problem is therefore to solve the two simultaneous, first order, non-linear, ordinary differential equations (25), (27) subject to the initial conditions

$$\xi = \eta = 0, \qquad \tau = 0 \tag{28}$$

in the range $0 \leqslant \eta \leqslant 1$. The complexity of these equations necessitates the use of a numerical method of integration.

Note first from (25), (27) that

$$\lim_{\xi,\eta\to 0} A_i(\xi, \eta) = \lim_{\xi,\eta\to 0} B_i(\xi, \eta) = 0 \quad (i = 1, 2),$$

but that the corresponding limit for the right-hand-side of Eq. (25) cannot yet be deduced as it depends upon

$$\lim_{\tau\to 0} \{\xi(\tau)/\eta(\tau)\}.$$

Now inasmuch as this latter limit is unlikely to be zero, it follows that ξ_τ and η_τ cannot both be finite at $\tau = 0$. In fact it may be expected that ξ_τ and η_τ will have an integrable infinity at $\tau = 0$, and the nature of this singularity is now found. For sufficiently small values of ξ and η, (25), (27) are well approximated by

$$(\xi + \eta)_\tau/(\xi + \eta)^2 = 1/2\eta^2(3\xi + 2\eta) = 1/2\xi(2\xi^2 + 6\xi\eta + 3\eta^2) \quad (\xi, \eta \ll 1), \tag{29}$$

and therefore the ratio $\theta = \xi/\eta$ satisfies the cubic equation

$$\theta^3 + 3\theta^2 - 1 = 0. \tag{30}$$

Equation (30) has only one positive root, and this gives

$$\theta \approx 0{\cdot}584. \tag{31}$$

Further from (29), remembering that $\xi(0) = \eta(0) = 0$, it follows that

$$\left.\begin{aligned} \xi &= k\theta\tau^{\frac{1}{2}} \approx 0{\cdot}348\,\tau^{\frac{1}{2}}, \\ \eta &= k\tau^{\frac{1}{2}} \approx 0{\cdot}652\,\tau^{\frac{1}{2}}, \\ \text{where} \quad k &= \left(\frac{1+\theta}{2+3\theta}\right)^{\frac{1}{2}} \approx 0{\cdot}652, \end{aligned}\right\} \quad (\tau \ll 1). \tag{32}$$

Therefore both ξ_τ and η_τ have the integrable singularity of type $\tau^{-\frac{1}{2}}$ near $\tau = 0$. It is worthwhile to express the above important results in a different manner, viz.,

$$\left.\begin{aligned} r_0/R &= (1 - k\tau^{\frac{1}{2}})\exp(-k\theta\tau^{\frac{1}{2}}) \approx 1 - k(1+\theta)\tau^{\frac{1}{2}}, \\ r_1/R &= \exp(-k\theta\tau^{\frac{1}{2}}) \approx 1 - k\theta\tau^{\frac{1}{2}}, \end{aligned}\right\} \quad (\tau \ll 1). \tag{33}$$

Thus $r_0 < r_1 < R$, and the boundaries between the regions in regimes A, AB and BC start to move inwards with velocities proportional to $t^{-\frac{1}{2}}$. Such a result must apply if the condition $w(R, t) = 0$ is satisfied. Furthermore

$$(r_0)_t/(r_1)_t \approx (1 + 1/\theta) \approx 2{\cdot}87 \quad (t \ll 1), \tag{34}$$

so that the velocity of the inner boundary is only a little less than three times the velocity of the outer boundary. Accordingly the two boundaries may be expected to separate quite rapidly. It is also expected that the velocities will fall off from the above values but will always be such that the relative velocity is positive.

If ξ is regarded as a function of η then τ may be eliminated between (25), (27) to give the non-linear, first order, ordinary differential equation

$$\left.\begin{aligned} \frac{d\xi}{d\eta} &= -\frac{P(\xi,\eta)}{Q(\xi,\eta)} \quad (0 \leqslant \eta \leqslant 1), \\ \text{where} \\ P(\xi,\eta) &= 8(1+2\xi+2\xi^2-e^{2\xi}) + \eta\{(4-8\eta)\eta^2(1+\xi) \\ &\quad -4(\eta^2-3\eta+8)\xi^2\}, \\ Q(\xi,\eta) &= 8(1+2\xi+2\xi^2-e^{2\xi}) + \eta\{\eta^2(4-7\eta+3\eta^2) \\ &\quad +\eta^2(6-8\eta+3\eta^2)\xi-(12-18\eta+12\eta^2-3\eta^3)\xi^2\}. \end{aligned}\right\} \tag{35}$$

The solution of (25), (27) corresponds to the characteristic of (35) that passes through the origin with slope $\left(\frac{d\xi}{d\eta}\right)_{\xi=\eta=0} = \theta \approx 0{\cdot}534$. The method of isoclines is employed to find this solution.

The isoclines of (35) are the one-parameter family of curves $P(\xi,\eta) + mQ(\xi,\eta) = 0$, or simply $\eta = g(\xi; m)$. The isoclines have the defining property that along any one of them, say $\eta = g(\xi; m_1)$, const. $= m_1 = -P/Q$, and therefore any characteristic of (35) crosses this isocline with slope m_1. Two very important isoclines are $m = 0, \infty$. From (35) it can be shown that

$$\left.\begin{aligned} P &\approx 4(\eta^3 - 3\xi^2\eta - \xi^3) + 4\eta^2\xi(\eta+3\xi), \\ Q &\approx 4(\eta^3 - 3\xi^2\eta - \xi^3) + 6\eta^2\xi(\eta+3\xi), \end{aligned}\right\} \quad (\xi,\eta < 1). \tag{36}$$

It follows that the origin is a singular point through which all isoclines pass and, moreover, are there asymptotic to the completely degenerate cubic

$$\xi^3 + 3\xi^2\eta - \eta^3 = 0. \tag{37}$$

Now the equation

$$\theta^3 + 3\theta^2 - 1 = 0 \tag{38}$$

has only one positive root. Thus near the origin, as previously found, the characteristic is approximated by the straight line $\xi/\eta = \theta \approx 0{\cdot}534$. When the value of η is below 0·15 the isoclines $m = 0$, ∞ are virtually indistinguishable; and above this value of η the isoclines steadily separate, but even when $\eta = 0{\cdot}5$ the difference between them is still relatively small. As m increases uniformly from 0 the corresponding isocline moves uniformly from the curve $m = 0$ towards the curve $m = \infty$, and the origin is the only common point of the family of isoclines $0 \leqslant m \leqslant \infty$.

The method of isoclines cannot readily be used in the neighbourhood of the origin because here they remain close to one another. If it be assumed that

$$\eta = \xi \sum_{i=0}^{\infty} a_i \xi^i \quad (0 \leqslant \xi < 1), \tag{39}$$

remembering that $\eta/\xi \to$ const. as $\tau \to 0$, then the coefficients a_i are found through the elimination of η between (35) and (39), followed by equating to zero the coefficients of successive powers of ξ in the resulting equation. Values of the first six coefficients are

$$\left.\begin{aligned} &a_0 \approx 1{\cdot}8794, \quad a_1 \approx -0{\cdot}7946, \quad a_2 \approx 1{\cdot}9144, \\ &a_3 \approx -0{\cdot}7296, \quad a_4 \approx 2.209, \quad a_5 \approx 0{\cdot}0481. \end{aligned}\right\} \tag{40}$$

The approximation

$$\eta = \xi \sum_{i=0}^{5} a_i \xi^i \quad (0 \leqslant \xi < 1) \tag{41}$$

is taken to represent the characteristic in the above region. The continuation of this approximation outside this region is done by the isocline method in the following way.

Now ξ and η must be steadily increasing functions of τ, and hence $d\xi/d\eta > 0$ along the characteristic which must therefore always lie between the isoclines $m = 0, \infty$. The maximum gradient of the isocline $m = \infty$ is 0·564 approx. (when $\eta = 0{\cdot}18$ approx.). The characteristic must lie above the isocline $m = 0{\cdot}564$ because otherwise its gradient would always exceed 0·564 and it could not pass through the origin. Similar reasoning shows that the characteristic cannot lie below the locus c_1 of points of intersection between the isocline $m =$ const. and the tangent line with gradient m to the isocline $m = \infty$. The locus c_1 is therefore a

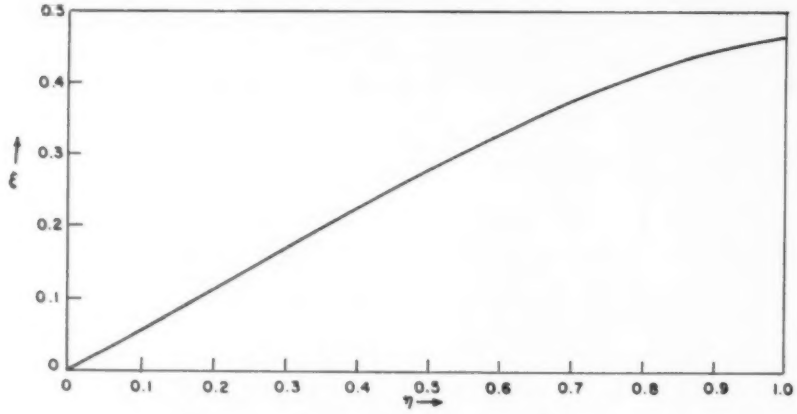

Fig. 2. The characteristic of (35). Phase 1.

lower bound. Moreover, the characteristic cannot intersect the isocline $m =$ const. before the slope of the isocline itself is equal to m, because, if it did, it would necessarily have to start on the isocline $m = 0$. The locus c_2 of such points on the isoclines where the slopes are equal to the corresponding values of m constitutes an upper bound. The characteristic lies between these two bounds which are found to define a comparatively narrow region. It was found necessary to graph only the isoclines $m = 0{\cdot}1\ (0{\cdot}1)\ 0{\cdot}5$ in order to determine the position of the characteristic as shown in Fig. 2. Note that $\xi \approx 0{\cdot}465$ when $\eta = 1$.

There is now the problem of determining ξ and η as functions of τ. If η is eliminated between (25) and (41) and the integration is made, then it is found that

$$\tau = \xi^2 \sum_{i=0}^{\infty} b_i \xi^i. \tag{42}$$

The coefficients b_i are given in terms of the a_i. Values of the first three coefficients are

$$b_0 \approx 8{\cdot}291, \qquad b_1 \approx -27{\cdot}51, \qquad b_2 \approx -20{\cdot}75. \tag{43}$$

The approximation

$$\tau = \xi^2 \sum_{i=0}^{2} b_i \xi^i \quad (0 \leqslant \xi < 1) \tag{44}$$

is taken in the neighborhood of the origin. Subsequent numerical results indicate that this approximation under-estimates τ by 2% when $\xi = 0{\cdot}05$ and by 10% when $\xi = 0{\cdot}10$, and it is not therefore very accurate when $\xi > 0{\cdot}10$ or, equivalently, when $\eta > 0{\cdot}20$. Beyond $\xi = 0{\cdot}10$ equations (25), (27) are solved approximately through step-by-step numerical integration as follows. However, note first that the 10% error in τ at $\xi = 0{\cdot}10$ is much smaller if expressed in terms of τ_1; and it is then about 1%. Let $\xi_0 = 0{\cdot}10$, and let η_0 be the corresponding value of η calculated from (41). Equations (25), (27) then enable $(\xi_0)_\tau$ and $(\eta_0)_\tau$ to be calculated. Now choose $\Delta\tau$ such that the point $\xi_1 = \xi_0 + (\xi_0)_\tau \Delta\tau$, $\eta_1 = \eta_0 + (\eta_0)_\tau \Delta\tau$ lies close to the characteristic (Fig. 2). Repeat the procedure until $\eta(\tau) = 1$ when by definition $\tau = \tau_1$ and the phase terminates. The accuracy is improved (and thereby partly checked) by taking progressively smaller intervals $\Delta\tau$. The quantity τ_1 is also

$$\int_0^{\xi(\tau_1)} \frac{d\xi}{\xi_\tau}, \tag{45}$$

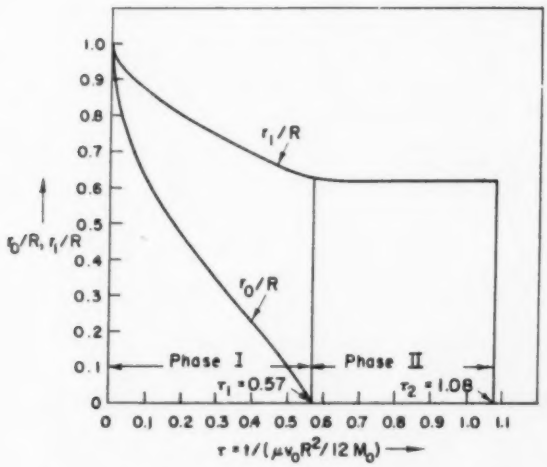

Fig. 3. Variation of r_0, r_1 with t. Phases I, II.

and this formula is employed as a check upon the previous result. The average of these two results is taken to be the best value for τ_1. The principal numerical results are

$$\tau_1 = 0{\cdot}57\ (\pm\ 0{\cdot}02), \tag{46}$$

$$\xi(\tau_1) = 0{\cdot}464\ (\pm\ 0{\cdot}001). \tag{47}$$

The quantities ξ and η may be plotted as functions of τ. The quantities r_0 and r_1 are then easily calculated, and the results are shown in Fig. 3.

Throughout this phase the plate centre is always in regime A. Thus the central

deflection at any time is simply $v_0 t$. However, other points do not always remain in the same regime, and care is needed in the evaluation of their displacements. This computation, although straightforward, has not been made.

It is straightforward to prove that the bending moment M decreases uniformly from M_0 to $-M_0$ as r increases uniformly from r_0 to R. The proof is omitted from the present paper.

The analysis of phase I is now complete.

Phase II : $t > t_1$.

Consider the motion described by

$$w_t = \left\{ \begin{array}{ll} V_0(t)\,(1 - \sigma r/r_1) & (0 \leqslant r \leqslant r_1(t)), \\ V_0(t)\,\sigma \ln (R/r) & (r_1(t) \leqslant r \leqslant R). \end{array} \right\} \tag{48}$$

This motion satisfies the condition $w_t\,(R, t) = 0$; also w_t and w_{rt} are continuous throughout $0 < r < R$ if σ is given by

$$1/\sigma = 1 + \ln (R/r_1) \qquad (\geqslant 0). \tag{49}$$

It is necessary that w_t is continuous at $t = t_1$, and this will be so if

$$r_1(t_1 + 0) = r_1(t_1 - 0), \qquad V_0(t_1) = v_0, \tag{50}$$

$r_1\,(t_1 - 0)$ being given from the analysis of the first phase. It is supposed that V_0 and r_1 are both montonically decreasing functions of the time, and then the end of the second phase is defined by

$$V_0\,(t) = 0, \qquad \text{say} \qquad t = t_2. \tag{51}$$

According to (48),

$$\left. \begin{array}{llll} \kappa = 0, & \lambda = \sigma V_0/r_1\, r & (\geqslant 0) & (0 < r \leqslant r_1), \\ \kappa = -\lambda = -\sigma V_0/r^2 & & (\leqslant 0) & (r_1 \leqslant r \leqslant R), \end{array} \right\} \tag{52}$$

so that λ is discontinuous only at $r = 0$, R where there are stationary hinge circles. Further from the flow rules (3)-(7), the regions $0 < r < r_1$ and $r_1 < r < R$ are in regimes AB and BC ; the edge and centre of the plate are respectively in regimes A and C. Thus

$$\left. \begin{array}{lll} 0 < M < M_0, & N = M_0 & (0 < r < r_1), \\ -M_0 < M < 0, & N = M_0 + M & (r_1 < r < R). \end{array} \right\} \tag{53}$$

Also from (48),

$$w_{tt} = \left\{ \begin{array}{ll} (V_0)_t - \left(\dfrac{V_0\,\sigma}{r_1}\right)_t r & (0 < r < r_1), \\ (V_0\sigma)_t \ln (R/r) & (r_1 < r < R); \end{array} \right\} \tag{54}$$

it is straightforward to verify that w_{tt} is continuous at $r = r_1$.

Subsequent analysis is simplified through the use of ρ, τ and ξ as defined in (19). Also let

$$\zeta = V_0/v_0. \tag{55}$$

In what follows w_t/v_0, M and N are again regarded principally as functions of ρ and τ, and ξ and ζ as functions of τ. The equation of motion (20) still applies. The velocity distribution (48) becomes

$$w_t/v_0 = \begin{cases} \zeta(1+\xi-\rho e^{\xi})/(1+\xi) & (0 \leqslant \rho \leqslant \rho_1 = e^{-\xi}), \\ -\zeta(\ln \rho)/(1+\xi) & (\rho_1 \leqslant \rho \leqslant 1). \end{cases} \tag{56}$$

The end of this phase is defined by

$$\zeta(\tau) = 0, \text{ say } \tau = \tau_2. \tag{57}$$

The conditions on the bending moment distributions become

$$\begin{aligned} 0 < M/M_0 < 1, \quad & N/M_0 = 1, && (0 < \rho < \rho_1), \\ -1 < M/M_0 < 0, \quad & N/M_0 = 1 + M/M_0, && (\rho_1 < \rho < 1). \end{aligned} \tag{58}$$

The dynamical equation (20) is now integrated throughout the region $0 < \rho < \rho_1$ with use of (56), (58) and the condition $M(0, \tau) = M_0$. This gives

$$\begin{aligned} M/M_0 &= 1 - \rho^2(-2\zeta_\tau + \gamma\rho) \qquad (0 \leqslant \rho < \rho_1), \\ \text{where} \qquad \gamma &= \{\zeta e^{\xi}/(1+\xi)\}_\tau. \end{aligned} \tag{59}$$

Now the regime AB terminates when $M(\rho, \tau) = 0$, i.e., $\rho = \rho_1 = e^{-\xi}$. Then from (59) it follows that ξ and ζ sati fy the first order, non-linear, ordinary differential equation

$$(1+\xi)(1+2\xi)\zeta_\tau - \xi\zeta\xi_\tau = -(1+\xi)^2 e^{2\xi}. \tag{60}$$

Next the dynamical equation (20) is integrated throughout the region $\rho_1 < \rho < 1$ with use of (56), (58) and the condition $M(\rho_1, \tau) = 0$. Thus

$$\begin{aligned} M/M_0 = {} & \{1 + \rho^2(6\zeta_\tau - 4\gamma\rho)\} \ln(\rho/\rho_1) \\ & - 3\delta\{\rho^2 \ln(\rho/e) - \rho_1^2 \ln(\rho_1/e) \\ & - \rho_1^2 \ln(\rho_1^2/e) \ln(\rho/\rho_1)\} \quad (\rho_1 < \rho < 1), \\ \text{where} \qquad \delta = {} & \{\zeta/(1+\xi)\}_\tau. \end{aligned} \tag{61}$$

The regime BC terminates when $M(\rho, \tau) = -M_0$; this must correspond to the plate edge, and so $\rho = 1$. Then from (61) as $M(1, \tau) = -M_0$ it follows that ξ and ζ satisfy a second equation similar in type to Eq. (60), viz.,

$$(1+\xi)(3e^{3\xi} - 3 - 4\xi)\zeta_\tau - (3e^{2\xi} - 3 - 6\xi - 2\xi^2)\zeta\xi_\tau = -(1+\xi)^3 e^{2\xi}. \tag{62}$$

The fundamental analytical problem is therefore to solve the two simultaneous, non-linear, ordinary differential equations (60), (62) subject to the initial conditions

$$\xi = \xi_1, \qquad \zeta = 1; \qquad \tau = \tau_1 \tag{63}$$

in the range $1 \geqslant \zeta \geqslant 0$. The complexity of these equations necessitates the use of a numerical method of integration. If ζ is regarded as a function of ξ then τ may be eliminated between (60) and (62) to give the separable equation

$$\frac{1}{\zeta}\frac{d\zeta}{d\xi} = (3 + 7\xi + 3\xi^2 - 3e^{2\xi})/(1+\xi)(4 + 7\xi + 2\xi^2 - 3e^{2\xi}), \tag{64}$$

Vol. 3 54/55

and therefore, remembering the conditions (63),

$$\zeta = \left(\frac{1+\xi}{1+\xi_1}\right) \exp\left\{-\int_{\xi_1}^{\xi} \frac{(1-\xi)\,d\xi}{(4+7\xi+2\xi^2-3e^{2\xi})}\right\}. \tag{65}$$

As ξ uniformly increases from ξ_1, ζ uniformly decreases from 1 and is zero when

$$4 + 7\xi + 2\xi^2 - 3e^{2\xi} = 0, \tag{66}$$

i.e.,

$$\xi(\tau_2) = \xi_2 \approx 0{\cdot}478. \tag{67}$$

Note that ξ changes but little during this phase as it varies only between 0·464 and 0·478. The relationship between ξ and ζ is shown in Fig. 4.

There is now the problem of determining ξ and ζ as functions of τ. For any point (ξ, ζ) lying on the curve of Fig. 4. the values of ξ_τ and ζ_τ are known from (60), (62). Now the formula

$$\tau_2 - \tau_1 = \int_1^0 \frac{d\zeta}{\zeta_\tau} \left(= \int_{\xi_1}^{\xi_2} \frac{d\xi}{\xi_\tau}\right) \tag{68}$$

enables $\tau_2 - \tau_1$ to be evaluated graphically, and this method gives the result

$$\tau_2 - \tau_1 \approx 0{\cdot}51\ (\pm\ 0{\cdot}005). \tag{69}$$

Note that the second phase is only slightly shorter than the first phase. The central deflection of the plate at the end of the second phase is, remembering (46),

$$w\,(0, t_2) = \frac{\mu v_0^2\, R^2}{12 M_0}\left(0{\cdot}57 + \int_{\tau_1}^{\tau_2} \zeta d\tau\right) \tag{70}$$

$$\approx 0{\cdot}84\ (\mu v_0^2\, R^2/12 M_0), \tag{71}$$

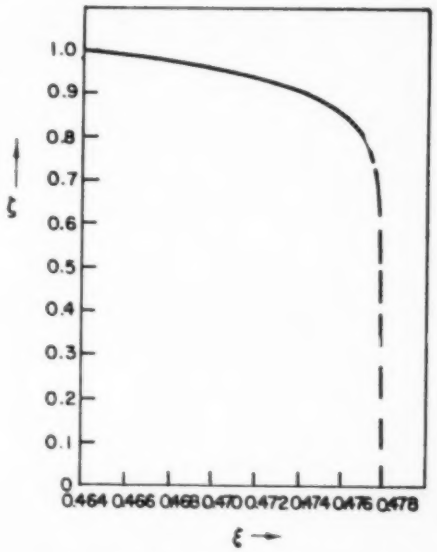

Fig. 4. Variation of ζ with ξ. Phase II.

the numerical coefficient again being found by graphical integration. The quantity ζ can be plotted as a function of τ. A very accurate approximation to V_0 is found to be the linear relationship in time,

$$V_0(t) = v_0\,(t - t_2)/(t_1 - t_2). \tag{72}$$

Lastly, in Fig. (3), the quantity r_1/R is plotted as a function of τ. Note that r_1 varies almost inappreciably during the major part of this phase.

The computation of the plate displacement (except that at the centre) has not been made.

It is straightforward to prove that the bending moment M decreases uniformly from M_0 to $-M_0$ as r increases uniformly from 0 to R. The proof is omitted from the present paper.

When $\tau = \tau_2$ all elements of the plate are instantaneously at rest. The plate

must now remain at rest. The bending moment distribution undergoes an instantaneous change to one of equilibrium not violating the yield condition.

The analysis of phase II is now complete.

Acknowledgment

The results presented in this paper were obtained in the course of research sponsored by the Norfolk Naval Shipyard under Contract No. N189s – 92558.

References

Bakhshiyan, F. A.	1948	*Prikl. Mat. Mekh.*, **12**, 47.
Kochetkov, A. M.	1950	*Prikl. Mat. Mekh.*, **14**, 203.
Hopkins, H. G.	1953	Brown University Technical Report DA-2598/7.
Hopkins, H. G. and Prager, W.	1953	*J. Mech. Phys. Solids*, **2**, 1.
	1954	*Zeit. f. Angew. Math. u. Phys.*, in press.
Wang, A. J.	1953	Brown University Technical Report DA-798/7.

Vol.
3
54/55

Journal of the Mechanics and Physics of Solids, 1954, Vol. 3, pp. 38 to 46. Pergamon Press Ltd., London.

THE DYNAMIC STRAINING OF METALS HAVING DEFINITE YIELD POINTS

By D. B. C. Taylor
Department of Engineering, University of Cambridge

(*Received 27th April*, 1954)

Summary

Strain rate during non-uniform yielding of metals under repeated dynamic loading is analysed and it is deduced that the time-yield stress relationship appears to be described better by a "delay period" effect than by a simple strain rate phenomenon.

The criterion for dynamic yield is discussed and appears to be of the form $\int_0^{t_1} \sigma^n \, dt = \text{constant}$, though some evidence is given which suggests that a term dependent exclusively upon stress should be included.

1. Introduction

It is now a well-established fact that many metals under dynamic straining offer a resistance to deformation which increases with the applied strain rate. The precise part played by this strain rate in determining the magnitude of the resistance offered is not as yet fully understood, but study of the phenomenon is rendered more difficult if the metal under test yields non-uniformly, the strain rate therefore varying from point to point along the specimen. The importance of this is emphasized by the fact that it is those very metals (e.g. mild steel and pure iron) that yield non-uniformly under both static and dynamic straining which show the greatest reaction to increase of strain rate.

The purpose of this paper is therefore to analyse the strain rate effect in such metals and to offer some further experimental evidence of their behaviour.

2. Previous Experimental Work

Researches into the dynamic properties of metals have in general been directed towards obtaining dynamic stress-strain diagrams which, as a result of dynamometer vibration, almost invariably show large superimposed vibrations. In testing yield-point metals these obscure the initial yield phenomenon and since straining is carried straight through to fracture, study of the non-uniform yielding aspect is also impossible.

To overcome these difficulties, in recent years such dynamic tests have been carried out in a series of steps, the dynamic yield stress and the resulting permanent strain being measured for each loading and from the results a yield stress-permanent strain diagram plotted. It is therefore to the results of such repeated

dynamic loading tests that we must turn for evidence of the dynamic behaviour of metals which yield non-uniformly.

WARNOCK and TAYLOR (1949) and GIBSON (1953) have shown that there is a marked similarity between such dynamic curves and the corresponding ones obtained under static conditions, since both have upper and lower yield points followed by rising strain hardening curves. The mode of deformation during the lower yield range is also the same for both types of straining and is represented approximately by Fig. 1, though the actual amplitude of the non-uniform yielding is greater for dynamic straining.

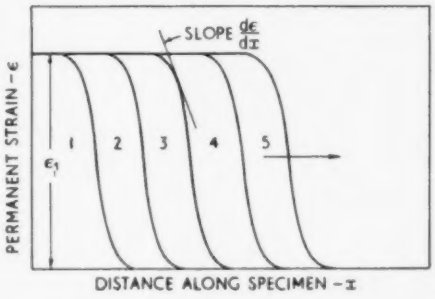

Fig. 1. Distribution of permanent strain in gauge length of yield point metal under repeated dynamic loading.

The permanent strain would seem to rise quickly towards a critical value ϵ_1 and then to spread along the gauge length with a more or less constant shape of front until the entire gauge length is yielded. For such a mode of deformation the plastic strain rate $\dot{\epsilon}$ of the metal at any point in the front can be shown to be given by

$$\dot{\epsilon} = \frac{V}{\epsilon_1} \times \frac{d\epsilon}{dx} \times \frac{I}{N} \tag{1}$$

where V = velocity of straining applied to the specimen ends,
x = distance along the specimen gauge length.
ϵ = permanent strain.
N = number of fronts.

The plastic strain rate therefore varies from point to point in the plastic front by change of slope $d\epsilon/dx$, but WARNOCK and TAYLOR showed, at least for a normalized 0·31% carbon steel which they tested, that the yield stress for repeated dynamic loading in this lower yield range remained constant. So long as the number of plastic fronts N remains the same this can perhaps be explained by assuming the dynamic properties of the metal to vary with the degree of permanent strain, and equilibrium to be established between the externally applied load on the specimen and the slope and dynamic properties of the metal at each point in the plastic front. However, WARNOCK and TAYLOR showed also that the steel in the "as received" state deformed less regularly; subsequent tests indicated that, while there was a tendency to follow a regular pattern, considerable variation in the shape and number of fronts could take place, but that, so long as unyielded material remained in the gauge length, the dynamic yield point remained substantially constant. This would seem to suggest that for repeated dynamic loading of partially strained metal in the lower yield range the yield points were not the stresses necessary to ensure plastic flow at the imposed strain rate, but instead were determined by some property of the unyielded material remaining in the gauge length.

Vol. 3 54/55

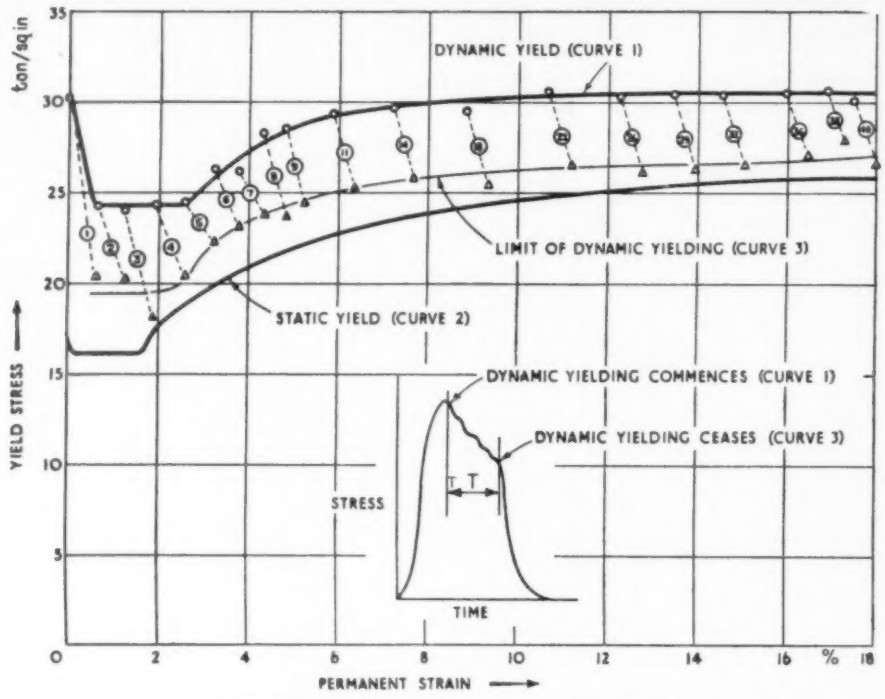

Fig. 2. Yield of mild steel under repeated dynamic loading.

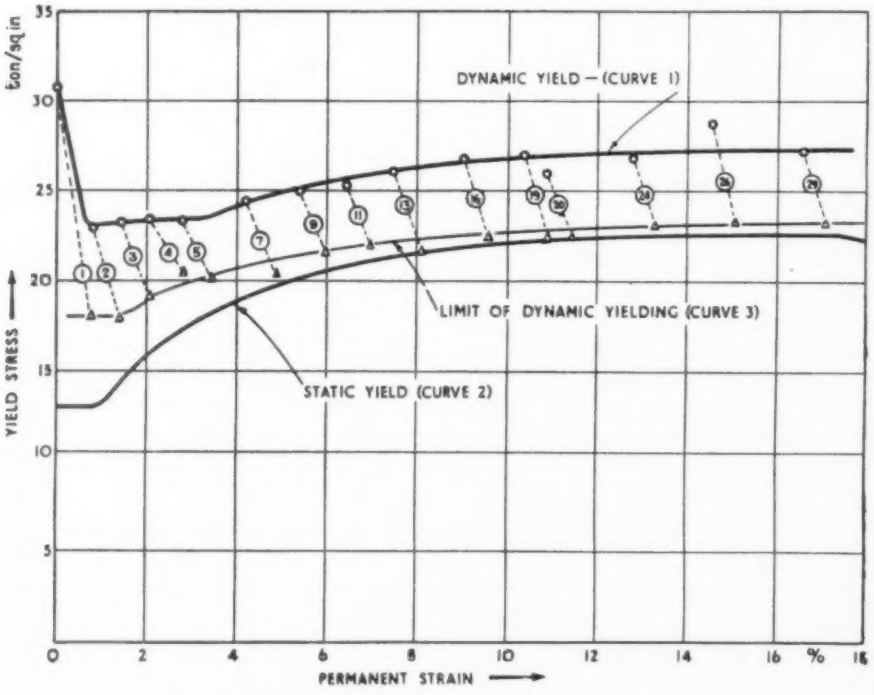

Fig. 3. Yield of pure iron under repeated dynamic loading.

3. Further Experimental Work

With the same " falling weight " type of impact testing machine as that used by Warnock and Taylor (1949) similar repeated dynamic loading tests were carried out on specimens of a mild steel, a pure iron and a carbon manganese

Table 1.
Mechanical Properties and Chemical Analyses of steels tested

Mechanical Properties	*Mild Steel*	*Pure Iron*	*Carbon Manganese Steel*
Yield Stress (tons/sq. in.)	16·6	13·2	25·2*
Maximum Stress (tons/sq. in.)	27·4	22·7	43·3
Elongation per cent.	41·0	36·0	27·0
Reduction in area per cent.	65·7	47·2	44·7
Brinell Hardness No.	131	116	215
Chemical Analysis			
Carbon per cent.	0·14	0·049	0·23
Silicon ,,	0·19	0·16	0·25
Manganese ,,	0·54	0·02	1·56
Sulphur ,,	0·010	0·004	0·014
Phosphorus ,,	0·011	0·083	0·012
Nickel ,,	0·19	—	0·18
Chromium ,,	0·14	—	0·06

* 0·2 per cent. Proof Stress
Specimen : 0·564 in. diameter, 2 in. gauge length.

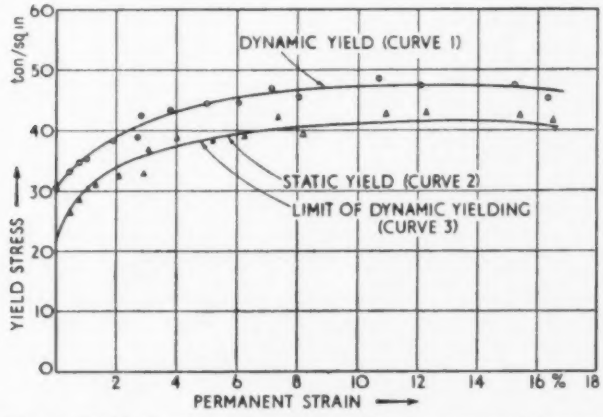

Fig. 4. Yield of carbon manganese steel under repeated dynamic loading

steel. All were tested in the " as received " condition their mechanical properties and chemical analyses being given in Table 1.

Curve 1 in Figs. 2, 3 and 4 shows the variation of dynamic yield stress of the metals when repeatedly loaded at an initial straining velocity of $V = 4{\cdot}5$ ft./sec.

which fell to zero after the metal had plastically yielded for T millisecs. A typical stress time record is included in Fig. 2. Figs. 5a, 6a, and 7a show the resulting permanent strains in the specimen gauge lengths, the numbers corresponding to those on the dynamic stress curves. Figs. 5b, 6b and 7b show the effect of repreated static loading on these three metals.

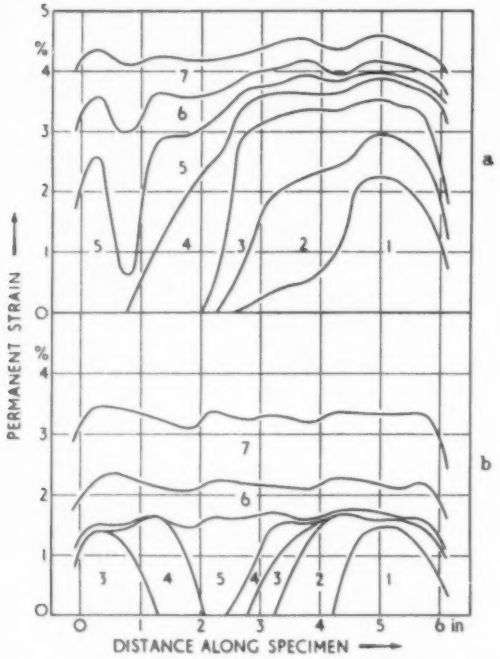

Fig. 5. Growth of permanent strain in mild steel specimen.
(a) Dynamic straining. (b) Static straining.

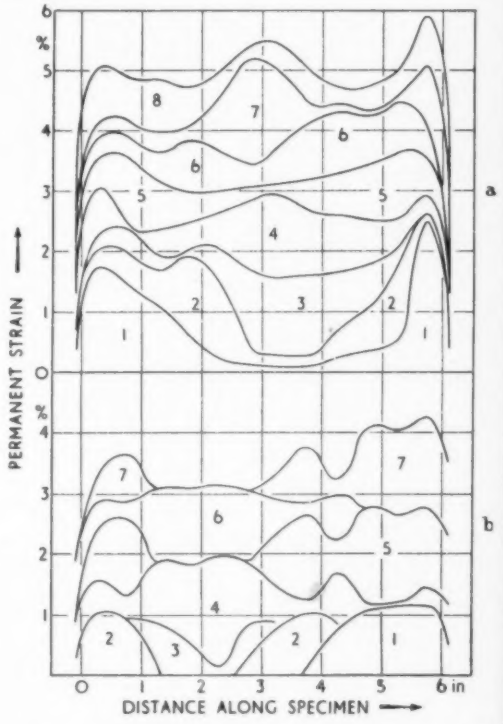

Fig. 6. Growth of permanent strain in pure iron specimen.
(a) Dynamic straining. (b) Static straining.

Behaving in a similar manner to the 0·31% carbon steel of Warnock and Taylor, both the mild steel and the pure iron showed dynamic upper and lower yield points together with increased amplitude of non-uniform yielding during the dynamic lower yield stress range. The carbon manganese steel which had no definite yield point when statically tested (curve 2, Fig. 4), strained quite uniformly under both static and dynamic straining and showed no exaggerated dynamic yield phenomenon. This is typical of the behaviour of such uniformly straining metals, the increases in resisting stress being less than those noted for yield point metals under equal dynamic straining conditions.

4. Discussion of Results

A study of the dynamic non-uniform yielding of the mild steel (Fig. 5a) and the pure iron (Fig. 6a) shows that the pattern of deformation varied from loading to

loading while the lower yield stress in both cases (Figs. 2 and 3) remained more or less constant. This again suggests that the dynamic yield stress is associated with the persistance of unyielded material in the gauge length, or, putting it more generally, is dependent upon that portion of the gauge length which has been least strain hardened and is therefore the weakest part of the specimen.

Such sympathetic movement of the dynamic yield point can perhaps be noted in the results for the dynamic straining of the pure iron (Figs. 3 and 6a), where once the dynamic upper yield point has been passed the yield stress for subsequent loadings rose slowly as the weakest portion of the gauge length continued to strain slightly. This should be compared with the mild steel (Figs. 2 and 5a), and with the carbon steel of WARNOCK and TAYLOR where the yield point remained constant in sympathy with the unyielded material remaining in the gauge length.

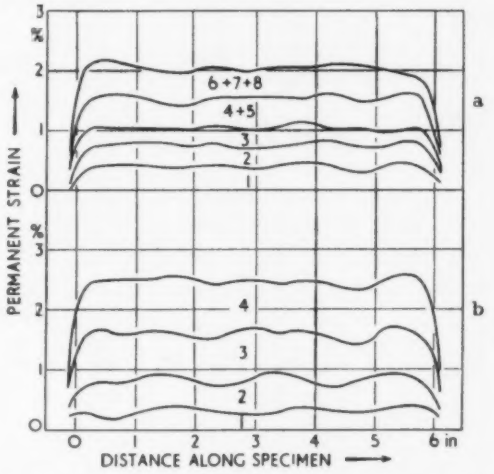

Fig. 7. Growth of permanent strain in carbon manganese steel specimen.
(a) Dynamic straining. (b) Static straining.

As a result of this, and again supposing a strain rate effect for the increased resistance, we might be led to conclude that the yield stress was a strain rate effect in the weakest portion of the gauge length. However, as more and more of the specimen is yielded so this portion is reduced in length, the effect being particularly noticable when varying amounts of gauge length remain completely unyielded, and it must therefore be concluded that the dynamic yield stress is not the result of a strain rate effect here either.

5. DELAY PERIOD

The basis of a new approach to this problem is to be found in the ' delay period ' work of CLARK and WOOD (1949) who studied the effect of suddenly applying a constant value of stress in excess of the static upper yield point to an annealed low carbon steel. They showed that for a particular value of stress there was a characteristic delay period prior to the initiation of plastic yield in an unstrained specimen. As the value of this applied stress was increased so the delay period was reduced. By measuring the plastic and anelastic microstrains in the metal during such delay periods VREELAND, WOOD and CLARK (1952) found that prior to the initiation of plastic yield a critical value of pre-yield microstrain of approximately 30×10^{-6} was attained and that this strain was uniformly spread along the gauge length.

Under such conditions of constant applied stress the microstrain is therefore a function of time only. Should the stress be other than constant during this delay

period, e.g. continually increasing with time either linearly or otherwise one might logically expect the critical value of microstrain to be eventually attained also, and yield to be initiated. This state of affairs may be expressed approximately by an equation of the form

$$\int_0^{t_1} \sigma^n \, dt = C \tag{2}$$

where

σ = applied stress in excess of the static yield stress (some function of time)
t_1 = duration of the delay period
n and C = constants, both positive, whose values would depend upon the material under test.

In the discussion of the paper by Gibson (1953) the author pointed out that the relationship between delay period and applied stress for the mild steel could be expressed by an equation of this form. More recently Campbell (1953) taking a critical value of the density of released dislocation as the criterion for yield, derived the following very similar relationship between the delay period t_1 and the applied stress

$$\int_0^{t_1} (\sigma/\sigma_0)^\alpha \, dt = C, \tag{3}$$

α, σ_0 and C being constants of the material. This equation differs from equation (2) in that σ is the full value of the applied stress and not simply that in excess of the static yield stress. However, since there is a lower limit to the stress at which yield can take place, Campbell discusses some experimental evidence which suggests that equation (3) is only applicable for values of t_1 less than approximately 1 sec.

If we consider, like Vreeland, Wood and Clark (1952), that the anelastic microstrains are produced by the concentration of free dislocations at the grain boundaries, then the similarity between equations (2) and (3) becomes more pronounced. However, these investigators did not detect any microstrain below a value of stress equal to approximately 60% of the static lower yield stress, a value which agrees fairly well with the limit of proportionality obtained by Roberts, Carruthers and Averbach (1952) for a similar material. This would seem to suggest that the correct value of σ in both equations (2) and (3) is the applied stress in excess of this limit of proportionality, though theoretical and experimental justification for this must await further work in this field.

6. Application of the Delay Period Hypothesis to Experimental Work

The large values of dynamic upper yield stress recorded for the mild steel and the pure iron in this paper (curve 1, Figs. 2 and 3), for the carbon steel of Warnock and Taylor, and in other dynamic straining tests on materials having definite static yield points, may be described on this basis. Both the applied stress and time increase until an equation of a form similar to either (2) or (3) is satisfied, when plastic yield will be initiated. The work of Vreeland, Wood and Clark (1953) would seem to suggest that at this point the value of pre-yield microstrain again reached the critical value noted immediately prior to the initiation of yield under constant applied stress.

It would seem that a similar phenomenon takes place during subsequent dynamic loading of partially strained metal, the material in the weakest portion of the gauge length again displaying a delay period effect. However, since the dynamic yield stresses recorded in the lower yield range are considerably lower than the dynamic upper yield, it must be concluded that the delay period effect is much less pronounced in this region.

The dynamic yield point for both the unstrained and partially strained metal would therefore seem to be the stress at which the appropriate delay period was overcome. Previously yielded portions of the gauge length would tend to yield at rates dependent upon local conditions and the extent to which they could yield (the critical value of dynamic non-uniform yielding ϵ_1 in equation (1)) being limited by the value of this yield stress.

This would seem to be a more reasonable explanation for the dynamic non-uniform yielding, since annealed materials, being more homogeneous, would tend to deform under a regular pattern, whereas " as received " materials would tend to yield much less uniformly as a result of internal strains etc.

7. Limit of Dynamic Yielding

Evidence that the plastic resisting stresses subsequent to the yield point in any particular dynamic loading are not directly dependent upon strain rate either is shown when we plot the values of stress at which yielding ceased. The variation of this stress is given by curve 3 in Figs. 2, 3 and 4. Since these values of stress correspond to zero strain rate (the external straining velocity having fallen to zero at this point) one would expect, on the basis of a strain rate effect, the points to coincide with the static permanent strain curves (curve 2). This was only found to be true for the carbon manganese steel (Fig. 4). For the mild steel and the pure iron (yield-point materials) the curve was in excess of the static curve.

Warnock and Taylor showed that for the carbon steel tested, part of this discrepancy could be accounted for by excessive strain hardening under dynamic straining but this was almost entirely confined to the strain hardening curve, the above experimental evidence showing that the effect was particularly noticeable during the early stages of straining. A tentative explanation of this can be put forward if it is assumed that the value of the microstrain, or, using Campbell's criterion for yield, the density of the released dislocations, is not simply a function of stress and time alone as has been suggested, but that it has a component dependent upon stress only. That is,

$$\text{microstrain } \epsilon' = f(\sigma, t) + F(\sigma). \tag{4}$$

Under this hypothesis, for very rapid straining (small values of time) the critical value of microstrain ϵ_c' would be attained almost exclusively by the $F(\sigma)$ component which is independent of time. As time increased the $f(\sigma, t)$ component would increase in value so that ϵ_c' could be maintained at a lower and lower value of stress, hence the fall in stress from the yield point noted in the stress-time record on Fig. 2.

The explanation of curve 3 in Figs. 2 and 3 would seem to be that even after time T, the duration of yielding (see record on Fig. 2), ϵ_c' was not attained by the

$f(\sigma, t)$ component, so that it was necessary for the applied stress to be maintained in excess of static values as the strain rate approached zero. On this basis, the fall in stress after yield is not, as was supposed by WARNOCK and TAYLOR, the result of the fall in velocity of straining from the initial value V to zero.

7. CONCLUSIONS

(i) The series of dynamic yield points obtained by the repeated dynamic loading of yield point metals do not appear to be dependent upon a straightforward strain rate effect but can be accounted for on the basis of a delay period effect in not only the unyielded but also the partially yielded material.

(ii) The non-uniform yielding noted during dynamic straining is simply the result of an inherent tendency of such metals to yield in this manner, the maximum amplitude of the permanent strains being determined by the above delay period stress.

(iii) The criterion for yield is expressed by an equation of the form (2), though there is some evidence that a term dependent exclusively upon stress should be included.

REFERENCES

CAMPBELL, J. D.	1953	*Acta Metallurgica*, **1**, 706.
CLARK, D. S. and WOOD, D. S.	1949	*Proc. A.S.T.M.*, **49**, 717.
GIBSON, J.	1953	*Proc. Inst. Mech. Eng.*, **1B**, 536.
ROBERTS, C. S., CARRUTHERS, R. C. and AVERBACH, B. L.	1952	*Trans. Am. Soc. Metals*, **44**, 1150.
VREELAND, T., WOOD, D. S. and CLARK, D. S.	1952	*Sixth Technical Report*, California Institute of Technology, Pasadena, U.S.A.
VREELAND, T., WOOD, D. S. and CLARK, D. S.	1953	*Trans. Am. Soc. Metals*, **45**, 620.
WARNOCK, F. V. and TAYLOR, D. B. C.	1949	*Proc. Inst., Mech. Eng.*, **161**, 165.

VOL 3 1954/

Journal of the Mechanics and Physics of Solids, 1954, Vol. 3, pp. 47 to 53. Pergamon Press Ltd., London.

THE MECHANICS OF MACHINING: A NEW APPROACH

By R. Hill
Department of Mathematics, University of Nottingham

(*Received* 10th *June*, 1954)

Summary

It is suggested that infinitely many steady states of the single shear-plane type are possible, for different initial conditions. If this is so, the search for a unique steady state (the aim of previous theories) is misplaced. Here the possible range of inclinations of the shear plane is obtained by excluding configurations that imply overstressing of material at the singularities of stress. The method makes use of a theorem (Hill 1954) on the maximum intensity of singularities in a material that yields when the shear stress attains a critical value.

Vol. 3 54/55

1. Aim of the Present Investigation

It is notorious that the extant theories of the mechanics of machining do not agree well with experiment. Evident reasons may be that (i) the assumptions basic to the analysis are not sufficiently realistic, though they serve well enough for many other forming processes (e.g. isotropy, no work-hardening, infinite shear modulus, constant angle of friction, no thermal effects); (ii) the experimental technique is inadequate, the geometry of the distortion being difficult to determine during motion and under plane-strain conditions; (iii) the theory is unsound, even within its self-imposed limits. This last is the aspect of the matter taken up here.

There seem to be only two theories of any significance in the field: those due respectively to Ernst and Merchant (1941) and to Lee and Shaffer (1951). Both are directed towards determining a unique steady-state configuration for given tool rake and friction angle; both are incomplete (in the sense that the entire state of stress is not investigated), and both introduce an ad hoc 'minimum load' hypothesis in order to secure uniqueness. This hypothesis has been sufficiently criticised by Bishop and McDougall (1953) and need not be considered further.

However, no one appears to have envisaged the possibility that the search for uniqueness is fruitless: that is, there may be many, even infinitely many, steady-state configurations of a given type (e.g. with a single plane of shear, or with a 'false cap' of given shape adhering to the tool). Indeed, in a process such as machining where there is so little constraint on the flow, it seems certain that the initial conditions must influence the ultimate steady state. Granted this, the logical approach to the problem is radically different. The ultimate objective now becomes, not a single unique solution, but a whole range of steady-state solutions of (let us say) the shear-plane type, each complete in the technical sense

and each associated with a set (or sets) of initial conditions by an intervening non-steady transitional flow*. One may proceed towards this objective in three stages of ascending difficulty : (i) establish the extent of the forbidden range of the shear-plane inclination ; (ii) guided by this information, construct permissible solutions in the range not excluded ; (iii) determine the initial conditions associated with each such solution.

Here only stage (i) is examined in any detail. The method depends on a recent theorem (HILL 1954) on the permissible singularities of stress in an ideal plastic-rigid material. Singularities are present at each end of the shear-plane where it intersects the tool and free surface respectively. Their role in the mechanics of the problem is so fundamental that the exclusion of configurations implying overstressed material at a singularity leaves a comparatively small range for examination in stage (ii).

2. EXCLUDED RANGES

In the machining process considered here a wedge-shaped tool is moved in a direction normal to its cutting edge and parallel to the plane surface of the workpiece (Fig. 1). The depth of cut is small compared with its width. We examine the possibility of steady states in which the zone of deformation is concentrated in a single plane (ST) springing from the tip of the tool (T). The inclination of the shear-plane to the surface of the workpiece is denoted by ϕ, and its inclination to the tool face by ψ. Nothing need be assumed about the geometry of the chip, other than that its free surface QS is parallel at S to the tool face RT. Relative sliding between chip and tool is supposed to occur is some unspecified neighbourhood of the tip, the angle of friction being λ at every point.

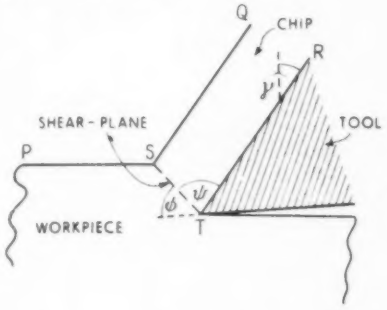

Fig. 1.

Since the velocity is tangentially discontinuous across the shear-plane, this must be a direction of maximum shear stress k. Moreover, by Hencky's theorem, the pressure acting across it is uniformly distributed, with magnitude p say. Evidently

$$p = k \cot (\psi - \lambda), \text{ with } \psi > \lambda, \tag{1}$$

since the resultant traction across the shear plane must balance the force exerted by the tool (no other forces being applied to the chip). The loading of the material within each of the three angles PST, QST, RTS in the immediate neighbourhood of their vertices can now be detailed as in Fig. 2.

(a) *Angle RTS.*

Let the frictional stress exerted by the tool on the chip at T be written as $k \sin 2\theta$. For present purposes we must envisage θ having any value in the range

* A much more limited, but still worthwhile, objective would be to determine a single steady state by tracing its development from one given set of initial conditions common in actual practice.

$(0, \frac{1}{4}\pi)$; its actual value in a valid steady-state is of course furnished by the corresponding complete solution.

According to HILL (1954, equations (6) and (7)) the material in the angle RTS would definitely be overstressed if the configuration were such that $\theta > \psi - \frac{1}{4}\pi$ or if the difference between the pressures on ST and RT, namely

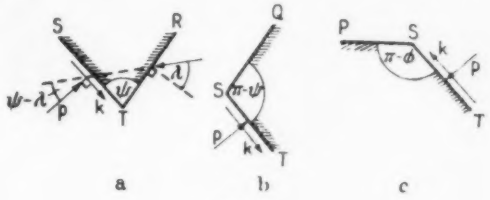

a b c

Fig. 2.

$$k\left[\cot(\psi - \lambda) - \cot\lambda \sin 2\theta\right]$$

exceeded $\quad k\left[\cos 2\theta - 2\cos(\theta + \psi - \frac{1}{4}\pi)\right] \quad$ when $\quad \theta + \psi \leqslant \frac{3}{4}\pi$

or $\quad k\left[\cos 2\theta + 2(\theta + \psi - \frac{3}{4}\pi)\right] \quad$ when $\quad \theta + \psi > \frac{3}{4}\pi$

for *all* values of θ in $(0, \psi - \frac{1}{4}\pi)$. We prove that this is so when

$$\lambda < \psi < \tfrac{1}{4}\pi + \lambda, \quad \text{if} \quad 0 \leqslant \lambda \leqslant \tfrac{1}{4}\pi. \tag{2a}$$

Since $0 < \psi - \lambda < \frac{1}{4}\pi$,

$$\begin{aligned}\cot(\psi - \lambda) - \cot\lambda \sin 2\theta &> 1 - \cot\lambda \sin 2\theta \\ &= \cos 2\theta - 2\sin\theta\cos(\theta + \lambda)/\sin\lambda \\ &> \cos 2\theta - 2\cos(\theta + \lambda)\end{aligned}$$

since $0 \leqslant \theta < \lambda \leqslant \frac{1}{4}\pi$,

$$> \cos 2\theta - 2\cos(\theta + \psi - \tfrac{1}{4}\pi)$$

since $|\theta + \psi - \frac{1}{4}\pi| < \lambda + \theta$. The stated result follows since $\theta + \psi \leqslant \frac{3}{4}\pi$. It is also true when

$$\lambda < \psi \leqslant \tfrac{1}{2}\pi, \quad \text{if} \quad \lambda > \tfrac{1}{4}\pi, \tag{2b}$$

the proof differing only slightly from the foregoing. When $\psi > \frac{1}{2}\pi$, however, values of θ have to be considered such that $\theta + \psi > \frac{3}{4}\pi$; calculation shows that the angle is overstressed for values of ψ below 103·6° when $\lambda = 60°$, below 115·7° when $\lambda = 75°$, and below 127·5° when $\lambda = 90°$. Above these limits values of θ exist such that the angle is not overstressed.

LEE and SHAFFER state that ψ must not be less than $\frac{1}{4}\pi + \lambda$, but their proof is invalid since the possibility of a stress sigularity is not allowed for.

(b) *Angle QST.*

From (1) and (2) we note that the pressure p across the shear-plane can not exceed k. On the other hand if

$$p/k = \cot(\psi - \lambda < 2\sin(\psi - \tfrac{1}{4}\pi) - 1, \qquad (3)$$

or if $\psi > \frac{3}{4}\pi$, the material at the vertex of angle QST (Fig. 2b) is definitely overstressed (HILL 1954, equation (12)). Thus, for a given λ, a lower limit is set to p and correspondingly an upper limit to ψ (Table 1). Equations (2) and (3) together define the range outside which ψ cannot fall.

TABLE 1.

λ	*Upper limit to* ψ (*equ.* 3)	*Lower limit to* p/k
0°	80·6°	0·165
10°	84·7°	0·274
20°	88·9°	0·386
30°	93·5°	0·499
40°	98·6°	0·610
50°	104·3°	0·719
60°	110·6°	0·821
70°	117·7°	0·910
80°	125·7°	0·976
90°	135°	1

(c) *Angle PST.*

The material at the vertex of the angle PST (Fig. 2c) is overstressed if the inclination ϕ of the shear-plane is so large that

$$p/k = \cot(\psi - \lambda) > 1 - 2\sin(\phi - \tfrac{1}{4}\pi). \qquad (4)$$

The greatest possible values of ϕ are given in Table 2.

TABLE 2.

$\psi - \lambda$	*Upper limit to* ϕ (*equ.* 4)
45°	45°
50°	49·6°
55°	53·6°
60°	57·2°
65°	60·5°
70°	63·5°
75°	66·5°
80°	69·4°
85°	72·2°
90°	75°

The values of ϕ and ψ not excluded by equations (2), (3) and (4) are shown as the shaded area in Fig. 3a. This is a schematic diagram for some given value of λ which, to be definite, is taken less than $\frac{1}{4}\pi$. It is customary to plot ϕ against

$\lambda - \gamma$, where γ is the rake of the tool. For this purpose it is necessary to take sections of Fig. 3a by lines $\phi + \psi = \frac{1}{2}\pi + \gamma$ for various values of γ, positive and negative. The result is shown schematically in Fig. 3b. Results to scale for $\lambda = 0°$, 15°, 30°, 45° are given in Fig. 4 ; it should be noted that boundaries

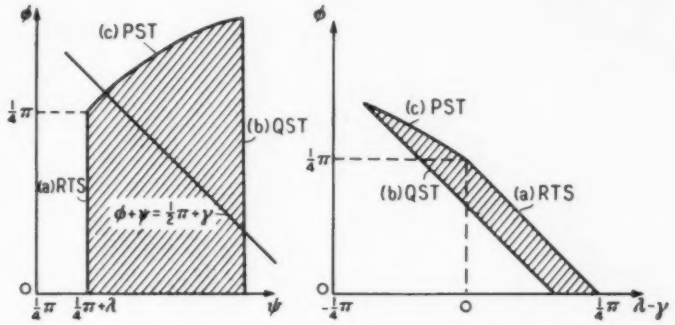

a b

Fig. 3.

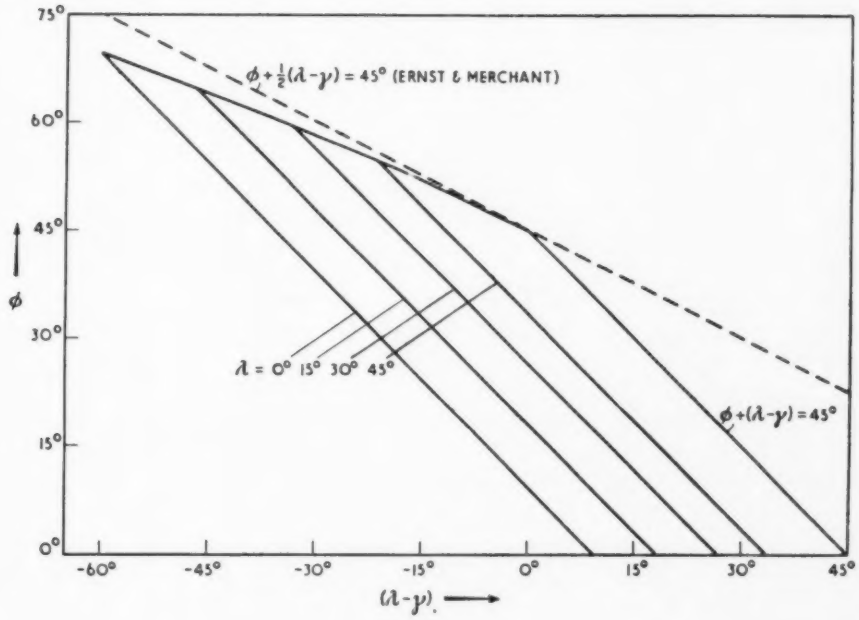

Fig. 4.

(a) and (c) are the same for all $\lambda \leqslant \frac{1}{4}\pi$, but that boundary (b) is different for each λ. When $\lambda = 0$ the greatest value of γ on the boundary (c) is 60·3°, the corresponding ϕ being 69·7°. Thus, no steady-state configuration of the shear-plane type is possible for smooth tools of rake greater than 60·3° (nor less than $-45°$).

Also shown is the ERNST and MERCHANT relation

$$\phi + \tfrac{1}{2}(\lambda - \gamma) = \tfrac{1}{4}\pi.$$

This falls in the excluded area (except when $\lambda = \gamma$) and is thus invalid. In fact, when $\lambda < \gamma$ the angle PST would be overstressed, while when $\lambda > \gamma$ the angle RTS would. The relation

$$\phi + (\lambda - \gamma) = \tfrac{1}{4}\pi,$$

mentioned by HILL (1950, p. 209 footnote) and incorporated by LEE and SHAFFER in their composite solution (op. cit.), coincides with the boundary (a) when $\lambda \geqslant \gamma$ but is invalid when $\lambda < \gamma$*.

3. PERMISSIBLE RANGES

By considering the singularities of stress it has been shown that the shear-plane inclination ϕ must lie within a certain range for each given pair λ, γ. It remains to examine whether all, or only some, values within the range are actually permissible (stage (ii) of the procedure suggested in Section 1). For this it is necessary to be able to construct some equilibrium state of stress throughout the entire chip and workpiece such that the yield limit is nowhere exceeded (HILL 1951 ; HODGE and PRAGER 1951). To any value of ϕ for which this can be done corresponds a possible steady-state configuration. The range of initial conditions from which such a steady state could be reached is yet another question for investigation (stage (iii))†.

These matters are outside the scope of the present paper. However, as it is an easy matter to construct a permissible state of stress in the workpiece (supposed infinite in extent) this will be briefly described here. The stresses p and k along the shear-plane ST can be balanced by two uniaxially-stressed columns $UVWS$ and $XYTW$ (Fig. 5). In the former the stress is a compression $2k$; in the latter it is a tension k-p (it will be recalled that $0 < p \leqslant k$). In triangle SWT the stress is identical with that on the shear-plane itself. The remainder of the workpiece is unstressed. WT and WS are stress discontinuities, WT being inclined at 45° to ST while WS bisects the angle between the two columns (it is a property of a stress discontinuity in a plane plastic state that the principal axes in the two fields are equally inclined to it). The angle VWX is

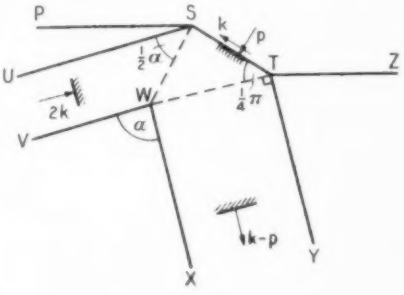

Fig. 5.

$$\alpha = \tfrac{1}{2}\pi - \sin^{-1}\left(\frac{1 - p/k}{2}\right).$$

The angle between US and TS produced being $\frac{3}{4}\pi - \alpha$, this artificial stress state is geometrically possible when $\phi < \frac{3}{4}\pi - \alpha$; that is, for all shear-plane inclinations not excluded by (4).

* The ' false cap ' type of steady state proposed by LEE and SHAFFER may be shown to imply overstressing of angle PST over a substantial range of the variables. This is so, for example, when the friction coefficient on the false cap is less than 1 when $\lambda - \gamma = 0$, 0·767 when $\lambda - \gamma = 29{\cdot}8°$, and 0·637 when $\lambda - \gamma = 49{\cdot}2°$.

† Obviously one way to reach a given steady-state configuration is to *start* with a workpiece of that shape !

In particular, when $\phi = \frac{1}{4}\pi - (\lambda - \gamma)$ and $\lambda \geqslant \gamma$ (boundary (a) in Fig. 3b) the pressure p is equal to k from equation (1) since $\psi - \lambda = \frac{1}{4}\pi$. In this case all the load is carried by one supporting column. Moreover, as BISHOP and MCDOUGALL (op. cit.) have remarked, by continuing this column up to the tool face a permissible state of stress is obtained in the chip (compatible with the given angle of friction) provided the contact with the tool extends sufficiently far.

REFERENCES

BISHOP, J. F. W. and MCDOUGALL, W. S.	1953	*Mech. Eng. Res. Lab.*, Report MF/MS 74.
ERNST, H. and MERCHANT, M. E.	1941	*Trans. Am. Soc. Metals*, **29**, 299.
HILL, R.	1950	*Mathematical Theory of Plasticity* (Clarendon Press).
	1951	*Phil. Mag.*, **42**, 868.
	1954	*J. Mech. Phys. Solids*, **2**, 278.
HODGE, P. G. and PRAGER, W.	1951	*Theory of Perfectly Plastic Solids* (Wiley).
LEE, E. H. and SHAFFER, B. W.	1951	*J. Appl. Mech.*, **73**, 405.

Vol. 3 54/55

Journal of the Mechanics and Physics of Solids, 1954, Vol. 3, pp. 54 to 62. Pergamon Press Ltd., London.

THE YIELD OF MILD STEEL UNDER IMPACT LOADING

By J. D. Campbell
Department of Engineering Science, University of Oxford

(*Received 20th July*, 1954)

Summary

Results are given of impact tests on mild steel specimens using a method of test described in a previous paper. A dynamic stress-strain curve is derived which indicates that the upper and lower yield stresses are about double those obtaining under normal static conditions. The results are compared with those of other investigators.

1. Introduction

In a previous paper (Campbell 1953a) a method of impact testing was described in which a free cylindrical specimen is subjected to longitudinal impact, and the results for an aluminium alloy were given. The present paper reports some results for mild steel specimens using the same method of test.

It was to be expected that there would be considerable differences between the behaviour of the two materials under impact loading, for two reasons. Firstly, it has been shown (White and Griffis 1948) that in a material with a drop of stress at yield, plastic strains in thin rods are propagated in the form of ' shock fronts ' across which the strain and velocity are discontinuous ; and secondly, it is known that in mild steel a small but finite time elapses before the initiation of yield in constant stress tests (Clark and Wood 1949). It is at present impossible to develop a theory of plastic wave propagation in which account is taken of this finite ' delay period,' since the behaviour of the material after the initiation of yielding is not known. It is, however, clear that both the effects mentioned above result in the plastic deformation being localized near the impact end of the specimen. For the velocity of propagation of a shock front, unless of great intensity, is small compared with the elastic wave velocity ; and the time during which the stress is maintained diminishes with increasing distance from the impact end. Owing to the resultant rapid variation of plastic strain along the specimen near its impact end, the use of strain gauges on the specimen is not so satisfactory as it was in the tests on light alloy specimens. The strain recorded by the gauges is an average over their length (8 mm) and, although the discontinuities predicted by the plastic wave theory are smoothed out owing to the effect of lateral inertia, the variation of plastic strain within the gauge length may be considerable. It was realized that for this reason the accuracy of the method used in the earlier work for obtaining data on the post-yield behaviour of the metal would not be very great. However, in mild steel considerable interest attaches to the value of the dynamic yield stress, i.e. the stress at which yield is first initiated in a dynamic

test. It was therefore decided to test a series of mild steel specimens in the same manner as before.

2. Experimental Results

(i) *Static Tests*

The steel used was a mild steel supplied by W. T. Flather & Co., Sheffield, and had the following composition :

C	Si	S	P	Mn
0·14%	0·02%	0·038%	0·027%	0·76%

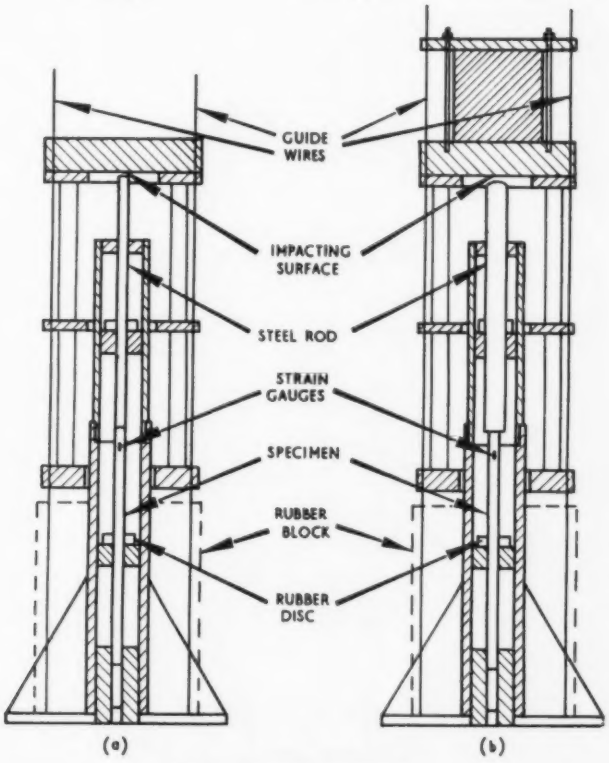

Fig. 1. Impact apparatus.
(a) Arrangement using $\frac{1}{2}$ inch diameter steel rod.
(b) Arrangement using 1 inch diameter steel rod and modified design of hammer.

Three static (tension) specimens and six impact specimens were machined from the same rod. All nine specimens were annealed together for 1 hour at 900°C. in a high vacuum furnace.

Static tension tests gave the following results :

Modulus of elasticity	$30{\cdot}3 \times 10^6$ lb./in.^{2}
Upper yield stress	40,000 lb./in.^{2}
Lower yield stress	30,000 lb./in.^{2}
Ultimate tensile strength	58,000 lb./in.^{2}

Vol. 3 54/55

(ii) *Impact Tests*

The impact apparatus (Fig. 1) was a modified form of that described in the previous paper. The specimens were $\frac{1}{2}$ inch in diameter and $10\frac{1}{2}$ inches in length, and the impact stress was transmitted through a coaxial hardened steel rod, in order to minimize eccentricity of loading. At first, a steel rod of the same diameter as the specimen was used, as shown in Fig. 1(a). The design of the falling weight was modified so as to increase its length ; this reduced tilting oscillations during its descent and also simplified the arrangement of the arresting block.

Assuming that the specimen and steel rod have the same diameter, modulus of elasticity E and density ρ, the stress σ' and strain ϵ' propagated into the specimen under elastic conditions are given by

$$\sigma' = V\sqrt{(E\rho)} \tag{1}$$

and

$$\epsilon' = \frac{V}{\sqrt{(E/\rho)}} \tag{2}$$

where V is the impact velocity.

Impact specimen No. 1 was subjected to a series of impacts at increasing velocities. No measurable permanent strain occurred at the gauge position (1 inch from the impact end) even at the maximum height of drop, which gave an impact velocity of 400 in./sec. The stress due to an impact at this velocity, according

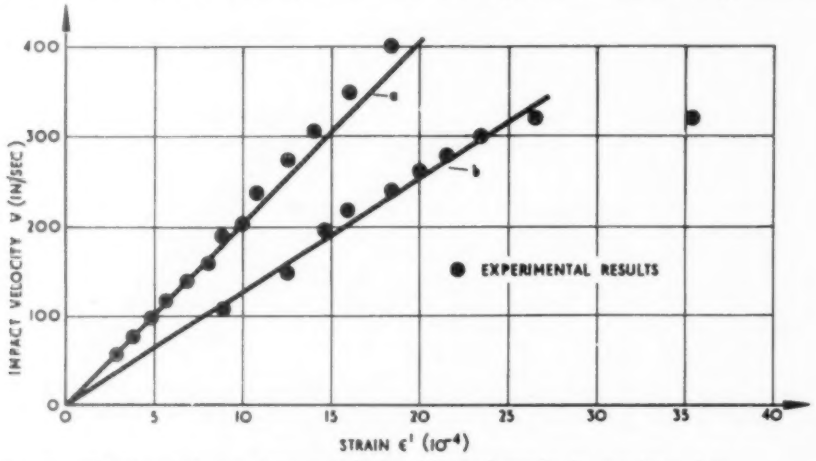

Fig. 2. Relation between impact velocity (V) and strain in specimen (ϵ').
(a) Theoretical relation for impact through $\frac{1}{2}$ inch diameter steel rod (Equation 2).
(b) Theoretical relation for impact through 1 inch diameter steel rod (Equation 4a).

to equation (1), is 60,000 lb./in.^{2}. The peak strains obtained from the gauge records are plotted in Fig. 2 against the impact velocity, together with the line corresponding to equation (2), in which E has been taken as $30{\cdot}3 \times 10^6$ lb./in.^{2}. It is seen that at the higher impact velocities, the measured strains are consistently 6 to 7 per cent lower than those calculated. The discrepancy is too great to be due to the difference between the dynamic and static moduli ; it is thought to be due to deformation of the impacting hammer under the very considerable force at the point of impact, with consequent loss of velocity.

From these results it was evident that considerably greater stresses would be required to cause yield in the specimen. Since the height of fall could not conveniently be increased by more than a few feet, it was decided to transmit the impact through a steel rod of larger diameter. The stress and strain propagated into the specimen, under elastic conditions, are then given by

$$\sigma' = V\sqrt{(E\rho)} \cdot \frac{2}{1 + A_2/A_1} \tag{3}$$

and

$$\epsilon' = \frac{V}{\sqrt{(E/\rho)}} \cdot \frac{2}{1 + A_2/A_1} \tag{4}$$

where V is the impact velocity and A_1, A_2 are the cross-sectional areas of the steel rod and specimen respectively. The diameter of the steel rod used was 0·990 in. and that of the specimen was 0·500 in., so equations (3) and (4) become

$$\sigma' = 1{\cdot}594\, V\sqrt{(E\rho)} \tag{3a}$$

and

$$\epsilon' = \frac{1{\cdot}594\, V}{\sqrt{(E/\rho)}}. \tag{4a}$$

Thus the arrangement gives an increase of nearly 60 per cent in maximum stress, which would require the height of drop to be increased some $2\frac{1}{2}$ times if the $\frac{1}{2}$ inch diameter rod were used.

The force exerted on the falling hammer by the larger rod was of course nearly four times that due to the smaller rod, so it was considered necessary to back the $1\frac{1}{2}$ inch thick impact disc with a solid steel block 4 inches in diameter and 4 inches in length, as shown in Fig. 1(b). This block was lapped on to the disc and bolted down, and it was hoped that with this arrangement the inertia and stiffness would be sufficiently great to ensure that no appreciable loss of velocity would occur during impact.

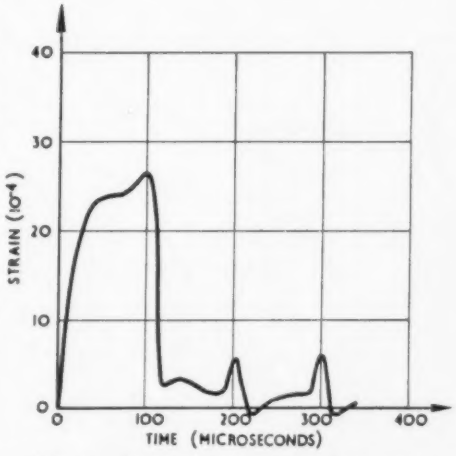

Fig. 3. Strain-time curve showing yield.

Owing to the stress concentration due to using a spherically-ended specimen, there was considerable local plastic deformation at the impact end. Before continuing the tests on specimen No. 1, therefore, it was decided to cut a piece of length $\frac{1}{2}$ inch from this end, and to use a plane end. It was found that by lapping together the contacting surfaces of the steel rod and specimen the stress concentration could be eliminated without any appreciable increase in the eccentricity of loading. The other specimens were also used with plane ends.

Specimen No. 1 was then subjected to a second series of impacts at increasing velocities, and the results of these tests are also plotted in Fig. 2, together with

the line corresponding to equation (4a). No measurable permanent strain occurred at the gauge position until the impact velocity was raised to 320 in./sec. It thus appears that the dynamic yield stress under these conditions lay between the stresses corresponding to velocities of 300 in./sec. and 320 in./sec. Using equation (3a), these are found to be 71,000 and 75,600 lb./in.^{2} respectively. The strain-time curve for the first impact in which permanent strain occurred at the gauge position is shown in Fig. 3. It will be noticed that the strain increases rapidly to about 24×10^{-4}, remains approximately constant at this value for 30 or 40 microseconds, and then increases again before being reduced by the unloading wave from the free end. This form of strain-time curve may be due either to the arrival after about 70 microseconds of a plastic shock front, or to the ' delayed yield ' phenomenon reported by CLARK and WOOD. It is not possible from a single record to determine which of these two mechanisms is responsible for the second increase of strain, though the latter seems the more likely ; but in either case it follows that the strain up to the second increase may be taken as elastic. Thus the dynamic yield stress may be obtained by multiplying the strain just before yield ($24{\cdot}0 \times 10^{-4}$) by the modulus of elasticity. Taking the latter as $30{\cdot}3 \times 10^6$ lb./in.^{2}, this gives the yield stress as 73,000 lb./in.^{2}, which lies between the limits of 71,000 and 75,600 lb./in.^{2} obtained by calculation from the impact velocities.

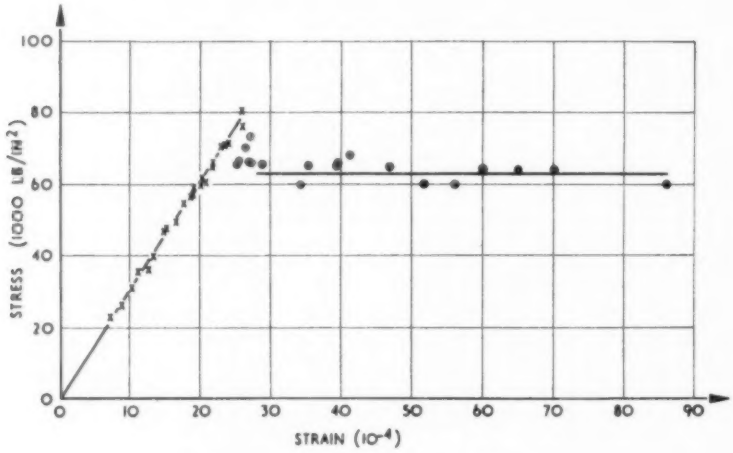

Fig. 4. Dynamic stress-strain curve.

In the earlier work on aluminium alloy specimens, the stress corresponding to maximum strain was derived on the assumption that unloading was elastic. With mild steel, however, it is known that unloading is not entirely elastic owing to the inhomogeneity of yielding. This was shown in a static test, in which a specimen was unloaded after yielding to a strain of about 80×10^{-4} ; the unloading line was appreciably curved, the slope of the straight line connecting its ends being about 27×10^6 lb./in.^{2}. It seems likely, however, that under the conditions of the impact tests, in which the plastic strains are much smaller, the unloading line approximates more closely to a straight line of slope equal to the elastic modulus. As a basis for estimating the post-yield stresses, therefore, the value

28×10^6 lb./in.^{2} was taken for the slope of the unloading line. From the record of Fig. 3, the maximum strain is $26{\cdot}5 \times 10^{-4}$; the permanent strain was $3{\cdot}3 \times 10^{-4}$ and thus the stress corresponding to the maximum strain may be estimated as $28 \times 10^6 \times (26{\cdot}5 - 3{\cdot}3) \times 10^{-4} = 65{,}000$ lb./in.^{2}. A second impact at 320 in./sec. on specimen No. 1 gave peak and permanent strains of $35{\cdot}3 \times 10^{-4}$ and $12{\cdot}4 \times 10^{-4}$, and hence a stress at the peak strain of $28 \times 10^6 \times (35{\cdot}3 - 12{\cdot}4) \times 10^{-4} = 64{,}000$ lb./in.^{2}. As a check on these estimates of the dynamic lower yield stress, the specimen was subjected to impacts at lower velocities. It was found that impacts at velocities up to 240 in./sec. caused negligible permanent strain; an

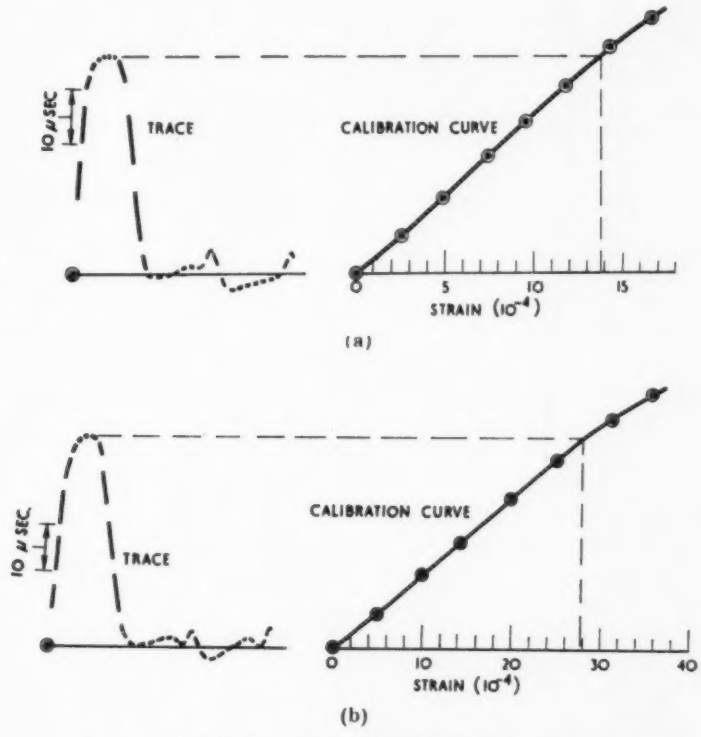

Fig. 5. Strain-time records for impacts on specimen No. 6.
(a) Impact at 172 in./sec.
(b) Impact at 400 in./sec.

impact at 260 in./sec. caused a permanent strain of $1{\cdot}7 \times 10^{-4}$; and impacts at 280 in./sec. caused considerable permanent strain. Thus the dynamic lower yield stress may be estimated as that corresponding to an elastic impact at 260 in./sec., i.e. 62,000 lb./in.^{2}. This is in reasonable agreement with the estimates obtained from the difference between peak and permanent strains.

The results derived by the above methods from tests on specimens 1, 3, 4, and 5 are plotted in Fig. 4. In this figure the results represented by crosses are those of tests in which no measurable permanent strain occurred and the stress was calculated by equation (3a); the results represented by circles are those of tests in which

measurable permanent strain occurred and the stress was calculated from the difference between peak and permanent strains.

No useful results were obtained from specimen No. 2 owing to misalignment of the specimen guides and consequent bending of the specimen.

In order to obtain a value for the dynamic upper yield stress of a specimen which had not previously been stressed appreciably above the static upper yield stress, specimen No. 6 was tested as follows. A preliminary test was made at an impact velocity of 172 in./sec., giving a theoretical maximum stress of 40,600 lb./in.^{2}. The strain-time trace and calibration curve for this test are shown in Fig. 5 (a). The peak strain is $13{\cdot}8 \times 10^{-4}$, using the makers' gauge factor. Assuming a modulus of $30{\cdot}3 \times 10^6$ lb./in.^{2}, this gives a peak stress of 41,800 lb./in.^{2}. The discrepancy (3 per cent) is probably at least partly due to the gauge factor of the gauges being slightly greater than that quoted by the makers for the mean of the batch.

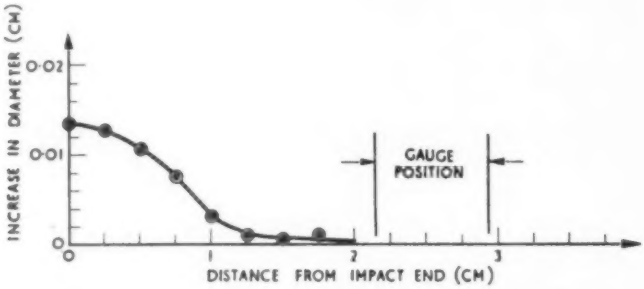

Fig. 6. Distribution of permanent strain in specimen No. 6.

The specimen was then subjected to an impact at the maximum velocity of 400 in./sec., for which the theoretical (elastic) peak stress is 95,000 lb./in.^{2}. The strain-time trace and calibration curve for this test are shown in Fig. 5(b). The measured peak strain at the gauge position is $27{\cdot}9 \times 10^{-4}$, and the permanent strain is very small. Thus assuming elastic conditions at the gauge position the peak stress there is 85,000 lb./in.^{2}. In view of the 3 per cent discrepancy in the earlier test, it is possible that this figure is two or three per cent too large. In order to determine whether yield had occurred at the impact end of the specimen, measurements of two perpendicular diameters of the specimen were made before the second impact, at intervals of 0·25 cm from its end, by means of a travelling microscope reading to 0·001 cm. These measurements were repeated after the impact and the mean increase of diameter is plotted in Fig. 6. From this it may be seen that the specimen yielded at its end (the longitudinal permanent strain there being about 0·02) but that this yielding was confined to within about 1 cm. of the end. This confirms the prediction that with mild steel the plastic deformation would be very localized.

It is evident that the maximum stress transmitted into the specimen under the conditions of this impact is the dynamic upper yield stress; so the peak stress occurring at the gauge position may be taken as this yield stress. The value thus derived, say 83,000 lb./in.^{2}, is somewhat higher than the values obtained in the repeated impact tests on the other four specimens. It appears likely that this is

due to incomplete ageing between the repeated impacts. No attempt was made to control this ageing, since it was not appreciated until later that even when the permanent strain was too small to be measurable with the apparatus used, the effects of the repeated impacts could be to a certain extent cumulative (see VREELAND, WOOD and CLARK 1958).

3. DISCUSSION

The results of the tests described above show that the stress necessary to cause yield of the steel tested is about twice as great under the conditions of the impact tests as that necessary under normal static conditions. The stress required to continue plastic deformation after the initial yield is also about twice that required under static conditions.

These results may be compared with those of HOPKINSON (1905) and MASON (1934), whose tests were of a similar type. In each case a wire was subjected to tensile impact by means of a falling weight, the stress being calculated from the theory of elastic wave propagation. In HOPKINSON's tests the theoretical stress-time curve shows a very sharp peak (see TAYLOR 1946), so that the maximum stress is only attained instantaneously. HOPKINSON found that an iron wire of static yield stress 40,000 lb./in.^{2} did not yield under an impact of peak stress 74,000 lb./in.^{2}.

Vol. 3 54/55

In the work of MASON the calculated stress-time curves show a rounded top, the stress falling gradually after the peak. MASON found that the yield stress of the steel wire tested was greater for small durations of load than for larger durations; he suggested that there existed a maximum yield stress for infinitely small duration of loading. The greatest yield stress obtained by MASON was 67,000 lb./in.^{2} in a test on a steel wire with a static yield stress of 37,000 lb./in.^{2}; in this test loading took place in about 100 microseconds and unloading in about 40 microseconds. This result agrees reasonably with those of the author's tests, in which the duration of the load was rather less than that of MASON.

Other more recent work includes that of DAVIES (1949), in which a steel ball was dropped on to a mild steel plate and the resulting dynamic stress in the plate calculated. The minimum stress required to cause permanent deformation of the plate was found to be 2·04 times that required under static conditions. The times of loading and unloading in these tests were each about 15 microseconds.

W. R. CAMPBELL (1953) has reported the results of longitudinal impact tests on mild steel bars of static yield stress about 50,000 lb./in.^{2}. No yield occurred at an impact velocity of 57 ft./sec., at which the maximum stresses were computed by a special method to be about 80,000 lb./in.^{2} and 90,000 lb./in.^{2} for the two specimens tested. The time to reach maximum strain in these tests was 35 microseconds.

In all these tests, therefore, there is considerable agreement, remarkable in view of the widely differing methods of test and of interpretation of results, that in cases where an impact load of duration of the order of 100 microseconds is applied to mild steel the stress required to initiate yield is about double that required under static conditions.

In addition to the impact tests referred to above, constant strain-rate and constant stress tests have been employed. These have shown that the yield stress

increases as the speed of loading increases or duration of loading decreases.

A method for correlating the results of tests of various types, based on COTTRELL and BILBY's (1949) theory of yield, has been put forward (CAMPBELL 1953b). In order to apply this method, it is necessary that the specimen contain no free dislocations before test, i.e. that it be fully aged ; this condition was not satisfied in the tests described in the present paper, since with one exception each specimen was subjected to a number of impacts before yielding and there may not have been complete ageing between impacts. It is also necessary to obtain an accurate stress-time curve up to the time of yielding, if the proposed method is to be used. The electrical amplifier used in the present tests was not considered to have a good enough high frequency response to ensure sufficiently faithful reproduction of the very rapid initial rise of strain. Further tests are in progress using a wide band amplifier with improved high frequency response and it is hoped to report the results of these tests in a later paper.

ACKNOWLEDGMENT

I am indebted to Professor J. L. M. MORRISON of Bristol University for the use of the high vacuum furnace in which the specimens were annealed.

REFERENCES

CAMPBELL, J. D.	1953a	*J. Mech. Phys. Solids*, **1**, 113.
	1953b	*Acta Metallurgica*, **1**, 706.
CAMPBELL, W. R.	1953	*J. Wash. Acad. Sci.*, **43**, 102.
CLARK, D. S. and WOOD, D. S.	1949	*Proc. Am. Soc. Test. Mat.*, **49**, 717.
COTTRELL, A. H. and BILBY, B. A.	1949	*Proc. Phys. Soc. A*, **62**, 49.
DAVIES, R. M.	1949	*Proc. Roy. Soc. A*, **197**, 416.
HOPKINSON, B.	1905	*Proc. Roy. Soc. A*, **74**, 498.
MASON, W.	1934	*Proc. Inst. Mech. Eng.*, **128**, 409.
TAYLOR, G. I.	1946	*J. Inst. Civ. Eng.*, **26**, 486.
VREELAND, T., WOOD, D. S. and CLARK, D. S.	1953	*Trans. Am. Soc. Met.*, **45**, 620.
WHITE, M. P. and GRIFFIS, L.	1948	*J. Appl. Mech.*, **15**, 256.

Journal of the Mechanics and Physics of Solids, 1954, Vol. 3, pp. 63 to 80. Pergamon Press Ltd., London.

AN EXPERIMENTAL STUDY OF BIAXIAL STRESS-STRAIN RELATIONS IN PLASTICITY*

By P. M. Naghdi and J. C. Rowley
Department of Engineering Mechanics, University of Michigan

(*Received* 20th *May*, 1954)

Summary

Experimental results for ten tubular 24 S-T4 aluminium-alloy specimens which possessed severe initial anisotropy are reported. These variable-loading path tests, where tension alone was followed by torsion, permitted the determination of the initial shear modulus when twist began. The results are discussed with reference to both initial and strain-hardening anisotropy.

Vol. 3 54/55

1. Introduction

Although considerable progress has been made in recent years in the development of isotropic theories of plasticity for strain-hardening materials (Prager 1948, 1949), relatively little is known about theories of plasticity which account for initial anisotropy and for such phenomena as the Bauschinger effect. This is not surprising, as the available experimental results are too few. In this connection, mention should be made of the illuminating discussion of the role of the experiments, as well as their interpretation and correlation with the mathematical theory of plasticity, given by Drucker (1949) and Prager (1948).

The present paper contains experimental results for ten tubular specimens possessing a rather severe initial anisotropy. The specimens, made of 24 S-T4 aluminium alloy, were subjected to combined action of tension and torsion with variable loading paths. The loading was such that tension alone was followed by torsion (accompanied with various amounts of tension) and permitted the determination of the initial shear modulus G_i when twist began. Also included is a discussion of the experimental results in the light of the incremental-strain (flow) theories of plasticity.

2. General Background

For purposes of clarity, we discuss briefly plastic stress-strain relations of incremental-strain theories of plasticity and their consequences relevant to the experimental results given here.

On the assumption that the increment of plastic strains is linear in the increment of stresses, the plastic strain tensor, when expressed in terms of a plastic potential

* The results presented in this paper were obtained in the course of research sponsored by the Office of Ordnance Research under Contract DA-20-018-ORD-12099 with University of Michigan.

f, reads as follows :

$$\left.\begin{aligned} \dot{\epsilon}_{ij}'' &= H \frac{\partial f}{\partial \sigma_{ij}} \frac{\partial f}{\partial \sigma_{kl}} \dot{\sigma}_{kl} && \text{during loading i.e., } \frac{\partial f}{\partial \sigma_{kl}} \dot{\sigma}_{kl} > 0 \\ &= 0 && \text{for unloading or neutral loading, i.e., } \frac{\partial f}{\partial \sigma_{kl}} \dot{\sigma}_{kl} \leqslant 0 \end{aligned}\right\} \quad (1)$$

where repeated indices imply summation over all the values the index may take ; H is a scalar function which may depend on the state of stress (σ_{ij}), strain (ϵ_{ij}), as well as history of loading ; the dot denotes differentiation with respect to time, and prime and double primes refer to the elastic and plastic components of the strain, since it is tacitly assumed that the total strain tensor $\epsilon_{ij} = \epsilon_{ij}' + \epsilon_{ij}''$.

The loading function f in (1) may be such as to account for various degrees of initial and strain-hardening anisotropy. A few loading functions exhibiting this character have been suggested by HILL (1950) and EDLEMAN and DRUCKER (1951). A simple example is

$$f = C_{ijkl}\, \sigma_{ij}\, \sigma_{kl} \quad (2)$$

which is quadratic in σ_{ij} and accounts for small initial anisotropy. In (2), C_{ijkl} is a fourth-order symmetric tensor, i.e., $C_{ijkl} = C_{klij}$, $C_{ijkl} = C_{jikl}$, $C_{ijkl} = C_{ijlk}$. From the assumption of incompressibility of plastic strains, $\dfrac{\partial f}{\partial \sigma_{pp}} = C_{ppkl}\, \sigma_{kl} = 0$ for all σ_{kl} ; hence $C_{ppkl} = 0$ for all k, l.

For isotropic theories of plasticity, f may be a function of both σ_{ij} and ϵ_{ij}. When f is a function of σ_{ij} alone, the stress-strain relations (1) may be referred to as isotropic stress theories. In particular, it is easily seen that the simple incremental-strain theory

$$\dot{\epsilon}_{ij}'' = H(J_2)\, s_{ij}\, \dot{J}_2 \quad (3)$$

is a special case of (1), when H is assumed to depend only on J_2 and $f = J_2$, i.e.,

$$J_2 = \tfrac{1}{2}\, s_{ij}\, s_{ij} \quad (4)$$

where

$$s_{ij} = \sigma_{ij} - s\delta_{ij} ; \qquad s = \tfrac{1}{3}\, \sigma_{ii} \quad (5)$$

and δ_{ij} is the Kronecker delta.

In the experimental results which are to be described, the determination of the initial shear modulus G_i when twist began is included (the loading was such that tension alone was followed by torsion). For this reason, it is desirable to examine the predictions for G_i by various theories of plasticity, appropriate for such loading paths.

All isotropic incremental-strain theories of plasticity imply that (PRAGER 1948 ; PETERS, DOW and BATDORF 1949)

$$G_i = G_0 \text{ for both loading and unloading} \quad (6)$$

for all ratios of the increments of axial stress to shear stress, $d\sigma_{33}/d\sigma_{23}$ or simply $d\sigma/d\tau$. Similarly, all isotropic total strain (deformation) theories predict that (PETERS, DOW and BATDORF 1949)

Vol.
3
54/55

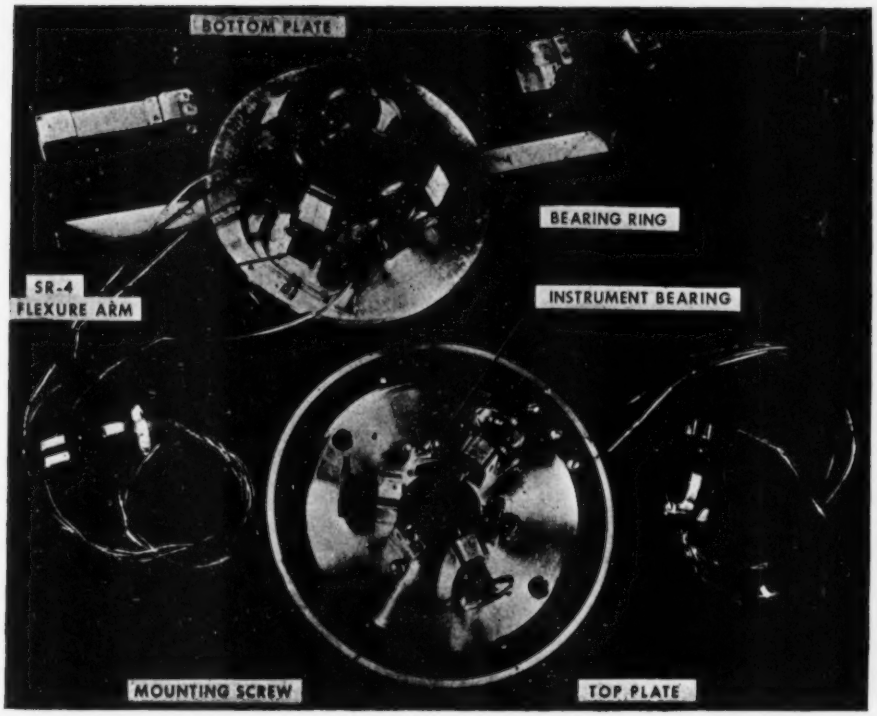

Fig. 1.

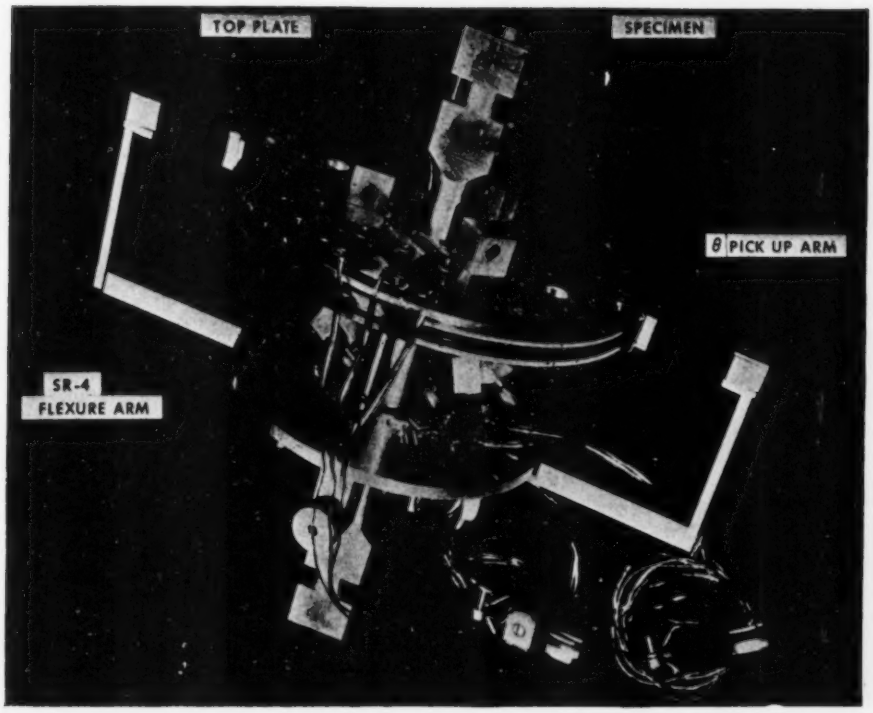

Fig. 2.

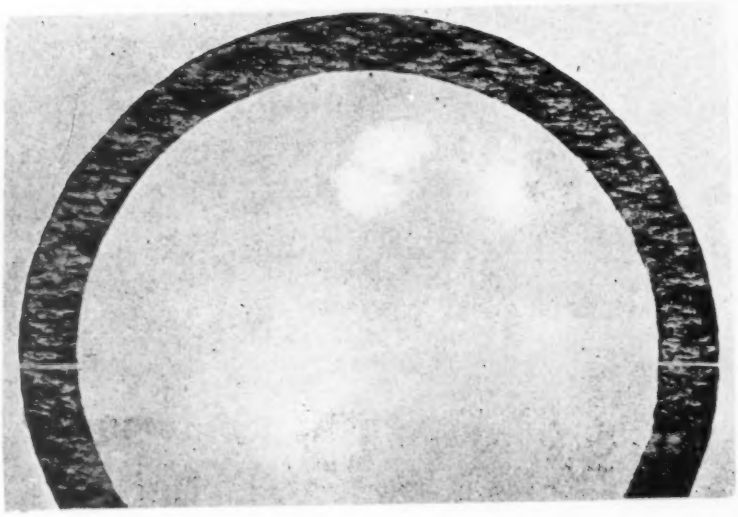

Fig. 4.

Vol
3
1954/

$$G_i = \frac{G_0}{1 + 3\,G_0\,(1/E_s - 1/E_0)} \qquad \text{for loading}$$
$$= G_0 \qquad \text{for unloading} \tag{7}$$

where E_s is the secant modulus with reference to the initiation of twist, and E_0 and G_0 are the elastic moduli in tension and shear.

If, however, in equation (1) f is an anisotropic loading function, then during loading G_i will in general be less than G_0. To demonstrate this point, let f be of the form given by (2); then it follows that

$$G_i = \left[\frac{d\sigma_{23}}{2\,(d\epsilon_{23}' + d\epsilon_{23}'')}\right]_{\sigma_{23}=0} \qquad \text{during loading} \tag{8}$$
$$= \frac{G_0}{1 + 2G_0\,HC_{2333}\,\sigma_{33}^{\,2}\,[2C_{2338} + C_{3333}\,d\sigma_{33}/d\sigma_{23}]}$$

3. Equipment and Specimens

The accuracy requirements and attendant difficulties peculiar to experimental investigations in plasticity, as opposed to the usual testing procedures in materials testing, have been emphasized recently by Drucker and Stockton (1952). In this section, we outline briefly the experimental set-up developed to include features necessary to meet these rather special requirements.

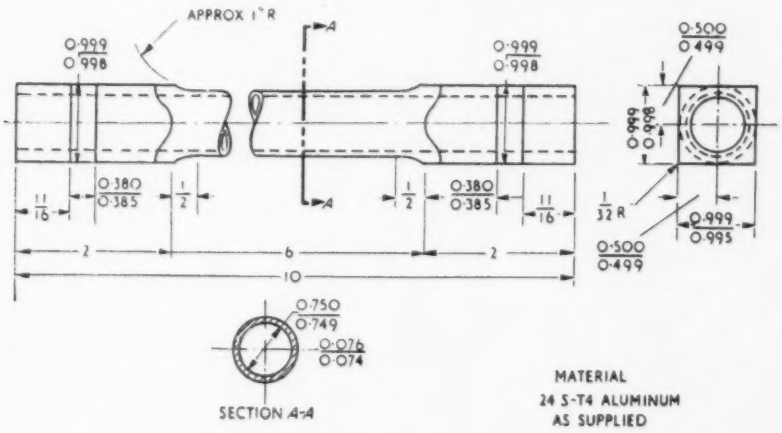

Fig. 3. Drawing of thin-walled specimen.

The testing machine used in this study to apply the combined tension and torsion loads is powered by electric motors which drive the loading bar through variable speed transmissions. The load ranges of 10,000 lbs. in tension and 10,000 inch-lbs. in torsion, together with the wide continuous range of strain rates available, make the machine particularly suited to this type of investigation. The magnitudes of the loads are indicated on dynamometers having both a dial for direct visual readings and a resistance strain gauge bridge for electrical recording.

The extensometer for the indication of the deformations of the tubular specimens was developed under the following considerations: it should preferably have linear characteristics; the deformation measurements should be independent; backlash and lag must be negligible; a wide range of plastic deformations must be covered with a precision comparable to that required for elastic strains; and finally, the output of the extensometer should be such that electrical recording

would be possible. Fig. 1 and 2 show the extensometer as used in these tests. The instrument has a nominal gauge length of 2·84 inches and consists of two aluminium disc fastened to the specimen with spring loaded screws. The screw contact force is roughly 5 lbs. and the weight of the extensometer is approximately $2\frac{1}{2}$ lbs. The relative angle of twist of the two discs is measured by a resistance slide wire wound on the periphery of the upper plate and two contacts fastened to the lower disc but allowed free axial motion through a thin spring brass cantilever system. The axial deformation is indicated by an extension unit made up of a steel ring attached to the bottom disc by four thin bronze flexure strips, each having two SR-4 strain gauges attached at a reduced section. As the extensometer is placed on the specimen, this extension unit is slightly compressed and the top disc rides on the steel ring through three small instrument bearings. Unfortunately, a means for indicating the circumferential deformations was not successfully developed, these attempts being principally thwarted by the difficulty of obtaining a reproducible calibration and the fact that the tubular specimens tended to distort to non-circular cross-sections.

The dimensions of the specimens are indicated in the drawing reproduced in Fig. 3. Tolerances were held to 0·001 inch in both eccentricity of bore and wall-thickness taper. The specimens were taken from the centre of two-inch thick rolled plates of 24 S-T4 aluminium alloy having a grain size of roughly 500 grains per inch, and considerable intial anisotropy was present, as

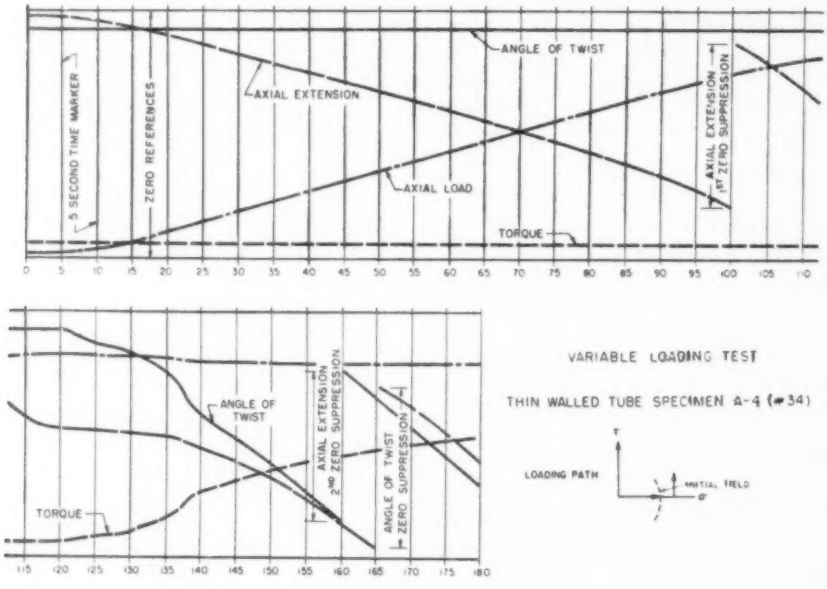
5 SECOND TIME MARKER
ZERO REFERENCES
AXIAL EXTENSION
ANGLE OF TWIST
AXIAL LOAD
TORQUE
AXIAL EXTENSION 1st ZERO SUPPRESSION
0 5 10 15 20 25 30 35 40 45 50 55 60 65 70 75 80 85 90 95 100 105 110
ANGLE OF TWIST
AXIAL EXTENSION 2nd ZERO SUPPRESSION
ANGLE OF TWIST ZERO SUPPRESSION
TORQUE
115 120 125 130 135 140 145 150 155 160 165 170 175 180
VARIABLE LOADING TEST
THIN WALLED TUBE SPECIMEN A-4 (#34)
LOADING PATH
INITIAL YIELD

Fig. 5.

indicated by Fig. 4 which shows one half of a cross-section. The design requirements on wall thickness were dictated by (i) elastic and plastic buckling in torsion (MOORE 1943) ; (ii) dimensions of the extensometer ; and (iii) the available loading range of the tension-torsion machine. The influence of the effects introduced by the fillets at the ends of the specimens was investigated by placing several strain gauges along the length of a tube. The variation of strain reading in tension over the region occupied by the extensometer gauge length was found to be only about $\frac{1}{2}\%$.

The accuracy of the load indications is limited to about $\pm$ 2% since the calibration was made against a laboratory testing machine, although relative values of load are probably better. The slight interaction of the extension and twist measurements reduced the precision at the corresponding strain readings to at most $\pm$ 50 micro-inches, although individually, the calibration and resolution were to about $\pm$ 10 micro-inches or better.

Continuous recording of both deformation and load was performed on photographic film, using mirror galvanometers in an oscillograph (HATHAWAY model S14-A). A facsimile of one such film for a variable loading path test is shown in Fig. 5. All recording circuits were of the Wheatstone bridge type, thus affording inherent temperature stability and ease of calibration by chopping fixed resistors across the fixed bridge arms.

4. EXPERIMENTAL RESULTS

The variable loading path tests, performed on ten thin-walled tubular specimens, consists of tension alone followed by torsion with varying amounts of accompanying tension. The test specimens and their data have been arranged in four groups (designated as *A*, *B*, *C*, *D*) according to the value of the ratio of additional tension to torsion at the initiation of the torque. This grouping is indicated in Fig. 6, where, in conformity with engineering notation, σ_z and $\tau_{\theta z}$ (or simply σ and τ) denote the axial and shearing stresses in the tubular specimen. Also shown in Fig. 6 is the approximate value of the initial slope $d\sigma/d\tau$ for each group.

The test data obtained are presented in the form of curves in Figs. 7-16. For each group of specimens, three sets of curves are plotted : axial stress vs. axial strain, showing where twist began ; elastic and initial shear moduli, including two elastic runs before and after each experiment (the first run was performed on the virgin tube in each case) ; and plastic strains occurring after initiation of twist. In each group, the secant modulus was computed to be approximately 7×10^6 psi.

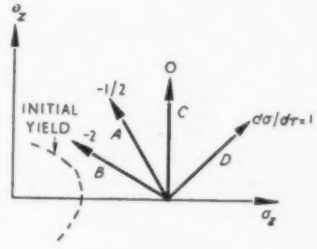

Fig. 6.

The uniformity of the dimensions of the specimens used was very good. As inidicated in Fig. 3, all tubes had an 0·075 inch nominal wall thickness and 0·75 inch inside diameter, with the exception of *D*-1 and *D*-2 tubes which had the same inside diameter but a wall thickness of 0·055 inch.

The curves of Figs. 7-16 also illustrate several limitations of the experimental set-up. First, a glance at the loading paths as plotted indicates the difficulty encountered in maintaining a linear stress path with a machine that is essentially a straining machine. Second, a slight tendency for the shear stress to lag occasionally in the initial portions of both elastic and plastic shear stress – shear strain curves (e.g., Fig. 12b) is a reflection of a small residual stickiness of the loading ram. Finally, the data for tube *B*-1 (Fig. 12) affords an excellent evaluation of the small amount of interaction that remains between the axial-extension and angle-of-twist measurements. The deviations of the plastic strain from the zero axis (Fig. 12c) occurring before the deformation has become plastic are probably due to this interaction.

5. DISCUSSION OF RESULTS

With reference to Figs. 7-16, it is seen that the repeatability of the experimental results is good and that for Group *A* specimens this extends over five tubes. In this connexion it should be mentioned that the agreement in the values of elastic

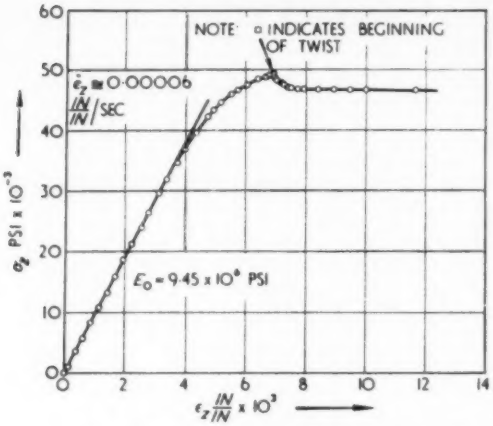
NOTE: ▫ INDICATES BEGINNING OF TWIST
$\dot{\epsilon}_z \cong 0.00006$ $\frac{IN}{IN}$/SEC
$E_0 = 9.45 \times 10^6$ PSI
σ_z PSI x 10^{-3}
$\epsilon_z \frac{IN}{IN} \times 10^3$

Fig 7a. Axial stress vs. axial strain tube A-1 (No. 27).

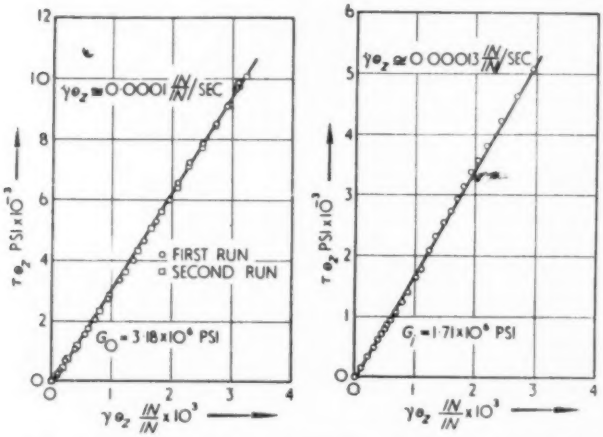
$\dot{\gamma}_{\theta z} \cong 0.0001$ $\frac{IN}{IN}$/SEC
▫ FIRST RUN
▫ SECOND RUN
$G_0 = 3.18 \times 10^6$ PSI
$\tau_{\theta z}$ PSI x 10^{-3}
$\gamma_{\theta z} \frac{IN}{IN} \times 10^3$
$\dot{\gamma}_{\theta z} \cong 0.00013$ $\frac{IN}{IN}$/SEC
$G_i = 1.71 \times 10^6$ PSI

Fig. 7b. Elastic and initial shear moduli tube A-1 (No. 27).

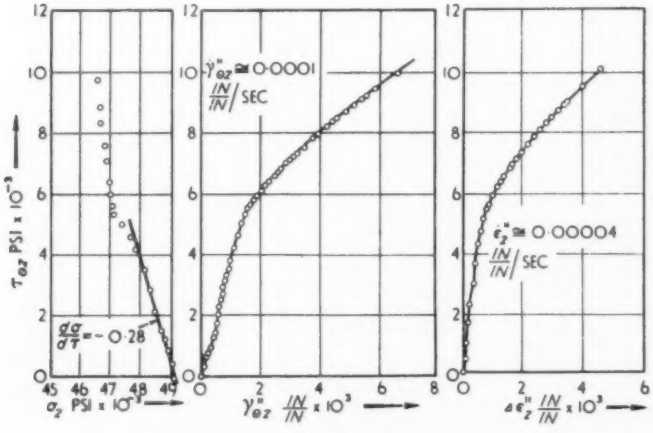
$\frac{dq}{dT} = -0.28$
σ_z PSI x 10^{-3}
$\tau_{\theta z}$ PSI x 10^{-3}
$\dot{\gamma}''_{\theta z} \cong 0.0001$ $\frac{IN}{IN}$/SEC
$\gamma''_{\theta z} \frac{IN}{IN} \times 10^3$
$\dot{\epsilon}''_z \cong 0.00004$ $\frac{IN}{IN}$/SEC
$\Delta\epsilon''_z \frac{IN}{IN} \times 10^3$

Fig 7c. Plastic strains and loading path tube A-1 (No. 27).

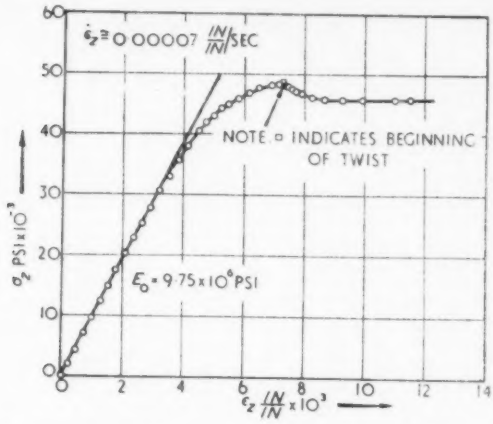
$\dot{\epsilon}_z \cong 0.00007$ IN/IN/SEC
NOTE ▫ INDICATES BEGINNING OF TWIST
$E_0 = 9.75 \times 10^6$ PSI
σ_z PSI x 10^{-3}
ϵ_z IN/IN x 10^3

Fig. 8a. Axial stress vs. axial strain tube A-2 (No. 29).

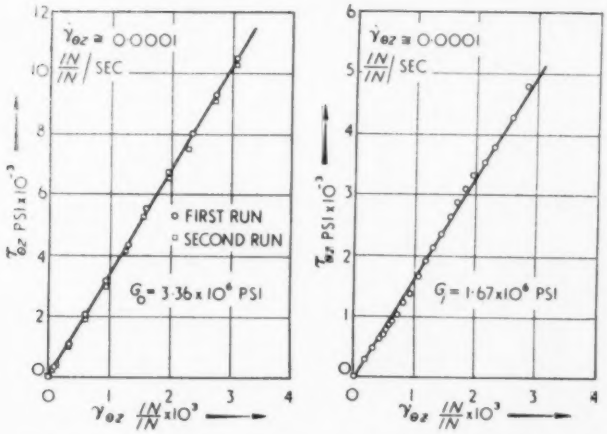
$\dot{\gamma}_{\theta z} \cong 0.0001$ IN/IN/SEC
○ FIRST RUN
▫ SECOND RUN
$G_0 = 3.36 \times 10^6$ PSI
$G_1 = 1.67 \times 10^6$ PSI
$\tau_{\theta z}$ PSI x 10^{-3}
$\gamma_{\theta z}$ IN/IN x 10^3

Fig. 8b. Elastic and initial shear moduli tube A-2 (No 29).

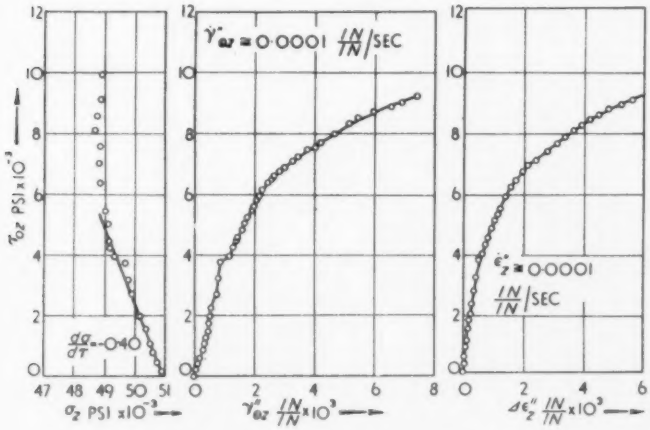
$\dot{\gamma}_{\theta z} \cong 0.0001$ IN/IN/SEC
$\frac{dq}{dT} = -0.40$
$\dot{\epsilon}_z'' \cong 0.0001$ IN/IN/SEC
$\tau_{\theta z}$ PSI x 10^{-3}
σ_z PSI x 10^{-3}
$\gamma''_{\theta z}$ IN/IN x 10^3
$\Delta\epsilon_z''$ IN/IN x 10^3

Fig. 8c. Plastic strains and loading path tube A-2 (No 29).

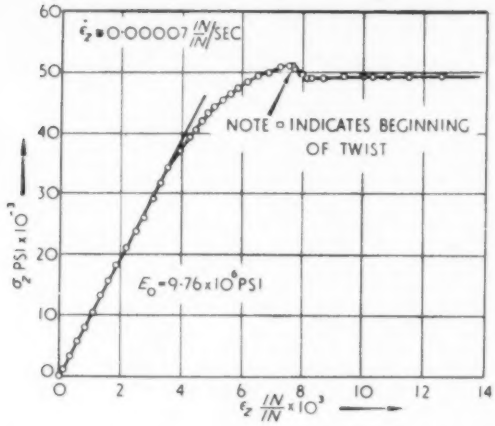

Fig. 9a. Axial stress vs. axial strain tube A-3 (No. 31).

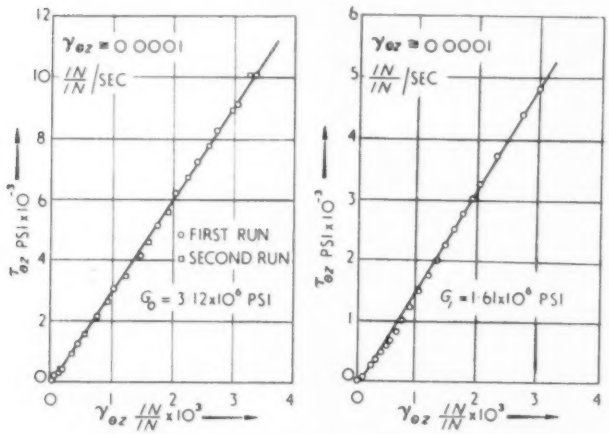

Fig. 9b. Elastic and initial shear moduli tube A-3 (No. 31).

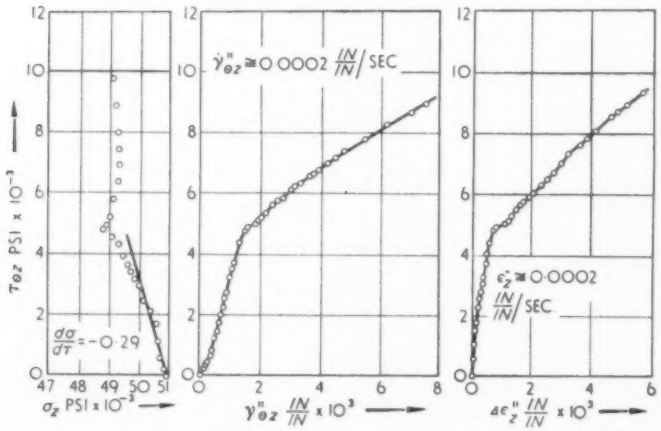
$\dot{\gamma}''_{\theta z}$ = 0·0002 IN/IN/SEC
$\frac{d\sigma}{dT}$ = −0·29
$\dot{\epsilon}''_z$ = 0·0002 IN/IN/SEC
$\tau_{\theta z}$ PSI x 10⁻³
σ_z PSI x 10⁻³
$\gamma''_{\theta z}$ IN/IN x 10³
$\Delta\epsilon''_z$ IN/IN x 10³

Fig. 9c. Plastic strains and loading path tube A-3 (No. 31).

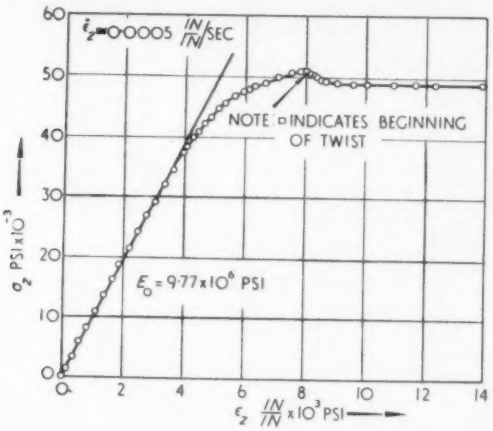

Fig. 10a. Axial stress vs. axial strain tube A-4 (No. 34).

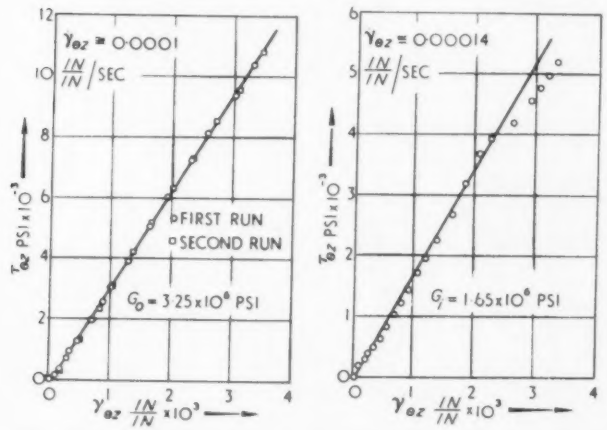
$\gamma_{\theta z}$ = 0·0001 IN/IN/SEC
•FIRST RUN
▫SECOND RUN
G_0 = 3·25 x 10⁶ PSI
$\tau_{\theta z}$ PSI x 10⁻³
$\gamma_{\theta z}$ IN/IN x 10³
$\gamma_{\theta z}$ = 0·00014 IN/IN/SEC
G_i = 1·65 x 10⁶ PSI

Fig. 10b. Elastic and initial shear moduli tube A-4 (No. 34).

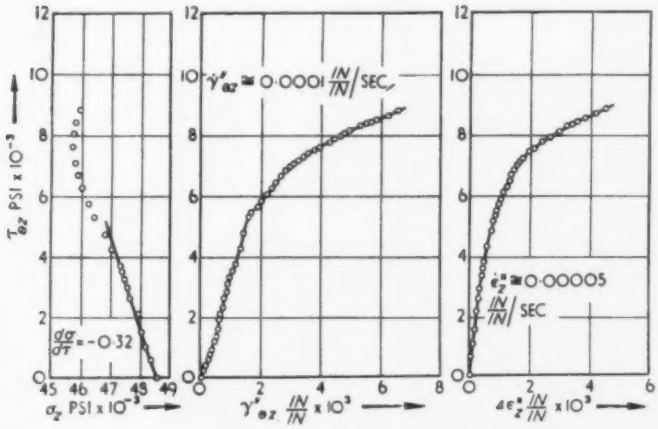
$\frac{d\sigma}{d\tau}$ = -0·32
$\gamma'_{\theta z}$ = 0·0001 IN/IN/SEC
$\dot{\epsilon}''_z$ = 0·00005 IN/IN/SEC
$\tau_{\theta z}$ PSI x 10⁻³
σ_z PSI x 10⁻³
$\gamma'_{\theta z}$ IN/IN x 10³
$\Delta\epsilon''_z$ IN/IN x 10³

Fig. 10c. Plastic strains and loading path tube A-4 (No. 34).

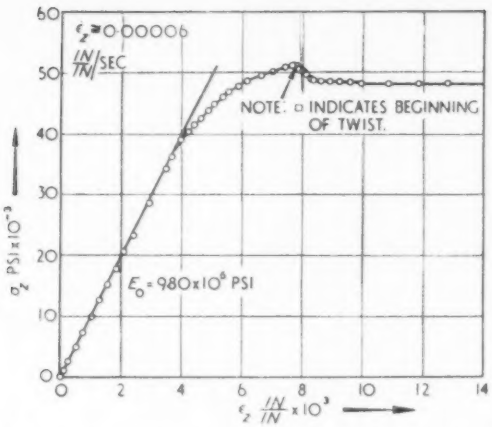
$\dot{\epsilon}_z \cong 0.00006$ IN/IN/SEC
NOTE: □ INDICATES BEGINNING OF TWIST.
$E_0 = 9.80 \times 10^6$ PSI
σ_z PSI x 10^{-3}
ϵ_z IN/IN x 10^3

Fig. 11a. Axial stress vs. axial strain tube A-5 (No. 35).

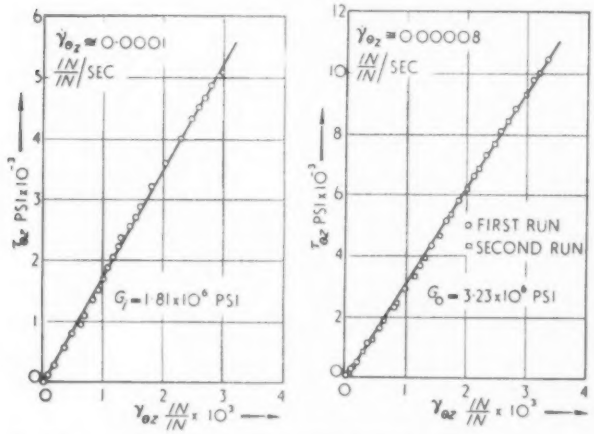
$\dot{\gamma}_{\theta z} \cong 0.0001$ IN/IN/SEC
$G_i = 1.81 \times 10^6$ PSI
$\tau_{\theta z}$ PSI x 10^{-3}
$\gamma_{\theta z}$ IN/IN x 10^3
$\dot{\gamma}_{\theta z} \cong 0.00008$ IN/IN/SEC
○ FIRST RUN
□ SECOND RUN
$G_0 = 3.23 \times 10^6$ PSI

Fig. 11b. Elastic and initial shear moduli tube A-5 (No. 35).

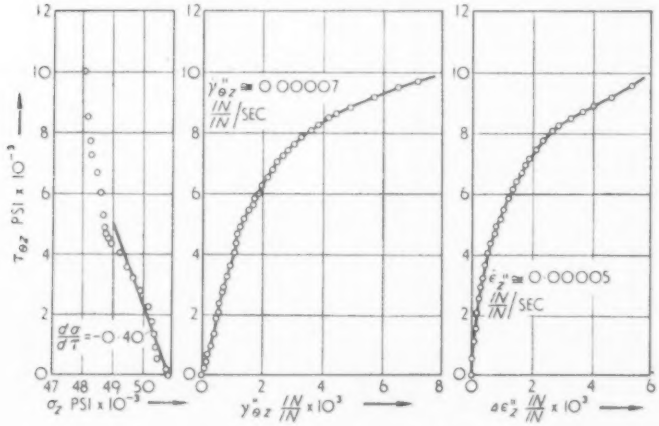
$\tau_{\theta z}$ PSI x 10^{-3}
$\frac{d\sigma}{d\tau} = -0.40$
σ_z PSI x 10^{-3}
$\dot{\gamma}''_{\theta z} \cong 0.00007$ IN/IN/SEC
$\gamma''_{\theta z}$ IN/IN x 10^3
$\dot{\epsilon}''_z \cong 0.00005$ IN/IN/SEC
$\Delta\epsilon''_z$ IN/IN x 10^3

Fig. 11c. Plastic strains and loading path tube A-5 (No. 35).

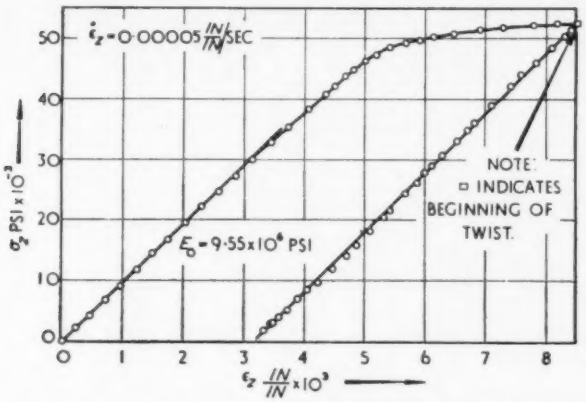

Fig. 12a. Axial stress vs. axial strain tube B-1 (No. 51).

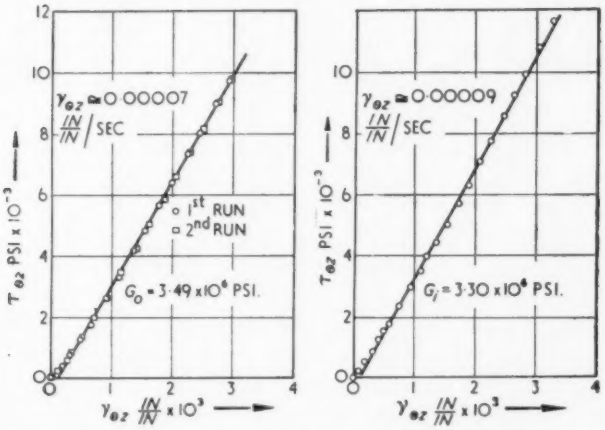
$\gamma_{\theta z}$ ≅ 0·00007 IN/IN/SEC
○ 1st RUN
□ 2nd RUN
G_0 = 3·49 x 10⁶ PSI.
$\gamma_{\theta z}$ ≅ 0·00009 IN/IN/SEC
G_i = 3·30 x 10⁶ PSI.
$\tau_{\theta z}$ PSI x 10⁻³
$\gamma_{\theta z}$ IN/IN x 10³

Fig. 12b. Elastic and initial shear moduli tube B-1 (No. 51).

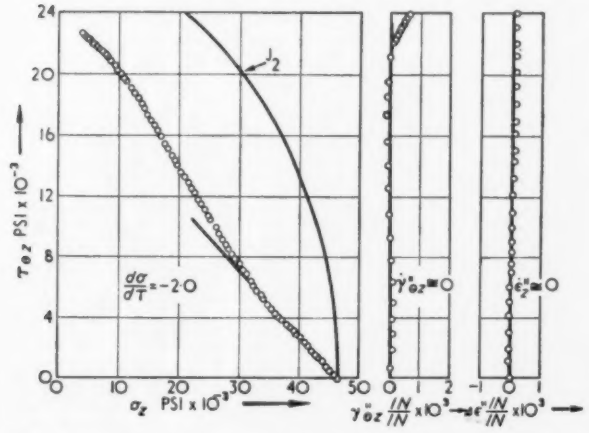

Fig. 12c. Plastic strains and loading path tube B-1 (No. 51).

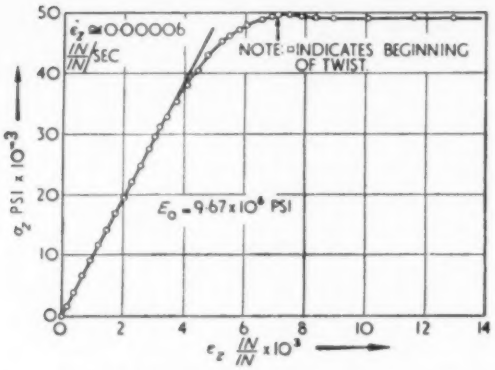
$\dot{\epsilon}_z \cong 0.00006$ IN/IN/SEC
NOTE: □ INDICATES BEGINNING OF TWIST
$E_0 = 9.67 \times 10^6$ PSI
σ_z PSI x 10^{-3}
ϵ_z IN/IN x 10^3

Fig. 13a. Axial stress vs. axial strain tube C-1 (No. 36).

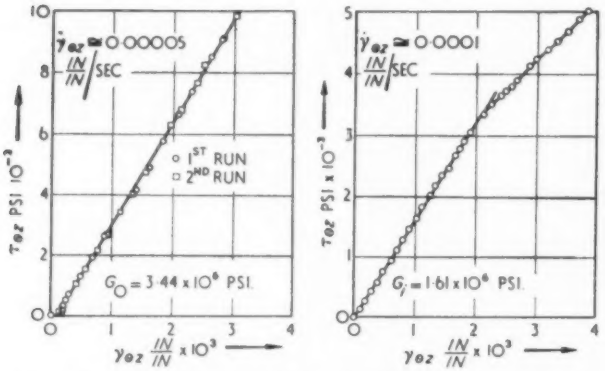
$\dot{\gamma}_{\theta z} \cong 0.00005$ IN/IN/SEC
○ 1ST RUN
□ 2ND RUN
$G_0 = 3.44 \times 10^6$ PSI
$\tau_{\theta z}$ PSI 10^{-3}
$\gamma_{\theta z}$ IN/IN x 10^3
$\dot{\gamma}_{\theta z} \cong 0.0001$ IN/IN/SEC
$G_i = 1.61 \times 10^6$ PSI

Fig. 13b. Elastic and initial shear moduli tube C-1 (No. 36).

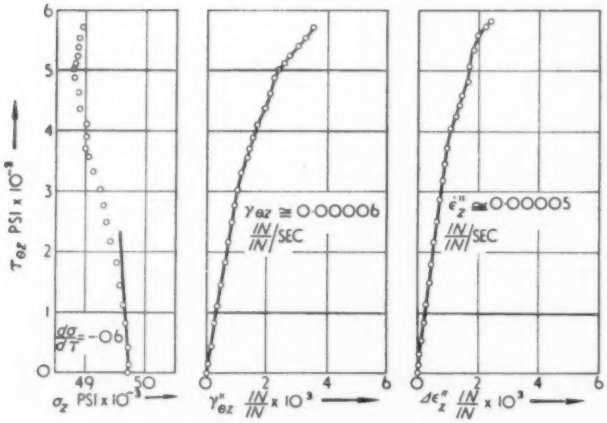
$\tau_{\theta z}$ PSI x 10^{-3}
$\frac{d\sigma_z}{dT} = -06$
σ_z PSI x 10^{-3}
$\gamma_{\theta z} \cong 0.00006$ IN/IN/SEC
$\gamma''_{\theta z}$ IN/IN x 10^3
$\dot{\epsilon}''_z \cong 0.00005$ IN/IN/SEC
$\Delta\epsilon''_z$ IN/IN x 10^3

Fig. 13c. Plastic strains and loading path tube C-1 (No. 36).

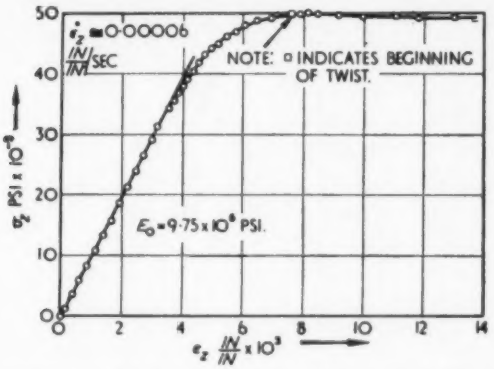
$\dot{\epsilon}_z \cong 0{\cdot}00006$ IN/IN/SEC
NOTE: □ INDICATES BEGINNING OF TWIST.
$E_0 = 9{\cdot}75 \times 10^6$ PSI.
σ_z PSI x 10^{-3}
ϵ_z IN/IN x 10^3

Fig. 14a. Axial stress vs. axial strain tube C-2 (No. 50).

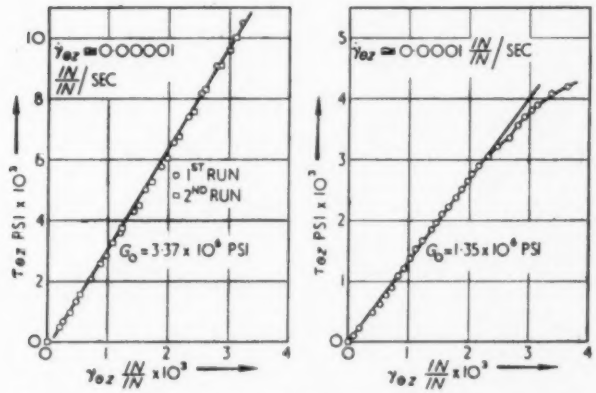
$\dot{\gamma}_{\theta z} \cong 0{\cdot}00001$ IN/IN/SEC
1ST RUN
2ND RUN
$G_0 = 3{\cdot}37 \times 10^6$ PSI
$\tau_{\theta z}$ PSI x 10^3
$\gamma_{\theta z}$ IN/IN x 10^3
$\dot{\gamma}_{\theta z} \cong 0{\cdot}0001$ IN/IN/SEC
$G_0 = 1{\cdot}35 \times 10^6$ PSI

Fig. 14b. Elastic and initial shear moduli tube C-2 (No. 50).

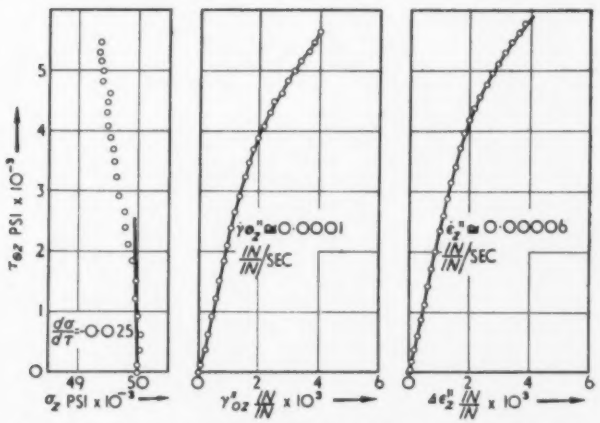
$\tau_{\theta z}$ PSI x 10^{-3}
$\frac{d\sigma}{d\tau} = 0{\cdot}025$
σ_z PSI x 10^{-3}
$\dot{\gamma}^p_{\theta z} \cong 0{\cdot}0001$ IN/IN/SEC
$\gamma^p_{\theta z}$ IN/IN x 10^3
$\dot{\epsilon}^p_z \cong 0{\cdot}00006$ IN/IN/SEC
ϵ^p_z IN/IN x 10^3

Fig. 14c. Plastic strains and loading path tube C-2 (No. 50).

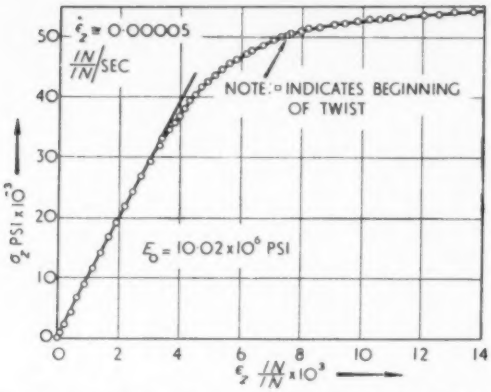

Fig. 15a. Axial stress vs. axial strain tube D-1 (No. 55).

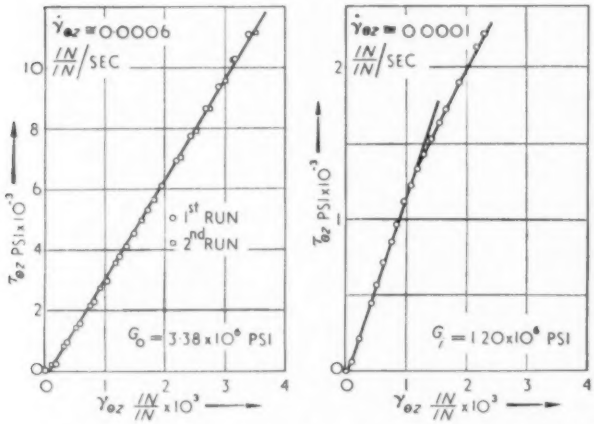
$\dot{\gamma}_{\theta z}$ = 0·0006
IN/IN/SEC
○ 1st RUN
○ 2nd RUN
G_0 = 3·38 x 10⁶ PSI
$\tau_{\theta z}$ PSI x 10⁻³
$\gamma_{\theta z}$ IN/IN x 10³
$\dot{\gamma}_{\theta z}$ = 0·0001
G_i = 1·20 x 10⁶ PSI

Fig. 15b. Elastic and initial shear moduli tube D-1 (No. 55).

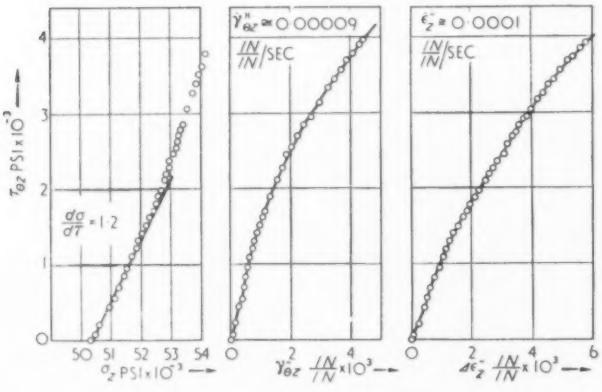

Fig. 15c. Plastic strains and loading path tube D-1 (No. 55).

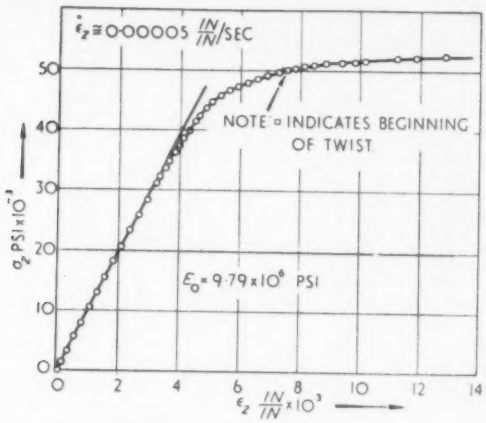
$\dot{\epsilon}_z \cong 0.00005$ IN/IN/SEC
NOTE ▫ INDICATES BEGINNING OF TWIST
$E_0 = 9.79 \times 10^6$ PSI
σ_z PSI $\times 10^{-3}$
ϵ_z IN/IN $\times 10^3$

Fig. 16a. Axial stress vs. axial strain tube D-2 (No. 56).

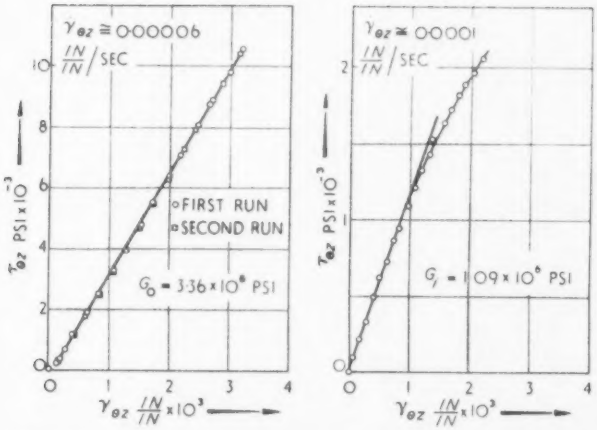
$\gamma_{\theta z} \cong 0.00006$ IN/IN/SEC
◦FIRST RUN
▫SECOND RUN
$G_0 = 3.36 \times 10^6$ PSI
$\gamma_{\theta z} \cong .0001$ IN/IN/SEC
$G_i = 1.09 \times 10^6$ PSI
$\tau_{\theta z}$ PSI $\times 10^{-3}$
$\gamma_{\theta z}$ IN/IN $\times 10^3$

Fig. 16b. Elastic and initial shear moduli tube D-2 (No. 56).

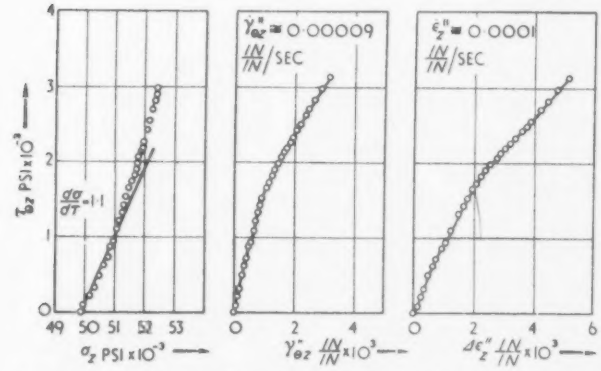
$\frac{d\sigma}{d\tau} = 1.1$
$\gamma''_{\theta z} \cong 0.00009$ IN/IN/SEC
$\epsilon''_z \cong 0.0001$ IN/IN/SEC
$\tau_{\theta z}$ PSI $\times 10^{-3}$
σ_z PSI $\times 10^{-3}$
$\gamma''_{\theta z}$ IN/IN $\times 10^3$
$\Delta\epsilon''_z$ IN/IN $\times 10^3$

Fig. 16c. Plastic strains and loading path tube D-2 (No. 56).

Vol. 3 54/55

constants (Figs. 7-16) is remarkable in view of the presence of rather severe initial anisotropy in the tubular specimens.

For Group A the shear modulus G_i is less than the elastic shear modulus G_0 (Figs. 7-11) by about a factor of 2. Apparently such a phenomenon has not been reported by previous investigators. This effect may be attributed in the main to the prescence of both initial and strain-hardening anisotropy and/or the non-existence of smooth yield loci.

For purposes of discussion, let us assume the existence of smooth yield loci and accept the validity of the linearity of the plastic strains in the increment of stresses (DRUCKER and STOCKTON 1952; STOCKTON 1953). Consider the subsequent yield surface f_2 for an initially anisotropic strain-hardening material, as shown

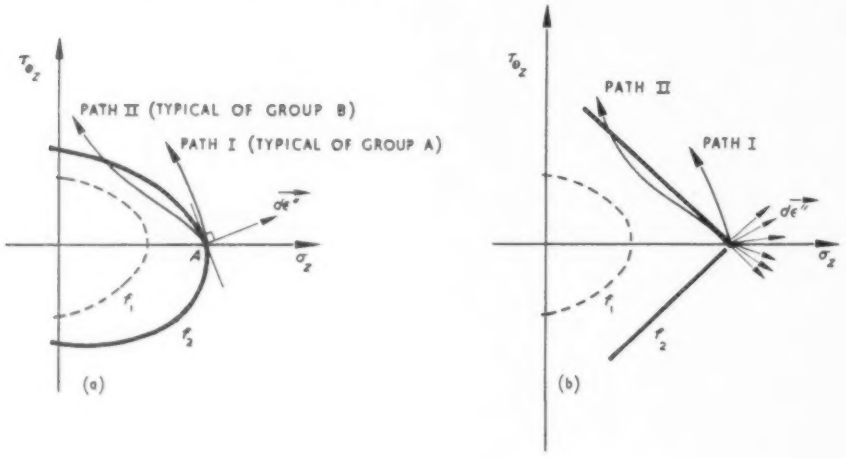

Fig. 17.

in Fig. 17a. This hypothetical loading surface is drawn so that the tangent at A (when travelling in a counterclockwise direction) makes an obtuse angle with the axis σ_z. Also shown in Fig. 17a are typical loading paths for Groups A and B specimens.

As pointed out by BISHOP and HILL (1951) and DRUCKER (1951), when the loading surface has neither corners nor pointed vertices, the increment of the plastic strain vector is normal to the loading surface. Hence, the plastic strain vector $d\epsilon''$ at A in Fig. 17a is along the external normal to f_2 and has both axial and shearing components. Clearly, then, G_i at A (beginning of twist) should not be equal to G_0. Furthermore, along the loading path I, additional plastic deformation should be produced. Thus, if the yield locus f_2 is smooth, then, according to the results for Group A specimens, it must be oblique to the σ_z-axis as shown in Fig. 17a. This, however, implies that (i) experimental results for a loading path, such as I in Fig. 17a, and its image about the σ_z-axis are not the same; and (ii) under a pure tensile load, the tubes would twist as well as extend, which definitely did not occur. In view of these faulty characters of the smooth locus f_2 in Fig. 17a, one may alternatively reach the conclusion that the existence of a corner at A on a yield locus symmetrically situated about the σ_z-axis is plausible (Fig. 17b). In

Fig. 17b, it should be noted that the direction of the plastic strain vector $d\epsilon''$ is not uniquely defined and is restricted only to the directions included between the normals to the adjacent surfaces at A.

With reference to Fig. 17b, if the loading path is as in Group B, then G_i would be expected to have the elastic value G_0, considering that unloading has definitely occurred. That this is indeed the case can be seen from Fig. 12 where $G_i \simeq G_0$. The small amount of deviation in these values is not unreasonable in view of the presence of initial anisotropy.

For Groups C and D, where loading would normally be assumed to occur, the existence of plastic strains after the application of torque is verified. Again the value of G_i for these groups is about $\frac{1}{2}$ of G_0, contrary to the results predicted by isotropic theories of plasticity.

It is the opinion of the present authors that the experimental results given here are explained in the main by the presence of initial and strain-hardening anisotropy and the existence of corners on the yield loci of the material. It may, of course, be possible that other factors, such as strain rate and time effects, grain size, homogeneity of stress state, and machining of specimens may have influenced the results. However, these effects are felt to be small.

Aside from the initial value of the shear modulus G_i and its consequences discussed above, the general trend of the results agrees favourably with those of other investigators (Budiansky, Dow, Peters and Shepherd 1951; Morrison and Shepherd 1950). Comparisons between experimentally determined plastic strains with those predicted by simple incremental and total strain theories are not plotted in Fig. 7-16 since, in view of the discussion concerning the effects of anisotropy and the yield surface, such comparisons appear to be useless.

Vol. 3 54/55

Acknowledgment

The authors wish to express their appreciation to Messrs C. W. Beadle and G. A. Shifrin, Research Assistants in Engineering Mechanics, for thier valuable assistance, both in the improvement of the extensometer and other equipment and in the running of tests.

References

Bishop, J. F. W. and Hill, R.	1951	*Phil. Mag.*, **42**, 414 and 1298.
Budiansky, B. Dow, N. F., Peters, R. W. and Shepherd, R. P.	1951	*Proc. First U.S. Nat. Cong. Appl. Mech.*, 503.
Drucker, D. C.	1949	*J. Appl. Mech.*, **16**, 349.
	1949	*Proc. First Symp. Appl. Math.*, **1**, 181.
	1949	*J. Colloid Science*, **4**, 229.
	1951	*Proc. First U.S. Nat. Cong. Appl. Mech.*, 487.
Drucker, D. C. and Stockton, F. D.	1952	To appear in *Proc. Soc. Exp. Stress Anal.*; also *ONR Tech. Rept.* 68, Brown University.
Edelman, F. and Drucker, D. C.	1951	*J. Franklin Inst.*, **251**, 581.

HILL, R.	1950	*Mathematical Theory of Plasticity* (Clarendon Press)
MOORE, R. L.	1943	*NACA TN*, 879.
MORRISON, J. L. M. and SHEPHERD, W. M.	1950	*Proc. Inst. Mech. Eng.*, **163**, 1.
PRAGER, W.	1948	*J. Appl. Mech.*, **15**, 226.
	1948	*NACA TN*, 1501.
	1949	*J. Appl. Phys.*, **20**, 235.
PETERS, R. W., DOW, N. F. and BATDORF, S. B.	1949	*Proc. Soc. Exp. Stress Anal.*, **7**, 127.
STOCKTON, F. D.	1953	*ONR Tech. Rept.*, 88, Brown University.

Vol
3
1954/

BOOK REVIEWS

T. Vogel : Les fonctions orthogonales dans les problèmes aux limites de la physique mathématique. Centre National de la Recherche Scientifique, Paris. 1953. 191 pp.

This book is the second of a series on mathematical physics from the " Centre d'études mathématique en vue des applications," apparently published with the purpose of enabling physicists and engineers to solve mathematical problems with the aid of the most modern theoretical concepts and techniques. As the title suggests, the author has considered the theory of orthogonal functions with particular emphasis on their application in solving boundary-value problems, and has produced what is called in the preface, written by Prof. A. Lichnerowicz of the Collège de France, the most up-to-date monograph on this subject.

The work begins with an account of the mathematical analysis which is an essential prelude to the general study of orthogonal functions and the algebraic theory of differential systems, continues with a detailed discussion of particular types of these functions, and ends with examples chosen to illustrate their use. The theoretical structure is given logically and carefully in the first chapter. The second chapter is devoted to the treatment of some of the well-known functions usually associated with boundary-value problems, including Fourier series, the functions of Bessel, Legendre, Mathieu, and the polynomials of Jacobi, Tchebycheff, Laguerre, Hermite and Charlier. The author intentionally omits much of the detail in the proofs of certain theorems, and occasionally simply states his results. However, this is no great disadvantage, since there is a comprehensive list of references at the end of each chapter. Much thought has evidently been given to the choice of the illustrative examples. They have been picked from various fields of modern research, with the intention of interesting and instructing the reader in the use of these special functions to help solve typical problems. The reviewer would like to have seen a little more space devoted to the method of conformal representation, and in this connexion would like to point out that the solution of a three-dimensional problem involving axial symmetry on pp. 163-4 is not the same as that of the corresponding two-dimensional problem.

Monsieur Vogel has produced a little book that should be of interest to applied mathematicians. The reader, however, must be fairly advanced in the art of mathematical analysis in order to digest the theoretical parts of this monograph ; which leads the reviewer to wonder how many engineers and physicists in this country will really appreciate the author's efforts.

There are a number of obvious typographical errors and omissions of a minor nature which could have been eliminated by more careful proof-reading. Finally, the paper covers may prove to be a serious disadvantage if the book is used frequently.

G. Power

R. J. Roark : Formulas for Stress and Strain. (Third Edition). McGraw-Hill Publishing Co. Ltd. 1954. xiii + 381 pp. Tables XIX. 53s. 6d.

This valuable book of reference had its first edition in 1938 and its second in 1943. This third edition differs from the second in minor detail only, except for the inclusion of more material on pressure vessels and shells, and a short treatment of circular arches, which are dealt with for the first time. References dated since the second edition are also given.

Individual sections of the book will doubtless be considered inadequate by specialists in the appropriate subjects, but such a result is inevitable when a single author attempts to cover in a small compass such an extraordinarily wide field, including as it does the flexure, torsion and instability of beams, columns, plates and shells, the bending of curved beams, rings and arches, bearing pressure, factors of stress concentration for elastic stress, fatigue and rupture, and dynamic and temperature stresses. Information has been carefully selected, and the manner of tabulating the results makes for easy reference. The book is on the whole well balanced, but certain omissions are difficult to understand. Despite the title, there is no analysis of strain

as such. The complete omission of this subject is strange in view of its great importance in experimental stress analysis. It also appears odd that no mention is made of MOHR's circle as an aid to calculations for two-dimensional stresses.

The book is avowedly a hand-book of formulae, and does not pretend to be a substitute for a text-book. There may however be a tendency to use the information given in Part II (" Facts ; Principles ; Methods ") to serve as a reminder of fundamental methods. It is therefore a pity that the error of justifying strain energy methods for calculating deflections and redundant forces by reference to a " Theorem of Least Work " is here perpetuated. Such methods can only be justified by reference to " complementary energy," and the subsequent observation that, in elastic structures, complementary energy and strain energy are identical. In this section the author also fails to make it clear that all problems involving redundant forces and stresses are ultimately solved by satisfying the two conditions of equilibrium and strain compatibility. The various methods of analysis are essentially different means of achieving strain compatibility. These criticisms are not however major ones, and do not detract from the high standard and utility of the book as a whole.

M. R. HORNE

W. T. READ : **Dislocations in Crystals.** McGraw Hill Publishing Co. Ltd., London, 1953. 228pp. Price 36s.

ALL who are concerned with the mechanisms of plastic flow in crystals will be aware of the dominant position that dislocation theory has come to assume in recent years. For the sake of those who may wish to approach the subject from first principles, Dr. READ has provided a book in which there is a rigorous progression from fundamentals to applications. The first part is concerned with a discussion of the geometry and crystallography of dislocations, with their modes of movement, multiplication and interaction, with the forces acting on them and with their associated stress fields.

The successful use of dislocation theory is illustrated in the second part by reference to crystal growth and, in greater detail, to the structure of grain-boundaries. Emphasis is laid throughout upon the presentation of clear physical pictures, upon the derivation of quantitative results (using " no mathematics beyond the calculus "), and upon unambiguous comparison of theory with experiment. Much of recent work on the rôle of dislocations in determining mechanical properties is regarded by Dr. READ as somewhat speculative and is not discussed.

The book may be unhesitatingly recommended as an imaginatively written text book on dislocation theory suitable for post-graduate study. Textual comments continually challenge the reader to test his comprehension of the subject matter ; numerous problems are set.

T. BROOM

AJIT RAM VERMA : **Crystal Growth and Dislocations.** Butterworths Scientific Publication 1953. 182 pp. 76 figures. 30s.

THIS book is about the role of screw dislocations in crystal growth – a limited field for a book, but one of great topical interest. In 1949, F. C. FRANK pointed out that on a perfect close-packed crystal face in contact with supersaturated vapour, the probability of formation of a surface nucleus to start off a new layer (calculated from considerations of thermodynamic fluctuations at the surface) is extremely small unless the supersaturation is very great – 25 to 50 per cent. (Similar considerations presumably apply to solutions.) But crystals do grow even in very slightly supersaturated vapours and solutions ; and according to this theory their ability to grow must be due to their imperfections – the dislocations which now play an important part in theories of the properties of metal crystals. In particular, there is one type of dislocation – the screw dislocation – which is self-perpetuating : the crystal grows, so to speak, up a spiral staircase, and does not have to wait for new surface nuclei to be formed. Accordingly, FRANK suggested that the screw dislocation plays an important part in keeping crystal growth going.

This suggestion inspired a number of people including Dr. VERMA to look closely at crystal surfaces by all the most powerful methods – interference methods of optical microscopy, and of course, electron microscopy – and their observations have revealed, on crystals of several different substances, spiral layers which indicate that growth did indeed occur by the screw dislocation mechanism.

The book begins with a condensed account of the theory of surface nucleation, and then, after describing the new methods of optical microscopy, it passes in review all the evidence on screw dislocation features which has accumulated in the last few years. The writing is on the whole fairly clear, though not distinguished. My first thought about the book is that Dr. VERMA has performed a very useful service in collecting and discussing all this evidence. It is fascinating to see all the beautiful photographs and to realise how much valuable information about growth has been gained by studying them and thinking about their implications. To take only two examples (apart from the general conclusion that some crystals do undoubtedly make use of screw dislocations in their growth) : the interlaced systems of spirals seen on silicon carbide crystals have been beautifully correlated with the very complex polymorphic crystallography of this substance (this is one of VERMA's own contributions to the subject) ; and the curvature of the layers on natural emeralds has been used by GRIFFIN to calculate the temperature at which these crystals grew.

The chief value of the book is the opportunity it affords for stocktaking in this subject : where do we now stand in the theory of crystal growth ? The spectacular photographs of spiral layers and the enthusiasm of the protagonists of the dislocation theory have led to a general impression that all crystals grow in this way and that if it were not for screw dislocations no crystal would be able to grow. But this would be going much too far ; to entertain such an idea is to ignore some of the facts of crystal surface structure and to forget the limitations of the surface nucleation theory. I am sorry to see that VERMA says nothing to dispel this impression. He does not even mention the even more spectacular photographs of protein crystals showing clearly the individual molecules but no signs of screw dislocations ; and he makes no attempt to emphasize (as anyone concerned with the general problem of crystal growth would be expected to do) that the theory of surface nucleation in its present form applies only to simple close-packed surfaces and therefore only to a small minority of crystals. For most of the more complex crystals, no surface could be described as close-packed ; surface nucleation would be expected to be much easier and take place at a much lower supersaturation on an uneven surface than on a relatively smooth one. (And what about ionic crystals ? Does the surface nucleation theory apply to any ionic crystal other than a " layer " crystal like CdI_2 in which the forces between layers are molecular in character ?) Of course, these considerations do not mean that growth of such crystals will take place entirely by surface nucleation : if dislocations occur, they will undoubtedly be utilised, and both mechanisms will operate. These are the questions which demand discussion in any serious consideration of the mechanism of crystal growth.

In short, VERMA's book is not an impartial discussion of fundamental crystal growth problems ; it is a piece of special pleading in favour of one particular theory. Those interested in the subject will find it a useful summary of the evidence of spiral surface layers, but they should not accept without question the implication that growth at screw dislocations is " the " mechanism of crystal growth.

C. W. BUNN

H. KOLSKY : **Stress Waves in Solids.** Clarendon Press, Oxford. 1953. 211 pp. 25s.

THIS book contains an excellent survey of theoretical and experimental investigations of the propagation of stress waves in solids. Much of it is concerned with work that otherwise appears only in research publications, and so the author has fulfilled a valuable service in collecting this work in book form.

A concise survey of the classical theory of wave propagation in linear elastic media is given, followed by the theoretical analysis of the propagation of longitudinal, lateral and torsional waves in rods, and other similar problems. This discussion includes the simplest one-dimensional theories and the more complicated theories, including their link with three-dimensional elasticity. There follows a discussion of experimental work which has been made possible by the development

of electronic methods of producing and recording strain variations. Such work has also made possible quantitative evaluation of non-elastic properties of materials, and a discussion of stress waves in such materials forms the second part of the book. The theory of the relation between stress and strain in imperfectly elastic materials is first given, including the spring and dash-pot models which lead to differential relations, and the more general heredity theory which is expressed by integral relations corresponding to a spectrum of relaxation times. The propagation of sinusoidal waves through such materials is considered. There follows a particularly extensive chapter on experimental methods of determining such relations based on both wave propagation and oscillatory tests. In contrast to these rate-dependent materials, there follows a discussion of non-linear plastic waves and shock waves, and finally a chapter on experimental investigations of fracture caused by stress wave reflections. A bibliography of 165 references to books and papers is given, more than half having been published after 1939 .

The only chapter of the book that the reviewer would like to have seen treated differently is that on plastic waves, where the emphasis is on the wave system produced by constant-velocity impact on the end of a semi-infinite rod. This is treated by both Lagrange and Euler coordinates, and the reader might get the impression that this represents the main achievement of this theory. Restriction to Lagrangian coordinates, and the presentation of a discussion of the method of characteristics first applied to this problem by KARMAN, BOHNENBLUST and HYERS, would seem to me to have been preferable.

In a pioneering book such as this, one expects to meet points that leave one unsatisfied ; for example, in the case of the propagation of an exponential pressure pulse in a conical bar (p. 78) the restriction to characteristic lengths long compared with the diameter when the front of the pulse involves a stress discontinuity ; and the implied limitation on p. 165 to two solutions in the analysis of the plastic-wave impact problem. I think that such points should be considered as emphasizing the development to be expected in this field, and should not be considered as a criticism of this valuable contribution to the literature.

E. H. LEE

Vol
3
1954

Journal of the Mechanics and Physics of Solids, 1954, Vol. 3, pp. 85 to 116. Pergamon Press Ltd., London.

SOME FUNDAMENTAL EXPERIMENTS ON HIGH TEMPERATURE CREEP

By J. E. Dorn
University of California, Berkeley

(*Received 14th May*, 1954)

Summary

At high temperatures, the creep strain, ϵ, appears to be a function of a temperature (T), compensated time (t), namely $te^{-\Delta H/RT}$, and the stress. X-ray analyses and plastic properties reveal that the same structures are developed at the same values of $te^{-\Delta H/RT}$ following creep at the same stress. Thus $\epsilon = f(te^{-\Delta H/RT})$, for the same stress. When the creep rate, ϵ, is evaluated as a function of stress, σ, for the same structure

$$\dot{\epsilon} = Se^{-\Delta H/RT}\phi(\sigma)$$

where S depends on the structure and

$$S\phi(\sigma) = \begin{cases} S' e^{B\sigma} & B\sigma \geqslant \sim 1{\cdot}4 \\ S'' \sigma^n & B\sigma \leqslant \sim 1{\cdot}4 \end{cases}$$

Although B and n appear to be insensitive to structural changes attending creep of annealed alloys, they decrease with increasing solute additions and cold working. Transients attending loading and unloading and the coincidence of the activation energy for creep, ΔH, with that for self-diffusion suggest that high temperature creep might be ascribed to a dislocation climb process.

Vol. 3 54/55

1. Introduction

The principal thesis of this paper is contained in a quotation from Voltaire : " We must not say, let us begin by inventing principles whereby we may be able to explain everything ; rather we must say, let us make an exact analysis of the matter and then we shall try to see, with much diffidence, if it fits in with any principle." Many theories of creep have been formulated ; but the deductions based on these theories are not always in complete harmony with the experimental facts. Undoubtedly some of the assumptions on which such theories are based must be unrealistic and perhaps even fictional.

In this paper a critical analysis will be attempted on some previously published and some, as yet, unpublished experimental observations on high temperature creep. It is the author's hope that these reflections might serve to stimulate additional research which will eventually culminate in a realistic theory for high temperature creep.

2. Creep Curves

Three significant characteristics of the phenomenon of high temperature creep are illustrated in the typical constant true stress creep curves of Figs. 1 and 2.

(1) During loading, an initial creep strain is imposed on the specimen, the magnitude of which is determined by the stress and temperature, The subsequent portions of each creep curve exhibit three ranges; a primary stage over which the creep rate diminishes, a secondary stage yielding a minimum creep rate, and a tertiary stage, over which the creep rate increases until creep is terminated by rupture. Since, in general, the specimen does not exhibit local plastic deformation

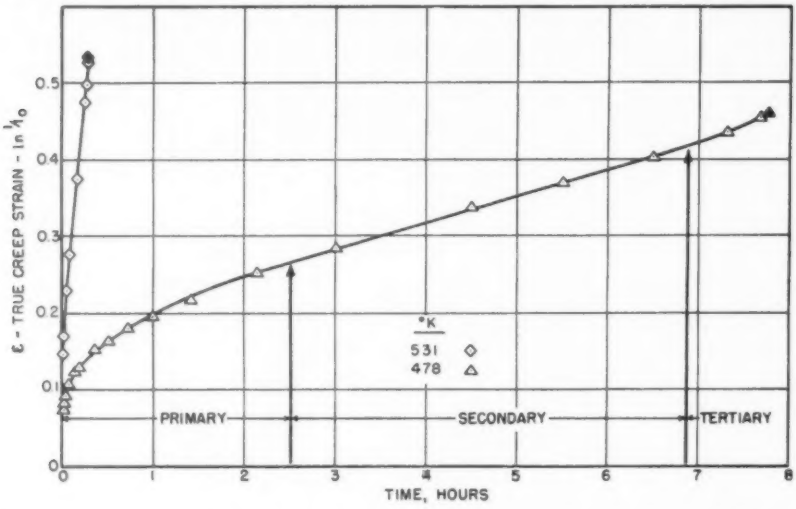

Fig. 1. Creep curves of high purity aluminium under a constant true stress of 3,000 psi.

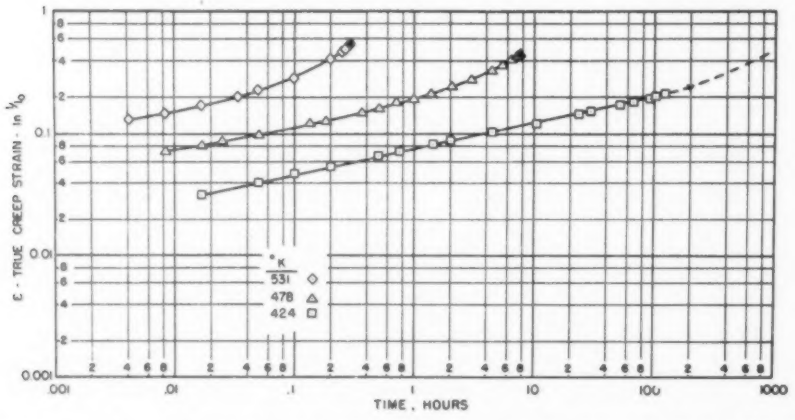

Fig. 2. Creep curves of high purity aluminium under a constant true stress of 3,000 psi.

until creep is well within the tertiary stage, the observed changes in the creep rate cannot be ascribed to changes in any of the externally controlled variables of the test. Assuming that the structure of the specimen had remained constant throughout the creep process, as it does during viscous flow of a Newtonian liquid, the creep rate should also have remained constant in a constant true stress constant

temperature test. Consequently the observed changes in the creep rate must arise from the structural changes that occur during creep. (The original investigations of Wood and Wilms 1949; Wood, Wilms and Rachinger 1951 as well as those of Servi and Grant (1951), Wyon and Crussard (1951), Greenough

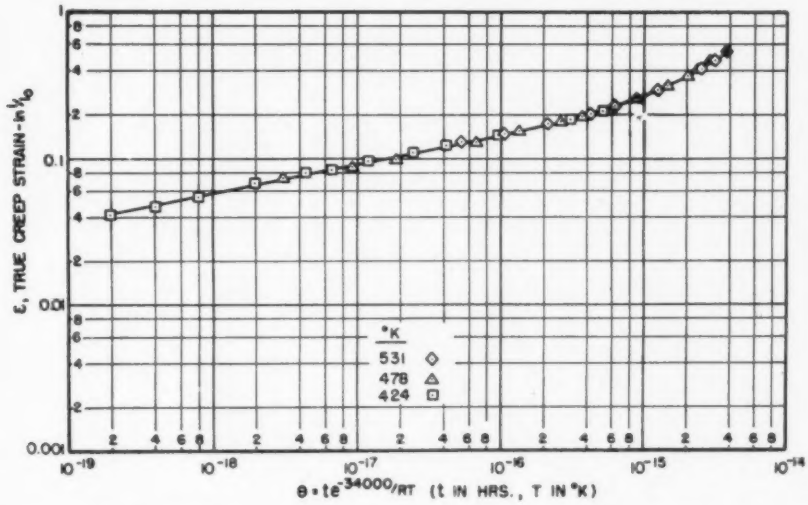

Fig. 3. Creep strain as a function of the temperature compensated time for a constant true stress of 3,000 psi.

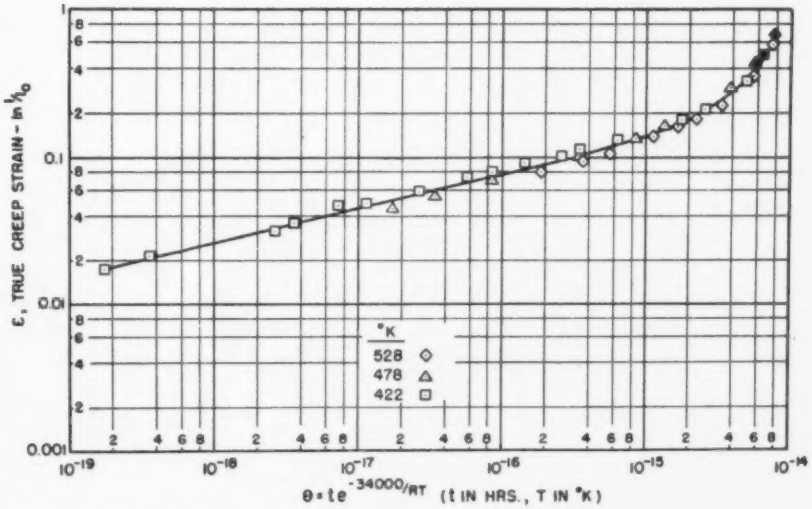

Fig. 4. Creep strain as a function of the temperature-compensated time for a constant load of 2,000 psi. (Data of Sherby and Dorn 1953).

and Smith (1950), and Sherby and Dorn (1953) have served to identify those structural changes which are directly detectable by metallographic and X-ray diffraction techniques.)

(2) The creep rate increases rapidly with an increase in test temperature, suggesting that the creep rate is controlled by some process involving thermal activation.

(3) When the total creep strains are plotted as a function of the logarithm of the time under test (vide Fig. 2), the creep curves for the same stress and different temperatures are identical excepting for parallel displacements along the time axis. Consequently the same total creep strains are obtained for identical values of

$$\ln t + \psi(T)$$

where t is the duration of the test and ψ is some function of the temperature T. But if the rate-controlling process be one of thermal activation, the function $\psi(T)$ might be replaced by $-\Delta H/RT$, where ΔH is the activation energy and R is the gas constant. Under such assumptions the total creep strain, ϵ, would be given by the functional relationship

$$\epsilon = f(te^{-\Delta H/RT}) = f(\theta), \qquad \sigma = \text{constant} \tag{1}$$

In this event the activation energy for creep could be determined from two creep tests conducted under the same stress at two different temperatures. If the times to reach the same strains at temperatures T_1 and T_2 are t_1 and t_2 respectively,

$$t_1 e^{-\Delta H/RT_1} = t_2 e^{-\Delta H/RT_2} \tag{2}$$

and ΔH can be evaluated. Knowing ΔH, the creep strains can now be plotted as a function of θ. The data recorded in Fig. 3 confirm the validity of equation 1. As revealed by the data recorded in Fig. 4, (1) is also applicable to constant load creep data. The only difference between constant load and constant true stress data arises from appropriate differences in the form of the function f.

It was considered possible that the coincidence of the $\epsilon - \theta$ curves for creep over a range of temperatures at constant stress (or load) might have been accidental and therefore of limited significance and import. But the excellence of the agreement between the $\epsilon - \theta$ curves over a series of temperatures and various stresses suggested that these correlations might have some fundamental origin. In view of the dependence of the creep rate on the structure, the basic reason for the observed correlations might be sought in the possible identity of structures obtained during creep under a given stress at the same values of θ independent of the test temperature. In order to test this concept a series of creep tests were made on the same coarse-grained high purity aluminium from which the constant load creep data of Fig. 4 were obtained. The tests were conducted at three temperatures (422, 477 and 528°K) under the same constant load of 2,000 psi. Specimens were removed from test at true strains of 0·082, 0·14, 0·22 and at fracture for each temperature and then cooled rapidly to room temperature for examination :

(1) The X-ray back-reflection Debye-Scherrer diagrams of Fig. 5 reveal that the X-ray patterns are somewhat sensitive to the creep strain and, within the scatter inherent in the X-ray sampling, approximately the same patterns are obtained at the same creep strains independent of the temperature of test. According to the correlations recorded in Fig. 4, therefore, almost identical structures are obtained at the same values of θ for creep under the same load.

(2) Metallographic examinations also confirmed the nominal identity of

Vol.
3
54/55

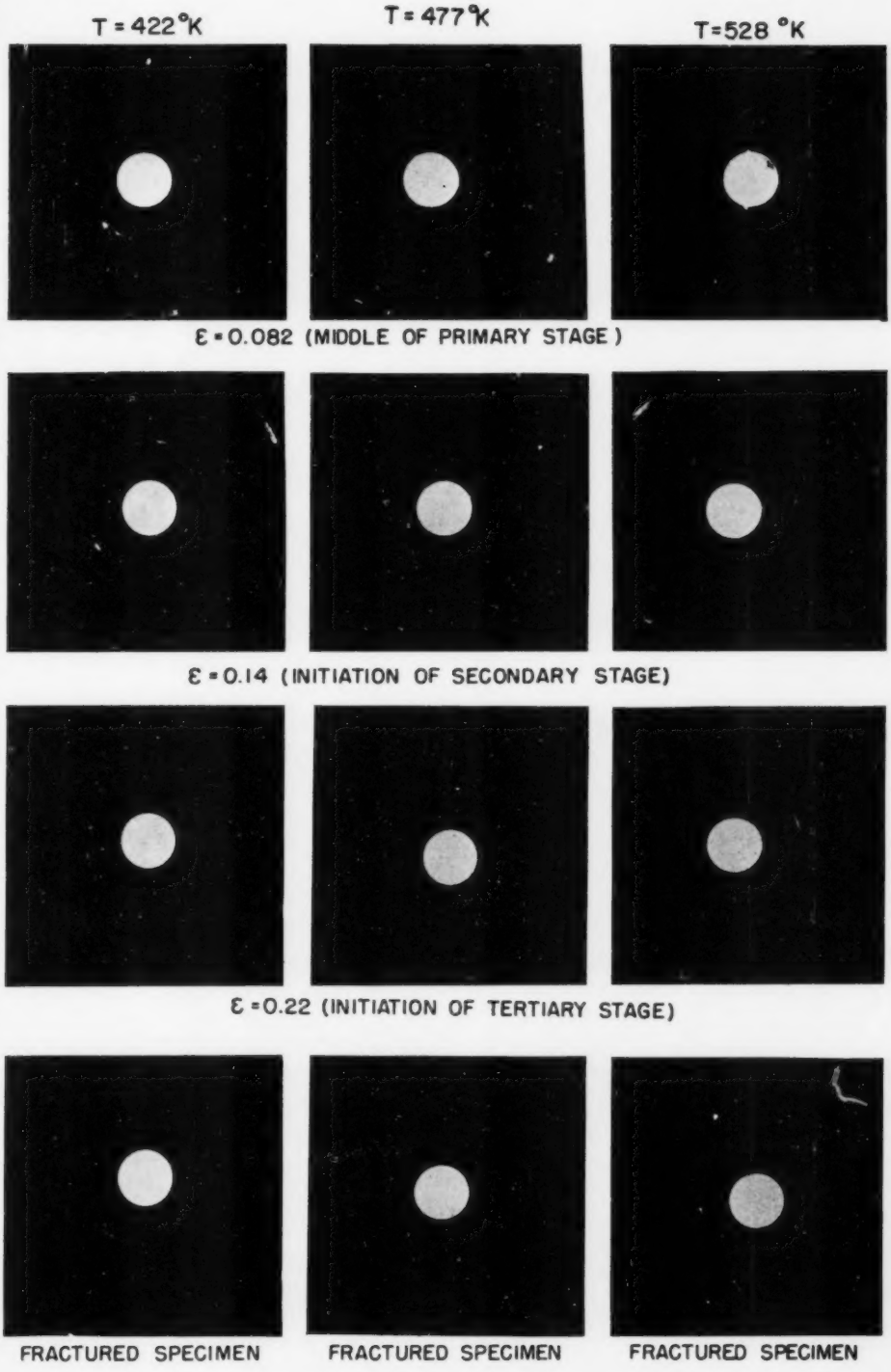
T = 422°K
T = 477°K
T = 528 °K
ε = 0.082 (MIDDLE OF PRIMARY STAGE)
ε = 0.14 (INITIATION OF SECONDARY STAGE)
ε = 0.22 (INITIATION OF TERTIARY STAGE)
FRACTURED SPECIMEN
FRACTURED SPECIMEN
FRACTURED SPECIMEN

Fig. 5. X-ray back reflection photograms of high purity aluminium under a constant load of 2,000 psi for various temperatures as a function of strain.

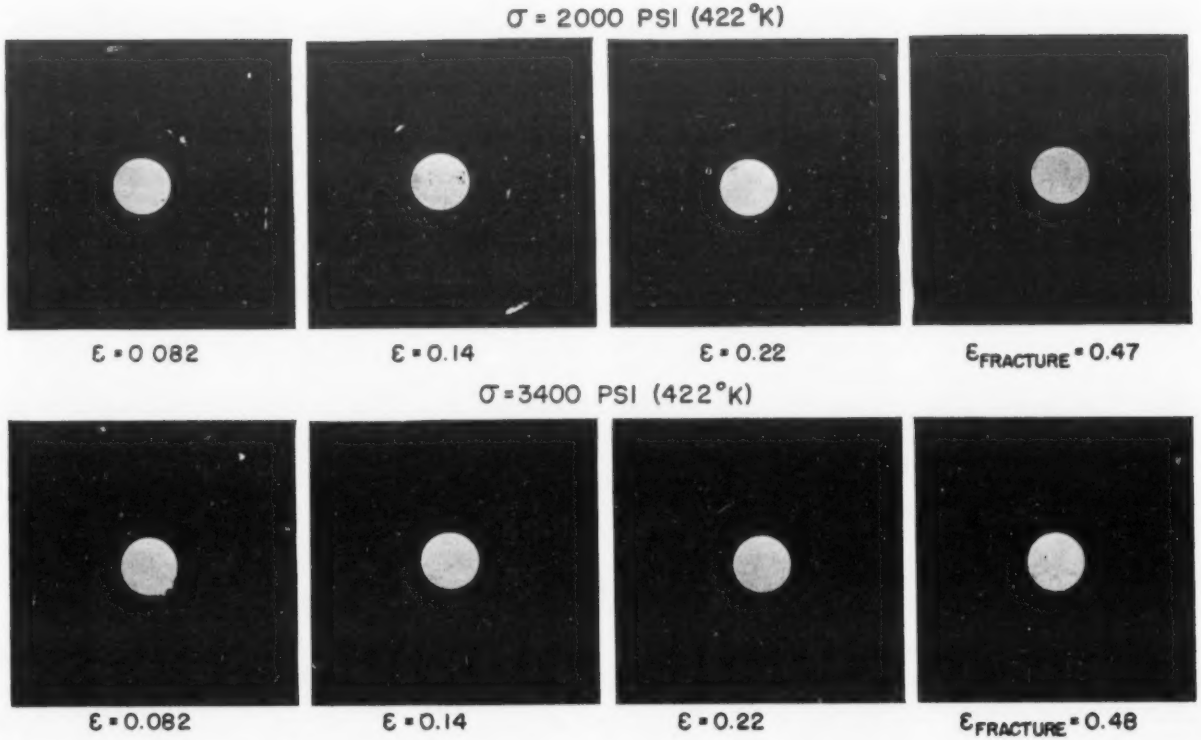

Fig. 6. X-ray back reflection photograms of high purity aluminium for two different stresses as a function of the strain.

VOL
3
1954/

structures at the same values of ϵ and therefore θ. At $\epsilon = 0{\cdot}082$ the metallographic structures exhibited approximately the same evidence of extensive deformation banding independent of test temperature in harmony with the short diffuse arcs in the X-ray patterns arising from bending and distortions of the grains. At $\epsilon = 0{\cdot}22$, however, the metallographic structures exhibited approximately the same extensive subgrain formation independent of test temperature in complete harmony with the extensive polygonization shown by the greater Debye-Scherrer arcs composed of sharp reflections arising from a series of nearly perfect subgrains. At the intermediate strains almost identical intermediate structures were obtained independent of the test temperature.

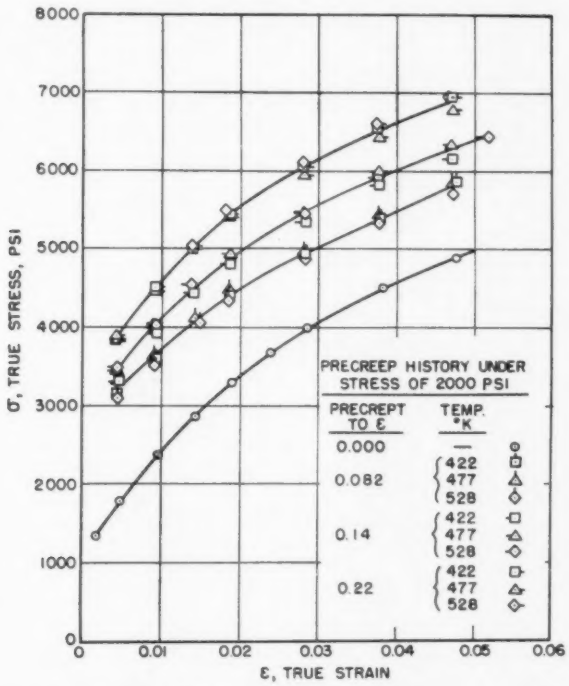

Fig. 7. Tensile properties at 298°K following creep under a constant load of 2,000 psi to strains indicated above. (Data of SHERBY and DORN 1953).

(3) Both X-ray and metallographic examination support the thesis that identical structures are obtained for the same values of ϵ or θ in a constant stress (or load) creep test, independent of the test temperature. But sampling difficulties and insensitivity inherent in these techniques suggested that a more definitive quantitative test of this concept be made; this was deemed particularly necessary inasmuch as only certain gross structural details can be revealed by X-ray diffraction and metallographic techniques. Since the plastic properties of metals are highly structure-sensitive, atmospheric temperature stress-strain curves following identical creep strains were selected for this test. As shown in Fig. 7, the stress-strain curves were sensitive to the previous creep history; and the same stress-strain curves were obtained following identical creep strains under the same

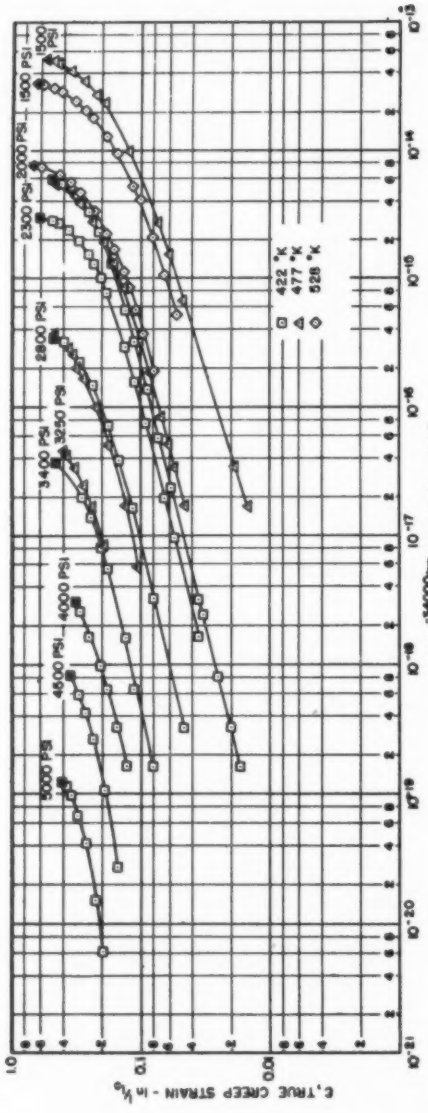
1500 PSI
2300 PSI
2000 PSI
1500 PSI
2800 PSI
3400 PSI
3250 PSI
4000 PSI
4500 PSI
5000 PSI
422 °K
477 °K
526 °K
ε, TRUE CREEP STRAIN - in %
1.0
0.1
0.01
10⁻¹³
10⁻¹⁴
10⁻¹⁵
10⁻¹⁶
10⁻¹⁷
10⁻¹⁸
10⁻¹⁹
10⁻²⁰
10⁻²¹
θ = te^(-34000/RT) (t IN HRS., T IN °K)

Fig. 8.

stress, independent of the test temperature. Consequently the validity of equation 1 arises from the identity of the total structure at equal values of θ and ϵ in a constant stress creep test, independent of the test temperature.

An increase in stress causes an increase in the initial strain and the subsequent creep rate, as shown by the data recorded in Fig. 8. These data also reveal that

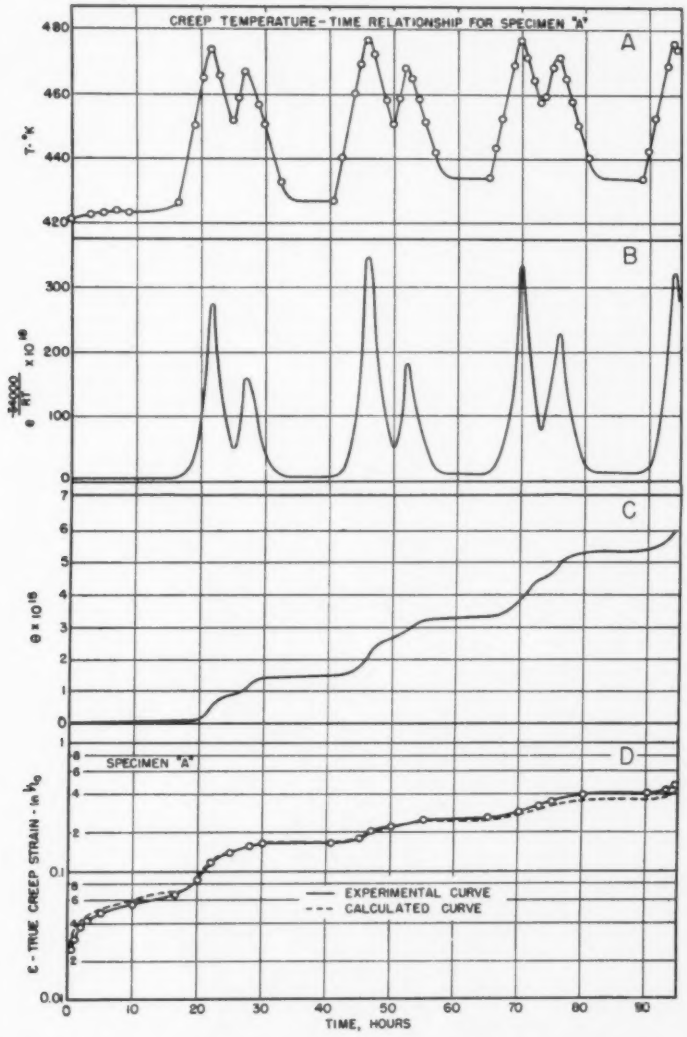

Fig. 9. Creep at a constant load of 2,000 psi under variable temperature conditions.

the activation energy for creep is insensitive to differences in the stress. As shown by the back-reflection Debye-Scherrer photograms of Fig. 6, creep to the same strain under a higher stress resulted in more diffuse arcs and finer subgrain sizes. Metallographic examination revealed more extensive deformation banding over the first portion of the creep curve at the higher stress, followed over the last

portion of the creep curve at higher stress by finer polygonized subgrain sizes. These observations suggest that the substructures developed during creep at higher stresses appear never to coincide with those developed at any strain during creep at lower stresses.

3. Deductions based on Equation (1)

Several deductions follow directly from equation (1).

1. *Creep under Variable Temperature.* For constant stress (or constant load) creep under conditions where the temperature is varied with time, the evaluation of θ can be generalized according to

$$\theta = \int_0^t e^{-\Delta H/RT}\, dt \tag{3}$$

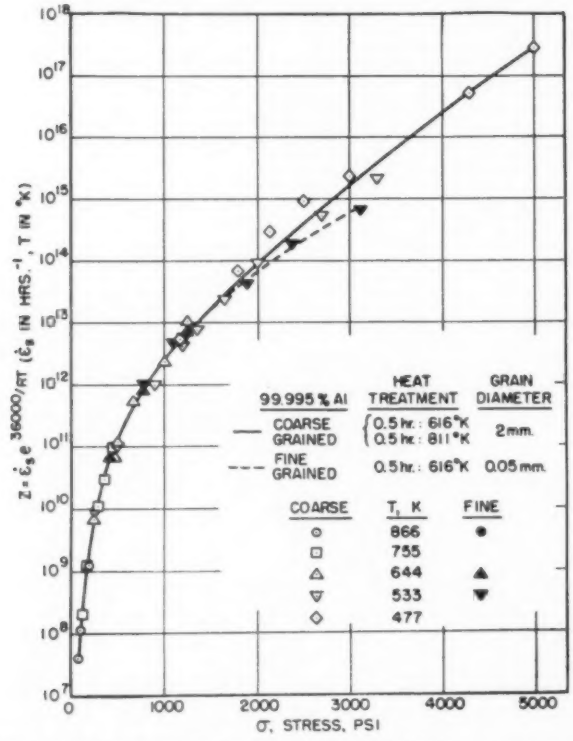

Fig. 10. Correlation between stress and the Zener-Hollomon parameter for high purity aluminium. (Data from SERVI and GRANT 1951).

which reduces to $\theta = te^{-\Delta H/RT}$ for constant temperature creep. Fig. 4 gives the $\epsilon - \theta$ curve of high purity Al under a constant load of 2,000 psi illustrating that ΔH is about 34,000 cal/mole. When the temperature is varied according to cut *A* of Fig. 9, the solid creep curve of cut *D* of Fig. 9 is obtained for a constant load of 2,000 psi. In cut *B* is shown the value of $e^{-\Delta H/RT}$ as a function of time from which the θ values shown in cut *C* are obtained by the graphical integration

suggested by (3). The strains corresponding to the calculated values of θ were obtained from the constant temperature $\epsilon - \theta$ curve of Fig. 4 and plotted as a function of time in the broken curve of cut D of Fig. 9. The good agreement between the calculated and experimental curves attests the validity of this method of prediction.

2. *Zener-Hollomon Parameter.* According to equation (1), the creep rate is given by

$$\dot{\epsilon} = \left(\frac{\partial f}{\partial \theta}\right)\left(\frac{d\theta}{df}\right) = f'(\theta)\, e^{-\Delta H/RT}, \qquad \sigma = \text{constant}. \tag{4}$$

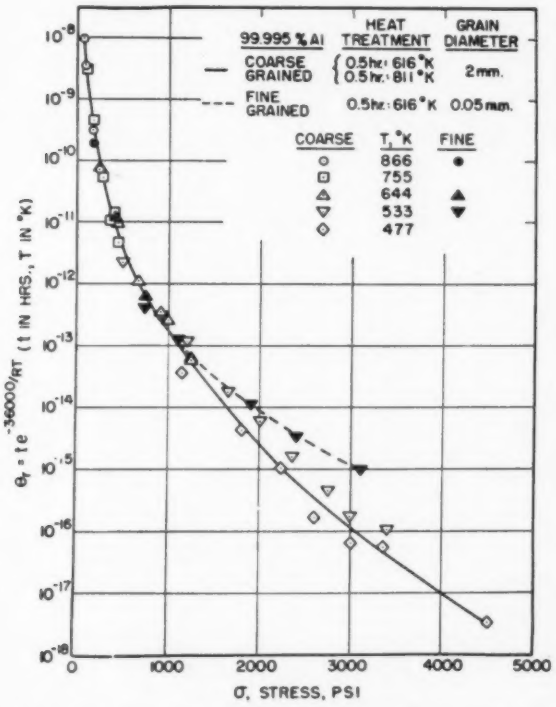

Fig. 11. Correlation between stress and θ at rupture for high purity aluminium. (Data from SERVI and GRANT 1951).

Therefore, at the secondary creep rate, designated by subscripts " s,"

$$\dot{\epsilon}_s\, e^{\Delta H/RT} = f(\theta_s), \qquad \sigma = \text{constant}. \tag{5}$$

But as shown by (1) as well as the data recorded in Figs. 3 and 4, θ_s has the same value independent of temperature for the same stress. As the stress is increased, however, θ_s decreases, whence θ_s is a function of the stress. Consequently

$$Z = \dot{\epsilon}_s\, e^{\Delta H/RT} = F(\sigma) \tag{6}$$

where Z is the well-known Zener-Hollomon parameter (ZENER and HOLLOMON 1944). A typical correlation of Z as a function of σ is shown in Fig. 10. The ΔH obtained by this method agrees well with that obtained from $\epsilon - \theta$ data.

3. *Stress-Rupture.* Assuming that the strain damage leading to rupture at a given stress is dependent only on the strain to rupture, the value of θ_r at rupture should be the same for all tests under the same stress independent of temperature. This conclusion is verified by the data of Figs. 3 and 4 where the termini of the

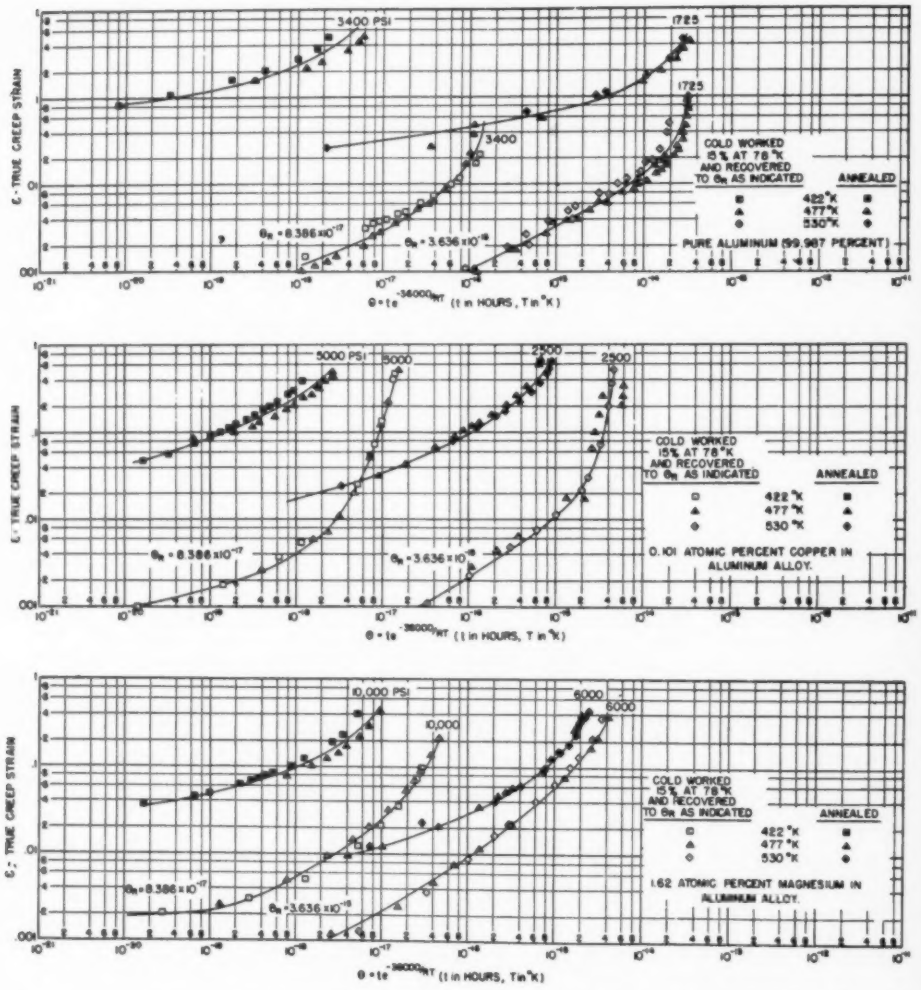

Fig. 12. Correlation of creep strain-time data for annealed and cold-worked states of dilute aluminium alloys by means of the relation $\epsilon = f(\theta_r)$ at constant load. (Data of FRENKEL, SHERBY and DORN 1953).

$\epsilon - \theta$ curves for each temperature are represented by the solid points shown on the graph. Consequently stress-rupture should obey the functional relationship (ORR, SHERBY and DORN 1954a)

$$\theta_r = t_r e^{-\Delta H/RT} = G(\sigma) \tag{7}$$

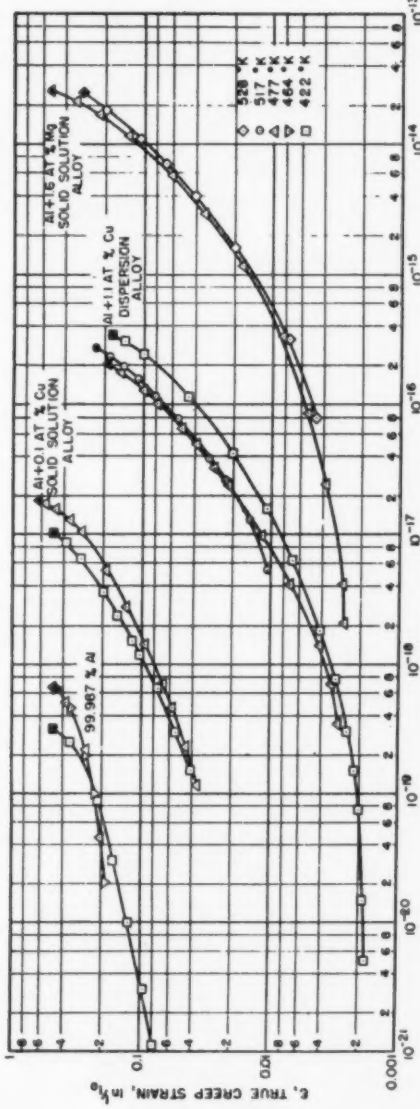
Al+0.1 AT % Cu SOLID SOLUTION ALLOY
Al+11 AT % Cu DISPERSION ALLOY
Al+15 AT % Mg SOLID SOLUTION ALLOY
99.987 % Al
528 °K
517 °K
477 °K
464 °K
422 °K
ε, TRUE CREEP STRAIN, in %
θ = te^-36000/RT (t IN HRS., T IN °K)

Fig. 13. Correlation of creep strain-time data for aluminium and dilute aluminium alloys bymeans of the relation for a constant load of 4,000 psi. (Data of SHERBY and DORN 1953, 1952; and GIEDT, SHERBY and DORN 1953).

A typical example of the validity of this relationship is given in Fig. 11. Again the activation energy so obtained agrees well with those obtained from $\epsilon - \theta$ and $Z - \sigma$ types of data.

4. Activation Energy for Creep

The methods of analyses described above are not universally applicable to all types of creep data. First they apply only when the temperature is above that for rapid crystal recovery (about one-half of the melting temperature for high purity metals). Creep data obtained at lower temperatures do not correlate with the higher temperature creep data (SHERBY and DORN 1952), suggesting that two alternate mechanisms for creep might exist, one predominating at the higher

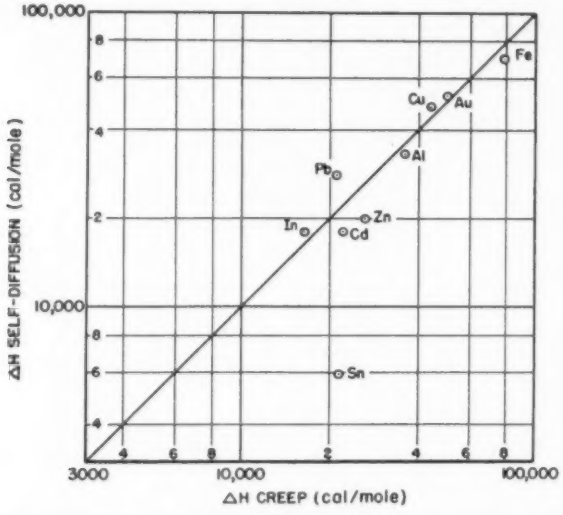

Fig. 14. Correlation between the activation energies for creep and self-diffusion.

temperatures and the other predominating over the lower ranges of temperature. Secondly the analyses described above are invalid when applied to thermally unstable systems such as precipitation hardened alloys. Such failures are ascribable to the possibility that the structures developed in these alloys following creep at a given stress are not simple functions of a single θ parameter. It is suspected that these simple correlations might not be applicable over the entire range of binary alpha solid solutions wherein two activation energies might be operative.

Within the limits of validity of (1), however, ΔH appears to be insensitive to temperature (vide Fig. 10), stress (vide Figs. 8 and 10), strain and the structure developed during creep of annealed metals (vide Figs. 3 and 4), cold worked state (FRENKEL, SHERBY and DORN 1953) (vide Fig. 12), grain size (vide Fig. 10), minor alloying additions (SHERBY and DORN 1952) (vide Fig. 13), and relatively stable dispersions of hard intermetallic compounds in dilute alpha solid solution matrices (GIEDT, SHERBY and DORN 1953) (vide Fig. 13). Since ΔH appears to be a structure-sensitive property it might be assumed that ΔH for creep of relatively pure metals approaches that of the elements.

TABLE 1.
Activation Energy for Creep.

Atomic No.	*Metal*	*Type of Correlation*	*ΔH (cal/mole)*	*Reference*
4	Be (99·7%)	$\theta_r - \sigma$	65,000	KAUFMAN, GORDON and LILLIE (1950)
12	Mg (99·93%)	$\epsilon - \theta$ $Z - \sigma$	31,000	ROBERTS (1953)
13	Al (99·99%)	$\epsilon - \theta$ $Z - \sigma$ $\theta_r - \sigma$	34,000 to 36,000	SHERBY and DORN (1952); ORR, SHERBY and DORN (1954a)
	Al-Mg Solid Solution Alloy (1·6% Mg)	$\epsilon - \theta$ $Z - \sigma$ $\theta_r - \sigma$	36,000	SHERBY and DORN (1952); ORR, SHERBY and DORN (1954a)
	Al-Cu Solid Solution Alloy (0·1% Cu)	$\epsilon - \theta$ $Z - \sigma$ $\theta_r - \sigma$	36,000	SHERBY and DORN (1952); ORR, SHERBY and DORN (1954a)
	Al-Cu Dispersion Alloy (1·1% Cu)	$\epsilon - \theta$ $Z - \sigma$ $\theta_r - \sigma$	36,000	GIEDT, SHERBY and DORN (1953)
	Al (99·99%)	$Z - \sigma$ $\theta_r - \sigma$	36,000	SERVI and GRANT (1951)
22	Ti (99·6%)	$\theta_r - \sigma$	60,000	CUFF and GRANT (1952)
26	Fe (99·93%)	$Z - \sigma$	78,000	TAPSELL and CLENSHAW (1927)
28	Ni (98·7%)	$\epsilon - \theta$	65,400	HAZLETT, PARKER and NATHANS (1950)
	Ni (99·5%)	$\theta_r - \sigma$	65,000	Battelle Memorial Institute
29	Cu (pure)	$Z - \sigma$	44,000	NADAI and MANJOINE (1941)
	Cu-Ni Solid Solution Alloy (45% Ni)	$Z - \sigma$	41,800	DUSHMAN, DUNBAR and HUTHSTEINER (1944)
30	Zn (99·0%)	$\epsilon - \theta$ $Z - \sigma$	26,000	POMP and LANGE (1936)
	Zn (99·99%)	$Z - \sigma$	26,000	GRAESER, HANEMANN and HOFMAN (1943)
41	Nb (99·8%)	$\theta_r - \sigma$	75,000	GRASSI, BAINBRIDGE and HARMON (1951); ORR and BAINBRIDGE (1953)
42	Mo	$\theta_r - \sigma$	120,000	PARKE (1951)
	Mo-Nb (0·34% Nb)	$\theta_r - \sigma$	120,000	SEMCHYSHEN and HOSTETTER (1952)
	Mo-V (0·87% V)	$\theta_r - \sigma$	120,000	SEMCHYSHEN and HOSTETTER (1952)
48	Cd (99·96%)	$\epsilon - \theta$ $Z - \sigma$	22,000	FRENKEL (1954)
49	In (99·86%)	$\epsilon - \theta$ $Z - \sigma$	16,500	FRENKEL (1954)
50	Sn (99·94%)	$\epsilon - \theta$ $Z - \sigma$	21,000	FRENKEL (1954)
78	Pt (99·98%)	$\epsilon - \theta$	56,000	CARREKER (1950)
	Pt (pure)	$Z - \sigma$	56,000	DUSHMAN, DUNBAR and HUTHSTEINER (1944)
79	Au (pure)	$Z - \sigma$	50,000	ALEXANDER, DAWSON and KING (1951)
82	Pb (99·9998%)	$\epsilon - \theta$ $Z - \sigma$	19,000	SMITH (1941)
	Pb (99·997%)	$\epsilon - \theta$ $Z - \sigma$	19,000	MCKEOWN (1937)
	Pb (99·92%)	$Z - \sigma$	23,000	SMITH and HOWE (1945)

TABLE 2.
*Data on Activation Energies for Self-Diffusion of Metals**

Metal Atomic No.	*ΔH self-diffusion, cal. per mol*		*Remarks (Data are for Polycrystals unless otherwise noted)*
	Reported Values (Source Indicated)	*Best or Average Value*	
Lithium	9,800 (a)		Deduced from nuclear resonance data
(3)	9,300 (b)		Deduced from electrical resistance data
		9,500	
Carbon	114,000 (c)	114,000	
(6)			
Sodium	10,450 (d)		
(11)	9,500 (e)		Deduced from nuclear resonance data
	9,100 (b)		Deduced from electrical resistance data
		10,450	
Aluminium	33,000 (f)	33,000	Estimated from diffusion data of other metals in aluminium
(13)			
Potassium	9,100 (b)	9,100	Deduced from electrical resistance data
(19)			
α-Iron	77,200 (g)		
(26)	73,200 (h)		Extensive data, 720° to 900°C
	59,700 (i)		800° to 900°C
		73,000	
γ-Iron	48,000 (g)		Superseded by later work (h)
(26)	74,200 (h)		
	67,900 (i)		
		71,000	
Cobalt	67,000 (j)		
(27)	61,900 (k)		
		75,000	
Copper	45,100 (l)		
(29)	49,000 (l)		Single crystal
	46,800 (m)		
	44,000 (n)		Based on diffusion data for copper in copper alloys extrapolated to zero concentration of alloying element
	57,200 (o)		
	61,400 (p)		Incomplete work, based on complete data at two temperatures only
	47,000 (f)		Based on reinterpretation of published data
		48,000	
Zinc	20,400∥*C* (q)		Single crystal, $\Delta H \parallel C$ used in correlations with creep data
(30)	31,000⊥*C* (q)	20,400	
Silver	45,950 (r)		Large grained polycrystals
(47)	45,950 (s)		Single crystal
	45,500 (t)		Large grained polycrystals
	46,000 (f)		Based on reinterpretation of published data
		46,000	

*Note added in proof: SHEWNON and RHINNES, A.I.M.M.E., 1954 have determined the activation energy for self-diffusion in Mg (12) to be 32,000 cal/mole.

TABLE 2.—*continued.*

Data on Activation Energies for Self-Diffusion of Metals

Metal Atomic No.	*ΔH Self-Diffusion, cal per mol*		*Remarks (Data are for Polycrystals unless otherwise noted)*
	Reported Values (Source Indicated)	*Best or Average Value*	
Cadmium (49)	18,900⊥*C* (u)		Single crystal, $\Delta H \perp C$ used in correlations with creep data
	17,300∥*C* (u)		
		17,300	
Indium (49)	17,900 (v)	17,900	
Tin (50)	10,500∥*C* (w)		Single crystal, $\Delta H \parallel a$ used inc orrelations with creep data
	5,900∥*a* (w)		
		5,900	
Tungsten (74)	140,000 (x)	140,000	Diffusion of Fe in *W* extrapolated to 100 pct. *W*
Gold (79)	51,000 (y)		Extensive data, 721° to 966°C
	62,900 (z)		Data at three temperatures only
	53,000 (a′)		
		52,000	
Lead (82)	27,900 (b′)		Single crystal
	27,000 (f)		Based on reinterpretation of published data
		28,000	
Bismuth (83)	31,000∥*C*(c′)		Single crystal, $\Delta H \parallel C$ used in correlations with creep data
	140,000⊥*C*(c′)		
		31,000	

(a) H. S. GUTOWSKY and B. R. MCGARVEY : *J. Appl. Phys.* 1952 **20**, p. 1472.
(b) D. K. C. MACDONALD : *J. Chem. Phys.* 1953 **21**, pp. 177-178.
(c) L. GREEN, Jr. : *J. Appl. Mech.* 1952 **19**, pp. 320-326.
(d) N. H. NACHTRIEB, E. CATALANO and J. A. WEIL : *J. Chem. Phys.* 1952 **20**, pp. 1185-1188.
(e) H. S. GUTOWSKY : *Phys. Rev.* 1951 **83**, p. 1073.
(f) A. S. NOWICK : *J. Appl. Phys.* 1951 **22**, pp.1182-1186.
(g) C. E. BIRCHENALL and R. F. MEHL : *J. Appl. Phys.* 1948 **19**, p. 217.
(h) C. E. BIRCHENALL and R. F. MEHL : *Trans. AIME* 1950 **188**, pp. 144-149 ; *J. Metals* (January 1950).
(i) F. S. BUFFINGTON, I. D. BAKALAR and M. COHEN : *Trans. AIME* 1950 **188**, pp. 1374-1375; *J. Metals* (November 1950).
(j) F. C. NIX and F. E. JAUMOT, Jr. : *Phys. Rev.* 1951 **82**, pp. 72-74.
(k) R. C. RUDER and C. E. BIRCHENALL : *Trans. AIME* 1951 **191**, pp. 142-146 ; *J. Metals* (February 1951).
(l) M. S. MAIER and H. R. NELSON : *Trans. AIME* 1942 **147**, pp. 39-47.
(m) C. L. RAYNOR, L. THOMASSEN and L. J. ROUSE : *Trans. ASM* 1942 **30**, pp. 313-325.
(n) R. N. RHINES and R. F. MEHL : *Trans. AIME* 1938 **128**, pp. 185-221.
(o) J. STEIGMAN, W. SHOCKLEY and F. C. NIX : *Phys. Rev.* 1939 **56**, pp. 13-21.
(p) B. V. ROLLIN : *Phys. Rev.* 1939 **55**, p. 231.
(q) P. H. MILLER, Jr. and F. R. BANKS : *Phys. Rev.* 1942 **61**, pp. 648-652.
(r) W. A. JOHNSON : *Trans. AIME* 1941 **143**, pp. 107-111.
(s) R. E. HOFFMAN and D. TURNBULL : *J. Appl. Phys.* 1951 **22**, pp. 634-639.
(t) L. SLIFKIN, D. LAZARUS and T. TOMIZUKA : *J. Appl. Phys.* 1952 **23**, pp. 1032-1033.

Vol. 3 54/55

(u) H. B. HUNTINGTON, J. S. SHIRN and E. S. WAJDA : *Anisotropic Diffusion*, Rensselaer Polytechnic Institute, Troy, New York, Progress Report No. 2, July 1, 1953.
(v) R. E. ECKERT and H. G. DRICKAMER : *J. Chem. Phys.* 1952 **20**, pp. 13-17.
(w) P. J. FENSHAM : *Australian J. Sci. Res.* 1950 **3A**, pp. 91-104.
(x) J. A. M. VAN LIEMPT : *Rec. Trav. Chim.* 1945 **64**, pp. 239-249.
(y) H. A. C. MCKAY : *Trans. Faraday Soc.* 1938 **34**, pp. 845-849.
(z) A. M. SAGRUBSKIJ : *Phys. Zeit. Sowjet Union* 1937 **12**, pp. 118-119.
(a′) A. M. SAGRUBSKIJ : *Bull. Acad. Sci.* U.S.S.R. 1937 p. 903.
(b′) G. VON HEVESY, W. SEITH and A. KEIL : *Ztsch. Physik.* 1932 **79**, pp. 197-202.
(c′) W. SEITH : *Ztsch. Elektrochem.* 1933 **39**, pp. 538-542.

As outlined in Table 1 a complete survey was made (ORR, SHERBY and DORN 1954a ; 1954b) of creep and stress-rupture data on pure metals and binary solid solution alloys found to be sufficiently extensive for determination of the activation energy. In several cases approximately the same value of the activation energy for creep was obtained from data presented by different investigators using different

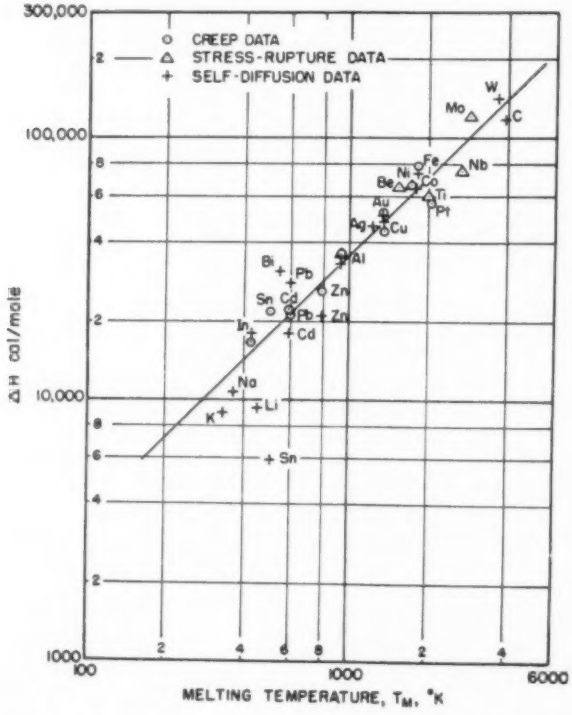

Fig. 15. Correlation of the activation energies for creep, stress-rupture and self-diffusion with the melting temperature.

purities and different pretreatments of the same base metal. In Table 2 are recorded the values of the activation energies for self-diffusion. As shown in Fig. 14, the activation energy for creep generally agrees well with that for self-diffusion. The Sn data deviate most seriously from the general correlation. As shown in Fig. 15, however, the activation energy for self-diffusion of Sn does not

correlate well with the usual trends of increasing activation energies for self-diffusion or creep with melting temperature, whereas the activation energy for creep of Sn coincides well with the general pattern. This suggests that despite the care that was exercised, some error might nevertheless have intruded into the evaluation of the activation energy for self-diffusion of Sn.

Neglecting the obviously important factor of crystal structure, some insight into the creep resistance of the elements might be gained by reviewing the periodic variation of the activation energies for creep and self-diffusion with atomic number as shown in Fig. 16. These empirical trends suggest that the highest creep resistant

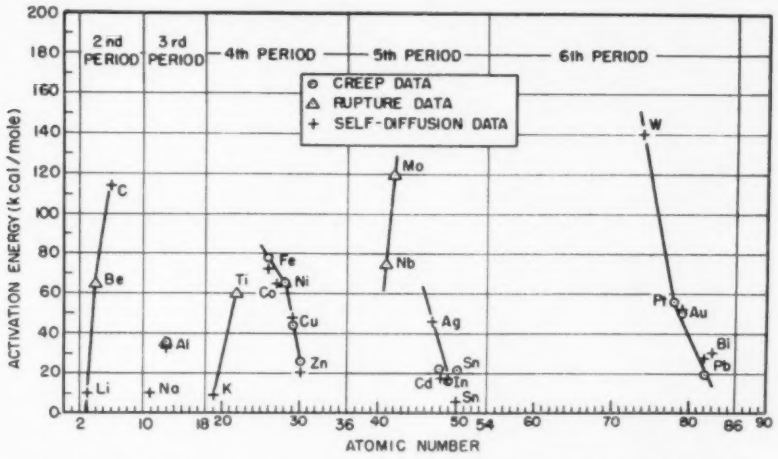

Fig. 16. Correlation of the activation energies for creep, rupture and self-diffusion with atomic number.

metals occur among those transition elements which exhibit the highest activation energies namely *W*, *Mo* and perhaps *V* in each series. Of course, as shown by the data of Fig. 13, a high activation energy is not the only factor responsible for high creep resistance. In fact introduction of minor alloying elements and stable dispersions also serve to improve the creep resistance even when the activation energy remains unaltered.

The apparent identity of the activation energy for creep with that for self-diffusion does not mean that high temperature creep is due to self-diffusion. But this apparent identity infers that the rate-controlling process for high temperature creep might be that of self-diffusion. Assuming that self-diffusion occurs by atom-vacancy interchanges, the activation energy for self-diffusion should arise from two terms. According to the Boltzmann distribution the number of vacancies in thermal equilibrium with the metal lattice should be proportional to $e^{-W/kT}$ where W is the energy required to produce a vacancy. If E be the activation energy for a vacancy-atom interchange, the frequency of such interchanges will be proportional to $e^{-E/kT}$. Consequently the activation energy for self-diffusion becomes $\Delta H = NW + NE$ per mole where N is Avogadro's number. (A similar expression applies for interstitial diffusion where W is the energy to produce an interstitial atom.) Since the activation energy for high temperature creep appears to agree

with that for self-diffusion, the number of vacancies participating in the rate-controlling self-diffusion process during creep must closely approximate the equilibrium number. This observation suggests that such excess vacancies (or interstitials) which are believed to be generated by Seitz's types of mechanisms (SEITZ 1952) are rapidly eliminated during high temperature creep.

Most formal theories of creep (KAUZMAN 1941; NOWICK and MACKLIN 1947) are predicted on thermal activation of dislocations over free energy barriers. As demanded by reaction rate theory, the creep rate for such processes give relations of the type

$$\dot{\epsilon} = Ae^{-\Delta H/RT} \sinh\left(\frac{V\sigma}{2kT}\right) \tag{8}$$

where A and V and ΔH might be taken as structure-sensitive parameters. Here the stress enters the equation for creep as a function of σ/T. But the observed $\epsilon - \theta$, $Z - \sigma$ and $\theta_r - \sigma$ relations all contain the stress and not σ/T as the appropriate variable for correlation. More conclusive evidence for the belief that stress alone and not σ/T enters the creep relationship will be presented in the following section. These observations suggest then that high temperature creep does not take place by thermal activation of dislocations over a barrier.

If high temperature creep were due to thermal activation of dislocations over a barrier it would be reasonable to expect ΔH to increase with increased barrier strengths introduced during creep or as a result of previous cold work. The constancy of ΔH with creep strain and cold work therefore support the hypothesis that high temperature creep does not involve thermal activation of dislocations over a free energy barrier.

Since high temperature creep is a continuing process, dislocations must either surmount barriers or move around barriers. Surmounting barriers by thermal activation does not, at present, appear to be a process that coincides deductions based on experimental observation. On the other hand as suggested by MOTT (1951, 1953) dislocations arrested at a barrier might undertake a climb process involving self-diffusion until they move to a plane where the barrier strength is equal to the applied stress. Under these conditions the dislocations would then circulate around the barrier. Thus the activation energy for high temperature creep could well be that for self-diffusion and the stress might enter the creep relationship as stress alone and not as σ/T.

5. GRAIN BOUNDARY SHEARING

In view of the complexity of the various processes occurring during creep of polycrystalline aggregates, it is somewhat surprising that creep can be correlated by such a simple functional relationship as that given by (1). In a series of unique investigations MCLEAN (1951-1952; 1952-1953a, b, c) has shown that creep of polycrystalline aggregates occurs by means of migration of dislocations (resulting in slip and subgrain tilting) and by means of grain boundary shearing. Under a given stress the ratio of the fraction of the creep strain arising from grain boundary shearing to the total creep strain, $\epsilon_{g.b.}/\epsilon$, remains essentially constant. But this ratio increases as the stress decreases. Using MCLEAN's techniques, the effect of temperature on grain boundary shearing was evaluated (FAZAN, SHERBY and

DORN) as recorded by the data in Table 3 for a constant load of 250 psi. The approximately constant values of $\epsilon_{g.b.}/\epsilon$ again confirm MCLEAN's observations. Furthermore the same values of $\epsilon_{g.b.}$ were obtained at the same values of ϵ independent of the test temperature. Consequently, within the limits of experimental error, the same θ parameter and the same value of ΔH applies to grain boundary shearing as to the total creep strain. Consequently (1) is shown to be applicable to grain boundary shearing as well as to the total creep strain.

TABLE 3.

Results on Grain Boundary Shearing in High Purity Aluminium under 250 psi (FAZAN, SHERBY and DORN).

Temp. °*K*	*Time Hours*	ϵ	$\epsilon_{g.b.}$	$\epsilon_{g.b.}/\epsilon$	ΔH *cal/mole*
610	9·7	0·037	0·0035	0·095	38,500
747	0·029	0·037	0·0031	0·085	
610	20·4	0·07	0·0055	0·079	35,000
747	0·105	0·07	0·0051	0·073	
610	55·5	0·11	0·0085	0·076	
640	14·42	0·11	0·0071	0·065	38,000
700	1·215	0·11	0·0071	0·065	
747	0·15	0·11	0·0075	0·068	

The fact that the activation energy for grain boundary shearing is practically identical with that for the total creep strain suggests that grain boundary shearing might be attributed to localized crystallographic mechanisms of deformation in the vicinity of the grain boundary, rather than such a process as viscous shearing. This hypothesis is further substantiated by the fact that $\epsilon_{g.b.}/\epsilon$ is constant for creep at a given stress. Consequently, as demonstrated by MCLEAN, the shape of the $\epsilon_{g.b.} - t$ curve is similar to that of the $\epsilon - t$ curve, suggesting that the same structural changes serve to decrease the rate of grain boundary shearing as operate to reduce the creep rate over the primary stage of creep. If grain boundary shearing were attributable to viscous flow $\epsilon_{g.b.}$ would have been a linear function of t and the ratio $\epsilon_{g.b.}/\epsilon$ should have increased with ϵ.

Since $\epsilon_{g.b.}$ is a function of θ for a given stress, independent of temperature, the localized strain damage in and about the grain boundary region, such as might lead to intergranular fracturing, should also depend on θ independent of the temperature. Such independence of the temperature suggests that the " so-called " equicohesive temperature (below which failures are transcrystalline and above which they are intergranular) might be a highly fictional concept. MCLEAN's data, which reveal that the ratio of $\epsilon_{g.b.}/\epsilon$ increases as the stress is decreased, suggest that the strain damage becomes concentrated more and more in the vicinity of the grain boundary as the stress is reduced. Perhaps future investigations will more conclusively reveal that " so-called " intergranular fracturing occurs below some critical stress rather than above some critical temperature.

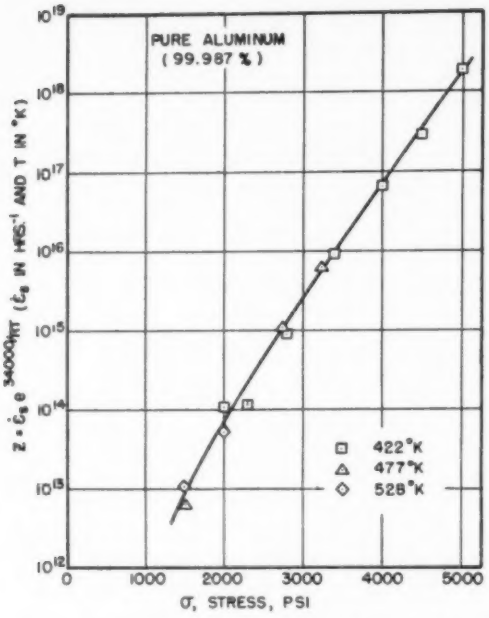

Fig. 17. Effect of stress on the Zener-Hollomon parameter for secondary creep. (Data of SHERBY and DORN 1953).

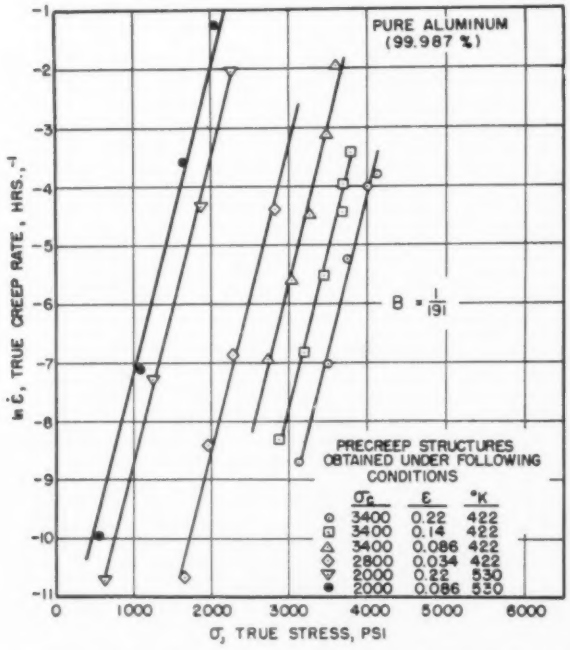

Fig. 18. Effect of stress on the creep rate for a constant structures (Data of SHERBY, FRENKEL, NADEAU and DORN 1954).

VOL. 3
54/55

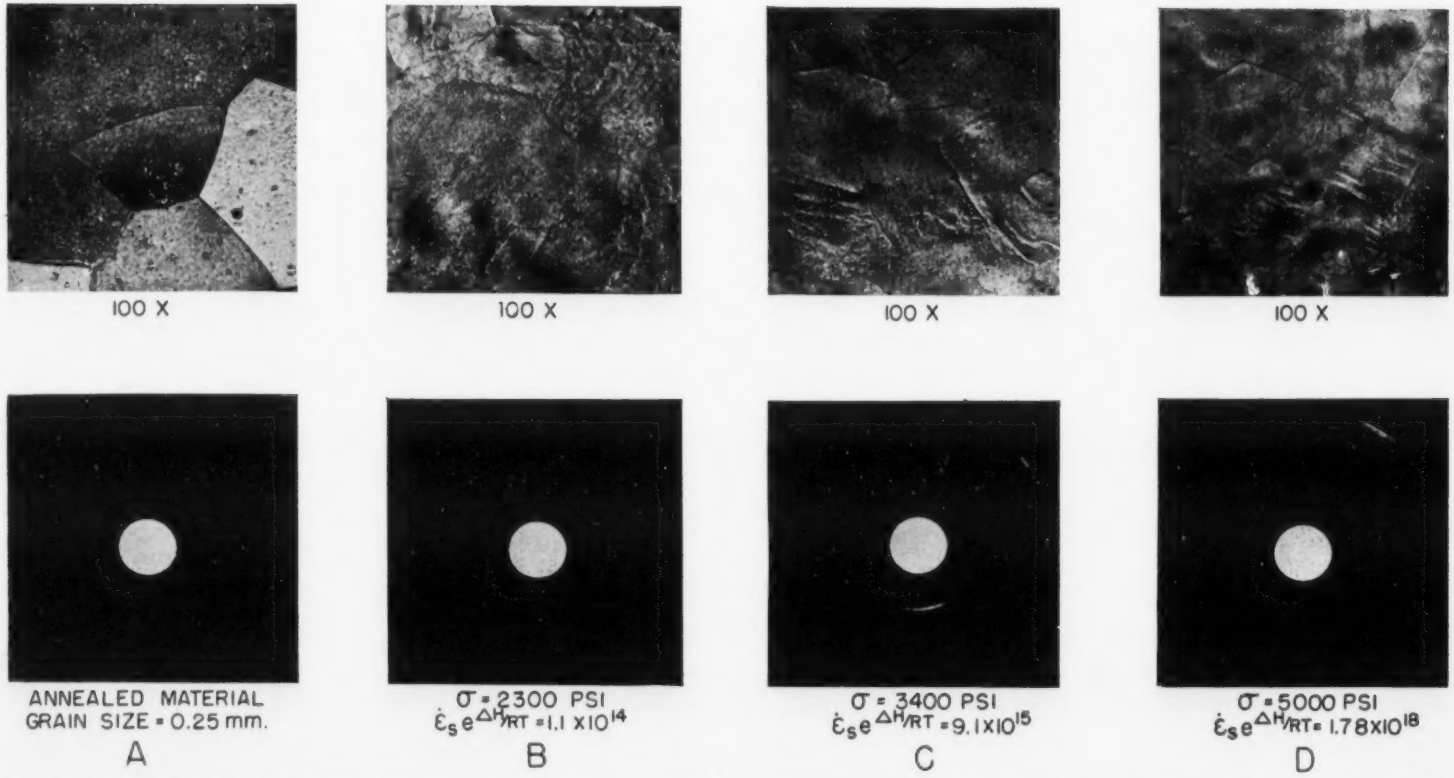

Fig. 19. Metallographic and X-ray photograms of creem specimens of high purity aluminium as a function of the parameter (SHERBY and DORN 1953).

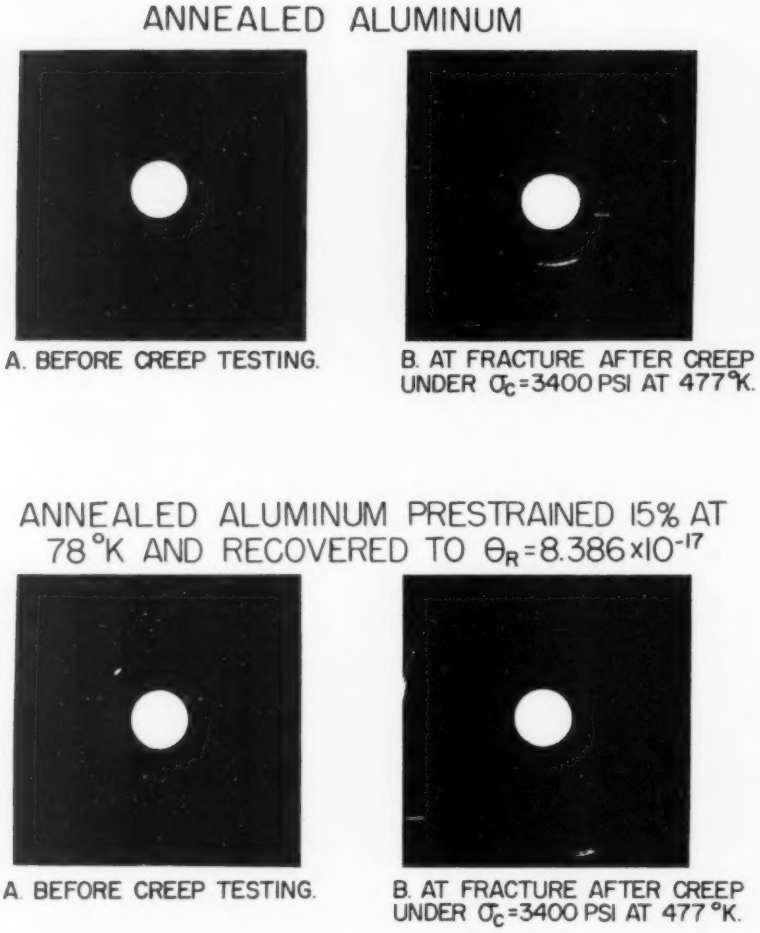
ANNEALED ALUMINUM
A. BEFORE CREEP TESTING.
B. AT FRACTURE AFTER CREEP UNDER σ_c=3400 PSI AT 477°K.
ANNEALED ALUMINUM PRESTRAINED 15% AT 78°K AND RECOVERED TO $\Theta_R = 8.386 \times 10^{-17}$
A. BEFORE CREEP TESTING.
B. AT FRACTURE AFTER CREEP UNDER σ_c=3400 PSI AT 477°K.

Fig. 20. X-ray back reflection photograms of annealed and worked aluminium before and after creep testing (FRENKEL, SHERBY and DORN 1953).

6. Stress Law for Creep

Many attempts have been made to determine the effect of stress on creep. In general this has been done by determining the effect of stress on the secondary creep rate, as shown by the $Z - \sigma$ data presented in Fig. 17. Although, as previously described, the same structure is obtained during secondary creep at the same stress independent of the test temperature, a systematic sequence of different structures are developed as a function of stress. Thus as shown by the back-reflection Debye-Scherrer diagrams and photomicrographs of Fig. 19, the $Z - \sigma$ data of Fig. 17 reflect not only the effect of stress but also the effect of structural differences on the creep rate.

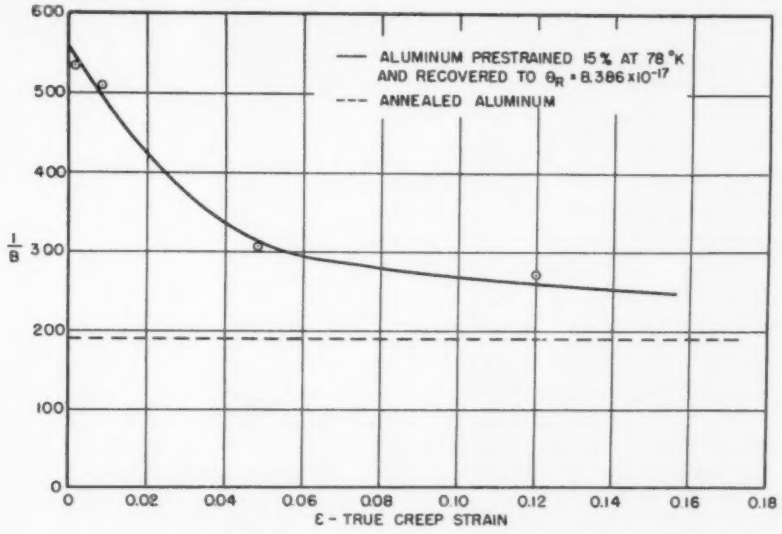

Fig. 21. Effect of creep on $1/B$ for cold-worked aluminium under a constant load of 4,000 psi at 447°K. (Data of Frenkel, Sherby and Dorn 1953).

The stress law for creep can be isolated only by employing test procedures that permit the evaluation of the effect of stress on the creep rate for the same structure. Preliminary tests (Sherby, Frenkel, Nadeau and Dorn 1954) having this objective in mind were conducted by prestraining a series of specimens under the same constant load to the same strain and then reducing the true stress to a series of lower values. Following the drop in true stress the instantaneous creep rate was determined as a function of the new true stress. Inasmuch as each specimen of the series was crept the same amount under the same load, each specimen had the same structure developed in it at the instant the stress was reduced. Increasing the stress was avoided because the instantaneous creep strain introduced upon increase of the stress would have modified the structure in a way dependent upon the magnitude of the adjusted stress. When the natural logarithm of the instantaneous creep rate was plotted as a function of the stress, the linear correlation illustrated in Fig. 18 was obtained. These data reveal that

$$\dot{\epsilon} = Ae^{B\sigma} \tag{9}$$

where B is the slope of the $\ln\dot{\epsilon} - \sigma$ plot. In general B appears to be approximately constant, independent of the precreep conditions of loads or strains. Since the structure generated during creep is dependent on the precreep conditions of load and strain, it follows that B is insensitive to the structural changes attending the creep of initially annealed metals. Furthermore, the data of Fig. 9 reveal that B is insensitive to the test temperature. Therefore the creep rate following a decrease in stress can be correlated by

$$\dot{\epsilon} = S' e^{-\Delta H/RT} e^{B\sigma} \tag{10}$$

where, within the limits of experimental error, ΔH and B are substantially constant for a given material. Thus S' is the only-structure sensitive parameter of (10).

Although B is insensitive to the structural changes occurring during high temperature creep of annealed specimens, it is sensitive to cold work (FRENKEL, SHERBY and DORN 1953). The back-reflection Debye-Scherrer X-ray photograms of Fig. 20 reveal in part the structural modifications introduced in a cold worked and partially recovered specimen of aluminium. The $1/B$ values from such initially cold worked and partially recovered specimens are given by the data of Fig. 21. Thus cold working increases $1/B$ and the $1/B$ value changes during subsequent creep, finally approaching the value appropriate for that obtained from an initially annealed specimen. The X-ray photograms of Fig. 20 reveal that almost identical subgrain structures are obtained following extensive creep under identical conditions, independent of the initial state of the material. As shown in Fig. 22, $1/B$ increases almost linearly with the atomic percent of alpha solid solution alloying additions.

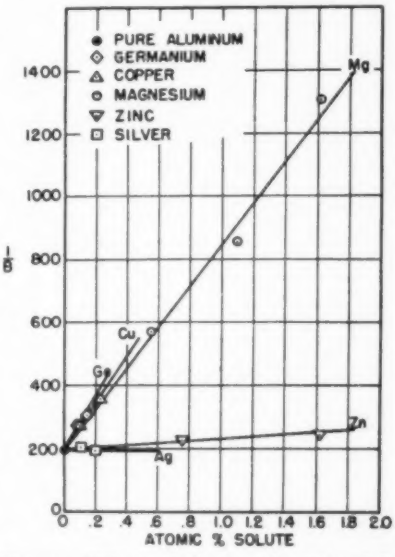

Fig. 22. Effects of alloying elements of the parameter $1/B$ for creep. (Data of SHERBY, FRENKEL, NADEAU and DORN 1954).

Obviously (10) cannot be valid for low stresses since $\dot{\epsilon}$ must vanish as σ approaches zero. A new series of investigations were therefore conducted (LAKS 1953) to ascertain what the stress law for creep might be at very low stresses. If the applied stresses are sufficiently low, the initial creep strain is zero, as shown in Fig. 23, and the initial creep rate is therefore that appropriate to the annealed state. The linear relationship that was obtained between the logarithm of the initial creep rate and the logarithm of the true stress, as shown in Fig. 24, suggests that over the low range of stresses

$$\dot{\epsilon} = S'' e^{-\Delta H/RT} \sigma^n. \tag{11}$$

Additional confirmation of the nominal validity of this relationship is contained in the low stress-zero initial creep strain data for a series of alpha solid solutions

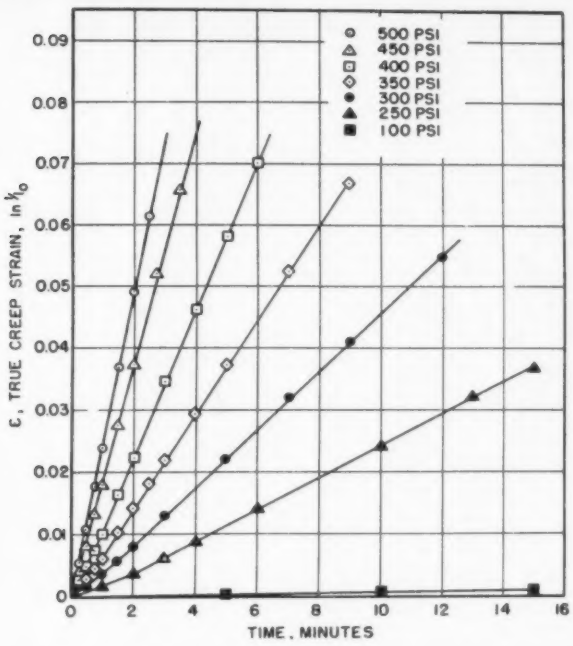

Fig. 23. Constant load creep of aluminium containing 3·1 atomic percent magnesium at low stresses. (Data of H. LAKS 1953).

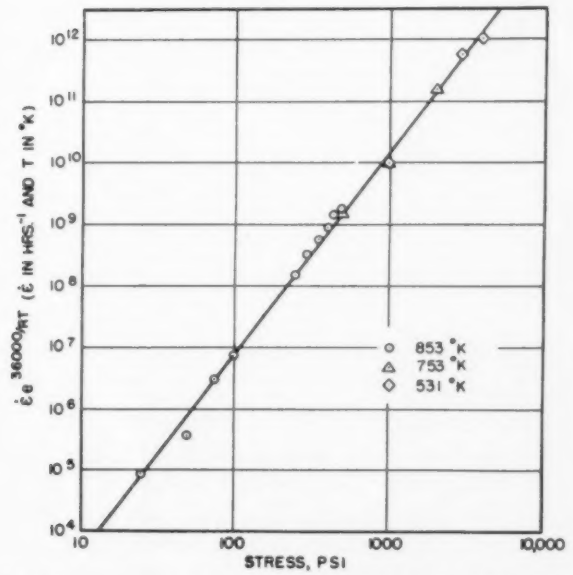

Fig. 24. Effect of small stresses on the creep rate of aluminium containing 3·1 atomic percent magnesium. (Data of H. LAKS 1953).

of Mg in Al shown in Fig. 25. These data reveal that n of (11) decreases with increasing amounts of alloying whereas S'' for the annealed state is practically independent of alloying.

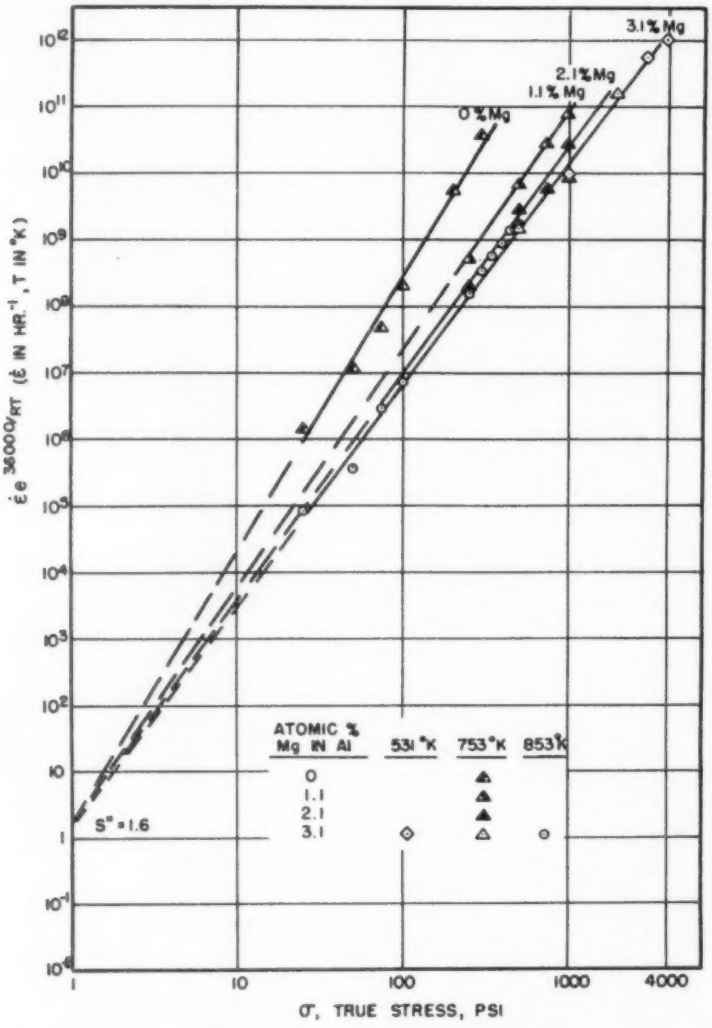

Fig. 25. Effect of solid solution alloying on the initial rate at low stresses.

It is indeed rational to suspect that the high and low stress creep laws defined by (10) and (11) are in no way due to any abrupt change in the mechanism of creep and therefore merely reflect two limiting conditions of a single law for creep. A preliminary test of this hypothesis was obtained by precreeping a series of specimens of aluminium containing 3·1 atomic percent magnesium to a strain of 0·077 at a constant load of 10,000 psi and at 531°K following which the new initial creep rates at various reduced stresses were obtained. As shown by cut *A*

of Fig. 26 the creep rate is proportional to $e^{B\sigma}$ at high stresses whereas cut B of Fig. 26 reveals that it is proportional to σ^n at low stresses under otherwise identical conditions of test. Thus it appears possible to generalize (10) and (11) to read

$$\dot{\epsilon} = S\, e^{-\Delta H/RT}\, \phi(\sigma) \tag{12}$$

where

$$S\,\phi(\sigma) = S'\, e^{B\sigma} \quad \text{for high stresses, and}$$

$$S\,\phi(\sigma) = S''\, \sigma^n \quad \text{for low stresses.}$$

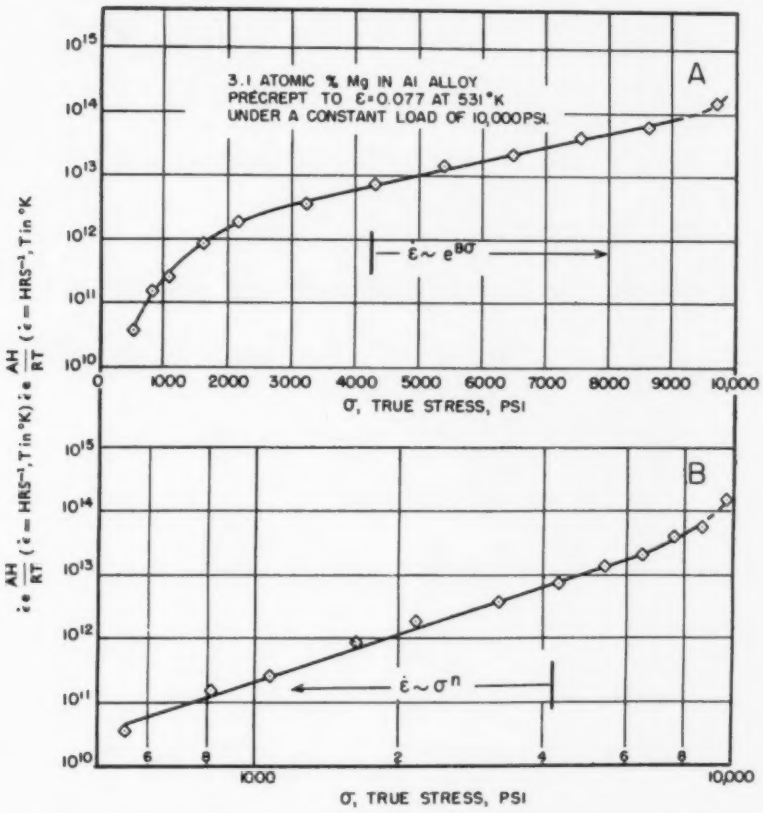
3.1 ATOMIC % Mg IN Al ALLOY
PRECREPT TO ε=0.077 AT 531°K
UNDER A CONSTANT LOAD OF 10,000PSI
A
$\dot{\epsilon} \sim e^{B\sigma}$
$\dot{\epsilon} e^{\frac{\Delta H}{RT}}$ ($\dot{\epsilon}$ = HRS^{-1}, T in °K)
σ, TRUE STRESS, PSI
B
$\dot{\epsilon} \sim \sigma^n$

Fig. 26. Effect of stress on the creep rate for the same structure.

Additional confirmation of this hypothesis is also contained by the data recorded in Fig. 27. For alloys exhibiting vastly dissimilar values of B the transition from $e^{B\sigma}$ to σ^n types of laws should occur at the same values of the total argument $B\sigma$, if a single function exists. The data of Fig. 27 reveal that the high stress creep law is valid above about $B\sigma = 1{\cdot}4$ independent of the value of B.

7. Transient Phenomena

The observations made above suggest that the law for high temperature creep of annealed simple metallic systems might now be fairly simply formulated in

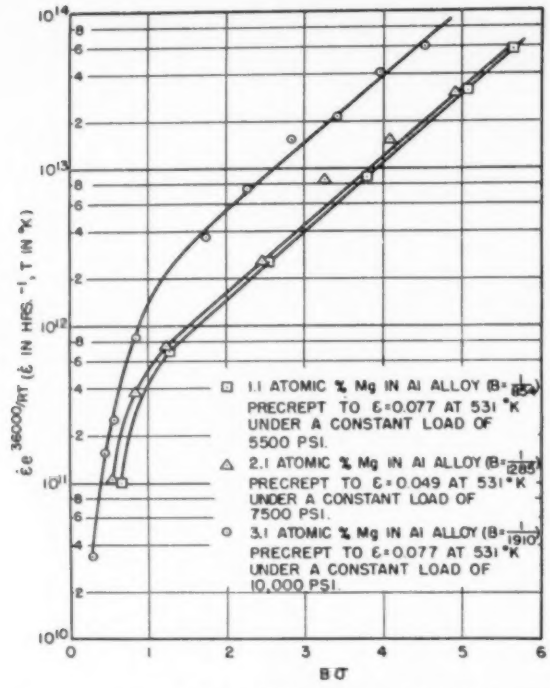
1.1 ATOMIC % Mg IN Al ALLOY (B=1/854)
PRECREPT TO ε=0.077 AT 531 °K
UNDER A CONSTANT LOAD OF
5500 PSI.
2.1 ATOMIC % Mg IN Al ALLOY (B=1/285)
PRECREPT TO ε=0.049 AT 531 °K
UNDER A CONSTANT LOAD OF
7500 PSI.
3.1 ATOMIC % Mg IN Al ALLOY (B=1/1910)
PRECREPT TO ε=0.077 AT 531 °K
UNDER A CONSTANT LOAD OF
10,000 PSI.
Bσ

Fig. 27. Range of validity of high stress creep law in terms of σ.

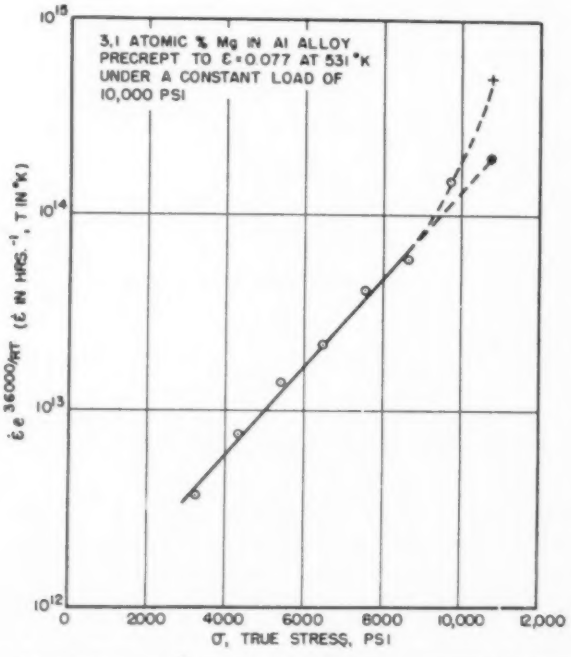

Fig. 28. Failure of $\dot{\epsilon}^{B\sigma}$ reltaionship for small decreases in stress.

terms of (12) where S is the major structure-sensitive parameter. This, however, is not true and much yet remains to be done to clarify some of the details of creep phenomena. In fact it is some of these details which might eventually lead to a more complete understanding of the phenomenon of high temperature creep.

For example (10) was found to be valid for the initial creep strain rate following reduction of the original creep stress. But it is not yet certain that it applies rigorously to the original creep process preceding reduction in stress. In fact the typical example given in Fig. 28 strongly suggests that the linear ln $\dot{\epsilon}$ versus σ curve does not include the last point on the original creep curve (shown by $+$) just preceding the time the stress was decreased. The discrepancy between the actual datum and the extrapolated value (shown by $\oplus$) increases as the original creep stress increases. Inasmuch as the structure must be identical immediately preceding and immediately following a decrease in stress, the reason for this

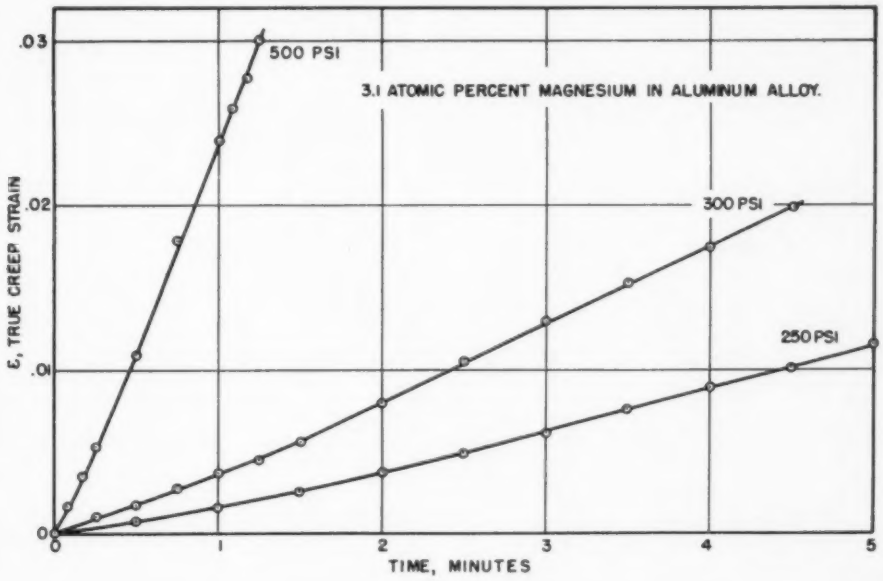

Fig. 29.

somewhat anomalous observation is not readily resolved. It is possible that as the creep stress is decreased only slightly, more barriers of lower strengths become effective in blocking the motion of dislocations thus decreasing the creep rate more rapidly than prescribed by the $e^{B\sigma}$ law. This should continue until the newly applied stress drops below the strength of the weakest barrier. Any additional decrease in stress would no longer cause any additional change in the pattern of effective barriers and therefore for all lower stresses the same stress law, namely $e^{B\sigma}$ or σ^n might apply.

It appears quite definite that an initial creep rate is obtained immediately upon applying the stress even at very low stress (as low as 10 psi). It is this initial creep rate that was used in establishing (11). But over the initial portion of the creep curve this rate increases and reaches a steady-state creep rate before

it exhibits the usual trend of decreasing creep rates over the primary stage. Typical examples of this behaviour are recorded in Fig. 29.

This behaviour might possibly be explained in terms of MOTT's model for high temperature creep (MOTT 1951). Dislocations begin to migrate immediately upon application of the stress. But if high temperature creep occurs primarily as a result of dislocation climb past barriers, some time interval will be required before a steady-state pattern of climbing dislocations can be established. Thus the initial creep rate should at first increase before the primary stage of decelerating creep rates is obtained.

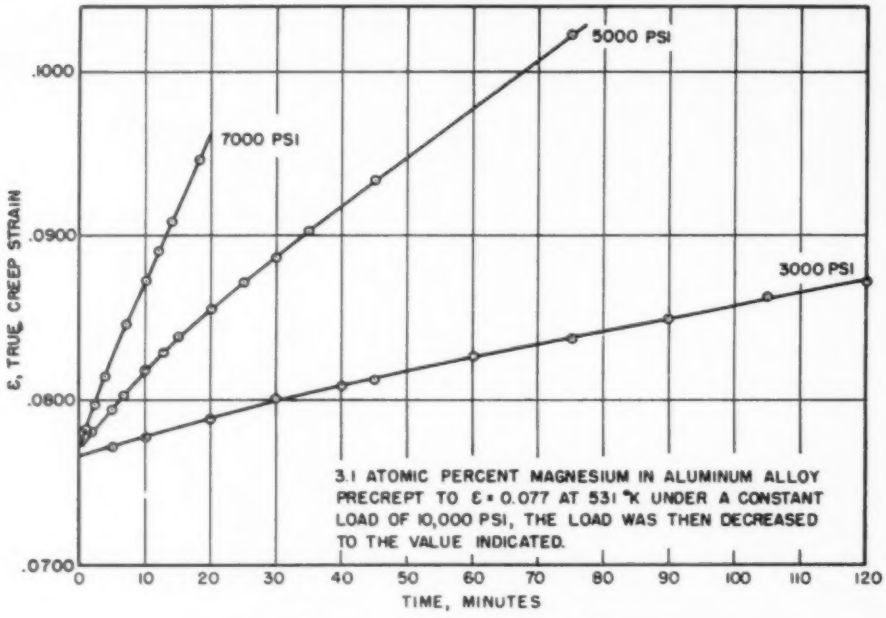

Fig. 30. Transients upon decreasing the stress.

Transients are also observed when the stress is decreased. But in the realm of high temperature creep under discussion here the transients are distinctly different from those previously reported by other investigators (CARREKER, LESCHEN and LUBAHN 1949; COTTRELL and AYTEKIN 1950). As shown by the typical examples of Fig. 30, the creep rate decreases with time following a drop in stress until some steady state is reached. This phenomenon cannot be explained by the crystal recovery mechanisms for transients at lower temperatures postulated by COTTRELL and AYTEKIN (1950) and also KUHLMANN (1951). or by the possible effects of creep recovery. It appears as if these observations might also be explained by MOTT's model for high temperature creep. Under the original high stress a large number of dislocations are in the process of climbing. Inasmuch as the climbing dislocations exist on a series of slip planes they cannot migrate back to their FRANK-READ sources immediately upon reduction of the stress. Consequently more than the steady-state number of dislocations for the new stress are climbing

to circumvent the barriers immediately following a reduction of stress. After an appropriate interval of time, however, the steady-state number for the new stress will be reached.

The two upper curves of Fig. 31 give the relationship between the estimated values of the instantaneous creep rate as well as the steady-state creep rate after the stress was reduced to the reported values. The difference between the instantaneous and steady-state creep rates is minor in the high stress range but it becomes

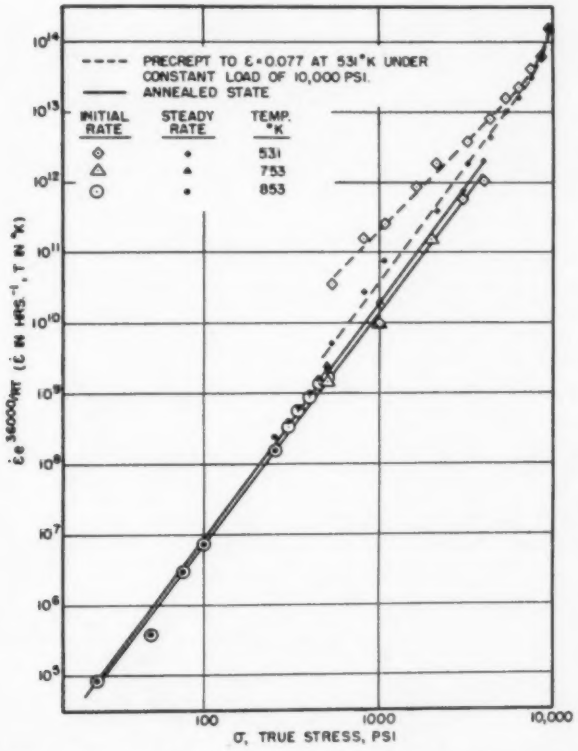

Fig. 31. Comparison of instantaneous and steady state creep rates.

pronounced at the lower stresses. Thus approximately the same values of B and S' are obtained for either the instantaneous or the steady-state creep rates. But in the range of lower stresses where the σ^n law applies n and S'' are quite different for the instantaneous and steady-state creep rates.

The two lower curves of Fig. 31 refer to the steady-state and instantaneous creep rates for the same material in the annealed state immediately following the first application of the stress. In this range the differences between the steady-state and instantaneous creep rates are small and increase only slightly with increase in stress. It may be significant to note that the steady-state value of n on decreasing the stress following precreep agrees well with the steady-state value of n upon first application of the stress, as evidenced by the parallelism between the $\ln \dot{\epsilon}\, e^{\Delta H/RT}$ versus $\ln \sigma$ curves. This agreement in the values of n

for the two steady-state sets of data might have been anticipated inasmuch as the steady-state pattern of dislocations migrating past barriers are presumably the same at the same stress. The difference in the elevation of these curves, however, arises from the fact that S'' is different in the two cases due to the possibility that their patterns of barriers are dissimilar as a result of the dissimilar strain histories in each case.

8. CONCLUSIONS

1. High temperature creep of thermally stable alloys is correlatable by the functional relationship

$$\epsilon = f(\theta), \qquad \sigma = \text{constant}$$

where ϵ = total creep strain
$\theta = t\, e^{-\Delta H/RT}$
t = duration of test
ΔH = activation energy for creep
R = gas constant
T = absolute temperature.

2. Grain boundary shearing obeys a similar functional relationship having the same activation energy.

3. The activation energy for high temperature creep approximates that for self-diffusion.

4. The stress appears to enter the high temperature creep law as σ and not as σ/T.

5. Conclusions 3 and 4 suggest that high temperature creep is not due to thermal activation of dislocations over a barrier but rather occurs as a result of dislocation climb by a self-diffusion process.

6. After an appropriate decrease in stress, the new creep rate is given by

$$\dot{\epsilon} = Se^{-\Delta H/RT}\phi(\sigma)$$

where S appears to depend on the barrier pattern and where

$$\phi(\sigma) \sim e^{B\sigma} \text{ at high stresses}$$

$$\phi(\sigma) \sim \sigma^n \text{ at low stresses.}$$

7. Transients encountered during changes in stress suggest that high temperature creep might be ascribed to a dislocation climb process.

ACKNOWLEDGMENTS

The author wishes to express his sincere appreciation to the Office of Naval Research for their wholehearted support of the investigations on high temperature creep reviewed here. The success of many of these studies were due to enthusiastic cooperation of several colleagues and numerous graduate students at the University of California. The author particularly wishes to acknowledge the substantial contributions made by his colleague, Mr. O. SHERBY, to this programme of investigation.

References

Alexander, B. M., Dawson, M. H. and Kling, H. P.	1951	*J. Appl. Phys.*, **22**, 439-443.
Carreker, R. P., Leschen, J. G. and Lubahn, J. D.	1949	*Transactions, A.I.M.E.*, **180**, 139-146.
Carreker, R. P.	1950	*J. Appl. Phys.*, **21**, 1286-1296.
Cottrell, A. H. and Aytekin, V.	1950	*J. Inst. Metals*, **77**, 389-422.
Cuff, F. B., Jr. and Grant, N. J.	1953	*The Iron Age* **170**, 134-139.
Dushman, S., Dunbar, L. W. and Huthsteiner, H. H.	1944	*J. Appl. Phys.*, **15**, 108-124.
Fazan, B., Sherby, O. D. and Dorn, J. E.	—	*AIME*, to be published in *Journal of Metals*.
Frenkel, R. E., Sherby, O. D. and Dorn, J. E.	1953	Institute of Engineering Research Report, University of California, Berkeley, California, Series No. 22, Issue 29, August 1st.
Giedt, W. H., Sherby, O. D. and Dorn, J. E.	1953	To be published in *Trans. ASME*.
Graeser, W., Hanemann, H. and Hofmann, W.	1943	*Z. Metallkunde*, **35**, 1-13.
Grassi, R. C., Bainbridge, D. W. and Harmon, J. W.	1951	Institute of Engineering Research Report, University of California, Berkeley, Series No. 22, Issue No. 28, July 1st.
Greenough, G. B. and Smith, Edna	1950	*J. Inst. Metals*, **77**, 435-443.
Hazlett, T. H., Parker, E. R. and Nathans, M.	1950	Institute of Engineering Research Report, University of California, Berkeley, Series No. 28, Issue No. 8.
Kaufman, A. R., Gordon, P. and Lillie, D. W.	1950	*Trans. ASM.*, **42**, 785-844.
Kauzman, W.	1941	*Trans. AIME.*, **143**, 57-83.
Kuhlmann, D.	1951	*Proc. Phys. Soc.*, **64A**, 140-155.
Laks, H.	1953	M.S. Thesis, College of Engineering, University of California, Berkeley, California.
McKeown, J.	1937	*J. Inst. Metals*, **60**, 201-228.
McLean, D.	1951	*J. Inst. Metals*, **80**, 507-519.
	1952	*J. Inst. Metals*, **81**, 133-144.
	1952	*J. Inst. Metals*, **81**, 287-292.
	1952	*J. Inst. Metals*, **81**, 293-300.
Mott, N. F.	1951	*Proc. Phys. Soc.*, **64**, 729-741.
Mott, N. F.	1953	*Phil. Mag.*, **44**, series 7, 742-765.
Nadai, A. and Manjoine, M. J.	1941	*Trans. ASME.*, **63**, A-77-A-91.
Nowick, A. S. and Machlin, E. S.	1947	*J. Appl. Phys.*, **18**, 79-87.
Orr, R. L. and Bainbridge, D. W.	1953	Institute of Engineering Research Report, University of California, Berkeley, Series No. 22, Issue No. 28, July 1st.
Orr, R. L., Sherby, O. D. and Dorn, J. E.	1954	*Trans. ASM.*, **46**.
Orr, R. L., Sherby, O. D. and Dorn, J. E.	1954	*J. Metals, AIME.*, 71-80.
Parke, R. M.	1951	*Met. Prog.*, **60**, No. 1, 81-96.
Pomp, A. and Lange, W.	1936	Mitt. Kaiser-Wilhelm Institute Eisenforschung Zu Dusseldorf, **18**, 51-63.
Roberts, C. S.	1953	*J. Metals, AIME*, 1121-1125; see discussion of paper by O. D. Sherby and R. E. Frenkel.

Vol. 3 54/55

SCHWOPE, A. D.		Personal communication. Battelle Memorial Institute, Columbus, Ohio.
SEITZ, R. and READ, T. A.	1941	*J. Appl. Phys.*, **12**, 57-83.
SEITZ, R.	1952	*Advances in Physics*, **1**, 43-89.
SEMCHYSHEN, M. and HOSTETTER, H.	1952	Third Annual Report, NR-O34-401, Climax Molybdenum Company of Michigan.
SERVI, I. S. and GRANT, N. J.	1951	*Trans. AIME.*, **191**, 917-922.
SERVI, I. S. and GRANT, N. J.	1951	*Trans. AIME.*, **191**, 909-916.
SHERBY, O. D. and DORN, J. E.	1952	*Trans. AIME*, **194**, 959-964.
SHERBY, O. D. and DORN, J. E.	1953	*J. Metals, AIME.*, **5**, 324-330.
SHERBY, O. D., FRENKEL, R., NADEAU, J. and DORN, J. E.	1954	*J. Metals, AIME.*, 275-279.
SMITH, A. A., Jr.	1941	*Trans. AIME.*, **143**, 165-171.
SMITH, A. A., Jr. and HOWE, H. E.	1945	*Trans. AIME.*, **161**, 472-477.
TAPSELL, H. J. and GLENSHAW, W. J.	1927	Great Britain Dept. of Science and Industrial Research, Special Report No. 1.
WOOD, W. A. and WILMS, G. R.	1949	*J. Inst. Met.*, **75**, 693-706.
WOOD, W. A., WILMS, G. R. and RACHINGER, W. A.	1949	*J. Inst. Metals*, **79**, 159-172.
WYON, G. and CRUSSARD, C.	1951	*Revue de Metallurgie*, **48** (2), 121-130.
ZENER, C. and HOLLOMON, J. H.	1944	*Trans. ASM.*, **33**, 163-235.
ZENER, C. and HOLLOMON, J. H.	1944	*J. Appl. Phys.*, **15**, 22-32.

VOL 3 1954

Journal of the Mechanics and Physics of Solids, 1954, Vol. 3, pp. 117 to 129. Pergamon Press Ltd., London.

LOAD-CARRYING CAPACITIES FOR CIRCULAR PLATES OF PERFECTLY-PLASTIC MATERIAL WITH ARBITRARY YIELD CONDITION

By H. G. Hopkins and A. J. Wang
Division of Applied Mathematics, Brown University

(*Received 5th August*, 1954)

Summary

This paper is concerned with the load-carrying capacities of thin circular plates made of a perfectly-plastic material that obeys an arbitrary yield condition and the associated flow rule. Attention is confined to support conditions and fairly general loading distributions that are rotationally-symmetric. In certain special cases only is it possible to derive solutions in simple closed form but, in general, it is always straightforward to derive approximations, correct to within any desired degree of accuracy, to the exact solutions through routine numerical integration of the basic equations. The procedure is illustrated through a discussion of problems involving the von Mises and parabolic yield conditions.

Vol. 3 54/55

1. Introduction

The load-carrying capacities of perfectly-plastic circular plates have been discussed by Pell and Prager (1951), Hopkins and Prager (1953), and Drucker and Hopkins (1954). Pell and Prager (1951) discussed this problem for material obeying the von Mises yield condition, and took the plate to be simply-supported and subjected to uniformly-distributed loading. Their analysis involved the use of the limit design theorems of Drucker, Greenberg and Prager (*see* Prager and Hodge 1951), and only an approximate value of the load-carrying capacity was found. Hopkins and Prager (1953) discussed the problem for material obeying the Tresca yield condition, and gave exact solutions of problems in which the plate was either simply-supported or built-in at its edge, and was subjected to certain simple types of rotationally-symmetric loading. Drucker and Hopkins (1954) have observed recently that it is straightforward to determine numerical results, to within any desired degree of accuracy, for more general rotationally-symmetric problems involving any yield condition and a loading distribution of a fairly general type. As an example of this extension of the work of Pell and Prager (1951) and Hopkins and Prager (1953), these authors treated the following problem. The Tresca yield condition was assumed. The load-carrying capacity was then found for an over-hanging plate subjected to both a central force and a uniformly-distributed load within the support circle. This solution is exact. The essential feature in all the above problems occurs also in the problem of the cylindrical shell under radial pressure treated by Drucker (1953). In both classes

of problems direct integration of the equations of equilibrium, after use of the yield condition, leads simply to the determination of the load-carrying capacity once certain boundary conditions are specified. The associated flow rule only needs to be considered if the velocity field is to be found, although of course the bending moment field is only admissible if there is a velocity field which is compatible with this bending moment field. In other words the analysis of the present paper refers to problems in which the load-carrying capacity of the plate is found through integration of an equation of equilibrium between two points on the yield curve, these points corresponding in the simplest case to the plate centre and edge. Only in certain special cases is it possible to derive solutions in simple closed form, but, in general, it is always straightforward to derive approximations (correct to within any desired degree of accuracy) to the exact solutions through routine numerical integration of the basic equations. The purpose of this paper is to illustrate this procedure through the treatment of certain fundamental problems. In general the determination of the load-carrying capacity for a plate is simplest when the yield curve is polygonal in shape as is the case, for example, with the Tresca yield condition. This is due to the fact that only linear equations then need to be considered. In other cases non-linear equations occur, and now in general numerical techniques must be used. Thus, as will be seen, the replacement of the Tresca yield condition by that of von Mises usually renders an analytical solution impractical. HILL (1952) has discussed the question of determining bounds to the errors committed when any approximate theory of plasticity is used to estimate load-carrying capacities. In particular if the von Mises yield function and plastic potential are the standard of comparison, and if both are approximated by the Tresca yield function, then the error in the load-carrying capacity can in certain cases be limited to within $\pm 8\%$. In the problems considered here the maximum possible magnitude of such errors will be intuitively obvious, and a formal proof is unnecessary.

The present theory only treats a greatly simplified model of the actual physical problem of the behaviour of a plate under load, because elastic and plastic deformation, and bending and membrane action, all influence in varying degrees the deformation versus load characteristics of the plate. Although a number of papers have been published on various aspects of this general problem, there is, owing to its complexity, as yet no completely satisfactory theory. A complete discussion of previous work in this field is outside the scope of this paper. However, some brief remarks are appropriate on the interpretation to be given to the loads obtained by the present analysis. Firstly, the loads are correctly those loads required to initiate plastic deformation when the material is plastic-rigid. In this case the subsequent behaviour of the plate depends upon whether or not there is strain-hardening. If there is strain-hardening then the deformation will not proceed save under immediate increase in applied load. Further, whether or not there is strain-hardening, increase in applied load will be required as soon as membrane action becomes a significant factor. Secondly, if the plate material is non-hardening plastic-elastic, and if membrane action be neglected, then the ultimate load-carrying capacity of the plate is that given by the present theory. These remarks need to be borne in mind when comparison is made with experimental results. SOKOLOVSKY (1944) has discussed the elastic-plastic bending of circular plates. The analysis is

based upon Hencky's deformation theory applied to a strain-hardening material obeying the von Mises yield condition, and the usual assumptions of the conventional theory of thin elastic plates are made. Load versus deflection curves are given for various cases. Although it is well-known that in general a deformation theory is incorrect, some of the results obtained in this way are in good agreement with the analysis of HOPKINS and PRAGER (1953) and of this paper. In particular there is exact agreement with the results for a concentrated load acting on a simply-supported plate whose material obeys the Tresca yield condition.

2. EQUATIONS OF EQUILIBRIUM AND FLOW RULE

The notation used in this paper is now described. It is convenient to think of the plate as being horizontal. Let r be distance measured from the plate centre, with $r = R$ corresponding to the plate edge. The pressure applied to the plate is $p(r)$, downwards-acting pressure being reckoned as positive. The radial and circumferential bending moments $M(r)$ and $N(r)$, respectively, are reckoned positive when these moments tend to stress the lower surface of the plate in tension. The vertical shear force, $Q(r)$ per unit arc length, transmitted across the section $r = \text{const.}$ is reckoned positive when the tendency is to produce downwards deflections of the middle surface. Finally, let $w(r)$ be the downwards velocity of points in the middle surface.

Vol. 3 54/55

The analysis given here is in the spirit of the theory of thin plates. Thus the state of stress and motion at initial yielding of the plate is expressed entirely through the quantities M, N, Q and w, all functions only of r.

The equations of equilibrium are

$$\frac{d}{dr}(rQ) + rp = 0, \tag{1}$$

$$\frac{d}{dr}(rM) = N + rQ. \tag{2}$$

If the boundary conditions do not involve Q then it is sufficient to consider the equation found through the elimination of Q between equations (1) and (2), i.e.

$$\frac{d}{dr}(rM) = N - \int_0^r rp(r)\,dr. \tag{3}$$

The yield condition is expressed analytically by giving the relationship between M/M_0 and N/M_0, say

$$f(M/M_0, N/M_0) = 0, \tag{4}$$

where M_0 is the fully-plastic bending moment, i.e. $M_0 = \sigma_0 h^2$ where σ_0 is the yield stress in tension (or compression) and $2h$ is the plate thickness. The yield condition $f = 0$ corresponds to a curve drawn in a plane in which the radial and circumferential bending moments are taken as rectangular cartesian co-ordinates. This curve must be closed and must contain the origin. No restriction is involved in choosing the sign of f so that $f < 0$ or > 0 at a point $P(M, N)$ according as P lies inside or outside the yield curve. Further, general theory requires the curve to be symmetrical about the bisectors of the co-ordinate axes and to be everywhere

concave towards the origin. Two particularly important yield conditions are those of Tresca (*see* Fig. 1 (a)) and von Mises (*see* Fig. 1 (b)). In the first case the yield curve is a hexagon and in the second it is an ellipse. Note that the value of M_0 may be so chosen that the bending moment states A, B, C, D, E, F separately coincide for both cases. A parabolic yield condition (see Fig. 1 (c)) has also been suggested by VON MISES (1949) but this yield condition, unlike the other two, does not appear to have any simple physical interpretation and was devised for purely mathematical reasons. The reader should note that, although reference is made here to theoretical yield conditions, any empirical yield condition based directly upon experimental data may always be used in connection with the present analysis if a better approximation to the actual yield curve is required.

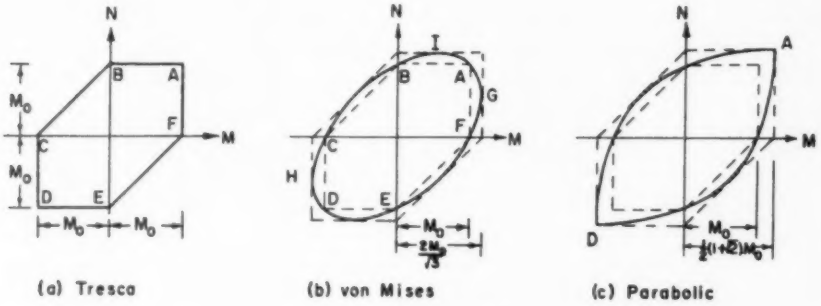

Fig. 1. Yield conditions.

The state of stress at any section $r = \text{const.}$ of the plate is represented by a point P with co-ordinates M, N. This point lies either within or on the yield curve, but in the absence of strain-hardening cannot lie outside. In the former case the plate must remain rigid at that section, but in the latter case it may deform plastically. If the latter situation applies then, taking the plastic potential to coincide with the yield function, the associated flow rule demands that the curvature-rate vector with components

$$\kappa = -\frac{d^2 w}{dr^2}, \qquad \lambda = -\frac{1}{r}\frac{dw}{dr}, \tag{5}$$

is parallel to the outwards-drawn normal at P to the yield curve. Thus

$$\kappa = A\frac{\partial f}{\partial M}, \qquad \lambda = A\frac{\partial f}{\partial N}, \tag{6}$$

where A is non-negative but is otherwise indeterminate. The above assumes that the yield curve has a continuously-turning tangent at P so that there is a well-defined normal at P. This is true of course everywhere for the von Mises yield condition (*see* Fig. 1 (b)), but it is not true for the Tresca yield condition at the vertices of the hexagon $ABCDEF$ (*see* Fig. 1 (a)). The yield curve is said to be regular at a point if $\partial f/\partial M$ and $\partial f/\partial N$ are continuous there, and otherwise is said to be singular there. The flow rule represented by equations (5) and (6) needs modification at a singular point. Two points of view appear permissible. On the

one hand, from a geometrical viewpoint, a singularity may be regarded as a limiting condition. On the other hand, from a physical viewpoint, a singularity may be regarded as due to the simultaneous operation of two flow mechanisms. In either case the generalization of the flow rule is

$$\left.\begin{aligned} \kappa &= A(1-\theta)\left(\frac{\partial f}{\partial M}\right)_1 + A\theta\left(\frac{\partial f}{\partial M}\right)_2, \\ \lambda &= A(1-\theta)\left(\frac{\partial f}{\partial N}\right)_1 + A\theta\left(\frac{\partial f}{\partial N}\right)_2, \end{aligned}\right\} \quad (0 \leqslant \theta \leqslant 1), \tag{7}$$

where the subscripts refer to limiting values immediately to either side of the (isolated) singular point. Equations (6) and (7) coincide at regular points.

3. Tresca Yield Condition

As already mentioned a number of problems have been solved for the case of the Tresca yield condition. These solutions are of interest here only in so far as comparison may be made with the solutions obtained here for the corresponding problems that involve either the von Mises or the parabolic yield condition. In this way the influence of the yield condition on the load-carrying capacity may be estimated. Note that with the Tresca yield condition the relation $f(M/M_0, N/M_0) = 0$ is always linear, and hence the elimination of N between the equilibrium equation (3) and the yield condition always results in a linear differential equation. Thus the solution of the problem is necessarily simple.

4. Von Mises Yield Condition

The von Mises yield condition is given by

$$f = (M^2 - MN + N^2)/M_0^2 - 1 = 0 \tag{8}$$

or, equivalently,

$$2N/M_0 = M/M_0 \pm (4 - 3M^2/M_0^2)^{1/2} \tag{9}$$

where the positive or negative sign is to be taken according as the point $P(M, N)$ lies on either the arc $GABCH$ or the arc $HDEFG$ (*see* Fig. 1 (b)). Equation (3) therefore becomes

$$\frac{d}{dr}(rM) = \tfrac{1}{2}M \pm \tfrac{1}{2}(4M_0^2 - 3M^2)^{1/2} - \int_0^r rp(r)\,dr \tag{10}$$

which is a first order, non-linear, ordinary differential equation. Although integration of this equation in simple closed form is seldom possible, approximate numerical integration is always straightforward. The simplest approach is through the method of isoclines but step-by-step methods may also be used (*see*, for example, Hartree 1952). The integration of (10) will now be discussed for some specific problems in which the plate is entirely plastic.

(a) *Simple edge support*

If the plate edge is simply-supported then

$$M(R) = 0, \tag{11}$$

and as there is stress isotropy at the plate centre

$$M(0) = N(0) = M_0, \tag{12}$$

these bending moments being positive. Thus the centre and edge of the plate are in plastic regimes A and B, respectively.

Consider first the case when there is uniform load p over the entire plate so that (10) is

$$\frac{d}{dr}(rM) = \tfrac{1}{2}M + \tfrac{1}{2}(4M_0^2 - 3M^2)^{1/2} - \tfrac{1}{2}pr^2 \quad (0 \leqslant r \leqslant R). \tag{13}$$

Introduce the non-dimensional independent and dependent variables x and y respectively defined by

$$y = M/M_0, \qquad x = (pr^2/M_0)^{1/2} = (P/\pi M_0)^{1/2}\, r/R, \tag{14}$$

P being the total applied load. Then $y = y(x)$ satisfies the equation

$$\frac{d}{dx}(xy) = \tfrac{1}{2}y + \tfrac{1}{2}(4 - 3y^2)^{1/2} - \tfrac{1}{2}x^2 \quad (0 \leqslant x \leqslant x_2 = (P/\pi M_0)^{1/2}) \tag{15}$$

and the condition

$$y(0) = 1. \tag{16}$$

Further the value of P is found from the requirement (equation (11)) $y(x_2) = 0$.

Now when the Tresca yield condition is assumed, the solution is known to be

$$y = 1 - x^2/6 \qquad (0 \leqslant x \leqslant x_2 = \sqrt{6}) \tag{17}$$

(*see* HOPKINS and PRAGER 1953). It is reasonable to regard this solution with the value of x_2 left free as a first approximation in the development of an iterative solution of (15). In this case a second approximation results from the integration of

$$\frac{d}{dx}(xy) = \tfrac{1}{2} - \frac{7}{12}x^2 + \tfrac{1}{2}\{4 - 3(1 - x^2/6)^2\}^{1/2} \qquad (0 \leqslant x \leqslant x_2) \tag{18}$$

subject to $y(0) = 1$ and x_2 now being derived from the condition $y(x_2) = 0$. Therefore

$$\left.\begin{aligned} y &= \tfrac{1}{2} - \frac{7}{36}x^2 + \frac{1}{2x}I_1(x), \\ I_1(x) &= \int_0^x [4 - 3(1 - x^2/6)^2]^{1/2}\, dx, \end{aligned}\right\} \quad (0 \leqslant x \leqslant x_2), \tag{19}$$

and

$$\tfrac{1}{2} - \frac{7}{36}x_2^2 + \frac{1}{2x_2}I_1(x_2) = 0. \tag{20}$$

It is straightforward to establish that

$$\left.\begin{aligned} I_1(x) = 2(1 + \alpha)\,\alpha^{-3/2} \Bigg[&\left(\frac{1}{k^2} - 1\right)\{F(\tfrac{1}{2}\pi, k) - F(\phi, k)\} \\ &+ \left(2 - \frac{1}{k^2}\right)\{E(\tfrac{1}{2}\pi, k) - E(\phi, k)\} + \sin\phi\cos\phi\,(1 - k^2\sin^2\phi)^{1/2}\Bigg] \end{aligned}\right\} \tag{21}$$

where

$$\alpha = \tfrac{1}{2}\sqrt{3}, \qquad k = \left(\frac{1 + \alpha}{2}\right)^{1/2} = \sin(75°), \qquad \phi = \arccos\left(\frac{x}{\sqrt{4\sqrt{3} + 6}}\right)$$

$$(0 \leqslant \phi \leqslant \tfrac{1}{2}\pi),$$

F and E being elliptic integrals of the first and second kinds, respectively, with k as modulus. Calculation shows that

$$x_2 \approx 2{\cdot}55\ (> \sqrt{6} \approx 2{\cdot}45) \tag{22}$$

so that

$$p = M_0 x_2^2/R^2 \approx 6{\cdot}51\ M_0/R^2. \tag{23}$$

This result lies between the two results for the Tresca yield hexagons inscribed and escribed to the von Mises ellipse, i.e.

$$p = 6M_0/R^2, \qquad p = 12M_0/\sqrt{3}\ R^2 \approx 6{\cdot}83\ M_0/R^2. \tag{24}$$

Further iterations are not practical, but as will be seen in a moment the result (23) is in very good agreement with that obtained by the isocline method.

The numerical integration of (18) through the method of isoclines is now discussed. Equation (15) is written in the form

$$\left.\begin{aligned} \frac{dy}{dx} &= \frac{1}{x}\,P(x, y), \\ 2P(x, y) &= -y + (4 - 3y^2)^{1/2} - x^2, \end{aligned}\right\} \quad (0 \leqslant x \leqslant x_2). \tag{25}$$

The isolcines of (25) are the family of curves defined by

$$P(x, y) - mx = 0, \tag{26}$$

m being an arbitrary parameter. These isoclines possess the property that any characteristic of (25) must cross the isocline $m = \text{const.}$ with slope m. The point (0,1) is a singular point of the differential equation (25). The isocline $m = \infty$ is the line $x = 0$ (i.e. the y-axis), and the isocline $m = 0$ is the curve $P(x, y) = 0$, i.e. $4y^2 + 2yx^2 + x^4 = 4$. This curve has a very simple shape in the first quadrant. It passes through the point (0,1) with zero slope, and to the right of this point the slope uniformly decreases to the value $-2\sqrt{2}$ when the curve passes through the point $(\sqrt{2},0)$. Now the radial bending moment must uniformly decrease with uniform increase in distance from the plate centre. Hence $dy/dx < 0$ $(x > 0)$ and so only the isoclines

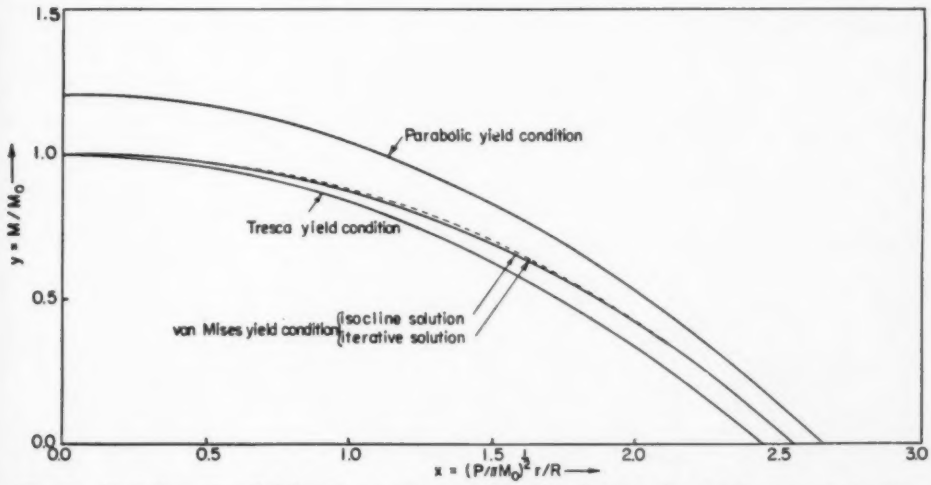

Fig. 2. Variation of radial bending moment with radial distance for simply-supported plate under uniformly-distributed load. Tresca, von Mises and parabolic yield conditions.

for negative m are relevant, these lying outside the isocline $m = 0$. The graphical determination of the required characteristic of (25) is straightforward once a few of these isoclines have been drawn. The result obtained is shown in Fig. 2, and for comparison the results corresponding to

the Tresca yield condition (equation (17)) and the iteration solution (equation (19)) are also shown. Thus it is found that

$$x_2 \approx 2{\cdot}55\ (4) \tag{27}$$

and hence

$$p \approx 6{\cdot}52\ M_0/R^2\ ; \tag{28}$$

these results do not differ significantly from the corresponding results based on the iterative solution (*see* (22) and (23)). The lower and upper bounds obtained from the use of the Tresca yield condition are in error by -8% and $+6\%$, respectively. The accuracy of the iterative solution is very striking. The approximate result of PELL and PRAGER (1951), viz. $p \approx 6{\cdot}33\ M_0/R^2$ is therefore in error by about -3%.

It is straightforward to extend the above analysis to the case when the loading is given by

$$p(r) = \begin{cases} p = \text{const.} & (0 \leqslant r < a), \\ 0 & (a < r \leqslant R), \end{cases} \tag{29}$$

i.e. circular loading. The governing differential equations are now

$$x\frac{dy}{dx} = \begin{cases} -\tfrac{1}{2}y + \tfrac{1}{2}(4-3y^2)^{1/2} - \tfrac{1}{2}x^2 \left(0 \leqslant x \leqslant x_1 = \left(\frac{P}{\pi M_0}\right)^{1/2}\right), \\ -\tfrac{1}{2}y + \tfrac{1}{2}(4-3y^2)^{1/2} - \tfrac{1}{2}x_1^{\,2} \left(x_1 \leqslant x \leqslant x_2 = \left(\frac{P}{\pi M_0}\right)^{1/2}\frac{R}{a}\right), \end{cases} \tag{30}$$

where

$$x = \left(\frac{P}{\pi M_0}\right)^{1/2}\frac{r}{a}, \qquad y = M/M_0, \quad P = \pi a^2 p.$$

In the region $0 \leqslant x \leqslant x_1$ the method of isoclines may be used. However, in this region an iterative solution, based upon the solution for the Tresca yield condition (which, within the loaded region, is still $y = 1 - x^2/6$), is found to yield a close approximation. This procedure considerably simplifies the numerical work with little resulting loss of accuracy. In the region $x_1 \leqslant x \leqslant x_2$ the differential equation is immediately integrable for it can be written in the separable form

$$\frac{dx}{2x} = \frac{dy}{(4-3y^2)^{1/2} - y - x_1^{\,2}}. \tag{31}$$

Hence, as $y(x_2) = 0$, it follows that

$$\tfrac{1}{2}\ln(x_2/x) = I_2(y) = \int_0^y \frac{dy}{x_1^{\,2} - [(4-3y^2)^{1/2} - y]} \qquad (x_1 \leqslant x \leqslant x_2). \tag{32}$$

It is straightforward to establish the result

$$I_2(y) = \tfrac{1}{4}\ln\left\{\frac{b - \sin\phi}{b - \frac{1}{2}\sqrt{3}}\right\} + \tfrac{1}{4}\sqrt{3}\,\{(\phi - \tfrac{1}{3}\pi) + \Phi(\phi)\},$$

$$\Phi(\phi) = \begin{cases} \dfrac{b}{\sqrt{1-b^2}}\ln\left[\left\{\dfrac{1 - b\tan(\phi/2) - \sqrt{1-b^2}}{1 - b\tan(\phi/2) + \sqrt{1-b^2}}\right\}\left\{\dfrac{1 - b/\sqrt{3} + \sqrt{1-b^2}}{1 - b/\sqrt{3} - \sqrt{1-b^2}}\right\}\right] (b<1), \\ 2\left\{\dfrac{1}{(1 - 1/\sqrt{3})} - \dfrac{1}{(1 - \tan(\phi/2))}\right\} (b = 1), \\ \dfrac{2b}{\sqrt{b^2-1}}\left[\arctan\left\{\dfrac{1 - b\tan(\phi/2)}{\sqrt{b^2-1}}\right\} - \arctan\left\{\dfrac{1 - b/\sqrt{3}}{\sqrt{b^2-1}}\right\}\right] (b > 1), \end{cases} \tag{33}$$

where

$$b = \frac{\sqrt{3}}{4}x_1^{\,2} = \frac{\sqrt{3}}{2}(P/2\pi M_0), \qquad \phi = \tfrac{1}{3}\pi - \arcsin\left(\frac{\sqrt{3}y}{2}\right),$$

the inverse tangent and sine lying in the ranges $-\frac{1}{2}\pi$ to $+\frac{1}{2}\pi$ and 0 to $\frac{1}{2}\pi$, respectively. The required continuity of y, i.e. of radial bending moment, at $x = x_1$ expresses a relationship between x_1 and x_2 which corresponds of course to a relationship between $P/2\pi M_0$ and a/R. The corresponding relationship for the case of the Tresca yield condition is simply

$$P/2\pi M_0 = \frac{1}{1 - \frac{1}{3}\frac{a}{R}}, \tag{34}$$

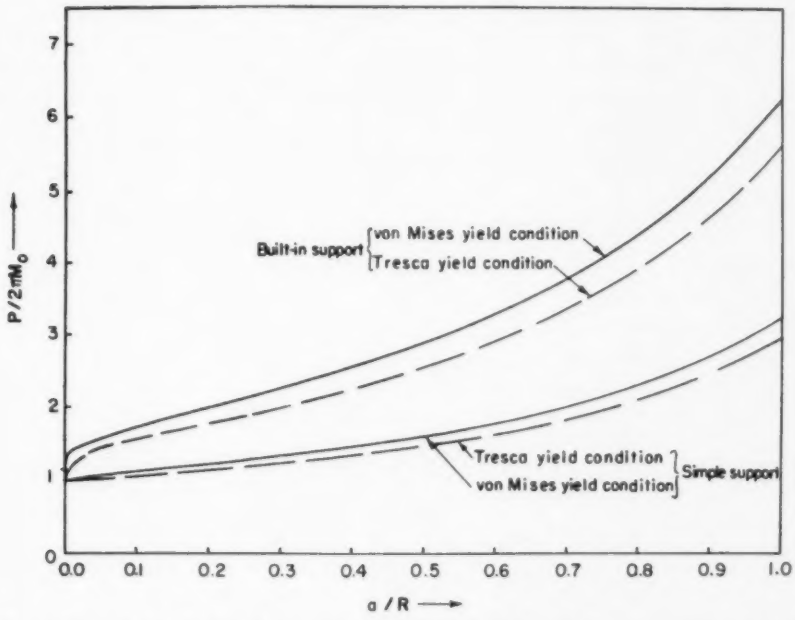

Fig. 3. Variation of load-carrying capacity with size of loaded region. Simple and built-in support conditions. Tresca and von Mises yield conditions.

These relationships for the two yield conditions are shown in Fig. 3. It will be noted that the results for the limiting case of a concentrated load coincide. These special results merit the following discussion. The governing differential equations are (30) with x_2 infinite; and, as before, the first of these equations admits only of numerical integration, but the second equation is separable and therefore is simply integrated. Examination of (32) and (33), after matching of the solution at $x = x_1$, shows that, for $y > 0$, $I_2(y) \to +\infty$ as $b \to \frac{1}{2}\sqrt{2} + 0$ or, equivalently, as $x_1 \to \sqrt{2} + 0$. Thus

$$x_2/x_1 \to +\infty, \qquad P \to 2\pi M_0 + 0, \qquad x_1 \to \sqrt{2} \qquad \text{as} \qquad a \to 0. \tag{35}$$

The same result applies in the case of the Tresca yield condition. In the latter case it may be shown that

$$y = \begin{cases} 1 - x^2/6 & (0 \leqslant x \leqslant \sqrt{2}), \\ 2\sqrt{2}/3x & (x \geqslant \sqrt{2}). \end{cases} \tag{36}$$

Accordingly the radial bending moment $M(r)$ has a discontinuity of amount $-M_0$ at $r = 0$, i.e.

$$M(r) = \begin{cases} M_0 & (r = 0), \\ 0 & (0 < r \leqslant R). \end{cases} \tag{37}$$

The presence of a concentrated load therefore introduces a singularity. It is simple to establish the formula for the concentrated load. A finite discontinuity must now be admitted in $M(r)$; then $M(0) = M_0$ and $M(+0) < M_0$. Also

$$(rM)_r = \left(M_0 - \frac{P}{2\pi}\right) \qquad (0 < r \leqslant R), \tag{38}$$

and, hence if $M(+0)$ is to be finite, it follows that

$$M = \left(M_0 - \frac{P}{2\pi}\right) \qquad (0 < r \leqslant R). \tag{39}$$

The boundary condition $M(R) = 0$ then gives the result. Note that the very centre of the plate is in regime A, and that the remainder of the plate is in regime B. A similar situation applies in the case of the von Mises yield condition.

The reader should note that the case of a 'concentrated' load is not physically realizable. Moreover, near the limit the problem should strictly be treated through a more elaborate analysis that takes into account shearing as well as bending deformations. However, the present results may be expected to be a good approximation if $h < a \leqslant R$. Further the results obviously hold more generally for $p = p(r) \geqslant 0$ $(0 \leqslant r < a)$ where now $P = 2\pi \int_0^a rp(r)\,dr$.

(b) *Built-in edge support*

The extension of the analysis given in (*a*) to treat corresponding problems for built-in edge support does not present difficulties. As before the plate centre is in regime A but the plate edge is now in regime H, this point corresponding to the algebraically-smallest radial bending moment, i.e. $-2M_0/\sqrt{3}$.

If there is uniformly-distributed loading over the entire plate then the isocline method gives

$$x_2 \approx 3{\cdot}54 \tag{40}$$

so that

$$p \approx 12{\cdot}5\, M_0/R^2. \tag{41}$$

This latter result may be compared with the lower and upper bounds obtained through the use of the Tresca yield criterion, viz.

$$p \approx 11{\cdot}26\, M_0/R^2, \qquad p \approx 13{\cdot}00\, M_0/R^2, \tag{42}$$

these being in error by approximately -10% and $+4\%$, respectively. An approximation may also be obtained through an iterative process based on the known solution for the Tresca yield condition, and this agrees within graphical error with the isocline approximation.

It is straightforward to solve the problem when there is circular loading (defined by equation (29)) by the same method described for the case of simple support. Thus within the loaded region the Tresca solution (see HOPKINS and PRAGER 1953) is taken as an approximation; and outside the loaded region the governing differential equation (30) is integrated exactly to give (32) where now the lower limit in the integral is $-2/\sqrt{3}$, results similar to (33) applying. The values obtained for the load-carrying capacity of the plate are shown in Fig. 3, and for purposes of comparison the corresponding results for the Tresca yield condition are also shown. It will be noted that the results for the limiting case of a concentrated load do not coincide, and

$$(P/2\pi M_0)_{\text{Tresca}} = 1, \qquad (P/2\pi M_0)_{\text{von Mises}} = \frac{2}{\sqrt{3}} \approx 1{\cdot}155. \tag{43}$$

These latter results will now be discussed. Examination of the results corresponding to (32) and (33), after matching of the solution at $x = x_1$, shows that for $y > -2/\sqrt{3}$, $I_2(y) \to +\infty$ as $b \to 1 + 0$ or , equivalently, $x_1 \to (16/3)^{1/4} + 0$. Thus

$$x_2/x_1 \to +\infty, \qquad P \to \frac{4}{\sqrt{3}}\,\pi M_0 + 0, \qquad \text{and} \qquad x_1 \to (16/3)^{1/4} \qquad \text{as } a \to 0. \tag{44}$$

The value of the concentrated load for the case of von Mises yield condition therefore exceeds that for the case of the Tresca yield condition by about 16% which is clearly a significant difference. The results corresponding to (36) are easily deduced from HOPKINS and PRAGER (1953). Further, with the Tresca and von Mises yield conditions there are discontinuities in the radial bending moment in the immediate neighbourhood of the plate centre of amounts $-2M_0$ and $-(1+2/\sqrt{3})\,M_0$, respectively.

5. Parabolic Yield Condition

The parabolic yield condition of von Mises (1949) is now considered briefly as a final example. The equation to the yield curve is

$$\left.\begin{aligned} &\frac{N-M}{M_0} = \pm\tfrac{1}{2}\left\{\beta - \frac{1}{\beta}\left(\frac{M+N}{M_0}\right)^2\right\} \\ \text{or, equivalently,}\quad &N/M_0 = -M/M_0 \mp \beta\left[1-\left\{2 \pm \frac{4}{\beta}M/M_0\right\}^{1/2}\right], \\ \text{where}\quad &\beta = \sqrt{2}+1, \end{aligned}\right\} \tag{45}$$

the upper or lower signs being taken according as $N > M$ or $< M$, respectively. Note that the points $A\,(\frac{1}{2}\beta M_0, \frac{1}{2}\beta M_0)$ and D (*see* Fig. 1 (c)) are singular but elsewhere the yield curve is regular. The Tresca, von Mises and parabolic yield conditions have all been made here to fit at the points corresponding to $M = 0$. Note that the parabolic yield curve has a discontinuity in slope of its tangent of amount $\frac{1}{2}\pi$ at the two singular points.

It is obvious that the load-carrying capacity P for the parabolic yield condition must satisfy the relations

$$P_T < P < \tfrac{1}{2}\beta P_T \approx 1{\cdot}20\,P_T, \tag{46}$$

where P_T is the load-carrying capacity for the Tresca yield condition (*see* Fig. 1(c)).

As an example consider the case of a simply-supported plate subjected to uniformly-distributed load over its entire surface. The plate is entirely plastic at initial yielding. Then from equation (45) and previous work, it follows that the problem involves the integration of

$$\left.\begin{aligned} &\frac{dy}{dx} = \frac{1}{x}\,P(x,y), \\ &P(x,y) = -2y - \beta\left\{1-\left(2+\frac{4}{\beta}y\right)^{1/2}\right\} - \tfrac{1}{2}x^2, \end{aligned}\right\} \quad (0 \leqslant x \leqslant x_2), \tag{47}$$

subject to $y(0) = \beta/2$ and $y(x_2) = 0$, x and y being defined as before by (14). This equation is similar in type to (25), and the point $(0, \beta/2)$ is a singular point. Numerical integration through the use of the method of isoclines is straightforward, and this procedure leads to the result

$$x_2 \approx 2{\cdot}66 \tag{48}$$

so that

$$P \approx 7{\cdot}08\,M_0/R^2. \tag{49}$$

This latter result lies between the two results based on the Tresca yield condition,

these being in error by about $-15\frac{1}{2}\%$ and $+1\frac{1}{2}\%$. It should be noted that such *errors* are not in any way absolute because the points of coincidence of the Tresca and parabolic yield curve are arbitrary to some extent. The variation of M with r is shown in Fig. 2.

The examples that have now been discussed establish that in general the basic problem is to integrate a first order, non-linear, ordinary differential equation of type

$$\frac{dy}{dx} = \frac{P(x, y)}{x}, \tag{50}$$

the integration proceeding outwards from a singular point (which may always be taken as (0,1) so that $P(0,1) = 0$). This is always a straightforward numerical problem.

6. Determination of Velocity Fields

It is very important to remember that the results obtained through the preceding analysis may be accepted only if the bending moment field (appropriate to any particular case) can be associated with a velocity field that satisfies the boundary conditions. Only if the yield curve is polygonal in shape (as is the case, for example, with that of Tresca) is the determination of the velocity field simple, and this simplicity is due in turn to the simplicity of the flow rule.

In the case of the von Mises yield condition the flow rule shows that

$$\frac{d^2w}{dr^2} \Big/ \frac{dw}{dr} = \frac{1}{r}\left(\frac{2M - N}{2N - M}\right) = \frac{1}{2r}\left\{\frac{3M}{(4M_0^2 - 3M^2)^{1/2}} - 1\right\}, \tag{51}$$

confining attention to a regime within AH, where M is regarded as a known function of r. Note that $w \geqslant 0$, $dw/dr \leqslant 0$, throughout AH but that $d^2w/dr^2 \leqslant 0$ throughout AI (*see* Fig. 1 (b)) and $d^2w/dr^2 \geqslant 0$ throughout IH, I being the point $\left(\frac{M_0}{\sqrt{3}}, \frac{2M_0}{\sqrt{3}}\right)$, i.e. both w and dw/dr are one-signed but d^2w/dr^2 changes sign at I. It is straightforward to integrate (51) formally under the boundary conditions $w(0) = w_0 (> 0)$ and $w(R) = 0$. The result may be expressed in the form

$$\left.\begin{aligned} w(x) &= w_0 \int_x^{x_2} f(x)\,dx \Big/ \int_0^{x_2} f(x)\,dx \\ \text{where} \qquad f(x) &= \frac{1}{x^{1/2}} \exp\left(-\frac{3}{2}\int_x^{x_2} \frac{1}{x}\frac{y}{\sqrt{4 - 3y^2}}\,dx\right), \end{aligned}\right\} \tag{52}$$

and x, $y = y(x)$ and x_2 are defined as before by equation (14). Therefore the determination of w involves double quadratures. The numerical calculations are straightforward but have not been made. Results similar to (52) will apply for other yield conditions. However, the important fact is that the existence of the velocity field is established, and therefore the previous bending moment fields are correct.

Acknowledgment

The results presented in this paper were obtained in the course of research

sponsored by the Ballistic Research Laboratories, Aberdeen Proving Ground, under Contract DA-19-020-ORD-798.

References

Drucker, D. C.	1953	Proc. 1st Midwestern Conf. Solid Mech. (University of Illinois, Urbana), 158.
Drucker, D. C. and Hopkins, H. G.	1954	Proc. 2nd U.S. Nat. Cong. Appl. Mech. (Amer. Soc. Mech. Engrs., New York), in press.
Hartree, D. R.	1952	*Numerical Analysis* (The Clarendon Press, Oxford).
Hill, R.	1952	*Phil. Mag.*, **43**, 353.
Hopkins, H. G. and Prager, W.	1953	*J. Mech. Phys. Solids*, **2**, 1.
Mises, R. von	1949	Reissner Anniversary Volume, 415 (J. W. Edwards, Ann Arbor).
Pell, W. H. and Prager, W.	1951	Proc. 1st U.S. Nat. Cong. Appl. Mech. (Amer. Soc. Mech. Engrs., New York), 547.
Prager, W. and Hodge, P. G.	1951	*Theory of Perfectly Plastic Solids* (John Wiley and Sons, Inc., New York).
Sokolovsky, V. V.	1944	*Prikl. Mat. Mekh.*, **8**, 141.

Vol. 3 54/55

Journal of the Mechanics and Physics of Solids, 1954, Vol. 3, pp. 130 to 142. Pergamon Press Ltd., London.

A THEORY OF THE TENSILE AND COMPRESSIVE TEXTURES OF FACE-CENTRED CUBIC METALS

By J. F. W. Bishop
Mechanical Engineering Research Laboratory, East Kilbride.

(*Received* 14*th June*, 1954)

Summary

The theory assumes that each grain in the aggregate undergoes the macroscopic strain. The possible rotations of a representative set of grains due to a small increment of strain are computed. It is found that in each grain a range of rotations can occur. A hypothesis is advanced to account for the different textures observed under similar straining conditions by metals of the same lattice type. This is to the effect that the texture developed is determined by the relative hardening of active and latent glide systems. A further hypothesis enables the influence of specific types of hardening to be assessed. Diagrams compare observed and predicted textures.

Vol 3 1954/

1. Introduction

Previous theories of the deformation textures of polcrystalline aggregates of face-centred cubic metals have been of two main kinds depending on whether assumptions are made about the stress or the strain in each grain. Theories of the former kind include those of Boas and Schmid (1931), Pickus and Mathewson (1939) and Calnan and Clews (1950). The latter theory is due to Taylor (1938a). The reader is referred to Barrett (1953) for an account and critical evaluation of these theories. The theory of Boas and Schmid can be criticised on the grounds that the resolved shear stresses on the glide planes which are taken to be active do not obey the critical shear stress law. Further the assumed mechanism of deformation would not allow of the aggregate remaining cohesive after straining. Similar objections apply to the theory of Pickus and Mathewson. Calnan and Clews formulate a theory which solves the difficulty of unequal resolved shear stresses on the active glide-planes, but is then open to the objection that the stresses assumed to operate in each grain are not in equilibrium across grain boundaries. Their model is also open to the objection that it would result in a lack of cohesion on straining, although in this respect it is considerably more realistic than the previous theories of this type. The theory of Taylor assumes that each grain undergoes the same strain as the aggregate. Taylor advances a minimum shear hypothesis which enables the operative glide systems to be found. The objections to this theory are firstly that stress and stress equilibrium are not considered at all, and secondly that the minimum shear hypothesis is proposed by analogy with non-conservative mechanical systems. All of these theories lead to predicted deformation textures which are in general qualitative agreement with observed results, although none accounts for the different textures developed by

metals of similar lattice structure undergoing similar distortions. CALNAN and CLEWS put forward a tentative suggestion that this latter effect may be attributable to the operation of a temperature dependent mechanism. The most satisfactory of these theories from the physical viewpoint is that of TAYLOR in that there is no immediately obvious inconsistency either in displacement continuity at grain boundaries or in violation of the Schmid Law.

2. EXPERIMENTAL EVIDENCE

In this paper only the tensile and compressive textures of face-centred cubic metals are considered. It is convenient to represent the preferred orientation on a sterographic diagram as follows. Consider a sterographic projection of each grain made relative to the cubic axes with the (100) direction as pole. The compressive or tensile axis, hereafter called the specimen axis, can be represented by a point on the projection. The symmetry of the lattice ensures that this point can be taken

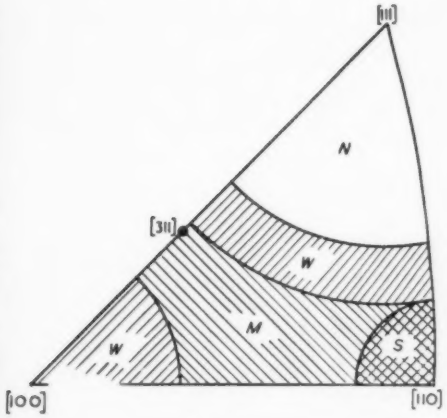

Fig. 1.

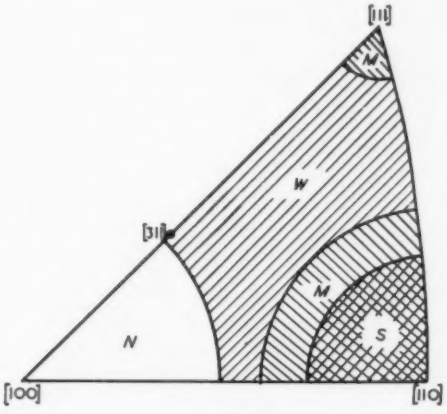

Fig. 2.

to lie within or upon the curvilinear triangle specified by vertices at (100), (110) and (111). If the projections for all the grains of an isotropic aggregate are superposed, the points representing the specimen axes will correspond to a uniform distribution on the projection sphere. The development of a deformation texture can be characterized by a probability distribution giving the likelihood of finding a specific orientation relative to the specimen axis. On the superposed sterographic projections this will appear as a non-uniform distribution of the specimen axis projections. Fig. 1, due to BARRETT and LEVENSON (1940), shows the compression texture developed in 99.95% pure aluminium after 99·9% reduction in height by compression to 84% followed by compression rolling, i.e. compression by repeated rolling in different directions with a small reduction at each pass. The preferred orientation was determined by X-ray diffraction, and the code N = none, W = weak, M = medium and S = strong refers to the intensity of the X-ray lines. The authors state that the boundaries between the regions are not well defined and for convenience are represented by circular arcs with suitable radii.

The general texture is (110) with a spread from (110) to (311). BARRETT and LEVENSON state that a half of the orientations differ by more than 10° from (110). According to BARRETT (1953, p. 447), unpublished work by BARRETT and LAYLAND shows that the compression textures of nickel and copper are almost identical to that of aluminium. The texture of 70-30 brass differs from these although it is also face-centred cubic. Fig. 2 given by BARRETT (1953, p. 448) shows the results obtained in his unpublished work on α-brass. The results are for compression rolling with a 97% reduction and were obtained by X-ray methods. Again the boundaries must be regarded as rather tentative, but the spread from (110) to (311) obtained with aluminium, nickel and copper is by no means so well defined. According to HIBBARD and TROUT (1949) a texture similar to that reported for α-brass is developed under compression by a 3·69% and a 7·76% alloy of aluminium in copper. The reduction was 90% and the textures were found by X-rays. The deformations leading to all these results were very heavy, and the textures can reasonably be regarded as 'end' textures. BARRETT and LEVENSON investigated the deformation of specific grains with increasing strain. They found that each grain *invariably* deformed inhomogeneously and developed a *range* of new orientations. The reader is referred to the original excellent paper for the actual results. This topic will be reverted to later in the present paper. It is remarked here that the spread of orientations in each grain relative to the specimen axis after a 30% reduction in thickness is considerable, of the order of 10° to 30°. Fig. 3 is reproduced from a diagram given by BARRETT and LEVENSON and is a typical result. The percentage reduction in thickness corresponding to each orientation contour is included in the Figure.

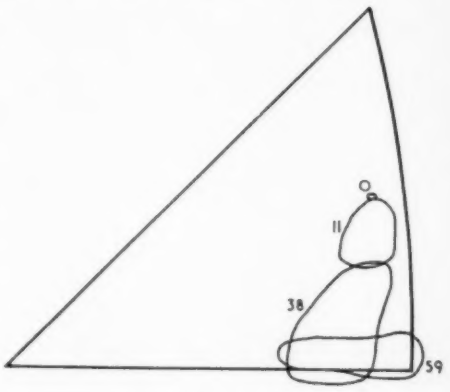

Fig. 3.

The experimental data for tension textures is not so conclusive. There is reason to believe that the development of deformation textures is primarily a function of the deformation occurring, irrespective of the force employed. (See for example BARRETT (1953, p. 445) and BARRETT and LEVENSON (1939)). On this basis it is common practice to take the textures of drawn wires and extruded rods to be a good approximation to tension textures. While this is probably reasonably true in certain circumstances, the theoretical solutions of HILL (1947) for plane strain extrusion and the experimental work reported in PEARSON (1953 Ch.V.), GREEN (1951), TAYLOR and QUINNEY (1932), and PURCHASE and TUPPER (1950), shows that in fact the deformation in extrusion and drawing can be considerably different from that in simple tension. In the following review of experimental work, it must be borne in mind that the textures found are *not* pure tension textures.

The early work of ETTISCH, POLANYI and WEISSENBERG (1921), SCHMID and WASSERMAN (1927) and others (for references see BARRETT 1953) gives the drawing

textures of face-centred cubic metals as a combination of (111) and (100) of varying amounts. Much of this work gives results which disgree with later investigations. It should therefore be realized that the results quoted below must be regarded as not entirely unexceptionable, although corroborative work exists in some cases. HIBBARD and YEN (1948) have investigated the drawing textures of copper and its binary alpha solid solution alloys with aluminium, nickel and zinc. They report a mixed (111) and (100) texture for all the alloys considered. For pure copper, copper-zinc alloys containing less than c.8% zinc, copper-aluminium alloys with less than 2% aluminium, and a 31% copper-nickel alloy, the texture is (111) and (110) of comparable order, with the (111) predominant. (The result given in Table 2 of their paper for a 5% brass is in error as reported in HIBBARD and TROUT (1949)). Alloys containing higher percentages of aluminium and copper exhibit primarily a (111) texture. According to GREENWOOD (1929), the texture of drawn nickel wires is a double (111), (100) fibre texture with the (111) component the stronger. CALNAN and WILLIAMS (1952) have published the only data on pure tension textures of which the author is aware. In experiments on high-purity and commercial aluminium they found a mixed (111), (100) texture. They conclude from progressive investigation that the final texture is between these two. The present author feels that there is an alternative explanation to their observations and that (111), (100) is the end texture in the sense implied here. This topic will be reverted to later.

Vol. 3 54/55

It appears that the position may be summarized as follows. The group of metals comprising aluminium, copper, nickel, alloys of less than 2% aluminium or 8% zinc in copper, and a 30%* copper-nickel alloy, exhibit a compression texture of the type shown in Fig. 1 and a mixed (111), (100) tension texture, the (111) component being predominant but not overwhelmingly so. Alloys of copper containing greater percentages of aluminium or zinc give a compression texture of the type shown in Fig. 2 and a tension texture which is primarily (111) with a weak (100) component. For all these metals it is to be expected that of the order of 50% of the grains will have orientations appreciably different from these.

3. THE PHYSICS OF POLYCRYSTALLINE DEFORMATION

Before developing the current theory, it will be helpful to have a physical picture of the deformation of an aggregate. The following remarks are intended primarily to refer to lattices for which an arbitrary deformation can be imposed by glide alone. Consider the uniform loading of an aggregate under increasing proportional loads. Initially all the grains will be stressed elastically until at some stage one grain is stressed such that any increase in stress following the previous stress history would lead to the violation of the critical shear stress law. This is the proportional point. Thereafter the stressing of individual grains follows a non-uniform pattern determined by considerations of stress equilibrium and yield. There is in general a range between the proportional point and the yield point in which although a proportion of the grains are stressed to the yield point, nevertheless the aggregate as a whole suffers strains of elastic order only. This is due to the constraining influence of the grains which are not stressed to the yield-point. This picture is

* All the percentages quoted are not intended to be critical.

consistent with a proportional point and a yield point which are not sharply defined. Consider now an individual grain. If it deforms plastically its surface displacements must be consistent with the strains occurring in adjacent grains. Moreover there must be continuity of forces across the grain boundaries. BISHOP and HILL (1951b) have shown that for the arbitrary strain of a face-centred cubic crystal one of a finite set of stress states must exist in the crystal. Consider the hypothesis that each grain in the aggregate undergoes the macroscopic strain. This ensures continuity of displacement throughout. However, according to BISHOP and HILL it implies that each grain is (in general) stressed under one of a finite set of stress systems. It is not difficult to show that stress equilibrium is not possible in these circumstances. This leads to the conclusion that in general each grain does *not* undergo the macroscopic strain. Consideration of special cases leads to the further conclusion that stress and displacement continuity cannot be obtained merely by allowing each grain to suffer a homogeneous but *individual* strain. Hence it is to be expected that each grain will undergo an inhomogeneous strain. This in turn implies that different areas of particular grains will undergo different rotations on straining. This is consistent with the observations of BARRETT and LEVENSON quoted in Section 2 and with those of YAMAGUCHI (1927) and ASTON (1925) on the inhomogeneity of deformation.

Although the above considerations lead to the conclusion that the deformation of each aggregate can be examined *exactly* only by treating it as an individual problem with a large number of variables, nevertheless the large number of grains present suggests that the aggregate will exhibit statistical properties. In particular it appears reasonable to suppose that the preferred orientation developed, assuming that each grain undergoes the macroscopic strain, will be a good first approximation to the actual deformation texture. This assumption is made in the present work. It will be realized that this is the model adopted by TAYLOR (1938a). The results obtained in the next section differ from TAYLOR's in that the complexity of his analysis resulted in certain alternative sets of shears being overlooked (see BISHOP and HILL, 1951b). The current treatment is based on their maximum work principle (1951a).

4. PRESENT THEORY

The present theory is based on the assumption that each grain deforms homogeneously, undergoing the macroscopic strain. The mechanism of distortion is taken to be glide on the octahedral planes in the direction of the face diagonals. For a discussion of this type of deformation the reader is referred to BISHOP and HILL (1951b). In this section it will be assumed that glide is stress-activated under a critical shear stress which is the same for all glide-planes and glide directions. Consider a grain in a polycrystalline aggregate. The directions of the cubic axes relative to the specimen axes can be specified by a transformation matrix with components a_{ij}. If an increment of specimen strain is dE_{ij}, the strain increment $d\epsilon_{ij}$ relative to the cubic axes is given by

$$d\epsilon_{ij} = a_{ik}\, a_{jl}\, dE_{kl}$$

where the repeated indices are summed. In a face-centred cubic aggregate undergoing compression or tension, there is no preferred transverse direction at any

stage. Hence the strain increment dE_{ij} will be given by

$$dE_{ij} = \pm \begin{bmatrix} dE & 0 & 0 \\ 0 & -\frac{1}{2}\,dE & 0 \\ 0 & 0 & -\frac{1}{2}\,dE \end{bmatrix}$$

where the transverse directions are any two (fixed) orthogonal directions. According to the maximum work principle of Bishop and Hill (1951a), the stress system (relative to the cubic axes) required to impose this strain can be found from a discrete set (given by Bishop 1953, p. 61). Hence from equations (10) of Bishop and Hill (1951b) the operative glide planes and directions can be found. It is found that either six or eight glides will be available in each grain. Since only five are required to impose an arbitrary strain with zero dilation, either one or three shears is redundant. If these redundant shears are treated as parameters, the remaining shears may be expressed in terms of the strain-increment components and these parameters (the relevant equations can be obtained from Bishop (1953)). The operative stress system will achieve the critical shear stress on the active planes in a specific sense. Since the shear magnitudes must be either non-negative or non-positive according as to whether the glide direction is operated in a positive or a negative sense, the parameters can be varied only in so far as they satisfy these requirements. In general, as will appear later, a *range* of shear magnitudes satisfy these conditions. The three rotation components of the principal axes of strain-increment relative to the reference axes are given by

$$\zeta = \tfrac{1}{2}\,\mathrm{curl}\,\boldsymbol{u}$$

where $\boldsymbol{u}$ is the displacement vector and ζ the rotation vector. These are expressible in terms of the shear magnitudes as shown by Taylor (1938b). Let the angles θ and ϕ specify the specimen axis relative to the cubic axis as in Fig. 4. It has been stated that it is necessary only to consider the traingle bounded by the (100), (110) and (111) directions. Since one of the principal axes of strain increment and the specimen axis coincide, the rotation of the specimen axis relative to the cubic axes can be expressed as a function of the ζ_i. This corresponds to increments $d\theta$ and $d\phi$ in θ and ϕ. Thus the rotation of the lattice relative to the specimen axis can be found. This computation has been carried out for 5° increments in θ and ϕ for a 1·78% compression. The results are reported in the next section.

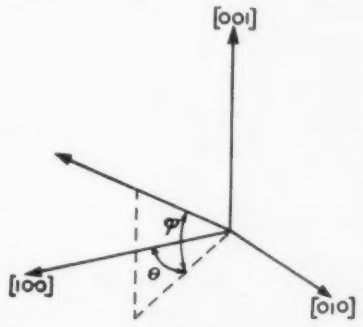

Fig. 4.

5. Results

The predicted rotations for compression are shown in Fig. 5. It is seen that two types of behaviour occur. Either the compressive axis is located along a line (as at P) or within or upon a domain (as at Q). These cases correspond to the operation of six and eight shears respectively. The rotations shown are obtained

from letting the parametric shears vary between the widest possible limits. It is seen that for many orientations the range of permissible rotations may result in the specimen axis moving in opposite directions. This point will be reverted to later when the large observed scatter in final orientations is discussed. If the strain in each grain is not the homogeneous macroscopic strain considered here, the rotations will differ from those illustrated. Nevertheless, having regard to the fact that qualitatively the strain in the bulk of the grain is not largely different from a uniform compression, it is reasonable to infer that both the types and ranges of rotations shown are close to the actual possible rotations. It is not proposed

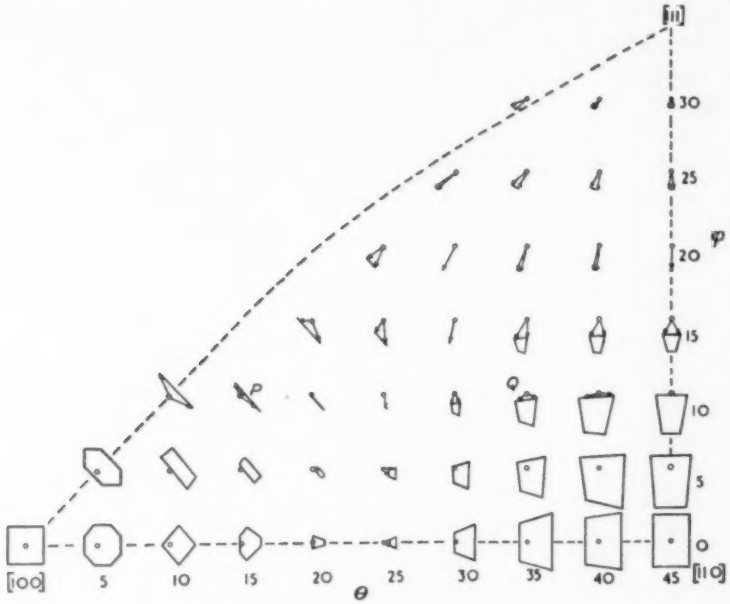

Fig. 5.

to examine in detail at this stage the correspondence between the observed textures and those which could be produced by rotations of the types predicted. Bearing in mind that the rotations in tension are the reverse of those shown in Fig. 5, it is seen that qualitatively the observed textures could be obtained save for the (111) component of the brass-type compression texture. There is still one outstanding experimental observation which has not been accounted for, namely the different preferred orientations developed under similar conditions by metals of the same lattice type. In the next section this topic is discussed and a hypothesis advanced to account for it.

6. Influence of Work-Hardening

The computations made so far in this paper have been based on a model for a face-centred cubic crystal for which glide is activated by a critical shear stress which is the same for each glide-plane and direction. In this section the effect of differential hardening will be examined. Consider the incremental deformation

of a specific grain. Two effects will result. Firstly a rotation of the cubic axes relative to the specimen axes will occur and secondly the physical properties of the grain will be modified. As to the former effect : if continued deformation is to occur, the grain must be stressed such that it is still at the yield point. This will entail a modification of the stress system specified relative to the specimen axes. The effect of hardening is more difficult to assess. The experimental evidence on the hardening of metal crystals does not lead to a very clear picture of the detailed nature of hardening within grains. The reader is referred to COTTRELL (1953, Ch.V) for a survey of this topic. In this section it is assumed that the position may be assessed as follows : the hardening of a glide system in a face-centred cubic crystal is a function both of the *total* shear which has occurred in the grain and of the amount of shear which has taken place on the glide-system in question. This assumption is briefly examined later in the light of the experimental evidence. In general this type of hardening will lead to a change both in size and shape of the yield surface of the crystal. It is required therefore to examine how the effects of strain-hardening on the yield locus will affect further straining. Consider firstly the case in which latent glide systems do not harden as rapidly as the active systems. Suppose, as is true in the present case, that there is a multiplicity of available shears (both from geometrical consideration and in that the critical shear stress is achieved in the correct sense), not *all* of which *need* operate simultaneously in order to impose a fixed (but arbitrary) strain. The actual selection of shears which is activated in a *very small* initial strain increment will be determined by inhomogeneties at the dislocation level. In general at least five shears will be activated. This incremental strain will result in the critical shear stress for the active shears becoming proportionately larger than that for the latent systems. It can be shown that continued gliding on these same systems would result in one of two consequences, depending both on the strain occuring and on the precise nature of the hardening relation. Either the critical shear stress on one or more of the latent glide-systems would be exceeded or the grain would remain at the yield point. It is not proposed to pursue this point here since the precise nature of the hardening relation is not known. It is remarked that if the active systems harden *equally*, the yield point will *always* be exceeded in these circumstances. If further glide on the original systems maintains the grain at the yield-point, it can continue so to deform. On the other hand, if it would result in the critical shear stress being exceeded on a latent system then gliding will cease in some of the active systems and previously latent shears will become active.

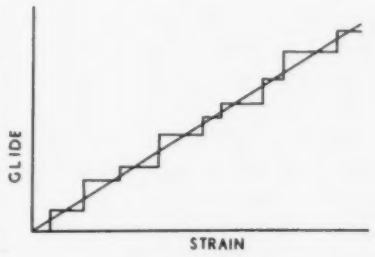

Fig. 6.

Thus, by repeating this process in a small but finite strain, the amount of glide occurring on a given system as a function of strain will be as indicated diagrammatically in Fig. 6. In the absence of other considerations this process would lead to the amounts of glide occurring on each system being very nearly equal after a small but finite strain. The overall requirement that a specified strain must occur will of course prevent this. The considerations given above lead to the conclusion

that the shear magnitudes will be as near equality as the constraint permits, i.e., the *smallest* shear magnitude (or magnitudes depending on the available degrees of freedom) will be as *large* as possible. This is the situation which will always obtain if active systems harden equally. If active systems harden by different amounts, this picture will be modified by the operation in certain instances of the alternative mode, leading to a scatter in the results. Consider now the case in which latent hardening is greater than active hardening. Again the effect of a second very small increment of strain is considered following an initial increment in which the latent glide-systems harden more rapidly than the active ones. Again, depending on the strain and the law of hardening, two effects could result. Either the grain hardens such that the active systems remain at the yield point with the critical shear stress not achieved on the latent systems or the critical shear stress would be exceeded on some of the latent systems. This latter alternative will again result in scatter. The former alternative will always occur if the active shears harden equally. The requirement that a specified strain must occur limits the magnitudes of the possible shears. Suppose that all available shears occur in an initial small strain. Since the glide system upon which the greatest shear has occurred becomes the least hardened, it is to be expected that after the initial phase the glide system(s) upon which the least shear has occurred will harden so as not be to stressed critically. Thus, under these circumstances, the *largest* shear magnitudes will be as *large* as possible. This condition does not necessarily imply that a unique set of shears operates. It will be realized that the above arguments are not rigorous in the sense that the effect of rotation of both the grain and its neighbours on the stress state has been neglected.

The argument can clearly be given a precise mathematical formulation if the effects of rotation are assumed to be secondary compared with the effects of hardening and some functional relationship between hardening and shear is postulated. However, the approximations involved in the present work render such a formulation rather an academic exercise.

The idea of determining *physically* possible deformation modes from ones which are merely *geometrically* possible by the type of argument used here is not of course new. Identically these arguments are employed both in explaining the yielding of mild steel (Lomer 1952) and the necking of work-hardening notched strips (Hill 1952). It should perhaps be pointed out that the maximum work principle (Bishop and Hill 1952a) holds at all stages of the deformation. This principle is essentially concerned with *first*-order effects, the work done in an infinitesimal strain-increment being the entity considered. The hypotheses advanced here are based on a *second*-order effect involving stress-*increment*. The position may be summarized as follows : if latent systems do not harden more rapidly than active ones, the *least* shear magnitudes will be as *large* as possible. If latent systems harden *more* rapidly than active ones, the *largest* shear magnitudes will be as *large* as possible. The precise nature of the hardening law will determine the scatter to be expected in both cases.

Consider now the experimental evidence on the hardening of crystals. According to Taylor and Elam (1925) for aluminium, Elam (1926) for copper, and Osswald (1933) for nickel, the latent and active planes harden by similar amounts. On the other hand, Elam (1927 a, b) reports than in 70-30 brass and 5% copper-

aluminium solid solutions the latent planes undergo appreciably greater hardening than the active ones. Thus, for example, ELAM reports a difference of 32% in the latent and active hardening for the 38% tensile strain of α-brass.

The hardening of indivudal systems as a function of strain varies considerably with circumstances. In simple glide in face-centred cubic metals a parabolic hardening law is taken to be normal, but ANDRADE and HENDERSON (1951) have shown that 'easy glide' in which the hardening is linear can be obtained under controlled conditions. It is significant that 'easy glide' occurs very readily in α-brass. As has been seen, latent hardening is appreciably greater than active hardening in this metal. The tendency for what COTTRELL calls 'Turbulent plastic flow' to occur is probably less than in metals such as aluminium in which latent and active hardening are similar.

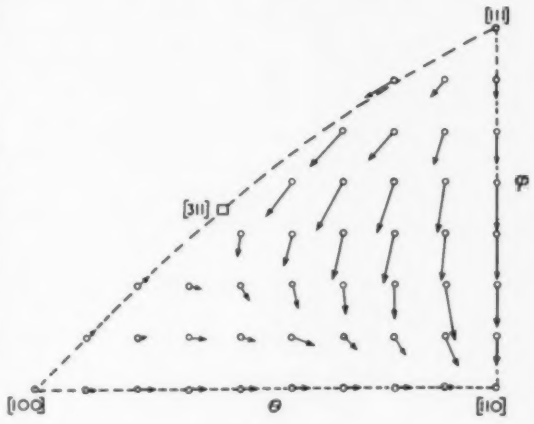

Fig. 7.

On the strength of the hypothesis advanced that the differential hardening of the glide systems affects the deformation textures, it is to be expected that the textures exhibited by aluminium, copper and nickel would be similar as would be those of α-brass containing more than 8% zinc and aluminium bronzes with more than 2% aluminium. Differences would be expected between these two types of behaviour. These are in fact the results reported in Section 2. In the following section the predictions of the hypotheses as regards the detailed effects of differential hardening are given and compared with the observed textures.

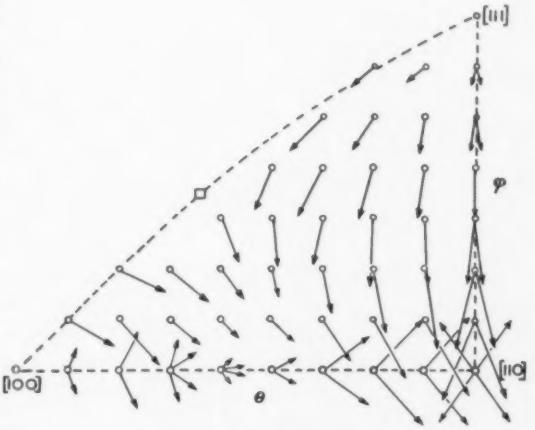

Fig. 8.

7. PREDICTED TEXTURES

The rotations shown in Fig. 7 and 8 corresponding to a 5% compression are obtained from maximising the *least* and the *greatest* shear magnitudes respectively. The density of orientations corresponding to a 15% compressive strain where these rotations occur are shown in Figs. 9 and 10 respectively. Consider the

rotations predicted in Figs. 7 and 8. The essential difference between them is that while a (110) texture is the ultimate texture predicted in both cases, there is a definite difference in behaviour of those grains originally located near the (100) direction. In Fig. 7, corresponding to equal active and latent hardening, the specimen axis firstly moves in the (311) direction and subsequently in the (110) direction: when the latent hardening exceeds the active hardening, the specimen axis moves directly in the general (110) direction. Comparison with the results given in Barrett (1953, pp. 447-448) and Hibbard and Trout (1949) shows these trends to be observed in the metals displaying these hardening characteristics.

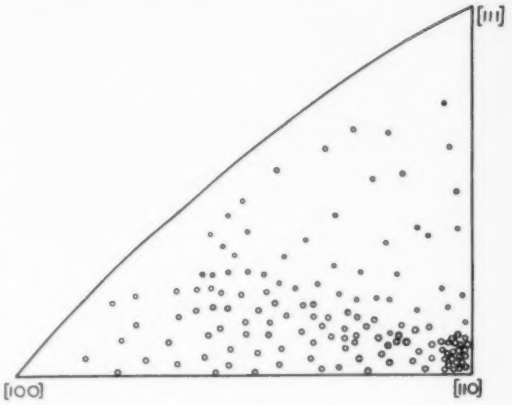

Fig. 9.

In tension the predicted rotations are the reverse of those shown in Figs. 7 and 8. The chief difference between the two types is that while the rotations of Fig. 7 would lead to a dominant (111) texture with a weaker (100) component, those of Fig. 8 would lead to a texture which is primarily (111). Again these correspond to the orientations observed for those materials which harden as specified.

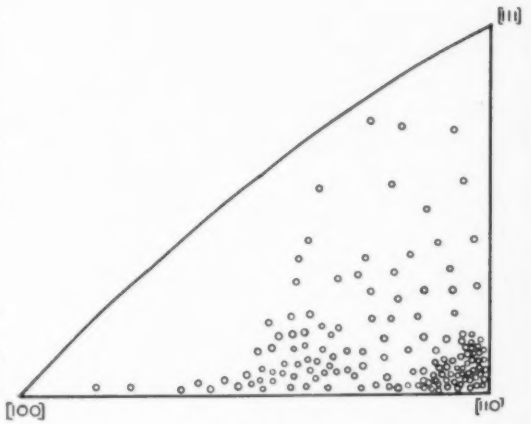

Fig. 10.

8. Summary and Discussion

In the foregoing work three hypotheses have been advanced :—

(i) The deformation textures developed are closely approximated by assuming that each grain undergoes the macroscopic strain.

(ii) The texture developed is determined by the differential hardening of latent and active glide systems.

(iii) If the latent systems harden less rapidly than the active ones, the glides are such that the least shear magnitudes are as large as possible ; if latent systems harden more rapidly than active ones, the largest shear magnitudes are as large as possible. A scatter about these predictions is to be expected depending on the hardening law.

The first of these hypotheses was originally advanced by Taylor (1938a).

It has already been discussed in Section 3. The evidence of BARRETT and LEVENSON (1940) demonstrates that each grain does not undergo the macroscopic strain but a range of strains leading to a spread of orientations. In comparing the predictions of the last hypothesis with observation the influence of inhomogeneity of distortion must be allowed for.

The second hypothesis is supported by the evidence quoted for the uniaxial deformation of aluminium, copper, nickel, brass and aluminium bronze. Similar effects are observed in rolling. HU, SPERRY and BECK (1952) report that copper and aluminium develop essentially similar rolling textures which are markedly different from that of 70-30 brass.

The third hypothesis leads to predictions which are qualitatively in close agreement with observations. The quantitative agreement is not so good. This is not surprising in view of the large scatter of orientations in individual grains observed in practice. This scatter appears to be a direct function of strain. It does not appear to be possible to give a meaningful theoretical estimate of the magnitude of scatter to be expected. In general the rotations predicted in Figs. 7 and 8 are to be expected subject to the modifying influences of scatter. If the dislocation model of plastic deformation is accepted, scatter is to be expected even in single crystals. The aggregation of dislocations of one sign and type causes distortion of the lattice and bending of the glide-planes. With large strains the fragmentation of either single crystals or grains in an aggregate will result in a increasingly large scatter. The ' end textures ' will probably be, as BARRETT and LEVENSON (1940) suggest, a statistical equilibrium between parts of grains moving towards and away from certain preferred orientations. It seems to the present author that this explanation accounts for the observations of CALNAN and WILLIAMS mentioned in Section 2.

A final point seems worthwhile making. BARRETT (1953, p. 458) remarks that different observers list different ideal orientations for textures which are essentially similar. This has become apparent on several occasions in the course of the present work. The procedure of HU, SPERRY and BECK in giving quantitative pole figures obviates this difficulty and enables a true comparison, free of subjective and interpretative difficulties to be made.

Vol. 3 54/55

ACKNOWLEDGMENTS

This work was carried out in the Plasticity Division of the Mechanical Engineering Research Laboratory as part of the programme of the Mechanical Engineering Research Board. This paper is published by permission of the Director of the Laboratory. The author wishes to express his thanks to Professor R. HILL of the University of Nottingham for many helpful suggestions to improve the original manuscript.

REFERENCES

ANDRADE, E. N. DA C., and HENDERSON, C. 1951 *Phil. Trans. Roy. Soc.*, *A*, **244**, 177.

ASTON, R. L. 1925 *Proc. Camb. Phil. Soc.*, **23**, 549.

BARRETT, C. S. 1923 *Structure of Metals* (McGraw-Hill, London).

Barrett, C. S. and Levenson, L. H.	1939	*Trans. A.I.M.E.*, **135**, 327.
	1940	*Trans. A.I.M.E.*, **185**, 620.
Bishop, J. F. W.	1953	*Phil. Mag.*, **44**, 51.
Bishop, J. F. W. and Hill, R.	1951a	*Phil. Mag.*, **42**, 414.
	1951b	*Phil. Mag.*, **42**, 1298.
Boas, W., and Schmid, E.	1931	*Z. tech. Physik*, **12**, 71.
Calnan, E. A. and Clews, C. J. B.	1950	*Phil. Mag.*, **41**, 1085.
Calnan, E. A. and Williams, B. E.	1952	*J. Metals.*, **4**, 743.
Cottrell, A. H.	1953	*Dislocations and Plastic Flow in Crystals* (Oxford : Clarendon Press).
Elam, C. F.	1927a	*Proc. Roy. Soc.*, A, **115**, 148.
	1927b	*Proc. Roy. Soc.*, A, **116**, 694.
Green, A. P.	1951	*Phil. Mag.*, **42**, 365.
Greenwood, G.	1929	*Z. Krist.*, **72**, 309.
Hibbard, W. R. and Trout, D. E.	1949	*Trans. A.I.M.E.*, **185**, 620.
Hibbard, W. R. and Yen, Ming-Kao	1948	*Trans. A.I.M.E.*, **175**, 126.
Hill, R.	1947	*J. Iron and Steel Inst.*, **156**, 177.
	1952	*J. Mech. Phys. Solids.*, **1**, 19.
Hu, H., Sperry, P. R. and Beck, P. A.	1952	*J. Mets.*, **4**, 76.
Lomer, W. M.	1952	*J. Mech. Phys. Solids*, **1**, 64.
Pearson, C. E.	1953	*The Extrusion of Metals* (Chapman and Hall : London)
Pickus, M. R. and Mathewson, C. H.	1939	*J. Inst. Metals*, **64**, 237.
Purchase, N. W. and Tupper, S. J.	1950	*A.R.E.*, Report No. 20/50.
Taylor, G. I.	1938a	*J. Inst. Metals*, **62**, 307.
	1938b	*S. Timoshenko Anniversary Volume*, p. 218 (Macmillan : New York).
Taylor, G. I. and Elam, C. F.	1925	*Proc. Roy. Soc.*, A, **108**, 28.
Taylor, G. I. and Quinney, H.	1932	*J. Inst. Metals*, **49**, 187.
Yamaguchi, K.	1927	*Sci. Papers Inst. Phys. Chem. Research*, Tokyo, **6**, 271.

Vol 3 1954/

Journal of the Mechanics and Physics of Solids, 1954, Vol. 3, pp. 143 to 155. Pergamon Press Ltd., London.

A THEORY OF THE PLASTIC YIELDING DUE TO BENDING OF CANTILEVERS AND BEAMS. PART II.

By A. P. Green
British Iron and Steel Research Association Metal Working Laboratories, Sheffield

(*Received 8th November*, 1954)

Summary

The group of solutions for the plastic yielding of cantilevers of rectangular cross section described in Part I of this paper is completed here by consideration of the effect of weak end support under conditions of plane stress. These solutions are applied to the problems of yielding of centrally or uniformly loaded beams, either fixed at both ends or simply supported. The plane stress solutions are applied to corresponding problems for beams of I-section, bent about an axis perpendicular to the web. The theoretical deformation modes for cantilevers are shown to agree well with experiments by Hundy (1954, rectangular section) and Frankl (1950, I-section). Empirical equations obtained for the shear loads under which I-beams yield are roughly confirmed by some experiments of Hendry (1950).

VOL. 3 54/55

1. Introduction

In Part I of this paper (Green 1954, hereafter referred to as Part I) solutions were described for the plastic yielding of end-loaded cantilevers. Broad and narrow cantilevers of rectangular cross section were treated by plane strain and plane stress solutions respectively. The plane strain solutions were constructed for both strong and weak end supports, but the plane stress solutions were for strong support only.

This group of solutions is first completed here by considering the effect of weak support under conditions of plane stress. The solutions for uniform, as opposed to tapering, cantilevers are then applied to problems of similarly shaped fixed ended beams. Finally, the plane stress solutions are applied to corresponding problems for beams and cantilevers of I-section bent about an axis perpendicular to the web.

2. Plane Stress Solutions (continued)

The type of weak support considered is the same as that assumed for plane strain in Part I (Section 3a), i.e. the top edge of the cantilever in a stress-free surface in the plastic region while the bottom edge is strongly supported behind the point B (Fig. 1) which is thus a point of stress singularity. The cantilever is assumed to be of uniform depth t and of length l with a shear load St acting perpendicular to its axis at its free end, 0.

A type I solution only has been constructed, having a stress discontinuity at Y, the point about which the cantilever rotates as yielding is initiated. The

characteristic field (Fig. 2) differs from the similar type *I* field for strong support only in that there is no singularity on the stress-free upper surface, and the method of solution is as described in Part I.

As $l/t \to \infty$, $S/k \to 0$ and angle $YBT \to 0$. The opposite limit to the solution is taken to be when angle $YBT = \beta = \tan^{-1}\sqrt{2}$; then $l/t = 1{\cdot}33$ and $S/k = 0{\cdot}328$. As this limit is approached with decreasing l/t the angle between the two characteristics BY and TY tends to zero, and in the limit TY approaches BY asymptotically (i.e. $\psi = \pi/2$ where ψ is defined as in Part I). Hence the solution degenerates to the coincident characteristics TY and BY while the region BTE dwindles to nothing. The fact that the solution degenerates, however, is not

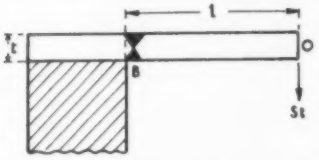

Fig. 1. Weakly supported uniform cantilever.

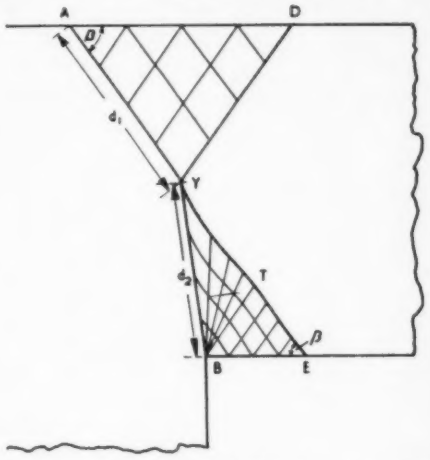

Fig. 2. Plane stress solution for a weakly supported uniform cantilever.

the reason for choosing this particular lower limit. The reason is that the discontinuous change of stress across Y for this solution is the same as it would be if AY and BY were continuously connected by a curved characteristic inserted at Y (as in the type II solutions described in Part I). In plane strain this criterion gives the limit to the change of stress which can be supported round a stress singularity without violating the yield criterion (HILL 1954). The validity of the criterion in plane stress can be proved by application of HILL's general theorem.

The calculated dimensions of the fields and the corresponding values of l/t and S/k are given in Table 1 together with some additional results for similar strongly supported cantilevers which were not given in Part I. Comparison between the two sets of results shows that the reduction in S/k with weak support is slightly greater than in plane strain, being about 6 per cent when $l/t \sim 1{\cdot}3$ and decreasing to about 1 per cent when $l/t \sim 5{\cdot}5$ and to zero as $l/t \to \infty$.

3. Summary of Results for Uniform Cantilevers

The results of all the solutions for uniform cantilevers are most conveniently compared with the simple theory of pure bending in terms of the bending moment at the fixed end. Let M and M_0 be the yield-point bending moments per unit width acting over the fixed end of a uniform cantilever according to the present theory and to the simple theory of pure bending without axial pressure respectively. Then $M = Slt$ and the simple theory gives

$$M_0 = \tfrac{1}{2} kt^2 \quad \text{in plane strain,}$$

and
$$M_0 = \frac{\sqrt{3}}{4} kt^2 \quad \text{in plane stress.} \tag{1}$$

where k is the yield stress in pure shear, and in plane stress the Mises yield criterion is assumed.

TABLE 1. PLANE STRESS
Uniform cantilever yielding under shear loads

	l/t	S/k	d_1/t	d_2/t	$\delta_2{}^c$
Weak support	1·33	0·328	0·656	0·492	0·955[c]
	1·62	0·275	0·651	0·482	0·855
	2·00	0·224	0·646	0·477	0·755
	2·55	0·177	0·640	0·477	0·655
	3·36	0·134	0·635	0·482	0·555
	4·72	0·0952	0·630	0·492	0·455
	5·77	0·0776	0·627	0·499	0·405
	7·26	0·0614	0·624	0·507	0·355
	8·25	0·0538	0·623	0·512	0·325
	9·49	0·0467	0·622	0·517	0·305
	13·10	0·0337	0·619	0·528	0·255
	19·52	0·0225	0·617	0·541	0·205
	33·47	0·0131	0·615	0·555	0·105
	l/t	S/k	d/t	$\delta°$	
Strong support	6·30	0·0714	0·533	15°	
	7·14	0·0628	0·536	14	
	8·17	0·0547	0·540	13	
	9·46	0·0470	0·544	12	
	11·11	0·0399	0·548	11	
	13·26	0·0333	0·553	10	
	16·15	0·0273	0·558	9	
	20·16	0·0218	0·562	8	

The two theories for zero axial pressure are compared in Fig. 3 where the percentage by which M exceeds M_0 is plotted against S/k. It is remarkable that M should be greater than M_0 over such a large range of S/k. Except for the lowest curve, $M > M_0$ for all values of S/k up to about 0·5, the corresponding value of l/t being about 1·0. With strong support the maximum increase in this range is about 12 per cent at $S/k \sim 0{\cdot}3$ in plane strain, and 7·5 per cent at $S/k \sim 0{\cdot}25$ in plane stress. Thus it appears that the constraining effect of the end support can outweigh the weakening effect of shear stress for all except very short cantilevers.

The curves all pass through the origin and are nearly parabolic in shape. Empirical equations have been constructed for both the plane stress curves. With strong support the equation

$$\left(\frac{M}{M_0} - 1\right) = 1{\cdot}23\left(\frac{S}{k}\right)\left(0{\cdot}5 - \frac{S}{k}\right) \tag{2}$$

gives M/M_0 accurate to within about $\frac{1}{4}$ per cent up to $S/k \sim 0{\cdot}62$, the value at which yielding first extends to the free end. With weak support the equation

$$\left(\frac{M}{M_0} - 1\right) = 1{\cdot}45\left(\frac{S}{k}\right)\left(0{\cdot}35 - S/k\right) \tag{3}$$

gives M/M_0 accurate to within about $\frac{1}{2}$ per cent up to $S/k \sim 0{\cdot}33$, the limit of the present solution.

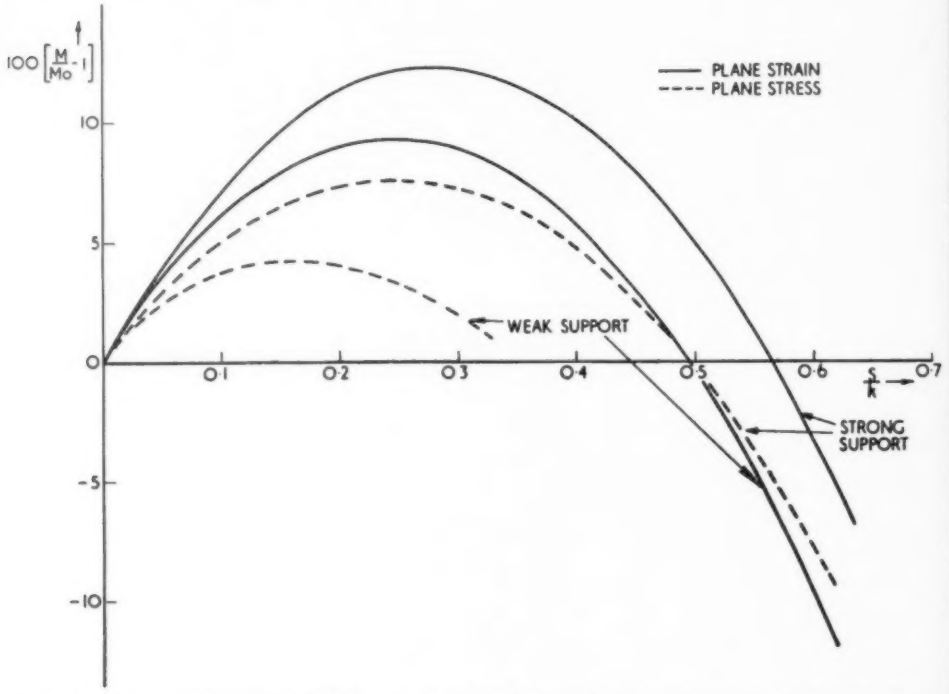

Fig. 3. Relations between 100 $(M/M_0 - 1)$ and S/k for uniform cantilevers under shear loading.

The effect of axial pressure, P, on M for a strongly supported cantilever in plane strain is shown in Fig. 4 where M/M_0 is plotted against P/k for various selected values of l/t. All the curves lie above that for an indefinitely large value of l/t which is the curve given by the simple theory taking account of axial pressure and has the equation

$$\frac{M}{M_0} = 1 - \left(\frac{P}{2k}\right)^2. \tag{4}$$

However long the cantilever is, M lies within about 12 per cent of the value given by this equation for all $P/k < 0{\cdot}7$.

All the results for end-loaded cantilevers can be applied directly to similar uniformly loaded cantilevers if we neglect in the latter, the surface pressure at

the regions of deformation, which will be small except at low values of l/t. Since the resultant vertical load, W per unit width say, now acts half way along the cantilever, W/kt is equal to S/k for a similar end-loaded cantilever of half the length.

We now go on to discuss the application of the above results to other problems of practical interest.

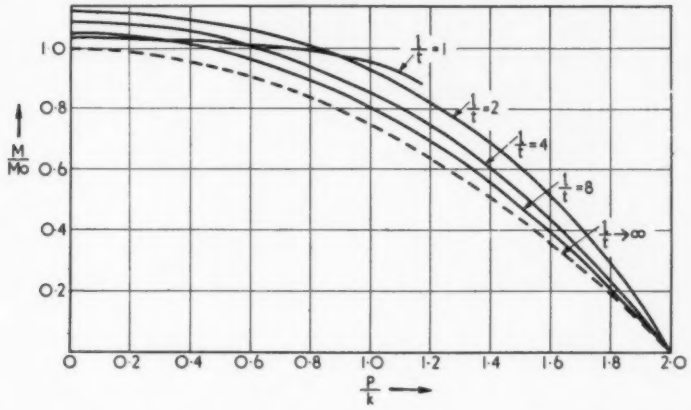

Fig 4. Relations between M/M_0 and P/k for strongly supported cantilevers in plane strain.

4. Uniform Beams of Rectangular Section

Consider a uniform beam AA of rectangular section, length $2l$, and thickness t, whose ends are either (a) supported in position and direction (fixed end) or (b) simply supported, and which is either (i) centrally loaded or (ii) uniformly loaded. In each case we wish to calculate the total load W per unit width which will cause yielding.

(a) *Fixed end beams*

(i) *Central loading.* We suppose that the load is supported over a small length $DD = a$ and that the region below DD remains rigid so that yielding takes place by rotation of the two halves of the beam about this ' pivot ' B and about ' pivots ' at either end A (Fig. 5). The resultant forces acting on unit width of the half to the left of the load at yielding are shown in the same figure. The shear forces are $W/2 = St$ at each end, the equal and opposite end thrusts are denoted by Pt, and the bending moments at A and B are denoted by M_A and M_B respectively.

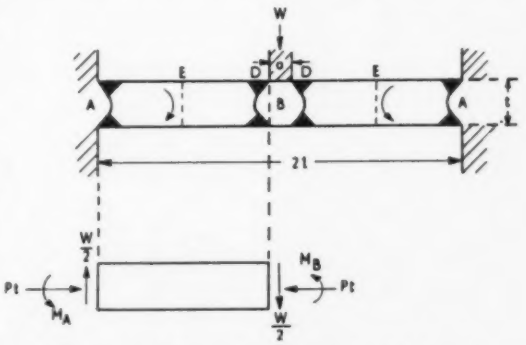

Fig. 5. Yielding of a centrally loaded fixed ended beam.

As a first approximation, for simplicity, a is neglected in comparison with l

and the length of the half beam to the left of the load is taken to be l. Taking moments

$$M_A + M_B = \frac{Wl}{2}. \tag{5}$$

The regions of deformation at the sections D will be of the kind shown in Fig. 2 for a cantilever with weak end support, modified if necessary for end thrust. At A we suppose that there is either strong support (Part I, Fig. 2) or weak support.

The end thrust is zero if free lateral motion of the ends is permitted. If, however, such motion is rigidly restrained, the thrust is determined by the condition that the pivot B must, by symmetry, move vertically downwards. This condition

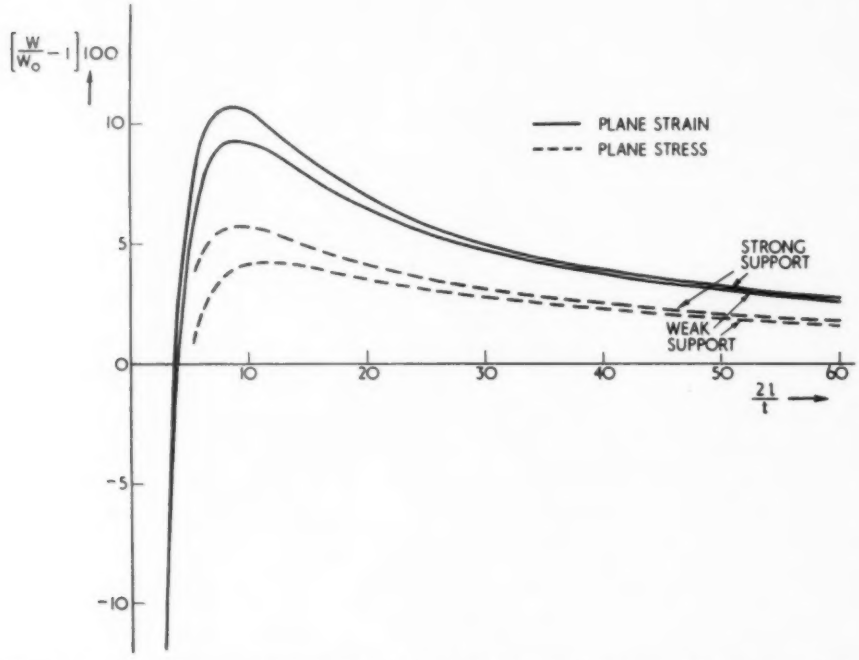

Fig. 6. Relations between $100\,(W/W_0 - 1)$ and $2l/t$ for centrally loaded fixed ended beams.

demands that the line joining the two instantaneous centres of rotation C_A and C_B of each half relative to its support at A and the pivot B, must be horizontal. The positions of C_A and C_B depend on the end thrust; the larger the thrust the higher is C_A and the lower is C_B. However, with zero end thrust C_B is less than $0{\cdot}07\,t$, above the central axis of the beam in plane strain for all values of l/t, and C_A lies on the axis or an equal distance below according as the end support is strong or weak. It is clear that though there is a positive thrust little error in W will be introduced by neglecting it.

The relationships between M_A (or M_B) and $W/2kt\,(= S/k)$ are assumed, therefore, to be given by one of the curves in Fig. 3. With these curves equation (5) is most conveniently solved by rewriting it in the form

$$\left(\frac{M_A + M_B}{2M_0} - 1\right) 100 = \left(\frac{W}{W_0} - 1\right) 100 = \left(\frac{cSl}{kt} - 1\right) 100, \tag{5a}$$

where $W_0 = 4M_0/l$ is the load predicted by the simple theory, and $c = 1$ in plane strain or $2/\sqrt{3}$ in plane stress. The L.H.S. of this equation is the ordinate either of a curve for weak support or of the mean of a pair of curves for strong and weak support according as there is weak or strong support at A. The corresponding value of S/k is obtained either from Fig. 3 or from one of the tables, and l/t is calculated by means of equation (5a). The present theory is compared in Fig. 6 with the simple theory by plotting curves of $100\left(\frac{W}{W_0} - 1\right)$ against $2l/t$.

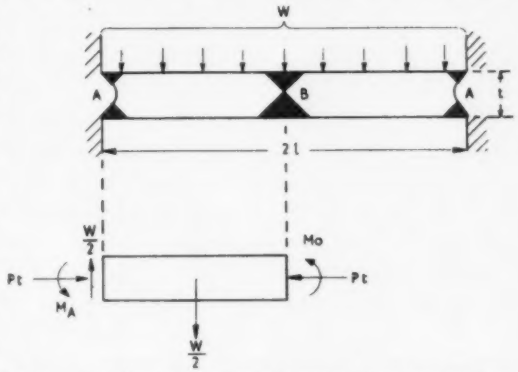

Fig. 7. Yielding of a uniformly loaded fixed ended beam.

(ii) *Uniform loading.* Similar calculations have been made for uniform loading (Fig. 7). Neglecting the effect of surface pressure on the regions of plastic deformation, there is now pure bending at

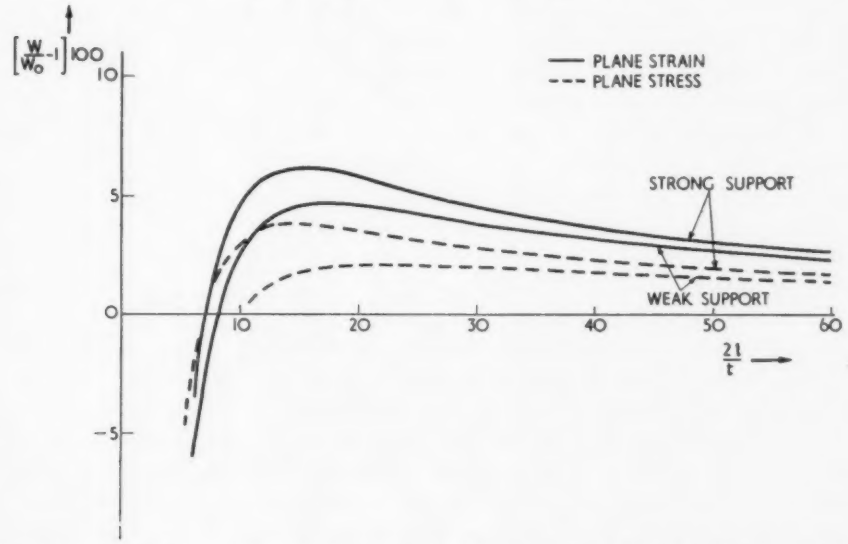

Fig. 8. Relations between $100\,(W/W_0 - 1)$ and $2l/t$ for uniformly loaded fixed ended beams.

the centre so that $M_B = M_0$. Taking moments for half the beam

$$M_A + M_B = Wl/4. \tag{6}$$

If there is strong support C_A and C_B both lie on the horizontal axis and there is no end thrust. Weak end support results in positive end thrust which we neglect.

Equation (6) is solved in a similar manner to (5) and the results are compared in Fig. 8 with the simple theory, which gives $W_0 = 8M_0/l$, i.e. twice the value for the same beam under concentrated loading.

(b) *Simply supported beams*

(i) *Central loading.* The beam is equivalent to the central half of a centrally loaded fixed-ended beam (the portion EE shown in Fig. 5) with weak end support and no axial constraint. Hence, neglecting a in comparison with l as before, W for a beam of length l is given by one of the curves for weak end support in Fig. 6.

(ii) *Uniform loading.* Provided that l/t is greater than about 1 a beam of length $2l$ yields by pure bending at the centre where the bending moment is a maximum. If the effect of surface pressure on the zone of deformation is neglected the simple theory holds and $W = 2M_0/l$. This is reasonably accurate except at low values of l/t when the surface pressure is large and effectively strengthens the beam. In plane strain, for example, W exceeds $2M_0/l$ by about 2, 4, and 9 per cent when $l/t = 4$, 3, and 2 respectively.

5. Cantilevers and Beams of I-Section

All the plane stress solutions for uniform cantilevers and beams can be used to give solutions for corresponding I-beams. We suppose that the flanges of the I-beam yield in pure tension or compression over the lengths adjacent to the regions of tension or compression in the web, where stresses and deformation correspond to one of the plane stress solutions. The flanges thereby increase the bending moment which can be supported by the given web under given shear and axial loads. Only when the mean shear stress over the web is greater than about $0{\cdot}6\,k$, or the mean axial stress approaches $\pm 2k$, does the region of pure tension or compression in the web dwindle to nothing and the flanges are forced to support some of the shear or axial load.

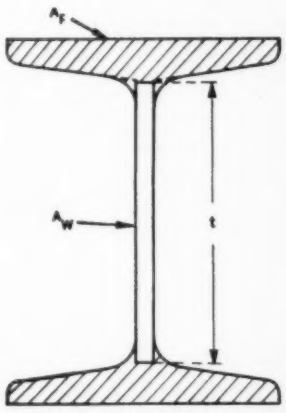

Fig. 9. Transverse section of an I-beam showing the notation used.

The following notation (Fig. 9) is used : A_W is the transverse sectional area of the web, t its depth, and S, P, and M_W the mean shear stress, mean axial pressure, and total bending moment respectively that it supports ; A_F is the area of each of each flange including the fillets, t_F is the distance perpendicular to the beam axis between the centroids of these areas, and the product $A_F t_F$ is denoted by B the bending modulus of the flanges alone. With one flange in tension and the other equal flange in compression the total bending moment supported is

$$M_F = Yt_F A_F = \sqrt{3}kB. \tag{7}$$

We now discuss the modification of the plane stress solutions.

(a) *End loaded cantilevers*

The total bending moment which an end-loaded I-beam of length l_i will support at its fixed end is

$$M_F + M_W = \sqrt{3}kB + SlA_W = Sl_i A_W, \tag{8}$$

where l is the length which the web alone would have to be to support the same vertical end-load SA_W. The value of l/t depends on S, P, and the strength of the end support, and may be interpolated from plane stress solutions. Two problems commonly arise in practice.

First, if S is given, then from (8) the length of the cantilever must be

$$l_i = l + \frac{\sqrt{3}kB}{SA_W}. \tag{9}$$

Second, if l_i and P are given, the vertical component of the end-load is

$$SA_W = \frac{\sqrt{3}kB}{l_i - l}. \tag{10}$$

Since both S and l are unknown this equation must be solved by trial and error unless a convenient empirical relation is known between S/k and l/t for the given value of P.

When $P = 0$, and there is strong end support, the following quadratic for S/k can be deduced from equation (2):

$$1{\cdot}23\left(\frac{S}{k}\right)^2 + \left(\frac{4l_i}{\sqrt{3}t} - 0{\cdot}62\right)\left(\frac{S}{k}\right) - \frac{4B}{tA_W} - 1 = 0 \tag{11}$$

which is valid up to $S/k \sim 0{\cdot}62$. However, since the web is strengthened by the flanges, the critical value of S/k at which yielding first extends to the free end of the beam is now greater than 0·62. For $S/k > 0{\cdot}62$ the plane stress solution in the web consists of a single curved characteristic (like PYQ in Part I, Fig. 11) and it is found that

$$l/t = \tfrac{1}{2}\tan\lambda, \qquad \text{and} \qquad S/k = \cos\lambda, \tag{12}$$

where λ is defined in Part I (Section 4). Applying this to an I-beam and neglecting the fact that some of the shear load will be supported by the flanges, S/k is given approximately by the equation

$$\left[4\left(\frac{l_i}{t}\right)^2 + 1\right]\left(\frac{S}{k}\right)^2 - \frac{8\sqrt{3}B}{tA_W}\left(\frac{l_i}{t}\right)\left(\frac{S}{k}\right) + \frac{12B^2}{t^2 A_W{}^2} - 1 = 0 \tag{13}$$

When $P = 0$ and there is weak end support the quadratic for S/k deduced from equation (3) is

$$1{\cdot}45\left(\frac{S}{k}\right)^2 + \left(\frac{4l_i}{\sqrt{3}t} - 0{\cdot}51\right)\left(\frac{S}{k}\right) - \frac{4B}{tA_W} - 1 = 0, \tag{14}$$

which is certainly valid up to $S/k = 0{\cdot}33$ and probably a reasonable approximation up to twice this value.

(b) *Fixed ended beams*

The modification of equations (5) and (6) for centrally and uniformly loaded I-beams respectively leads to the equations

$$w(M_A + M_B) + 2\sqrt{3}kB = Wl_i/2, \tag{15}$$

and

$$w(M_A + M_0) + 2\sqrt{3}kB = Wl_i/4, \tag{16}$$

where W is now the total load, M_A and M_B are the bending moments per unit width for the web alone, and the length of the beam is $2l_i$. These equations can be solved in a manner similar to that described in Section 4 (a), M_A and M_B being given by one or other of the plane stress solutions.

(c) *Simply supported beams*

The discussion of simply supported beams of rectangular section (Section 2 (b)) is equally applicable to beams of I-section. With central loading W is approximately the same as that for a similar fixed ended beam of twice the length with weak end support. With uniform loading, unless the beam is very short, $W = 2(wM_0 + \sqrt{3}kB)/l_i$ according to the simple theory.

6. Comparison of Theory with Experiment

In this section the theory is compared with the small amount of relevant experimental work known to the writer, under two headings (a) modes of deformation, and (b) yield-point loads.

(a) *Mode of deformation*

The mode of deformation under shearing load of a uniform cantilever of rectangular section has been demonstrated in mild steel by Hundy (1954). Each steel specimen was annealed, deformed just past the yield-point, aged at 250°C for about half an hour, and finally etched with Wazeau's reagent to reveal the regions where plastic deformation had taken place. The wide plane strain specimen was cut in half so that the central longitudinal section could be polished and etched.

The resulting comparisons between theory and experiment for $l/t = 2$, under conditions of both plane strain ($w/t \sim 8$) and plane stress ($w/t \sim 1/6$) are shown in Figs. 10a and 10b. They demonstrate the general validity of the assumed regions of deformation. The striated pattern of yielding in plane strain is characteristic of mild steel and the bands appear to run approximately parallel to the slip lines.

Further confirmation of the theory is provided by some tests carried out by Frankl (1950) on I-beams. Two horizontal 6 in. × 3 in. R.S.J.'s were welded by fillet welds round their whole profiles at A and A' to the flanges of a vertical 8 in. × 6 in. R.S.J., CD, and loaded past the yield-point in the manner shown in Fig. 11. Near the joints the metal was coated with plumber's resin which roughly revealed the regions of plastic deformation. Yielding was first observed in the web of the stanchion with the central load $W \sim 6$ tons and later in the horizontal beams with $W \sim 7{\cdot}5$ tons. The pattern in the stanchion web (Fig. 12a)

VOL. 3
54/55

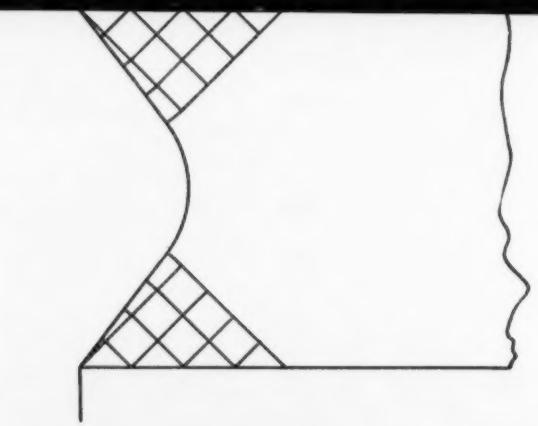

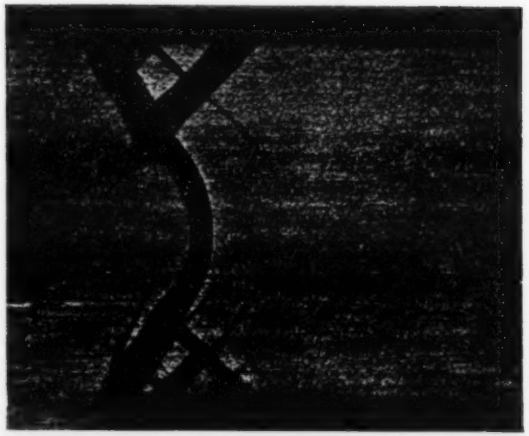

a

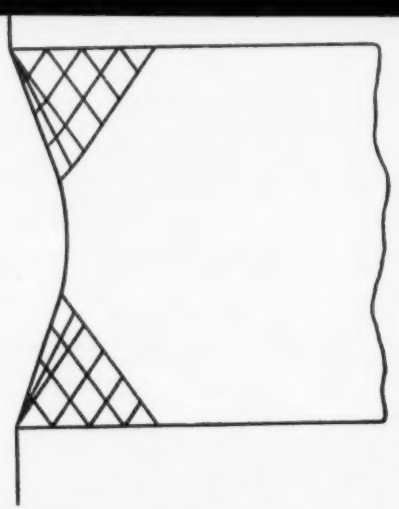

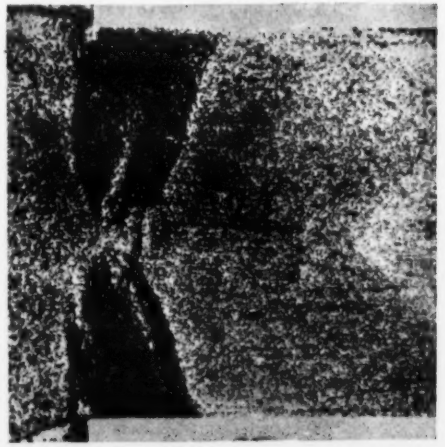

b

Fig. 10. Theoretical and experimental regions of deformation in uniform cantilevers of rectangular section, yielding under shear loading. (*a*) Plane strain, $l/t = 2$. $w/t = 8$; (*b*) Plane stress, $l/t = 2$, $w/t = 1/6$.

a

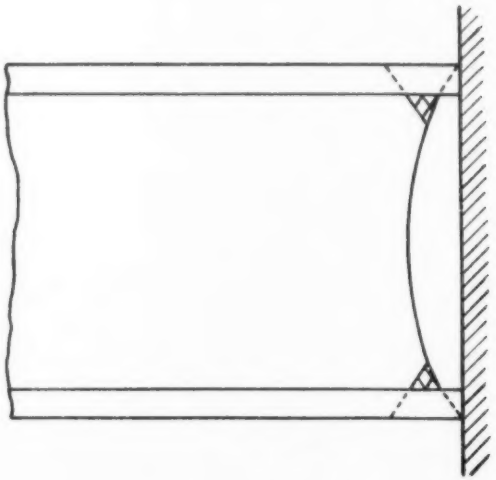

b

Fig. 12. Resin patterns due to plastic yielding obtained by FRANKL. (*a*) In the web of a stanchion; (*b*) In the web of a cantilever at its welded end, compared with the theoretical region of deformation.

is the plane stress equivalent of the alternative mode shown in Part I (Fig. 4). No calculations have been made, but it is not surprising that yielding should occur here first because, in contrast to the horizontal beams, the stanchion flanges add little strength to their web under this loading system. In later experiments, horizontal stiffeners, introduced between the flanges along the dotted lines shown in Fig. 11 effectively prevented yielding in the stanchion. A typical pattern in the web of a horizontal beam adjacent to the stanchion is compared in Fig. 12b with the characteristic field predicted by the present theory.

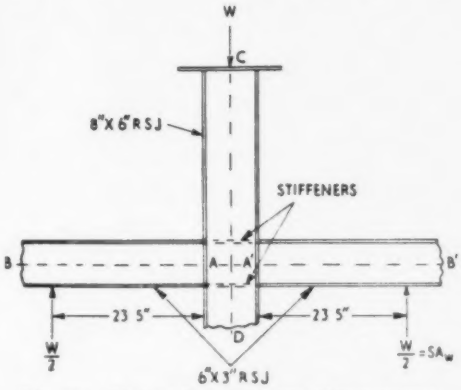

Fig. 11. FRANKL's experimental arrangment.

(b) *Yield-point loads*

It is not possible to compare FRANKL's experimental results closely with the theory because he does not give the yield stress of his material. However, if it is assumed that $Y \sim \sqrt{3}k \sim 16$ tons/in.^{2}, using equation (11) we obtain a theoretical value of 11 tons for W. This is midway between the value of 7·5 tons at which the first crack was noticed in the resin on the web, and 14·3 tons the average maximum value at which the load deflection curve flattened out; it corresponds to the 'knee' of the load-

TABLE 2

Comparison of HENDRY'S *experimental results for centrally loaded, simply supported, I-beams with theoretical calculations*

Section	l_i *(ins.)*	*Theory*					*Experiment*
		t *(ins.)*	B *(ins.*^{3}*)*	A_w *(ins.*^{2}*)*	S/k	M/M_0	M/M_0
4 in. × 3 in. RSJ	15	3·08	4·01	0·739	0·70	0·98	0·95
	12				0·85	0·95	1·0
3 in. × 1½ in. RSJ	12	2·39	1·10	0·38	0·50	1·00	1·00
	7·5				0·76	0·95	0·97
	5				1·00	0·87	0·88
1¼ in. × 1 in. (welded section made from 3 1 × 1⅛ in. flats)	10	1·0	0·141	0·125	0·24	1·01	1·00
	5				0·48	1·00	1·00
	3				0·76	0·96	0·97

deflection curve given by FRANKL. At the theoretical yield-point the mean shear stress in the web was $S = 0{\cdot}52\,k$, and $M/M_0 = 1{\cdot}0$.

In an investigation by HENDRY (1950) of the effect of shear on the carrying capacity of I-beams a number of simply supported beams were centrally loaded

The beams were stiffened under the load points to prevent severe local distortions. The set-up is equivalent to the central half of a centrally loaded fixed ended beam with weak end support, as was remarked in Section 3 (b). Unfortunately the present plane stress theory for weak support extends only up to $S/k \sim 0{\cdot}33$. The theoretical calculations were, therefore, based on equations (11) or (13) according as S/k was less than or greater than 0·62; no calculations could be made for $S/k \sim 1$ when the flanges must support an appreciable part of the shear load. Since these equations are for strong support one would expect the yield-point loads to be over-estimated.

Theory and experiment are compared in Table 2, and it can be seen that there is approximate agreement, though the experimental values of M/M_0 tend to be slightly higher. The experimental loads were not, however, measured at the 'knee' of the load-deflection curve but correspond to a later stage when the deflection of the beam was equal to 1/50th of the total span, $2l_i$. This is made clear in Fig. 13, which shows the point on each experimental load deflection curve of the 3 in. × 1½ in. RSJ selected by HENDRY, and that corresponding to the theoretical calculations. In fact the theory overestimates the load corresponding to the knee of the curve by roughly the percentage one would expect. It is interesting that the higher rate of increase of load with deflection for the shorter beams tends to offset the greater reduction in carrying capacity due to the higher shear loads.

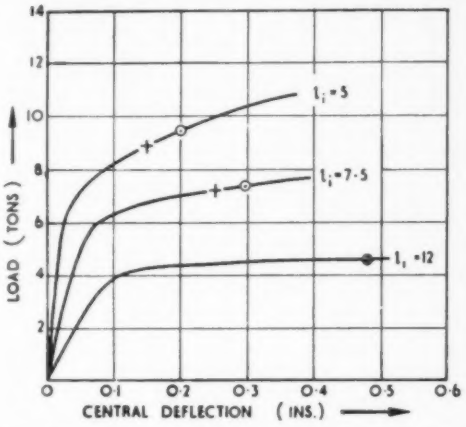

Fig. 13. HENDRY's load deflection curves for simply supported beams of 3 in. × 1½ in. I-section showing: (i) Points ⊙ corresponding to deflections equal to 1/50th of the span; (ii) Points + corresponding to the theoretical calculations.

7. DISCUSSION

The simple theory of pure bending is, in effect, the limit of the present theory as $l/t \to \infty$. This latter theory shows that the simple theory may be more in error for small values of S/k than has hitherto been supposed, and that it is certainly inaccurate for large values of S/k. The discrepancy between the two theories depends not only on the value of S/k but also on the strength of the end support and the precise manner of loading.

The present theory needs to be completed by constructing equilibrium stress distributions which do not violate the yield criterion in the assumed rigid regions. Until this is done, it is not certain that the yield-point loads are not over-estimated, though this seems unlikely.

The main aim of the more detailed theory is to obtain an accurate knowledge of the corrections which must be applied to the simple theory. With this aim still in view, it would be useful to extend the results of this paper, and to construct simple empirical equations where possible to cover the following problems:

(i) Weakly supported uniform cantilever in plane stress under shear loading with $S/k > 0{\cdot}33$.

(ii) Non-symmetrically loaded fixed-ended beams.

(iii) Effect of combined axial and shear loads in plane stress and application of the results to I-beams.

(iv) I-beams bent about axes perpendicular to the flanges.

Problems like (ii) require simultaneous consideration of load and displacement boundary conditions, a difficulty which has only been lightly touched upon here in the discussion of the yielding of fixed ended beams.

Finally, the amount of relevant experimental work is at present small and needs to be extended to test effectively the reliability of the theory.

Acknowledgment

I am grateful to Mr. D. Spenceley of the General Plasticity Section of B.I.S.R.A. for his assistance in calculating the results and drawing the diagrams for this paper, which is based on B.I.S.R.A. Reports MW/B/14/53 and MW/B/9/54.

References

Frankl, E. K. 1950 *Welding Research*, **4**, 27.

Green, A. P. 1954 *J. Mech. Phys. Solids*, **3**, 1.

Hendry, A. W. 1950 *The Structural Engineer*, **28**, 311.

Hill, R. 1954 *J. Mech. Phys. Solids*, **2**, 278.

Hundy, B. B. 1954 *Metallurgia*, **49**, 109.

Vol. 3 54/55

Journal of the Mechanics and Physics of Solids, 1954, Vol. 3, pp. 156 to 166. Pergamon Press Ltd., London

THE PLASTIC BENDING AND TWISTING OF SQUARE SECTION MEMBERS

By M. C. Steele
Department of Theoretical and Applied Mechanics, University of Illinois

(*Received 2nd July*, 1954)

Summary

A long prismatic member is acted on by combinations of bending moments and torques of such a magnitude as to render the member just fully plastic. This problem was originally discussed by Handelman, who, assuming a Lévy-Mises material, derived a nonlinear, partial differential equation to describe it.

The present paper takes Handelman's equation and solves it numerically for a square section member. The moments and tor ues computed from the numerical solution are compared with a bounded solution due to Hill and Siebel. Finally, the stress distributions (shear and bending) are given in a member for two critical combinations of moment and torque.

1. Introduction

A straight uniform square section member is acted on by combinations of bending moments and torques applied at the two ends. The bending moments lie in one of the planes of symmetry parallel to the sides and torques act about the centre of twist. It is required to find the critical combinations of moments and torques which render the member fully plastic and the corresponding distributions of stresses.

It is assumed that the member is composed of an ideally plastic-rigid material. Thus, there is no deformation until every element is yielded, at which stage plastic-flow commences under constant values of the applied force actions and the corresponding stresses (change in geometry being neglected).

This problem was originally discussed by Handelman (1944). Considering a Levy-Mises body, Handelman derived a second order, nonlinear, partial differential equation in a stress function ϕ to describe the problem. The same equation was derived by Hill (1948) to illustrate the use of his principle of maximum plastic work. So far as the author knows, a solution to this differential equation has not appeared in the literature.

From a practical point of view, an approximate knowledge of the critical combinations of moments and torques is all that is required. Hill and Siebel (1953) supplied this information by bounding the critical combinations from above and below using variational principles. They applied their theory to a circular cross section member and supported it by experimental data which showed good agreement.

The present work applies the general theory of HILL and SIEBEL to obtaining upper and lower bounds on the critical combinations of moments and torques for a square cross section member. A numerical solution is then given for the partial differential equation of HANDELMAN and HILL for two values of a parameter ($\dot{\theta}/\dot{\rho}$) which is the ratio of rate of twist to rate of curvature. The moments and torques computed from the numerical solution are compared with the bounded solution due to HILL and SIEBEL. Finally, the stress distributions (shear and bending) are given in a member composed of this hypothetical material for the two values of $\dot{\theta}/\dot{\rho}$.

2. MATHEMATICAL FORMULATION OF PROBLEM

1. *Partial Differential Equation of* HANDELMAN

The rate of work of the external forces is given by

$$\dot{W} = \int\int [\tau_{xz} v_x + \tau_{yz} v_y + \sigma_z v_z]\, dx\, dy \tag{1}$$

the integral being taken over the ends of the member. σ_x, σ_y, and τ_{xy} are assumed to be zero (twist is about the z-axis) and v_x, v_y, and v_z are assumed to satisfy

$$\left.\begin{aligned} v_x &= \tfrac{1}{4}(x^2 - y^2 + 2z^2)\,\dot{\rho} - yz\dot{\theta}, \\ v_y &= \tfrac{1}{2}\, xy\dot{\rho} + xz\dot{\theta}, \\ v_z &= -\,xz\dot{\rho} + \dot{w}\,(x, y). \end{aligned}\right\} \tag{2}$$

Expression (1) is maximized for varying stresses σ_z, τ_{xz}, τ_{yz} which satisfy

$$\tau_{xz} = -\,k\,\frac{\partial\phi}{\partial y}, \qquad \tau_{yz} = k\,\frac{\partial\phi}{\partial x}, \qquad \sigma_z = \pm\sqrt{3}k\sqrt{1 - \left(\frac{\partial\phi}{\partial x}\right)^2 - \left(\frac{\partial\phi}{\partial y}\right)^2}, \tag{3}$$

where $\phi(x, y)$ is a stress function. ϕ is zero on the boundary curve of the cross section to meet the requirement that the lateral surface of the member is free from stress. k is the yield stress in pure shear.

The stresses and strain rates are independent of z as is the warping function. In the integral in (1) terms not involving z cancel out at opposite ends of the member. Substitution of the expressions given in (2) and (3) into (1) and using the Euler-Lagrange formula of the calculus of variations, stationary values of $\dot{W}$ corresponding to functions ϕ satisfy

$$\left.\begin{aligned} &\frac{\partial}{\partial x}\left[x\,\frac{\partial\phi}{\partial x}\right] + \frac{\partial}{\partial y}\left[x\,\frac{\partial\phi}{\partial y}\right] + \frac{2}{\sqrt{3}}\,\frac{\dot{\theta}}{\dot{\rho}} = 0 \\ &\text{where} \\ &x = \frac{y}{\sqrt{1 - \left(\frac{\partial\phi}{\partial x}\right)^2 - \left(\frac{\partial\phi}{\partial y}\right)^2}}. \end{aligned}\right\} \tag{4}$$

This derivation is due to HILL (1948) who treated the more general case of bending couples, twisting couples and longitudinal forces applied to the ends. It is recognized as an application of HILL's principle of maximum plastic work for

a Lévy-Mises material. HILL verified that the original assumptions made with regard to velocities and stresess are justified.

It is (4) together with $\phi = 0$ on the boundary curve which is solved numerically in this paper for two values of the parameter $\dot{\theta}/\dot{\rho}$.

It can readily be shown that the moments (M) and torques (T) are given by

$$M = \sqrt{3}\,k \iint y \sqrt{1 - \phi_x{}^2 - \phi_y{}^2}\, dx\, dy, \qquad T = 2k \iint \phi\, dx\, dy, \tag{5}$$

where the sign of the radical is taken as positive when y is positive and negative when y is negative. ϕ_x and ϕ_y denote $\partial\phi/\partial x$ and $\partial\phi/\partial y$.

2. *Upper and Lower Bound Solutions*

(i) *Lower Bound.* For any system of stresses which satisfy (3) and the stress boundary conditions, the rate of work of the external forces given by (1) is either less than or equal to the rate of work performed by the actual external forces. This enables us to find lower bounds for M and T, i.e., we can select an admissible stress system and be assured that the M and T computed from these stresses is always a combination which is less than or equal to the actual initial combination causing yield. In a recent paper, HILL and SIEBEL (1953) have shown that a good approximation for a lower bound for any given section is given by the interaction equation

$$(M/M_0)^2 + (T/T_0)^2 = 1 \tag{6}$$

in which M_0 is the " yield " moment with no torque acting and T_0 is the " yield " torque with no moment acting.

(ii) *Upper Bound.* HILL and SIEBEL have also shown that an application of HILL's (1950, p. 67) inequality provides an upper bound for the critical moments and torques. Thus

$$M\dot{\rho} + T\dot{\theta} \leqslant k \iint [3x^2\,\dot{\rho}^2 + (x^2 + y^2)\,\dot{\theta}^2]^{\frac{1}{2}}\, dx\, dy = \lambda, \text{ say,} \tag{7}$$

where the left-hand side represents the rate of work of the actual external forces and the right-hand side is derived from a fictitious velocity distribution which is the same as (2) with the warping function zero.

If M^* and T^* are moments and torques providing an upper bound, then it can be shown that

$$M^* = \partial\lambda/\partial\dot{\rho}, \qquad T^* = \partial\lambda/\partial\dot{\theta}, \qquad \text{where } M^*/T^* = M/T. \tag{7}$$

If A is the side of the square cross section,

$$\left.\begin{aligned} \frac{M^*}{M_0} &= \frac{4}{\sqrt{3}A^3} \iint \frac{3x^2\,\lambda\, dx\, dy}{\sqrt{3x^2\,\lambda^2 + x^2 + y^2}}, \\ \frac{T^*}{T_0} &= \frac{3}{A^2} \iint \frac{(x^2 + y^2)\, dx\, dy}{\sqrt{3x^2\,\lambda^2 + x^2 + y^2}}, \\ \text{where} \qquad \lambda &= \dot{\rho}/\dot{\theta}. \end{aligned}\right\} \tag{8}$$

Expressions (8) are both integrable. The combined results of the lower and upper bound solutions may be plotted on an interaction curve of T/T_0 versus

M/M_0, as in Fig. 12. The maximum difference occurs for pure torsion and is approximately 14%.

3. Numerical Formulation of Problem

1. *Preliminary Discussion of Partial Differential Equation*

A numerical solution is sought for

$$\left.\begin{aligned} &\frac{\partial}{\partial x}\left[x\frac{\partial \phi}{\partial x}\right]+\frac{\partial}{\partial y}\left[x\frac{\partial \phi}{\partial y}\right]+\frac{2}{\sqrt{3}}\frac{\theta}{\dot{\rho}}=0 \\ \text{where}\quad &x=\frac{y}{\sqrt{1-\phi_x^{\,2}-\phi_y^{\,2}}} \end{aligned}\right\} \tag{9}$$

and $\phi = 0$ on the boundary curve.

If $\dot{\theta}/\dot{\rho} = \infty$ ($\dot{\rho} = 0$, $\dot{\theta} \neq 0$) (9) reduces to

$$\phi_x^{\,2} + \phi_y^{\,2} = 1$$

which is recognized as the governing equation for pure torsion. If $\dot{\theta}/\dot{\rho} = 0$ ($\dot{\theta} = 0$, $\dot{\rho} \neq 0$), then ϕ = constant satisfies (9) and the constant is zero from the boundary conditions. This is the case for pure bending.

If x is always positive, i.e., the sign of the radical is taken the same as the sign of y, then ϕ is symmetrical about axes x and y. Regarding ϕ as a stress surface built up over the cross section, the possible nature of singularities on the bending axis ($y = 0$) may be visualized. When $y = 0$ $x = 0$ unless $\phi_x^{\,2} + \phi_y^{\,2} = 1$ in which case x is indeterminate. If the ϕ-surface is smooth at $y = 0$, then $\phi_y = 0$, in which case $\phi_x = 1$ and x is again indeterminate. From an examination of the expanded form of (9), it appears likely that the ϕ-surface comes to a cusp along the y-axis or part of it and the numerical solution has been approached with this point in mind. A numerical procedure, then, which would essentially smooth out any ridges in the ϕ-surface may be in considerable error near the bending axis. The error will be shown up most severely in the stresses τ_{xz}, τ_{yz}, σ_z near the x-axis, but their effect on the corresponding moments and torques is likely to be negligible.

2. *Non-dimensional Form of Equation*

It is advisable to write (9) in a non-dimensional form before proceeding to the numerical solution for the square cross section. To do this we put

$$x = Ax', \qquad y = Ay', \qquad \phi = A\phi', \qquad x = Ax', \tag{10}$$

where A is the side of the square cross section. Thus :

$$\frac{\partial}{\partial x} = \frac{1}{A}\cdot\frac{\partial}{\partial x'}, \ldots\ldots \qquad \frac{\partial \phi}{\partial x} = \frac{\partial \phi'}{\partial x'}, \ldots\ldots$$

Substitution in (9) shows that the original form of the equation is retained in the new variables :

$$\left.\begin{aligned} &\frac{\partial}{\partial x'}\left[x' \cdot \frac{\partial \phi}{\partial x'}\right] + \frac{\partial}{\partial y'}\left[x' \cdot \frac{\partial \phi'}{\partial y'}\right] + \frac{2\dot{\theta}}{\sqrt{3}\dot{\rho}} = 0 \\ \text{where} \qquad &x' = \frac{y'}{\sqrt{1 - \left(\frac{\partial \phi'}{\partial x'}\right)^2 - \left(\frac{\partial \phi'}{\partial x'}\right)^2}} \end{aligned}\right\} \tag{11}$$

and $\phi' = 0$ on the boundary curve. In what follows the primes will be dropped for convenience.

3. *Finite Difference Approximation*

Equation (11) is of the "quasi-plane-harmonic" type which is treated by SOUTHWELL (1946, page 187) or GREEN and SOUTHWELL (1944). Using the simplest finite difference approximation, we have at an internal point (0) (square mesh) that (11) is approximated by

$$\tfrac{1}{2}\left\{\Sigma\left[\phi_1\left(x_1 + x_0\right)\right] - \phi_0\,\Sigma\left[x_1 + x_0\right]\right\} + a^2 \cdot \frac{2}{\sqrt{3}}\frac{\dot{\theta}}{\dot{\rho}} = 0 \tag{12}$$

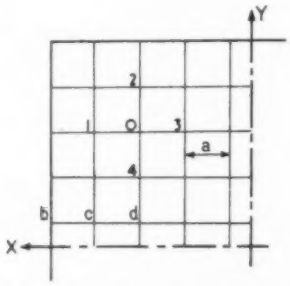

Fig. 1. Notation for finite difference approximations.

where the subscript numbers are as shown in Fig. 1 and 'a' is the mesh side. x for an internal mesh point is given by

$$x = \frac{y}{\sqrt{1 - \frac{2}{a^2}\left[\phi_0{}^2 + \tfrac{1}{4}\left\{\Sigma\left(\phi^2\right) - 2\phi_0\,\Sigma\left(\phi\right)\right\}\right]}} \tag{13}$$

and x at a point on the boundary curve (e.g. b in Fig. 1) is given by the ended formula approximation as

$$x = \frac{y}{\sqrt{1 - \frac{1}{4a^2}\left[\phi_a - 4\phi_c\right]^2}} \tag{14}$$

where ϕ_b is zero from boundary conditions.

4. *Relaxation Pattern and Procedure*

For any chosen ϕ distribution consistent with boundary conditions, we can write down for each mesh point, an equation of the form

$$\tfrac{1}{2}\{\Sigma[\phi_1(x_1+x_0)]-\phi_0\,\Sigma[x_1+x_0]\}+a^2\cdot\frac{2}{\sqrt{3}}\cdot\frac{\dot\theta}{\dot\rho}=F_0 \tag{15}$$

where F_0 is the "residual force." A solution is obtained when F_0 for all mesh points are reduced to zero. The method for reducing F_0 to zero or a negligible quantity is a relaxation procedure as used by SOUTHWELL for this type of problem. The relaxation pattern is shown in Fig. 2. This gives the change in residual forces at the points 0, 1, 2, 3, 4 for a unit (positive) change in ϕ_0.

The numerical solution is carried out for specific values of the parameter $\dot\theta/\dot\rho$ which is regarded as known in (15). A ϕ-distribution is assumed which then allows the computation of x's according to (13) or (14). Then the pattern appropriate to each mesh point is defined and the liquidation of residuals F_0 may proceed. Changes in ϕ during the liquidation process inflict changes in x and new x values must be computed from time to time. In the later stages of the work more attention must be given to accurate values for x, since the residuals must finally be computed accurately (i.e., within the limits of the finite difference approximations).

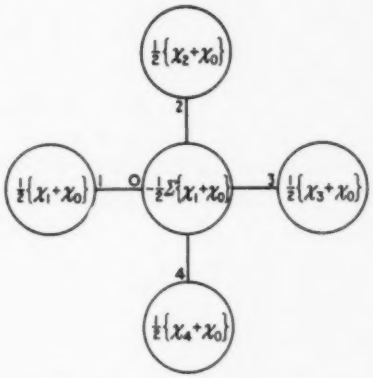

Fig. 2. Relaxation pattern.

A grid-size of $a = 1/9$ has been used mostly throughout the work. An uneven division of the square side was taken so that mesh points did not appear on the bending axis where singularities exist. A multiplying factor of 8,100 is employed for (15) and residuals deemed negligible when $F_0 = \pm 1$. Multiplying (15) by 8,100 we have

$$\Sigma[\bar\phi_1(x_1+x_0)]-\bar\phi_0\,\Sigma(x_1+x_0)+100\cdot\frac{2}{\sqrt{3}}\cdot\frac{\dot\theta}{\dot\rho}=F_0 \tag{16}$$

where $\bar\phi$'s are the ϕ's multiplied by 4,050. The bars will be dropped for convenience.

It is found that, due to the functional relation betsween x and ϕ, at some localities in the square region very small changes in ϕ produce comparatively large changes in x. Consequently to reduce F_0 to ± 1 at these localities, we must have a relatively high accuracy in ϕ. For the solutions reported the liquidation process was stopped when a unit change in ϕ at a point produced a larger residual of opposite sign at that point.

5. *Computation of Moments and Torques*

Moments and torques for a square cross section of side A are computed from the actual ϕ-solutions by noting that

$$T = 2kA^3\,(\text{volume under } \phi\text{-surface})$$

$$M = \sqrt{3}\,kA^3\,(\text{volume under } \psi\text{-surface}) \tag{17}$$

where $$\psi = y\sqrt{1-\phi_x{}^2-\phi_y{}^2}$$

Vol. 3 54/55

and the ϕ values used are the non-dimensional ones obtained from the solution divided by the multiplying factor of 4,050. The double use of SIMPSON's rule was employed to calculate the volumes in (17).

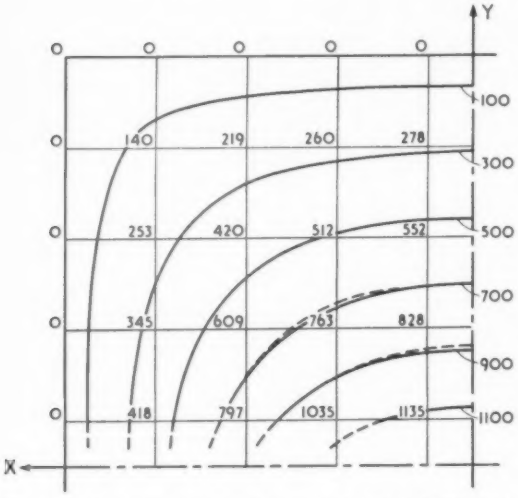

Fig. 3. Contour curves of constant ϕ ($\times$ 4050) and nodal point ϕ ($\times$ 4050) values ($\dot{\theta}/\dot{\rho} = \sqrt{3}/2$; $a = 1/9$ (full lines); $a = 1/13$ (dotted lines)).

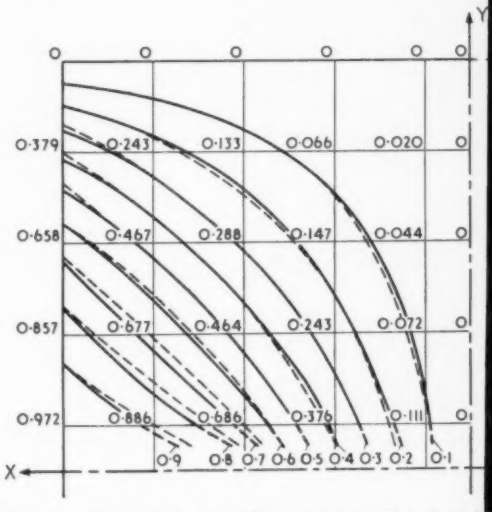

Fig. 4. Contour curves of constant τ_{yz}/k and nodal point τ_{yz}/k values ($\dot{\theta}/\dot{\rho} = \sqrt{3}/2$; $a = 1/9$ (full lines); $a = 1/13$ (dotted lines)).

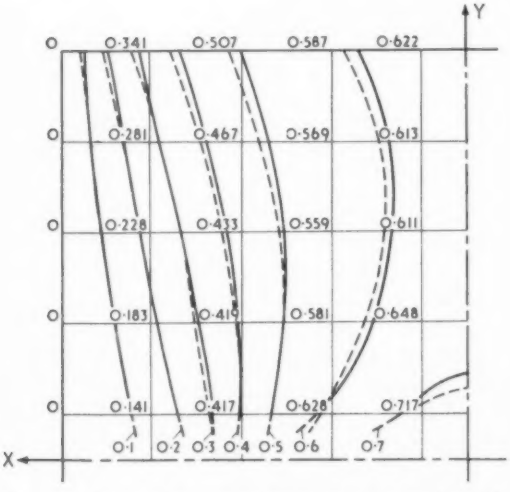

Fig. 5. Contour curves of constant τ_{xz}/k and nodal point τ_{xz}/k values ($\dot{\theta}/\dot{\rho} = \sqrt{3}/2$; $a = 1/9$ (full lines); $a = 1/13$ (dotted lines)).

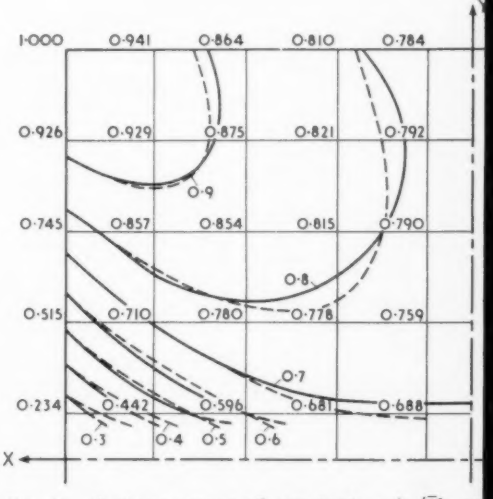

Fig. 6. Contour curves of constant $\sigma_z/\sqrt{3}k$ and nodal point $\sigma_z/\sqrt{3}k$ values ($\dot{\theta}/\dot{\rho} = \sqrt{3}/2$; $a = 1/9$ (full lines); $a = 1/13$ (dotted lines)).

4. RESULTS AND DISCUSSIONS

1. *Results*

Fig. 3 shows nodal values and contour curves for a ϕ-solution when $\dot{\theta}/\dot{\rho} = \sqrt{3}/2$,

and mesh size is one ninth of the square side. A plot of ϕ on mesh lines $x = 1/18$, $3/18$, etc. assists in visualizing the shape of the ϕ-surface in the y-direction and in particular in recognizing that the surface tends towards a cusp over part of the neutral axis of bending, i.e. the x-axis. Since the numerical method ignores

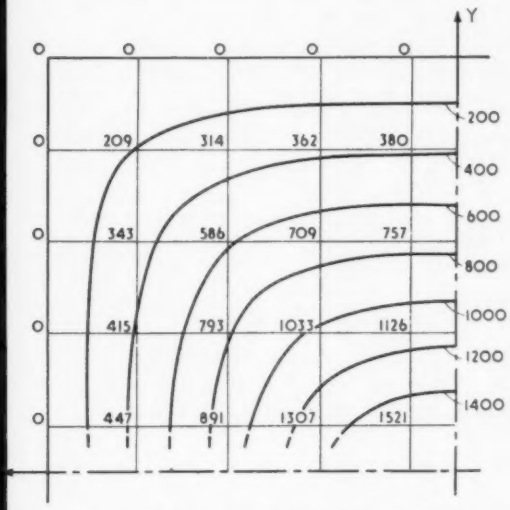

Fig. 7. Contour curves of constant ϕ ($\times$ 4050) and nodal point ϕ ($\times$ 4050) ($\dot{\theta}/\dot{\rho} = \sqrt{3}$; $a = 1/9$).

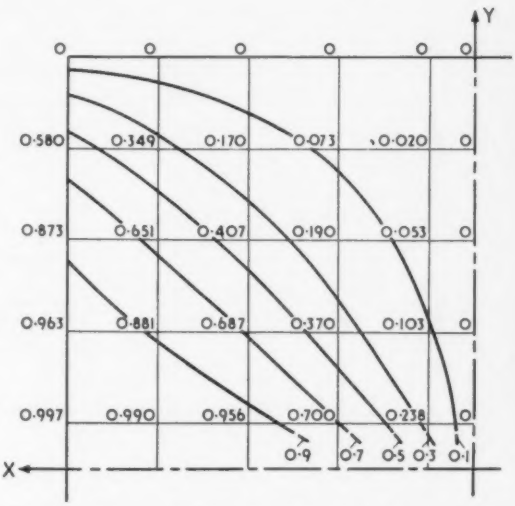

Fig. 8. Contour curves of constant τ_{yz}/k and nodal point τ_{yz}/k values ($\dot{\theta}/\dot{\rho} = \sqrt{3}$; $a = 1/9$).

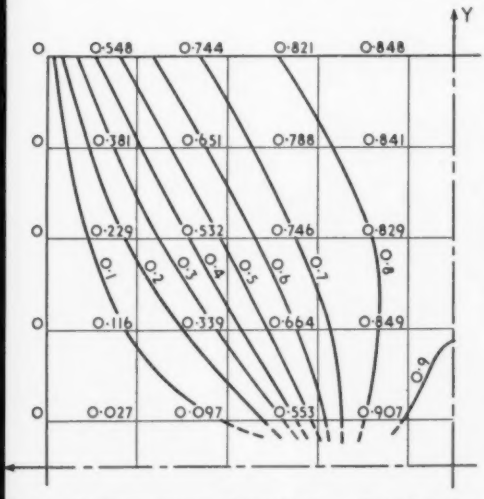

Fig. 9. Contour curves of constant τ_{xz}/k and nodal point τ_{xz}/k values ($\dot{\theta}/\dot{\rho} = \sqrt{3}$; $a = 1/9$).

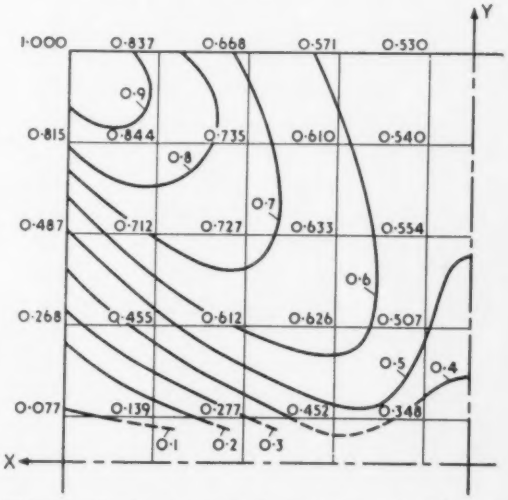

Fig. 10. Contour curves of constant $\sigma_z/\sqrt{3}k$ and nodal point $\sigma_z/\sqrt{3}k$ values ($\dot{\theta}/\dot{\rho} = \sqrt{3}$; $a = 1/9$).

this curvature discontinuity on the x-axis, the accuracy of the results are open to question. It is reasonable to assume that large errors may be localized in the region close to the x-axis, and hence a solution using a smaller mesh would indicate the significance of such errors. To this end, a numerical solution was completed

for a 13 × 13 mesh as compared to the previous 9 × 9 mesh ($\dot{\theta}/\dot{\rho} = \sqrt{3}/2$). Fig. 11 shows nodal values only for the 13 × 13 solution. Contours curves for the 13 × 13 solution are shown (dotted) superimposed in Figs. 3, 4, 5, 6; where full lines only are shown, it is to be assumed, that the dotted curves are coincident. Figs. 4, 5, 6 give results for τ_{yz}/k, τ_{xz}/k and $\sigma_z/\sqrt{3}k$ respectively, when $\dot{\theta}/\dot{\rho}$ has the value $\sqrt{3}/2$.

Figs. 7, 8, 9, 10 give corresponding results for a different value of $\dot{\theta}/\dot{\rho}$, that of $\sqrt{3}$. A 9 × 9 mesh was used in the solution. Lastly, Fig. 12 compares the numerical results for M and T with the bounds established on them using variational principles.

2. *Accuracy of Solutions*

The question of absolute accuracy is always a debatable one where numerical work is concerned. In this case, the existence of singularities in the given region complicates matters even further. A 9 × 9 mesh was chosen as a possible mesh size which would give sufficiently accurate results without an exorbitant amount of work. Since this was no more than a reasonable guess, it was decided to carry out a solution using a 13 × 13 mesh which involved approximately twice as many mesh points in the solution. Graphical interpolation was used to compare these two solutions and the error in ϕ was no more than $\pm 2\%$ which is within the limits of error to be expected in the comparison procedure. It is important that no relatively significant errors were located in the regions closest to the axis of singularities.

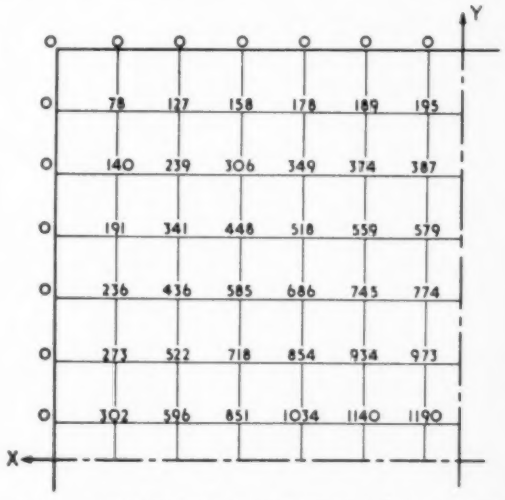

Fig. 11. Nodal point ϕ ($\times$ 4050) values ($\dot{\theta}/\dot{\rho} = 1/13$).

The shape of the ϕ surfaces indicates the nature of the singularities on the x-axis. The surfaces form a cusp on the x-axis and this shows up in the numerical solution in spite of the fact that its existence was ignored in obtaining the solution. The ridge or cusp on the x-axis, however, cannot be ignored in computing slopes of the ϕ surface in the y-direction on the y-grid adjacent to the x-axis. ($\partial\phi/\partial y \propto \tau_{xz}$). In computations for Figs. 4 and 8, $\partial\phi/\partial y$ values for points on the y-grid adjacent to the x-axis were found using ended finite difference formulae. Elsewhere the same approximations for slopes were used as in the numerical solution.

Figs. 4, 5, and 6 show comparisons of τ_{yz}/k, τ_{xz}/k, $\sigma_z/\sqrt{3}k$ respectively using 9 × 9 and 13 × 13 meshes when $\dot{\theta}/\dot{\rho} = \sqrt{3}/2$. The differences in τ_{yz}/k and τ_{xz}/k (assuming ϕ solutions to be sensibly the same) are undoubtedly due to the greater accuracy obtainable for the slopes using the finer mesh. The differences

are small and it is realized that a 9×9 mesh solution together with a four or five point formula for differentiation instead of the three point formula as used here, would give close comparison. The widest discrepancies occur for the $\sigma_z/\sqrt{3}k$ contour curves (Fig. 6). This is understandable when the nature of the relation between σ_z and ϕ is examined. It is readily shown that

$$\frac{\Delta(\sigma_z/\sqrt{3}k)}{\sigma_z/\sqrt{3}k} = \left|\frac{\Delta x}{x}\right| = \left|\frac{\phi_x^2}{(1-\phi_x^2-\phi_y^2)} \cdot \left(\frac{\Delta\phi_x}{\phi_x}\right) + \frac{\phi_y^2}{(1-\phi_x^2-\phi_y^2)} \cdot \left(\frac{\Delta\phi_y}{\phi_y}\right)\right|$$

For a 1% error in ϕ_x and ϕ_y, this gives for the per cent error in $\sigma_z/\sqrt{3}k$:

$$\frac{\Delta(\sigma_z/\sqrt{3}k)}{\sigma_z/\sqrt{3}k} = \left|\frac{1}{\left[\frac{1}{(\phi_x^2+\phi_y^2)} - 1\right]}\right|$$

Now in some regions $\phi_x^2 + \phi_y^2$ approaches unity and hence the possibility of large percentage errors in $\sigma_z/\sqrt{3}k$ must be accepted.

The τ_{yz} stresses are seen from Figs. 4 and 8 to be largest in the region surrounding the point where the x-axis meets the square section boundary. Because of symmetry, τ_{yz} stresses are zero on the y-axis. On the other hand, the τ_{xz} stresses are largest at regions removed from the square section boundary parallel to the y-axis. τ_{xz} stresses are not zero at all points on the x-axis because of the aforementioned cusp shape of the ϕ surface.

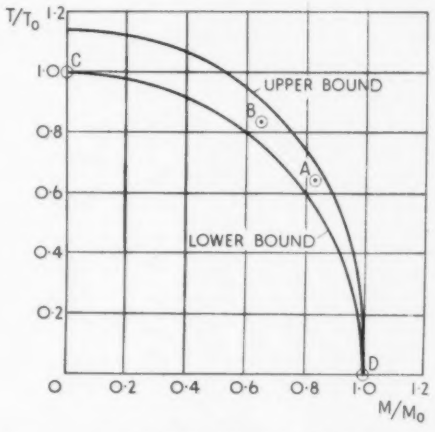

Fig. 12. Interaction diagram showing comparison of variational and numerical results.

The full lines in Fig. 12 show the upper and lower bound combinations of moment and torque causing " yield " of the square section member. The largest difference occurs for pure torque and is approximately 14%. Points A and B are the results from numerical computations for $\dot{\theta}/\dot{\rho} = \sqrt{3}/2$ and $\sqrt{3}$ respectively. It is worth mentioning that moments and torques for point A were computed for the solutions from both the 9×9 and 13×13 mesh sizes. Comparisons are shown in Table 1.

TABLE 1.

Comparison of T/T_0 and M/M_0 for 9×9 and 13×13 mesh size solutions ($\dot{\theta}/\dot{\rho} = \sqrt{3}/2$).

	9×9 *mesh*	13×13 *mesh*	*difference*
T/T_0	0·643	0·644	0·15%
M/M_0	0·828	0·825	0·36%

Points C and D represent, respectively, the correct yield torque for zero moment and the correct yield moment for zero torque. The fact that the points A and B lie between the upper and lower bound solutions lends support to the numerical solution given in the paper.

ACKNOWLEDGMENTS

The author is indebted to L. C. EICHBERGER, Research Assistant, Department of Theoretical and Applied Mechanics, University of Illinois, for his generous assistance in the preparation of the illustrations.

REFERENCES

HANDELMAN, G. H. 1944 *Quart. J. Appl. Math.*, **1**, 351.

HILL, R. 1948 *Quart. J. Mech. Appl. Math.*, **1**, 18.

HILL, R. and SIEBEL, M. P. L. 1953 *J. Mech. Phys. Solids*, **1**, 207.

HILL, R. 1950 *The Mathematical Theory of Plasticity* (Clarendon Press).

SOUTHWELL, R. V. 1946 *Relaxation Methods in Theoretical Physics* (Clarendon Press).

GREEN, J. R. and SOUTHWELL, R. V. 1944 *Phil. Trans. Roy. Soc.* A, **239**, 367.

Vol 3 1954/

BOOK REVIEWS

E. O. Hall : Twinning and Diffusionless Transformations in Metals. Butterworths Scientific Publications. 1954. pp. ix + 181, with 98 figures. 30s. net.

The great interest shown in the process of slip in crystals, quickened in recent years by the many signs that dislocation theory is at last on the right track, should not blind us to the fact that there are other modes of plastic deformation in crystals. Deformation twinning and shear transformations, which respectively produce new orientations and new crystal structures in the sheared region, also deserve attention. It is most unlikely that these modes of deformation will ever be dismissable with a mere ' etcetera,' once the slip process is understood, since they involve certain features distinctive from slip, e.g. homogeneous shear, complex habit planes and localized inhomogeneous atomic movements.

It was considerations such as these that led Dr. Hall to write this book and one must agree wholeheartedly with the opinion expressed in his preface, that ' a comprehensive and critical review (of twinning) would not be out of place.' The author has recognized the close connection between twinning and shear transformations by including a detailed account of the latter, although under the rather questionable title of ' diffusionless transformations.' Surely the absence of diffusion, i.e. of composition changes in the transformed regions, is irrelevant ; and the real reason for discussing these transformations alongside deformation twinning is that both cause plastic shear ? Moreover, as the bainite transformation shows, shear transformations exist which are not of the diffusionless kind.

The interesting part of the book begins in Chapter 4. The first three chapters provide a general background, dealing with topics such as space lattices, Miller indices, stereographic projection, the preparation of single crystals, slip deformation, and the formal crystallography of twinning. It is difficult to see the author's purpose here, since nearly everyone having the specialized interest necessary for the book will already be familiar with ' Barrett ' and ' Schmid and Boas.' Furthermore, the beginner may find himself confused at places in these introductory chapters. The rotation of the specimen axis in Figure 29 (a), for example, contradicts that in Figure 29 (b). On the same page (p. 36) the reader is led to believe that the lattice rotation accompanying an extension due to single slip causes a decrease in the component of unit tensile load resolved on the active slip system, whereas in fact it always causes an increase.

Chapters 4 to 7 deal with deformation twins, annealing twins, and shear transformations in various metals and alloys. These chapters are comprehensive, up-to-date, and well-documented reviews of both experimental and theoretical work in these fields. As guides to the literature they will prove most valuable, especially as the author gives an impartial and balanced survey of all the main points of view. It is a pity, however, that the author has found it necessary to suppress so much of his own personal opinion in order to reach this state of impartiality, for such views, coming from Dr. Hall and after such a thorough study of the literature, could not fail to be both valuable and interesting.

A. H. Cottrell

Structure and Properties of Solid Surfaces : Edited by Robert Gomer and Cyril Stanley Smith ; University of Chicago Press 1953 (Cambridge Univ. Press). XVI + 491 pp. Well illustrated. 64s.

This book reports a Conference arranged by the National Research Council in September 1952, in the form of fourteen prepared chapters each followed by contributions to discussion. The first by Conyers Herring on The Use of Classical Macroscopic Concepts in Surface-Energy Problems contains quite the most powerful study of the thermodynamics of solid surfaces yet available, and gives some consolation for the regretted fact that Gibbs was less expansive on the subject than he might have been. When next one hears nonsense talked about it (as one surely will) one will now know where to direct the speaker for education. The reviewer welcomes

HERRING's decision to re-instate the term "surface tension" (though, to be safe, he usually calls it γ) because no better term exists: "specific surface free energy," besides being lengthy, is, as he shows, only exact for single component systems.

The second chapter, on the Atomic Theory of Surface Energy, by EWALD and JURETSCHKE, contains original work in its first half, on the evaluation of lattice potentials near a surface. This will be of chief interest to those who try to calculate such quantities, who will find it has all the virtues and disadvantages of generality. The second half of this chapter reviews wave-mechanical calculations of the surface energy of metals: a survey of this rather difficult subject is welcome.

The third chapter, on the Mechanical Properties of Crystalline Metal Surfaces is by A. J. SHALER. Having been one of the initiators of the beautiful series of measurements of the surface tension of solids at M.I.T., SHALER has been wondering ever since what they really measured; but, for lack of precise definition of his terms, this reviewer got little profit from following his speculations.

Chapter IV by W. A. WEYL, on the Wetting of Solids as Influenced by Polarizability of Surface Ions, is more stimulating, though less drastically unconventional than its author thinks, except when wrong (as when his electrostatic theory conflicts with GAUSS's theorem). His arguments for a significantly distorted layer some hundreds of lattice spacings deep at the surface are in part invalid (elastic theory) and for the rest unconvincing (indirect inferences from observation). But it is not uncommon to find that the points most stressed by the author are not necessarily the most important in a paper. The treatment is quite unmathematical, and the penultimate sentence on p. 184 illustrates rather neatly the limit of his mathematical powers.

Chapter V by Sir GEORGE THOMSON gives a brief and illuminating account of the study of solid surfaces by electron diffraction, and Chapter VI by BOWDEN and TABOR on the Adhesion of Solids provides a typically interesting selection from the well-known studies of the Cambridge group of workers on this subject.

There are two chapters on Crystal Growth. That of A. F. WELLS contains in addition to older material some interesting new work on the geometry (in fact, mainly, the topology) of framework structures, which is helpful in understanding the structure of the more complex crystals. The second of these chapters is by H. E. BUCKLEY. His miscellaneous observations always make interesting reading to one interested in crystals. With regard to interpretations he displays a staunch and admirable conservatism blended with a mystic faith in the capabilities of vortices – but, of course, one who disclaims the making of theories can always make them more lightheartedly than if he acknowledges some obligation to work out their consequences in detail.

H. SEIFERT's chapter on epitaxy is an extensive review with many references, assuming considerable prior knowledge of the subject.

The remaining five chapters are on adsorption and catalysis, respectively by T. L. HILL, M. BOUDART, P. H. EMMETT, A. WHEELER, and G. M. SCHWAB *et al.* The study of adsorption can in principle give a great deal of information about the condition of surfaces, and it appears that one can at least deduce surface areas on the atomic scale in a fairly reliable way, but that the interpretation of results indicating heterogeneity of the surface or otherwise remains very much a matter of dispute. These chapters and the accompanying discussion provide a good opportunity to assess the position.

On the whole, except for specialists closely concerned, most chapters in this work can be regarded as dispensible, but anyone who can afford the purchase price is cordially recommended to buy it rather than to wait for the collected works of CONYERS HERRING.

F. C. FRANK

Vol 3 1954

Journal of the Mechanics and Physics of Solids, 1955, Vol. 3, pp. 169 to 175. Pergamon Press Ltd., London.

PLASTIC TWISTING OF A CIRCULAR RING SECTOR

By A. J. Wang and W. Prager
Division of Applied Mathematics, Brown University

(*Received 28th September*, 1954)

Summary

The fully plastic twisting of a circular ring sector of an arbitrary solid cross section is discussed. Graphical methods for the determination of the shear lines and the rate of warping are developed. Square and rectangular cross sections are treated as examples.

Vol. 3 54/55

1. Introduction

The elastic twisting of a circular ring sector is a problem of obvious importance for the determination of the stresses and strains in closely coiled helical springs (see, for instance, Timoshenko and Goodier 1953). While plastic deformations would be undesirable in a spring during normal conditions of service, they may be produced inadvertently through overloading or deliberately as part of the manufacturing process (" scragging "). In this connection the following analysis of the fully plastic twisting of a circular ring sector may be of interest.

For a circular cross section this problem has been treated by Freiberger (1953). The present analysis follows Freiberger's as far as the stress distribution is concerned. A geometrical interpretation of Freiberger's equations leads to a simple construction of the characteristics. The shear lines, which are the orthogonal trajectories of the characteristics, can thus be constructed for a cross section of arbitrary shape.

The present analysis differs from Freiberger's with respect to the circumferential velocity, which produces the warping of the cross sections. Freiberger assumes that this velocity vanishes along the line of stress discontinuity. As is shown below, this condition is not compatible with the general equations of the theory of perfectly plastic solids : not the circumferential velocity but the shear rate must vanish along the line of stress discontinuity. To within a rigid body rotation of the ring sector, this condition yields the circumferential velocities of the points on the line of discontinuity. The circumferential velocity of any other point can then be determined by integrating the differential equation for the circumferential velocity along the characteristic arc joining the considered point to a point on the line of discontinuity where the circumferential velocity is known.

To illustrate the general techniques suggested for the determination of stresses and circumferential velocities, square and rectangular cross sections are treated in some detail.

2. STRESSES

With respect to the cylindrical coordinates indicated in Fig. 1, all stress components except $\tau_{r\theta}$ and $\tau_{z\theta}$ are supposed to vanish. For simplicity, these will be denoted by τ_r and τ_z in the following. For the determination of these stresses, we have the equation of equilibrium,

$$\frac{\partial}{\partial r}(r^2\,\tau_r) + \frac{\partial}{\partial z}(r^2\,\tau_z) = 0, \tag{1}$$

the yield condition,

$$\tau_r^{\,2} + \tau_z^{\,2} = k^2, \tag{2}$$

where k is the yield stress in simple shear, and the boundary condition

$$\tau_z\,dr - \tau_r\,dz = 0. \tag{3}$$

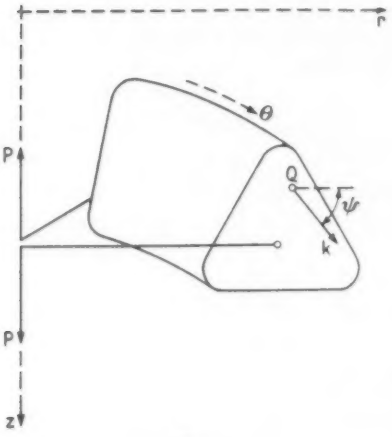

Fig. 1.

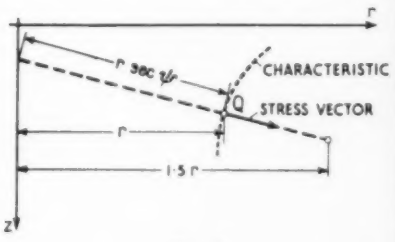

Fig. 2.

The yield condition (2) can be satisfied by setting

$$\tau_r = k\cos\psi, \qquad \tau_z = k\sin\psi, \tag{4}$$

where ψ is the angle formed by the resultant shearing stress and the axis of r. Substitution of (4) into the equation of equilibrium (1) yields the following partial differential equation for ψ :

$$\sin\psi\,\frac{\partial\psi}{\partial r} - \cos\psi\,\frac{\partial\psi}{\partial z} - \frac{2\cos\psi}{r} = 0. \tag{5}$$

The characteristic equations of (5) are

$$\frac{dr}{ds} = \sin\psi, \qquad \frac{dz}{ds} = -\cos\psi, \qquad \frac{d\psi}{ds} = \frac{2\cos\psi}{r}, \tag{6}$$

where ds is the line element of the characteristic. The first two equations (6) show that the characteristic through a generic point Q of the cross section is normal to the stress vector at Q. To obtain the positive direction of the characteristic,

we must rotate the stress vector by 90° in the sense which transforms the positive z direction into the positive r direction. The last equation (6) shows that the characteristic has the radius of curvature

$$\rho = \frac{r}{2} \sec \psi. \tag{7}$$

Fig. 2 indicates how the centre of curvature C at a point Q of the characteristic is determined when the stress vector at Q is known : C lies on the line of action of the stress vector, and its distance from the z axis equals 1·5 times the distance of Q from the z axis.

At a point Q on the contour of the cross section, the stress vector is tangential to the contour. The centre of curvature C of the characteristic through Q can therefore be determined and, in the neighbourhood of Q, the characteristic can be replaced by a short arc QQ' of its circle of curvature. The stress vector at Q' has the line of action $Q'C$. The centre of curvature C' of the characteristic at Q' can therefore be determined as before. Proceeding in this manner, we can approximate the characteristic by a sequence of short circular arcs.

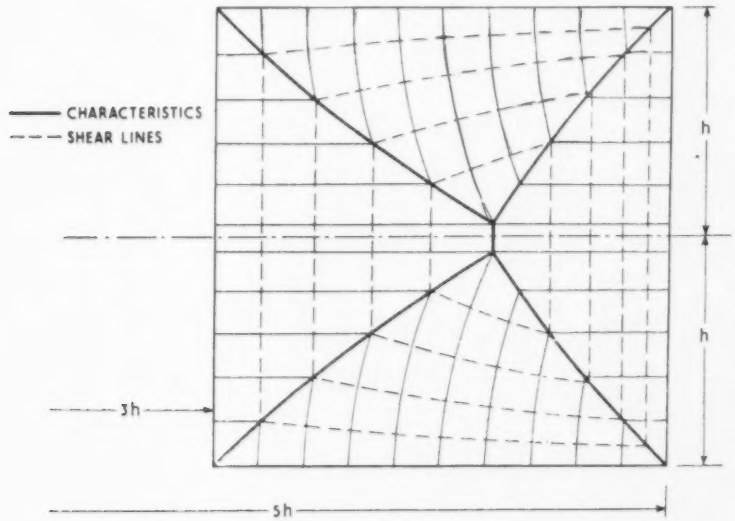

Fig. 3.

In treating a given cross section, it is advisable to start a number of characteristics from more or less equidistant points on the contour and extend all thesecharacteristics gradually into the interior of the cross section. It will then be found that characteristics emanating from different parts of the contour will intersect in the points of a line of discontinuity of the stress field. This phenomenon is well known from the problem of the fully plastic torsion of a prismatic bar, where the characteristics are the projections, on the cross sectional plane, of the lines of steepest descent on Nadai's sandhill, and the lines of discontinuity are the projections of the ridges of the sandhill (see NADAI 1923).

At a generic point of a line of discontinuity, the shear stress component normal to this line must be continuous for equilibrium. Since moreover the shear stress has the same value k on both sides of the line of discontinuity, the tangential components on the two sides must have the same magnitude but opposite directions. The tangent at a point Q of the line of discontinuity therefore bisects the angle formed by the tangents of the shear lines meeting at Q.

Figs. 3 and 4 show the characteristics and shear lines for a square and a rectangular section. The general pattern resembles that for the fully plastic torsion of these sections.

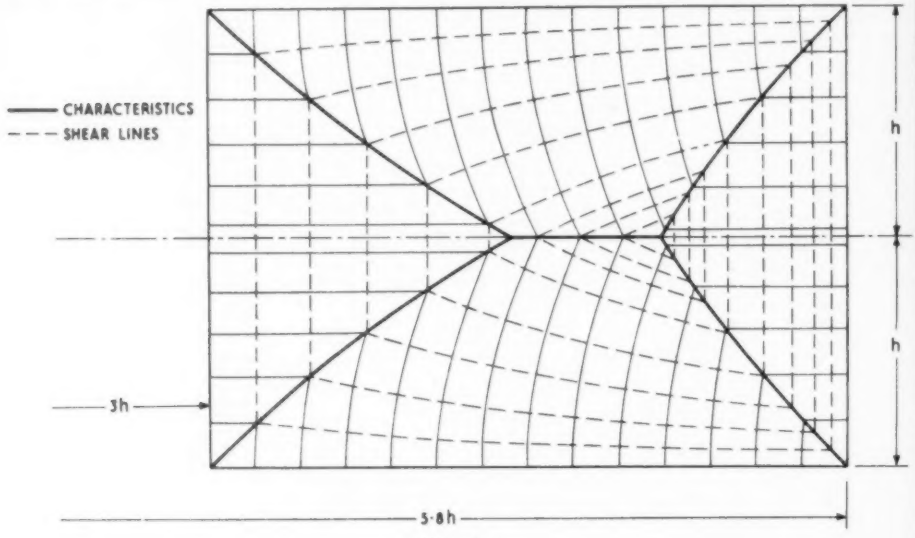

Fig. 4.

3. Stress Resultant

It remains to be shown that the shearing stresses obtained in this manner have as resultant a force acting along the z axis. Since these shearing stresses satisfy the equation of equilibrium (1), they are derivable from a stress function $\phi(r, z)$ in accordance with

$$\tau_r = \frac{1}{r^2}\frac{\partial \phi}{\partial z}; \qquad \tau_z = -\frac{1}{r^2}\frac{\partial \phi}{\partial r}. \tag{8}$$

The boundary condition (3) then shows that ϕ must be constant on the contour of the cross section, and for a simply connected cross section the constant value of ϕ on the contour may be taken as zero. At a line of discontinuity in the stress field, the stress function and its tangential derivative are continuous, but the normal derivative is discontinuous.

The resultant of the radial shearing stresses is given by

$$\int\int \tau_r \, dr \, dz = \int\int \frac{1}{r^2}\frac{\partial \phi}{\partial z} \, dr \, dz, \tag{9}$$

where the integration is extended over the entire cross section. Performing the

integration with respect to z and taking into account that ϕ vanishes on the contour of the cross section and is continuous across any line of discontinuity, we find that the resultant of the radial shearing stresses vanishes.

The resulting moment of the shearing stresses with respect to the origin of the r, z plane is given by

$$M = \int\int (r\tau_z - z\tau_r)\, dr\, dz = -\int\int \left(\frac{1}{r}\frac{\partial \phi}{\partial r} + \frac{z}{r^2}\frac{\partial \phi}{\partial z}\right) dr\, dz. \tag{10}$$

In view of the boundary and continuity conditions for ϕ, integration by parts of the right-hand integral in (10) shows the moment M to be zero.

The resultant of the shearing stresses in the cross section must therefore be a force acting along the z axis. According to the second equation (4) the intensity P of this force is given by

$$P = \int\int \tau_z\, dr\, dz = k \int\int \sin\psi\, dr\, dz. \tag{11}$$

When ψ has been determined by the graphical method described in the preceding section, the integration in (11) is best performed graphically. For the examples discussed in connection with Figs. 3 and 4, the following results were obtained :

$$P = 0{\cdot}66\, kh^2 \text{ for the square of Fig. 3.}$$

and

$$P = 1{\cdot}00\, kh^2 \text{ for the rectangle of Fig. 4.}$$

4. Velocities

According to Freiberger, the velocities of the plastic flow in the ring sector are of the form

$$v_r = 0, \qquad v_z = a\theta, \qquad v_\theta = a w\,(r, z), \tag{12}$$

where a is an arbitrary velocity and w is the rate of warping of the cross section when $a = 1$. Since the considered perfectly plastic material is inviscid, the velocities are determined only to within the arbitrary factor a.

Except for the shear rates $\gamma_{r\theta}$ and $\gamma_{z\theta}$ all strain rates associated with the velocities (12) are found to vanish. These shear rates, which will be denoted by γ_r and γ_z in the following, are given by

$$\begin{aligned} \gamma_r &= \frac{1}{r}\frac{\partial v_r}{\partial \theta} + \frac{\partial v_\theta}{\partial r} - \frac{v_\theta}{r} = a\left(\frac{\partial w}{\partial r} - \frac{w}{r}\right), \\ \gamma_z &= \frac{\partial v_\theta}{\partial z} + \frac{1}{r}\frac{\partial v_z}{\partial \theta} = a\left(\frac{\partial w}{\partial z} + \frac{1}{r}\right). \end{aligned} \tag{13}$$

The flow rule of von Mises requires that

$$\gamma_r/\gamma_z = \tau_r/\tau_z \qquad \text{and} \qquad \operatorname{sgn}\gamma_z = \operatorname{sgn}\tau_z. \tag{14}$$

When (4) and (13) are substituted into (14), the following partial differential equation for the rate of warping w is obtained :

$$\sin\psi\frac{\partial w}{\partial r} - \cos\psi\frac{\partial w}{\partial z} - \frac{1}{r}(w\sin\psi + \cos\psi) = 0. \tag{15}$$

This equation has the same characteristics as (5). Along any characteristic the following equation holds :

$$\frac{dw}{ds} = \frac{1}{r}(w \sin \psi + \cos \psi), \tag{16}$$

where the positive direction of the characteristic is defined in the same manner as before (see the discussion following (6)). Since r and ψ are known along the characteristic, graphical integration of (16) furnishes w along the characteristic provided that w is known at some point of the characteristic.

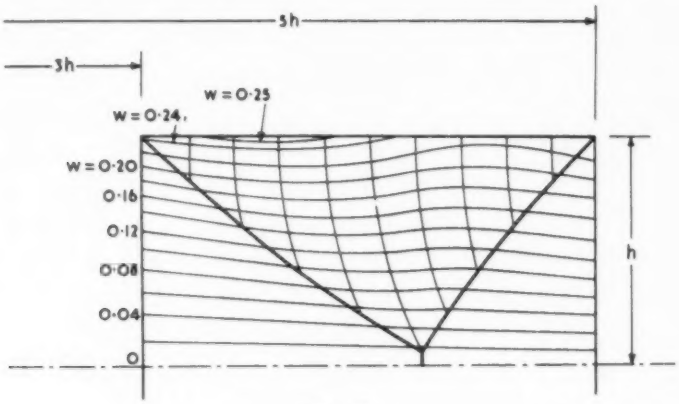

Fig. 5.

This initial information necessary for the graphical integration of (16) along the characteristic is obtained from the analysis of the rate of warping w on the line of discontinuity D. As has been shown in Section 2, the normal component of the shearing stress is continuous across D, but the tangential component reverses its sign. If the line of stress discontinuity is considered as the limiting case of a narrow zone of rapidly but continuously varying stress, the resulting shear stress at interior points of this zone will therefore not have the yield intensity k. Accordingly, the shear rate must vanish in the interior of this zone. In the limiting case of a line of discontinuity, it is therefore the shear rate that must vanish and not the rate of warping as assumed by FREIBERGER.*

According to (13), the following relations therefore hold along the line of discontinuity :

$$\frac{\partial w}{\partial r} = \frac{w}{r}, \qquad \frac{\partial w}{\partial z} = -\frac{1}{r}. \tag{17}$$

Graphical integration of

$$dw = \frac{1}{r}(w dr - dz) \tag{18}$$

along the line of discontinuity therefore furnishes w along this line provided that the value of w at some point of this line is known. Since the circumferential

* For the corresponding intuitive argument in the case of plane plastic strain see HILL (1950) and LEE (1950). Formal proofs have been given by HILL (1952) for plane plastic stress, GEIRINGER (1953) for plane plastic strain, HILL (1954) for plastic torsion, and PRAGER (1954) for perfectly plastic continua of one, two, and three dimensions.

velocity v_θ is determined only to within an arbitrary constant corresponding to a rigid body rotation about the z axis, w may be assumed to be zero at an arbitrarily chosen point of the line of discontinuity. Figs. 5 and 6 show the contour lines of w determined in this manner for the cross sections of Figs. 3 and 4; in each case w has been assumed to vanish at the centre of the cross section. At corresponding points of the upper and lower halves, w has the same absolute value but opposite

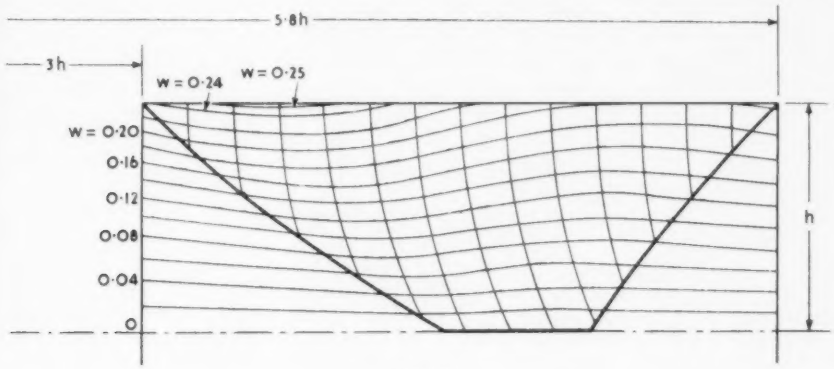

Fig. 6.

Vol. 3 54/55

signs. Inspection of Figs. 5 and 6 reveals that circumferential velocity w corresponds primarily to a skewing of the cross sectional plane with respect to the centroidal axis of the ring; superimposed on this skewing is some warping as is indicated by the fact that the contour lines of w are not parallel and equidistant straight lines.

Acknowledgment

The results presented in this paper were obtained in the course of research sponsored by Watertown Arsenal Laboratories under Contract DA-19-020-ORD-259 with Brown University.

References

Freiberger, W.	1953	Commonwealth of Australia, Aeron. Res. Labs. Report A.R.L./SM 213.
Geiringer, H.	1953	*Advances in Appl. Mech.*, **3**, 276.
Hill, R.	1950	*The Mathematical Theory of Plasticity* (Clarendon Press, Oxford), p. 160.
	1952	*J. Mech. Phys. Solids*, **1**, 19.
	1954	*Ibid.*, **2**, 87.
Lee, E. H.	1950	*Proc. Symp. Appl. Math.*, **3**, 213.
Mises, R. von	1913	*Goettinger Nachrichten, Math. Phys. Kl.* **1913**, 582.
Nadai, A.	1923	*Zeitschrift angew. Math. Mech.*, **3**, 442.
Prager, W.	1954	2nd U. S. National Congress, Appl. Mech., General Lecture.
Timoshenko, S. and Goodier, J. N.	1951	*Theory of Elasticity* (McGraw-Hill Book Co., New York).

Journal of the Mechanics and Physics of Solids, 1955, Vol. 3, pp. 176 to 188. Pergamon Press Ltd., London.

IMPACT PRESSURE LOADING OF RIGID-PLASTIC CYLINDRICAL SHELLS

By P. G. Hodge, Jr.
Department of Aeronautical Engineering and Applied Mechanics, Polytechnic Institute of Brooklyn

(*Received 28th September*, 1954)

Summary

The collapse load of a rigid-plastic body is defined as the smallest load at which deformations become possible. If a load greater than the collapse load is applied, the material of the body will undergo accelerated plastic flow. The present report considers a rigid-plastic cylindrical shell, loaded for a short time with a pressure greater than the collapse load. It is found that the shell is still specified by a single parameter depending on its dimensions, and that four different types of solution exist depending upon whether the load is "medium" or "high," and the shell is "short" or "long." Expressions for the stresses, velocities, and displacements are found in each case, and typical results are presented graphically.

1. Introduction

If an infinitely long cylindrical shell which is reinforced with equally spaced rigid reinforcing rings is instantaneously loaded with a finite pressure pulse, the stress and velocity distribution in any one bay of the shell may be regarded as typical. The phenomena which actually take place under such a loading will be quite complex, but certain simplifications may be made, depending upon the magnitude and duration of the pressure pulse. The present paper is concerned with a load which is greater than the static collapse load of the shell so that the elastic strains, both static and dynamic, may reasonably be neglected. On the other hand, the duration of the pulse is assumed to be sufficiently short for the total strains to be regarded as small compared with unity.

The static analysis of thin-walled shells under the above assumptions has been considered by Drucker (1953) and Hodge (1954). On the other hand, the dynamic behaviour of plates under similar assumptions has recently been considered by Hopkins and Prager (1953, 1954) while Lee and Symonds (1952), Symonds and Leth (1953), Owens and Symonds (1954), and Hopkins (1953) have considered similar problems for beams. However, the present paper is believed to be the first extension of plastic-rigid dynamic theory to cylindrical shells.

The mechanical state of a thin walled cylindrical shell under uniform radial pressure is entirely characterized by two stress resultants and a displacement. Let M_x and N_ϕ be, respectively, the bending moment and circumferential force per unit length of circumference, and let w be the radial displacement of the centroidal surface. M_x will be taken positive if it corresponds to tensile stresses

at the inner surface, N_ϕ will be positive in tension, and w will be positive when directed inwards. These three unknown functions depend only upon the axial distance x along a generator of the shell and the time t. They must be determined so as to satisfy the equation of equilibrium, certain yield conditions, and the plastic flow law. The formulation of these latter two conditions leads to certain inequalities as well as equations. Thus the obtaining of a solution becomes somewhat complex as the equations alone are insufficient to provide a unique result. All of these conditions will be given in Section 2.

Section 3 begins with a qualitative discussion of the type of solution to be expected for loads slightly greater than the collapse load. Such a " preview " to the mathematical methods for actually obtaining the solution may not be strictly necessary, in that the exhibition of a set of functions which satisfy all equations and inequalities defines a solution. However, from a practical viewpoint the obtaining of such a set of functions without a clear intuitive picture of what is happening in the shell is virtually impossible. Of course, it will often happen that the first intuitive picture is incorrect. If this is the case, a reference to the equations and inequalities will usually indicate the necessary changes to be made.

This is exemplified by the treatment of " long " shells. Intuitively, the solution of Section 3 might seem to apply, but this solution does not satisfy all inequalities. In Section 4 the correct solution is deduced for this case. Sections 5 and 6 are concerned with short and long shells, respectively, under the action of very high loads. Finally, an example is considered in Section 7, and several results are presented graphically.

Vol. 3 54/55

2. Defining Equations

It will prove convenient to discuss the title problem in terms of dimensionless variables defined in terms of the physical constants of the problem. The dimensions of a typical bay of the shell are given in Fig. 1. The surface density of the material is denoted by s, and the yield stress in pure shear of the material by k. The pressure pulse is assumed to have constant magnitude p and to act for a time t_0. The distance x is measured from the reinforcing ring and the time t from the instant of application of the pressure. Dimensionless quantities are then defined by

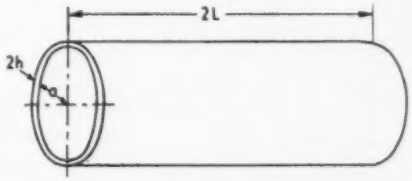

Fig. 1. Dimensions of shell.

$$\left.\begin{aligned} n &= N_\phi/4kh, & m &= M_x/2kh^2, \\ P &= pa/4kh, & W &= wsa/4kht_0^2, \\ y &= x/L, & \tau &= t/t_0, \\ & c = L/\sqrt{ah}. \end{aligned}\right\} \tag{1}$$

The equations of motion for a cylindrical shell are obtained by adding appropriate inertia terms to the static equations of equilibrium. The only modes of motion which are not prohibited by symmetry are radial motion and rotation

about a circumference. The elimination of shear force between the resulting equations of motion leads to

$$d^2 M_x/dx^2 + N_\phi/a + p - sd^2 w/dt^2 = 0,$$

or, in terms of the dimensionless variables defined by (1),

$$m''/2c^2 + n + P - \ddot{W} = 0, \tag{2}$$

where primes indicate differentiation with respect to y and dots with respect to τ.

For a perfectly plastic material, the reduced stress resultants must satisfy certain inequalities which depend upon the yield condition and the cross-section of the shell. This may be expressed in geometrical terms by stating that the stress point with coordinates (n, m) must lie within a certain bounded domain called the yield domain. For the particular case of Tresca's (maximum shearing stress) yield condition, Drucker (1953) has found the yield domain of Fig. 2a for a uniform section, and Hodge (1954) has found the curve of Fig. 2b for an ideal sandwich section. In the analysis to follow, a simplified yield domain as shown in Fig. 2c will be considered. Drucker has shown that by suitable choice of the yield stress k the collapse load can be determined to within $\pm$ 12·5% by this simple domain, but Hill (1954) has pointed out that similar accuracy may not apply to displacements.

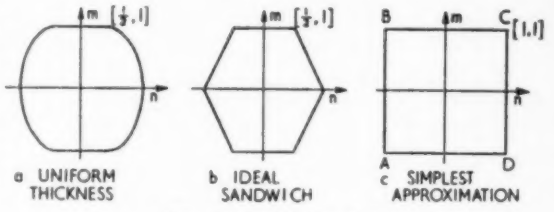

Fig. 2. Yield domains.

The image of the stress resultants along a typical generator of the shell in the stress resultant plane is called the stress profile. For a perfectly plastic material it must lie in or on the yield domain. Points of the shell where the stress profile lies within the yield domain must remain rigid, while at a boundary point a certain strain rate vector must be normal to the boundary. For the problem under consideration, this vector is

$$\dot{E} = \lambda\left[-\dot{W}, -\dot{W}''/2c^2\right] \tag{3}$$

where λ is arbitrary but must be positive. At a corner, the vector must lie between the two extreme normals there defined.

In the following, it will turn out that only the sides DA and AB and the vertices A and B of the yield domain are appropriate, and these will be denoted by plastic regime DA, plastic regime A, etc. The resulting stresses and strain-rates are listed in Table 1, together with the equations and inequalities which derive from them.

Table 1, together with the equilibrium equation (2), and certain continuity and boundary conditions to be expressed immediately completely define the mathematical problem to be solved.

In problems where the entire shell lies in one plastic regime, the substitution of the appropriate line of Table 1 into (2) leads immediately to a solution. However, in general, the stress profile includes two or more plastic regimes and it is

necessary to discuss the conditions of continuity. Considerations of equilibrium demand that the moment and the shear both be continuous, hence

$$m] = m'] = 0 \tag{4a, b}$$

TABLE 1

Plastic regime	*Stress resultants*			*Strain-rate vector*			
	Components n m		*Inequalities*	*Components* $\dot{W}$ $\dot{W}''/2c^2$		*Equations*	*Inequalities*
AD	*	-1	$-1 \leqslant n \leqslant 1$	0	λ	$\dot{W} = 0$	$\dot{W}'' \geqslant 0$
A	-1	-1	*	μ	λ	*	$\dot{W} \geqslant 0, \dot{W}'' \geqslant 0$
AB	-1	*	$-1 \leqslant m \leqslant 1$	μ	0	$\dot{W}'' = 0$	$\dot{W} \geqslant 0$
B	-1	$+1$	*	μ	$-\nu$	*	$\dot{W} \geqslant 0, \dot{W}'' \leqslant 0$

where the symbol] denotes the jump in the quantity preceding. Similarly, cohesion of the material requires that

$$W] = \dot{W}] = 0. \tag{4c, d}$$

Equations (4) must hold across any boundary, moving or stationary. Further relations may be obtained by taking the total derivatives of equations (4) with respect to time; this will be done in special cases as required.

Equations (4) are the only continuity requirements that have a direct physical basis. For actual materials, a certain degree of "smoothness" of results is expected that is often lost in the mathematical model due to simplifying assumptions. Where this occurs, the mathematical discontinuity must be regarded as the limiting case of a narrow region of rapid change for the real material. From this viewpoint if discontinuities in the velocity slope $\dot{W}'$ occur, they must correspond to finite values of the velocity $\dot{W}$ and infinite values of $\dot{W}''$. Such conditions can hold only at the corner plastic regimes *A* and *B*. The sign of the discontinuity is specified by the requirement that λ, μ, ν are all positive in Table 1, but its magnitude is indeterminate.

If the pressure variation were continuous, all quantities of interest would be continuous functions of time. However, for the pressure step function here considered, the time discontinuity of pressure can produce time discontinuities of all quantities except the displacement and velocity.

Finally, the initial and boundary conditions must be stated. Due to symmetry only half the shell need be considered. At $y = 0$, the rigid ring permits no displacement, and by symmetry the slope is either zero or discontinuous. Thus

$$W(0, \tau) = \dot{W}(0, \tau) = 0, \tag{5a}$$

$$W'(0^-, \tau) = \dot{W}'(0^-, \tau) = 0. \tag{5b}$$

At the centre of the shell $y = 1$, the shear and average slope must vanish, so that

$$W'(1^+, \tau) = \dot{W}'(1^+, \tau) = 0, \tag{5c}$$

$$m'(1, \tau) = 0. \tag{5d}$$

Finally, since there is no deformation prior to the application of the load,

$$W(y, 0) = \dot{W}(y, 0) = 0. \tag{5e}$$

3. Short shells under medium loads

If the magnitude of the pressure pulse is less than the collapse pressure, then according to the assumptions of the problem no motion will take place. It follows that the first problem is to determine the collapse load. Using the techniques proposed by HODGE (1954) for the yield domain Fig. 2c, it is easily seen that the stress profile at collapse occupies the entire regime AB with $y = 0$ corresponding to A and $y = 1$ to B. The necessary collapse pressure is

$$P_0 = (c^2 + 2)/c^2, \tag{6a}$$

and the corresponding velocity field is

$$\dot{W} = \dot{W}_0 y. \tag{6b}$$

If the pressure is slightly greater than P_0, it is reasonable to expect that the same plastic regime is applicable for dynamic loading. This hypothesis is tested by solving (2) and the two equations in the third line of Table 1, using the boundary conditions (5). The resulting solution is

$$\left.\begin{aligned} &m = \left[(c^2/2)(P-1) - 1\right] y^3 - c^2 (P-1) y^2 + \left[(c^2/2)(P-1) + 3\right] y - 1, \\ &n = -1, \qquad W = (3/2c^2)\left[(c^2/2)(P-1) - 1\right] \tau^2 y, \\ &0 \leqslant \tau \leqslant 1, \qquad P_0 \leqslant P \leqslant P_1, \end{aligned}\right\} \tag{7}$$

where P_1 will be defined in (9) following. The solution given by (7) is now checked against the inequalities in the third line of Table 1, and the requirement that the slope discontinuities at the hinge circles be in the proper direction. The latter condition, and the inequality $\dot{W} \geqslant 0$ are obviously satisfied for $P \geqslant P_0$. With regards to the stress, since m is a cubic in y and since

$$m(0) = -1, \qquad m(1) = 1, \qquad m'(1) = 0,$$

a necessary and sufficient condition that $-1 \leqslant m \leqslant 1$ for all $0 \leqslant y \leqslant 1$ is that

$$m''(1) \leqslant 0. \tag{8}$$

This condition is readily seen to hold for all $P \leqslant P_1$ where

$$P_1 = (c^2 + 6)/c^2 = P_0 + 4/c^2. \tag{9}$$

It follows then that the "medium" loads referred to in the title of this section are defined by

$$P_0 < P \leqslant P_1. \tag{10}$$

At $\tau = 1$, the pressure pulse instantaneously passes and no external load is applied to the shell. However, since the shell is already in motion, it must continue until all of the kinetic energy present has been dissipated into plastic work. If it is assumed that plastic regime AB continues to apply during this second stage of motion, the same equations are now to be solved with $P = 0$. The resulting solution is

$$\left.\begin{aligned} &m = -(c^2/2 + 1) y^3 + c^2 y^2 + (3 - c^2/2) y - 1, \qquad n = -1, \\ &W = \left[-(3/2c^2)(c^2/2 + 1) \tau^2 + (3P/2) \tau - 3P/4\right] y, \\ &1 < \tau \leqslant T, \qquad P_0 < P \leqslant P_1, \qquad 0 < c < \sqrt{6}. \end{aligned}\right\} \tag{11}$$

Here T is defined in (13) following, and the condition on c is derived in (12).

When the solution given by (11) is examined with reference to the stress inequalities in Table 1 it is evident that a necessary and sufficient condition that $-1 \leqslant m \leqslant 1$ for all $0 \leqslant y \leqslant 1$ is that

$$m'(0, \tau) = (6 - c^2)/2 \geqslant 0.$$

Therefore, the present analysis is valid only for " short " shells such that

$$0 < c^2 < 6. \tag{12}$$

For such short shells, the velocity condition $\dot{W} > 0$ and the conditions at the hinge circles both lead to requirement that τ be less than T where

$$T = Pc^2/(c^2 + 2) = P/P_0. \tag{13}$$

Therefore, for loads satisfying (10) and shells satisfying (12), the complete solution is given by (7) for $0 \leqslant \tau \leqslant 1$, by (11) for $1 \leqslant \tau \leqslant P/P_0$, and by $\dot{W} \equiv 0$ for $P/P_0 < \tau$.

4. Long Shells Under Medium Loads

The solution given in (7) is valid for $0 \leqslant \tau \leqslant 1$ for all shells provided that P satisfies (10). However, if $c^2 > 6$, then (11) predict that $m < -1$ near the end $y = 0$. Since this is not possible for a perfectly plastic material, some other hypothesis for the stress profile must be considered. One possibility might be to take the profile at A for $0 \leqslant y < u$ and along AB for $u < y < 1$. However, the substitution of the second line of Table 1 together with $P = 0$ into (2) leads to $\ddot{W} = -1$ for $0 < y < u$, and the boundary conditions (5a) cannot be satisfied. Therefore this possibility must be discarded.

An alternative suggestion is that the stress profile is in plastic regime DA for $0 < y < u$ and in AB for $u < y < 1$. In this case it follows immediately from the first line of Table 1 that the shell is rigid for $0 < y < u$. Since the entire shell is in motion at $\tau = 1$, u must be zero at $\tau = 1$ and hence the boundary between the two regimes must move as the deformation progresses. Thus, immediately when the load is removed motion stops in an infinitesimal region next to the rigid reinforcing rings. As time goes on the region of no motion grows and the deformation is confined to the ever narrowing centre section of the shell. A schematic representation of such a stress profile history is shown in Fig. 3b.

Under this hypothesis, the solution of the equations containing certain arbitrary functions of time A, B, C, D as integration constants is

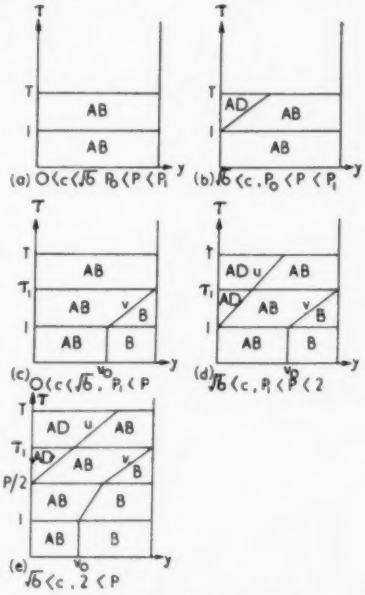

Fig. 3. Stress profile histories.

$$\left.\begin{aligned} &0 < y < u: \quad m = -1, \quad n = 0, \quad \dot{W} = 0 \\ &u < y < 1: \quad m = c^2\left[(\ddot{A}/3)\,y^3 + (1 + \ddot{B})\,y^2\right] + Cy + D, \\ &\qquad\qquad n = -1, \quad \dot{W} = \dot{A}y + \dot{B}. \end{aligned}\right\} \tag{14}$$

The boundary conditions on m for $u < y < 1$ are

$$m(u) = -1, \qquad m'(u) = 0, \qquad m(1) = +1, \qquad m'(1) = 0. \tag{15}$$

These four conditions can be utilized to find the integration functions in terms of the as yet unknown moving hinge circle u :

$$\left.\begin{aligned} \ddot{A} &= -(12/c^2)\,(1 - u)^{-3}, \\ \ddot{B} &= -1 + (6/c^2)\,(1 + u)\,(1 - u)^{-3}, \\ C &= -12u\,(1 - u)^{-3}, \\ D &= 1 - 2\,(1 - 3u)\,(1 - u)^{-3}. \end{aligned}\right\} \tag{16}$$

The velocity must be continuous at $y = u$ and must also be continuous in time with the solution given by (7) for $\tau = 1$. From the first of these requirements,

$$\dot{B} = -\dot{A}\,u. \tag{17}$$

If (17) is differentiated with respect to time, and second derivatives replaced by their values from (16), $\dot{A}$ may be written explicity as a function of u and $\dot{u}$:

$$A = (6/c^2\,\dot{u})\,[c^2/6 - (1-u)^{-2}]. \tag{18}$$

Differentiation of (18) and further use of (16) then leads to the following differential equation for u :

$$\ddot{u}\,[c^2/6 - (1-u)^{-2}] = 0. \tag{19}$$

Now, in view of (18) the bracketed expression in (19) cannot vanish since this would predict no motion. Therefore u is a linear function of τ. The values of the constants of integration are determined from the continuity of W at $\tau = 1$. Thus, from (14) and (7),

$$\dot{W}(y, 1) = \dot{A}(1)\,y + \dot{B}(1) = (3/2c^2)\,[(c^2/2)\,(P-1) - 1]\,y,$$

hence

$$\dot{A}(1) = (3/2c^2)\,[(c^2/2)\,(P-1) - 1], \qquad \dot{B}(1) = 0.$$

These conditions may be expressed in terms of u by means of (17) and (18), the resulting expressions being

$$u(1) = 0, \qquad \dot{u}(1) = \frac{2\,(c^2-6)}{3\,[(c^2/2)\,(P-1) - 1]}.$$

Therefore, the position of the hinge circle is given by

$$u = \frac{2\,(c^2-6)\,(\tau-1)}{3\,[(c^2/2)\,(P-1) - 1]}. \tag{20}$$

The preceding equations may now be combined to give the solution in the form

$$\left.\begin{aligned}
&0 < y < u: \quad m = -1, \qquad n = 0, \qquad \dot{W} = 0,\\
&u < y < 1: \quad m = 1 + (1-u)^{-3}\,[-4y^3 + 6\,(1+u)\,y^2 - 12uy - 2\,(1-3u)],\\
&\qquad\qquad n = -1, \qquad W = (6/c^2\,\dot{u})\,[c^2/6 - (1-u)^{-2}]\,(y-u),\\
&\qquad\qquad u = (2/3)\,(c^2-6)\,(\tau-1)\,[(c^2/2)\,(P-1) - 1]^{-1},\\
&\qquad\qquad 1 < \tau \leqslant T, \qquad P_0 < P \leqslant P_1, \qquad \sqrt{6} < c.
\end{aligned}\right\} \tag{21}$$

This solution must be tested in the inequalities of Table 1. It follows immediately from the boundary conditions (15) on m that $-1 \leqslant m \leqslant 1$ for $u \leqslant y \leqslant 1$. Further, the conditions $W \geqslant 0$ and proper discontinuities of the hinge circles are necessarily satisfied when $u = 0$ at $\tau = 1$, and will continue to be valid as long as

$$u < 1 - \sqrt{6}/c.$$

Therefore, in view of (20), the above solution will be valid for $1 < \tau < T$ where

$$T = \frac{3\,[(c^2/2)\,(P-1) - 1]}{2c\,(c + \sqrt{6})} + 1. \tag{22}$$

For $\tau = T$, $\dot{A} = 0$, hence the velocity everywhere vanishes and the motion is terminated.

5. Short Shells Under High Loads

If P is greater than P_1, inequality (8) is no longer satisfied and the solution given by (7) predicts a bending moment greater than one near the centre of the shell. Since this is inadmissible it seems reasonable to set $m = 1$ for some finite part of the shell. Obviously the centre of the

shell cannot remain rigid so that the only reasonable choice is for the stress profile to be in plastic regime AB for $0 < y < v_0$ and in regime B for $v_0 < y < 1$.

From Table 1 and equation (2) the solution is seen to be

$$\left.\begin{aligned} 0 < y < v_0 : \quad & m = (c^2/3)\,\ddot{A}y^3 - c^2\,(P-1)\,y^2 + Cy - 1, \\ & n = -1,\ \dot{W} = \dot{A}y\,; \\ v_0 < y < 1 : \quad & m = 1,\ n = -1,\ \dot{W} = (P-1)\,\tau. \end{aligned}\right\} \tag{23}$$

Here the boundary conditions at $y = 0$ and $y = 1$ have been accounted for, and the quantities A, C, and v_0 are to be determined from the continuity of m, m', and $\dot{W}$ at $y = v_0$. Evidently v_0 will be constant under these conditions. The final solution is then obtained in the form

$$\left.\begin{aligned} 0 < y < v_0 : \quad & m = 2\,(y/v_0 - 1)^3 + 1, \qquad n = -1, \\ & W = (1/2)\,(P-1)\,\tau^2\,(y/v_0)\,; \\ v_0 < y < 1 : \quad & m = 1, \qquad n = -1, \qquad W = (1/2)\,(P-1)\,\tau^2\,; \\ & v_0 = (1/c)\,\sqrt{6/(P-1)}, \\ & P_1 < P,\ 0 < \tau < 1. \end{aligned}\right\} \tag{24}$$

Obviously the greater the load the smaller the value of v_0, but for any finite load greater than P_1 there exists a value of v_0 between zero and one. The centre section of the shell moves uniformly inward and the end sections deform into truncated cones. It is readily verified that (24) satisfy all of the appropriate inequalities of Section 2.

At $\tau = 1$ the load is suddenly removed and (2) must be solved with $P = 0$. If the stress profile is assumed to have the same character as when $\tau < 1$, it turns out that the hinge circle separating the two regions is no longer stationary. After some computation the solution in this case is obtained in the form

$$\left.\begin{aligned} 0 < y < v : \quad & m = -(c^2 v^2 + 1)\,(y/v)^3 + c^2 v^2\,(y/v)^2 + (3 - c^2 v^2/2)\,(y/v) - 1, \\ & n = -1, \qquad \dot{W} = (P-\tau)\,(y/v)\,; \\ v < y < 1 : \quad & m = 1, \qquad n = -1, \qquad \dot{W} = P - \tau\,; \\ & v = (1/c)\,\sqrt{6\tau/(P-\tau)}\,; \\ & P_1 < P, \qquad 1 < \tau < \tau_1, \qquad 0 < c < \sqrt{6}. \end{aligned}\right\} \tag{25}$$

In order for this solution to be valid it must satisfy the inequalities of Section 2. Evidently a necessary and sufficient condition that m be less than one in magnitude is that $m'(0) > 0$. This will be initially true only if $P > 2$ and will be true for all $v_0 < v < 1$ only if $c^2 < 6$. However, for the loads considered here, $P > 1 + 6/c^2$ so that the second condition implies the first. Equations (25), then satisfy the stress inequalities for all $v_0 < v < 1$ for all "short" shells as defined in Section 3.

The velocity inequalities are all valid provided that $\tau < P$. However, this restriction is weaker than the geometrical condition that v be less than one. Indeed, it follows from this latter requirement and the last equation (25) that

$$\tau < \tau_1 = Pc^2/(c^2 + 6).$$

At $\tau = \tau_1$ the moving hinge circle v reaches the centre and can go no further. However, the velocity $\dot{W}$ is not yet equal to zero, so that the motion must continue. Since the entire stress profile is now in plastic regime AB the analysis of Section 3 is applicable, although with different initial conditions. After some computation the complete solution is found in the form

$$\left.\begin{aligned} & m = -(c^2/2 + 1)\,y^3 + c^2 y^2 + (3 - c^2/2)\,y - 1, \qquad n = -1, \\ & \dot{W} = (3y/2)\,[P - \tau\,(c^2+2)/c^2], \\ & P_1 < P, \qquad Pc^2/(c^2+6) < \tau < T, \qquad 0 < c < \sqrt{6}. \end{aligned}\right\} \tag{27}$$

This solution will be valid as long as the velocity is greater than zero, i.e. as long as

$$\tau < T = P/P_0. \tag{28}$$

Comparison with (13) shows that the same formula for the total time of deformation applies for both medium and high loads. The stress profile history for short shells with high loads is indicated in Fig. 3c.

In order to complete equations (25) or (27) by finding the displacement W, it is necessary to integrate $\dot{W}$. For $v < y < 1$ in (25) this is trivial, but for $0 < y < v$ some care must be taken with the boundary conditions. The general solution may be written

$$\left.\begin{aligned} 0 < y < v: \quad & W = y\{(\sqrt{6}\,P^2/8)\,[\sin^{-1}\sqrt{\tau/P} - \sin^{-1}\sqrt{1/P}] \\ & + (1/4\sqrt{6})\,[(5P-2\tau)\sqrt{\tau(P-\tau)} - (5P-2)\sqrt{P-1}]\} \\ & + h(y), \\ v < y < 1: \quad & W = (1/2)(-P + 2P\tau - \tau^2). \end{aligned}\right\} \tag{29}$$

A schematic diagram of the plastic regimes as functions of time is shown in Fig. 3c. For $0 < y < v_0$, it is evident that W must be continuous with the value given by [24] for $\tau = 1$. This leads easily to

$$h(y) = 3y/c^2 v_0^3 \qquad \text{for} \qquad 0 < y < v_0. \tag{30}$$

However, for $v_0 < v < 1$, Fig. 3c shows that the solution considered does not adjoin that given by (24), and the proper continuity consideration is at the hinge circle $y = v$. If y is set equal to v in (25) and the two values of W equated, the resulting equation may be solved for $h(v)$. In order to exhibit $h(v)$ explicitly, τ must be written in terms of v as defined by (25). The resulting expression will be the correct functional form of h for all $v_0 < v < 1$. Therefore, the desired expression for $h(y)$ is obtained by replacing v by y wherever it occurs. The final result is

$$\left.\begin{aligned} h(y) = & -\frac{P}{2}\left[1 - \frac{2c^2y^2P}{6+c^2y^2} + \frac{c^4y^4P}{(6+c^2y^2)^2}\right] \\ & - \frac{\sqrt{6}\,P^2y}{8}\left[\tan^{-1}\frac{cy}{\sqrt{6}} - \sin^{-1}\sqrt{\frac{1}{P}}\right] \\ & - \frac{y}{4\sqrt{6}}\left[3\sqrt{6}\,P^2cy\frac{10+c^2y^2}{(6+c^2y^2)^2} - (5P-2)\sqrt{P-1}\right], \\ & \text{for } v_0 < y < v. \end{aligned}\right\} \tag{31}$$

A similar computation for $\tau_1 < \tau < T$ shows that the displacement is given by

$$\left.\begin{aligned} W = & (3y/2)\,[P\tau - \tau^2(c^2+2)/2c^2] + k(y), \\ k(y) = & y\left[\frac{3}{4}\frac{P^2c(1-c)(10+c^2)}{(6+c^2)^2} + \frac{\sqrt{6}P^2}{8}\left(\tan^{-1}\frac{c}{\sqrt{6}} - \sin^{-1}\sqrt{\frac{1}{P}}\right)\right. \\ & \left. - (5P-2)\sqrt{P-1}/4\sqrt{6} + (P-1)/2v_0\right], \qquad 0 < y < v_0, \\ k(y) = & y\left\{\frac{3P^2c}{4}\left[\frac{(1-c)(10+c^2)}{(6+c^2)^2} - y\frac{c^2y^2+10}{(c^2y^2+6)^2}\right]\right. \\ & + \frac{\sqrt{6}P^2}{8}\left[\left[\tan^{-1}\frac{c}{\sqrt{6}} - \tan^{-1}\frac{cy}{\sqrt{6}}\right)\right. \\ & \left. - \frac{P}{2}\left[1 - \frac{2c^2y^2P}{6+c^2y^2} + \frac{c^4y^4P}{(6+c^2y^2)^2}\right], \qquad v_0 < y < 1. \right. \end{aligned}\right\} \tag{32}$$

6. Long Shells Under High Loads

For $c^2 > 6$ and $P > 1 + 6/c^2$, the solution for $0 < \tau < 1$ is still given by (24). However, after the load is removed a variety of behaviour can occur, depending upon the precise values of c and P. If P is less than 2, then (25) are inapplicable for any part of the remaining deformation. The correct stress profile to use in this case involves three plastic regimes as indicated in Fig. 3d. The corresponding solution is

$$\left.\begin{aligned} &0 < y < u: \quad m = -1, \quad n = 0, \quad \dot{W} = 0; \\ &u < y < v: \quad m = c^2\left[\ddot{A}y^3/3 + (1 + \ddot{B})\,y^2\right] + Cy + D, \\ &\qquad\qquad n = -1, \quad \dot{W} = \dot{A}y + \dot{B}; \\ &v < y < 1: \quad m = 1, \quad n = -1, \quad \dot{W} = P - \tau; \\ &\qquad P_1 < P < 2, \quad 1 < \tau < \tau_1, \quad \sqrt{6} < c. \end{aligned}\right\} \tag{33}$$

Here the integration functions of time are defined in equations (34), (35), and (37) following, u and v are given by equations (34) and (38) following, and τ_1 is defined by equations (38a) and (39) following.

As in Section 4, the substitution of (33) into the conditions expressing the continuity of m and m' at $y = u$ and $y = v$ leads to the relations

$$\left.\begin{aligned} &\ddot{A} = -12/c^2 z^3, \\ &B = -1 + 6(z + 2u)/c^2 z^3 \\ &C = -12uv/z^3, \qquad D = -(u + v)(v^2 - 4uv + u^2)/z^3, \end{aligned}\right\} \tag{34a}$$

where

$$z = v - u. \tag{34b}$$

Continuity of the velocity at u and at v then furnishes

$$\dot{W}(u, \tau) = \dot{A}u + \dot{B} = 0, \tag{35}$$

$$\dot{W}(v, \tau) = \dot{A}v + \dot{B} = P - \tau. \tag{36}$$

These relations may be combined to yield

$$\dot{A} = (P - \tau)/z. \tag{37}$$

If (37) is differentiated and $\ddot{A}$ replaced by its value from the first equation (34) the resulting first order differential equation in z is easily solved to furnish.

$$z^2 = (6/c^2)\left[2 - (2P - 3)(P - \tau)^2 (P - 1)^{-3}\right]. \tag{38a}$$

Here the initial condition $z = v_0$ (see (24)) at $\tau = 1$ was used to determine the integration constant.

With z known, u can be found by differentiating (37), using (34) and (38a), and taking the boundary condition $u(1) = 0$. The result is

$$u = v_0 - z - \frac{\sqrt{3}}{2c}\log\frac{z + 2\sqrt{3}/c}{z - 2\sqrt{3}/c}\,\frac{v_0 - 2\sqrt{3}/c}{v_0 + 2\sqrt{3}/c}. \tag{38b}$$

Finally, v is then given by (34b).

An analysis of (38) shows that for $P < 2$ (the only case now being considered), u and v both increase monotonically with time, and remain finite for all $\tau < P$. Further, it is evident from (37) and (33) that the velocity inequalities are all satisfied. Therefore the solution defined above remains valid until $v = 1$. The corresponding value of z is determined from (38b).

$$z_1 = \frac{2\sqrt{3}}{c}\,\frac{(-2\sqrt{3}/c)\sinh c(1 - v_0)/\sqrt{3} + v_0\cosh c(1 - v_0)/\sqrt{3}}{(2\sqrt{3}/c)\cosh c(1 - v_0)/\sqrt{3} - v_0\sinh c(1 - v_0)/\sqrt{3}}, \tag{39}$$

and the time τ_1 is then given by (38a).

For $\tau > \tau_1$ the stress profile is indicated in Fig. 3d. Except for the initial conditions, the problem is the same as that discussed in Section 4, and may be analysed in similar fashion. The appropriate initial conditions are obtained from the continuity of $\dot{W}$ at $\tau = \tau_1$ for all values of y. Evidently this is equivalent to the continuity of u and $\dot{u}$ so that for $\tau > \tau_1$ the position of the hinge circle is given by

$$u = \dot{u}(\tau_1)(\tau - \tau_1) + u(\tau_1)$$

$$= \frac{c^2 z_1^2 - 6}{(P - \tau_1) c^2 z_1} (\tau - \tau_1) + 1 - z_1 \tag{40}$$

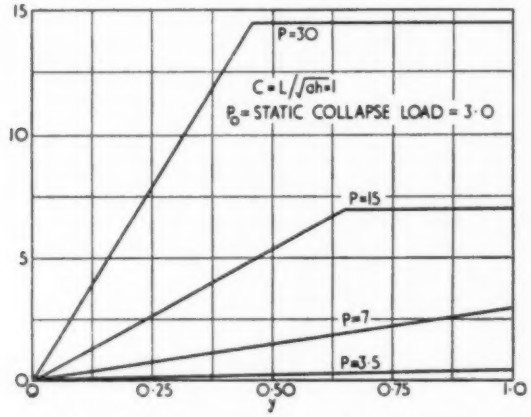

Fig. 4. Deformed shape of half-shell at instant load is removed.

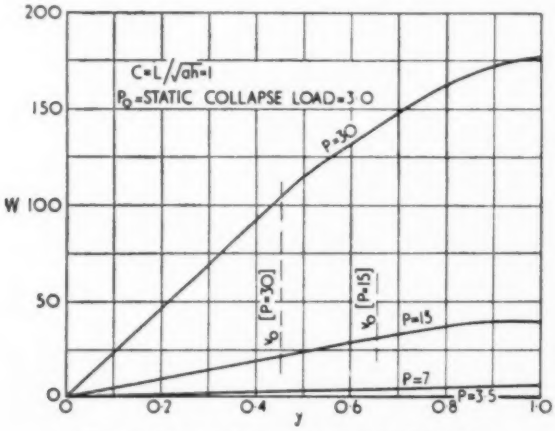

Fig. 5. Final deformed shape of half-shell.

where z_1 is given by (39). Since $\dot{A}$ is again given by (18), the above equation remains valid until as long as

$$u < 1 - \sqrt{6}/c,$$

i.e., for

$$\tau_1 < \tau < T = \frac{cz_1(P - \tau_1)}{cz_1 + \sqrt{6}} + \tau_1 \tag{41}$$

where z_1 is given by (39).

The final case to be considered is when $c^2 > 6$ but $P > 2$. In this case, (25) are valid for the initial stages after the load is removed. However, the stress distribution depends upon the

position of the hinge circle v and hence varies with time. In particular, $m'(0, \tau)$ decreases with time and becomes negative for $v^2 > 6/c^2$. Therefore, in view of the last equation (25) the solution is valid only for

$$1 < \tau < P/2.$$

For $\tau > P/2$, the solution will have the same general character as that discussed in the beginning of this section. A typical stress profile history is indicated in Fig. 3e.

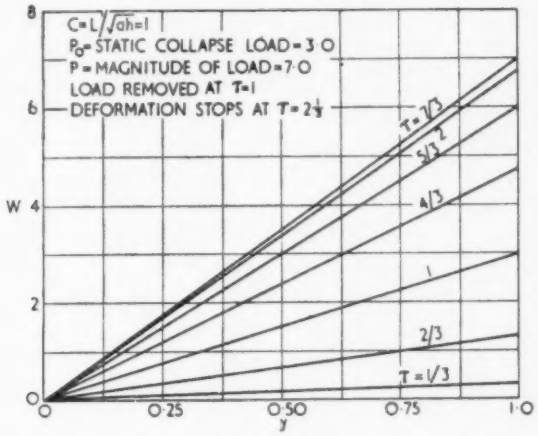

Fig. 6. Progress of deformation of half-shell.

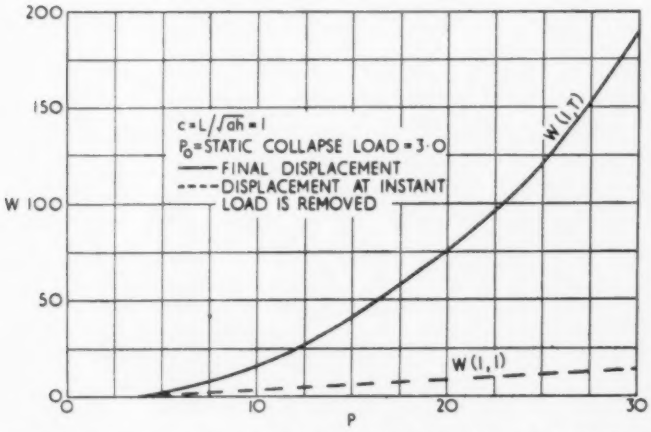

Fig. 7. Displacement at centre of shell as a function of the load.

7. Example

As a particular example the value $c = 1$ has been chosen and the results are summarized in Figs. 4-7. Fig. 4 shows the deformation of the half-shell at $\tau = 1$ when the load is removed. For $c = 1$, the dividing point between medium and high loads is $P = 7$. For $P \leqslant 7$ the deformation at $\tau = 1$ is obtained from (7) and is linear across the half length of the shell. There are hinge circles at the ends and centre of the shell. For $P > 7$, (24) must be used. The centre hinge circle is now

located at the value $v_0 = \sqrt{6/(P-1)}$. For $y < v_0$ there is no rotation, and for $y < v_0$ the deformation is linear.

Fig. 5 shows the corresponding final deformation patterns. For medium loads ($P \leqslant 7$) equations (11) are applicable and show that the entire half-shell remains linear with hinge circles at the ends and centre of the shell. For $P > 7$ the discontinuity is slope at v_0 remains constant but the total deformation has increased so much that the slope discontinuity is scarcely observable at $\tau = T$. The difference in scale between Figs. 4 and 5 should be observed.

The deformation at various times has been plotted in Fig. 6 for the particular load $P = 7$. It is evident that the rate of deformation increases while the load is being applied and then decreases, as is required by the conservation of energy. It is worth noting that the deformation without load continues for a longer than the deformation with load, and that the total deformation is more than double that when the load is removed.

The extent to which the deformation occurs after removal of the load is brought out more strikingly in Fig. 7. Here the displacement at the centre of the shell is shown as a function of the load, both the final displacement and that at the instant of load removal. As the magnitude of the load pulse is increased the displacment during application varies linearly, as is evident from (7). However, the length of time for which the deformation continues and the resulting total displacement increase rapidly with increasing load. For a load $P = 30$ more than 90% of the final displacement has occurred after the pressure pulse has passed.

Vol 3 1954/

Acknowledgments

The results presented in this paper were obtained in the course of research conducted under Contract Nonr-267 (00) between the Office of Naval Research and The Polytechnic Institute of Brooklyn. Appreciation is expressed for permission to publish the results.

The author would like to thank Mr. J. Glicksman-Felix for checking the formulas and for carrying out the computations called for in the final section (Figs. 4-7).

References

Drucker, D. C. 1953 *Proc. 1st Midwest Conf. on Solid Mech.*, 158.
Hill, R. 1954 *J. Appl. Mech.*, **21**, 93.
Hodge, P. G., Jr. 1954 *J. Appl. Mech.*, **21**, 336.
Hopkins, H. G. and Prager, W. 1953 *J. Appl. Math. Phys.*, **5**, 317.
Hopkins, H. G. 1953 Tech. Rep. DA-19-020-ORD-2598/4, Brown University.
1954 Tech. Rep. DA-19-020-ORD-2598/7, Brown University.
Lee, E. H. and Symonds, P. S. 1952 *J. Appl. Mech.* **19**, 308.
Owens, R. H. and Symonds, P. S. 1954 Tech. Rep. B11-21, Brown University.
Symonds, P. S. and Leth, C.-F. A. 1953 Tech. Rep. B11-20, Brown University.

Journal of the Mechanics and Physics of Solids, 1955, Vol. 3, pp. 189 to 196. Pergamon Press Ltd., London.

ON UNSYMMETRICAL EXTRUSION IN PLANE STRAIN

By A. P. Green
Tube Investments Research Laboratories, Hinxton Hall, Cambridge

(*Received 2nd February*, 1955)

Summary

Slip-line fields are proposed and extrusion pressures are calculated for unsymmetrical extrusion through a square die, situated either at the end or in the side of a container with smooth or rough walls. A plastic-rigid non-hardening material is assumed. Plasticine experiments are described which reveal the deformation and confirm the theory.

Vol. 3 54/55

1. Introduction

Plane strain solutions* have been proposed by Hill (1948) for extrusion through a square die placed symmetrically at the end of a straight parallel-sided container which has either smooth or rough walls. A non-hardening plastic-rigid material is assumed. The state of stress in a plane of flow is pure shear combined with a hydrostatic pressure, p. In the plastic regions the maximum shear stress is a constant, k, but in general p varies.

In this paper we discuss how these solutions must be modified if the aperture of the die is not central with respect to the container. Calculations of extrusion pressures include those for symmetrical extrusion from a rough container, which were not calculated by Hill. Solutions are also proposed for extrusion through an aperture in the side instead of at the end of the container.

It often happens in extrusion that regions of " dead " material are left behind in the corners of the container as a steady state of flow is initiated (see for example Fig. 2), and thereafter constrain the flow as if they formed a rough die. As Hill (1948) has remarked, the shapes of these regions depend on so many variables, such as friction over the die, temperature and speed of extrusion, etc., that it is impossible to predict them theoretically. Therefore, we assume boundaries for the dead regions which satisfy frictional conditions only where they meet the container walls, and are reasonably close to what is actually observed, but are otherwise chosen for simplicity. They are also assumed, in the solutions presented here, to be continuous slip lines. The stresses are not examined in the rigid regions, including the dead regions, and to this extent the solutions are theoretically incomplete.

In spite of the simplifying assumptions and the incompleteness of the theory, the deformation predicted corresponds closely to that observed in various model experiments with plasticine, which deforms in plane strain like a metal (Green

*For an account of the theory of plane plastic strain, see R. Hill, *The Mathematical Theory of Plasticity*, Ch. VI (Clarendon Press 1950).

1951). The deformation of the plasticine is revealed by a square grid (1/10 or 1/5 inch squares) stamped in ink on a central plane of flow before extrusion.

2. End Extrusion

The widths of the container and die aperture are denoted by D and $2d$ respectively, and the widths of the die on either side of the aperture by b and c. The fractional reduction, r, is $(D - 2d)/D$ and the eccentricity of the die is conveniently defined as $\epsilon = (b - c)/(b + c)$, ranging from zero (symmetrical) to a maximum of one.

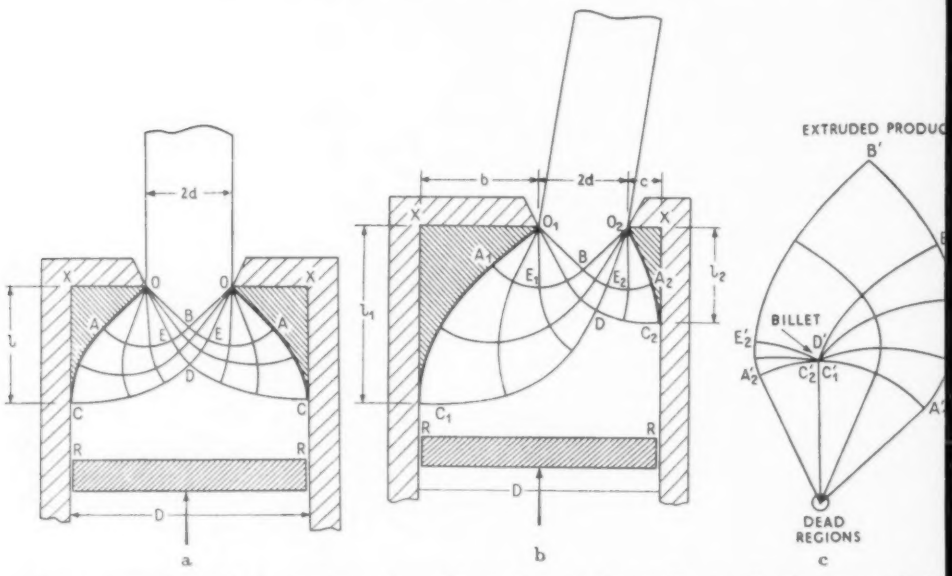

Fig. 1. Slip-line fields for end-extrusion with rough container walls : (a) HILL's symmetrical field ; (b) an unsymmetrical field and (c) its hodograph.

(a) *Rough container walls.* The term ' rough ' is taken to mean that, under the high pressure involved, the frictional stress reaches the value k wherever the billet moves relative to the container walls. Hence, the slip lines of one family meet the walls tangentially.

A simple modification of HILL's symmetrical slip-line field (Fig. 1a) is shown in Fig. 1b (slip lines across which the velocity is discontinuous are drawn thicker in this as in other Figures). The form of the field is unaltered, being defined by the equal circular arcs BE_1A_1 and BE_2A_2 but it now extends farther on one side than on the other, with corresponding unequal dead regions in the corners. Equilibrium of the extruded material demands that $p = k$ on the straight slip lines BO_1 and BO_2. The stress at any other point in the field is deduced by means of the well known Hencky relations along the slip lines. The hodograph of the velocity field (GREEN 1954, PRAGER 1953) is shown in Fig. 1c, from which it is clear that the boundary conditions are satisfied and the material is extruded straight but obliquely towards the side to which the aperture is closer.

HILL's symmetrical solution has already been closely confirmed, including the assumed shape of the dead region, by a plasticine experiment (GREEN 1951), The present unsymmetrical solution is not so precisely compared with experiment, but Fig. 2 shows that the extent of the plastic regions and the shapes of the dead regions in the plasticine specimens correspond qualitatively to the theory.

The pressures, P, on the extrusion ram and the depths of the dead regions, $CX = l$, have been calculated between $r = 0$ and $r = 0{\cdot}78$ for the symmetrical case by integrating the components of force parallel to the container walls acting across the slip lines OAC. These pressures correspond to positions of the ram RR coinciding with the ends of the dead regions CC; if the ram is further back

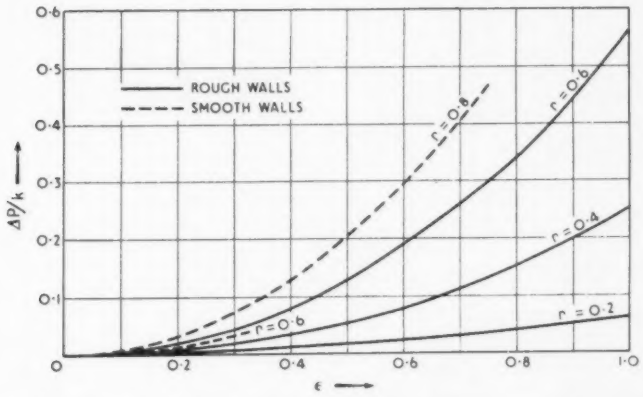

Fig. 3. Increase in extrusion pressure due to eccentricity, versus eccentricity.

an additional term $2k \times RC/D$ must be added, representing the friction between the wall and the remaining length of billet, RC. The calculated values of $P/2k$ and l/d are given in the Table. The following empirical equation gives $P/2k$ to within $2\frac{1}{2}\%$ over the range of r considered :—

$$P/2k = 1/\sqrt{2} + 1{\cdot}33 \ln\left(\frac{1}{1-r}\right). \tag{1}$$

The pressure in eccentric extrusion can be deduced from equation (1) without further integration. The slip lines OA_1C_1 and OA_2C_2, with depths of dead regions l_1 and l_2 correspond respectively in symmetrical extrusion to reductions

$$r_1 = \frac{r(1+\epsilon)}{1+\epsilon r}, \qquad \text{and} \qquad r_2 = \frac{r(1-\epsilon)}{1-\epsilon r}, \tag{2}$$

and to extrusion pressures P_1 and P_2, say. Adding the forces across both these slip lines, the resultant pressure is found to be

$$P_\epsilon = \tfrac{1}{2}[P_1 + P_2 + \epsilon r(P_1 - P_2]. \tag{3}$$

To this must be added the pressure $k\,(2RX - l_1 - l_2)/D$ due to the frictional drag between the billet and the walls, the values of l_1/d and l_2/d being interpolated from the Table. Hence, using equations (1) and (2) to express P_1 and P_2 in terms of r and ϵ, the amount by which the *total* pressure in unsymmetrical extrusion

exceeds that in symmetrical extrusion for the same reduction and position of ram is

$$\left.\begin{aligned}\Delta P = {} & 1{\cdot}33k\left[(1+\epsilon r)\ln(1+\epsilon r)+(1-\epsilon r)\ln(1-\epsilon r)\right] \\ & +k(1-r)(2l-l_1-l_2)/d\end{aligned}\right\} \qquad (4)$$

The plots of $\Delta P/k$ against ϵ in Fig. 3, for $r = 0{\cdot}2$, $0{\cdot}4$, and $0{\cdot}6$, show that it increases with increasing reduction and eccentricity. It is unaffected by the position of the ram until the ram approaches close to, or reaches, a dead region, when the slip line field will depend on frictional conditions on the ram. The problem is then no longer one of steady motion and its solution has not been attempted.

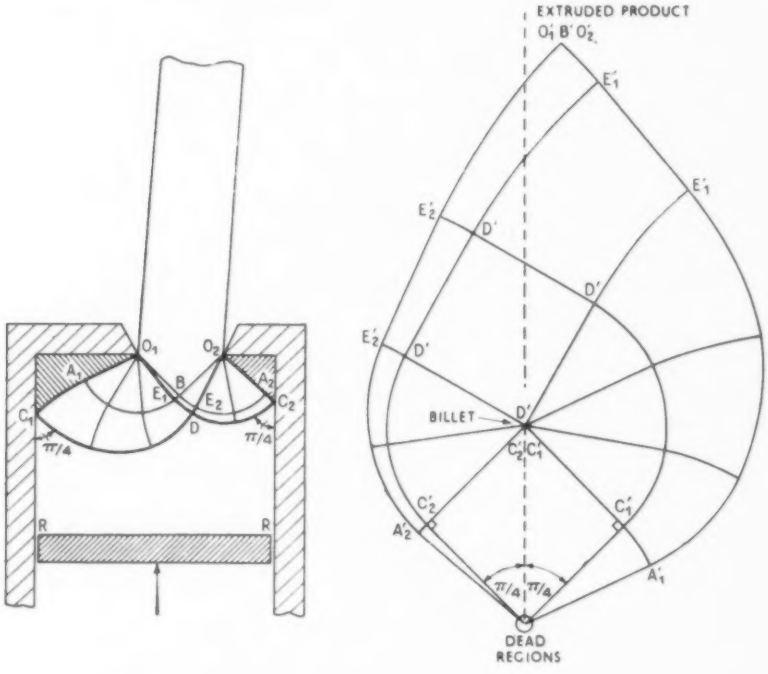

a b

Fig. 4. (a) Slip-line field, and (b) its hodograph for unsymmetrical end-extrusion with smooth container walls in range (i).

(b) *Smooth container walls.* Two types of solution for symmetrical extrusion were constructed by HILL, one for $r \leqslant 0{\cdot}5$ and the other for $r \geqslant 0{\cdot}5$. The following empirical equation, similar to equation (1), gives the extrusion pressures calculated by HILL to within about 2% :—

$$P/2k = 0{\cdot}13 + r(1-r) + 1{\cdot}33\ln\left(\frac{1}{1-r}\right). \qquad (5)$$

In unsymmetrical extrusion three ranges must be considered i.e. (i) b and $c > d$, (ii) b and $c < d$, (iii) $b > d$, $c < d$.

Vol.
3
54/55

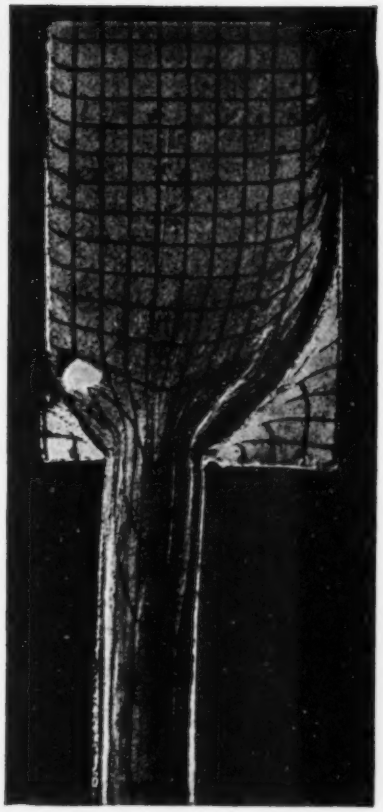

(a)

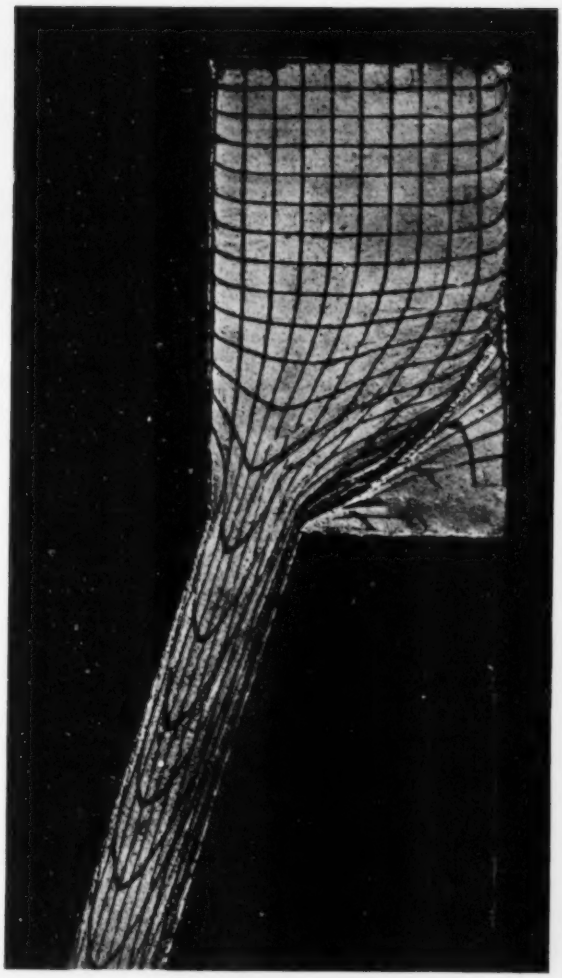

(b)

Fig. 2. Unsymmetrical end-extrusion of plasticine with rough container walls : (a) $r = 0{\cdot}67$, $\epsilon = 0{\cdot}31$; (b) $r = 0{\cdot}67$, $\epsilon = 1{\cdot}0$.

Vol
3
1954/

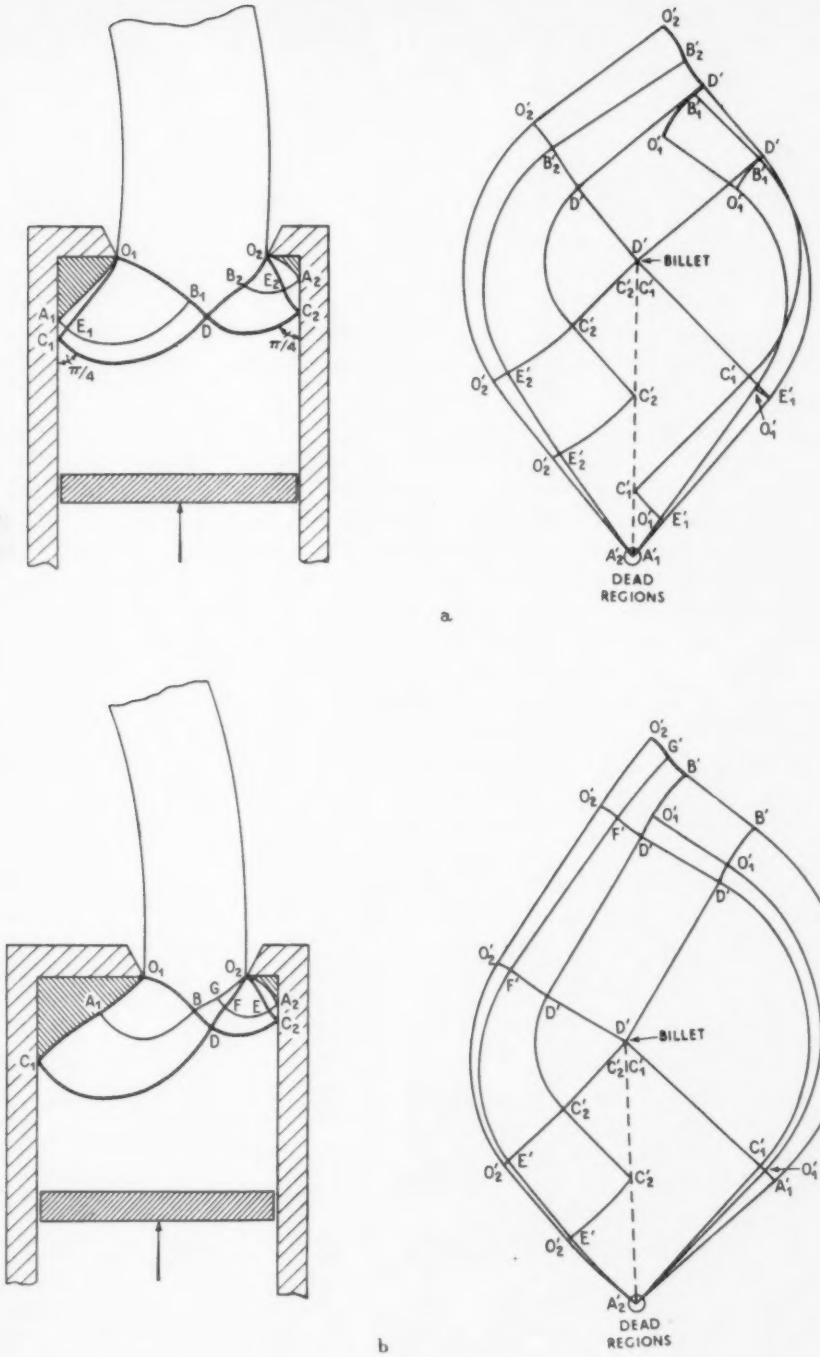

Fig. 5. Possible slip-line fields and their hodographs for unsymmetrical end-extrusion with smooth container walls in (a) range (ii), and (b) range (iii).

Range (i) is covered by the same kind of straightforward modification as that already used in Section 2 (a). The proposed slip line field, shown in Fig. 4a, is an unsymmetrical version of HILL's field for $r \geqslant 0{\cdot}5$. The hodograph (Fig. 4b) shows that the velocity boundary conditions are satisfied, and that the extruded portion emerges straight but obliquely. The pressure is deduced from (5), as in Section 2 (a), by use of (2) and (3), and the amount by which the pressure in unsymmetrical extrusion exceeds that in symmetrical extrusion is found to be

$$\left.\begin{aligned}\Delta P = 1{\cdot}33k\,[(1+\epsilon r)\ln(1+\epsilon r) + (1-\epsilon r)\ln(1-\epsilon r)] \\ - 2k\,\epsilon^2 r^2 (1-r)^2/(1-\epsilon^2 r^2)\end{aligned}\right\} \quad (6)$$

where $|\epsilon| < 2 - 1/r$ since b and $c > d$. $\Delta P/k$ is again plotted against ϵ in Fig. 3, for $r = 0{\cdot}6$ and $0{\cdot}8$, and it is evident that the effect of eccentricity is slightly less than with rough container walls.

In ranges (ii) and (iii) neither of HILL's fields can be modified without upsetting the symmetry of the exit slip lines. However, two more complex forms of slip-line field have been qualitatively constructed, one for each range, with which it seems very likely that all boundary conditions could be satisfied. These fields and their hodographs are shown diagramatically in Fig. 5. In both fields the rigid material emerging from the plastic region rotates to form an extruded product with constant curvature. The centre of rotation is towards the side with the larger dead region. Such rotation imposes the condition that the exit slip lines must be geometrically similar to the corresponding lines in the hodograph (GREEN 1953). This condition, alone, limits the choice of shapes for the dead regions. Those shown in Fig. 5 are the only ones that the writer could find which produce the correct correspondence of directions of curvature between slip line field and hodograph.

No exact calculations of these fields have been attempted since there is at present no general method of solution and it would be a formidable task to satisfy the mixed stress and velocity boundary conditions using trial and error methods. However, the extruded plasticine specimens, shown in Fig. 6, roughly confirm the theoretical forms of the fields. In numerous experiments a curved product always resulted in ranges (ii) and (iii), whereas in range (i) the extrusion was straight.

3. SIDE EXTRUSION

We now consider extrusion through an aperture of width $2d$ in one wall of a container of width D (Fig. 7). The closed end of the container is assumed to be sufficiently far from the aperture not to affect the nature of the flow.

The slip line field for this problem shown in Fig. 7 was originally proposed by HILL*, and satisfies all stress and velocity boundary conditions relating to the deforming regions. Its shape is defined by the equal circular arcs CD and CE. The point F at which it meets the wall opposite the aperture is adjusted to fit the frictional conditions on that wall. With no friction the slip line EF meets the wall at the angle $\beta = \pi/4$ and the field is symmetrical about CF. As the friction increases β decreases and F moves up the wall until, when the wall is rough, $\beta = 0$. The hodograph, shown alongside the field, is also defined by circular arcs, the ratio of whose radii is tan β equal to the ratio of the velocity discontinuities

*Private communication (1949).

Vol.
3
54/55

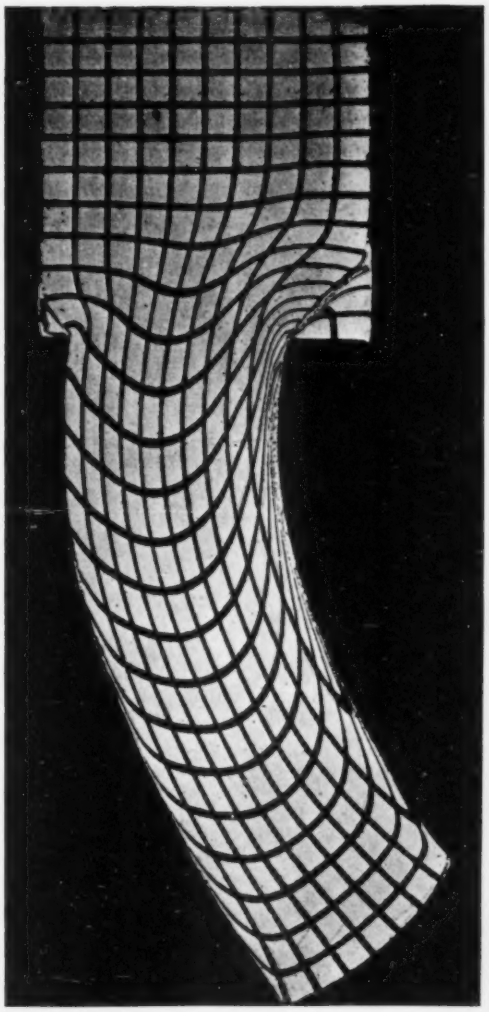

(a)

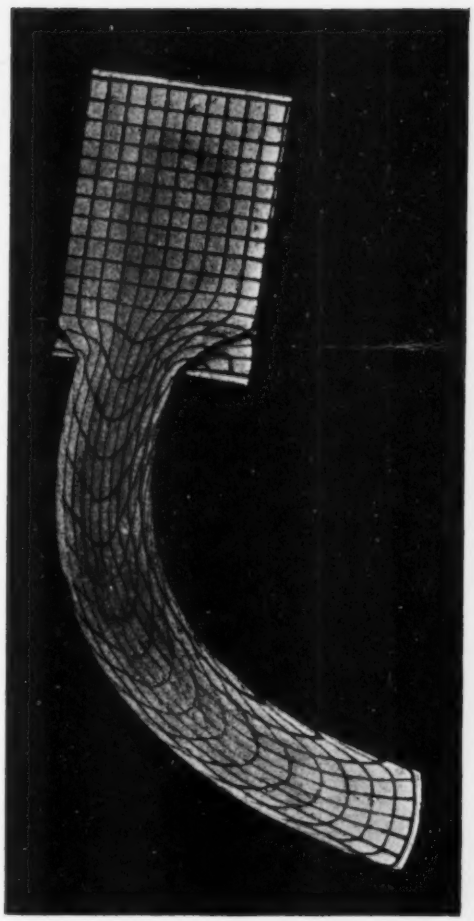

(b)

Fig. 6. Unsymmetrical end-extrusion of plasticine with smooth container walls in (a) range (ii), $r = 0{\cdot}34$, $\epsilon = 0{\cdot}45$, and (b) range (iii), $r = 0{\cdot}5$, $\epsilon = 0{\cdot}42$.

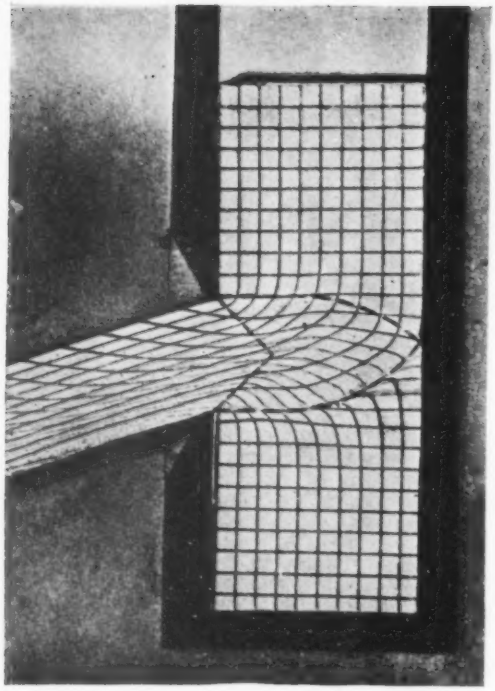

(a)

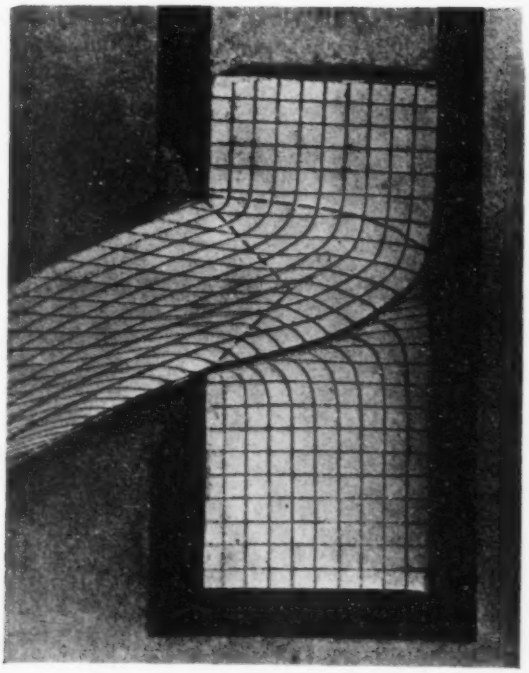

(b)

Fig. 8. Side extrusion of plasticine with low friction ($\mu \approx 0{\cdot}1$) at the container walls : (a) $D/d = 1{\cdot}90$, (b) $D/d = 1{\cdot}34$.

across FDA and FEB respectively. Thus, the slip-line field and hodograph are identical only if there is no friction. The extruded product is straight and the angle θ which it makes with the wall beyond the aperture depends on the ratio d/D and the wall friction. When there is no friction $\tan\theta = D/d$; there is no simple expression for other frictional conditions.

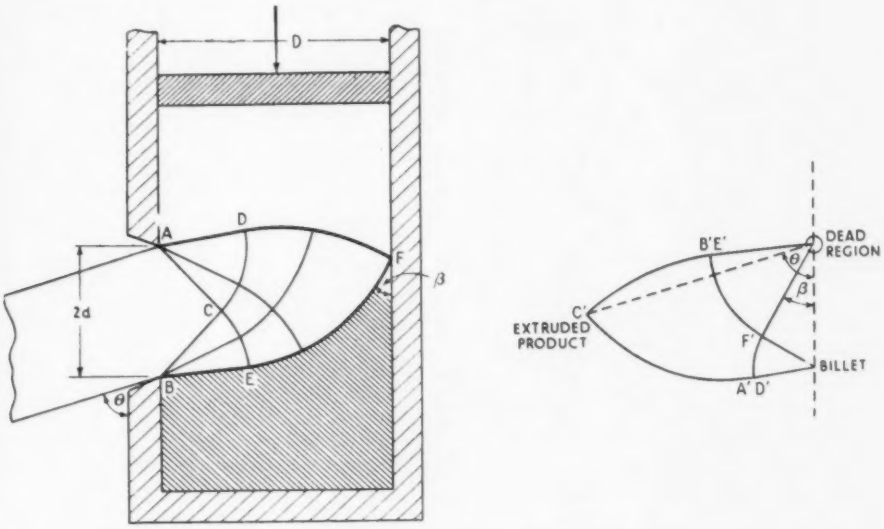

Fig. 7. Slip-line field and hodograph for side extrusion.

The upper limit of D/d for which the solution is valid is determined by the condition that the angle at which AD is inclined to the container wall at A must not be less than β, otherwise the yield criterion would be violated in the rigid material in that corner. The lower limit is $D/d = \sqrt{2}\cos\beta$ when angle $CBE = 0$.

The extrusion pressure with *smooth* container walls can readily be shown to be identical to the pressure required to compress an unconstrained rectangular block of thickness $2D$ between two opposing dies of width $2d$ under conditions of plane strain. Half the slip-line field for the latter problem when $8{\cdot}74 > D/d > 1$ (Hill 1950) is identical to that proposed for the present problem; the aperture corresponds to one indenting die and the opposite wall to the axis of symmetry in the block parallel to the die faces. Hill's calculated values of the pressure extend from $2k$ when $D/d = 1$ to $2k\,(1 + \pi/2)$ when $D/d = 8{\cdot}74$. The upper limit, $D/d = 8{\cdot}74$, does not apply to the extrusion problem but the calculations have not been extended. It should be noted that the solution of the compression problem for $D/d < 1$ (Green 1951) cannot be applied to the present problem, since, unlike Hill's solution, it involves deformation adjacent to the die, whereas the extruding material is obviously rigid as it crosses the line of the aperture AB. No pressures have been calculated for side extrusion with friction between the billet and the container walls.

Plasticine experiments, two examples of which are shown in Fig. 8, confirm the solution fairly closely. The dashed lines drawn on the photographs are the theoretical boundaries of the slip-line fields, calculated with F in the position

given by the experiments. The boundaries of the dead regions coincide with slip lines and deformation is mostly confined to the theoretical region, though naturally the other boundaries are not so sharply defined in the plasticine, since it does not have a sharp yield point. The experimental values of θ are about 3° less than $\tan^{-1}(D/d)$, but this may be due to the friction on the walls : calculations based on the position of F give $\mu \approx 0{\cdot}1$.

TABLE

r	0	0·118	0·225	0·320	0·406	0·483	0·550	0·610	0·662	0·708	0·748	0·782
$P/2k$	1·414	1·777	2·137	2·497	2·856	3·213	3·568	3·925	4·280	4·637	4·987	5·341
l/d	1·414	1·646	1·905	2·195	2·522	2·891	3·311	3·789	4·336	4·962	5·682	6·511

Data for symmetrical end-extrusion with rough container walls.

ACKNOWLEDGMENTS

The author is indebted to Tube Investments Ltd. for permission to publish this paper ; to Mr. F. T. M. SMITH for some assistance with the calculations ; and to Mr. D. SPENCELEY for his help with the experiments. Part of the work was carried out while the author was employed by the British Iron and Steel Research Association.

REFERENCES

GREEN, A. P. 1951a *Phil. Mag.*, **42**, 365
1951b *Phil. Mag.*, **42**, 900.
1954 *J. Mech. Phys. Solids*, **2**, 73.
HILL, R. 1948 *J. Iron Steel Inst.*, **158**, 177.
1950 *The Mathematical Theory of Plasticity* (Clarendon Press).
PRAGER, W. 1953 *Trans. Royal Inst. Tech. Stockholm*, No. 65.

Journal of the Mechanics and Physics of Solids, 1955, Vol. 3, pp. 197 to 205. Pergamon Press Ltd., London.

EXPERIMENTS WITH PYRAMIDAL INDENTERS—PART I

By D. S. DUGDALE*
Department of Mechanical Engineering, University of Bristol

(*Received* 14*th February*, 1955)

SUMMARY

EFFICIENTLY lubricated indenters of pyramidal form have been used to produce impressions in cold-drawn steel, cold-rolled copper and silicon-aluminium. Care was taken to avoid possible errors due to finite size of specimen and to directional and time-dependent properties of the material. Measurements of the shape of the impression were recorded. Indentation pressures were compared with shear yield stresses obtained from torsion tests, and ratios common to the three materials were found.

Vol. 3 54/55

1. INTRODUCTION

IN the study of the plastic deformation of metals it is often found useful to postulate an ideal material whose shear and bulk moduli of elasticity are infinitely great and whose rate of strain-hardening is zero. Perhaps it is also necessary to specify that the yield criterion and stress-strain relations should follow simple forms, say the MISES criterion and the LEVY-MISES equations. Then the material can be completely defined by its shear yield stress. Therefore, for a frictionless pyramidal indenter of a given vertex angle, there should be a ratio of indentation pressure to shear yield stress common to all such materials, and also a common shape of the deformed surface around the impression. There should be another pressure-ratio and shape appropriate to an indenter whose surface is sufficiently rough to prevent relative motion between the indenter and the material in contact with it.

It may be conjectured that if the rate of strain-hardening is small, the material would still behave in a similar way to the ideal material. The material could then be idealized as an equivalent non-hardening material having a yield stress suitably chosen from the actual stress-strain curve. It would then be a simple matter to calculate the pressure required to enforce the penetration of any particular kind of indenter, provided that the appropriate pressure-ratio for the ideal material was known. The purpose of the present work is to investigate how far this simple method is valid for various materials and various indenters of pyramidal form.

2. MATERIALS

Experiments were carried out on cold-drawn steel, cold-rolled copper and silicon-aluminium. The cold-drawn steel bar was 8 feet long by 1 inch square. Chemical analysis gave 0·15% carbon and 0·7% manganese. The high-conductivity copper slab was of cross-section 5 × 1½ inches, and it had been reduced in thickness

*Now at Mechanical Engineering Research Laboratory, East Kilbride.

by about 25% by cold rolling. The silicon-aluminium had been cast in the form of a cylinder 3 feet long by 5 inches diameter. Analysis gave 10·9% silicon, 0·3% iron and 0·02% copper. This material was annealed by heating for 2 hours at 400°C, followed by cooling in the furnace.

The uniformity of these materials was investigated by taking Vickers hardness readings over sections cut from the bar or slab. As a result of these tests it was decided that a strip one inch wide from the side of the copper slab should be discarded, as this material was about 2% softer than the rest. Material lying within a radius of one inch from the centre of the silicon-aluminium casting was discarded, as it was about 4% harder than the rest. The centre of the cold-drawn steel bar was about 8% harder than the outside. As the section was too small to allow of any selection of material, it was arranged that indentations were made in the centre of the bar, and that torsion test specimens were also cut from the central part.

The results of these tests are summarized below :—

	Number of sections	*Total number of tests*	*Average Vickers hardness number*
Steel	5	500	194·6
Copper	2	500	102·6
Aluminium	3	900	55·0

When compression tests were carried out on the cold-worked materials, it was found that the specimens did not remain of circular cross-section, which indicated that these materials were not isotropic. For this reason it was decided that all indentation tests should be carried out in triplicate, with the axis of the indenter positioned along each of the principal axes of the bar.

3. Apparatus

Pyramidal indenting tools were made from high-carbon steel. After being hardened they were ground in a fixture which ensured that an accurate form was obtained. The vertex angles were considered to be accurate to within $\frac{1}{4}$ degree, and the surface finish was ± 3 micro-inches. It was found that after indenting steel, the indenters became blunted by amounts up to 0·001 inches measured in an axial direction. The indenting tool was accommodated in a subpress situated between the platens of a Buckton single-lever testing machine. A light spring lifted the indenting tool clear of the specimen when the load was removed. Stops fitted to the subpress allowed the specimen to be replaced in exactly the same position after each application of load.

4. Torsion Tests

Solid specimens of nominal diameter 0·3 inches and gauge length $1\frac{1}{4}$ inches were tested. The testing machine and procedure have been previously described (Dugdale 1954). The specimen was fixed in tandem with a master-specimen of stiffness 4 ton-inches per radian. Tests of two kinds were carried out. For tests

of the first kind, the specimen was twisted at a fairly rapid rate so as to produce an increment of shear strain of about 0·2 in the outer fibre of the specimen. Two minutes then elapsed before the torque reading was recorded. Shear yield stresses found from these tests are denoted k_a. For tests of the second kind the spindle of the machine was driven at a controlled speed such that the rate of straining produced in the outer fibres of the specimen was 10^{-4} per second. Shear yield stresses found from these tests are denoted k_b. The results are shown in Fig. 1. The results for silicon-aluminium were obtained from specimens tested under a hydraulic pressure of 20 tons per square inch, for it was found that specimens tested at atmospheric pressure usually fractured before a strain of 0·5 was reached. These tests were carried out by Dr. B. Crossland at the University of Bristol (for a description of the apparatus see Crossland 1954). The results of these tests agreed well over the range of strain 0 to 0·5 with results from 10 specimens tested by the author at atmospheric pressure.

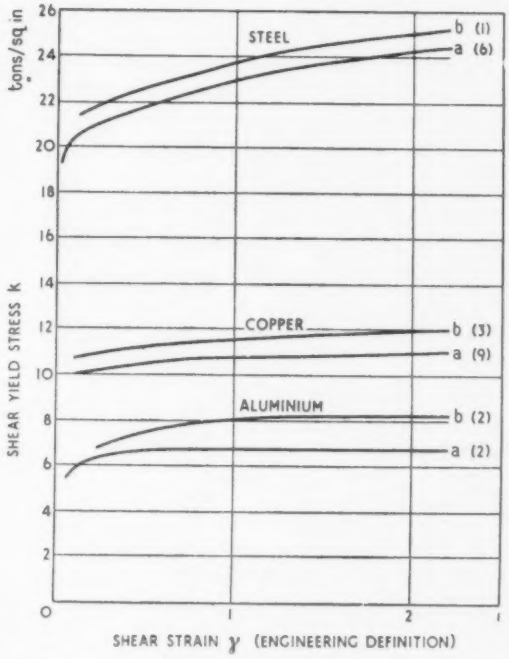

Fig. 1. Torsion test results. (a) From intermittent straining tests; (b) From continuous straining tests. Numbers of specimens tested are shown in brackets.

5. Indentation Specimens

Preliminary tests were carried out in order to determine suitable dimensions for the indentation specimens. First, effects of restricted lateral dimensions were investigated. The specimens for these tests were $\frac{1}{2}$ inch square by 1 inch deep, and the lubricated indentation was made in the centre of the square end. The impression was enlarged in about 10 steps, the lengths of the diagonals d and the lateral dimensions l ot the specimen being recorded. When the product of the diagonals was plotted against the applied load, the curve was straight up to some limiting size of impression. At this stage it was found that the lateral dimension, measured in the plane of the upper surface of the specimen, had increased by a fraction varying from 0·1% to 0·4%. The limiting ratios d/l are shown in Fig. 2. A second set of specimens of lateral dimensions 1 inch or more and thickness t about 0·1 inch were prepared. They were tested in a similar manner, the anvil being of polished mild steel. The limiting ratios d/t are also shown in Fig. 2. This information was utilised in fixing proportions of specimens. The steel and copper specimens

were 1 inch square by 0·6 inches deep, and one indentation was made in each specimen. The aluminium specimens were made in the form of cubes of side $1\frac{1}{2}$ inches, and an indentation was made on three faces of each specimen. The maximum length of diagonal for lubricated indentations was 0·2 inches.

6. Indentation Tests

So that equal unlubricated surfaces should be generated at the cutting edges of the pyramidal tool during each increment of penetration, uniformly increasing loads were applied. The impression was filled with calcium oleate before the indenter was introduced for each loading, and 13 loads were applied during each test. In all tests, the load was maintained for 2 minutes. Both diagonals were measured with a measuring microscope. When the product of the diagonals was plotted against the load, it was found that all the points, except the first one or two, lay on a straight line. It can be seen that twice the gradient of this line gives the pressure acting on the square defined by the corners of the impression. For each indenter, the values obtained from the three specimens were averaged to give the pressure denoted p_0 in Table 1.

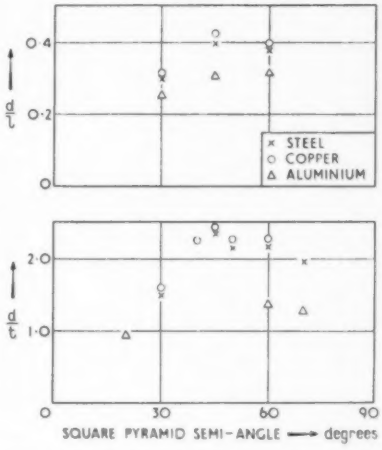

Fig. 2. Critical proportions of indentation specimens.

After each increment of penetration the following additional measurements of the impression were recorded. Both of the lateral dimensions B were measured. Then, with normal illumination of the polished surface of the specimen, the dimensions G across the apparently overstrained region were measured. Finally the heights h of the four raised lips were measured with a micrometer. For each test, the measurements B, G and h were plotted against the average length of the diagonal d. From these graphs average ratios b/s, g/s and h/s were found (see Fig. 3). Values for each set of 3 specimens were then averaged, the results being shown in Fig. 4. As a basic measure of the size of the impression it seems to be convenient to use the dimension s, defined as the perpendicular distance from the axis of the impression to the line joining two adjacent corners.

7. Friction

By means of the method described by Hill (1950) the following friction coefficients μ were determined : steel 0·03 ; copper 0·02 ; aluminium 0·02. The observed indentation pressures were corrected by means of the formula $p_n = p_0/(1 + \mu \cot \alpha)$, where α is the pyramid semi-angle. These nominal pressures p_n are given in Table 1.

8. Projected Area

A conventional measure of indentation-hardness might be obtained by dividing the applied load by the square of any dimension of the impression. However,

when the flow is of the kind in which the displaced material forms a raised lip, the average normal stress acting over the whole surface of contact seems to have the most direct physical significance. For a frictionless indentation, this pressure is clearly equal to that given by dividing the applied load by the area of the surface

TABLE 1

	Pyramid semi-angle (degrees)	*Indentation pressures (ton per sq. in.)* p_0	p_n	p_c	*Shear strain* γ_a	*Shear yield stresses* k_a	k_b
	Square pyramids						
	20	93·0	86·0	71·6	1·0	22·9	23·7
	30	105·5	100·0	80·3	1·3	23·4	24·2
	40	113·8	110·0	86·3	1·5	23·7	24·5
Steel	45	119·8	116·2	92·6	1·7	23·9	24·7
	50	123·8	120·8	97·2	1·8	24·0	24·8
	60	128·3	126·1	106·0	1·9	24·1	24·9
	70	124·5	123·2	109·0	1·9	24·1	24·9
	20	44·8	42·5	34·0	1·2	10·7	11·6
	30	47·5	45·9	35·0	1·4	10·8	11·7
	40	55·8	54·6	40·6	1·6	10·8	11·8
Copper	45	57·4	56·3	41·8	1·8	10·8	11·9
	50	60·7	59·8	44·9	2·0	10·9	11·9
	60	63·5	62·7	48·7	2·2	10·9	12·0
	70	65·4	65·0	53·4	2·3	11·0	12·0
	20	27·6	26·2	21·7	1·0	6·8	8·0
	30	31·5	30·4	24·4	1·3	6·8	8·2
	40	34·6	33·8	26·7	1·5	6·8	8·2
Aluminium	45	35·8	35·2	28·1	1·7	6·8	8·2
	50	36·4	35·8	30·0	1·8	6·8	8·2
	60	37·1	36·7	32·7	1·9	6·8	8·2
	70	34·8	34·6	33·6	1·9	6·8	8·2
	Triangular Pyramids						
	30	47·1	45·5	31·2	1·1	10·7	11·6
Copper	45	56·8	55·7	36·4	1·6	10·8	11·8
	60	65·2	64·5	44·5	2·0	10·9	11·9

of contact projected into a horizontal plane. In order to determine this area, it seems to be convenient to assume that the impression is bounded by parabolic arcs. CROW and HINSLEY (1946) found that this method gave very accurate results for impressions made with a Vickers diamond pyramid. However, it was observed during the present work that when the vertex angle was small, the profile tended towards a curve consisting of two straight lines. Nevertheless, it is estimated that the area calculated by assuming the curve to be parabolic should not be in error by more than 3%, even for impressions of small vertex angle. If this method is adopted, the nominal pressure p_n may be corrected for the effect of convexity of the sides of the impression by means of a simple relation, which follows from Fig. 3, $p_c = p_n/(1 + 4\,b/3s)$. Values of b/s are given in Fig. 4, and the pressures p_c are shown in Table 1.

9. AVERAGE STRAIN

When the displaced material flows to the surface, it must be heavily strained. From consideration of the work required to bring about this large strain, it can be seen that the work required to force the indenter into the material cannot be

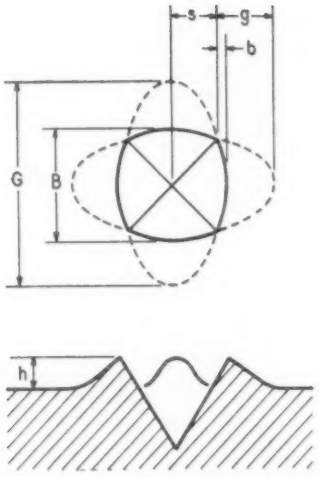

Fig. 3. Measurements of impression.

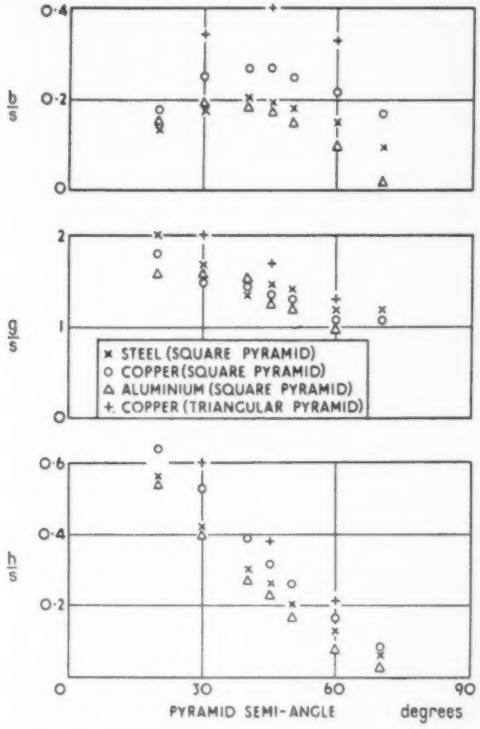

Fig. 4. Proportions of pyramidal impressions.

appreciably influenced by either the elastic constants of the material, or by the precise value of the initial yield stress. Some method is therefore required for estimating the average value of the shear strain in the deformed material, so that a reasonable value of the shear yield stress can be selected from the stress-strain curve. While the method to be described is crude, it represents an attempt to avoid arbitrariness in the choice of the relevant range of strain. First, some observed features of the deformed area around the impression may be mentioned. Indentations made with pyramidal indenters of square section showed four pronounced raised lips adjacent to the sides of the indenter. With normal illumination of the surface, the region between these lips appeared to be unstrained, but with oblique illumination, it could be seen that this surface was slightly raised. This means that the corners of the impression were slightly elevated above the plane of the original surface. However, indentations made with indenters of triangular section showed no such regions of diffused deformation between the raised lips, and the corners of the impression appeared to lie in the original surface, which retained its polished finish. If the material within the raised lips is considered,

without regard to the more widely diffused deformation, an attempt may be made to estimate the volume of the severely strained material. Visual observation suggested that the outline of these raised lips when viewed from above was roughly parabolic. The shape of the slip-lines below the surface is not known, so for simplicity it is assumed that they consisted of straight lines radiating from the vertex of the indenter. The volume of the strained material can then be written $fd^2\,(1 + 4g/3s)/6$, where f is the penetration of the vertex below the original surface. The work done during the penetration is given by $p_n\,fd^2/6$. For an ideal material of shear yield stress k_a, the work done in straining unit volume of material to an average strain γ_a is given by $\gamma_a k_a$. Hence an expression is obtained for the average strain, $\gamma_a = p_n/k_a\,(1 + 4g/3s)$. Values of g/s were taken from Fig. 4, and trial values of k_a were used initially. Values of strain γ_a and corresponding yield stress k_a (from Fig. 1) are shown in Table 1. The above equation gives slightly lower values of strain γ_b corresponding to yield stress k_b. These are not shown.

10. Indentation Pressures

It is thought that when torsion tests are carried out by intermittently straining a specimen which is attached to a fairly stiff master-specimen, the results must be similar to those which would be obtained from a test carried out with a fairly slow rate of continuous straining, say 10^{-6} or 10^{-7} units of shear strain per second in the outer fibres of the specimen. It seems to be a difficult matter to determine the precise rate of strain which would allow the time-dependent properties of the material to come into play to a corresponding degree in both torsion and indentation tests. So that these effects should not be lost to view, further torsion tests were carried out at the fairly high strain-rate of 10^{-4} per second, and gave the alternative shear yield stresses k_b shown in Fig. 1 and Table 1. The ratios of indentation pressure p_c to each of these shear yield stresses are plotted in Fig. 5. Of the three materials, aluminium, which exhibits the greatest time-effects (Fig. 1), gives the largest ratios in Fig. 5a, and the smallest in Fig. 5b. This suggests that if experiments could be carried out on an ideal material which exhibited no time-effects,

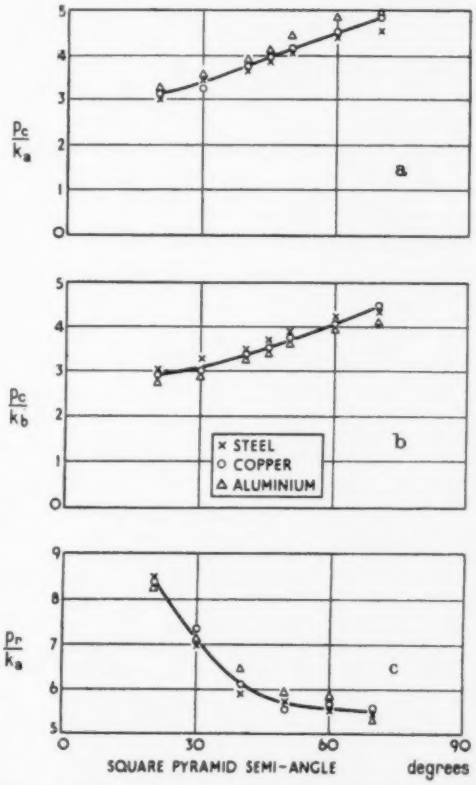

Fig. 5. Indentation pressure ratios. (a) and (b) For lubricated indenters with alternative shear yield stresses ; (c) For roughened indenters.

a curve lying between these two curves would be obtained. Further, when three widely different materials, such as those tested, give pressure ratios which agree fairly closely, it is inferred that the same ratios would be obtained from hypothetical tests carried out on an ideal plastic-rigid material.

11. ROUGHENED INDENTERS

It can be seen that indentation pressures determined from tests carried out with either perfectly smooth or perfectly rough indenters must be independent of the frictional properties of the indenter and the material. At the completion of the work described above, the highly finished surfaces of the indenters were etched with strong nitric acid for a period of a few minutes. This treatment produced a surface which under the microscope appeared non-reflecting and lightly pitted all over, but the accuracy of the pyramidal form was not impaired. New specimens of the kind previously used were prepared, i.e. three specimens for each indenter and for each material, variously oriented relative to the bar from which they were cut. The size of impression was restricted to a diagonal length of 0·1 inches, and the full load required to produce the indentation was applied once only, and was maintained for 2 minutes. The mean pressure acting on the projected area of the impression was then calculated, and the pressures p_r for each set of three specimens were averaged. The results are given in Table 2. Each of these pressures was divided by the corresponding shear yield stress k_a given in Table 1. These ratios are plotted in Fig. 5c. Agreement between ratios for the three materials suggests that the curve drawn through these points represents the results that would be obtained from an ideal plastic-rigid material with perfectly-rough indenters.

TABLE 2

Pyramid semi-angle (degrees)	*Indentation pressure* p_r *(tons per sq. in.)*		
	Cold-drawn steel	*Cold-rolled copper*	*Silicon-aluminium*
20	195	89·6	56·8
30	163	80·1	48·1
40	140	66·4	44·4
50	138	60·7	40·6
60	133	61·4	39·9
70	132	60·8	36·0

12. DISCUSSION OF RESULTS

Indentation pressure ratios based on the first set of torsion test results (shear yield stress k_a) are taken from Tables 1 and 2 and plotted together in Fig. 6. The curve for fully-lubricated conical indenters (DUGDALE 1954) is included. First, it can be seen that imperfectly-smooth indenters of the square-pyramid type must give pressures intermediate between those defined by curves a and b. Secondly the curves of Fig. 6 provide a basis for discussing the penetration into a plastic

medium of a frictionless body of general pyramidal form. Except for very small vertex angles, the pressure rises as the vertex angle is increased. It also rises as the angle between the planes of adjacent faces of the pyramid is increased, that is, as the indenter tends to deform the material more by expanding it and less by cutting it.

Reference to Fig. 5 shows that copper, the material whose stress-strain curve (Fig. 1) approaches nearest to that of an ideal non-hardening material, gives ratios that rise steadily with increasing vertex angle. However, the same rate of increase is not reproduced by the ratios for steel and aluminium for the 70° semi-angle. It appears that the pressure required to enforce flow of the plastic-rigid type around an indenter of this vertex angle is too great for these materials to bear, and that plastic-elastic flow involving subsidence of material beneath the indenter has begun. From Fig. 4 it can be seen that the convexity parameter b/s is almost zero for an impression of this vertex angle in aluminium, and that a further increase of angle would result in the impression being of the " sinking-in " type characterized by concave sides. This type of flow will be further discussed in Part II.

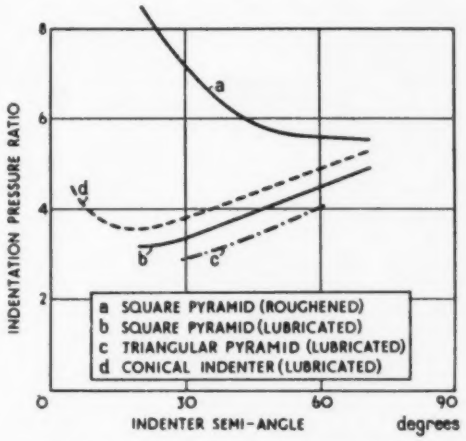

Fig. 6. Indentation pressure ratio curves for various indenters.

Vol. 3 54/55

Acknowledgments

The writer is grateful to Professor J. L. M. Morrison for advice given on many occasions. The silicon-aluminium was supplied by Aluminium Laboratories Ltd.

References

Crossland, B. 1954 *Proc. Inst. Mech. Eng.*, **168**, 935.
Crow, T. B. and Hinsley, J. F. 1946 *J. Inst. Metals*, **72**, 461.
Dugdale, D. S. 1954 *J. Mech. Phys. Solids*, **2**, 265.
Hill, R. 1950 *Phil. Mag.*, **41**, 733.

Journal of the Mechanics and Physics of Solids, 1955, Vol. 3, pp. 206 to 211. Pergamon Press Ltd., London.

EXPERIMENTS WITH PYRAMIDAL INDENTERS—PART II

By D. S. Dugdale
Department of Mechanical Engineering, University of Bristol

(*Received* 14*th February*, 1955)

Summary

Indenters of vertex semi-angles 20° to 80° have been used for making impressions in annealed copper and manganese steel. It was found that the indentation pressure decreased with increasing angle of indenter for semi-angles greater than 50°. Yield stresses were obtained from compression tests. The difference between the plastic-rigid and plastic-elastic types of flow is emphasized and a method is suggested for relating hardness to the stress-strain curve.

1. Introduction

When the material displaced by a penetrating indenter flows upwards to the free surface, there is a certain volume of material, more or less clearly defined, which is highly strained. It may be expected, therefore, that the identation pressure should be governed by some yield stress corresponding to this large strain. When, however, the displaced material sinks into the interior of the specimen, it is not at all clear that an average value of strain can be logically assigned to the material around the indentation, for the domain of the deformation has no definite boundary. Here, it may be expected that yield stresses from all parts of the stress-strain curve would make contributions to the indentation pressure.

Hankins (1925) used unlubricated conical indenters of various angles to investigate the hardness of annealed copper and manganese steel. Similar experiments were carried out on annealed copper by Krupkowski (1932). This work showed that there was a pronounced decrease of hardness with increasing indenter angle. However, data obtained for cold-rolled copper (Dugdale 1954) showed a pronounced *increase* of hardness with increasing indenter angle. So that these apparently conflicting results could be re-examined, further experiments were carried out on rapidly strain-hardening materials.

2. Materials

Two materials were used for the tests to be described. The annealed copper was of the ' Oxygen-free high conductivity ' grade, and was in the form of a hot-rolled bar of cross-section 4 × 2 inches. Specimens were annealed at 400°C for one hour, after they had been finish-machined. Manganese steel specimens were taken from a bar $1\frac{1}{8}$ inches diameter, 8 feet long. A chemical analysis gave the following composition : manganese 13·4%; carbon 0·80%. This material was heated at 1,000°C for $\frac{1}{2}$ hour and then quenched in water. After the material had been heat-treated, specimens were formed by grinding.

Two sections 0·3 inches thick were cut from the copper bar, and 180 Vickers

tests were carried out on each. Similar results were obtained for the two sections. The hardness distribution over one of the sections is shown in Fig. 1. The unduly soft part of the bar was discarded. About 400 Vickers tests were carried out on various transverse and longitudinal sections of the steel bar, but no abnormal variations of hardness were found. The Vickers number varied from 215 to 225.

From the deformed shape of compression specimens, it could be seen the materials were isotropic.

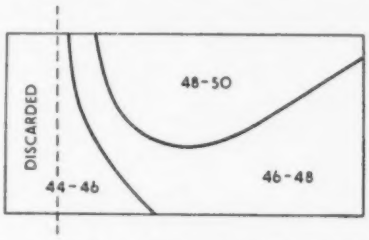

Fig. 1. Vickers hardness readings taken over section of annealed copper bar.

3. Compression Tests

Specimens of various sizes, ranging from 0·2 to 0·6 inch diameter were prepared. The length was approximately equal to the diameter. It was found that if the length was much greater than this, the specimens collapsed by rotating in a vertical plane. They were compressed between highly-polished steel platens of Vickers hardness number 1000. Calcium oleate was applied to the ends of the specimen before each application of load, and it was found that a film remained after the specimen was withdrawn from the testing machine for measurement. The load was maintained for 2 minutes. It was observed that the sides of the specimen remained parallel throughout the test. Two mutually perpendicular diameters D_1 and D_2 were measured in the central section of the specimen with a micrometer.

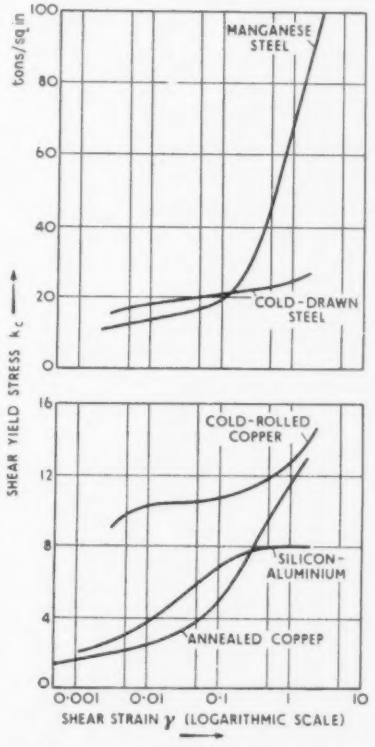

Fig. 2. Compression test results.

The shear yield stress in compression, k_c, was found from the formula $k_c = 4W/\sqrt{3}\,\pi D_1 D_2$ (W being the load in tons). Siebel's correction for the effect of friction was then applied (see Hill 1950 p. 277). The equivalent shear strain γ was found from the formula $\gamma = 2\sqrt{3}\ln(\overline{D}/D_0)$, where D_0 is the initial diameter of the specimen, and $\overline{D}$ the average of the current diameters, D_1 and D_2. As the total strain was required, the elastic component k/G was added to the observed value, G being the shear modulus. The results are shown in Fig. 2. Results for materials described in Part 1 of this work are included. In order to show, on one graph, yield stress for both very small and very large strains, it was necessary to use a logarithmic scale. For clarity, the experimental points have been omitted.

4. INDENTATION TESTS

Thirteen indenting tools of hardened steel were used. They were ground to an accurate pyramidal form. The force exerted by the testing machine was transmitted to the indenter by way of a subpress which ensured perpendicular penetration, and correct positioning of the specimen.

Specimens cut from the manganese steel bar were $1\frac{1}{8}$ inch diameter and 0·6 inch deep, and one indentation was made in each. The copper specimens were in the form of cubes of $1\frac{1}{4}$ inch side, and an indentation was made on three faces of each cube. Preliminary tests were carried out on small blocks of these materials to determine the ratio of impression-size to specimen-size at which expansion of the specimen commenced. The results indicated that there would be no finite-size effects if the impression-diagonal was restricted to 0·2 inch.

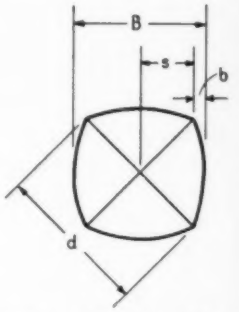

Fig. 3. Dimensions of pyramidal impression.

One lubricated indentation only was made with each indenter. For each indentation, about 12 uniformly increasing loads were applied to the indenter. At each stage, the impression was filled with lubricant (calcium oleate) before introducing the indenter. After each increment of penetration the two diagonals d, and two lateral dimensions B were measured (Fig. 3). When the product of the diagonals was plotted against the applied load it was found that the curve was straight.

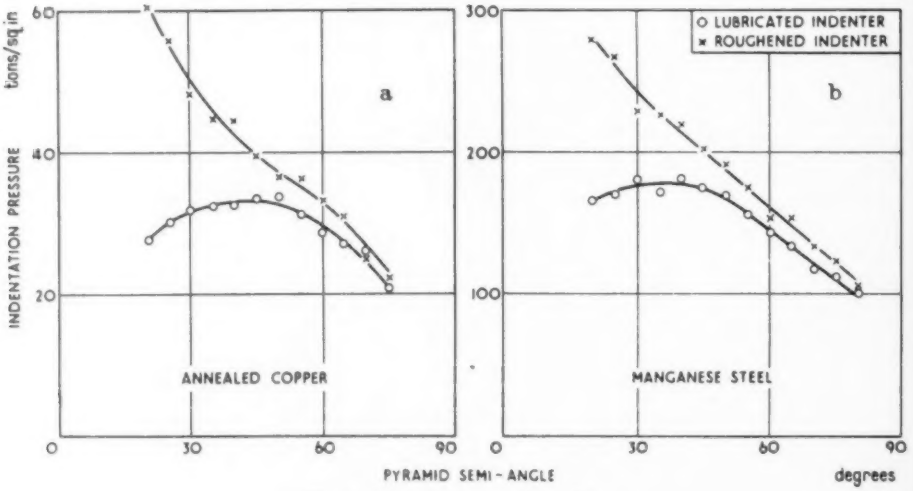

Fig. 4. Indentation test results.

The gradient of this curve gave the nominal pressure p_0 acting on the square defined by the corners of the impression. Values of the nominal pressure p_n corrected for the effect of friction were found from the relation $p_n = p_0/(1 + \mu \cot \alpha)$, where α is the semi-angle of the pyramid and μ is the friction coefficient. The friction coefficients used were : annealed copper 0·02 ; manganese steel 0·04. These values of p_n are plotted in Fig. 4.

For each impression the lateral dimension B was plotted against the diagonal length d to give the average value b/s (see Fig. 3). These values are plotted in Fig. 5.

Further tests were carried out on specimens of the same kind with the surface of the indenter roughened by etching in nitric acid. Load was applied to the indenter once only. The resulting indentation pressures calculated from the nominal areas of the impressions are plotted in Fig. 4.

5. Analytical Approach

Consider the impression made when load is applied to a conical or pyramidal indenter whose semi-angle is very nearly 90°. It is considered that only material near the point or sharp edges of the indenter will be permanently deformed, and that stresses in the remainder of the material will correspond to small elastic strains. Therefore, it is suggested that the hardness of an elastic material will fall to a low value, probably to zero, as the semi-angle tends towards 90°. At the other extreme, the average pressure acting on a lubricated indenter of vanishingly small angle must be equal to the pressure required to expand a long prismatic cavity in an infinite mass of material.

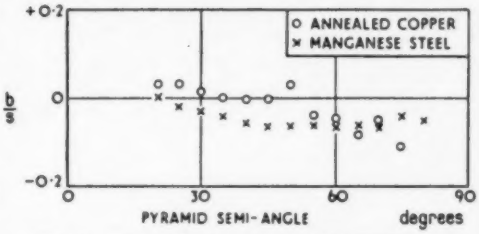

Fig. 5. Proportions of pyramidal impression.

For intermediate angles it seems likely that the indentation pressure should be similar to the average pressure required to expand indefinitely an octahedral cavity in an infinite mass of material. However, it would be expected that it would fall short of this pressure, for two reasons. First, the presence of a stress-free surface must relieve stresses in the material near the outside edge of the impression. Secondly, any slight elevation of the corners of the impression above the original surface must increase the dimensions of the impression, thereby lowering the observed pressure.

As there seems to be difficulty in calculating the average pressure to expand an octahedral cavity, a further simplification of the problem is sought. When the octahedron is regular (semi-angle of vertex about 35°) it is suggested that this pressure may not differ greatly from the analogous pressure for a spherical cavity. If this is true, one would expect the indentation pressure for an indenter of 35° semi-angle to be almost, but not quite, equal to the pressure required to expand a spherical cavity, provided, of course, that the impression is of the "sinking-in" type.

If the material is taken to be incompressible, the pressure p_s required to expand a spherical cavity can be readily computed from the stress-strain curve (Fig. 2) by integrating the radial equilibrium equation numerically (Dugdale 1954). These values are shown in Table 1, with the necessary values of elastic shear modulus G and initial yield stress k_0.

Vol. 3 54/55

TABLE 1

	G	k_0	p_s
Manganese Steel	5240	11·0	205
Annealed Copper	2930	1·7	41·0
Silicon-Aluminium	1720	2·0	44·4
Cold-Drawn Steel	5240	15·0	163
Cold-Rolled Copper	2930	9·0	85·0

6. DISCUSSION OF RESULTS

The object of this work was to investigate the relation between indentation-hardness and the yield stress-strain curve. When the impression is of the " sinking-in " type, there does not seem to be any good reason for calculating hardness from the projected area of the impression, so it is calculated here from the square defined by the corners of the impression. When material beneath the indenter

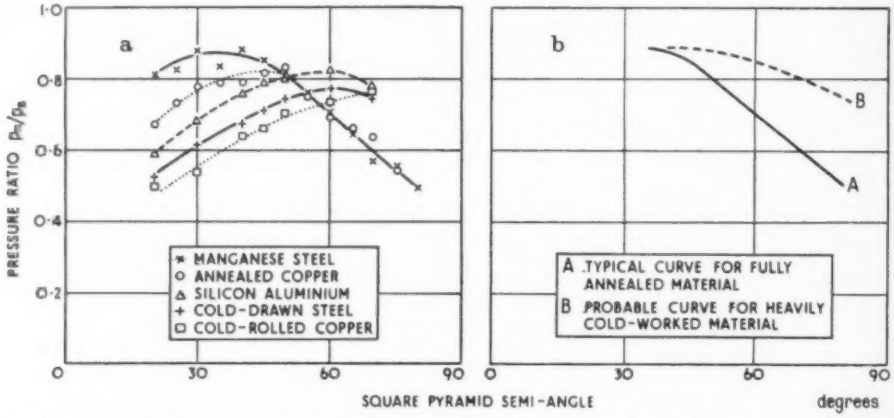

Fig. 6. Indentation pressure expressed as a fraction of pressure required to expand a spherical cavity.

subsides into the interior of the specimen, it seems likely that the average value of LODE's strain variable should be near to unity, and that shear yield stresses determined from compression tests should be more appropriate than those obtained from torsion tests. Indentation pressures p_n from Fig. 4 were divided by corresponding pressures p_s from Table 1, and the ratios are plotted in Fig. 6a. Indentation pressures for other materials are taken from Part 1 of this work.

This diagram is interpreted as follows. The displaced material may either escape to the free surface, or subside beneath the indenter. It is reasonable to suppose that the material would flow in the manner which requires least work for unit penetration of the indenter (see also HILL 1950, p. 259). For a particular indenter this work is in a fixed proportion to the pressure acting on the nominal area of impression, provided the corners of the impression remain in the original surface. Therefore, when this pressure reaches a certain magnitude depending on the particular material, transition from one type of flow to the other must

occur. It is characteristic of flow to the free surface that the pressure increases with increasing indenter angle (e.g. the curve for cold-rolled copper in Fig. 6a). It appears that the reverse is true when the flow is of the " sinking-in " kind (e.g. the curve for annealed copper).

This can be readily explained if the reasonable hypothesis is adopted that a shallow indentation strains the material around the impression less severely than a deep indentation. As the indenter angle is increased, it may be expected that the indentation pressure should be governed by correspondingly smaller yield stresses in every particle of the material. Therefore, for a material having a rapid rate of strain-hardening, the yield stresses in every particle, and consequently the indentation pressure, would fall rapidly as the indenter angle is increased. For a material having only a slow rate of strain-hardening, it might be expected that the indentation pressure would fall less rapidly with increasing indenter angle. So although the indentation pressure for an indenter of 35° may bear an almost constant ratio to the pressure p_s for materials of various rates of strain-hardening, it is evident that indentation pressures for indenters of larger angle will not.

Nevertheless, it appears that the experimental results for annealed copper and manganese steel lie on a common curve (Fig. 6a), for those indenters which produce impressions having concave sides (Fig. 5). This curve is re-drawn in Fig. 6b, and it seems likely that pressure ratios for other annealed materials should lie close to this curve. The upper curve in Fig. 6b is drawn so as to enclose the curves for the cold-worked materials.

Indentation pressures for the indenter of 68° semi-angle are of special interest, since this is the angle which has been adopted for the Vickers hardness testing apparatus. From Fig. 6b it can be seen that for this angle, the ratio p_n/p_s might be expected to take, for many materials, some value between 0·6 and 0·8, approximating to one or the other according to the rate of strain-hardening. In estimating the hardness numeral in this way, it would be necessary, of course, to make a small allowance for friction.

Vol. 3 54/55

Acknowledgment

The manganese steel bar was supplied by the British Iron and Steel Research Association, Sheffield.

References

Dugdale, D. S. 1954 *J. Mech. Phys. Solids*, **2**, 265.
Hankins, G. A. 1925 *Proc. Inst. Mech. Eng.*, 611.
Hill, R. 1950 *Mathematical Theory of Plasticity* (Clarendon Press).
Krupkowski, A. 1932 *Revue de Métallurgie*, **29**, 16.

Journal of the Mechanics and Physics of Solids, 1955, Vol. 3, pp. 212 to 217. Pergamon Press Ltd., London.

X-RAY MICROBEAM STUDIES OF BRITTLE FRACTURES OF METALS

By Lo-ching Chang*
Columbia University, New York, New York, U.S.A.

(*Received 4th October*, 1954)

Summary

X-ray microbeam studies of the fracture surfaces of polycrystalline iron and zinc reveal that the plastic strain associated with brittle fracture of both metals can be resolved into two parts : the pre-fracture strain and the fracture strain. Brittle fracture is therefore preceded by plastic strain. The energy associated with the fracture strain component is found to be approximately two orders of magnitude larger than the surface energy of the metal and can thus be regarded as the determining energy term for the propagation of a crack. The experimental results support the dislocation mechanism of crack nucleation in crystalline solids recently advanced by several investigators.

1. Introduction

The determination of plastic strain associated with brittle fracture of metals by means of X-ray diffraction methods has been attempted by a few investigators. Klier (1951) has shown that plastically deformed metal is obtained at the fracture surface of alpha iron cleaved under a variety of test conditions. Orowan (1950) estimated that a layer, strained to an average of two per cent, existed to a depth of 1/2 mm below the fracture surface of a brittle-failed polycrystalline steel specimen. In order to understand fully the mechanism of fracture of a metal, it is desirable to study separately the extent of plastic deformation associated with nucleation and growth of cracks during fracture of the metal. Such quantitative information, as pointed out recently by Hall (1953), is not yet available. It is the purpose of this study to reach the goal by means of X-ray diffraction methods.

2. Experimental Procedures

A back-reflection X-ray microbeam camera is used in this study. The X-ray beam is collimated to give a divergence of about one and one-half degrees. Micro-stages are provided to permit small horizontal and vertical motions, respectively, of the pinhole for beam alignment. The diameter of pinhole used in this study is about 150 microns. Filtered Cu radiation is used for zinc specimens and filtered Co radiation for iron specimens. The grain size of the specimen is such that only a few grains diffract in the high angle back reflection region.

A discussion of the physical significance of the broadening of Debye spots is given by Gay and Kelly (1953). In general, the total misorientation of a given

* Now at Rutgers University, New Brunswick, New Jersey, U.S.A.

grain, β, is related to the Bragg angle, θ, and the measured arc length, α (after correction for beam divergence, etc.), along the Debye ring, as follows :

$$\sin \frac{\beta}{2} = \cos \theta \, . \sin \frac{\alpha}{2}, \tag{1}$$

and when both α and β are small,

$$\beta \cong \alpha \cos \theta. \tag{1'}$$

It was found that the average arc length of diffracted spots measured along the Debye ring increases with increasing previous plastic deformation for small strains. The average misorientations of polycrystalline zinc and iron grains after various amounts of plastic strain are shown respectively in Fig. 1 (a, b).

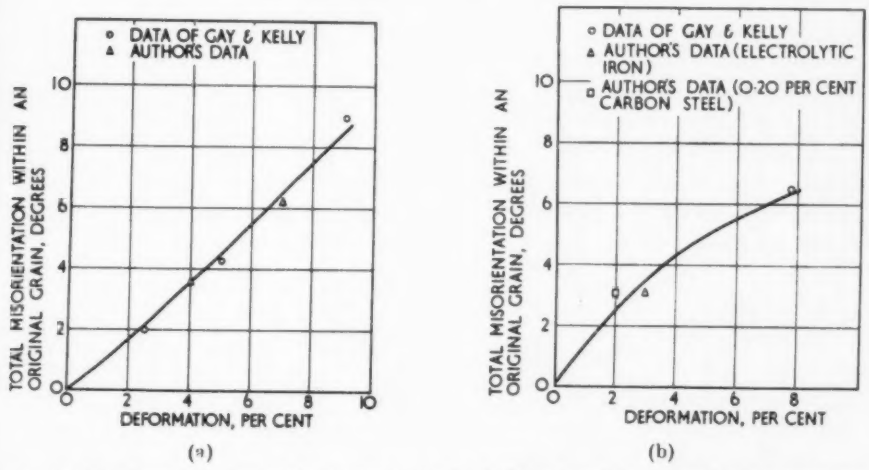
DATA OF GAY & KELLY
AUTHOR'S DATA
TOTAL MISORIENTATION WITHIN AN ORIGINAL GRAIN, DEGREES
DEFORMATION, PER CENT
(a)
DATA OF GAY & KELLY
AUTHOR'S DATA (ELECTROLYTIC IRON)
AUTHOR'S DATA (0·20 PER CENT CARBON STEEL)
TOTAL MISORIENTATION WITHIN AN ORIGINAL GRAIN, DEGREES
DEFORMATION, PER CENT
(b)

Fig. 1. (a) Misorientation versus plastic strain, zinc ; (b) Misorientation versus plastic strain, iron.

To estimate the average plastic strain within a given area of the fracture surface, several photograms are taken from the area of interest. The arc widths of all spots are measured and averaged. The corresponding plastic strain according to calibrated curves such as Fig. 1 is taken as the true average plastic strain of that portion of fracture surface under study. To find the average plastic strain of the metal at increasing distances from the fracture surface, successive layers of the metal are removed by etching in 1 : 1 aqueous hydrochloric acid at room temperature. X-ray photograms are taken of each newly exposed surface. The thickness of metal removed each time is found by chemical analysis of the etchant, assuming that etching removes uniformly successive layers of the metal.* By this means the distribution of plastic strain of a metal in a direction perpendicular to the fracture surface is obtained.

Typical back-reflection photograms taken near the centre of fracture surfaces of zinc and iron specimens after slow tension tests are shown in Fig. 2. For zinc specimens, the interpretation and measurement of arc widths are comparatively easy. For iron specimens, however, the spots spread both circumferentially and

* The appearance of the surface after repeated etches suggests that the assumption is reasonable.

radially along the Debye ring, making the measurement more difficult. Sufficient spots (about 40) are therefore measured in the case of iron specimens to yield a good average. A typical distribution curve of the spots obtained from an iron specimen is shown in Fig. 3. The $(21\bar{3}2)$ reflection of zinc and the (310) reflection of iron are studied.

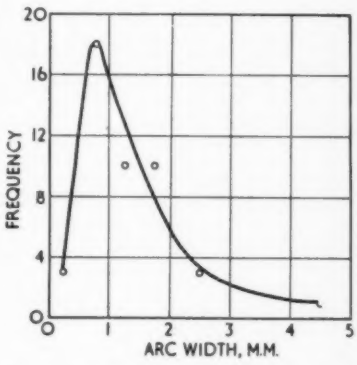

Fig. 3. Statistical distribution of spot widths, iron.

3. Data and Results

The strain distribution curves obtained by the above described experimental procedures for zinc specimens fractured in slow tension at 77, 195, and 225°K, respectively, are shown in Fig. 4. The specimens were made from chemically pure zinc, worked, and finally recrystallised to yield grains of 40 to 80 microns in diameter. The strain distribution curves of an electrolytic iron specimen (average grain diameter 30 microns, fractured in slow tension at 35°K) and a 0·20 per cent carbon steel specimen (average grain diameter 15 microns, fractured in slow tension at 38°K) are shown in Fig. 5.

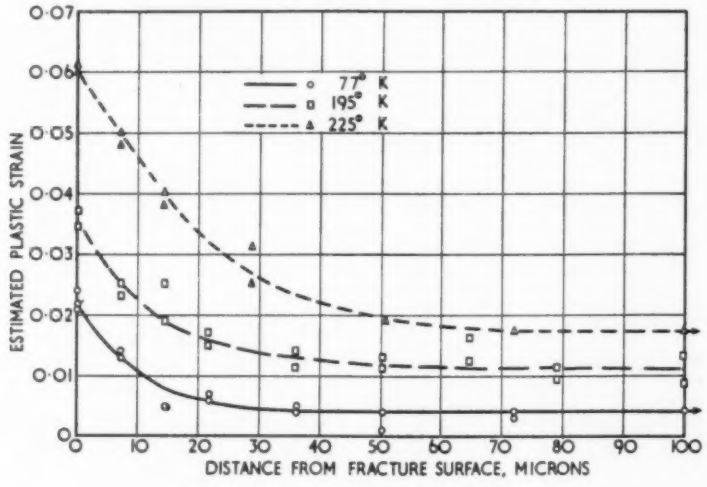

Fig. 4. Strain distribution curve, zinc.

4. Conclusion

It is interesting to note that the average plastic strain decreases rapidly within a short distance from the fracture surface and remains more or less constant at longer distances. X-ray photograms corresponding to these long distances show almost without exception a few distorted spots accompanied by several sharp spots along the Debye ring, indicating the straining of favourably oriented grains before fracture presumably during the tension test. The strain pattern is thus

VOL. 3
54/55

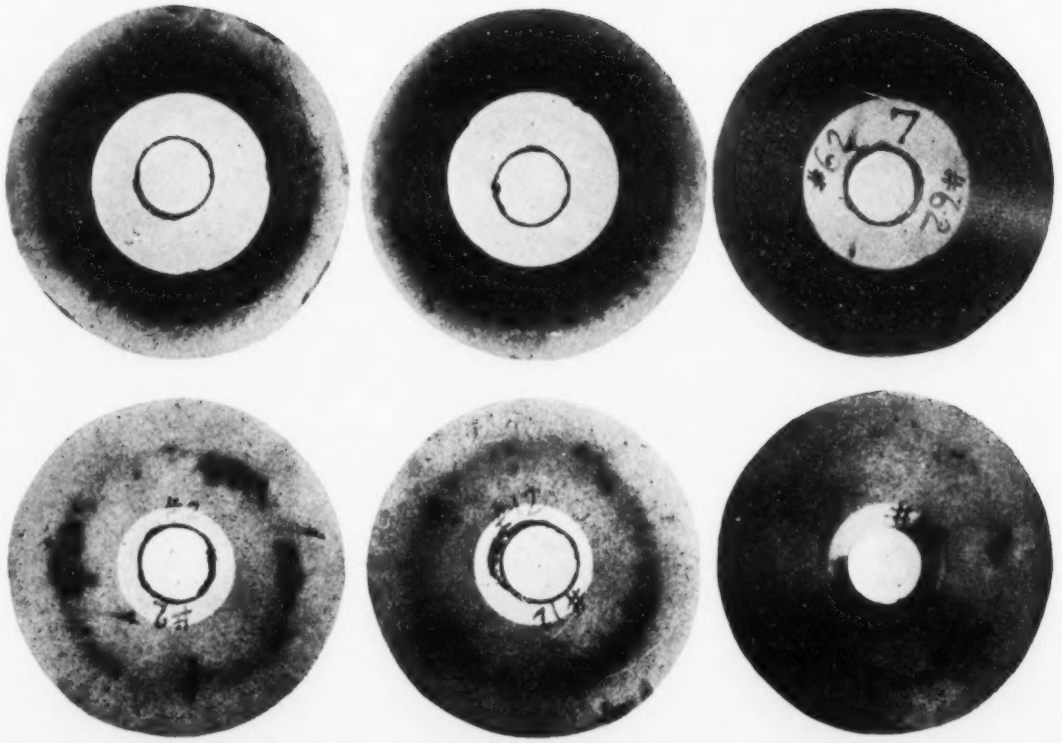

Fig. 2. Typical photograms (magnified approximately 2 times), zinc and iron.
Top row, Zinc ; bottom row, Iron. Left, as fractured, no etch. Centre, lightly etched. Right, heavily etched.

Vol
3
1954/

made of two parts : the pre-fracture strain, which is relatively small and remains constant over long distances, and the fracture strain, which is greatest near the fracture surface and drops rapidly within a short distance of the fracture surface. This is good evidence that uniformly distributed plastic strain precedes the plastic process resulting in brittle fracture.

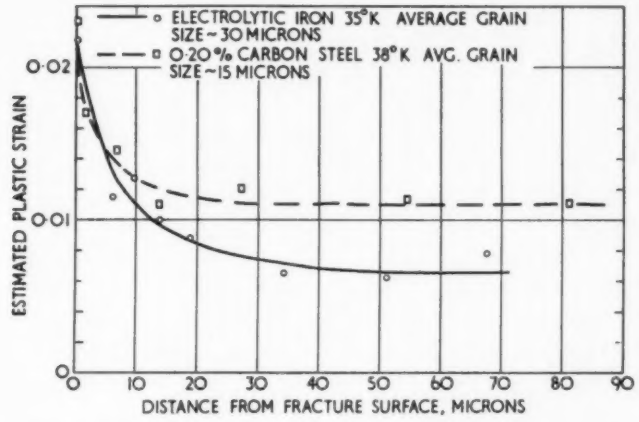

Fig. 5. Strain distribution curve, iron and 0·20 per cent carbon steel.

The work done to produce the plastic strain associated with fracture, or the plastic work factor w, is given by

$$w = \int_0^l \sigma\epsilon \, dx - \int_0^l \sigma\epsilon_p \, dx$$

$$= \int_0^l (\sigma_0 + b\,\epsilon)\,\epsilon \, dx - (\sigma_0 + b\,\epsilon_p)\,\epsilon_p\, l$$

$$= \sigma_0 \int_0^l \epsilon \, dx + b \int_0^l \epsilon^2 \, dx - (\sigma_0 + b\epsilon_p)\,\epsilon_p\, l \qquad (2)$$

where $\sigma = \sigma_0 + b\,\epsilon$, as is the case for small strains (σ_0, b are constants characteristic of the material), σ the flow stress corresponding to strain ϵ, ϵ_p the pre-fracture strain, and l the distance along a direction normal to the fracture surface.

An estimation of the plastic work factor w was accomplished graphically by measuring the area under curves of the strain and the square of strain plotted against the distance normal to the fracture surface and subtracting the pre-fracture strain component. A compilation of the w values obtained in this study is shown in Table 1.

5. Discussion

The present study reveals that brittle fracture is preceded by plastic deformation, indicating strongly that crack is nucleated by plastic strain. It further reveals that the plastic work factor w, instead of the surface energy γ, of a metal is the determining factor for the propagation of a crack. Table 1 shows that, first, the w values for zinc and iron are about two orders of magnitude larger than their

respective surface energies (γ), and second, w is seen to decrease slightly with decreasing temperature in the case of zinc.

According to the modified GRIFFITH's formula for the propagation of a crack (HALL 1953) :

$$\sigma_f \cong \sqrt{\frac{2E(w+\gamma)}{\pi C}} \tag{3}$$

where σ_f is the fracture stress, E the modulus of elasticity, w the plastic work factor, γ the surface energy (which is negligibly small compared with w), $2C$ the critical length of an internal crack, the critical crack length can be calculated from known values of σ_f, E and w. The calculated $2C$ values are inserted in the last column of Table 1. It is interesting to note that they are of the order of the grain diameters of the specimens studied.

It has been proposed that certain arrangement of dislocation arrays produced in crystalline materials resulting from plastic strain has the properties of cracks. ZENER (1948) has pointed out the significance of the crack nucleus associated with a dislocation. ESHELBY and FRANK (1951) have suggested the simulation of a crack by the following sequence of dislocations : a locked positive dislocation, a number of free positive dislocations, an equal number of free negative dislocations, a locked negative dislocation. The free dislocations are prevented from coalescing by an externally applied stress, while the locked dislocations prevent the free dislocations from spreading and define the length of an equivalent crack. It is quite possible that such arrays of dislocations act as nucleation sites for fracture. The present state of knowledge about fracture is, however, far from a true understanding of its mechanisms inasmuch as the nucleation and growth of cracks are concerned. Further work in this direction is needed.

Several published papers (LOW and FEUSTEL 1953 ; BILBY and ENTWISLE 1954) reveal that mechanical twinning, like brittle fracture, is also nucleated by plastic strain. Metals which form mechanical twins also fail brittlely. The close association between mechanical twinning and brittle fracture and their respective mechanisms should be interesting subjects for further investigation.

TABLE 1

Specimen	*Grain size (microns)*	*Temperature (°K)*	*Plastic work factor w (ergs/cm^2)*	*Surface energy γ, (ergs/cm^2)*	*Critical crack length $2C$ (microns)*
Zinc	40-80	77	30,000	$\sim$ 800	52
Zinc	40-80	195	100,000	$\sim$ 800	240
Zinc	40-80	225	140,000	$\sim$ 800	320
Iron	$\sim$ 30	35	150,000	$\sim$ 1,000	30
0·20%C Steel	$\sim$ 15	38	70,000	$\sim$ 1,000	12

ACKNOWLEDGMENT

This work was supported by Contract AF 18 (600)-898 with Air Research

Development Command under the direction of Professor MAXWELL GENSAMER, School of Mines, Columbia University.

REFERENCES

BILBY, B. A. and ENTWISLE, A. R.	1954	*Acta Metallurgica*, **2**, 15.
ESHELBY, J. D. and FRANK, F. C.	1951	*Phil. Mag.*, **42**, 351.
GAY, P. and KELLY, A.	1953	*Acta Crystallographica*, **6**, 165.
HALL, E. O.	1953	*J. Mech. Phys. Solids*, **1**, 227.
KLIER, E. P.	1951	*Trans. Amer. Soc. Metals*, **43**, 935.
LOW, J. R. Jr. and FEUSTEL, R. G.	1953	*Acta Metallurgica*, **1**, 185.
OROWAN, E.	1950	*Conference on Fatigue and Fracture of Metals*, *M.I.T.*, June.
ZENER, C.	1948	*A.S.M. Symposium on Fracturing of Metals*, 3.

Vol.
3
54/55

Journal of the Mechanics and Physics of Solids, 1955, Vol. 3, pp. 218 to 223. Pergamon Press Ltd., London.

EXTRUSION THROUGH WEDGE-SHAPED DIES. PART I.

By W. Johnson
Department of Mechanical Engineering, University of Sheffield

(*Received 7th March*, 1955)

Summary

The results of calculations of the steady-state pressure for the direct extrusion of sheet under plane strain conditions through square and wedge-shaped dies are given. The results depend upon whether a dead metal zone is formed on the die face or whether the metal slips over the die face.

1. Introduction

If the mode of deformation of metal during its extrusion through wedge-shaped dies is examined, the flow is seen to be accomplished in one or other of two ways :

(a) the metal slips, with or without friction along the die face ;

(b) a region of ' dead ' or ' trapped ' metal is seen to rest on the die face.

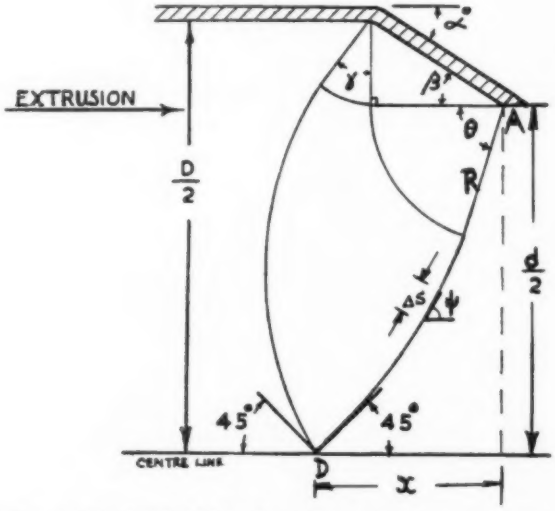

Fig. 1. Slip-line field for r less than $2 \sin \alpha/(1 + 2 \sin \alpha)$.

For both physical situations the theory of plane plastic strain can furnish slip-line fields over certain reductions and thereby enable one to calculate the steady-state extrusion pressure.

The theory of plane plastic strain has been given by Hill (1950) and the slip-line

fields used in the present calculations have been justified in the original paper (HILL 1948). The various slip-line fields used here were determined graphically using an equiangular net of 5°, the quantities required in the expressions below being easily obtained from them.

2. EXTRUSION BY SLIP ALONG THE DIE FACE

The results presented below are only for frictionless slip of the metal along the die; they are based on the slip-line fields shown in Figs. 1 and 2; the fields are symmetrical about the die centre-line.

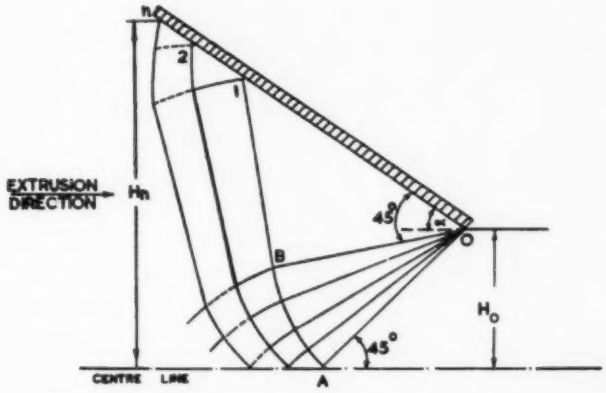

Fig. 2. Slip-line field for r greater than $2 \sin \alpha/(1 + 2 \sin \alpha)$.

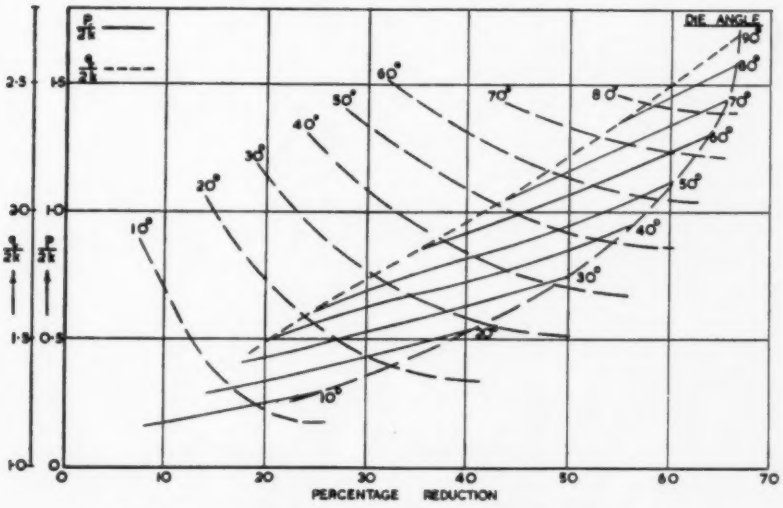

Fig. 3. Variation of $p/2k$ and $q/2k$ with r for values of α.

The field of Fig. 1 applies when the reduction, r, is larger than that at which bulging occurs but less than $2 \sin \alpha/(1 + 2 \sin \alpha)$, where α is the semi-angle of

the die. The region of large plastic strains intersects the axis in one point only. It is easily shown that

$$r = \frac{1}{1 + \dfrac{d \,.\, \operatorname{cosec} \alpha}{2\sqrt{2} \,.\, R}}, \tag{1}$$

$$\frac{q}{2k} = \frac{\frac{1}{2}x - \Sigma_B^A \psi \,.\, \sin \psi \,.\, \Delta s}{\frac{1}{2}d} + \tfrac{1}{4}\pi + \theta + \gamma + \tfrac{1}{2}, \tag{2}$$

and

$$\frac{p}{2k} = r\left(\frac{q}{2k}\right). \tag{3}$$

q is the die face pressure, p the extrusion pressure and k the yield shear stress of the material in plane strain. The meaning of the other quantities will be clear on inspecting Fig. 1 (similarly for equations (4), (5) and (6) see Fig. 2, and for (7), (8) and (9) see Fig. 5). The results are presented in Fig. 3, those for 10°, 20° and 30° having been previously given by HILL (1948).

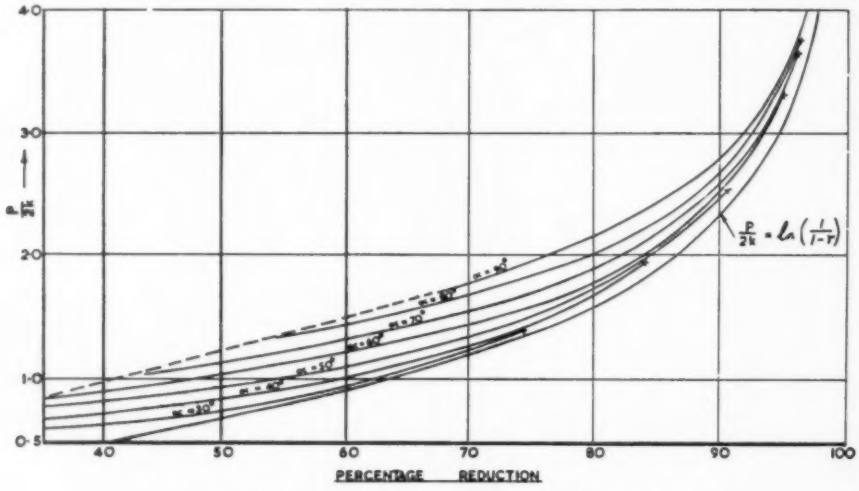

Fig. 4. Variation of $p/2k$ with r for values of α.

The corresponding expressions applying to Fig. 2, in which the region of large plastic strains now meets the axis over a finite length, and, when r is greater than $2 \sin \alpha/(1 + 2 \sin \alpha)$, are

$$r = \frac{H_n - H_0}{H_n}, \tag{4}$$

$$\frac{q_n}{2k} = 1 + \alpha + 2(n-1)\,\Delta\phi, \tag{5}$$

$$(\Delta\phi = 0{\cdot}0873^r \text{ for a } 5° \text{ net})$$

and

$$\frac{p}{2k} H_n \doteq (1+\alpha)(H_1 - H_0) + \tfrac{1}{2}\left(\frac{q_1}{2k} + \frac{q_2}{2k}\right)(H_2 - H_1) + \ldots + \tfrac{1}{2}\left(\frac{q_{n-1}}{2k} + \frac{q_n}{2k}\right)(H_n - H_{n-1}). \tag{6}$$

The results of these calculations are shown in Fig. 4; they have been combined with those in Fig. 3 for r greater than 0·35, and the curve of uniform compression, $p/2k = \ln(1/(1-r))$, has been inserted for purposes of comparison.

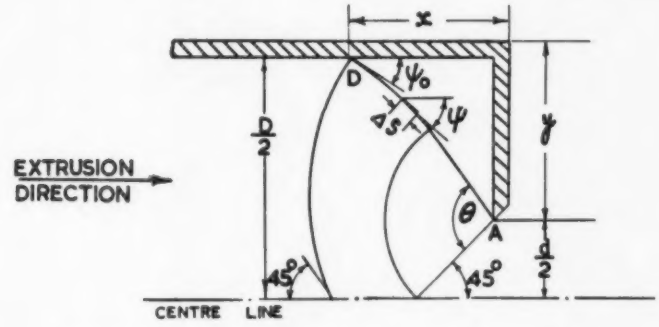

Fig. 5. Square dies, slip-line field for r greater than 0·5.

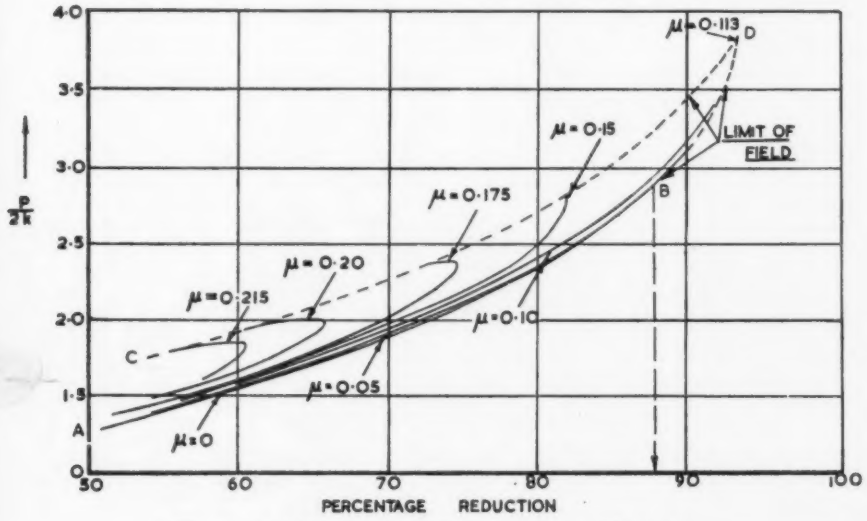

Fig. 6. Variation of $p/2k$ with r for various values of μ.

3. Extrusion with Dead Metal Zone on Die Face

(i) *Square Dies* ($\alpha = 90°$). When sheet of thickness D is extruded down to thickness d, and r is greater than 0·5, the slip-line field is as in Fig. 5. It can be shown that

$$r = \frac{y}{D/2}, \tag{7}$$

$$\frac{p}{2k} = \frac{1}{D}\left[x + y\left(1 - \tfrac{1}{2}\pi + 4\theta\right) - 2\Sigma_A^D \psi \,.\, \sin\psi \,.\, \Delta s\right], \tag{8}$$

and $$\mu = \frac{\cos 2\psi_0}{1 + 4\vartheta - \frac{1}{2}\pi - 2\psi_0 - \sin 2\psi_0}. \tag{9}$$

μ is the coefficient of friction between metal and container wall. By a process of graphical interpolation it was possible to derive values of $p/2k$ for certain values of r for selected values of μ. Fig. 6 shows the variation of $p/2k$ with r for various

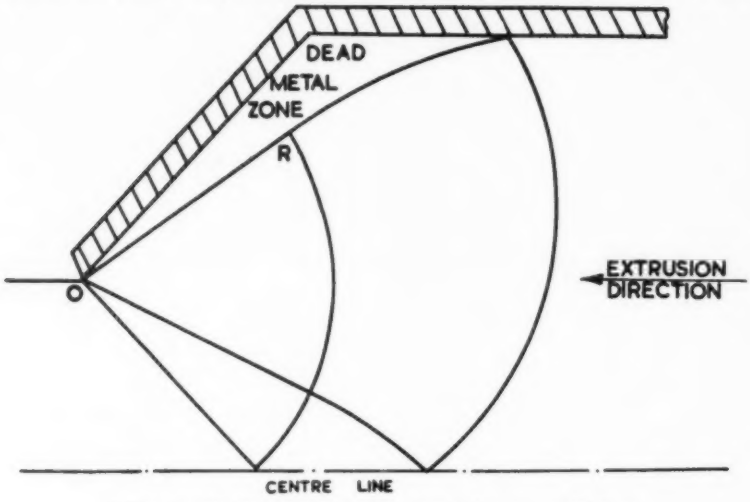

Fig. 7. Slip-line field with dead metal zone on die face.

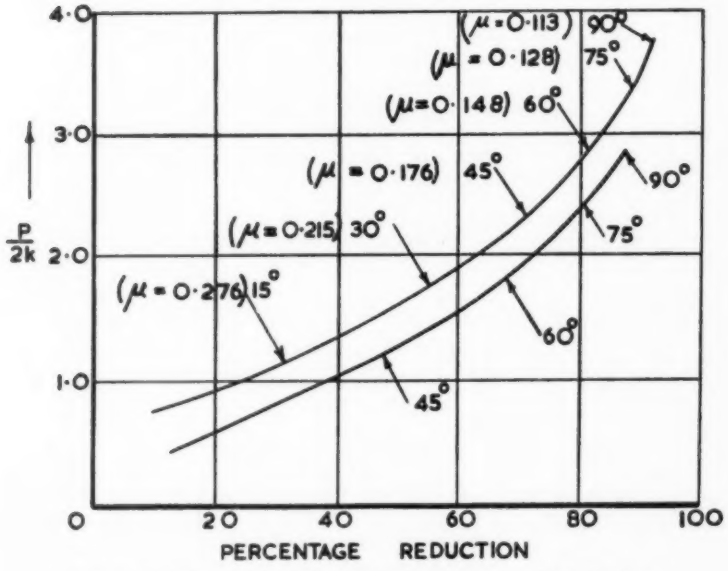

Fig. 8. Results when dead metal zones rest on conical die face.

values of μ. Curve AB corresponds to no friction between metal and container wall (slip-lines meet the wall at 45°), and curve CD to the configurations in which, for a given r, the slip-lines meet the container wall at 0° and 90°.

(ii) *Wedge-Shaped Dies.* It is obvious that dead metal zones will not be uniquely associated with square dies but may be presumed to exist when α is large, but not necessarily as large as 90°. We can assume the dead metal zones to be of the form shown in Fig. 7, in which case the slip-line field will be as indicated. The largest reduction corresponding to this field occurs when *OR* lies along the die face. The results for the square die comprise all those for α less than 90°; it is then a matter of giving the upper limits to r for each value of α and this is done in Fig. 8.

4. Comment

The results presented show no perceptible difference from those originally obtained by Hill at the points where comparison with his is possible. The degree of accuracy with which results can be obtained by means of this semi-graphical method is more than adequate for use in experimental investigation and it is thought they are correct to about 1%.

Acknowledgments

The author wishes to acknowledge the assistance of Mr. J. M. Clark with some of the calculations, the kindly encouragement of Professor H. W. Swift, and the permission of B.I.S.R.A. to publish these results, taken from the original report (Johnson 1953).

Vol. 3 54/55

References

Hill, R. 1950 *Mathematical Theory of Plasticity*, Chap. V (Clarendon Press).
Hill, R. 1948 *J. Iron Steel Inst.*, **158**, 177.
Johnson, W. 1953 B.I.S.R.A. Report MW/ E/ 56/53.

Journal of the Mechanics and Physics of Solids, 1955, Vol. 3, pp. 224 to 230. Pergamon Press Ltd., London.

EXTRUSION THROUGH WEDGE-SHAPED DIES. PART II.

By W. Johnson
Department of Mechanical Engineering, University of Sheffield

(*Received 7th March*, 1955)

Summary

Results are presented giving the variation of extrusion pressure with friction, for selected reductions for wedge-shaped dies of small angle, using the Hill-Tupper theory of sheet-drawing.

1. Introduction

Uniform sheet or bar, cold extruded or drawn through a wedge-shaped die under conditions of plane-strain at slow speeds, in practice appears to be subject to considerable frictional drag between the die and the metal, even when attempts to introduce a lubricant are made (Johnson and Collins 1954). As a preliminary to an experimental investigation of the effect of friction in these two operations, calculations of the variation of extrusion pressure with friction for some particular reductions have been made, using the exact theory for the slip-line field as given by Hill and Tupper (1948). This theory assumes an ideal plastic-rigid material deforming under constant maximum shear stress, k.

Calculations have already been given by Green and Hill (1952) for sheet-drawing when the coefficient of friction in drawing, μ_D, is less than 0·15, for dies of semi-angle between 5° and 15°, and for reductions larger than those at which bulging occurs ; the reductions covered by their calculations also extend to larger values than those presented here.

2. Type of Field and Calculations

The type of slip-line field used is that shown in Fig. 1 which was originally derived and justified by Hill and Tupper for sheet drawing through a rough die, though exact results were given for smooth dies only. Green and Hill have obtained results with this type of field for drawing through rough dies for such values of β as lead to μ_D being less than 0·15.

Beginning with values of $\beta = 45°$, 35°, 20° and 10°, equiangular 5° slip-line fields of this type were drawn (Hill 1950). Now it can be shown that, if q is the die pressure in extrusion (see Fig. 1) and the summation is taken from A to D, then

$$\frac{q}{2k} = \frac{\frac{1}{2}x - \Sigma_A^D \psi \sin \psi \, \Delta s}{\frac{1}{2}d} + \tfrac{1}{4}\pi + \theta + \gamma + \tfrac{1}{2}\sin 2\beta. \qquad (1)$$

$$\text{Coefficient of friction, } \mu_E = \tfrac{1}{2}\cos 2\beta \Big/ \frac{q}{2k}. \qquad (2)$$

$$\text{Reduction,} \qquad r = \frac{1}{\dfrac{d \cos \beta}{2R \sin \alpha}}. \tag{3}$$

$$\frac{\text{Extrusion pressure}}{2k}, \qquad \frac{p}{2k} = \left(\frac{q}{2k} + \frac{\cos 2\beta}{2 \tan \alpha}\right) r. \tag{4}$$

Determining these quantities by use of the drawn fields for each value of β (see Fig. 1) and for a chosen value of α, one obtains unique combinations of r,

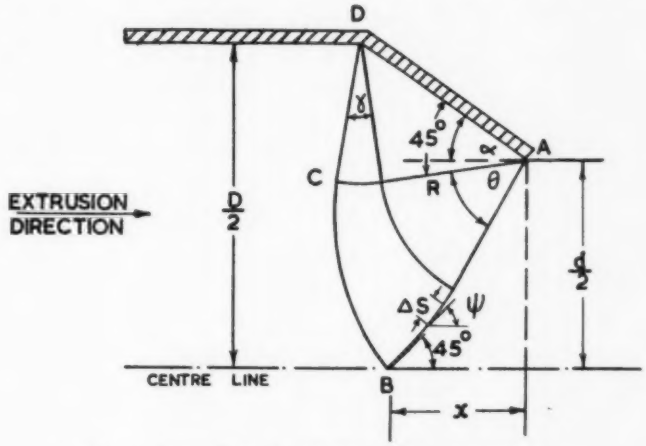

Fig. 1. Type of slip-line field used in calculations.

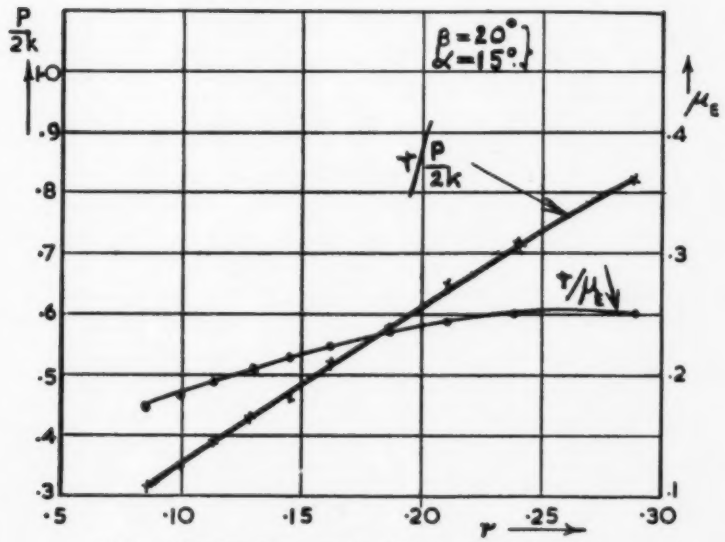

Fig. 2. Showing how μ varies with r, and $p/2k$ with r.

μ_E and $p/2k$; from these, curves can be plotted showing the variation of μ_E and $p/2k$ with r (see typical example in Fig. 2). For selected values of r one can now obtain corresponding values of μ_E and $p/2k$. In general four points are obtained,

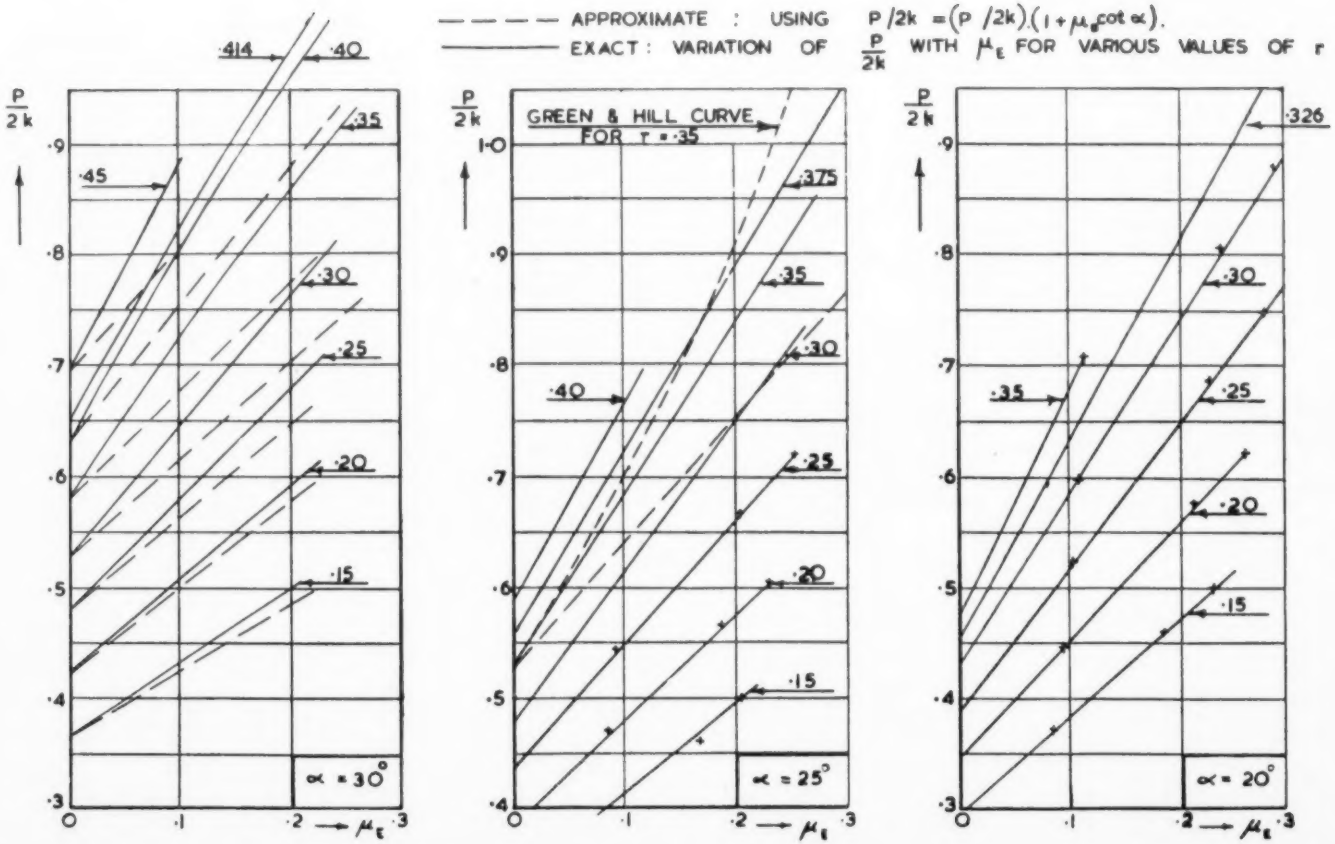

Figs. 3, 4 and 5. Variation of $p/2k$ with μ for various values of r.

VOL 3 1954/

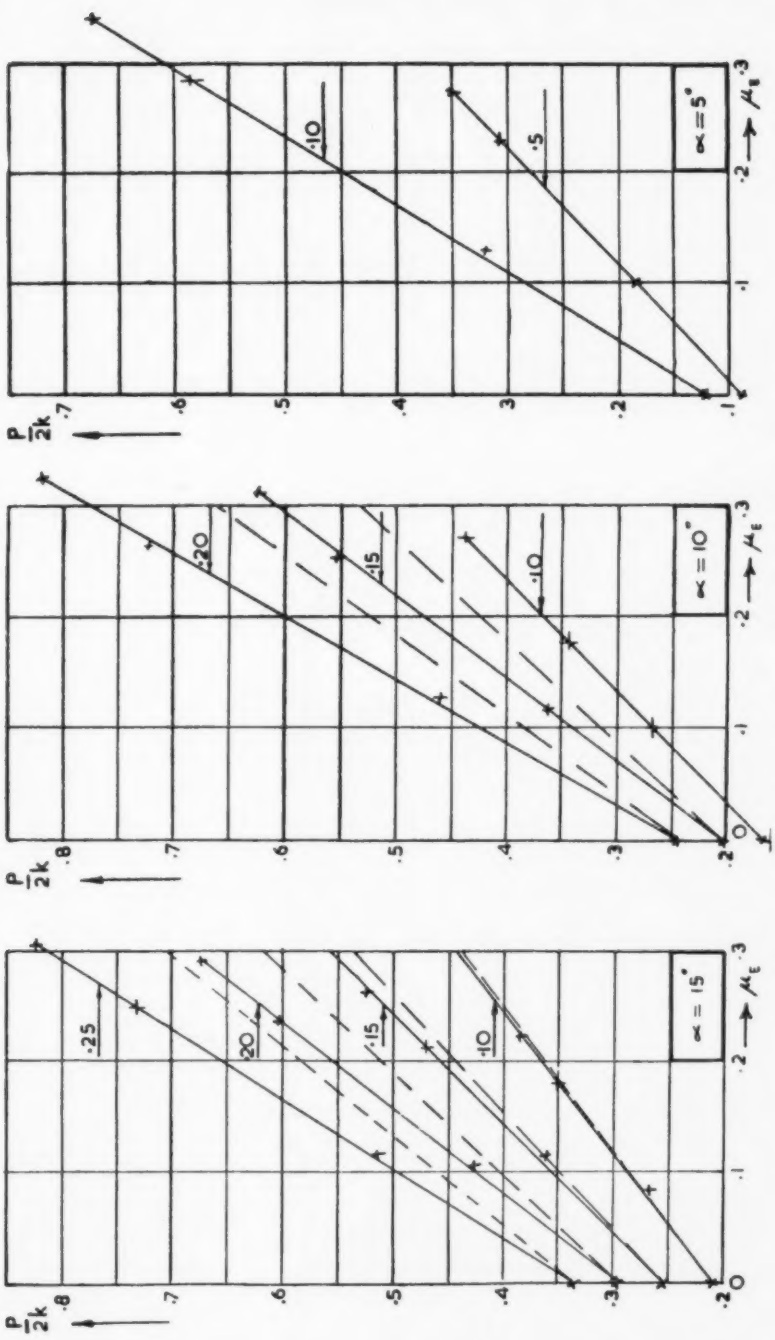

Figs. 6, 7 and 8. Variation of $p/2k$ with μ for various values of r.

Vol. 3 54/55

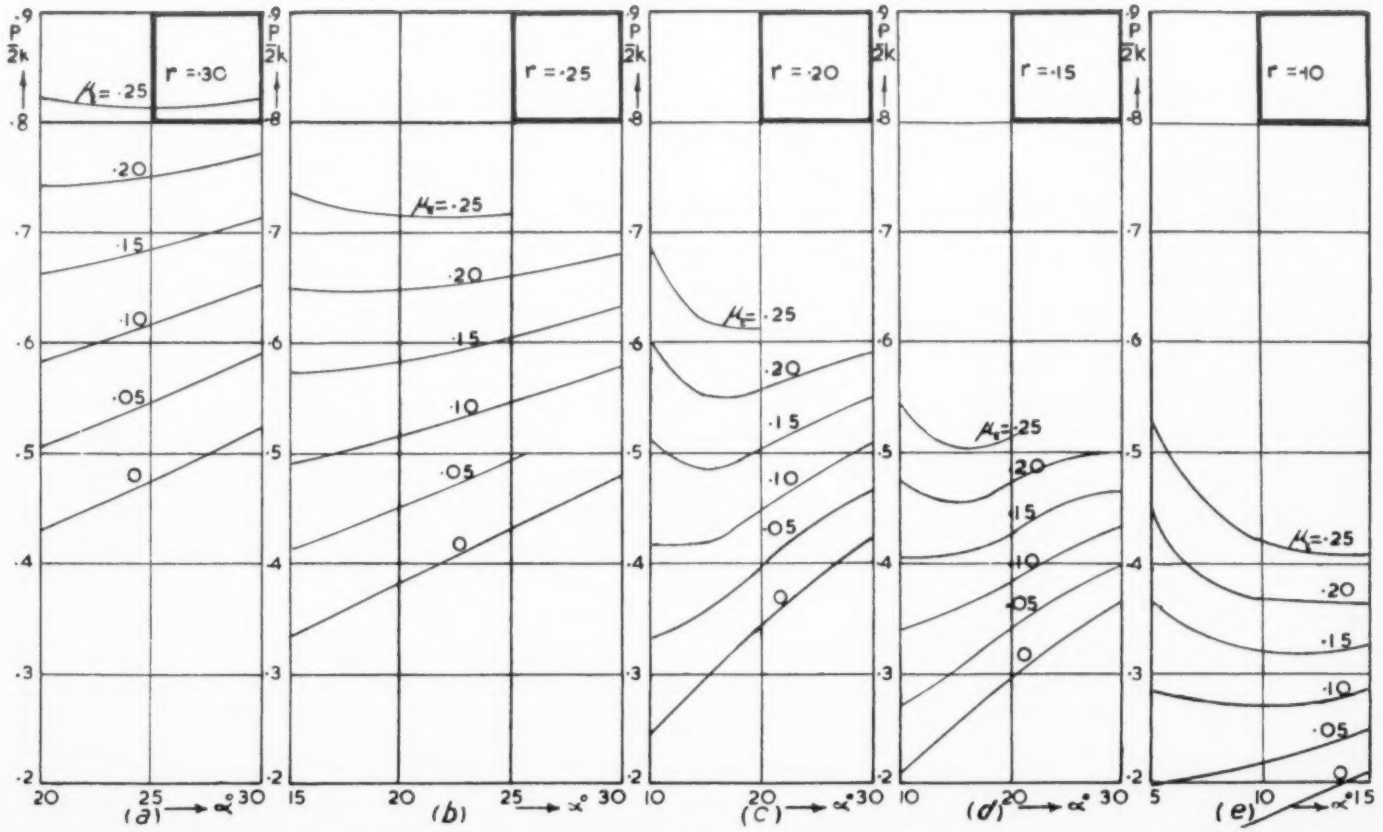

Fig. 9. Variation in pressure with friction.

corresponding to each of the values of β taken for a selected r and α, e.g. see Figs. 3 to 8.

3. Results

The results are presented in Figs. 3-8 and they are thought to be correct to between 1% and 2%. There is seen to be, for all practical purposes, a nearly linear relationship between μ_E and $p/2k$.

The variation of $p/2k$ with α for various values of μ_E may be deduced from the curves in Figs. 3 to 8 with a view to suggesting the best die angle for a given r and μ_E, to give near minimum extrusion pressures; examples are shown in Fig. 9.

4. Discussion

For the slip-line fields used, when the reduction is the same for drawing and extrusion, it may be shown that if the drawing stress for a rough die, with coefficient of friction μ_D, is equal to the extrusion pressure for a rough die of equal angle α and coefficient of friction μ_E, then

$$\mu_E = \frac{1 - r}{r \cot \alpha + 1/\mu_D},$$

We may now re-write the expression (4) of Green and Hill as

$$\frac{p'}{p} = \frac{(1 - r) - \mu_E \left[0{\cdot}2 - (1 - r) \cot \alpha + 0{\cdot}08\, r \cot^2 \alpha\right]}{1 - r\,(1 + \mu_E \cot \alpha)}, \tag{5}$$

where p is the extrusion pressure when $\mu_E = 0$ and p' is the extrusion pressure for the rough die.

The expression (5) has been inserted on Fig. 4 for $r = 0{\cdot}35$ and $\alpha = 25°$. Clearly there is here no very great error in using it, when μ_E is less than 0·15 ($\mu_D = 0{\cdot}28$),

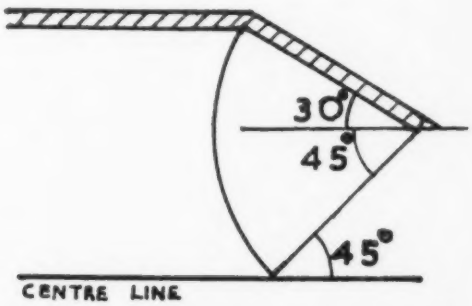

Fig. 10. Slip-line field for $r = 0{\cdot}414$ and $\alpha = 80°$.

at values of α beyond 15° for which it was originally derived.

It has often been suggested that a rough method of allowing for friction is to take

$$\frac{p'}{p} = 1 + \mu_E \cot \alpha.$$

This curve has also been inserted on Figs. 3, 4, 6 and 7. For large values of μ_E the error is, of course, considerable.

Some indication of the approximate correctness of the almost linear relationship between $p/2k$ and μ_E, for given values of r and α, is obtained by extrapolating as a straight line, on Fig. 3, for $r = 0{\cdot}414$; this gives, at $\mu_E = 0{\cdot}276$, a value of $p/2k = 1{\cdot}11$. In Fig. 10 is shown the slip-line field for $r = 0{\cdot}414$ and $\alpha = 30°$; shearing occurs along the whole die face and it is easy to show that here $\mu_E = 0{\cdot}276$ and $p/2k = 1{\cdot}107$. Similarly extrapolated values for $r = 0{\cdot}373$, $\alpha = 25°$ and $r = 0{\cdot}326$, $\alpha = 20°$, are inserted in Figs. 4 and 5 and are found to be correct to within about 2%.

Direct comparison with the results of GREEN and HILL reveal at worst a 2% disparity from those given here.

ACKNOWLEDGMENT

The author wishes to acknowledge the encouragement of Professor H. W. SWIFT during the making of these calculations.

REFERENCES

GREEN, A. P. and HILL, R. 1952 *J. Mech. Phys. Solids*, **1**, 331.

HILL, R. and TUPPER, S. J. 1948 *J. Iron Steel Inst.*, **159**, 353.

HILL, R. 1950 *Mathematical Theory of Plasticity*, p. 141 (Clarendon Press, Oxford).

JOHNSON, W. and COLLINS, A. G. 1954 B.I.S.R.A. Report MW/E/54/54.

BOOK REVIEWS

Max Born and Kun Huang : Dynamical Theory of Crystal Lattices. Oxford University Press, 1954, pp. xii + 420. 50s. net.

The authors are concerned with the dynamics of ionic and homopolar perfect lattices. As metals and physical properties depending on imperfections of the lattice are excluded, the book does not directly touch the particular interests of this Journal. Part I (Elementary Theories) briefly discusses the various kinds of interatomic force (Ch. I), gives a fairly simple account of lattice vibrations (Ch. II) and (for central forces) of elasticity and lattice stability (Ch. III). Particularly interesting is the discussion of the inter-relation of mechanical and electromagnetic waves in a lattice of ions coupled by short-range spring forces and long-range electromagnetic fields.

Part II (General Theories) starts from the quantum-mechanical problem of a set of ions and electrons. It is shown that the effect of the electrons can to a good approximation be replaced by an inter-ion potential (Ch. IV). Certain difficulties in discussing homogeneous deformation of an infinite lattice lead in Chapter V to " The Method of Long Waves." Chapter VI determines the free energy of a crystal as a function of distortion and electric field ; from it can be derived the thermal, elastic and dielectric properties and their inter-relations (pyro-electric and piezo-electric coefficients). The last chapter is devoted to dispersion, Raman scattering and other optical effects.

Compared with the introductory Part I, Part II is on the whole heavy reading, containing besides some rather subtle considerations a great deal of straightforward calculation in a necessarily forbidding notation. The non-specialist reader will perhaps be content merely to note the existence of the body of work which it presents.

J. D. Eshelby

Vol. 3 54/55

A. E. Green and W. Zerna : Theoretical Elasticity, Clarendon Press, Oxford, 1954, 437 pp. 50s. net.

This is not a comprehensive work on elasticity, but reflects the particular interests of the authors. Three main topics are treated : the theory of finite elastic strain ; two-dimensional problems of infinitesimal strain by means of functions of a complex variable ; and the infinitesimal distortion of thin shells by bending. The treatment is authoritative, and in various places is claimed to be an improvement on existing methods. Emphasis is laid on the advantages of tensor analysis from the point of view of mathematical elegance.

There are no concessions of any kind to make the book accessible or interesting to engineers. Even for a trained mathematician it is an extremely hard book to read – unnecessarily so, one feels, notwithstanding the intrinsic difficulties of the subject. There is no doubt, however. that the book is an inportant one, and indispensable to specialists in this field.

R. Hill

Edited by B. Chalmers and R. King : Progress in Metal Physics. Vol 5 ; Pergamon Press Ltd., 1954, viii + 324 pp. 60s. net.

The appearance of another volume in this excellent series is always an event of some interest, and this, the fifth, fully maintains the high standard of its predecessors. It is perhaps inevitable that contributions should gradually become more specialised in their appeal, but most people engaged in research in the field of metal physics will find something of interest and value.

Almost half of the space is occupied by a " Report on Precipitation " by H. K. Hardy and T. J. Heal. This falls into two distinct parts. The first, dealing with the thermodynamics and kinetics of the process has more the character of a monograph than a review of recent progress, and is not easy to follow in some places. The second part gives a detailed review of the structural

changes observed in a number of the better known systems : although easier to read than the first part, it will have appeal to a more restricted public.

Of the remaining contributions, that by R. MADDEN and N. K. CHEN on geometrical aspects of plastic deformation is a useful summary of recent work on various aspects of this, perhaps the earliest, branch of the subject ; it might be described as a supplement to SCHMID and BOAS. The other three papers are review articles on special branches ; N. J. PETCH writes on fracture, B. R. T. FROST on the structure of liquid metals, and A. M. MARTIUS on the solidification of metals. All three papers are well written and can be read with pleasure by the non-specialist.

The whole volume is printed and produced to the high standard which one has learned to expect from the publishers. There are in all 829 references to published papers.

N. F. MOTT

C. G. B. GARRETT : **Magnetic Cooling.** Harvard Monographs in Applied Science, Number 4. Harvard University Press ; John Wiley and Sons, Inc. Chapman and Hall. $4.50/36s. net.

As the term ' applied science ' is broadly interpreted by the Editorial Committee of the Harvard Monographs to comprise all phases of science that influence the lives of men, this book on Magnetic Cooling forms a most suitable volume in the series. It gives, within a reasonable compass, a very informative survey of the principles, techniques and applications of adiabatic demagnetization by one who himself has contributed markedly to the development of the subject. It can be confidently recommended, for it is pleasing and straightforward to read apart from some blemishes whose relative importance is probably a matter of taste. Some of us for example may not like expressing magnetic field strengths in oersteds, but nevertheless we do so as an international duty. Again, it is irritating to read about ' cooperative phenomena ' and ' coöperative phenomena' on the same page ; what is wrong with ' cooperative ' ? And, was it really necessary to foist upon the reader the hideous word ' erutarepmet ' ?

The author very wisely keeps to c.g.s. units throughout the book ; one wishes that in addition he followed more established custom in the use of certain letters. He uses B_0 to denote what most of us would term an applied magnetic field, and H to denote an effective field. He uses λ to denote the Curie constant, and some English readers will certainly be disconcerted thereby. They may also wonder what is meant by the somewhat bald sentence on p. 85 – " In the case of ferromagnetism and antiferromagnetism, the excitons, being associated with ' wrong ' spins, are called ' spin waves '." But when these minor irritations are overlooked the volume is well worth perusal.

L. F. BATES

D. N. DE G. ALLEN : **Relaxation Methods.** 1954, 257 pp. McGraw-Hill Publishing Co. 53s. 6d. net.

Dr. ALLEN has written a timely and extremely practical book. The Relaxation Method has now become an essential part of the equipment of researchers in Applied Physics but, in order to acquire the ability to use the method with confidence and economy of time and effort, a preliminary period of study and practice, particularly practice, is necessary. This period will be made much more profitable by the use of this admirable book written by an author who has taken a leading part in the development of the method.

All the main applications of the method, including the solution of linear algebraic and ordinary and partial differential equations are treated with the aid of detailed examples through which the reader is taken step by step and at the end of each chapter there are examples on which the reader can test his skill. There is a very useful bibliography.

The only criticism which the reviewer would like to make is the lack here and there of a word of warning to the unwary. A consideration of the unreliability of an apparently satisfactory solution of an ill-conditioned set of linear algebraic equations would have been welcome. Possibly the treatment of this sort of point would have expanded the book unduly.

The book is written in a clear and easy style and is well produced. The only misprint noticed is the substitution of χ for ψ in two places at the bottom of page 87.

W. M. SHEPHERD

Vol 3 1954/

Journal of the Mechanics and Physics of Solids, 1955, Vol. 3, pp. 238 to 245. Pergamon Press Ltd., London.

THE EFFECT OF COULOMB FRICTION IN THE PLANE-STRAIN COMPRESSION OF A PLASTIC-RIGID MATERIAL

By J. M. Alexander
Aluminium Laboratories Limited, Banbury

(*Received 25th March*, 1955)

Summary

The plane-strain compression of a plastic-rigid material is analysed on the assumption that the frictional conditions between the platens and the material are such that the shear stress is the same fraction of the normal stress everywhere on the platen surface, unless this value attains the yield shear stress of the metal, which it can never exceed. This is the condition known as Coulomb friction, the ratio being defined as the coefficient of friction μ. The solution has been determined by a geometrical method recently proposed by Prager (1953) for integral ratios of platen breadth/material thickness of 7 and 3, and for values of the coefficient of friction of 0·05, 0·1, 0·15, 0·225, 0·3 and the limiting value of $\frac{1}{1+\frac{1}{2}\pi} = 0{\cdot}389$, above which value the yield shear stress is always attained along the complete zone of contact. Comparison is made with an approximate theory in which the state of stress is assumed constant across any section. A simple test is described by means of which the coefficient of friction for material being deformed under plane strain conditions may be determined.

Vol. 3 54/55

1. Introduction

In all problems of deformation it is necessary to know the frictional conditions which exist between the deforming tool and the deformed metal. This is particularly true of the rolling process, in which frictional conditions profoundly affect the distribution of pressure along the arc of contact, and the plane strain compression test, in which friction increases the mean pressure on the platens above the theoretical value it is desired to measure.

The plane strain compression test, described in detail in the paper by Watts and Ford (1952) is a simple laboratory test which allows the determination of the yield strength of a strip of metal under test conditions very similar to actual rolling conditions. During such tests it had been observed that variation of surface conditions affected the stress-strain curves obtained due to the variation of the coefficient of friction.

It was therefore felt that, if an exact theoretical analysis of the deformation occurring in the test could be made, including the effect of friction, the test would itself allow the experimental determination of the coefficient of friction and its effect on the measured mean pressure. This argument carries the assumption that the equations of plastic flow do strictly represent the behaviour of the actual metal. For this particular mode of deformation (plane strain compression), comparison of the experimental results of Watts and Ford (1952) with the theoretical values derived by Green (1951) shows that this assumption is justified.

The problem of the plane strain compression of a ductile material between rough platens has been solved for those cases in which the slip lines of one family meet the platen surface at a constant angle (HILL, 1952; GREEN 1954). These solutions refer to the case in which the shear stresses acting on the boundary of the platen surface and deforming metal are all of equal magnitude. If a constant coefficient of friction is assumed, however, the shear stress is always the same fraction of the normal stress on this boundary and the slip lines no longer meet the platen surface at a constant angle along its length.

If a zero coefficient of friction is assumed, the slip lines meet the platen surface at an angle of 45°, and for integral ratios of platen breadth b to material thickness t, the solution is a simple criss-cross of slip lines terminating on the corners of the platens. There is a tangential velocity discontinuity of amount $u\sqrt{2}$ along each of the slip lines, where u is the downward velocity of the upper platen, and the material deforms momentarily as a series of rigid blocks, each block being bounded by the slip lines. The normal stress at all points along the platen surface is equal to $2k$, where k is the yield shear stress of the metal. If the material obeys the VON MISES criterion of yielding k must be put equal to $\sigma_0/\sqrt{3}$, where σ_0 is the uniaxial tensile yield stress, and if it obeys the TRESCA criterion k must be put equal to $\sigma_0/2$.

For non-integral ratios of b/t, it has been shown by GREEN (1951) that the slip-line field for the frictionless case becomes distorted, and the mean pressure on the platens exceeds $2k$. In discussing the effect of friction, therefore, it has been decided to solve the problem for integral ratios of b/t, so that direct comparison can be made with the frictionless case. GREEN'S analysis refers to values of b/t between 1 and 2, and the effect of the distortion of the slip-line field is not known for non-integral values of b/t outside this range. It is customary in performing plane strain compression tests to restrict b/t to lie between values of 2 and 4, where the effect of the distortion of the slip line field is known to be small, as shown by the upper bounds of HILL'S solution referred to in GREEN'S paper, and as determined experimentally by WATTS and FORD (1952). The upper limit of 4 has been dictated mainly by consideration of the increasing effect of friction as b/t is increased, but an accurate estimate of the increase of mean pressure due to frictional effects has not hitherto been available.

It was accordingly decided to estimate the effect of friction for an integral b/t ratio of 3, to assess the accuracy of the plane strain test in determining the mean yield stress at that ratio. It was also realized that an accurate value of the coefficient of friction would have to be known for this purpose, so the analysis was repeated for the integral ratio of $b/t = 7$. By taking the ratios of the mean yield pressures at the two b/t values, the coefficient of friction is uniquely defined. In this way, by carrying out two plane strain compression tests on the same strip of material, under identical conditions with the exception of the b/t ratio, an accurate value for the coefficient of friction under the desired conditions can be determined.

2. THE GENERAL SOLUTION

Fig. 1 shows the geometrical representation of the solution for a b/t ratio of 7, with $\mu = 0{\cdot}15$. Since the problem is symmetrical, all the features of the solution are shown by the one quadrant considered. If a straight slip line is assumed at

the edge of the deforming zone $A1$, and a singular point exists at A, the slip lines between $A1$ and $A3$ form a centred fan of straight lines and circular arcs. In the stress plane the pole of the Mohr's circle representing the state of stress along the slip line 123 traces out the cycloid 123 as it rolls along the bottom tangent to the stress plane. (For a detailed discussion of the method reference

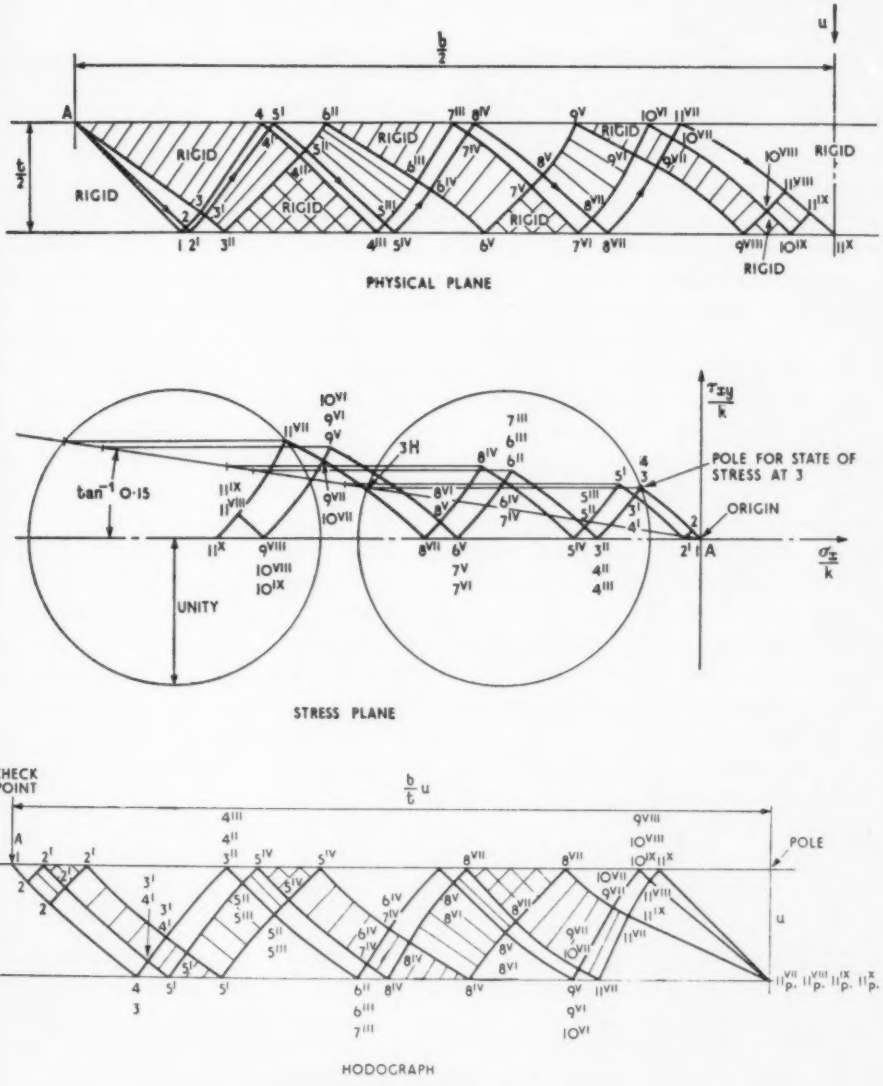

Fig. 1. Solution for $b/t = 7$, $\mu = 0{\cdot}15$.

should be made to PRAGER's paper (1953)). To determine the state of stress on the horizontal plane through the point 3, a horizontal line is drawn through the point 3 in the stress plane; the point at which it cuts the Mohr's circle then defines the state of stress. The condition that the ratio of shear stress/normal

stress acting in this plane should equal the coefficient of friction determines the position of 3 in the stress plane, since 3_H must lie on the line which makes an angle $\tan^{-1}\mu$ with the horizontal axis of the stress plane. Having located the point 3 in the stress plane it is possible to locate 3 in the physical plane, the angle being accurately determined from the cycloid construction. The slip lines adjacent to $A3$ and 34 are straight and the state of stress is identical for all points in the triangular zone $A34$.

The state of stress along the slip line $3\ 3^{I}\ 3^{II}$ is represented by the cycloid $3\ 3^{I}\ 3^{II}$ in the stress plane which is traced out by the Mohr's circle rolling along the top tangent to the stress plane. Since the slip line 34 is straight, neighbouring slip lines $3^{I}\ 4^{I}$, $3^{II}\ 4^{II}$ are also straight, the stress states being constant along these lines as shown in the stress plane.

The solution is built up in this way until the desired region is covered. By analogy with previous solutions there will be a central zone of rigid metal bounded by velocity discontinuities which will be propagated along the slip lines by " reflection " from the platen surfaces as shown by the arrowed slip lines in Fig. 1. The solution for problems of this type is only valid as long as the velocity discontinuity does not terminate on the platen surface or on the slip line $A1$. The discontinuity shown terminates on the singular point A, thus giving an acceptable solution. This condition restricts the ratios of b/t for which a solution can be obtained by a straight starting slip line $A1$, as can be seen by reference to the physical plane of Fig. 2. For instance, a solution could be obtained for the slip line field shown for values of b/t between 4·63 and 6·15 (points 7^{VI} and 9^{VIII}) but not for values of b/t between 6·15 and 6·57 (points 9^{VIII} and 10^{IX}). For such values a curved slip line $A1$ would have to be assumed which would make the analysis more complicated. It was found possible to obtain solutions for $b = 3$ and 7, and $\mu = 0$, 0·05, 0·1, 0·15, 0·225, 0·3 and 0·389 by adopting the simple straight slip line $A1$, the velocity discontinuity terminating at the singular point A in all cases.

The downward velocity u of the upper platen is mapped on the hodograph by the point 11_p^{VII} to 11_p^{X}, representing the downward velocity of the elements in the boundary of the rigid metal zone. The constant tangential velocity discontinuity of amount $u\sqrt{2}$ gives the points $11^{X}\ 11^{IX}\ 11^{VIII}\ 11^{VII}$, referring to the deforming metal, which lie on a circular arc centred at the end of the vector u. The magnitude of the tangential velocity discontinuity along the slip line $11^{VII}\ 10^{VII}$ is determined by the angle at which the slip line meets the platen surface as shown in the hodograph.

The magnitude of the tangential velocity discontinuity is gradually reduced by successive reflection at the platen surface depending on the angle at which the slip line meets the surface until its final value is given by the distance between the points 22 in the hodograph. In this case the hodograph has a different shape from the slip line field since the boundary conditions are not the simple ones which give equivalence between slip line field and transformed velocity field (see GREEN 1954). A check on the accuracy of the construction is given by the fact that the outward velocity of the metal crossing $A1$ should be bu/t, by consideration of constancy of volume. This " check point " is shown in Fig. 1 and exhibits fair agreement. By analogy with previous similar solutions it can be easily checked that the rate of plastic work is everywhere positive throughout the field.

3. Solutions for Other Cases

Fig. 2 shows the complete solution for the case $b/t = 7$, $\mu = 0{\cdot}3$. In this solution the slip line field is built up as before until the point 7^{II} is reached in the physical plane. At this point the normal stress on the platen surface is such that the shear stress induced is equal to the yield shear stress of the metal, and the slip line of one family meets the platen orthogonally. The solution then proceeds by the usual

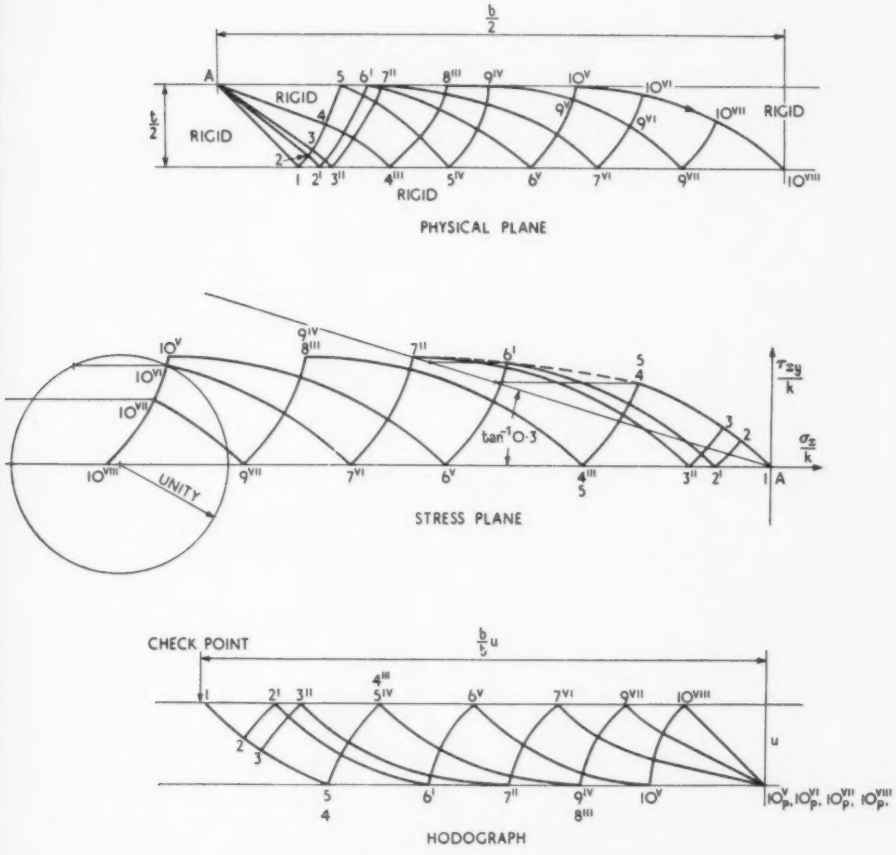

Fig. 2. Solution for $b/t = 7$, $\mu = 0{\cdot}3$.

procedure of making the slip lines of one family meet the platen orthogonally since the normal pressure inside the point 7^{II} is always sufficient to induce the yield shear stress of the material but which cannot, of course, be exceeded.

Fig. 3 shows the solution, due to Hill (1952), for the case $b/t = 7$, $\mu \geqslant \dfrac{1}{1 + \frac{1}{2}\pi} \simeq 0{\cdot}389$. In this case the normal pressure is always sufficient to allow the yield shear stress to be attained at the platen surface, the value of $\mu = \dfrac{1}{1 + \frac{1}{2}\pi}$ having been chosen so that the yield shear stress is just attained along the outermost

portion of the platen $A6$. The hodograph is, for this simple case, the same shape as the slip line field, but rotated through 180°, and has not been shown, for the sake of brevity. In both of these solutions, the velocity discontinuity along the central rigid zone disappears at the platen surface, since the slip line concerned meets the platen tangentially.

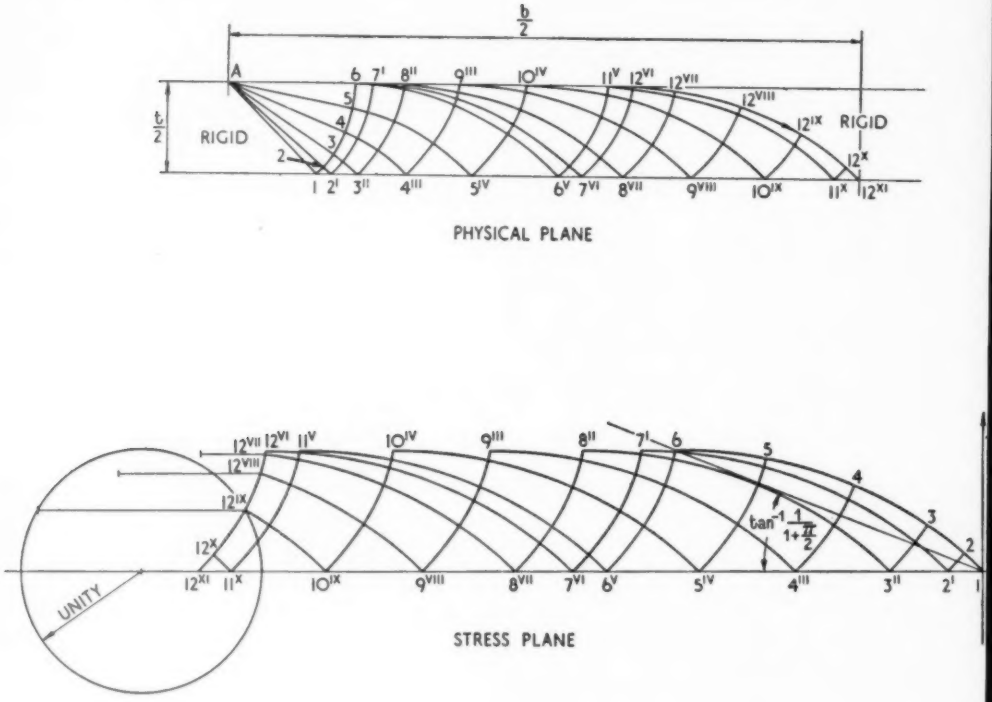

Fig. 3. Solution for $b/t = 7$, $\mu \geqslant \dfrac{1}{1+\frac{\pi}{2}} = \cdot 389$.

Fig. 4 shows the solution, due to HILL (1950), for the case $b/t = 3$, $\mu \geqslant 0{\cdot}389$. This is a special case since the central zone of rigid metal extends across the whole platen surface, and there is no "reflection" of the velocity discontinuity from the platen surface.

All the other solutions are similar in principle to those discussed in connection with Figs. 1 and 2, and are not therefore shown in detail.

4. DETERMINATION OF THE MEAN PRESSURE ON THE PLATENS

The distribution of normal stress along the surface of the platen can be determined directly from the stress plane, with the exception of the central rigid zone. To determine the mean pressure over this central zone it is necessary to integrate

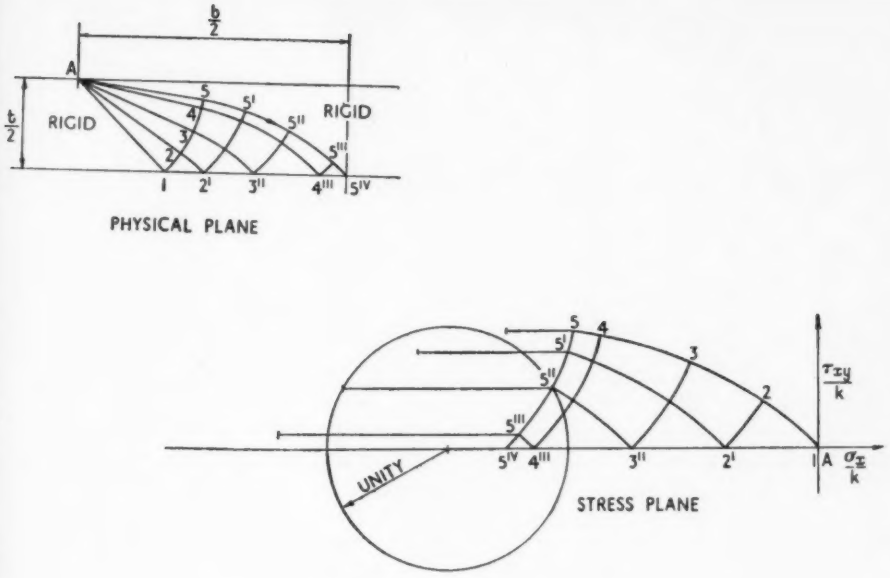

Fig. 4. Solution for $b/t = 3$, $\mu \geqslant \cdot 389$.

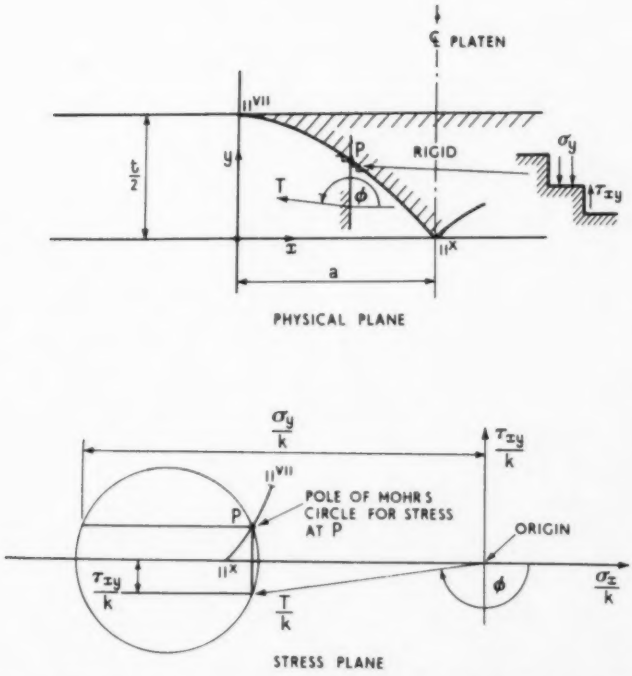

Fig. 5. Stresses on boundary between central rigid zone and plastically deforming metal.

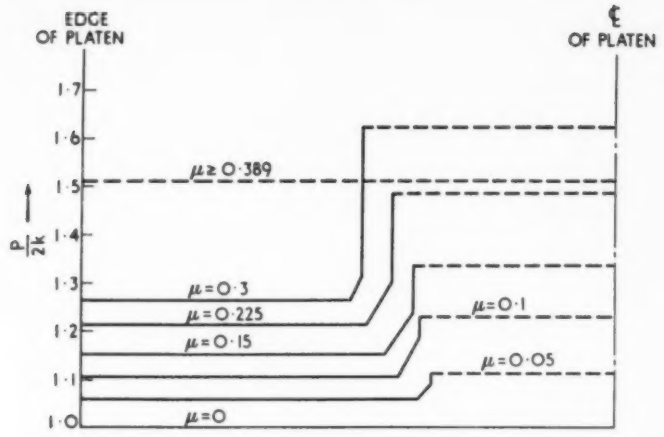

Fig. 6. Pressure distributions for $b/t = 3$. Mean pressures over central rigid zones indicated by broken lines.

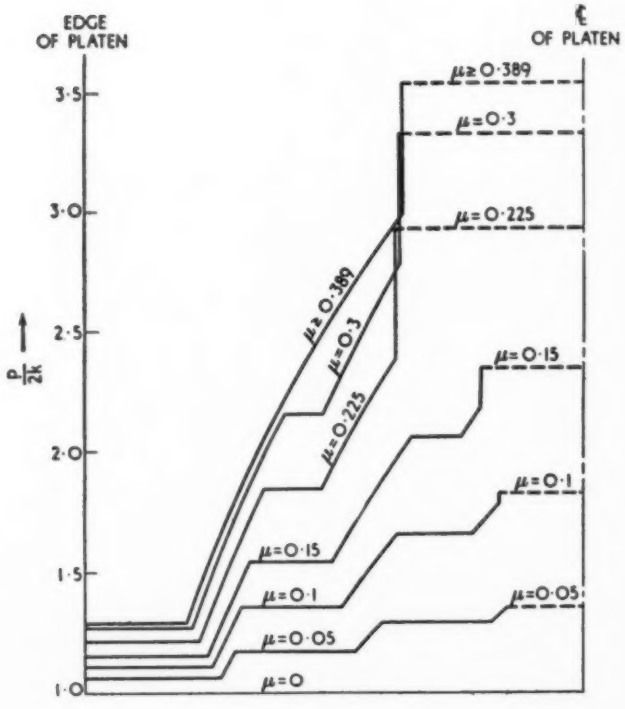

Fig. 7. Pressure distributions for $b/t = 7$. Mean pressures over central rigid zones indicated by broken lines.

the effect of the stresses along the boundary between it and the plastically deformed metal. The direction of the relevant stresses on this boundary is obtained from the stress plane in the manner shown in Fig. 5.

The shear stress on the vertical plane through the point P is determined from the fact that the traction T acting on the shaded element shown through P has the direction indicated. The angle ϕ in the physical plane is of equal magnitude but of opposite sense to the angle ϕ in the stress plane where ϕ is the angle through which the normal to the plane considered must be rotated to coincide with T in the physical plane, and is the angle through which the positive σ_x/k axis must be rotated to coincide with T in the stress plane. Thus on an elemental section of the slip line $11^{VII}\,11^{X}$ the stresses act as shown in the inset diagram, from which it can be seen that the mean pressure $\bar{p}_R$ transmitted normal to the platen must be given by

$$\frac{\bar{p}_R}{k} = \frac{\int_0^a \frac{\sigma_y}{k}\,dx - \int_0^{\frac{t}{2}} \frac{\tau_{xy}}{k}\,dy}{a}$$

where the x and y axes are as shown in the diagram and σ_y is regarded as positive if compressive.

TABLE I

μ	*Slip Line Field Theory*			*Approximate Theory*		
	$\frac{\bar{p}}{2k}$		$\bar{p}_7/\bar{p}_3$	$\frac{\bar{p}}{2k}$		$\bar{p}_7/\bar{p}_3$
	$\frac{b}{t}=3$	$\frac{b}{t}=7$		$\frac{b}{t}=3$	$\frac{b}{t}=7$	
0	1·0	1·0	1·0	1·0	1·0	1·0
0·05	1·076	1·205	1·120	1·078	1·197	1·110
0·1	1·151	1·450	1·260	1·166	1·448	1·242
0·15	1·222	1·713	1·402	1·262	1·770	1·402
0·161	—	—	—	1·286	1·870	1·456
0·2	—	—	—	1·370	2·142	1·564
0·225	1·328	2·110	1·589	1·429	2·293	1·606
0·242	—	—	—	1·468	2·380	1·622
0·25	—	—	—	1·489	2·420	1·627
0·3	1·434	2·370	1·653	1·599	2·583	1·619
0·35	—	—	—	1·678	2·670	1·592
0·389	1·510	2·520	1·669	1·716	2·710	1·580
0·4	1·510	2·520	1·669	1·726	2·715	1·574
0·5	1·510	2·520	1·669	1·75	2·750	1·571

The distributions of pressure p over the platens for $b/t = 3$ are shown in Fig. 6, and for $b/t = 7$ in Fig. 7. The calculated mean pressures $\bar{p}/2k$ for each case are tabulated in Table 1 and plotted against coefficient of friction in Fig. 8. The ratio $\bar{p}_7/\bar{p}_3$ of the yield point pressures for the two b/t values at any given coefficient of friction are also tabulated, $\bar{p}_7$ and $\bar{p}_3$ being the mean pressures for b/t ratios of 7 and 3 respectively, a curve of μ versus $\bar{p}_7/\bar{p}_3$ being shown in Fig. 9.

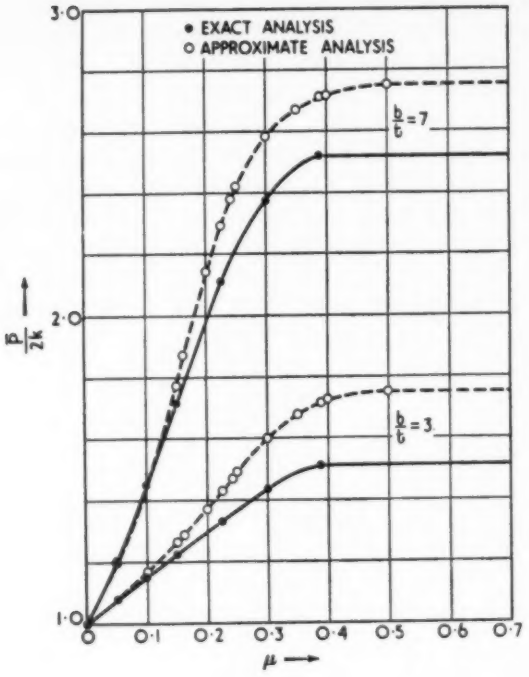
• EXACT ANALYSIS
○ APPROXIMATE ANALYSIS
b/c = 7
b/c = 3
P/2k
μ
3·0
2·0
1·0
0·1
0·2
0·3
0·4
0·5
0·6
0·7

Fig. 8.

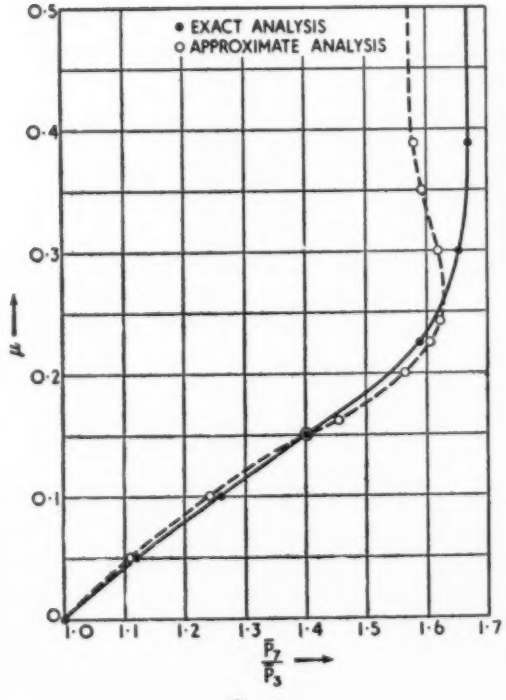
• EXACT ANALYSIS
○ APPROXIMATE ANALYSIS
μ
P7/P3
0·5
0·4
0·3
0·2
0·1
0
1·0
1·1
1·2
1·3
1·4
1·5
1·6
1·7

Fig. 9.

Also tabulated and plotted are values of mean pressure and ratio $\bar{p}_7/\bar{p}_8$ calculated from the approximate analysis outlined in the next section.

5. Approximate Analysis

Assuming that the state of stress across any section, distant x from the centre-line of the platens, is constant, it is easily shown that the equilibrium equation is

$$\frac{dq}{dx} = -\frac{2\mu p}{t} \tag{1}$$

where p and q are respectively the vertical and horizontal stresses at the section (assumed positive if compressive).

The criterion of yielding reduces to

$$p - q = 2k. \qquad (k = \sigma_0/\sqrt{3} \text{ von Mises}, \ \sigma_0/2 \text{ Tresca}) \tag{2}$$

Hence it can be shown that the distribution of pressure across the section is given by

$$p = 2k \exp \frac{\mu b}{t}\left(1 - \frac{2x}{b}\right) \tag{3}$$

and the mean pressure by

$$\frac{\bar{p}}{2k} = \frac{\exp\left(\dfrac{\mu b}{t}\right) - 1}{\dfrac{\mu b}{t}} \tag{4}$$

The first reference to this type of analysis for plane strain compression appears to be due to Stone and Greenberger (1943).

The distribution of shear stress τ acting along the platen and material interface is given by

$$\tau = \mu p. \tag{5}$$

Now the material cannot withstand a shear stress greater than the yield shear stress k. To determine the value of x ($= x'$, say) for which $\tau = k$, from equation (3)

$$k = 2k\mu \exp \frac{\mu b}{t}\left(1 - \frac{2x'}{b}\right). \tag{6}$$

Hence

$$x' = \frac{b}{2}\left(1 - \frac{\log (1/2\mu)}{\mu b/t}\right). \tag{7}$$

This equation only has meaning when x' is positive and equal or less than $\frac{1}{2}b$. It can only be positive so long as

$$\log (1/2\mu) < \frac{\mu b}{t}. \tag{8}$$

This condition is illustrated graphically in Fig. 10. For values of $\mu \geqslant 0{\cdot}5$, $x' = \dfrac{b}{2}$ and $\tau = k$ along the whole interface.

For the central zone in which $\tau = k$, the equilibrium equation becomes

$$\frac{dp}{dx} = -\frac{2k}{t}. \tag{9}$$

Hence

$$p = \frac{2k}{t}\left(\frac{b}{2} - x\right) + \frac{k}{\mu}\left(1 - \log\frac{1}{2\mu}\right),$$

where

$$0 < x < \frac{b}{2}\left(1 - \frac{\log(1/2\mu)}{\mu b/t}\right), \tag{10}$$

and

$$\frac{\bar{p}}{2k} = \frac{b}{4t}\left(1 - \frac{\log(1/2\mu)}{\mu b/t}\right)\left(1 + \frac{2 - \log(1/2\mu)}{\mu b/t}\right) + \frac{\frac{1}{2\mu} - 1}{\mu b/t} \tag{11}$$

when

$$\log\frac{1}{2\mu} < \frac{\mu b}{t}.$$

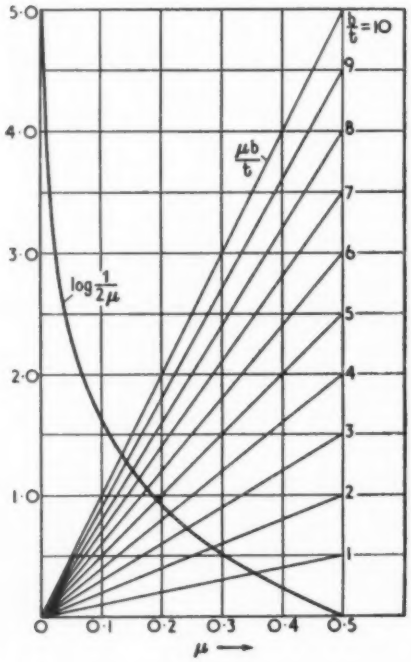

Fig. 10.

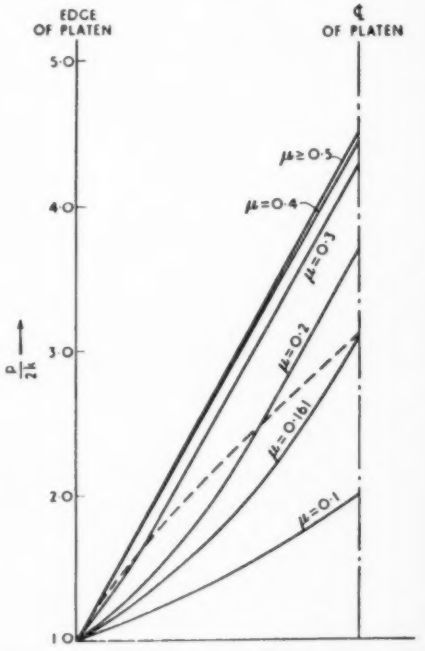

Fig. 11. Typical pressure distributions for $b/t = 7$. (approximate theory). Above the broken line the limiting yield shear stress is attained along the interface.

Summarizing, and rewriting these equations in their simplest form

$$\frac{\bar{p}}{2k} = \frac{\exp\left(\frac{\mu b}{t}\right) - 1}{\frac{\mu b}{t}} \qquad \text{when} \qquad \frac{\mu b}{t} < \log\frac{1}{2\mu}. \tag{4}$$

$$\frac{\bar{p}}{2k} = \left[\frac{(1+\alpha)^2+1}{4\mu} - 1\right] \Big/ \frac{\mu b}{t} \qquad \text{when} \qquad \frac{\mu b}{t} > \log \frac{1}{2\mu}. \tag{12}$$

where $$\alpha = \frac{\mu b}{t} - \log \frac{1}{2\mu}.$$

Typical pressure distributions calculated from these equations for the case $b/t = 7$ are shown in Fig. 11.

6. Discussion

The exact analysis shows that for a coefficient of friction of, say, $\mu = 0{\cdot}015$ (a reasonable value for graphite grease as generally used in these tests), using a b/t ratio of 3 will give a value of $\bar{p}/2k = 1{\cdot}024$. That is, the plane strain compression yield strength of the metal will be overestimated by about 2·4%. This means that uncorrected experimental values will be sufficiently accurate for most practical purposes.

To determine a value for the coefficient of friction between surfaces under these conditions it is suggested that a strip of material be rolled until it is work hardened and will have a fairly flat stress strain curve. Using the experimental technique described by Watts and Ford (1952), the yield point pressure could be determined for the same strip under two identical conditions, except that $b/t = 7$ in one case and 3 in the other, by extrapolating back to zero strain, after a finite compression of, say, 10%. The ratio of these two pressures, viz. $\bar{p}_7/\bar{p}_3$, would then give a fairly accurate estimate of the coefficient of friction by reference to Fig. 9.

The approximate analysis is significantly different from the exact analysis for values of $\mu > 0{\cdot}15$, and leads to a function $\bar{p}_7/\bar{p}_3$ which is not single valued with respect to μ. It should therefore be used with caution for values of $\mu > 0{\cdot}15$.

Vol. 3 54/55

Acknowledgment

Acknowledgment is made to Aluminium Laboratories Limited for permission to published this paper.

References

Green, A. P.	1951	*Phil. Mag.*, **42**, 900.
	1954	*J. Mech. Phys. Solids*, **2**, 73.
Hill, R.	1950	*Mathematical Theory of Plasticity*, p. 280. (Clarendon Press).
	1952	Strength and Testing of Materials, Part 1, Report No. 6. (H.M.S.O.).
Prager, W.	1953	*Trans. Royal Inst. Tech. Stockholm*, No. 65.
Stone, M. D. and Greenberger, J. I.	1943	*Iron and Steel Engineer*, February, 61.
Watts, A. B. and Ford, H.	1952	*Proc. Inst. Mech. Eng.*, (B), Vol. 1B, No. 10.

Journal of the Mechanics and Physics of Solids, 1955, Vol., 3 pp. 246 to 258. Pergamon Press Ltd., London.

PLASTIC FLOW IN A CONVERGING CONICAL CHANNEL

By R. T. Shield
A.R.D.E. Fort Halstead

(*Received 4th March*, 1955)

Summary

The flow of a plastic-rigid material forced through a rigid conical-shaped channel or die is considered. The method of solution is described for a general yield criterion. The particular yield conditions of von Mises and Tresca are considered in detail. Application of the theory is made to wire drawing.

1. Introduction

The flow of a plastic-rigid, non-hardening material forced through a wedge-shaped channel under conditions of plane strain has been considered by Nadai (1924). The solution for flow through a rigid conical-shaped channel or die is obtained here. A constant frictional force between the die and the material is assumed. The method of solution is outlined first using a general yield criterion for an isotropic, plastic-rigid, non-hardening material, the behaviour of which is independent of hydrostatic pressure. The particular cases of the yield conditions of von Mises (1913) and Tresca (1868) are then considered in detail. Finally the theory is applied to give an approximate description of wire drawing.

2. Converging Flow through a Conical Channel

We consider the flow of a plastic-rigid material forced through a conical-shaped channel or die. The flow is axially symmetric and the z-axis is taken along the axis of symmetry, Fig. 1. Spherical polar coordinates (R, ϕ, θ) will be used to describe the flow. In this coordinate system, the z-axis is given by $\phi = 0$ and the rigid channel is bounded by part of the surface $\phi = \alpha$, where α is a constant. It is assumed that the frictional stress exerted by the channel on the material has the constant value mk, where $0 \leqslant m \leqslant 1$ and k is the maximum shearing stress which can be supported by the material. The further assumptions are made that the channel is long enough to neglect the effect of the end conditions, and that the flow is steady and directed towards the virtual apex O of the channel.

The non-zero components of the stress tensor σ_{ij} are the components σ_R, σ_ϕ, σ_θ, and $\tau_{R\phi}$. They satisfy the equations of equilibrium

$$\left.\begin{aligned} &\frac{\partial \sigma_R}{\partial R} + \frac{1}{R}\frac{\partial \tau_{R\phi}}{\partial \phi} + \frac{1}{R}\{2\sigma_R - \sigma_\phi - \sigma_\theta + \tau_{R\phi}\cot\phi\} = 0, \\ &\frac{\partial \tau_{R\phi}}{\partial R} + \frac{1}{R}\frac{\partial \sigma_\phi}{\partial \phi} + \frac{1}{R}\{(\sigma_\phi - \sigma_\theta)\cot\phi + 3\tau_{R\phi}\} = 0, \end{aligned}\right\} \quad (1)$$

since body forces and inertial terms are neglected. The (outward) radial velocity will be denoted by U. The non-zero components of the rate of plastic strain tensor are then given by

$$\epsilon_R = \frac{\partial U}{\partial R}, \qquad \epsilon_\phi = \epsilon_\theta = \frac{U}{R}, \qquad \gamma_{R\phi} = \frac{1}{R}\frac{\partial U}{\partial \phi}. \tag{2}$$

The material is assumed to be isotropic and perfectly plastic (no workhardening), and the yield criterion is assumed to be independent of hydrostatic pressure, as is usual in the theory of metals. The yield function is then a function of the two invariants, $J_2 = \frac{1}{2} s_{ij} s_{ij}$ and $J_3 = \frac{1}{3} s_{ij} s_{jk} s_{ki}$, of the deviatoric stress tensor s_{ij}, and we shall write it in the form

$$f(J_2, J_3) = k^2, \tag{3}$$

where k is the maximum shearing stress permissible in the material. The material is rigid when $f < k^2$ and states of stress for which $f > k^2$ are not permissible. When $f = k^2$, plastic deformation is possible under the flow rule (see, for example, MISES 1928 and DRUCKER 1950):

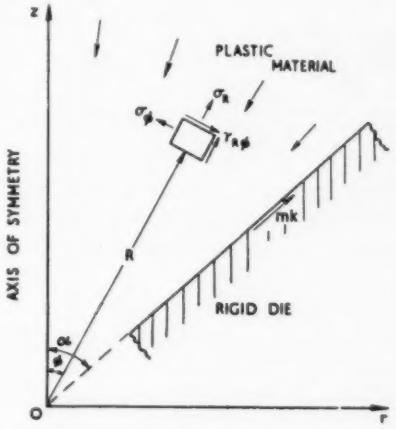

Fig. 1. Converging flow through a conical channel.

$$\epsilon_{ij} = \lambda \frac{\partial f}{\partial \sigma_{ij}} = \lambda \left(\frac{\partial f}{\partial J_2}\frac{\partial J_2}{\partial \sigma_{ij}} + \frac{\partial f}{\partial J_3}\frac{\partial J_3}{\partial \sigma_{ij}} \right), \tag{4}$$

where λ is an arbitrary positive scalar. The yield function (3) can be regarded as defining a surface in principal stress space. The flow rule (4) states that the vector with components proportional to the principal components of the plastic strain rate is in the direction of the (outwards-drawn) normal to the yield surface at the stress point. If the yield surface has a singular point where there is not a unique normal, then the strain rate vector must lie in the fan bounded by the normals to the yield surface at adjacent points.

For the axially symmetric stress field considered here, the invariants J_2, J_3 are given by

$$\left.\begin{aligned} 6J_2 &= (\sigma_R - \sigma_\phi)^2 + (\sigma_\phi - \sigma_\theta)^2 + (\sigma_\theta - \sigma_R)^2 + 6\tau^2_{R\phi}, \\ 27J_3 &= (2\sigma_\theta - \sigma_R - \sigma_\phi)\{(2\sigma_R - \sigma_\phi - \sigma_\theta)(2\sigma_\phi - \sigma_\theta - \sigma_R) - 9\tau^2_{R\phi}\}. \end{aligned}\right\} \tag{5}$$

The assumption of radial flow implies that the rate of strain components ϵ_ϕ, ϵ_θ are equal, as stated in (2), and with (4) this condition is

$$\frac{\partial f}{\partial J_2}\left(\frac{\partial J_2}{\partial \sigma_\phi} - \frac{\partial J_2}{\partial \sigma_\theta}\right) + \frac{\partial f}{\partial J_3}\left(\frac{\partial J_3}{\partial \sigma_\phi} - \frac{\partial J_3}{\partial \sigma_\theta}\right) = 0.$$

With the values (5) for the invariants J_2, J_3, this equation becomes, after some reduction,

$$\frac{\partial f}{\partial J_2}(\sigma_\phi - \sigma_\theta) + \tfrac{1}{3}\frac{\partial f}{\partial J_3}\{(2\sigma_R - \sigma_\phi - \sigma_\theta)(\sigma_\theta - \sigma_\phi) + 3\tau^2_{R\phi}\} = 0. \tag{6}$$

It can be seen from equation (6) that the condition $\epsilon_\phi = \epsilon_\theta$ enforces $\sigma_\phi = \sigma_\theta$ if f is independent of J_3.

We now introduce the quantities G and H defined by

$$\sigma_R - \sigma_\phi = G, \qquad \sigma_R - \sigma_\theta = H. \tag{7}$$

The invariants J_2, J_3 and the coefficients of $\partial f/\partial J_2$, $\partial f/\partial J_3$ in (6) can be expressed in terms of G, H and $\tau_{R\phi}$ only, so that (3) and (6) can be written in the form

$$\left.\begin{aligned} K(G, H, \tau_{R\phi}) &= 0, \\ L(G, H, \tau_{R\phi}) &= 0. \end{aligned}\right\} \tag{8}$$

Equations (1) and (8) form a set of four equations for the determination of the four components of stress. In order to solve these equations, it will be assumed that $\tau_{R\phi}$ is a function of ϕ only, and it is convenient to write

$$\tau_{R\phi} = k\tau, \tag{9}$$

where the parameter τ is a function of ϕ only. On the axis $\phi = 0$, symmetry requires that $\tau_{R\phi} = 0$, while on $\phi = \alpha$, $\tau_{R\phi} = mk$. The boundary conditions on τ are therefore

$$\tau(0) = 0, \qquad \tau(\alpha) = m. \tag{10}$$

The substitution of the value (9) for $\tau_{R\phi}$ into (8) gives two finite equations for G and H. Assuming that the yield function (3) is such that these equations have a unique solution, G and H will be functions of τ only, so that

$$\sigma_R - \sigma_\phi = G(\tau), \qquad \sigma_R - \sigma_\theta = H(\tau). \tag{11}$$

The second of the equations of equilibrium (1) is now

$$\frac{\partial \sigma_\phi}{\partial \phi} + (H - G)\cot\phi + 3k\tau = 0,$$

and therefore

$$\sigma_\phi = \sigma_R - G(\tau) = kg(R) - \int\{(H - G)\cot\phi + 3k\tau\}\, d\phi, \tag{12}$$

where g is a function of R to be determined.

Substitution in the first equation of equilibrium now leads to

$$kRg'(R) + k\tau'(\phi) + G + H + k\tau\cot\phi = 0,$$

and it follows that

$$g(R) = -c\ln R + A, \tag{13}$$

and

$$\tau'(\phi) + \tau\cot\phi + (G + H)/k = c. \tag{14}$$

Here c and A are constants of integration to be determined.

Equation (14) is a first order differential equation for $\tau(\phi)$ and the constant c must be chosen so that the function $\tau(\phi)$ determined by (14) satisfies the boundary conditions (10). When $\tau(\phi)$ and c are known for given values of α and m, the

stresses are given by (9), (11), (12) and (13), apart from an arbitrary hydrostatic pressure represented by the constant A in (13). It remains to determine the radial velocity U.

The function U satisfies the incompressibility condition

$$\frac{\partial U}{\partial R} + 2\frac{U}{R} = 0, \tag{15}$$

since the yield criterion (3) is independent of hydrostatic pressure. Equation (15) requires U to be of the form $U = h(\phi)/R^2$. The isotropy condition

$$\frac{\epsilon_R - \epsilon_\phi}{\gamma_{R\phi}} = \frac{\sigma_R - \sigma_\phi}{2\tau_{R\phi}}, \tag{16}$$

which can be derived from (4), shows that the function $h(\phi)$ is given by

$$-\frac{3h(\phi)/R^3}{h'(\phi)/R^3} = \frac{G(\tau)}{2k\tau}.$$

It follows that

$$U = \frac{h(\phi)}{R^2} = \frac{B}{R^2}\exp\left\{-6k\int \tau/G(\tau)\,d\phi\right\}. \tag{17}$$

The arbitrary constant B in this equation is negative since the flow is directed towards the apex.

In principle, the solution to the problem is now complete for a general yield criterion (3). We proceed to obtain the solutions for the particular yield conditions of von Mises and Tresca.

3. The von Mises Yield Criterion

The yield criterion of von Mises states that plastic flow can occur under states of stress such that $J_2 = k^2$, or

$$(\sigma_R - \sigma_\phi)^2 + (\sigma_\phi - \sigma_\theta)^2 + (\sigma_\theta - \sigma_R)^2 + 6\tau_{R\phi}^2 = 6k^2. \tag{18}$$

Thus in this case the yield function f is independent of J_3, and equation (6) shows that $\sigma_\phi = \sigma_\theta$. The yield condition (18) therefore reduces to

$$\tfrac{1}{3}(\sigma_R - \sigma_\phi)^2 + \tau_{R\phi}^2 = k^2,$$

and this is satisfied by the expressions

$$\tau_{R\phi} = k\tau, \qquad \sigma_R - \sigma_\phi = \sqrt{3}k(1 - \tau^2)^{1/2}. \tag{19}$$

In the notation of the previous section we have

$$G(\tau) = H(\tau) = \sqrt{3}k(1 - \tau^2)^{1/2} \tag{20}$$

as the solution of (8). In the same way that (12) was derived, or by substitution of (20) in (12), we obtain

$$\sigma_\theta = \sigma_\phi = \sigma_R - \sqrt{3}k(1 - \tau^2)^{1/2} = kg(R) - 3k\int \tau d\phi. \tag{21}$$

The function g is given by equation (13), while $\tau(\phi)$ satisfies the equation

$$\tau'(\phi) + \tau\cot\phi + 2\sqrt{3}(1 - \tau^2)^{1/2} = c. \tag{22}$$

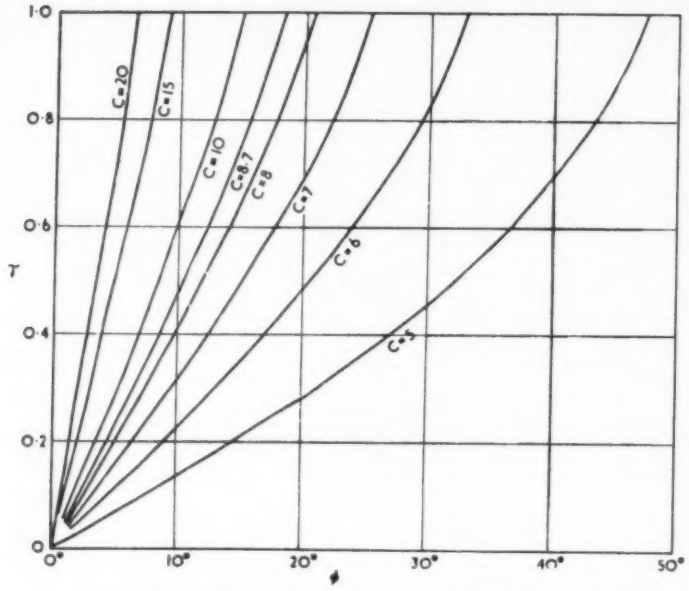

Fig. 2. The function $\tau(\phi)$ for various values of c (MISES material).

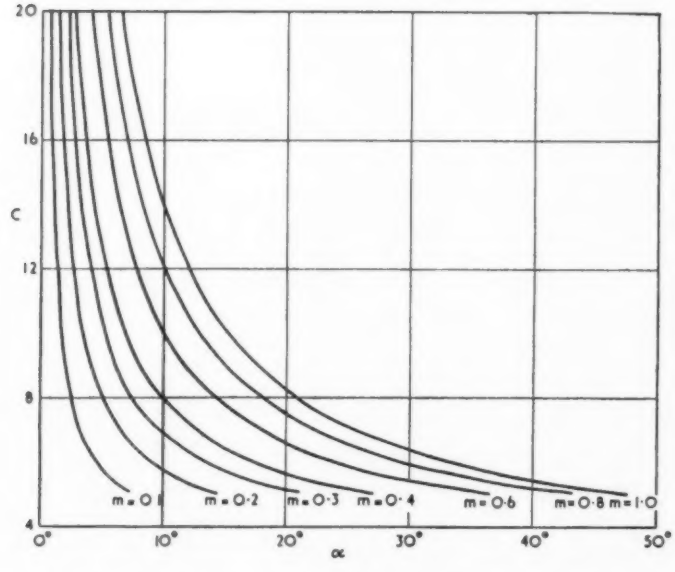

Fig. 3. Variation of c with α for values of m (MISES material).

Since τ has the same sign as ϕ, the constant c must be greater than $2\sqrt{3}$. As mentioned previously, the value of c must be such that the function τ determined by (22) satisfies the boundary conditions (10), so that c is a function of α and m. In order to integrate (22) numerically, it was taken as an equation determining ϕ as a function of τ, the boundary conditions being now $\phi(0) = 0$, $\phi(m) = \alpha$. A certain value of c was chosen, and the equation was integrated numerically to give $\phi(\tau)$ in the interval $0 \leqslant \tau \leqslant 1$, using the initial value $\phi(0) = 0$. Fig. 2 shows the function $\phi(\tau)$ for various values of c. For a particular value of c, the value of α corresponding to a given value of m is given by the value of $\phi(\tau)$ for $\tau = m$, so that the dependence of c on the quantities α, m can be obtained from the results shown in Fig. 2. The dependence of c on α, m is shown graphically in Figs. 3 and 4. It can be seen from Fig. 4 that the dependence of c (for fixed α) on m is almost linear.

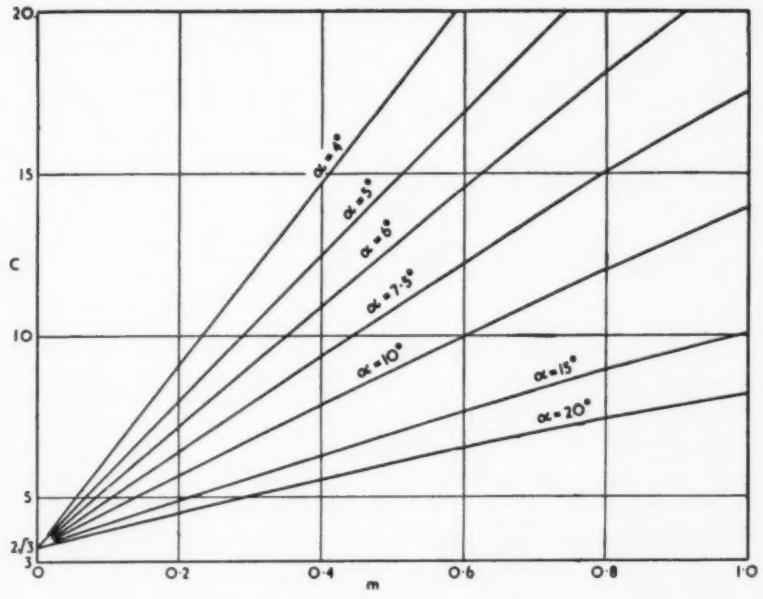

Fig. 4. Variation of c with m for values of α (MISES material).

For a smooth channel, $m = 0$, the plastic stress and velocity fields are spherically symmetric. The constant c now has the value $2\sqrt{3}$ for all α, and the parameter $\tau = \tau_{R\phi}/k$ is zero for all ϕ.

When $\tau(\phi)$ and c are known for given values of α, m, the stress components are given by equations (19) and (21), apart from an arbitrary hydrostatic pressure. As an example, the variation of the stresses with ϕ for a fixed value of R for the case $c = 7$ is shown in Fig. 5. The value $c = 7$ corresponds to a set of values of α and m, for example $\alpha = 25°24'$, $m = 1$.

The velocity component U is given, from (17) and (20), by

$$U = \frac{B}{R^2} \exp\left\{-2\sqrt{3}\int \tau (1-\tau^2)^{-1/2}\, d\phi\right\}, \tag{23}$$

where B is a negative constant.

4. The Tresca Yield Condition

The TRESCA yield condition states that during plastic flow the maximum shearing stress has a constant value k. In terms of the invariants J_2, J_3 this condition is complicated (see PRAGER and HODGE 1951), with a resulting complexity in equations (8). We shall simplify the analysis by assuming that the circumferential stress σ_θ is equal to the lesser of the other two principal stresses, in the spirit of the general hypothesis proposed by HAAR and VON KÁRMÁN (1909). The appropriateness of this assumption is shown later by the fact that the solution to the problem is obtained.

With this assumption, the yield condition reduces to

$$\left.\begin{aligned} &\tfrac{1}{4}(\sigma_R - \sigma_\phi)^2 + \tau^2_{R\phi} = k^2, \\ &\sigma_\theta = \tfrac{1}{2}(\sigma_R + \sigma_\phi) - k, \end{aligned}\right\} \tag{24}$$

and these equations replace (8). The analysis now proceeds as above for the MISES material after the introduction of the parameter $\tau(\phi)$ by the equations

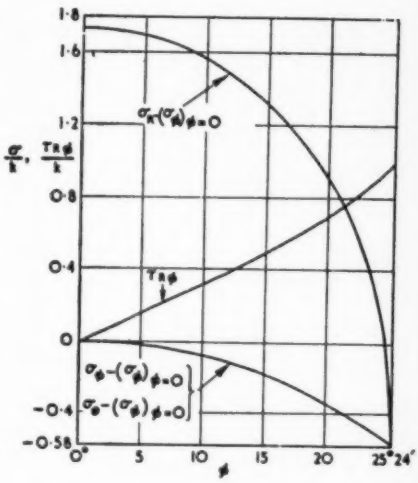

Fig. 5. Variation of stresses with ϕ for constant R for $c = 7$ (MISES material; $\alpha = 25°\,24'$, $m = 1$).

$$\tau_{R\phi} = k\tau, \qquad \sigma_R - \sigma_\phi = 2k(1-\tau^2)^{1/2}. \tag{25}$$

The function $\tau(\phi)$ is determined by

$$\tau'(\phi) + \tau \cot\phi + 1 + 3(1-\tau^2)^{1/2} = c, \tag{26}$$

where c is a constant greater than 4. The stresses are given by (24), (25) and the equation

$$\sigma_\phi = kg(R) - k\int \{3\tau + \cot\phi - \cot\phi\,(1-\tau^2)^{1/2}\}\, d\phi, \tag{27}$$

where $g(R)$ is given by (13).

The radial velocity U is determined, as before, by the incompressibility condition (15) and the isotropy condition (16), and is found to be given by

$$U = \frac{h(\phi)}{R^2} = \frac{D}{R^2} \exp\left\{-3\int \tau (1-\tau^2)^{-1/2}\, d\phi\right\}, \tag{28}$$

where D is a negative constant. However, the velocity field must also satisfy the restrictions

$$\epsilon_\theta \leqslant 0, \qquad (\epsilon_R - \epsilon_\phi)^2 + \gamma^2_{R\phi} \geqslant \epsilon^2_\theta. \tag{29}$$

These restrictions apply because the stresses satisfying the yield condition (24) lie on an edge of the TRESCA yield surface in principal stress space. The vector representing a plastic strain rate associated with the stresses satisfying (24) must lie between the normals to the two faces of the TRESCA yield surface which meet at the corner, and this condition enforces the restrictions (29). The first of these restrictions is satisfied since U is negative and the second restriction reduces to

$$9h^2 + \{h'(\phi)\}^2 \geqslant h^2,$$

which is obviously true.

Equation (26) was integrated numerically for certain values of c in order to obtain the dependence of c on the quantities α and m. The results are shown graphically in Fig. 6. For a smooth channel, $m = 0$, c has the value 4 for all values of α.

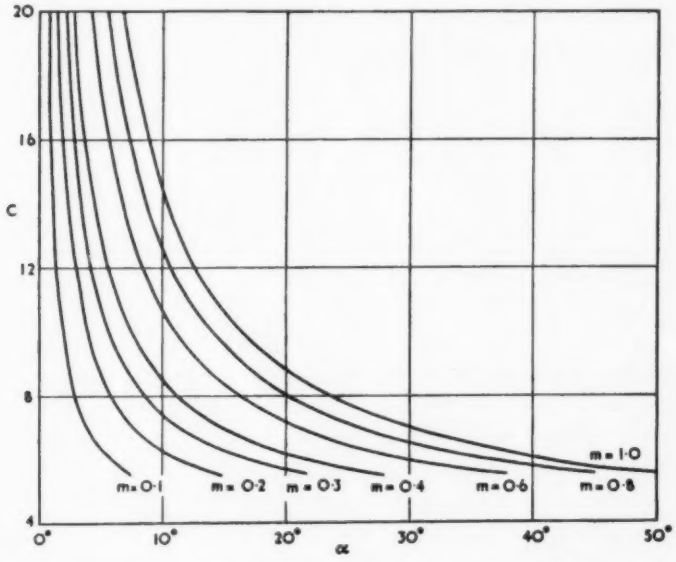

Fig. 6. Variation of c with α for values of m (TRESCA material).

The variation of the stresses with ϕ for a fixed value of R for the case $c = 8$ is shown in Fig. 7. The value $c = 8$ corresponds to a set of values of α and m, for example $\alpha = 23°27'$, $m = 1$. Comparison with Fig. 5 shows that the main difference between the behaviour of a MISES material and the behaviour of a TRESCA material in the present problem lies in the variation of the stress σ_θ with ϕ.

5. Application to Wire Drawing.

As an illustration, the solution to the problem of this paper will be used to give an approximate theory of wire drawing. The assumption is made that the

plastic stress and velocity fields of the metal flowing inside the conical die, region *ABCD* of Fig. 8, can be represented with sufficient accuracy by the converging flow field of Fig. 1. Accordingly there is neglect of the work expended in non-homogeneous distortion at entry and exit. However, it is to be expected that this approximation will be a good one for large reductions of the diameter of the wire since the end effects will then be small. It is implicit in the assumption that the frictional stress over the die surface has the constant value mk.

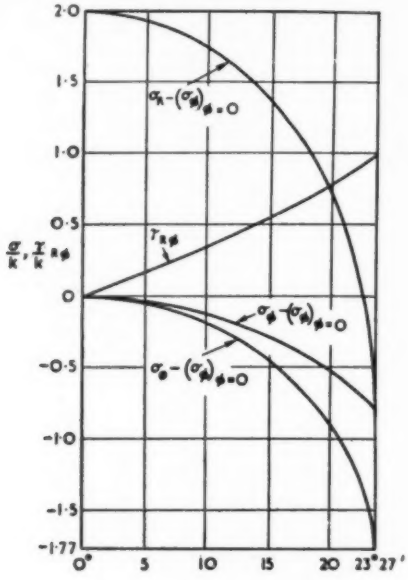

Fig. 7. Variation of stresses with ϕ for constant R for $c = 8$ (TRESCA material; $\alpha = 23° 27'$, $m = 1$).

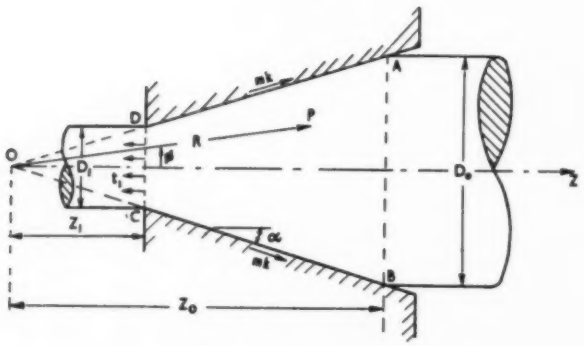

Fig. 8. Wire drawing.

The axial stress component σ_z at a point P inside the die is given in terms of the components σ_R, σ_ϕ, $\tau_{R\phi}$ by

$$\sigma_z = \tfrac{1}{2}(\sigma_R + \sigma_\phi) + \tfrac{1}{2}(\sigma_R - \sigma_\phi)\cos 2\phi - \tau_{R\phi}\sin 2\phi.$$

With (19) and (21) for a material which obeys the yield criterion of VON MISES, this gives

$$\sigma_z = -kc\ln R + kL(\phi), \tag{30}$$

where

$$L(\phi) = A + \tfrac{1}{2}\sqrt{3}(1-\tau^2)^{1/2}(1+\cos 2\phi) - 3\int \tau d\phi - \tau \sin 2\phi. \tag{31}$$

When the drawing is without backpull, the resultant axial force over the entry section AB is zero. Denoting by z_0 the distance of this section from the virtual apex O of the die, this condition is

$$\int_0^\alpha (\sigma_z)_{z=z_0}\, 2\pi z_0^2 \tan\phi \sec^2\phi\, d\phi = 0. \tag{32}$$

The mean drawing stress t_1 over the exit section CD is given by

$$\pi z_1^2 \tan^2\alpha\, t_1 = \int_0^\alpha (\sigma_z)_{z=z_1}\, 2\pi z_1^2 \tan\phi \sec^2\phi\, d\phi, \tag{33}$$

where z_1 is the distance of the exit section from 0. Equation (30) shows that

$$(\sigma_z)_{z=z_1} = (\sigma_z)_{z=z_0} + kc\ln\frac{z_0}{z_1}.$$

Vol. 3 54/55

Substituting this value of $(\sigma_z)_{z=z_1}$ in (33), using (32) and performing the integration, we obtain finally

$$t_1 = kc\ln\frac{z_0}{z_1}. \tag{34}$$

In terms of the diameters D_0, D_1 of the wire before and after drawing, the mean drawing stress is therefore

$$t_1 = \tfrac{1}{2}kc\ln\frac{D_0^2}{D_1^2}. \tag{35}$$

The constant c depends on the semi-angle α of the die and on the constant m occurring in the frictional stress value mk. For given values of α and m, the value of c can be derived from Figs. 3 and 4. (For a TRESCA material, formula (35) is unchanged but c is now given by Fig. 6). As mentioned previously, the variation of c with m is almost linear so that the mean drawing stress t_1 is a linear function of m approximately. Fig. 9 shows the variation of t_1 for values of c with the percentage reduction in area Q, given by

$$Q = 100\left(1 - \frac{D_1^2}{D_0^2}\right).$$

The curves in Fig. 9 show the variation of t_1 with Q for certain values of α and m; for example, the curve for $c = 8$ is also the curve for $\alpha = 5°$, $m = 0{\cdot}20$, or for $\alpha = 10°$, $m = 0{\cdot}41$, and so on. The curve for $c = 2\sqrt{3}$ applies to smooth dies, $m = 0$, for any angle of the die. The mean drawing stress must be less than the tensile yield stress, $\sqrt{3}k$, of the material, so that there is a maximum value of the reduction in area Q for each value of c. For smooth drawing the maximum reduction possible is 63 per cent.

The pressure p on the die is equal to $(-\sigma_\phi)_{\phi=\alpha}$. The stress component σ_ϕ

is given by (13) and (21) in which the constant A has the value determined by the condition (32). The die pressure depends logarithmically on R; in fact

$$p = p_0 + kc \ln \frac{R}{R_0},$$

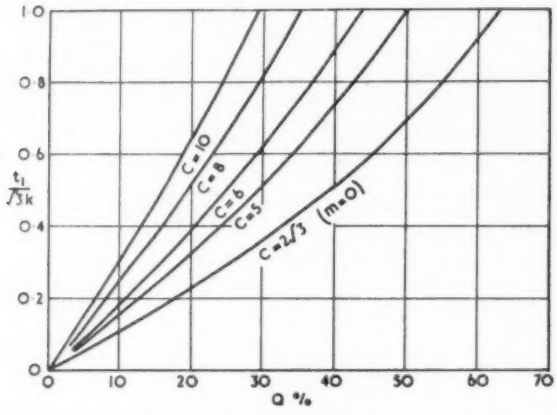

Fig. 9. Variation of drawing stress with percentage reduction in area (MISES material).

where p_0 and R_0 denote the values of p and R at the entry section. Since the frictional stress is assumed to have the constant value mk over the die, an average coefficient of friction μ can be defined by the equation

$$\mu = mkS \Big/ \int_S p dS,$$

where S is the area of the conical surface of contact between the wire and the die. Considerations of statical equilibrium show that

$$\tfrac{1}{4} t_1 \pi D_1^2 = \cos \alpha \, mkS + \sin \alpha \int_S p dS,$$

so that the coefficient μ is given by

$$\mu = \sin \alpha \, mkS / \{\tfrac{1}{4} t_1 \pi D_1^2 - \cos \alpha \, mkS\}.$$

The area of contact is

$$S = \tfrac{1}{4} \pi \operatorname{cosec} \alpha \, (D_0^2 - D_1^2),$$

and with the value (35) for t_1 we have

$$\mu = m \left(\frac{D_0^2}{D_1^2} - 1\right) \Big/ \left\{\tfrac{1}{2} c \ln \frac{D_0^2}{D_1^2} - m \cot \alpha \left(\frac{D_0^2}{D_1^2} - 1\right)\right\}.$$

If the reduction in area is small,

$$\mu \sim m/(\tfrac{1}{2} c - m \cot \alpha).$$

If m and α are also small, a reasonable approximation to c is

$$c = 2 \frac{m}{\alpha} + 2\sqrt{3},$$

so that in this case for small reductions

$$\mu \sim m/\sqrt{3}.$$

An approximate theory of wire drawing has been derived by SACHS (1927). SACHS assumed a Coulomb law of friction between the die and the wire and obtained the formula

$$t_1 = \sqrt{3}k\,(1 + \tan\alpha/\mu)\{1 - (D_1^2/D_0^2)^{\mu\cot\alpha}\}, \tag{36}$$

where μ is the coefficient of friction. In this formula, the tensile yield stress has been replaced by the MISES value $\sqrt{3}k$. Formulae (35) and (36) agree only when the frictional stress is zero. For drawing with backpull, in which there is a mean tensile stress t_0 over the entry section AB, the term $t_0\,(D_1^2/D_0^2)^{\mu\cot\alpha}$ is added to the right hand side of (36). According to the solution given here, which does not assume a Coulomb law of friction, the effect of backpull of amount t_0 increases the drawing stress t_1 by t_0. Fig. 10 shows the effect of backpull on the maximum reduction in area for $c = 5$. For comparison, the effect predicted by the theory of SACHS for $\mu\cot\alpha = 1$ is shown in the same figures (see HOFFMAN and SACHS 1953). Note that SACHS' theory with $\mu\cot\alpha = 1$ and the present theory with $c = 5$ predict the same value, 50 per cent, for the maximum reduction in area with zero backpull.

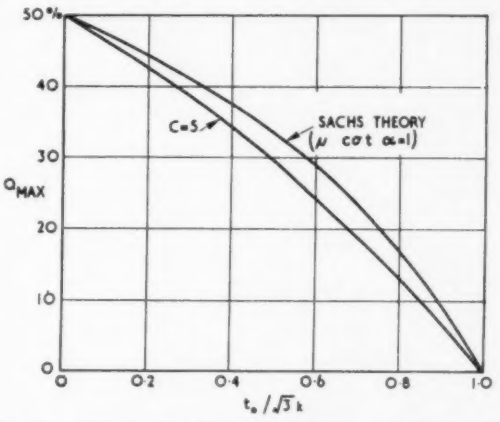

Fig. 10. Effect of backpull on maximum reduction in area according to present theory ($c = 5$) and theory of SACHS ($\mu\cot\alpha = 1$).

SACHS and VAN HORN (1940) have suggested the expression

$$t_1 = \sqrt{3}k\,(1 + \mu\cot\alpha)\ln\frac{D_0^2}{D_1^2} \tag{37}$$

as a convenient approximation to the mean drawing stress without backpull. Formulae (35) and (37) depend in the same way on the reduction in area.

ONAT (1954) has used a linearized theory of axially symmetric plastic stress and velocity fields to obtain the solution to a problem related to wire drawing without friction. In the only case considered, his solution predicts a drawing stress of amount $0{\cdot}430\,\sigma_0$, where σ_0 is the yield stress in tension, for a reduction in area of between 30·4 and 33·1 per cent. The inaccuracy in the amount of reduction in area is due to various approximations in the calculation. The present theory (with $m = 0$) predicts that the drawing stress lies between $0{\cdot}362\sigma_0$ and $0{\cdot}401\sigma_0$.

ACKNOWLEDGMENT

The writer would like to thank Mr. H. G. HOPKINS for a helpful discussion of this paper and the Chief Scientist, Ministry of Supply, for permission to publish.

(Crown Copyright reserved. Reproduced with the permission of the Controller, H.M.S.O.).

REFERENCES

DRUCKER, D. C.	1950	*Qu. Appl. Math.*, **7**, 411.
HAAR, A. and VON KÁRMÁN, TH.	1909	*Goettinger Nachr.*, math.-phys. Kl., **1909**, 204.
HOFFMAN, O. and SACHS, G.	1953	*Theory of Plasticity* (McGraw-Hill).
MISES, R. VON	1913	*Goettinger Nachr.*, math.-phys. Kl., **1913**, 582.
	1928	*Z. f. ang. Math. Mech.*, **8**, 161.
NADAI, A.	1924	*Z. f. Phys.*, **30**, 106.
ONAT, E. T.	1954	Brown Univ. Report DA 2598/14.
PRAGER, W. and HODGE, P. G.	1951	*Theory of Perfectly Plastic Solids* (Wiley).
SACHS, G.	1927	*Z. f. ang. Math. Mech.*, **7**, 235.
SACHS, G. and VAN HORN, K. R.	1940	*Practical Metallurgy* (Amer. Soc. for Metals, Cleveland).
TRESCA, H.	1868	*Mém. prés. par div. sav.*, **18**, 733.

Vol 3 1954/

Journal of the Mechanics and Physics of Solids, 1955, Vol. 3, pp. 259 to 266. Pergamon Press Ltd., London.

ON THE CONTRIBUTION OF CRYSTALLOGRAPHIC FIBRING TO HARDENING UNDER UNIAXIAL STRAINING CONDITIONS

By J. F. W. Bishop
Mechanical Engineering Research Laboratory, East Kilbride

(*Received 26th April, 1955*)

Summary

The effect of the development of a deformation texture in certain face-centred cubic metals on the tensile and compressive strength is examined. It is found that isotropic materials harden approximately equally in tension and compression for logarithmic strains up to 0·3. The theoretical ratio of the strengths at infinite strain is 1·13 : 1.

Vol. 3 54/55

1. Introduction

When a single crystal of a metal which deforms by glide is strained, the critical shear stress is found to be an increasing function of shear-strain. The precise nature of the hardening curve varies with the lattice structure and in many cases

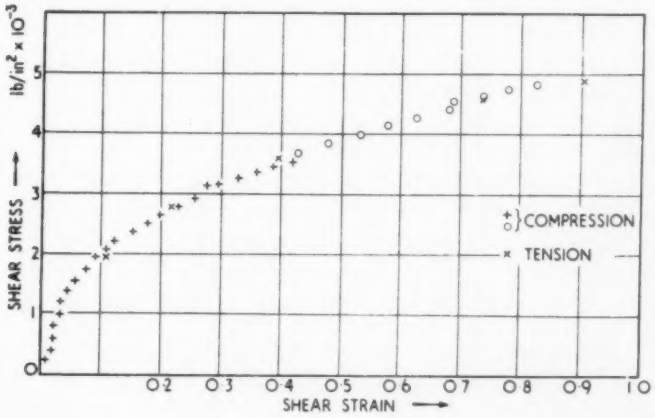

Fig. 1.

seems to be very sensitive to the conditions of test and the purity of the material. Thus G. I. Taylor (1927) found a parabolic hardening law for aluminium crystals in both tension and compression (Fig. 1), whereas Lücke and Lange (1952) obtained "easy glide" i.e. approximately linear hardening in 99·99% pure aluminium.

ANDRADE and HENDERSON (1951) were the originators of the term "easy glide" which they found to occur in very pure gold and silver. Fig. 2 shows the hardening curves given by SCHMID and BOAS (1950, p. 125) for magnesium, zinc, cadmium, aluminium, copper and nickel. The division between the face-centred cubic and hexagonal metals is clear. All these results are for simple slip. When multiple glide occurs, the hardening becomes more complex. TAYLOR and ELAM, for example, have shown that in aluminium active and latent glide planes harden by approximately the same amounts, whereas α-brass hardens more rapidly on latent planes than on active ones. According to KARNOP and SACHS (1927) the hardening of an aluminium single crystal in duplex slip is similar to that in simple slip if the amounts of glide occurring on each plane are summed to give the total glide-strain.

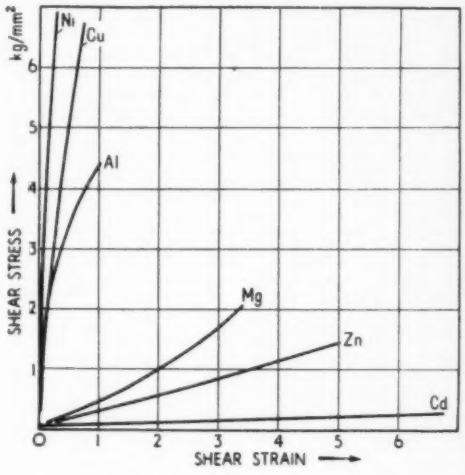

Fig. 2.

Multiple glide is the normal mechanism for the deformation of polycrystalline specimens. Here however two further factors affecting mechanical strength arise, namely crystallographic and mechanical fibring. The first of these effects is the result of the development of a preferred orientation and is of considerable importance in sheet material. Since the yield strength of each crystal is a function of its orientation the strength of an aggregate having a preferred orientation will vary with direction. The second effect is due to the alignment of inclusions, cavities and particular phases in certain directions due to mechanical working.

According to SACHS and VAN HORN (1940, p. 134) the properties of forgings are determined chiefly by mechanical fibring although they quote SCHMID as attributing the properties of magnesium forgings to perferred orientation. In this paper the hardening of certain face-centred cubic metals due to crystallographic fibring in uniaxial deformation is examined.

2. HARDENING OF POLYCRYSTALLINE AGGREGATES

When a tensile specimen is permanently extended, a record of stress against plastic strain can be obtained prior to the onset of necking and subsequent fracture. Any point on this curve gives the tensile yield stress at the associated state of work-hardening. In general the working of metals involves combined stress states and both tensile and compressive stresses. The question therefore arises as to the relative amounts of hardening which occur under different stress systems or straining conditions. In the present paper only two causes of hardening (or softening) are considered, namely a variation in the critical shear stress of the individual grains and the development of a preferred orientation. A brief description of the former is given in this section.

The experimental work of KARNOP and SACHS (1927) and TAYLOR (1927) suggests that in certain face-centred cubic metals the critical shear stress is a function of the total glide which has occurred. Assuming that each grain in an aggregate undergoes the macroscopic strain and that they all harden equally, TAYLOR (1938) showed that if the variation of the critical shear stress τ of a single crystal could be expressed as a function of the shear strain γ by

$$\tau = \tau(\gamma),$$

then the tensile strength of an isotropic aggregate could be expressed as a function of logarithmic strain E by

$$S = m\,\tau(mE) \tag{i}$$

m has been computed by BISHOP and HILL (1951) to be 3·06 for an initially isotropic aggregate for *small* strains. These authors have also shown that the assumption that each grain undergoes the macroscopic strain can be removed and that the above assumptions lead to the conclusion that the size of the yield locus is a function of plastic work.

If the aggregate does not remain isotropic, equation (i) is valid for small strains only. For larger strains the differential relations

$$\frac{S}{T} = \frac{d\gamma}{dE} = m(E)$$

must be considered, where m is now a function of E. Thus E is expressed in terms of γ through the integral equation

$$\gamma = \int m(E)\,dE,$$

and equation (i) is replaced by

$$S = m(E)\,\tau\left(\int m(E)\,dE\right). \tag{ii}$$

Equation (i) is valid for both tension and compression. TAYLOR (1927) has shown that for aluminium single crystals the tensile and compressive curves of critical shear-stress versus shear-strain are to all intents and purposes identical. Hence for an isotropic aggregate of aluminium crystals which remains isotropic (i.e. for small strains) the compressive and tensile curves plotted on a logarithmic strain basis should be identical. More generally this is true for an anisotropic aggregate for small strains. This conclusion was proved by HILL (1950, p. 23 *et seq.*) starting from the assumption that the size of the yield locus is a function of plastic work only. As stated above this property follows from the assumptions that the critical shear stress is a function of the total glide and that the grains harden equally. It is remarked that HILL's conclusions still obtain whether or not equation (i) is true, since they are based on a hypothesis made for the aggregate; they are not restricted to any particular lattice structure.

The value of m in equation (ii) would be expected to vary with strain if the material developed a preferred orientation. Hence at this stage it would not be surprising to find tensile and compressive curves diverging with increasing strain, i.e. with developing anisotropy.

Vol. 3 54/55

In Fig. 3 the results obtained by Ludwik and Scheu (1925) for annealed copper in tension and compression are shown. It is seen that they are sensibly identical up to strains of 0·3, and at a strain of nearly 0·4, at which necking commences, the discrepancy is no larger than is customarily obtained in very careful tests

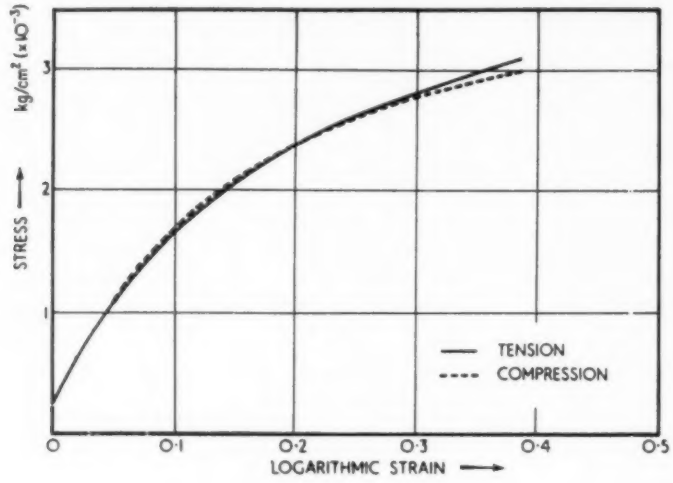

Fig. 3.

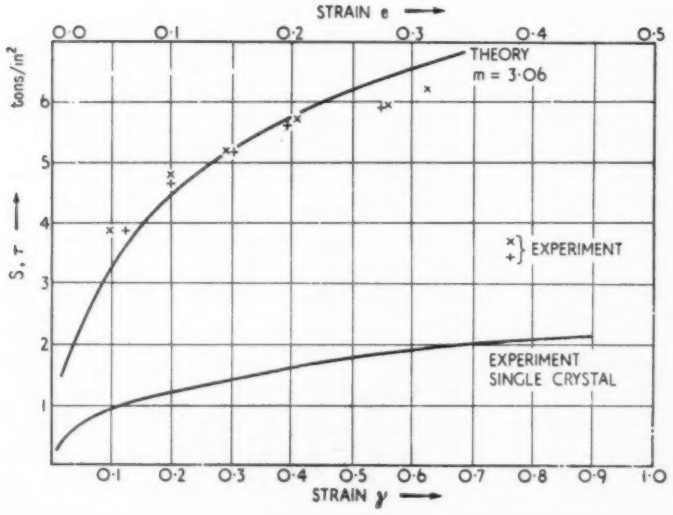

Fig. 4.

under identical straining conditions (see for example Davis and Parker 1948).

Fig. 4 shows the S, e curve (e is apparent strain) predicted by Taylor (1938) from data obtained for aluminium by Miss Elam. Also shown are the experimentally determined points for a polycrystalline specimen. The theoretical curve is predicted using a constant value for m.

3. Deformation Textures

Several theories have been advanced to account for the deformation textures of face-centred cubic metals. The one employed here is that due to Bishop (1954). It is assumed that each grain in the aggregate undergoes the macroscopic strain. From purely geometrical considerations, the relations between strain and shear on the glide planes can be stated. The maximum work principle of Bishop and Hill (1951) enables the physically possible set or sets of shears to be found. These will normally contain either one or three redundant shears giving a range of possible rotations of the grain. The hypothesis advanced by Bishop (1954) enables the operative shears to be found when the hardening characteristics of single crystals

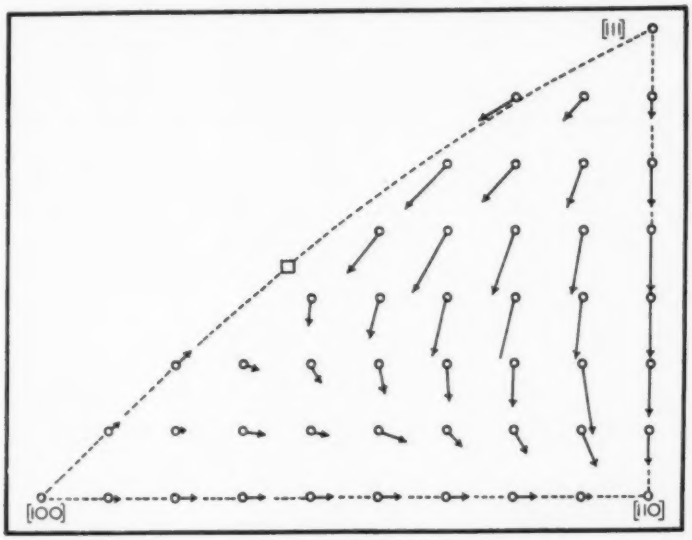

Fig. 5.

of the material involved are known. In Fig. 5 the rotations due to a 0·05 compressive strain of an isotropic aluminium or copper specimen are shown. Each point represents the initial orientation of the specimen axis relative to the crystal axes and the arrowhead the position subsequent to straining. The rotations in tension are the reverse of those in the Figure. It should be remarked that the rotations observed experimentally are consistent with those predicted by this theory but that the development of the texture is by no means as rapid as indicated theoretically. Possible reasons for this are given by Bishop in the paper cited. For the purposes of this paper it should be borne in mind that qualitatively the results obtained here are good. The quantitative value of the results will be reverted to in the discussion.

4. Method of the Present Work

Bishop and Hill (1951) have shown how the work done in imparting an arbitrary strain to a grain in an aggregate may be evaluated. This work varies both with

orientation and with strain. The yield stress of an aggregate undergoing a given strain can be found by equating the work done in the (known) macroscopic strain with the average work required to deform the grains of known orientations present.

In general the yield stress corresponding to a plastic strain increment can only be found from the establishment of an arc of the yield surface by enveloping it (see Bishop and Hill 1951). If however an initially isotropic aggregate is taken and loaded uniaxially the strain components are known at all stages since developed anisotropy is axially symmetrical about the loading direction. The average work done in a small increment of strain can be computed and the accompanying rotation of the grains found as shown by Bishop (1954). Thus the deformation texture and the current yield stress (in terms of the critical shear stress) can be evaluated. This procedure repeated for a series of strain-increments will lead to the establishment of a yield stress-strain curve which shows the influence of crystallographic fibring on the yield strength.

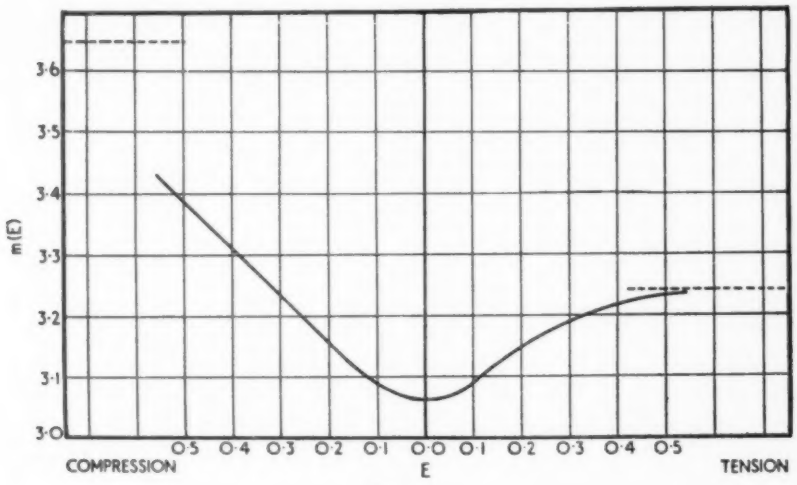

Fig. 6.

Computations have been carried out for an initially isotropic face-centred cubic material with equal latent and active hardening (e.g. copper and aluminium for 0·05 increments in uniaxial strain in both tension and compression up to 0·55 strain. The value of m as a function of logarithmic strain is shown in Fig. 6.

5. Discussion

It can be seen that up to 0·3 logarithmic strain, the function m is for all practical purposes symmetrical about the origin. The values at infinite strain were calculated giving the asymptotes indicated by the dotted lines. According to these computations the ratios of the yield points at infinite strain in compression and tension to that at zero strain taking account of crystallographic hardening only are 1·20 and 1·06 to 1·00. Hence the maximum discrepancy between the strengths in tension and compression predicted by this theory is about 13%. It is interesting to note

that in rolling where very heavy deformations occur in the length direction with zero strain in the cross direction, BARRETT (1953, p. 522) states that the anisotropy seldom amounts to as much as 10% in yield strength.

In considering the results obtained here, it must be remembered that the effects of inhomogenous strain within grains, and of strains differing from the macroscopic strain, are not taken into account. From a comparison with experimental data (e.g. BARRETT 1953, p. 447) it can be shown that the development of the textures predicted by the theory is considerably more rapid than is found in practice. Thus the function m shown in Fig. 6 should have a shallower gradient. It seems reasonable to suppose that the graph gives a good qualitative picture of the variation of m with strain. The results obtained here are therefore consistent with the experimental work of LUDWIK and SCHEU.

As stated in section 2, the theoretical curve in Fig. 4 was predicted by TAYLOR using a constant value for m. According to the present paper the value of m should increase with strain. This would give a rather poorer agreement between the experimental and theoretical curves. It should perhaps be remarked that the single crystal curve is rather sensitive to the conditions of test; (see for example COTTRELL 1953, Ch. V). The results obtained here can be regarded as the variation of a particular section through the yield locus of an anisotropic material with strain. The general problem of finding the tensile strength in various directions in an anisotropic material cannot be treated exactly by the method used here since the macroscopic strains which occur are a function of the anisotropy developed. It is hoped to give an approximate treatment of this problem based on the current theory in a later paper.

Vol. 3 54/55

6. ACKNOWLEDGMENTS

I should like to thank Professor HILL for critical comments on the original manuscript.

The work described forms part of the research programme of the Mechanical Engineering Research Board of the Department of Scientific and Industrial Research. It was carried out in the Plasticity Division of the Mechanical Engineering Research Laboratory and is published by permission of the Director.

REFERENCES

ANDRADE, E. N. da C. and HENDERSON, C. 1951 *Phil. Trans. Roy. Soc.*, A, **244**, 177.

BARRETT, C. S. 1953 *Structure of Metals* (London : McGraw-Hill).

BISHOP, J. F. W. 1955 *J. Mech. Phys Solids*, **3**, 130.

BISHOP, J. F. W. and HILL, R. 1951 *Phil. Mag.*, **42**, 1298.

COTTRELL, A. H. 1953 *Dislocations and Plastic Flow in Crystals* (Oxford : Clarendon Press).

DAVIS, H. E. and PARKER, E. R. 1948 *J. Appl. Mech.*, **15**, 201.

HILL, R. 1950 *Mathematical Theory of Plasticity* (Oxford : Clarendon Press).

KARNOP, R. and SACHS, G. 1927 *Z. Phys.*, **75**, 531.

Lücke, K. and Lange, H.	1952	*Z. Met.*, **43**, 55.
Ludwik, P. and Scheu, R.	1925	*Stahl und Eisen*, **45**, 373.
Sachs, G. and van Horn, K. R.	1940	*Practical Metallurgy* (Cleveland : A.S.M.).
Schmid, E. and Boas, W.	1950	*Plasticity of Crystals* (London : Hughes).
Taylor, G. I.	1927	*Proc. Roy. Soc.*, A, **116**, 39.
	1938	*S. Timoshenko Anniversary Vol.*, p. 218 (New York Macmillan).

Journal of the Mechanics and Physics of Solids, 1955, Vol. 3, pp. 267 to 274. Pergamon Press Ltd., London.

AVERAGE WARPING IN THE TORSION OF THIN-WALLED OPEN-SECTION BEAMS

By A. H. Chilver
Department of Engineering, University of Cambridge

(*Received 20th April*, 1955)

Summary

It is suggested that in the theory of non-uniform torsion of thin-walled beams of open cross-section it is strictly relevant to define average longitudinal warping as the mean value taken over the whole cross-sectional area, and not as the mean value taken over the centre-line of the wall, as suggested by Timoshenko (1945). This alternative concept was used earlier by Wagner (1929); it seems desirable at this stage to re-define the warping stiffness in the general case in terms of this alternative value of average warping.

Vol. 3 54/55

1. Introduction

The torsional properties of thin-walled beams of open cross-section have assumed considerable practical importance, largely as a result of the wider use of thin-walled metal structures. Interest in this field was revived recently by Timoshenko (1945) in an excellent series of articles covering a wide range of bending, torsion and buckling problems. In his analysis Timoshenko introduces the concept of average longitudinal warping of a twisted beam of open cross-section; this is defined as the mean value of longitudinal warping taken over the centre line of the wall of the section; a theory of non-uniform torsion is built up on this basis, and Timoshenko suggests that the average warping, defined in this way, is fundamental to the general problem of non-uniform torsion of a thin-walled open-section beam.

In the author's opinion Timoshenko's definition of average warping is not sufficiently adequate for dealing with the most general problems; it can be used only in discussing beams of constant wall thickness. The author suggests that in the general problem, concerning a beam of variable wall thickness, the definition of average warping should be based on the mean value taken over the whole area of the cross-section of the beam. This alternative value of average warping gives a warping stiffness which differs slightly in form from that of Timoshenko's; it may be shown that in general Timoshenko's value of warping stiffness always overestimates the correct value.

These thoughts led the author to study more closely the original work of Wagner (1929); it is apparent that Wagner uses implicitly an average value of warping based, as the author suggests, on a mean value taken over the whole area of the cross-section.

The purpose of this paper is to present simply and concisely the theory of non-uniform torsion of a beam of thin-walled open cross-section. Where necessary the

analysis of WAGNER is extended to show that, on the basis of the usual assumptions of the theory of torsion of open sections, average warping is most conveniently defined as the mean value taken over the whole cross-sectional area of the beam.

2. Position of the Shear-Centre Axis

A straight beam, uniform along its length, has a thin-walled open cross-section (Fig. 1); the centroid of the cross-section is at C, and Cx, Cy are the principal centroidal axes; the wall of the section is of variable thickness t; the second moments of area about the axes Cx, Cy are I_x, I_y, respectively. Only bending of the beam takes place if the resultant shear forces on all cross-sections pass through a point O having co-ordinates

$$x_0 = \frac{1}{I_x}\int_0^m yt\alpha_c\,ds, \qquad y_0 = -\frac{1}{I_y}\int_0^m xt\alpha_c\,ds, \tag{1}$$

in which (x, y) are the coordinates of any point on the centre line of the wall, s is the distance measured along the centre line from one extreme end of the centre line to that point, m is the total length of the centre line, and

$$\alpha_c = \int_0^s p\,ds, \tag{2}$$

where p is the perpendicular distance from the centroid to the tangent at that point of the wall; p is taken positive if a vector coincident with the tangent, and having the direction in which s is increasing, gives an anti-clockwise moment about C. The point O of the cross-section is called the shear centre; the longitudinal axis connecting points O is referred to as the shear-centre axis.

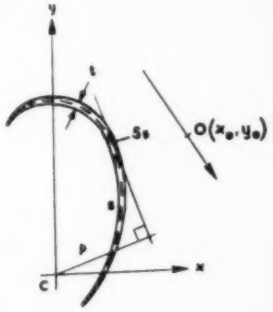

Fig. 1. Position of the shear centre in any cross-section of the beam.

3. Uniform Torsion of the Beam

In a condition of uniform torsion, torques applied at the ends of the beam produce a uniform twist along the length. Only shear stresses are induced in the walls of the beam, and the distribution of shear stresses is the same for all cross-sections.

Suppose cross-sections twist about a longitudinal axis BB', which is parallel to the centroidal axis Cz (Fig. 2); ρ is the length of the line joining the centre of twist at any cross-section and a point P of the centre line of the wall (Fig. 3); r is the length of the perpendicular from the centre of twist to the tangent to the centre line at P; the direction of the tangent at P in the xy-plane is $P\eta$. If B is the centre of twist of a cross-section, and if the whole cross-section twists by an amount θ, then in the xy-plane the point P is displaced a small amount $\rho\theta$ perpendicular to BP. The point P is also displaced longitudinally by an amount w, in a direction parallel to the Cz-axis.

In the pure torsion of a thin-walled open-section beam there is no shear strain in the centre line of the wall; this condition determines the value of w, or the amount of longitudinal warping, at any point of the cross-section for any rate of

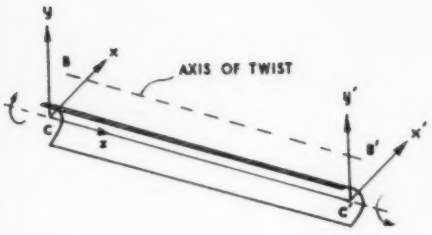

Fig. 2. Uniform torsion under equal and opposite end torques.

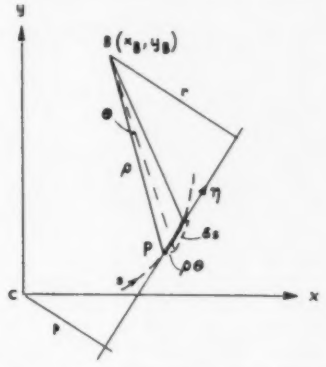

Fig. 3. Displacement of an element in the xy-plane.

twist of the beam. Consider an element of the wall in the ηz-plane (Fig. 4); the longitudinal displacement of the point P is w; the circumferential displacement is $r\theta$, or the component of $\rho\theta$ in the $P\eta$- direction. For no shear strain of the centre line of the wall

$$r\frac{d\theta}{dz} + \frac{\partial w}{\partial s} = 0.$$

Then

$$w = w_0 - \theta' \int_0^s r ds, \tag{3}$$

where w_0 is the longitudinal warping of the cross-section at the point $s = 0$, and $\theta' = d\theta/dz$. The value of w may be expressed also in terms of p, the length of the perpendicular from the centroid to the tangent at P. Suppose (x, y) are the coordinates of P, and (x_B, y_B) the coordinates of B, the centre of twist. Then

$$r = p + y_B\frac{dx}{ds} - x_B\frac{dy}{ds}, \tag{4}$$

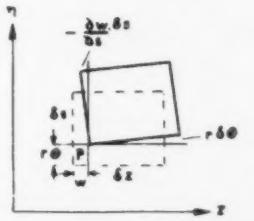

Fig. 4. Displacements of an element in the ηz-plane.

and, in terms of p, w becomes

$$w = w_0 - \theta'\left[\alpha_c + y_B(x - X_0) - x_B(y - Y_0)\right], \tag{5}$$

where (X_0, Y_0) are the coordinates, referred to Cx, Cy, of the point $s = 0$, and α_c is defined by equation (2).

4. Non-uniform Torsion of the Beam

In non-uniform torsion, equal and opposite torques are again applied at the ends of the beam; in this case, however, cross-sections of the beam are not necessarily

free to warp longitudinally. For this reason longitudinal stresses may exist, and there may be a variable rate of twist along the length of the beam.

Consider an elemental length δz of the section; suppose the element is completely free to warp on both cross-sectional faces. If θ' is the rate of change of angle of twist, then the warping at any point of the cross-section is

$$w = w_0 - \theta' \int_0^s r ds,$$

in which r is measured from the centre of twist. Suppose that an adjacent elemental length, at the section $(z + \delta z)$, is also free to warp; if the rate of change of angle of twist at this section is $(\theta' + \delta\theta')$, then the warping at any point of the cross-section is

$$w + \delta w = (w_0 + \delta w_0) - (\theta' + \delta\theta') \int_0^s r ds,$$

where r is measured from the same centre of twist. At the cross-section where the two elements meet, there is a longitudinal discontinuity at any point of the cross-section of amount

$$\delta w = \delta w_0 - \delta\theta' \int_0^s r ds.$$

Suppose this discontinuity is eliminated by introducing a longitudinal stress σ at any point of the cross-section; since it may be necessary to vary σ from one cross-section to another, equilibrating shear stresses τ are introduced on the longitudinal sides of an element of the wall in the ηz-plane (Fig. 5). Assume that circumferential stresses are negligible; then

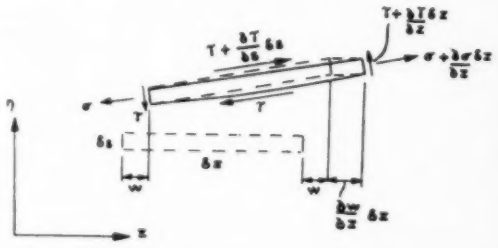

Fig. 5. Longitudinal and shear stress produced by non-uniform torsion.

$$\sigma = E \frac{\partial w}{\partial z} = E \left[w_0' - \theta'' \int_0^s r ds \right],$$

where E is Young's modulus for the material of the beam. The value of w_0 and the position of the centre of twist are chosen so that at all cross-sections of the beam we have

(i) no resultant longitudinal force,
(ii) no resultant bending moments about the axes Cx, Cy, and
(iii) no resultant transverse forces parallel to the axes Cx, Cy.

Condition (i) gives

$$\int_0^m \sigma t ds = E \int_0^m \left[w_0' - \theta'' \int_0^s r ds \right] t ds = 0. \tag{6}$$

Suppose

$$\alpha = \int_0^s r ds, \qquad \Gamma = \frac{1}{A} \int_0^m \alpha t ds, \tag{7}$$

where A is the total cross-sectional area of the beam. Then equation (6) gives

$$w_0' = \theta'' \Gamma,$$

and, therefore,

$$\sigma = E\theta''(\Gamma - \alpha).$$

The first of conditions (ii) gives

$$\int_0^m \sigma y t ds = E\theta'' \int_0^m (\Gamma - \alpha) y t ds = 0. \tag{8}$$

Suppose the coordinates of the centre of twist are (x_B, y_B); then

$$r = p + y_B \frac{dx}{ds} - x_B \frac{dy}{ds},$$

and

$$\alpha = \int_0^s r ds = \alpha_c + y_B (x - X_0) - x_B (y - Y_0).$$

Equation (8) then reduces to

$$\int_0^m y t \alpha_c \, ds - x_B I_x = 0.$$

But from equations (1), $\int_0^m y t \alpha_c \, ds = x_0 I_x$, so that $x_B = x_0$. Similarly the second of conditions (ii) gives $y_B = y_0$. The centre of twist is coincident, therefore, with the shear centre, (x_0, y_0).

The shear stresses τ on an element of the wall are found from the equilibrium equation

$$\frac{\partial}{\partial s}(\tau t) + t \frac{\partial \sigma}{\partial z} = 0.$$

The shear force parallel to Cx is

$$\int_0^m \tau t \frac{dx}{ds} ds = \int_0^m x t \frac{\partial \sigma}{\partial z} ds,$$

since τt vanishes at $s = 0$ and $s = m$. On substituting for σ, we find that the shear force vanishes if $y_B = y_0$. Similarly, the shear force parallel to Cy is zero if $x_B = x_0$.

5. The Warping Stiffness

Suppose Γ_0 and α_0 are the particular values of Γ and α when r is measured from the shear centre, (x_0, y_0). Then the longitudinal stress system

$$\sigma = E\theta''(\Gamma_0 - \alpha_0), \tag{9}$$

satisfies all the conditions (i), (ii) and (iii), above. The presence of the shear stresses τ implies an additional torque on any cross-section of amount

$$\int_0^m \tau t r ds = -E\theta''' \int_0^m \alpha_0 (\alpha_0 - \Gamma_0) t ds. \tag{10}$$

The geometrical constant in equation (10) may be written in the forms

$$\int_0^m \alpha_0 (\alpha_0 - \Gamma_0)\, t ds = \int_0^m (\Gamma_0 - \alpha_0)^2 t ds = \int_0^m \alpha_0^2 t ds - A\Gamma_0^2 = K, \quad \text{(say)}. \qquad (11)$$

K is called the warping constant; the warping stiffness is EK. The third form of K in equation (11) is probably the simplest to evaluate in practical problems.

6. Average Longitudinal Warping

The preceding analysis suggests that it is convenient to define average warping on any cross-section in the form

$$w = \theta' (\Gamma_0 - \alpha_0).$$

Longitudinal warping stresses, by equation (9), are proportional to the quantity $(\Gamma_0 - \alpha_0)$. Now, in full,

$$\Gamma_0 = \frac{1}{A} \int_0^m t \int_0^s r ds \, . \, ds,$$

where r is measured from the shear centre; Γ_0 is the mean value of $\int_0^s r ds$ taken over the whole cross-sectional area of the beam.

7. Comparisons with Timoshenko's Theory

In the problem of uniform torsion the warping of points of the centre line of the wall in any cross-section may be referred quite arbitrarily to any suitable datum. Timoshenko (1945) takes the warping over any cross-section in the form

$$w = \theta' \left(D - \int_0^s r ds \right),$$

where r is measured from the centre of twist, and D is defined by

$$D = \frac{1}{m} \int_0^m \int_0^s r ds. \; ds. \qquad (12)$$

Obviously D is the mean value of $\int_0^s r ds$ taken over the whole length of the centre line of the wall.

In the problem of non-uniform torsion, Timoshenko considers a longitudinal stress system of the type

$$\sigma = E\theta'' (D - \int_0^s r ds). \qquad (13)$$

He contends that the total longitudinal force produced by these stresses is zero; in fact

$$\int_0^m \sigma t ds = E\theta'' \int_0^m \left(D - \int_0^s r ds \right) t ds,$$

only vanishes when t is constant over the whole length of the centre line. In the more general case the stresses defined by equation (13) imply a resultant longitudinal force.

As a particular case, consider the zed-section of Fig. 6. The flanges of this section are geometrically similar; the shear centre and centroid are coincident at the centre of the web. The position of the shear centre is unaffected by the relative values of the thicknesses t_1 and t_2 of the flanges and web, respectively; so that according to TIMOSHENKO, the longitudinal warping stresses given by (13) are independent of the ratio (t_1/t_2). It is easily shown that the flanges of the section warp so that the stresses defined by (13) produce no longitudinal force only if $t_1 = t_2$.

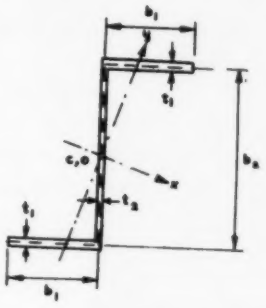

Fig. 6. Dimensions of a zed-section.

TIMOSHENKO's value of the warping constant, which is based on (13), is

$$\int_0^m \left(D - \int_0^s r\,ds\right)^2 t\,ds = K_T, \quad \text{(say)}, \tag{14}$$

where r is measured from the shear centre. It is easily demonstrated that

$$K_T = K + A\,(D - \Gamma_0)^2 \tag{15}$$

in which K is defined by (11), Γ_0 by (7), and A is the cross-sectional area of the beam. Then TIMOSHENKO's value of the warping constant is always greater than the true value K. The fractional error involved in K_T is

$$\frac{K_T}{K} - 1 = \frac{A}{K}(D - \Gamma_0)^2. \tag{16}$$

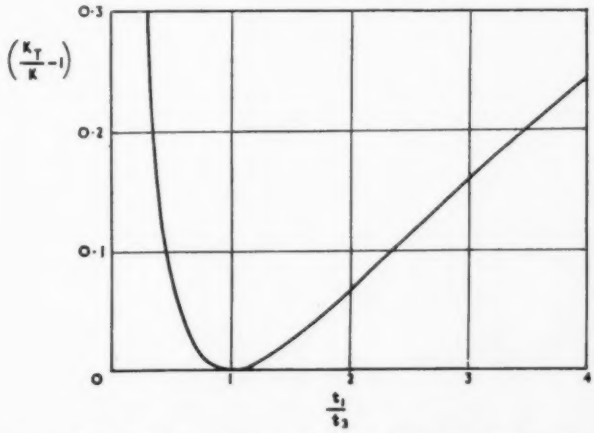

Fig. 7. Fractional error in K_T for a zed-section in which $b_2 = 3b_1$, for various values of (t_1/t_2).

When the walls of a section are of constant thickness, $D = \Gamma_0$, and it follows that $K_T = K$. For the zed-section shown in Fig. 6

$$A = 2b_1 t_1 + b_2 t_2,$$

$$\Gamma_0 = \frac{b_1 b_2 (b_1 t_1 + b_2 t_2)}{2\,(2b_1 t_1 + b_2 t_2)},$$

and

$$K = \tfrac{1}{12}\, b_1^{\,3}\, b_2^{\,2}\, t_1 \left[\frac{b_1\, t_1 + 2b_2\, t_2}{2b_1\, t_1 + b_2\, t_2}\right].$$

TIMOSHENKO's constant D is derived from Γ_0 by putting $t_1 = t_2$; this gives

$$D = \tfrac{1}{2}\, b_1\, b_2 \left[\frac{b_1 + b_2}{2b_1 + b_2}\right].$$

For the case in which $b_2 = 3b_1$ the variation of $(K_T/K - 1)$ with (t_1/t_2) has the form shown in Fig. 7; K_T overestimates the warping stiffness by about 24% when $t_1/t_2 = 4$.

REFERENCES

TIMOSHENKO, S. P.	1945	*J. Franklin Inst.*, **239** (3, 4, 5).
WAGNER, H.	1929	25th Anniversary Publication. Technische Hochschule, Danzig. (English translation in Tech. Mem. 807, Nat. Adv. Comm. Aero, 1936).

Journal of the Mechanics and Physics of Solids, 1955, Vol. 3, pp. 275 to 294. Pergamon Press Ltd., London.

THE EFFECT OF PRESTRAINING IN SIMPLE TENSION AND BIAXIAL TENSION ON FLOW AND FRACTURE BEHAVIOUR OF A LOW CARBON DEEP-DRAWING STEEL SHEET

By F. Garofalo* and J. R. Low, Jr.†

(*Received* 14*th February*, 1955)

Summary

The effect of prestraining in tension in the rolling direction of a fully killed deep drawing steel sheet has been determined in subsequent tension at 0°, 22·5°, 45°, 67·5° and 90° to the rolling direction. The effect of prestraining under biaxial tension, using a circular and an elliptical bulge tester, has been determined in subsequent tension at 0° and 45° to the original rolling direction.

The initial anisotropy of the material satisfied orthotropic symmetry, and is not affected by the prestrain. After prestraining under biaxial tension, or upon changing the direction of straining after prestraining in tension, the initial flow stress is greater than that predicted by the effective stress-strain concept, the strain-hardening coefficient is decreased, and, beyond a prestrain of 0·095 effective strain, the maximum load upon retesting is reached after approximately 0·01 strain. The angle between specimen axis and fracture surface is not affected by the prestrain, and is found to be approximately 50°, which is in agreement with the computed value of 51° for the rolling and transverse directions for the type of anisotropy found.

Vol. 3 54/55

1. Introduction

Experimental work on the effect of prestraining on flow and fracture behaviour has received particular attention in recent years (Swift 1939; Körber 1941; 1943; Hollomon 1944; Mehringer 1945; Lynch 1948; Liu 1949, 1951; Faupel 1951; Bridgman 1952; Marin *et al.* 1953a and b). Few investigations in this field have been devoted, however, to the study of the effect of prestraining on the plastic and fracture behaviour of sheet steels used in deep drawing operations. When subjecting a metal sheet to a deep drawing formation, a number of factors are encountered which may vary appreciably during the drawing operation. In non-symmetrical draws, for example, one factor which may vary appreciably is the strain or stress pattern. Although the true variation of this factor is not known, some useful information on the behaviour of deep drawing sheet materials can be obtained from controlled tests, in which the direction of straining or the

* F. Garofalo is now associated with the Fundamental Research Laboratory of the United States Steel Corporation, Kearny, New Jersey; formerly Carnegie-Illinois Graduate Fellow, The Pennsylvania State University.

† J. R. Low, Jr. is now associated with the Research Laboratory of the General Electric Company; formerly Professor of Metallurgy and Chief, Division of Metallurgy, The Pennsylvania State University.

This paper is based in part upon a thesis submitted by F. Garofalo to The Pennsylvania State University in partial fulfilment of the requirements for the degree of Doctor of Philosophy, June 1949.

state of stress is changed between prestraining and subsequent testing. Moreover, a check on the existing criteria of flow and fracture is possible by interpreting the test results in terms of fundamental mechanical properties.

The present investigation was undertaken to study the effect of pre-straining in simple tension, and under biaxial tension, on the flow and fracture characteristics of a fully killed, temper rolled, deep drawing steel sheet. Following prestraining in tension, tensile tests were made at 0, 22·5, 45, 67·5 and 90° to the direction of tensile prestrain. Two different bulge testers, one circular and one elliptical in shape, were used for prestraining under biaxial tension. Tensile tests at 0 and 45° to the original rolling direction were made after prestraining under biaxial tension.

2. Material and Testing Techniques

The test material used in this investigation is a temper-rolled, fully killed, deep-drawing steel sheet of nominal 0·037 in. thickness, and of the following nominal type composition : C, 0·05 per cent ; Mn, 0·35 ; P, 0·010 ; S, 0·025 ; Si, $< 0{\cdot}01$ and Al, 0·05. The material was received in the form of 36 in. square sheets cut from a continuous strip temper-rolled after anealling.

The two types of test methods employed in the prestraining operations are simple tension and bi-axial tension. In the latter, circular and elliptical bulge-testing apparatus is used. Following the various prestraining operations, subsequent tension tests were made at room temperature, employing high precision measurements of extension, contraction and load.

3. Prestraining in Simple Tension

Wide sheet blanks, 20 in. long and 9 in. wide, were cut with the longitudinal direction of the blanks coinciding with the direction of rolling. To minimize metallurgical variation, the centre line of each blank in the longitudinal direction coincided with one of the two longitudinal quarter lines parallel to the two edges of the strip.

The wide sheet blanks were strained in tension 5, 10, 15 or 20%. The extension during prestraining was determined with dividers by measuring the distortion of a 20 line to one inch photo-grid. A more accurate determination of the longitudinal extension and lateral contraction was made, following prestraining by using a micro-comparator.

Tensile test pieces, 8 in. long and 0·75 in. wide, which were subsequently machined into tensile specimens, were cut from the prestrained blanks. The longitudinal axes of these test pieces were inclined at various angles to the direction of initial tensile strain, and therefore rolling direction. These inclinations were : 0°, 22·5°, 45°, 67·5° and 90°. Three test pieces were removed from each blank, the longitudinal axes of these being parallel.

Nominal strain values after prestraining were computed from grid measurements within a 3 in. length located in the centre of each tensile test piece. The maximum variation in the strain for each test piece was found to be within ± 1 per cent of the mean value.

In order to minimize the occurrence of strain ageing after prestraining, the test pieces were kept at approximately 0°C, except when strain measurements were made or machining operations performed. The effect of time and temperature following prestraining on the plastic behaviour of the material has been investigated and is discussed later.

4. Prestraining under Bi-axial Tension

As mentioned previously, circular and elliptical hydraulic bulge testers were used for prestraining under biaxial tension. The hydraulic bulge-testing apparatus used was the same as that employed by Lankford, Low and Gensamer (1947).

The blanks prestrained under biaxial loads were cut from the large 36 in. square sheets in a manner similar to those prestrained in simple tension; that is, a line through the centre of each blank coincided with one of the quarter lines. The direction of initial rolling in each blank prestrained in the elliptical bulge tester coincided with the major axis of the ellipse. Because of rotational symmetry in the circular bulge tester, no preferred orientation of the blanks is necessary; however, the direction of initial rolling was clearly marked on each blank.

The desired amount of deformation during prestraining under biaxial tension was determined from the distortion of the photo-grid, measured again by means of dividers. The predetermined amounts of prestrain were 5, 10, 20 and 30% extension, computed from the elongation in a one inch initial gauge length in a direction coinciding with that of rolling in the circular bulge, and in a direction coinciding with the minor axis or transverse to that of rolling in the elliptical bulge.

Vol. 3 54/55

Two tensile test pieces, 8 in. in length and $\frac{3}{4}$ in. wide, were cut from each partially blown bulge. The test pieces were taken at 0 or 45° to the rolling direction. Only two amounts of prestrain, 5 and 10% extension, were employed for the test pieces cut at an inclination of 45°.

It is known from observation that the strain in a partially blown bulge varies from zero at the periphery to a maximum at the pole; however, in the region of the pole the strain is substantially homogeneous over an appreciable area (Chow, Dana and Sachs 1949). Grid measurements, using the micro-comparator on the two tensile test pieces cut from each partially blown bulge, show that the strain within a 3 in. central section is reasonably uniform, being within $\pm 3\%$ of the mean value. The slight curvature which resulted from the prestrain in the hydraulic bulges was eliminated upon clamping of the blanks for machining into tensile specimens.

5. Tensile Testing Procedures

The testing procedure and the special apparatus which enables precise measurement of load and extension by determining the elastic strain in a dynamometer and clip gauge by means of SR-4 resistance strain gauges have been described in an earlier paper by Low and Garofalo (1947). An additional clip gauge used for lateral contraction measurements is shown in Fig. 1. This strain gauge was designed to cover a range from 0 to 80% contraction in a 0·5 in. initial gauge length. From a number of calibrations over a range from 0 to 30% contraction,

the maximum error was found to be of the order of 0·5% and the clip gauge was found to be sensitive to less than 0·0001 in. change in contraction. The elastic strain in the beams of the clip gauge is proportional to the lateral strain of the specimen. The elastic strain is measured with SR-4 resistance strain gauges.

The initial resistance reading for the SR-4 gauges for zero elastic strain is found to vary slightly with time, although the gauges in each instrument compensate each other for temperature changes. The calibration results, however, show that the elastic strain-increment in the apparatus is proportional only to the increment in load or extension, and the relationship is independent of the initial resistance reading. Accordingly, load and strain values were computed from the increment in elastic strain measured on the strain indicator.

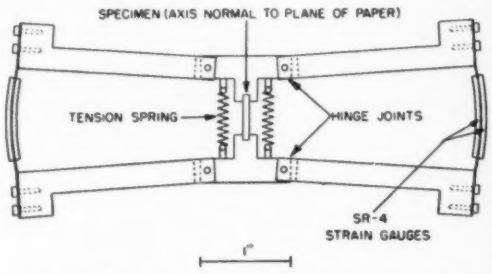

Fig. 1. Clip-gauge assembly for determining lateral strain.

A standard A.S.T.M. sheet tensile specimen was used. The width and thickness along the reduced section were measured at 0·5 in. intervals with a flat-end micrometer accurate to 0·0001 in. Samples showing a variation in width or thickness greater than $\pm$ 0·00025 in. were discarded.

As described by Low and GAROFALO (1947), before conducting each tensile test the axis of each specimen is aligned with the axis of tensile force. Following proper alignment, the load was reduced to approximately twenty pounds, and the two gauges for measuring extension and lateral contraction were clamped on to the specimen. The clip gauge for measuring strains in the width direction was clamped within the 2 in. initial gauge length. Initial readings for the clip gauges were then obtained. At predetermined extension values the load and strain in width direction were measured until the load reached a maximum and began to decrease. At this point the clip gauges were removed from the specimen, which was then strained to fracture. All tests were carried out at a constant cross-head speed of approximately 0·06 in. per minute.

Following each prestraining operation, two tensile tests were made. In each case the true stress in tension (σ_1) was computed from the relation

$$\sigma_1 = \frac{L}{A_0}(1 + \epsilon_1) \tag{1}$$

where L is the instantaneous load, A_0 the original cross-sectional area and ϵ_1 the nominal strain under load. The true plastic strain (δ_1) in a direction coinciding with that of the longitudinal axis of the tensile specimen was computed from the relation

$$\delta_1 = \ln(1 + \epsilon'_1) \tag{2}$$

where ϵ'_1 is the plastic nominal strain defined by $\epsilon'_1 = \epsilon_1 - \sigma_1/E$, where E is the elastic modulus in tension.

The true strain (δ_2) in the width direction was computed from the relation

$$\delta_2 = \ln (1 + \epsilon_2) \tag{3}$$

where ϵ_2 is the nominal strain in the width direction under load. The elastic correction in this case, using 0·3 for Poisson's ratio, was found to be insignificant. Since the strain in the width direction was measured at a single point, it may not represent, as is the case for the longitudinal direction, the average strain within the gauge length. It has been found, however, from tests on specimens inclined at 0, 22·5, 67·5 and 90° to the rolling direction, that the variation in δ_2 within the initial 2 in. gauge length was very small for most of the plastic range prior to necking.

6. Stress-Strain Relationship during Plastic Flow in Anisotropic Materials

The relationship between average true stress and strain in tension during plastic straining up to the point of maximum load has been found to be represented for various steels and non-ferrous alloys (Low 1947; Hollomon 1945; Gensamer 1946) by the power function

$$\sigma_1 = K \delta_1^n \tag{4}$$

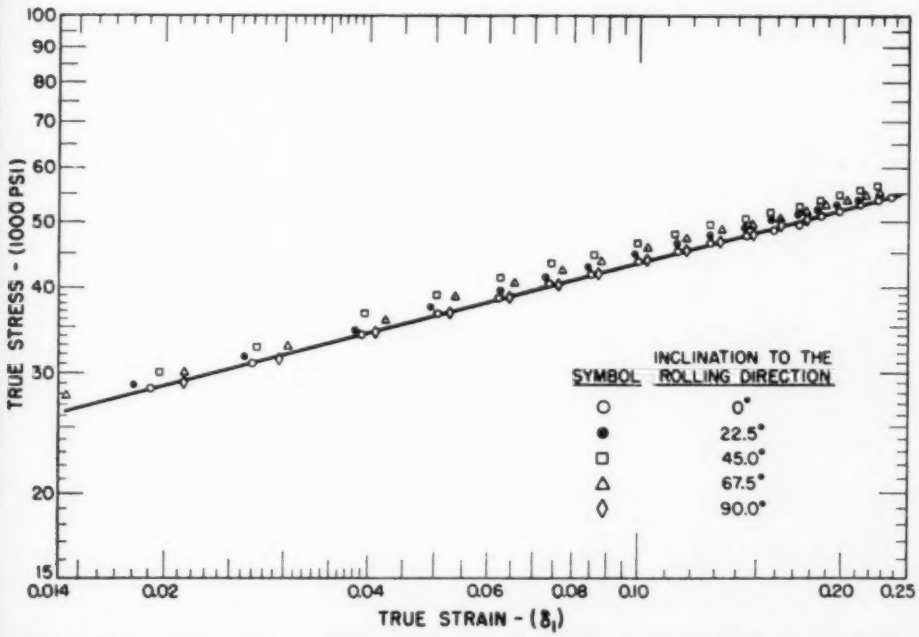

Fig. 2. True stress – true strain relationship for simple tension tests at various inclinations to the rolling direction.

where K and n are material constants. By plotting the logarithm of the true stress (σ_1) against the logarithm of true strain (δ_1), the data should result in a straight line with, slope (n) and ian intercept K at $\delta_1 = 1$.

Logarithmic true stress-strain curves in tension for the steel under investigation at various orientations to the rolling direction are presented in Fig. 2. To avoid

confusion only one straight line, following the results for 0° inclination, is shown in Fig. 2. In each case, however, the test results satisfy relation (4). The material constants n and K computed from these results are given in Table 1.

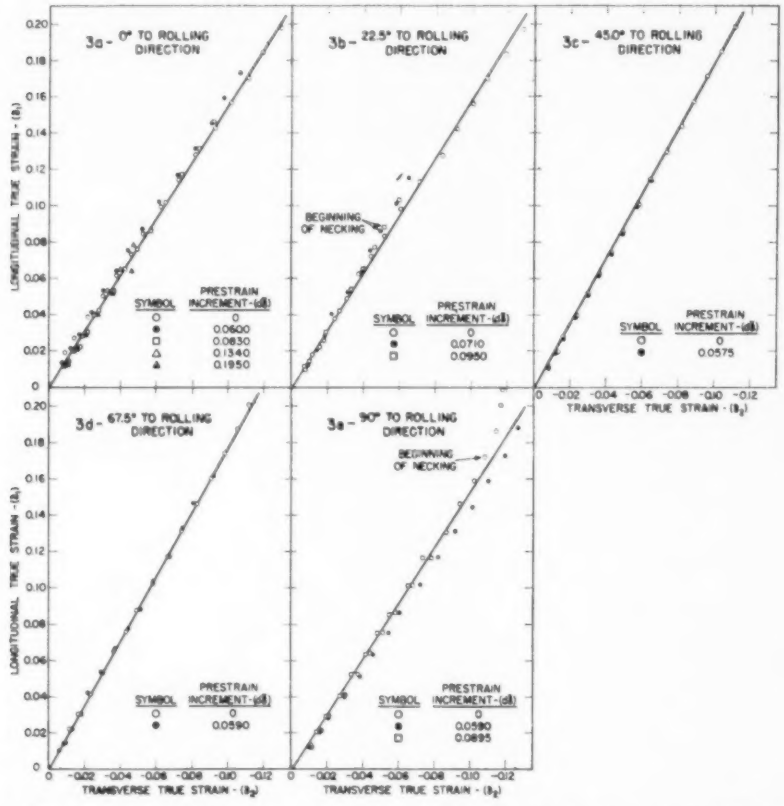
3a - 0° TO ROLLING DIRECTION
3b - 22.5° TO ROLLING DIRECTION
3c - 45.0° TO ROLLING DIRECTION
3d - 67.5° TO ROLLING DIRECTION
3e - 90° TO ROLLING DIRECTION
BEGINNING OF NECKING
SYMBOL
PRESTRAIN INCREMENT - (ε̄i)
LONGITUDINAL TRUE STRAIN - (δ1)
TRANSVERSE TRUE STRAIN - (δ2)

Fig. 3. Effect of pre-straining in tension in the rolling direction on the relationship between longitudinal true strain (δ_1) and transverse true strain (δ_2) in subsequent tension at various various orientations to the direction of rolling.

For an isotropic sheet material the true stress-strain curves in the plane of the sheet should coincide. These curves will also coincide, however, in case of rotational symmetry of anisotropy. The degree of anisotropy can be determined from the ratio of the true strain in the longitudinal direction to the true strain in the width direction. This ratio should be minus two for an isotropic material. The relationship between δ_1 in the longitudinal direction and δ_2 in the width direction is found to be linear up to the necking point for all orientations to the rolling direction, as shown by the open circles in Fig. 3. Apparently the degree of anisotropy does not change as straining proceeds. A similar behaviour has also been observed in a number of non-ferrous metals (BOURNE and HILL 1950; HAZLETT, ROBINSON and DORN 1950). The deviations found in Fig. 3b for results after prestraining in tension, and in Fig. 3c for results of as-received material, indicate the beginning of necking. The values of $-\delta_1/\delta_2$ for all orientations obtained from Fig. 3 are

included in Table 1. These values are appreciably less than minus two, and vary somewhat with orientation. As should be expected, variation with orientation is also found in the material constants, especially in the K values.

TABLE 1

Material constants obtained from simple tension tests of as-received steel sheet for various orientations to the initial rolling direction

Orientation to rolling direction – degrees	n	K (1,000 *psi*)	$-\delta_1/\delta_2$	k_{13}	k_{23}	*Limiting strain* δ_1
0	0·253	77·9	1·56	1·79	1·82	0·250
22·5	0·253	77·7	1·59	1·69	1·32	0·211
45·0	0·259	84·9	1·78	1·28	1·28	0·238
67·5	0·260	81·7	1·76	1·32	1·69	0·228
90·0	0·256	78·4	1·55	1·82	1·79	0·227

Prestrains at 0° to rolling direction seem to have very little effect on the anisotropy in subsequent tension in the same direction, as shown in Fig. 3a. As shown in Figs. 3b to 3e and in Figs. 4a and 4b, small amounts of prestrain in tension

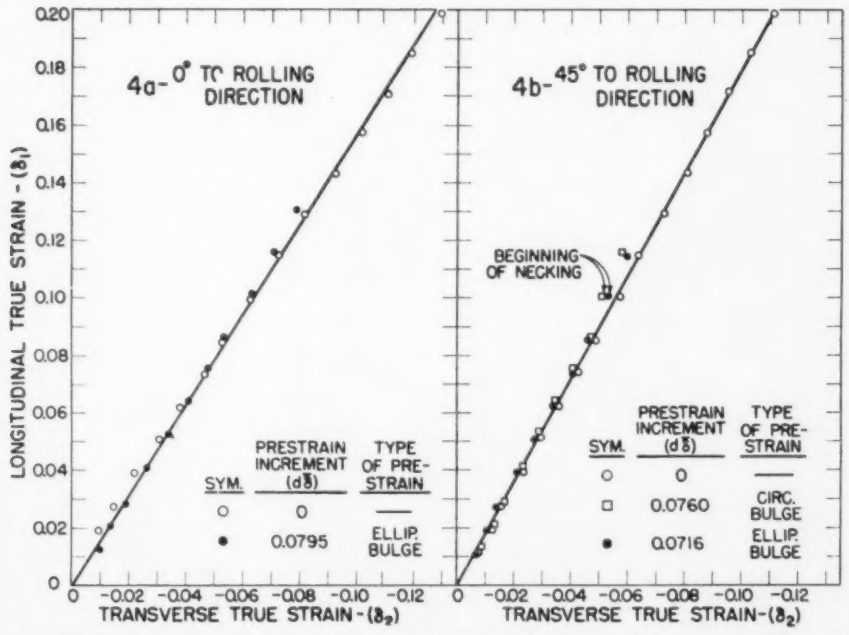

Fig. 4. Effect of prestraining under combined loads on the relationship between longitudinal true strain (δ_1) and transverse true strain (δ_2) at 0° and 45° to the direction of rolling.

or under biaxial tension have no marked effect on the anisotropy when changing the direction of straining or the state of stress. The values of $(-\delta_1/\delta_2)$ for all orientations given in Table 1 are employed later in the analysis on the effect of

prestrain on flow behaviour. Based on the results just discussed, it is assumed that they are not affected by prestraining.

Several generalized relations for anisotropic materials relating effective stress and strain-increment in the plastic range have been advanced (HILL 1948, 1950; JACKSON, SMITH and LANKFORD 1949; HAZLETT, ROBINSON and DORN 1950). It has been found for the material tested in this investigation that the anisotropy exhibited satisfies a special type of symmetry (HILL 1950; JACKSON, SMITH and LANKFORD 1949). This has been termed orthotropic symmetry, wherein the orthogonal planar axes of anisotropy are in the rolling and transverse directions, and the third axis is normal to the plane of the sheet. In formulating the orthotropic relations, it is assumed that the axes of symmetry remain fixed. Therefore, the variation in the material constants given in Table 1 as orientation is changed cannot be predicted with these relations. However, the more generalized theory proposed by HILL (BOURNE and HILL 1950) is to some extent in agreement with the experimental results. This theory predicts anisotropic symmetry about the axis at 45° to the rolling direction. Although the agreement is not exact, as may be seen in Table 1, the results are not sufficient for a thorough test of the theory. It should be noted also that the type of anisotropy exhibited by the material tested does not satisfy the conditions encountered in the relations of HAZLETT *et al.* Because the material constants and $-\delta_1/\delta_2$ values for 0° and 90° inclinations are essentially the same, the HAZLETT relations predict rotational symmetry of anisotropy. That is to say that n, K and $-\delta_1/\delta_2$ values should be independent of orientation.

The usefulness of the relations of JACKSON *et al.* may be enhanced, if it is found for various sheet materials that orthotropic anisotropy is not restricted to single-fold symmetry about the axis normal to the sheet. To prove the existence of many-fold symmetry, the anisotropy constants for each orientation with respect to a fixed direction, such as that of rolling, must be determined experimentally or determined from the relations presented by HILL. Following the method of JACKSON *et al.*, anisotropic constants for any orientation are computed from the relations

$$k_{13} = \frac{-1}{1 + \delta_1/\delta_2} \tag{5}$$

and

$$k_{23} = \frac{-1}{1 + \delta'_1/\delta'_2} \tag{6}$$

where the ratios δ_1/δ_2 and δ'_1/δ'_2 are determined from tensile tests of specimens whose axes are 90° apart in the plane of the sheet. Values of the computed anisotropy constants for the orientations included in this investigation are given in Table 1.

The effective stress according to JACKSON *et al.* becomes*

$$\bar{\sigma} = \left\{\frac{3}{2\,(k_{13} + k_{23} + k_{13}\,k_{23})}\,[k_{13}\,k_{23}\,(\sigma_1 - \sigma_2)^2 + k_{23}\,(\sigma_2 - \sigma_3)^2 + k_{13}\,(\sigma_3 - \sigma_1)^2]\right\}^{1/2} \tag{7}$$

and the effective strain-increment becomes*

$$d\bar{\delta} = \frac{\sigma_1 \, d\delta_1 + \sigma_2 \, d\delta_2 + \sigma_3 \, d\delta_3}{\bar{\sigma}} \tag{8}$$

where σ_1, σ_2 and σ_3 are principal true stresses and $d\delta_1$, $d\delta_2$ and $d\delta_3$ are the principal true strain-increments. By substituting, in relations (7) and (8), the appropriate constants of anisotropy, it is found, as shown in Fig. 5, that for all orientations a common logarithmic effective stress-strain curve is obtained. This finding indicates that, for the material tested, the anisotropy encountered has at least four-fold symmetry.

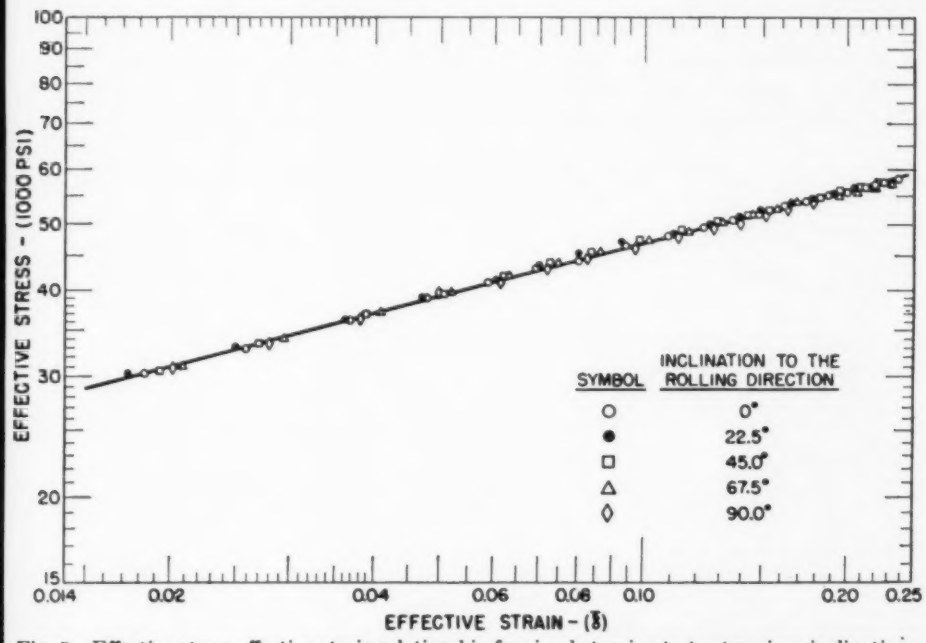

Fig. 5. Effective stress-effective strain relationship for simple tension tests at various inclinations to the rolling direction, assuming orthotropic symmetry.

The results in Fig. 5 also indicate that the function $\sigma = f(d\bar{\delta})$ is independent of orientation in the plane of the sheet, when the proper anisotropic constants are used. As shown by JACKSON *et al.*, this function is also independent of the strain path under conditions of constant strain ratios encountered in circular and elliptical bulge tests for the same anisotropic steel sheet as the one investigated here. It has also been found from experimental results on several non-ferrous materials that to a first approximation the function $\sigma = f(d\delta)$ is independent of the strain path under conditions of varying strain ratios, but assuming isotropic symmetry (FAUPEL and MARIN 1951; MARIN, HU and HAMBURG 1953; MARIN and WISEMAN 1953).

The experiments included in the present investigatoin, as discussed later, constitute testing under conditions of varying strain ratios. An analysis of the

* See also HILL 1950, p. 333.

experimental results is made later to determine whether, for an anisotropic steel sheet, the effective stress-strain concept is independent of the strain path. It should be noted, however, that the effective stress is not expected to be an explicit function of the effective strain in the presence of strain-ageing or recovery effects, the Bauschinger effect or upon changing the temperature (Dorn, Goldberg and Tietz 1949) or strain rate (Miller, Smith and Kehl 1943). In the present investigation the test temperature and strain rate were kept essentially constant. Complete reversal of the three principal strains was not involved, eliminating consideration of the Bauschinger effect. A recovery effect during the interval between the end of prestraining and retesting has been found, although the prestraining in tension was in the same direction as retesting in tension.

To determine the magnitude of the recovery effect, a number of longitudinal tensile specimens were strained 5, 10, 15 and 20%, and retested after holding for 7, 30 or 60 days at room temperature or at 0°C. A typical set of data shown as logarithmic true stress-true strain curves are given in Fig. 6. These results show

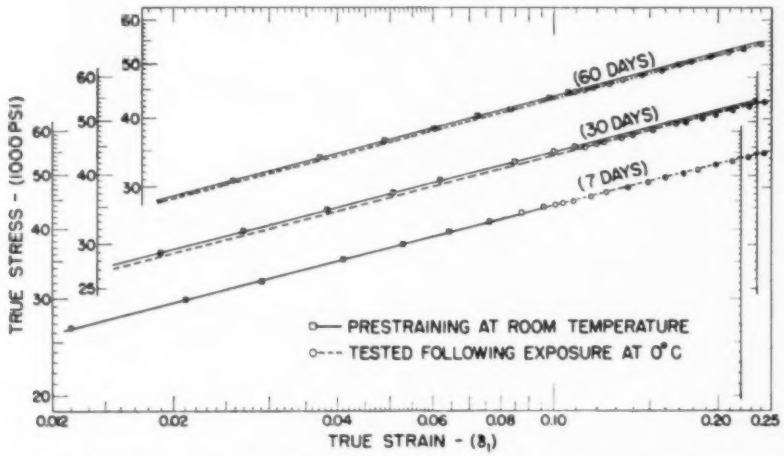

Fig. 6. Effect of time at approximately 0°C after pre-straining in tension on logarithmic stress-strain curve.

that, after a prestrain of approximately 0·1 true strain, holding at 0°C and retesting no change is found in the slope, or n, but a change in the intercept K is found after the 30 and 60 day interruptions. In all the other cases examined, the n value was unchanged, but the K value was found to vary except following 5% prestrain. The maximum deviation in K was found to be approximately 3%. However, this effect is small and will be neglected in the analysis of the experimental data.

7. Effect of Prestraining in Tension on Flow Behaviour in Tension

Upon close examination it is found that the strain path (that is, the relationship between δ_1 and δ_2) during prestraining in tension, is different from that during retesting in tension, except at 0° to the rolling direction. It is possible, therefore,

to determine from the results obtained in this investigation whether the function $\bar{\sigma} = f(d\bar{\delta})$ is independent of the strain path under conditions of varying strain ratios for an anisotropic steel sheet. If the effective stress depends only on the effective strain-increment, one logarithmic effective stress-strain curve should be obtained for as-received or prestrained material.

As discussed previously, the anisotropic characteristics of the material satisfy orthotropic symmetry and, therefore, the relations advanced by JACKSON *et al.* can be used during the retest to determine effective stress and strain-increment values, which for simple tension become

$$\bar{\sigma} = \sigma_1 \left\{ \frac{3\,(k_{13}\,k_{23} + k_{13})}{2\,(k_{13} + k_{23} + k_{13}\,k_{23})} \right\}^{1/2} \tag{9}$$

and

$$d\bar{\delta} = \frac{-1}{k_{13}} \left\{ \frac{2\,(k_{13} + k_{23} + k_{13}\,k_{23})\,(k_{12}\,k_{23} + k_{13})}{3} \right\}^{1/2} d\delta_3. \tag{10}$$

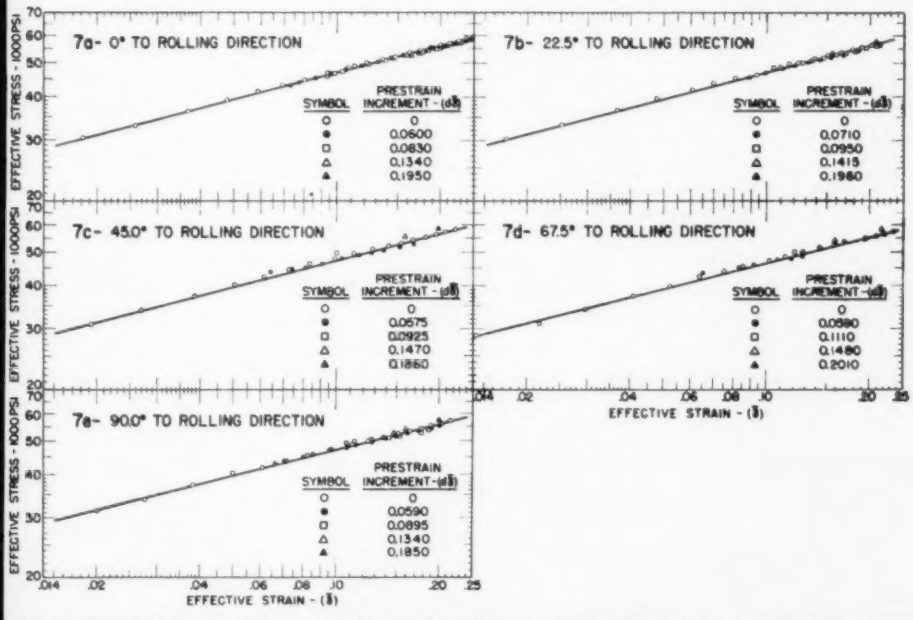

Fig. 7. Effect of pre-straining in tension in the rolling direction of flow behaviour in subsequent tension at various orientations to direction of rolling, assuming orthotrpoic symmetry.

In computing the effective stress and strain, the particular anisotropy constants for each orientation in the plane of the sheet are used. The direction of the strain-increment ($d\delta_3$) coincides with the axis perpendicular to the plane of the sheet, and is unchanged during the prestraining operation of during the retest, although the strain ratio ($-\delta_1/\delta_2$) or strain path is changed, except for the retest at 0° to the rolling direction.

The values of effective stress and strain for all inclinations are shown in Fig. 7. The effective strain represents the cumulative sum of the effective strain-increments during the prestrain and subsequent tensile test. The effective strain-increment

during the prestrain is computed from relation (10) by employing the anisotropy constants relating to straining in the rolling direction. Although duplicate tests were made in all cases, test results from only one test are given. For the test in the rolling direction, Fig. 7a, a downward shift is found in the logarithmic stress-strain curve. The slope is found unchanged following the prestrain. In obtaining these results the tensile prestrain was followed by testing in tension without altering the strain path. All experimental points should fall therefore on the original logarithmic stress-strain curve for 0° inclination, except for differences in properties arising between specimens or arising from recovery effects occurring before the retest. The increase that takes place in the downward shift of the flow curve the greater the prestrain, indicates from observations mentioned previously that a recovery effect is responsible for this behaviour.

The results for the other inclinations show, in Figs. 7b to 7e, that the computed values lie near the original flow curve, as should be expected for the condition that the effective stress is an explicit function of the effective strain. However, two important deviations are noted. The first is the observation that the initial flow stress determined upon retesting is higher than expected for all prestrains greater than 0·07, whereas the second is the finding that the slope of the logarithmic flow curve during the retest has been lowered appreciably. Moreover, it is found, as will be discussed in detail later, that beyond a prestrain of approximately 0·095, except for 0° inclination, maximum load on retest occurs after a tensile strain of about 0·01. For prestrain greaters than 0·095 only one experimental point is thus shown. It must be concluded therefore from these test results that, for the steel sheet studied here and for the type of tests included, the effective stress to a first approximation seems to depend only on the effective strain ; however, important deviations from expected behaviour are found. Somewhat similar indications have been interpreted by Brown, Millenson and Jones (1948) from limited results on copper alloys.

Vol
3
1954/

8. Effect of Prestrain under Biaxial Tension on Flow Behaviour in Tension

A circular and an elliptical bulge tester were used for prestraining under biaxial tension. As mentioned previously, tensile test pieces were taken from partially blown bulges at 0° and 45° to the original rolling direction of the sheet. For the test samples at 0° inclination, the prestrains included 5, 10, 20 and 30% in the rolling direction in the circular bulge, and transverse to the rolling direction in the elliptical bulge. For the 45° inclination, two extensions, 5 or 10% were employed. Upon removal of the blanks from the partially blown bulges, a permanent curvature was found in each blank. As mentioned, previously, the curvature was eliminated upon clamping of each blank during machining.

The experimental results have been treated in a manner similar to the analysis of the data obtained following tensile prestrains. Relations (9) and (10) apply again in this case during the retest in tension, whereas the total effective strain represents the cumulative sum of the effective strain-increment during the prestrain and subsequent tensile test. The effective strain-increment during the prestrain is computed from

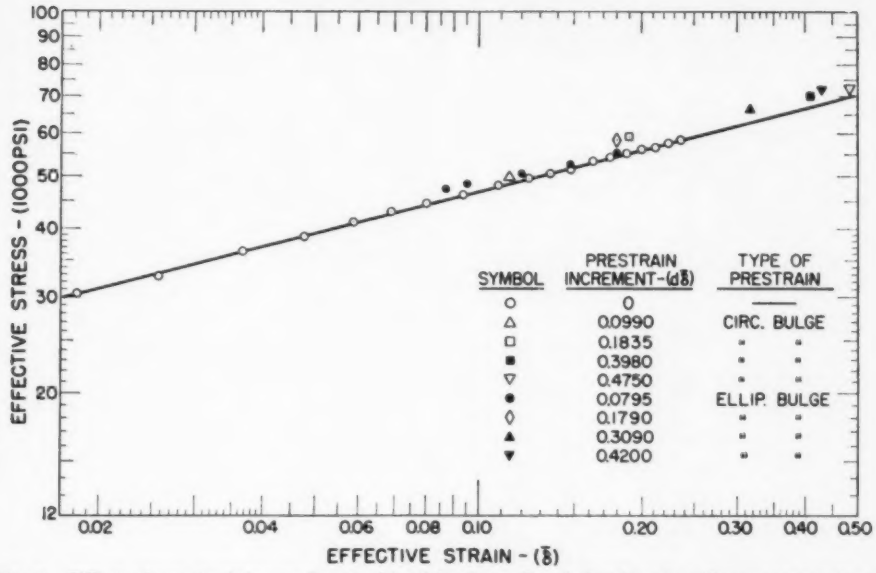

Fig. 8. Effect of pre-straining under combined loads on flow behaviour in subsequent tension at an inclination of 0° to direction of rolling, assuming orthotropic symmetry.

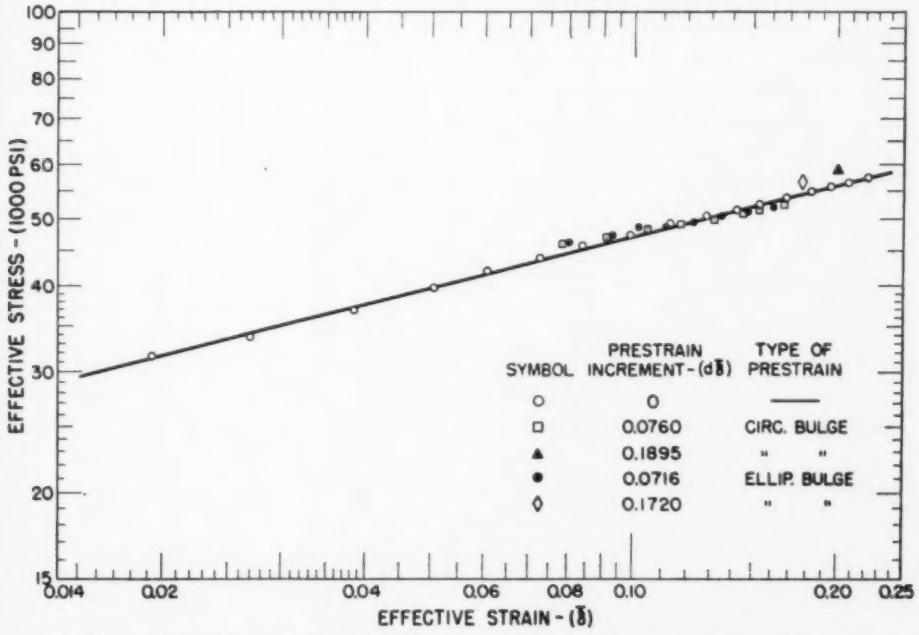

Fig. 9. Effect of pre-straining under combined loads on flow behaviour in subsequent tension at an inclination of 45° to direction of rolling, assuming orthotropic symmetry.

$$d\delta = \frac{-1}{(k_{13} + \alpha k_{23})} \left\{ \tfrac{2}{3} (k_{13} + k_{23} + k_{13} k_{23}) \left[k_{13} k_{23} (1 - 2\alpha + \alpha^2) + k_{13} + k_{23} \alpha^2 \right] \right\}^{1/2} \tag{11}$$

where $\alpha = \sigma_2/\sigma_1$.

The results for an inclination of 0° to the original rolling direction are shown in Fig. 8, and for 45° in Fig. 9. These results are somewhat similar to those following the tensile prestrain. The initial flow stress computed upon retesting in tension is appreciably greater than expected, if it is assumed that the effective stress depends only on the effective strain. The slope of the logarithmic flow curve is decreased again by the prestrain. The maximum load upon reloading, as shown later, is reached after an additional strain of 0·01 upon retesting when the effective prestrain is greater than about 0·095. Because of this effect, only one experimental point is shown for prestrains greater than this value.

9. Effect of Structural Changes during Prestraining on Subsequent Plastic Flow

From the results discussed above, it is concluded that it is not entirely possible to interpret the mechanical behaviour of metals by a single strain energy concept. Such behaviour must also be interpreted in the light of the structural changes which accompany plastic deformation.

The physical picture of the structural changes occurring during plastic deformation is not complete at present. Nevertheless, the information which is available indicates that the discrepancies found between theory and test results should be expected. This is based on the fact that in the effective stress-strain concept it is tacitly assumed that before or after plastic deformation metals are essentially homogeneous. Therefore, the complications arising from the very nature of the crystalline structure, the interactions between crystals in polycrystalline metals and the highly inhomogeneous nature of plastic deformation, are totally neglected. Some of the test results obtained in the present investigation are not unlike those observed for single crystals; therefore, the behaviour found after prestraining is related to fundamental aspects of plastic flow, which are not incorporated in the effective stress-strain concept.

Under conditions of simple tension in a single crystal, slip occurs when the resolved shear stress in a latent slip plane reaches a critical value. Upon further plastic deformation the active slip planes are rotated, thus becoming parallel to the direction of loading. If a second set of latent slip planes is present, these planes are subjected to this same rotation, and some therefore to an increasing component of resolved shear stress. Eventually, when the component of resolved shear stress is equal in both sets of planes, the latent slip planes are expected to become active, resulting in simultaneous or alternate slip on both sets. The actual behaviour in α-brass single crystals, for example, (Göler and Sachs 1929) shows that simultaneous slip does not occur as expected when the slip planes are rotated into a position where equal components of resolved shear stress are acting in both planes. In fact, slip is not observed in the second set of planes until these planes are rotated slightly beyond the position of equal resolved shear stress. Thus, the resolved shear stress component necessary to cause slip on the latent slip planes

has to be greater than the component necessary to enable the continuance of slip on active slip planes in which a certain amount of strain-hardening has occurred. This seems to imply that the structural changes occurring within one slip system has a strengthening effect on the second slip system. Moreover, it seems that this strengthening effect is greater in the latent slip planes than in the active ones. It should be noted, however, that strengthening of latent slip planes in α-brass is somewhat greater than in most metals (Bishop 1955).

Apparently, as shown by results on α-brass single crystals, after slip in the second slip system has spread across existing slip bands, appreciable deformation in the newly active planes occurs under an essentially constant resolved shear stress. Although little is known about the interactions between intersecting dislocations (Cottrell 1953; Read 1952), there is some indication that a certain amount of energy is required for the formation of a jog upon crossing each other. This may account for the higher resolved shear stress in the latent slip system for initiation of plastic flow.

The observations during slip in α-brass single crystals are not unlike those found in the tests included in the present investigation, as mentioned previously. In changing the direction of straining from tension during the prestrain to tension at a different orientation on retesting, a new set of latent slip planes, oriented at 45° to the new direction of loading which is a direction of maximum-resolved shear stress, becomes available. When slip occurs on these latent slip planes, it must cross the already existing slip bands, and as in the case of the α-brass single crystals, an initial flow stress greater than expected is found. Similarly, following prestraining under combined loads, new latent slip planes become available, and, again, it is observed experimentally that the initial flow stress in tension during the retest is greater than the expected value. It should also be noted that the discrepancy in this case between the predicted and observed values is greater than those following prestraining in simple tension.

The decrease, after prestraining, in the strain-hardening coefficient, which is discussed more completely later, is similar to the observed slip in the second slip system of the α-brass single crystals proceeding without any appreciable increase in the resolved shear stress.

10. Effect of Prestraining on Limiting Ductility

During a tensile test of a ductile metal it is generally found that, as straining progresses, the material strain-hardens at a decreasing rate, and the load supported by the specimen eventually reaches a maximum and begins to decrease. The lateral strain distribution within the reduced section does not remain exactly uniform up to the maximum load, at which point it is found that the specimen exhibits a well-defined neck. The true strain to the point of maximum load is defined here as the limiting ductility, since beyond this point the strain becomes completely localized within the neck.

The existence of a maximum in the load in a tensile test, and therefore the limiting ductility, as defined here, is related to the rate of strain hardening, and the rate of decrease in the load-carrying capacity of the specimen as the cross-sectional area decreases (Gensamer 1946; Hill 1950). This is shown by the relation

$$L_T = L + L_D \tag{12}$$

where L_T is the theoretical load, based on a constant cross-sectional area, that can be supported during strain-hardening, L the actual load supported by the specimen, and L_D the loss in load-carrying capacity or load decrement. The theoretical

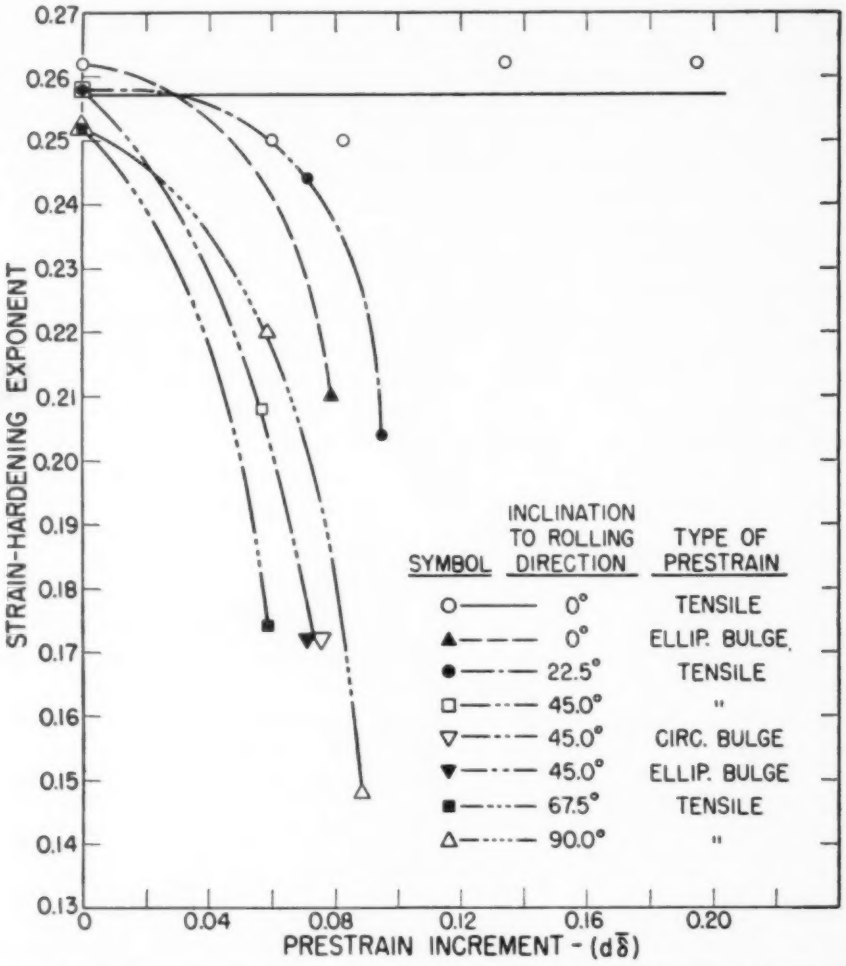

Fig. 10. Effect of pre-straining in tension or under biaxial tension on strain-hardening exponent determined from logarithmic effective stress-strain curves.

load L_T can be defined by $Ao\,\sigma_1$, where Ao is the original area and σ_1 the true stress. After substituting for L_T and differentiating with respect to the true strain, relation (12) becomes

$$\frac{dL}{d\delta_1} = Ao\frac{d\sigma_1}{d\delta_1} - \frac{dL_D}{d\delta_1} \tag{13}$$

This relation indicates that for an original area of unity the load in a tensile test

reaches a maximum when the rate of strain-hardening is equal to the rate of loss of load-carrying capacity. It is found experimentally that whereas $d\sigma_1/d\sigma_1$ decreases, $dL_D/d\delta_1$ increases as L increases. The rate at which these two quantities approach each other determines eventually the magnitude of the limiting strain.

As discussed previously, it has been found that upon prestraining and changing the strain path or state of stress, a decrease in the rate of strain-hardening in subsequent tension has been found for any equivalent effective strain. It is also found, although not understood, that the rate of loss of load-carrying capacity is increased for any equivalent effective strain after the prestrain. From the above relation it may be observed that these effects tend to decrease the magnitude of the limiting ductilit luring the retest.

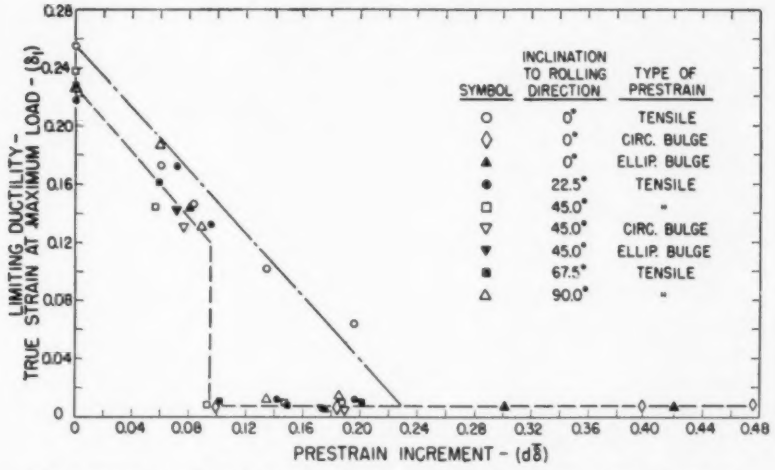

Fig. 11. Effect of pre-straining in tension and under biaxial tension on true strain at maximum load during the tensile re-test.

The effect of prestraining on the rate of strain-hardening, as indicated by the strain-hardening exponent, is shown in Fig. 10. Values of the strain-hardening exponent were determined from the results in Figs. 7, 8 and 9. It is observed from Fig. 10 that the strain-hardening exponent remains essentially constant after prestraining in tension, if the direction of testing during the retest is unchanged. For all other cases a sharp drop in the strain-hardening exponent is observed as the prestrain-increment approaches 0·10.

The effect of prestrain on the limiting ductility, that is, true strain at the maximum load, during the retest, is given in Fig. 11. As should be expected, the limiting ductility, after prestraining in tension, and retesting in tension in the same direction, varies linearly with the prestrain increment. A similar behaviour would be expected for all other cases studied. The experimental results, however, show that beyond a prestrain of approximately 0·095, the limiting strain during the retest is reduced to essentially 0·01. This sharp decrease in the limiting ductility is undoubtedly related to the drastic drop in the strain-hardening exponent shown in Fig. 10. It has been shown in the past by Hollomon (1945) and Gensamer (1946), that at the maximum load in tension the true strain is equal to the

strain-hardening exponent, although experimentally, as indicated in Table 1, this condition may not be completely satisfied.

11. Effect of Prestraining on Fracture Behaviour

A number of observations relating to the fracture behaviour during the simple tension tests are of particular interest. It was observed in the as-received material that, upon straining in tension up to the maximum load, the surface remains smooth without surface markings. During necking, however, a rectangular depression forms within the neck region. Upon further straining other strain markings appear, These are shallow depressions oriented along two planes normal to the specimen surface, and inclined at approximately 50° to the specimen axis. With further straining, a crack extending through the entire thickness of the specimen appears at the point of the depression, which is found at the intersection of the strain markings. In several cases this crack, which was in a plane normal to the specimen axis, spread at a fairly slow rate. Eventually, total separation occurs by a sliding action along one of the two strain markings. Prestraining seems to have no effect on the events leading to fracture. In all specimens tested the angle between the fracture surface and specimen axis remained constant, and is found to be approximately 50°.

The final rupture along one of the two strain markings is believed to be caused (Zener 1948) by localization of adiabatic shear strain. The fact that the maximum shear strain-increment occurs at 50° to the direction of loading is surprising, since it does not coincide with the direction of the maximum resolved shear stress, which is acting presumably at an angle of 45°. However, it has been shown by Hill (1948) that these directions do not generally coincide, and that the discrepancy depends on the type of anisotropy. For an isotropic material the direction of maximum shear strain-increment is at 55° to the direction of loading. Since in the direction of maximum shear strain-increment the incremental extension is zero, it results from the constancy of volume condition that the sheet material can contract only in the thickness direction. Thus the strain markings which were observed actually constitute a type of neck by localized thinning in a direction normal to the plane of the sheet.

The direction of the strain markings can be predicted for an anisotropic sheet tested in tension in the rolling or transverse direction from the following theoretical relation given by Hill (1950)

$$\tan \theta = (\delta_1/\delta_2)^{1/2} \tag{14}$$

where θ is the angle between the markings and the direction of loading. For the steel sheet tested in this investigation relation (14) predicts an angle of 51° which is in agreement with the 50° angle observed.

12. Summary and Conclusion

The effect of prestraining in simple tension on plastic flow and fracture in tension at 0°, 22·5°, 45°, 67·5° or 90° to the direction of the tensile prestrain has been determined for a fully killed, temper-rolled, deep-drawing steel sheet. In addition, the effect of prestrains under biaxial tension, using a circular and an

elliptical bulge tester, on flow and fracture behaviour in subsequent tension at 0° or 45° to the initial rolling direction, has been investigated. The following conclusions are indicated by the test results :

1. The initial anisotropy of the material in any orientation to the rolling direction is unaffected by straining in tension up to the point of maximum load. Small amounts of prestrain up to 0·095 effective strain-increment in simple tension or under biaxial tension do not affect the initial anisotropy when the direction of straining or state of stress is changed.

2. The type of anisotropy exhibited by the steel sheet studied satisfies orthotropic symmetry. However, this type of anisotropy is found to exhibit at least four-fold symmetry. To prove the existence of many-fold symmetry it is necessary for each new orientation to determine the anisotropic constants experimentally.

3. Upon prestraining in tension in the direction of rolling, and changing the direction of straining upon retesting in tension, it is found, in general, that the initially determined flow stress is greater than that predicted by the effective stress-strain concept : the strain-hardening coefficient, or rate of strain hardening, is decreased, and beyond a prestrain of 0·095 effective strain-increment the point of maximum load is reached upon retesting after about 0·01 strain. Similar observations are found after prestraining under conditions of biaxial tension and retesting in tension.

4. After prestraining in simple tension or under biaxial tension, and upon retesting in tension in a different direction, or when changing the state of stress, the strain-hardening coefficient decreases continually and sharply as the prestrain increases. Also, prestraining brings about an increase in the rate of loss of load-carrying capacity of the material for any equivalent effective strain, when compared to the as-received material.

5. The fracturing characteristics of the material in simple tension were unchanged by the prestrain. Final fracture occurred along strain markings which appeared during necking. These markings are formed by thinning in the thickness direction, and are in a direction of maximum shear strain-increment, which for the material studied is calculated to be at 51° to the direction of loading when testing in the rolling or transverse direction. Experimentally it is found that, for the as-received or prestrained material, the angle between the markings, or fracture surface, and direction of loading, remains constant and is approximately 50°.

Vol. 3 54/55

Acknowledgments

The authors are indebted to the United States Steel Corporation for supporting this investigation and supplying the test material. The valuable help of Messrs. H. E. Hartner and G. F. McCracken in conducting the experimental work is gratefully acknowledged.

References

Bishop, J. F. W. 1955 *J. Mech. Phys. Solids*, **3**, 130.

Bourne, L. and Hill, R. 1950 *Phil. Mag.*, **41**, 671.

Bridgman, P. W. 1952 *Studies in Large Plastic Flow and Fracture* (McGraw-Hill, New York).

BROWN, W. F., MILLENSON, M. B. and JONES, M. H.	1948	*Trans. AIME*, **175**, 462.
CHOW, C. C., DANA, A. W. and SACHS, G.	1949	*Trans. AIME*, **185**, 49.
COTTRELL, A. H.	1953	*Dislocations and Plastic Flow in Crystals* (Oxford University Press).
DORN, J. E., GOLDBERG, A. and TIETZ, T. E.	1949	*Trans. AIME*, **180**, 205.
FAUPEL, J. H. and MARIN, J.	1951	*Trans. ASM*, **43**, 993.
GENSAMER, M.	1946	*Trans. ASM*, **36**, 30.
GÖLER, V. and SACHS, G.	1929	*Z. Physik.*, **55**, 581.
HAZLETT, T. H., ROBINSON, T. A. and DORN, J. E.	1950	*Trans. ASM*, **42**, 1326.
HILL, R.	1948	*Proc. Roy. Soc.* A, **193**, 281.
	1950	*The Mathematical Theory of Plasticity* (Clarendon Press, Oxford).
HOLLOMON, J. H.	1945	*Trans. AIME*, **162**, 268.
HOLLOMON, J. H. and ZENER, C.	1944	*Trans. AIME*, **158**, 283.
JACKSON, L. R., SMITH, K. F. and LANKFORD, W. T.	1949	*Trans. AIME*, **180**, 415.
KÖRBER, F. EICHINGER, A. and MÖLLER, H.	1941	*Mitt. K.W.I.*, **23**, No. 29, 123.
	1943	*Mitt. K.W.I.*, **26**, No. 6, 71.
LANKFORD, W. T., LOW, J. R. and GENSAMER, M.	1947	*Trans. AIME*, **171**, 574.
LIU, S. I.	1951	*Trans. AIME*, **191**, 452.
LIU, S. I. and SACHS, G.	1949	*Trans. AIME*, **180**, 193.
LOW, J. R. and GAROFALO, F.	1947	*Proc. SESA*, **4**, No. **2**, 16.
LYNCH, J. J., RIPLING, E. J. and SACHS, G.	1948	*Trans. AIME*, **175**, 435.
MARIN, J., HU, L. W. and HAMBURG, J. F.	1953	*Trans. ASM*, **45**, 686.
MARIN, J. and WISEMAN, H. A. B.	1953	*Trans. AIME*, **197**, 1181.
MEHRINGER, F. J. and MACGREGOR, C. W.	1945	*Trans. AIME*, **162**, 291.
MILLER, R. F., SMITH, G. V. and KEHL, G. L.	1943	*Trans. ASM*, **31**, 817.
READ, W. T.	1953	*Dislocations in Crystals* (McGraw-Hill, New York).
SWIFT, H. W.	1939	*J. Iron and Steel Inst.*, **140**, 181.
ZENER, C.	1948	*Fracturing of Metals* (American Society for Metals, Cleveland).

Vol 3 1954/

BOOK REVIEWS

K. SWAINGER : **Analysis of Deformation, Volume 2.** Chapman and Hall, London, 1954, pp. xxxvi + 365. 70s.

IN the preface and in remarks scattered throughout the book, the author establishes the position that he has presented a unified linear theory of deformation embracing ' all substances which deform under applied loads.' It is implied that this theory is of sufficient novelty as to have met with difficulties of publication in the scientific literature, hence the need for this treatise. This position is not without precedent. The author cannot, however, complain if an impartial study of his ideas leads to the conclusion that his theory is limited or erroneous. In the following the reviewer has attempted to be impartial and objective.

This volume deals with experiment and applied theory. The author expresses the hope that it will supply a ' need of the research engineer, experimentalist and physicist without unduly emphasizing the mathematical aspect of the subject.' Obviously a very great deal of care and labour has been spent on the writing and setting out of the book. Nevertheless it is extremely difficult to follow. The author works in terms of dyadics, which, combined with an involved symbolism and an esoteric terminology, will deter all but the most persistent readers. It does not seem that this presentation of standard results is any advance on the many excellent presentations already to hand. Attention will therefore be focussed on those aspects of the book which present the author's own ideas. The two main aspects of these are presumably the formulation of a linear theory of finite strain, and secondly a (co-existent) unified elastic-plastic deformation theory. Dr. GORDON in a communication to ' *Nature* ' has shown that the author's finite strain theory is not general and is meaningful only for irrotational strains. The author's reply to this courteous scientific criticism is not encouraging. He describes it as a ' polemical letter ' (p. 178), and purports to answer it by confuting an argument which certainly Dr. GORDON has not advanced. Dr. GORDON's criticism is sound and the author has not formulated a general linear theory. There is a further detraction from the value of the book in that the author uses strain compatibility relations which are based on an error in the first volume. There the author wrongly applies the result that curl grad $\phi = 0$, where ϕ is a *scalar*, to his strain dyadic and obtains compatibility relations which are sufficient but not necessary. (If the argument is advanced that the strain dyadic is obtained from displacement D or from the displacement potential, and that this step is valid, the criticism that D is meaningful only for irrotational strains leads to the same conclusion.) The compatibility relations given are in fact restrictive to irrotational strains. Again, in considering stress, the author makes an unjustifiable assumption, namely that a *general* stress can be derived from a potential (ψ say) by $S_{ij} = \partial^2 \psi / \partial x_i \, \partial x_j$. This is restricting consideration to stress states having a constant hydrostatic part.

In his treatment of plastic flow the author again conflicts with contemporary thought. He appears to hold the view that plastic strain-increment and stress increment are related in terms of a material *constant* (e.g., pp. 51, 100, 121). This does not prevent his criticizing Professors HILL and PRAGER (p. 118 *et seq.*) for deviations from a third (and presumably also erroneous) theory involving 'Trouton's coefficient of viscous extension.' The truth here is that Dr. SWAINGER's criticisms are quite out of context and demonstrably wrong. Moreover, his own theory does not fit the facts.

It will be appreciated that this is an extremely critical review. Nevertheless the reviewer must not lose sight of his duty to the reader as well as to the author. The major criticisms advanced here and elsewhere render this book of very doubtful value as a text-book. As a statement of the author's ideas the book will have a limited appeal to those specialists who are able to ascertain precisely the validity of the statements made.

J. F. W. BISHOP

J. M. LESSELLS : **Strength and Resistance of Metals.** Wiley and Sons, Chapman and Hall, Ltd. 1954. xiv + 450. 80s.

ENGINEERING is as much an art as a science. While considerable advances have been made in

stress analysis, in both the elastic and plastic range, this advance is of little value unless an accurate knowledge and a full appreciation of the basic properties of the materials to be used are also available. Professor LESSELLS has set himself a formidable task in collecting this information into one volume, and the problem of editing the final manuscript must have been considerable.

The book deals mainly with steel, although attention is given to non-ferrous alloys. The obvious reason for this is that considerably more research has been carried out with steels than with any other group of metals. The tensile properties of metals at various rates of strain and temperature are adequately covered. The section dealing with " creep " gives the reader an accurate birds-eye view of a very complex phenomenon.

A whole chapter is devoted to impact, and while considerable attention is given to low temperature brittleness only brief reference is made to " cohesive strength " and its effect on ductility and mode of fracture.

The chapters on fatigue collate a large amount of experimental information on the more important factors affecting the phenomenon, which should be of great value to the designer and the research worker if supplemented by further reading.

It seems strange that the theories of strength should be included in the final chapter. One would have thought that, if these theories had been presented at the beginning, the understanding of certain phenomena reported in subsequent chapters would have been facilitated.

The section dealing with working stresses is weak, and one cannot but feel that more attention should have been given to plastic overstrain. These criticisms, however, in comparison with the major achievements, are minute.

Worked examples and adequate references to original works are given in each section for the reader who wishes to make a more detailed study. This book can be recommended to engineering undergraduates in their final year and to designers. It should also provide useful general reading for those undertaking research in the field of strength of materials.

J. A. POPE.

VOL 3 1954

END OF VOL.

Vol.
3
54/55